

THE BIOCHEMISTRY OF AMYLOIDS IN NEURODEGENERATIVE DISEASES, VOLUME I

EDITED BY: Cláudio M. Gomes, Wolfgang Hoyer and Jinghui Luo

PUBLISHED IN: Frontiers in Neuroscience and
Frontiers in Molecular Neuroscience



frontiers Research Topics



frontiers

Frontiers eBook Copyright Statement

The copyright in the text of individual articles in this eBook is the property of their respective authors or their respective institutions or funders. The copyright in graphics and images within each article may be subject to copyright of other parties. In both cases this is subject to a license granted to Frontiers.

The compilation of articles constituting this eBook is the property of Frontiers.

Each article within this eBook, and the eBook itself, are published under the most recent version of the Creative Commons CC-BY licence.

The version current at the date of publication of this eBook is CC-BY 4.0. If the CC-BY licence is updated, the licence granted by Frontiers is automatically updated to the new version.

When exercising any right under the CC-BY licence, Frontiers must be attributed as the original publisher of the article or eBook, as applicable.

Authors have the responsibility of ensuring that any graphics or other materials which are the property of others may be included in the CC-BY licence, but this should be checked before relying on the CC-BY licence to reproduce those materials. Any copyright notices relating to those materials must be complied with.

Copyright and source acknowledgement notices may not be removed and must be displayed in any copy, derivative work or partial copy which includes the elements in question.

All copyright, and all rights therein, are protected by national and international copyright laws. The above represents a summary only. For further information please read Frontiers' Conditions for Website Use and Copyright Statement, and the applicable CC-BY licence.

ISSN 1664-8714

ISBN 978-2-88974-251-6

DOI 10.3389/978-2-88974-251-6

About Frontiers

Frontiers is more than just an open-access publisher of scholarly articles: it is a pioneering approach to the world of academia, radically improving the way scholarly research is managed. The grand vision of Frontiers is a world where all people have an equal opportunity to seek, share and generate knowledge. Frontiers provides immediate and permanent online open access to all its publications, but this alone is not enough to realize our grand goals.

Frontiers Journal Series

The Frontiers Journal Series is a multi-tier and interdisciplinary set of open-access, online journals, promising a paradigm shift from the current review, selection and dissemination processes in academic publishing. All Frontiers journals are driven by researchers for researchers; therefore, they constitute a service to the scholarly community. At the same time, the Frontiers Journal Series operates on a revolutionary invention, the tiered publishing system, initially addressing specific communities of scholars, and gradually climbing up to broader public understanding, thus serving the interests of the lay society, too.

Dedication to Quality

Each Frontiers article is a landmark of the highest quality, thanks to genuinely collaborative interactions between authors and review editors, who include some of the world's best academicians. Research must be certified by peers before entering a stream of knowledge that may eventually reach the public - and shape society; therefore, Frontiers only applies the most rigorous and unbiased reviews. Frontiers revolutionizes research publishing by freely delivering the most outstanding research, evaluated with no bias from both the academic and social point of view. By applying the most advanced information technologies, Frontiers is catapulting scholarly publishing into a new generation.

What are Frontiers Research Topics?

Frontiers Research Topics are very popular trademarks of the Frontiers Journals Series: they are collections of at least ten articles, all centered on a particular subject. With their unique mix of varied contributions from Original Research to Review Articles, Frontiers Research Topics unify the most influential researchers, the latest key findings and historical advances in a hot research area! Find out more on how to host your own Frontiers Research Topic or contribute to one as an author by contacting the Frontiers Editorial Office: frontiersin.org/about/contact

THE BIOCHEMISTRY OF AMYLOIDS IN NEURODEGENERATIVE DISEASES, VOLUME I

Topic Editors:

Cláudio M. Gomes, University of Lisbon, Portugal

Wolfgang Hoyer, Heinrich Heine University of Düsseldorf, Germany

Jinghui Luo, Paul Scherrer Institut (PSI), Switzerland

Citation: Gomes, C. M., Hoyer, W., Luo, J., eds. (2022). The Biochemistry of Amyloids in Neurodegenerative Diseases, Volume I. Lausanne: Frontiers Media SA. doi: 10.3389/978-2-88974-251-6

Table of Contents

- 04 Editorial: The Biochemistry of Amyloids in Neurodegenerative Diseases, Volume I**
Cláudio M. Gomes, Wolfgang Hoyer and Jinghui Luo
- 06 Insights Into Peptide Inhibition of Alpha-Synuclein Aggregation**
James H. Torpey, Richard M. Meade, Ravina Mistry, Jody M. Mason and Jillian Madine
- 17 Comparison of Common and Disease-Specific Post-translational Modifications of Pathological Tau Associated With a Wide Range of Tauopathies**
Fuyuki Kametani, Mari Yoshida, Tomoyasu Matsubara, Shigeo Murayama, Yuko Saito, Ito Kawakami, Mitsumoto Onaya, Hidetomo Tanaka, Akiyoshi Kakita, Andrew C. Robinson, David M. A. Mann and Masato Hasegawa
- 26 Looking Beyond the Core: The Role of Flanking Regions in the Aggregation of Amyloidogenic Peptides and Proteins**
Sabine M. Ulamec, David J. Brockwell and Sheena E. Radford
- 49 Natural Compounds as Inhibitors of A β Peptide Aggregation: Chemical Requirements and Molecular Mechanisms**
Katuscia Pagano, Simona Tomaselli, Henriette Molinari and Laura Ragona
- 67 Novel Phosphorylation-State Specific Antibodies Reveal Differential Deposition of Ser26 Phosphorylated A β Species in a Mouse Model of Alzheimer's Disease**
Sathish Kumar, Akshay Kapadia, Sandra Theil, Pranav Joshi, Florian Riffel, Michael T. Heneka and Jochen Walter
- 79 Prediction of Transmembrane Regions, Cholesterol, and Ganglioside Binding Sites in Amyloid-Forming Proteins Indicate Potential for Amyloid Pore Formation**
Katja Venko, Marjana Novič, Veronika Stoka and Eva Žerovnik
- 94 A Novel SOD1 Intermediate Oligomer, Role of Free Thiols and Disulfide Exchange**
Bon-Kyung Koo, William Munroe, Edith B. Gralla, Joan Selverstone Valentine and Julian P. Whitelegge
- 106 Rationally Designed Bicyclic Peptides Prevent the Conversion of A β 42 Assemblies Into Fibrillar Structures**
Tatsuya Ikenoue, Francesco A. Aprile, Pietro Sormanni and Michele Vendruscolo
- 115 Identification of Two Novel Peptides That Inhibit α -Synuclein Toxicity and Aggregation**
Blagovesta Popova, Dan Wang, Abirami Rajavel, Karthikeyan Dhamotharan, Diana F. Lázaro, Jennifer Gerke, Joachim F. Uhrig, Michael Hoppert, Tiago F. Outeiro and Gerhard H. Braus
- 133 Arginine and Arginine-Rich Peptides as Modulators of Protein Aggregation and Cytotoxicity Associated With Alzheimer's Disease**
Somayra S. A. Mamsa and Bruno P. Meloni



Editorial: The Biochemistry of Amyloids in Neurodegenerative Diseases, Volume I

Cláudio M. Gomes^{1,2*}, Wolfgang Hoyer^{3,4*} and Jinghui Luo^{5*}

¹ Faculdade de Ciências, Biosystems and Integrative Sciences Institute, Universidade de Lisboa, Lisbon, Portugal,

² Departamento de Química e Bioquímica, Faculdade de Ciências, Universidade de Lisboa, Lisbon, Portugal, ³ Institute of Physical Biology, Heinrich Heine University Düsseldorf, Düsseldorf, Germany, ⁴ Institute of Biological Information Processing (IBI-7) and Jülich Center for Structural Biology, Forschungszentrum Jülich, Jülich, Germany, ⁵ Department of Biology and Chemistry, Paul Scherrer Institute, Villigen, Switzerland

Keywords: protein aggregation, tau, synuclein, SOD1, Alzheimer's disease, Parkinson's disease, aggregation inhibitors, amyloid beta

Editorial on the Research Topic

The Biochemistry of Amyloids in Neurodegenerative Diseases, Volume I

Protein aggregation and formation of amyloids is a key pathological hallmark across multiple neurodegenerative diseases such as Alzheimer's disease (AD) and Parkinson's Disease (PD). Understanding the structural conversions underlying the formation of amyloid oligomers and fibrils, as well as the relevant molecular mechanisms that dictate the rate and type of aggregation, is critical not only to establish the underlying fundamental biological processes related to amyloid aggregation *in vivo*, but also to envision the design of mechanism-based and/or structure-oriented therapeutics against amyloid-related neurodegenerative diseases. This Research Topic and e-book comprises a series of original papers and updated reviews that present advances in this direction and highlight trends in the field, covering aspects related to mechanisms of amyloid formation and toxicity, the role of post translational modifications, and inhibitors of protein aggregation.

The formation of fibrillar aggregates is triggered by aggregation prone regions within polypeptides whose misfolding will trigger self-assembly into an ordered amyloid core, now elucidated in several atomic-resolution structures of the amyloid fold. However, as reviewed by Ulamec et al. the regions that flank such amyloid cores, which often form dynamic fuzzy coats around the amyloid core, play key roles as modulators of function, toxicity, and aggregation. In this comprehensive analysis, the authors present and discuss the flanking regions that either protect or accelerate aggregation and provide a conceptual framework to understand their roles in regulating the mechanism of self-assembly, interactions with other amyloidogenic proteins, membranes, chaperones, and RNA. The authors convincingly argue that investigations on these flanking regions will lead to a better understanding of the molecular mechanism of fibril formation and to the identification of new targets for drug development beyond the ordered amyloid core and the aggregation hotspots.

Superoxide dismutase 1 (SOD1) typifies a protein whose destabilization triggers amyloid fibrillation as in amyotrophic lateral sclerosis. Destabilization of the SOD1 homodimer due to loss of the catalytic Cu and Zn ions greatly destabilizes the protein, favoring reduction of a conserved intra-molecular disulfide that aggravates dimer dissociation, resulting in exposure of otherwise solvent shielded aggregation prone regions. However, SOD1 contains two additional distal cysteines whose role in the aggregation pathway remained unclear. Koo et al. here report an investigation on the role of free thiols and disulfide exchange in the aggregation of SOD1, concluding that the

OPEN ACCESS

Edited and reviewed by:

Einar M. Sigurdsson,
New York University, United States

*Correspondence:

Cláudio M. Gomes
cmgomes@fc.ul.pt
Wolfgang Hoyer
wolfgang.hoyer@hhu.de
Jinghui Luo
jinghui.luo@psi.ch

Specialty section:

This article was submitted to
Neurodegeneration,
a section of the journal
Frontiers in Neuroscience

Received: 21 November 2021

Accepted: 29 November 2021

Published: 16 December 2021

Citation:

Gomes CM, Hoyer W and Luo J
(2021) Editorial: The Biochemistry of
Amyloids in Neurodegenerative
Diseases, Volume I.
Front. Neurosci. 15:819481.
doi: 10.3389/fnins.2021.819481

reduction status modulates the formation of a novel SOD1 oligomer with mixed disulfides, with implications in fibril formation. Amyloid induced toxicity is known to be also caused by amyloid pores. Venko et al. present predictive approaches to assess the propensity of amyloid forming proteins to form transmembrane channels, suggesting that many have such potential and that oligomerization and conformational transitions in lipid rafts may be critical common events.

Post translational modifications are known to impact in the formation of protein aggregates and to influence their structure and toxicity. However, the repertoire of disease-associated modifications is vast, and its study presents several challenges. Two contributions in this Research Topic are focused on post translational modifications of proteins implicated in neurodegeneration. Kumar et al. report the development of novel phosphorylation-state specific antibodies that can differentiate A β peptides depending on the phosphorylation state of Ser26. Such site- and phosphorylation state-specific A β antibodies have the potential to be employed as tools in studies aimed at investigating the spatio-temporal deposition of different A β variants in transgenic mouse models and human AD brains. Kametani et al. have compared common and disease-specific post-translational modifications of pathological tau associated with multiple tauopathies. For this, detergent insoluble tau inclusions prepared from brains of patients suffering from a wide range of tauopathies were investigated, resulting in the identification of new tau modifications and in the hypothesis that differences in PTMs may be related to the observed differences in the structures of tau filament core structures.

The ability to modulate amyloid formation by selectively targeting aggregation-prone proteins implicated in neurodegenerative diseases is of great interest in drug discovery programmes. Protein-based biologics are of particular relevance, as antibodies or peptides have the potential to be engineered toward increased molecular recognition and specificity. Reflecting this emerging trend, several contributions in this Research Topic are focused on the use of peptides to inhibit protein aggregation and toxicity. Along these lines, Mamsa and Meloniv review the potential of cationic arginine-rich peptides (CARPS) as an emergent class of promising neurotherapeutics in AD capable to prevent toxic aggregation of A β and tau. Departing from an analysis of the structural and physicochemical characteristics and of the emerging properties of the arginine moiety, the authors present a thorough overview of the types and mechanisms of action of several inhibitory peptides that attenuate the aggregation and cytotoxicity of A β and tau and may even prove to be useful to decrease soluble cytotoxic oligomers. Also in the context of AD, Ikenoue et al. describe the rational design of bicyclic peptides that target various epitopes along the most amyloidogenic region of the A β sequence. By combining kinetic and structural approaches, the authors show that these compounds have the potential to remodel the aggregation of A β by redirecting it toward non-fibrillar species. Indeed, at sub-stoichiometric levels the bicyclic peptides delay the condensation of A β and the subsequent formation of fibrils, a process which is inhibited at high compound

concentrations. Torpey et al. undertake a study focused on the inhibition of α -synuclein aggregation by the 4554W peptide, whose mechanism of action is investigated from a structural perspective. The authors use NMR to probe the interaction and conclude that 4,554W associates with a partially aggregated form of α -synuclein, with enhanced association occurring over time. Also, they report that this peptide reduces the formation of α -synuclein fibrils resulting from PD-associated mutations and that it disaggregates pre-formed fibrils, as inferred from an effect over fibril length. The article by Popova et al. describes a yeast based high-throughput screening for short peptides that inhibit α -synuclein aggregation, leading to the identification of several peptides capable to suppress aggregation and toxicity in living cells. Subsequent *in vitro* assays using two of these peptides established that they significantly inhibit α -synuclein oligomerization and aggregation at sub-stoichiometric molar ratios and that some are effective in inhibiting the formation of early oligomers. Finally, Pagano et al. reviewed natural compounds shown to interfere with A β aggregation by direct interaction with A β peptide and whose inhibitory mechanism has been investigated by means of biophysical and structural biology experimental approaches. This can provide a rationale for the selection of natural compounds as molecular scaffolds for the design of new therapeutic strategies against the progression of early and late stages of AD.

AUTHOR CONTRIBUTIONS

All authors have contributed to writing of the editorial and all have handled submissions to the Research Topic as topic editors.

ACKNOWLEDGMENTS

We are extremely grateful to all that made this Research Topic possible and that have contributed to its success. We thank the 56 authors that have chosen our Research Topic as the most adequate venue to disseminate their research in 10 published articles, and the 20 reviewers, for their valuable time, and for contributing to improve quality through constructive comments. We are also grateful to the Frontiers publishing team and editors for their support.

Conflict of Interest: The authors declare that the research was conducted in the absence of any commercial or financial relationships that could be construed as a potential conflict of interest.

Publisher's Note: All claims expressed in this article are solely those of the authors and do not necessarily represent those of their affiliated organizations, or those of the publisher, the editors and the reviewers. Any product that may be evaluated in this article, or claim that may be made by its manufacturer, is not guaranteed or endorsed by the publisher.

Copyright © 2021 Gomes, Hoyer and Luo. This is an open-access article distributed under the terms of the Creative Commons Attribution License (CC BY). The use, distribution or reproduction in other forums is permitted, provided the original author(s) and the copyright owner(s) are credited and that the original publication in this journal is cited, in accordance with accepted academic practice. No use, distribution or reproduction is permitted which does not comply with these terms.



Insights Into Peptide Inhibition of Alpha-Synuclein Aggregation

James H. Torpey¹, Richard M. Meade², Ravina Mistry¹, Jody M. Mason² and Jillian Madine^{1*}

¹ Institute of Integrative Biology, University of Liverpool, Liverpool, United Kingdom, ² Department of Biology and Biochemistry, University of Bath, Bath, United Kingdom

OPEN ACCESS

Edited by:

Wolfgang Hoyer,
Heinrich Heine University
of Düsseldorf, Germany

Reviewed by:

Marcos Dias Pereira,
Federal University of Rio de Janeiro,
Brazil

Sandrine Ongeré,
Université Paris-Saclay, France

*Correspondence:

Jillian Madine
j.madine@liverpool.ac.uk

Specialty section:

This article was submitted to
Neurodegeneration,
a section of the journal
Frontiers in Neuroscience

Received: 12 May 2020

Accepted: 21 September 2020

Published: 15 October 2020

Citation:

Torpey JH, Meade RM, Mistry R,
Mason JM and Madine J (2020)
Insights Into Peptide Inhibition
of Alpha-Synuclein Aggregation.
Front. Neurosci. 14:561462.
doi: 10.3389/fnins.2020.561462

α -Synuclein (aSyn) aggregation is an attractive target for therapeutic development for a range of neurodegenerative conditions, collectively termed synucleinopathies. Here, we probe the mechanism of action of a peptide 4554W, (KDGIVNGVKA), previously identified through intracellular library screening, to prevent aSyn aggregation and associated toxicity. We utilize NMR to probe association and identify that 4554W associates with a “partially aggregated” form of aSyn, with enhanced association occurring over time. We also report the ability of 4554W to undergo modification through deamidation of the central asparagine residue, occurring on the same timescale as aSyn aggregation *in vitro*, with peptide modification enhancing its association with aSyn. Additionally, we report that 4554W can act to reduce fibril formation of five Parkinson’s disease associated aSyn mutants. Inhibitory peptide binding to partially aggregated forms of aSyn, as identified here, is particularly attractive from a therapeutic perspective, as it would eliminate the need to administer the therapy at pre-aggregation stages, which are difficult to diagnose. Taken together the data suggest that 4554W could be a suitable candidate for future therapeutic development against wild-type, and most mutant aSyn aggregation.

Keywords: alpha-synuclein, electron microscopy, neurodegenerative disease, NMR, Parkinson disease, peptide interaction, protein aggregation

INTRODUCTION

Neurodegenerative diseases, such as Parkinson’s disease (PD), are associated with the self-assembly and aggregation of proteins (Goedert, 1999). They arguably represent one of the most significant challenges to modern medicine; they are prevalent and, as yet, there are no tools available to fight back against the gradual yet relentless progression of neurodegeneration. A range of strategies targeting toxicity associated with protein aggregation are being investigated (Dehay et al., 2015; Fields et al., 2019). These include the use of passive or active immunization (Lee and Lee, 2016; Vaikath et al., 2019). Another strategy is reduction of protein expression or enhancement of clearance mechanisms (Stefanis et al., 2019), together with methods to prevent cell to cell transmission of misfolded proteins (Hasegawa et al., 2017). Targeting the aggregation process directly presents an attractive therapeutic option and has been probed using chaperones

(Arosio et al., 2016; Burmann et al., 2020) or via modulation and inhibitor compounds (Singh et al., 2017; Pujols et al., 2018; Peña-Díaz et al., 2019). The majority of drugs currently on the market are small molecules, however there is an increasing level of interest in the use of peptides as pharmaceuticals. Peptides are generally more specific to a given target than small molecules and thus are considered less likely to have prohibitive side-effects. Many of the issues that have historically proved an impediment to the clinical development of peptides (e.g., proteolytic degradation and localization) are better understood and can now be circumvented (Mason, 2010; Fosgerau and Hoffmann, 2015). Peptides are particularly attractive to neurodegenerative research associated with protein aggregation due to their potential to impede these broad and shallow protein-protein interactions, and therefore fibril formation. Some peptides have been shown to form β -hairpin structures that can “cap” fibrils to prevent the addition of further monomeric units and thus blocking their elongation, as shown for amylin and α -synuclein (aSyn) (Huggins et al., 2011). An alternative approach has been to inhibit assembly on one side of the protein using N-methylated peptides to prevent the formation of hydrogen bonds (Madine et al., 2008) or using short peptides containing residues that prevent further protein attachment (Kim et al., 2009). There is therefore great interest in the development of new peptide-based inhibitors to combat the toxicity of aggregation-prone proteins, such as aSyn (Mason and Fairlie, 2015).

A 10-residue peptide candidate, 4554W (KDGIVNGVKA) has been previously identified by an intracellular library-screening technique, and showed a reduction in aSyn fibril formation and reduced cytotoxicity (Cheruvu et al., 2015). However, this work did not provide insight into the mode of action of the peptide. The work presented here aimed to employ NMR techniques to test the hypothesis that 4554W bound to aSyn, and to identify key residues involved in the interaction. The ability of 4554W to inhibit the fibrillation of PD-associated aSyn mutants was also explored. It was found that 4554W associates with partially aggregated forms of aSyn, preventing fibril growth. This is appealing for further therapeutic development since the mechanism need not inhibit the native function of aSyn, and could be administered following identification of disease initiation, instead of at a pre-diagnostic stage when no aggregation has occurred.

MATERIALS AND METHODS

Expression of aSyn

The pRK172 aSyn expression construct (kindly gifted by Michel Goedert) was freshly transformed into *E. coli* BL21 (DE3) cells, using the heat-shock method. These cells were used to inoculate 1 mL of super optimal broth with catabolite repression (SOC) (100 μ g/mL ampicillin), which was grown at 37°C with shaking at 200 rpm for 8 h. 150 μ L of this culture was used to inoculate 50 mL of minimal medium (Solution A: 12.5 g/L Na_2HPO_4 , 7.5 g/L KH_2PO_4 pH 7.2; Solution B (for 1 L): 4 g glucose, 1 g (^{15}N) NH_4Cl , 240 mg $\text{MgSO}_4 \cdot 7\text{H}_2\text{O}$, 20 mg $\text{CaCl}_2 \cdot 2\text{H}_2\text{O}$, 10 mg thiamine), and grown at 37°C overnight. This starter culture was

used to inoculate 1 L of minimal medium such that the starting optical density at 600 nm (OD600) was 0.1, with growth at 37°C with shaking at 180 rpm until the OD600 reached 0.8. At this point isopropyl- β -D-1-thiogalactopyranoside (IPTG) was added to the culture to a final concentration of 0.5 mM and the culture was then incubated with shaking overnight at 18°C. The cells were harvested by centrifugation at 4,000 g for 20 min at 4°C. The cell pellets were snap frozen in liquid nitrogen (LN_2) prior to storage at -80°C .

Site-Directed Mutagenesis of aSyn

The QuikChange II kit (Agilent Technologies) was used according to the manufacturer's instructions to prepare the six PD-linked aSyn mutants (A30P, E46K, H50Q, G51D, A53T, and A53E). The WT aSyn pRK172 expression construct was used as the template and the reaction carried out according to the manufacturer's instructions with the primer sequences shown in **Supplementary Table 1**. Successful mutagenesis was confirmed by sequencing (Source Bioscience) and proteins expressed and purified as for wild-type.

Purification of aSyn

Cell pellets were resuspended in 20 mL Buffer A [20 mM Tris-HCl pH 8.0, 1 mM ethylenediaminetetraacetic acid (EDTA)], and lysed by pressure homogenization, followed by a single cycle of ultra-sonication (30 s at 23 kHz). The lysate was incubated at 85°C for 10 min and then clarified by centrifugation at 18,000 g for 30 min at 4°C. The clarified lysate was applied directly to a 5 mL Q HiTrap anion exchange chromatography column (GE Healthcare Life Sciences) pre-equilibrated with Buffer A. Protein was eluted from the column via gradient elution with Buffer B (Buffer A + 1M NaCl). aSyn elutes from the column at approximately 300 mM NaCl. Fractions were analyzed by SDS-PAGE, pooled and filtered through an Amicon Ultra-15 centrifugal filter with a 30 kDa molecular weight cut-off (MWCO) (EMD Millipore). The flow-through was collected and applied to a 10 kDa MWCO centrifugal filter, and concentrated to 10 mg/mL. Protein concentration was determined using UV absorbance at 280 nm and purity assessed by SDS-PAGE and mass spectrometry. aSyn was buffer exchanged into double-distilled water (ddH_2O) using a PD-10 desalting column (GE Healthcare Life Sciences) and lyophilized. Lyophilized protein was monomerised by resuspension in hexafluoroisopropanol (HFIP) and thoroughly vortexed until transparent. The HFIP was then evaporated under a stream of nitrogen and resuspended in the required buffer.

Production and Purification of Peptides

4554W was synthesized using a Liberty Blue microwave peptide synthesizer (CEM). The peptide was synthesized on a Rink amide ChemMatrix resin (PCAS BioMatrix) employing Fmoc solid-phase technique, with repeated steps of coupling-deprotection-washing for each amino acid. The activator solution consisted of 26 g PyBOP in 100 mL DMF, and the deprotection solution was 20% Piperidine in DMF with the addition of 5% Formic acid to prevent aspartamide formation of the peptide.

The peptide was removed from the matrix by incubating in cleavage solution (95% TFA, 2.5% Triisopropylsilane, and 2.5% water), on a shaker at 25°C, for 4 h. The resin was removed by filtration, and the peptide precipitated using ice cold ether, with vortexing and centrifugation at 7,000 g for 3 rounds. The pellet was left overnight at room temperature to completely dry, and purified by HPLC using a Jupiter 4 μ m Proteo C-18 90 Å reverse phase semipreparative column.

The fractions of the HPLC peaks were examined by mass spectroscopy, using a microTOF (Bruker Daltonics) to confirm which fractions contained the purified peptide (**Supplementary Figure 1**). Fractions, containing the peptide were pooled, and lyophilized. The dry weight of the purified peptide was measured to 0.1 μ g accuracy using a Sartorius SE2 Ultra Micro Balance and stored at -80°C .

WaterLOGSY NMR Peptide-Binding Experiments

NMR spectra were collected on a Bruker Avance III 800 MHz spectrometer equipped with a TCI CryoProbe (Bruker) at 298 K in 5 mm glass tubes. Lyophilized aSyn and 4554W were reconstituted in NMR buffer (10 mM sodium phosphate pH 7.0, 100 mM KF, 0.05% NaN_3) with a final concentration of 5% D_2O (v/v) to a final concentration of 50 μM and 1 mM, respectively. Each experiment required multiple samples: 1 mM 4554W alone, 50 μM aSyn alone, 50 μM aSyn + 1 mM 4554W. 1D proton and WaterLOGSY spectra were collected on each sample every day for 6 days. Spectra were also obtained using aged peptide (following incubation with a flea at 37°C for 6 days) and aSyn fibrils (formed by incubation with a flea at 37°C for 7 days). The 1D proton spectra were collected with 128 scans, 20 dummy scans, an acquisition time of 0.734 s, and a sweep width of 13.9456 ppm. WaterLOGSY spectra were collected with 256 scans, 16 dummy scans, an acquisition time of 0.729 s, and a sweep width of 14.0396 ppm. 1D and WaterLOGSY spectra were compared in TopSpin 3.5 pl 7 (Bruker) with the control spectra to check for signs of binding. The integral volume for peaks corresponding to the aromatic region (6.5–9 ppm) and aliphatic region (0.5–4.5 ppm) were calculated in Origin and added together to give the peak area per spectra avoiding the water peak. Peak volumes were calculated for spectra obtained for 4554W alone and 4554W plus aSyn (following subtraction of aSyn alone). The difference between the total integral volumes for 4554W and 4554W plus aSyn were calculated and plotted.

Natural Abundance ^1H - ^{13}C Heteronuclear Single Quantum Coherence Spectroscopy (HSQC) of Peptides

4554W was dissolved in D_2O at 1 mM. 1D proton and ^1H - ^{13}C HSQC spectra were collected freshly prepared and following incubation at 37°C with agitation for 6 days. 1D proton spectra were collected with 128 scans, 100 dummy scans, an acquisition time of 0.557 s, and a sweep width of 9.1877

ppm. ^1H - ^{13}C HSQC spectra were collected with 16 scans, 16 dummy scans, an acquisition time of 0.100 s (^1H) and 0.014s (^{13}C), and a sweep width of 10.0122 ppm (^1H) and 65.0005 ppm (^{13}C). Spectra were processed in TopSpin and analyzed in CCPN Analysis.

Transmission Electron Microscopy

Hundred micrometer samples of aSyn were incubated in PBS pH 7.4 alone, or in the presence of equimolar 4554W at 37°C, with agitation with a flea for 1 week. 5 μL of each sample was mounted onto a carbon-coated copper grid for 2 min. Excess was blotted away, and grids stained with 4% uranyl acetate for 30 s. Images were collected on a 120 kV Tecnai G2 Spirit BioTWIN electron microscope (FEI) with a SIS Megaview III camera. Image and fibril length analysis was carried out using ImageJ and OriginLab, with the scale bar on each image used as the length reference. Four images were used for each analysis with number of measurements included in each analysis shown in **Supplementary Table 2**.

Mass Spectrometry Peptide Analysis

Fresh and aged 4554W samples were diluted to a concentration of 1 pmol/ μL in 50% acetonitrile, 0.1% formic acid and infused at 5 $\mu\text{L}/\text{min}$ onto the electrospray ionization (ESI) source of an Orbitrap Fusion. Comparison of theoretical and experimental m/z values showed that measurements were accurate to 3 ppm. Asparagine deamidation was probed using the corresponding 1Da mass shift, and the proportion of asparagine deamidated was determined through deconvolution of the isotope (^{13}C) cluster peaks. This was further confirmed through higher-energy C-trap dissociation (HCD) MS-MS.

Thioflavin T Fluorescence

aSyn (WT, A30P, E46K, H50Q, G51D, A53T, and A53E) were prepared in PBS pH 7.4 at a concentration of 100 μM alone and in the presence of 100 μM 4554W. Samples were incubated at 37°C with agitation for up to 1 week. Samples were transferred to a 96-well black-walled, clear bottom plate (Nunc) with 2 μM Thioflavin T and fluorescence measurements taken using $\lambda_{\text{ex}} = 440$ nm and $\lambda_{\text{em}} = 490$ nm on a Flexstation 3 microplate reader (Molecular Devices). Each sample was measured in triplicate and the final volume in each well was 50 μL . Data was processed and analyzed using OriginLab. Statistical significance of the differences was assessed using analysis of variance (ANOVA) with the Bonferroni *post hoc* test.

Addition of 4554W to Pre-formed Fibrils

WT aSyn fibrils were formed by incubating 100 μM aSyn in PBS pH 7.4 at 37°C, with agitation with a flea for 1 week. 4554W was added to equimolar concentration and samples further incubated for 5 days at 37°C with agitation with a flea. Thioflavin T and transmission electron microscopy with image analysis were carried out as described above.

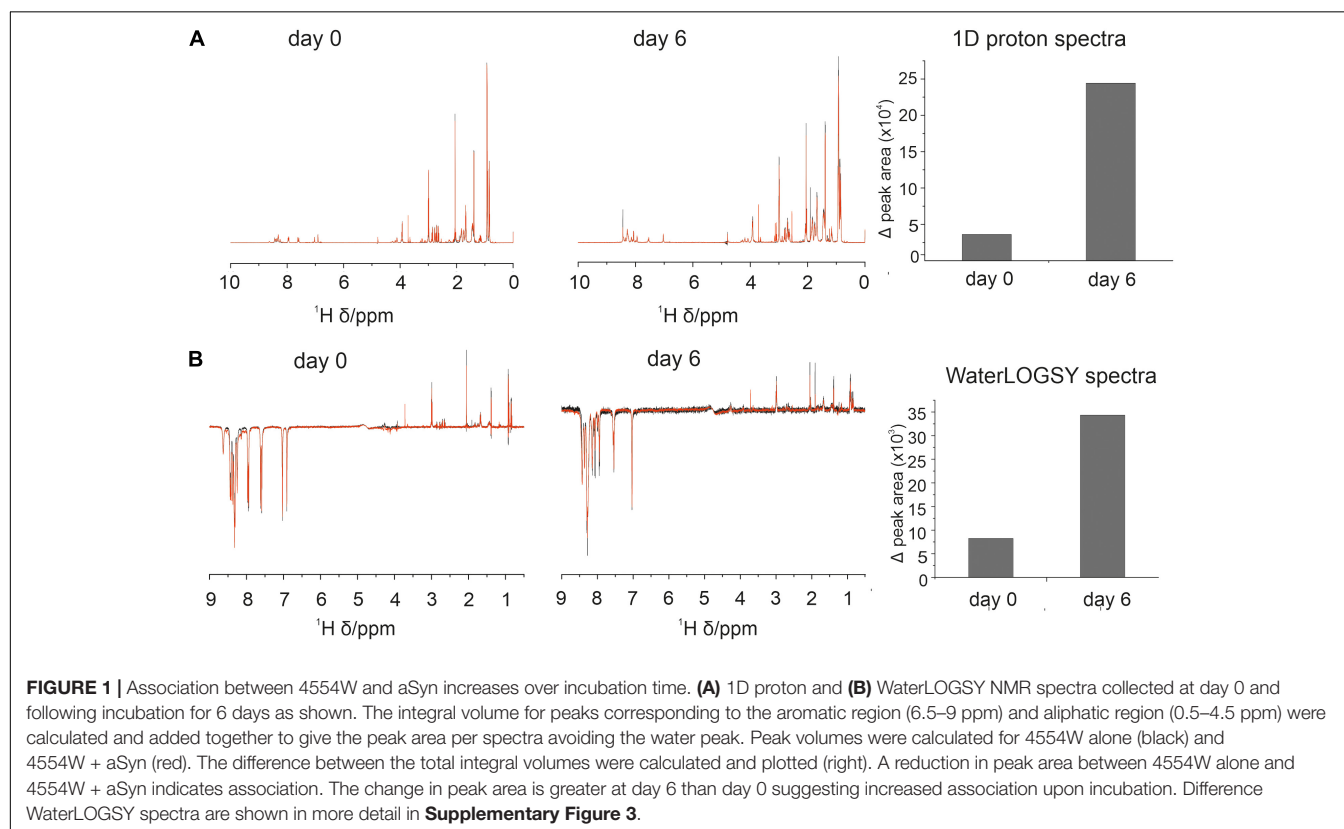
RESULTS

4554W Binds to ‘Partially Aggregated’ aSyn Species and Shows Increased Binding Over Time

We carried out Heteronuclear single quantum coherence spectroscopy (HSQC) experiments using ^{15}N labeled aSyn alone and in the presence of increasing concentrations of 4554W, up to a 20:1 peptide:protein ratio. No changes in intensity or chemical peak shifts were observed suggesting little or no binding to “NMR observable” aSyn species (**Supplementary Figure 2A**). We also observed that when aSyn alone or aSyn plus 4554W was incubated for 6 days the resulting spectra were the same irrespective of the presence or absence of 4554W (**Supplementary Figure 2B**). This suggests that 4554W does not bind with significant affinity to aSyn species within the NMR visible size range, i.e., oligomers of trimeric or less. It also indicates that the presence of 4554W does not alter the aggregation of these low- n aSyn oligomers, with observed loss of signal upon incubation consistent with aggregation. The peaks that remain correspond to the C-terminal region which is predicted to be outside of the core region of aSyn fibrils (Li et al., 2018) and may remain flexible and therefore NMR accessible upon aggregation. From this data we hypothesized that 4554W could be binding to a larger species of aSyn than cannot be detected via HSQC NMR experiments.

We therefore utilized 1D proton and WaterLOGSY (Water-Ligand Observed via Gradient Spectroscopy) NMR experiments to probe this hypothesis and observe interactions between 4554W and “NMR invisible” aSyn species. These experiments were designed to observe an NMR spectrum of 4554W, with association to aSyn resulting in a reduction in 1D signal as 4554W becomes “NMR invisible.” WaterLOGSY is often employed as a screening method to identify compounds that can interact with proteins or other macromolecules and can be used to probe binding affinities within the micromolar range. The experiment works by transferring magnetization from the bulk solution to the ligand which is then detected as the NMR signal (Dalvit et al., 2000). When some of the ligand is associated with protein, resonances from the bound ligand will be observed with the opposite sign to that of the unbound, identified as reduction in signal.

1D and WaterLOGSY data indicated some association between 4554W and aSyn at day 0 observed as a difference between the spectrum acquired for 4554W alone and that acquired in the presence of aSyn (**Figure 1**). Additionally, upon incubation for 6 days the observed difference increased, suggesting enhanced binding over time. This can be seen in the difference WaterLOGSY spectra obtained daily for up to 6 days (**Supplementary Figure 3A**), with greater peak areas present in the difference spectra at day 6 compared with day 0 (**Supplementary Figure 3B**). We therefore propose that the peptide “recognizes” and is able to bind to partially aggregated aSyn species and functions to prevent their further aggregation.



4554W Becomes Modified Upon Incubation

During the analysis of WaterLOGSY and 1D data we observed changes in the 4554W spectrum over time (**Supplementary Figure 4**). To probe this change further ^1H - ^{13}C natural abundance HSQC experiments of 4554W alone were performed. The spectra revealed clear shifts in the position of the $\text{C}\alpha$ and $\text{C}\beta$ peaks corresponding to the Asn residue (**Figure 2A**). Asn is prone to deamidation, resulting in a mass shift of 1Da, and is detectable by mass spectrometry (Yang and Zubarev, 2010). Fresh and aged

(pre-incubated for 6 days) 4554W, prepared under identical conditions to those used in the NMR experiments, were analyzed by MS through direct infusion revealing a primary ion with the m/z value 521.3079 corresponding to the 2 + species (**Figure 2B**). The fresh 4554W sample gave a predominant peak of 521.3079, with less abundant peaks at 521.8045 and 522.2999 which reflect those ions containing ^{13}C . In the aged sample the distribution of these peaks was different, with the predominant peak being the middle peak (521.8010). This suggests that partial deamidation of the sample had occurred, and the first ^{13}C peak of the

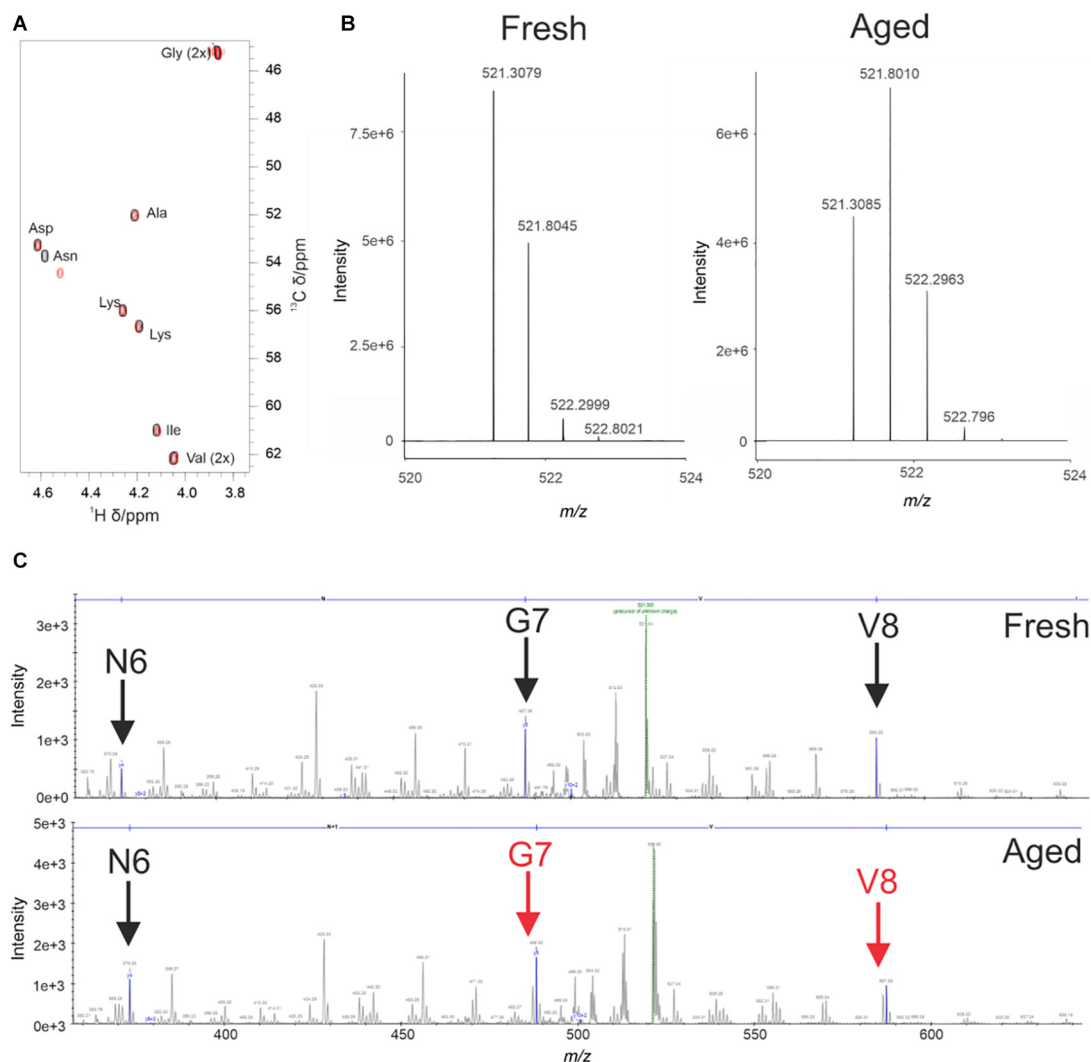


FIGURE 2 | Deamidation of 4554W upon incubation. **(A)** Natural abundance HSQC for fresh (black) and aged (red) 4554W shows a shift in Asn residue. **(B)** Deamidation results in a mass shift of 1Da. Direct infusion mass spectrometry of fresh and aged 4554W showed a shift from primary ion with m/z value 521.3079 (fresh), with less abundant peaks at 521.8045 and 522.2999 reflecting ions containing ^{13}C . The aged sample shows a different distribution of peaks, with the predominant peak being the middle peak (521.8010). This suggests that partial deamidation has occurred, and the first ^{13}C peak of the unmodified 4554W now overlaps with that of the deamidated 4554W. By looking at the ratio in the relative abundances of each peak in the two samples it was possible to determine the proportion of 4554W that had been deamidated to be approximately 50%. **(C)** Higher-energy collisional (HCD) MS-MS used to determine the location of deamidation by generating ion fragments of 4554W. The distribution of peaks showing a dual population (observed as a preceding peak prior to the main peak, red arrows) for the aged 4554W mimics that seen for the whole peptide at sites C-terminal to the modification site. The lack of preceding peaks in fresh 4554W (black arrows), and loss of the preceding peak corresponding to N6 in the aged 4554W sample indicates that this is the site responsible for the dual population with a difference in mass of 1Da.

unmodified peptide superimposed with that of the deamidated peptide (observed as + 0.5Da which corresponds to + 1Da in the + 1 species). By observing the ratio of each peak's relative abundance in the two samples it was possible to determine the proportion of 4554W that had been deamidated to be approximately 50%. Using higher-energy collisional (HCD) MS-MS (Olsen et al., 2007) the location of this deamidation was determined. Unlike in **Figure 2B** in which *m/z* values of the whole peptide were recorded, using HCD MS-MS ion fragments of the peptide were generated. As can be seen in **Figure 2C**, the distribution of peaks mimics that seen for the whole peptide until Asn is removed (**Figure 2C**). The loss of the preceding peak indicates that the Asn residue is responsible for the dual population (with a difference in mass of 1Da). This corresponds to the mass change induced by deamidation and confirms that Asn 6 in the 10-residue peptide is the site of deamidation. This data highlights that partial deamidation of Asn is taking place within a similar timeframe to the aggregation of aSyn *in vitro* and may be modulating the affinity of interaction between aSyn aggregates and 4554W. The data suggests that greatest binding is achieved between modified peptide and partially aggregated aSyn.

We collected WaterLOGSY NMR spectra using freshly prepared 4554W and following aging to induce deamidation in the presence of freshly prepared aSyn (presumed to be predominantly monomeric) and using aSyn fibrils. Assessment of the difference between 4554W alone and aSyn under these different conditions (**Supplementary Figure 5**) confirms that binding is enhanced following aging of the peptide, and that greatest binding is observed between fibrillar aSyn and aged 4554W.

4554W Prevents Aggregation of PD-Associated Mutants

The initial peptide screen was designed to target the region containing residues 45–54 of aSyn. This region contains all but one (A30P) of the currently identified PD-associated aSyn mutants (Meade et al., 2019). Here the ability of 4554W to prevent fibrillation of mutant aSyn variants *in vitro* was explored. Thioflavin T (ThT) was used to assess fibril formation of aSyn variants in the absence and presence of equimolar concentrations of 4554W. A significant reduction in ThT fluorescence was observed in the presence of 4554W at day 3 for WT ($p = 0.0003$), G51D ($p = 0.0023$) and A53T ($p = 0.01082$) (**Figure 3**). A53E took longer to aggregate showing a significant reduction in ThT fluorescence in the presence of 4554W by day 7 ($p = 0.0216$). In contrast A30P, E46K, and H50Q had low ThT fluorescence after 7 days incubation and showed no significant reduction in the presence of 4554W (**Figure 3**).

TEM analysis was used to observe changes in morphology of fibrils formed following incubation for 1 week *in vitro*. WT, A30P, H50Q, and A53T mutant aSyn variants form long fibrils when incubated alone (**Figure 4A**). When incubated in the presence of 4554W shorter fibrils/aggregate species were observed, with length analysis confirming most species < 150 nm in length (**Supplementary Figure 6**), and mean lengths significantly reduced compared to the aSyn variants alone (**Figure 5** and

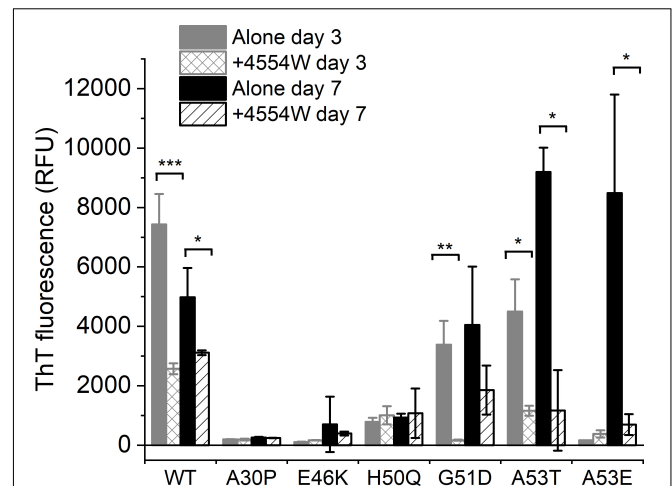


FIGURE 3 | Thioflavin T fluorescence for aSyn variants alone and incubated in the presence of 4554W. WT, G51D, A53T, and A53E show significant reduction in ThT fluorescence upon incubation in the presence of 4554W. Data is shown as mean \pm SD for triplicate readings following incubation for 3 and 7 days. Control 4554W alone samples do not show any ThT fluorescence (data not shown). * $p < 0.05$, ** $p < 0.01$, *** $p < 0.001$.

Supplementary Table 2). In contrast, addition of 4554W had little effect on the length of fibrils formed from E46K, G51D, or A53E mutants (**Figure 4B**). G51D and A53E alone produced short fibrils in comparison to WT and other mutant aSyn variants with approximately 50% of fibrils measured < 100 nm.

4554W Disaggregates Pre-formed aSyn Fibrils

Further to data showing 4554W preferentially associates with aggregated aSyn species (**Supplementary Figure 5**), the ability of 4554W to disaggregate pre-formed fibrils was probed. Incubation of 4554W with pre-formed WT aSyn fibrils for 5 days showed no alteration in ThT fluorescence (**Figure 6A**). However, TEM analysis showed a significant reduction in fibril length (**Figures 6B,C** and **Supplementary Figure 6**) resulting in fibrils of similar size to those produced when non-aggregated aSyn is incubated in the presence of 4554W (as shown in **Figures 4A, 5**). This indicated that 4554W can disaggregate pre-formed aSyn fibrils. Taken together work presented here showed that the presence of 4554W resulted in shortened fibrils independent of the starting aSyn species, consistent with the peptide acting to both prevent further aggregation and alter pre-formed aggregates.

DISCUSSION

4554W was previously shown to inhibit fibrillation and reduce cytotoxicity of aSyn showing potential biological and therapeutic benefit for 4554W (Cheruvu et al., 2015). Here we showed that 4554W can bind to partially or fully aggregated species of aSyn preventing further fibrillation and resulting in shorter fibrils. In contrast no association is observed with monomeric aSyn. We

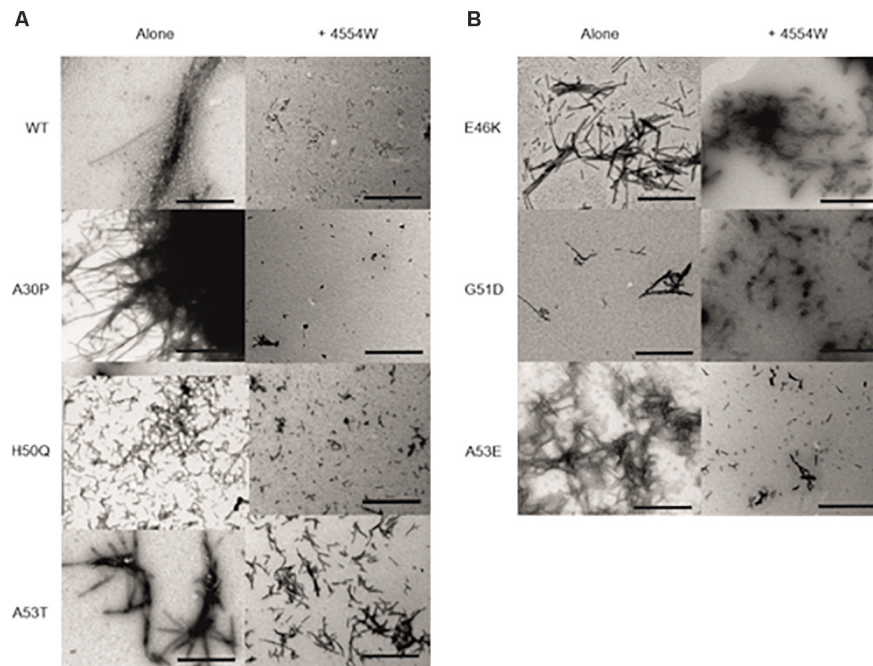


FIGURE 4 | Transmission electron microscopy images for aSyn mutant proteins incubated alone and in the presence of 4554W. **(A)** WT, A30P, H50Q, and A53T show significant reduction in fibril length upon incubation with 4554W. **(B)** E46K, G51D, and A53E do not show significantly altered length in the presence of 4554W. Scale bar is 1 μ m.

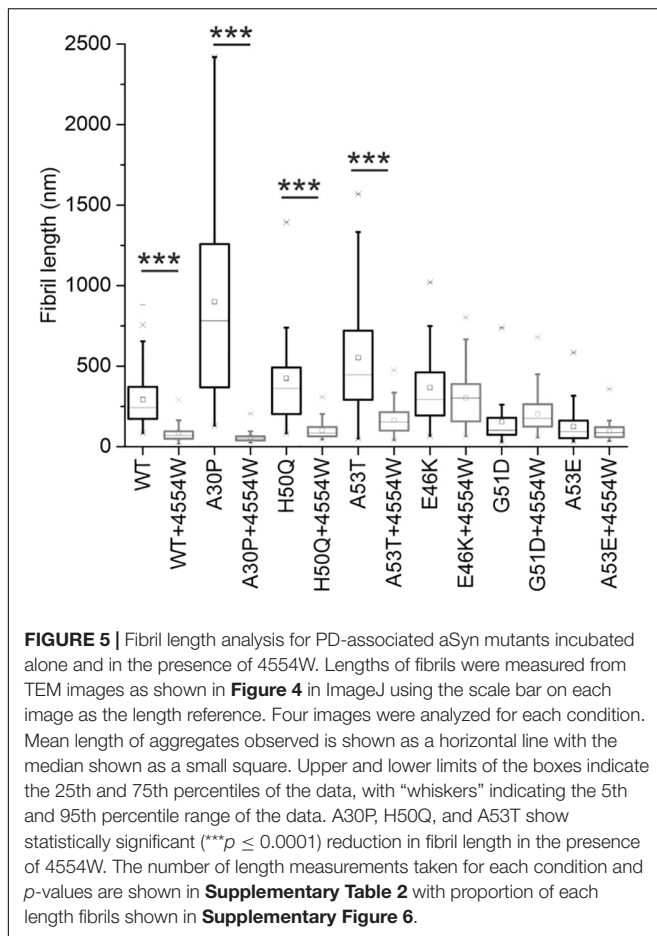
report that maximal binding was achieved when 50% of 4554W had undergone deamidation of the Asn 6 residue. Deamidation can affect the structural integrity of proteins and peptides through the introduction of a negative charge which may affect the ability of 4554W to interact with aSyn and alter self-association interactions. Given that deamidation occurred under *in vitro* conditions that promoted aSyn aggregation we believe that deamidation of the peptide would also occur *in vivo* if 4554W was to be utilized in the future as a therapeutic option. However, an alternative future strategy could involve synthesizing deamidated 4554W which may show improved association with aSyn.

Many avenues targeting aSyn aggregation are under investigation as disease-modifying therapeutic approaches. The small molecule inhibitor Fasudil has been shown to prevent aggregation of aSyn by binding to the C-terminal region identified via specific NMR chemical shifts (Tatenhorst et al., 2016). In this study we report a lack of chemical shift changes following addition of 4,454 W to aSyn showing 4554W doesn't associate with monomeric aSyn. The flavonoid epigallocatechin gallate and phenol curcumin have shown potential for inhibiting several aggregation-prone proteins (Ehrnhoefer et al., 2008; Ahmad et al., 2017). They also act via direct association to prevent the structural re-arrangement required for fibril formation (Meng et al., 2009; Takahashi et al., 2015). Other avenues being explored include the natural antimicrobial, squalamine which has shown promise as an inhibitor by competing with aSyn in binding lipid membranes, specifically inhibiting aggregation initiation and in turn reducing

aSyn toxicity in cell and animal models of Parkinson's disease (Perni et al., 2017).

4554W is observed to reduce fibril formation assessed by ThT or TEM against all known PD-associated mutants except E46K. aSyn mutants that result in shorter fibrils when incubated in the presence of 4554W (A30P, H50Q, and A53T) have been previously shown to enhance the formation of oligomers (Marvian et al., 2019). In contrast mutants that do not show an effect on fibril length have been shown to have no effect (E46K) or an inhibitory effect (G51D and A53E) on oligomer formation. Morphological and structural similarities have also been observed between WT, A30P, and A53T fibrils (Ruggeri et al., 2020). Recent studies have shown that small molecules SynuClean-D and ZPD-2 can reduce the aggregation of WT, H50Q, and A30P (Pujols et al., 2018; Peña-Díaz et al., 2019). These mutants affect aSyn oligomerization, therefore taken together data presented in this study and previous data suggest that 4554W could be acting during the oligomerization step targeting a common assembly pathway in WT, A30P, H50Q, and A53T to modulate fibrillation.

G51D is associated with earlier age of onset, and a slower rate of aggregation, therefore likely persisting in the oligomeric state for longer than WT aSyn (Fares et al., 2014). This is consistent with very few isolated patches of fibrils observed in our analysis. In the presence of 4554W fibrils were more prevalent suggesting that the presence of 4554W may influence G51D aSyn to follow an alternative aggregation pathway that favors the formation of amyloid fibrils, over that of oligomeric species. Therapeutically this may be beneficial as fibrils may represent a benign endpoint.



ThT fluorescence data for G51D suggests that oligomers that form in the absence of 4554W have high ThT fluorescence whereas fibrils produced in the presence of 4554W have lower ThT fluorescence. A53E is the most recently identified PD-linked point mutation in aSyn (Pasanen et al., 2014). It is thus the least characterized with little known about its rate of aggregation or fibril morphology. Here, we show that 4554W reduces ThT fluorescence of A53E fibrils but has little effect on fibril length assessed by TEM.

Interestingly, fibrils that show low ThT fluorescence with no significant alteration in the presence of 4554W (A30P and H50Q) show large fibrils with significant reduction by TEM. Whereas, in contrast G51D and A53E show significant reduction in ThT fluorescence with no show significant alteration in size by TEM. It is known that aSyn mutants likely aggregate by different pathways therefore it could be expected that 4554W may act on all mutants in different ways either altering fibril morphology or amount of fibrils formed. We report that mutants that do not show an effect on ThT fluorescence in the presence of 4554W (A30P, E46K, H50Q) had low ThT fluorescence in the absence of 4554W, in comparison to those mutants that showed an effect. The low ThT for these aSyn mutants alone may explain why a reduction in ThT fluorescence in the presence of 4554W was not observed. We also report that mutants that do not show a reduction in fibril length

(E46K, G51D, A53E) were smaller in the absence of 4554W, in comparison to those mutants that showed an effect. This suggests that 4554W is unable to reduce the length of mutants that already produce short fibrils. We therefore hypothesize that 4554W acts to reduce the length of long aSyn fibrils and to reduce ThT fluorescence of aSyn species that have high fluorescence.

We also report that addition of 4554W to pre-formed fibrils does not show a reduction in ThT fluorescence, whereas a significant reduction in length was observed by TEM. We hypothesize for pre-formed fibrils that the amount of fibrils remains the same, whereas the morphology and length of the fibrils is altered. Taken together this study highlights the need to investigate multiple aspects of aggregation to generate a holistic view of effect of addition of a potential aggregation inhibitor.

Data presented here is consistent with 4554W associating with partially aggregated aSyn species. This work highlights a key area of research that is hampered by a lack of reliable, readily available techniques available to study interactions with partially aggregated or oligomeric species directly. This barrier is largely due to the transient nature of these aggregation intermediates and the equilibrium that exists between monomeric, partially aggregated and fully formed fibrils. Any attempt to isolate aggregation intermediates to study their interactions causes disruption to this equilibrium and could result in alteration to the species present and an inaccurate representation of what is happening in the native heterogeneous system. Future experiments to probe association of 4554W with oligomeric aSyn species could include ion mobility mass spectrometry as utilized for a range of aggregating proteins (Woods et al., 2013; Young et al., 2015), including aSyn (Liu et al., 2015). Size exclusion chromatography enables isolation of oligomeric species (Daturpalli et al., 2013; Schonhofs et al., 2017) and if coupled with small angle X-ray scattering can provide structural information (Rekas et al., 2010). Employing fluorescent or other labeling approaches would also enable microscopy-based methods to probe and visualize peptide-oligomer interactions. We acknowledge that while we don't present evidence for direct binding the data we present confirms lack of binding to monomeric aSyn and shows enhanced association upon incubation of aSyn consistent with our conclusion.

The ability of a therapeutic to act after onset of symptoms in neurodegenerative diseases associated with protein aggregation is an important prerequisite for its use as a disease-modifying therapy. This has been shown previously with anle138b able to modulate oligomer formation and inhibit disease progression in a Parkinson mouse model even when treatment was started after disease onset (Levin et al., 2014). Previously identified small molecules have been shown to have different modes of action affecting different stages of aggregation, e.g., ZPD is more effective at early stages of aggregation (Peña-Díaz et al., 2019), whereas SynuClean-D can target later stages (Pujols et al., 2018). Data presented here suggests that 4554W acts following onset of aggregation and is able to disaggregate pre-formed fibrils highlighting its potential for future therapeutic development. Assessing the effect of 4554W on toxicity associated with mutant aSyn aggregation was beyond the scope of the current work. This represents the next stage in development

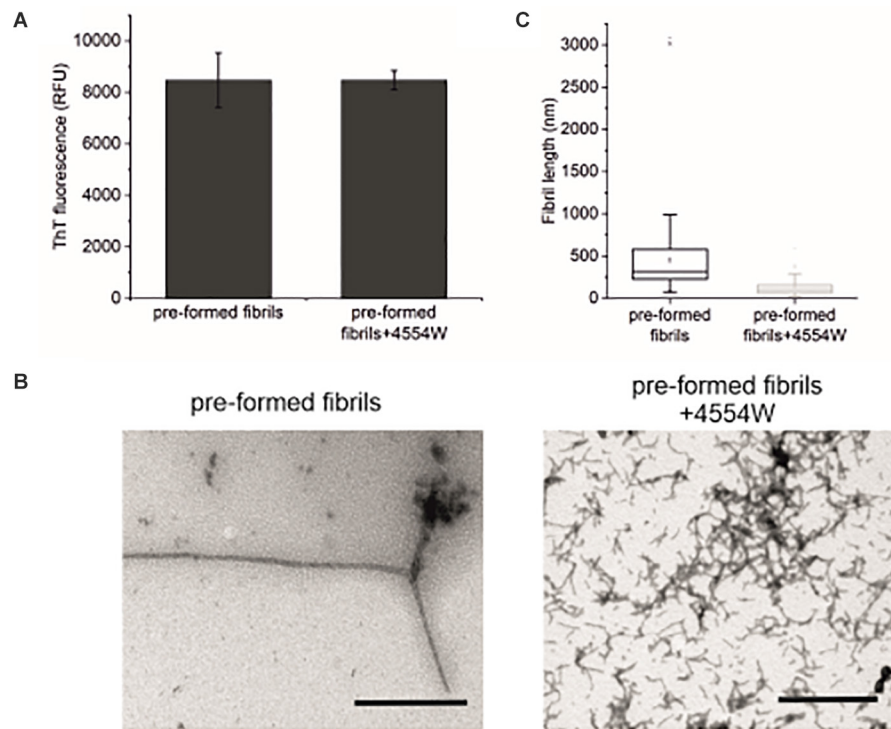


FIGURE 6 | Incubation of pre-formed aSyn fibrils with 4554W. **(A)** No difference in ThT fluorescence was observed following incubation of pre-formed aSyn fibrils with 4554W for 5 days. **(B)** TEM images show short fibrils upon incubation of pre-formed fibrils with 4554W. Scale bar 1 μ M. **(C)** Lengths of fibrils measured from 4 images using the scale bar as the length reference show a significant reduction in mean length compared to fibrils incubated alone. Mean length of aggregates observed is shown as a horizontal line with the median shown as a small square. Upper and lower limits of the boxes indicate the 25th and 75th percentiles of the data, with “whiskers” indicating the 5th and 95th percentile range of the data. The number of length measurements and *p*-values are shown in **Supplementary Table 2** with proportion of each length fibrils shown in **Supplementary Figure 6**.

of 4554W as a future therapeutic to confirm the preliminary data presented here highlighting its potential to alter WT and mutant aSyn aggregation. Taken together with additional studies as outlined above probing peptide-oligomer association, toxicity evaluation is required to enable assessment of the effectiveness of 4554W to reduce aggregation associated pathogenicity when added at advanced stages of aggregation and future therapeutic development.

Overall the data suggests that it may be feasible to target aSyn variants with similar fibril morphological properties (WT, A30P, H50Q, and A53T) by a single therapeutic strategy, instead of requiring individual approaches for each PD-associated mutation. The data also provides additional confirmation that peptide therapeutics may be a feasible option for modulating aSyn aggregation, and associated cytotoxicity. This is especially attractive if they can be targeted to pre/partially-aggregated species overcoming the need to administer them prior to signs of disease onset.

DATA AVAILABILITY STATEMENT

All datasets presented in this study are included in the article/Supplementary Material.

AUTHOR CONTRIBUTIONS

JT carried out all experiments included in the manuscript. RMe synthesized the peptides. RMi carried out sample preparation as part of a summer vacation studentship. JMas and JMad conceived the study and acquired funding. All authors were involved in scientific discussion throughout the project. JT and JMad wrote the initial draft with RMe and JMas was involved in re-drafting. All authors shared the responsibility for contributing to the final version of the manuscript.

FUNDING

We acknowledge Institute of Integrative Biology, University of Liverpool for funding a studentship to JT. We acknowledge a Biochemical Society Summer Vacation Studentship for RMe. JMas and RMi thank BRACE for award of a Ph.D. studentship (BR16/064).

ACKNOWLEDGMENTS

All MS analysis was carried out by Philip Brownridge and the Center for Proteome Research at the University of Liverpool.

We acknowledge Institute of Integrative Biology, University of Liverpool for funding a studentship to JT. RMI was funded by a Biochemical Society Summer Vacation Studentship. JMas and RMe thank BRACE for award of a Ph.D. studentship (BR16/064).

REFERENCES

- Ahmad, B., Borana, M. S., and Chaudhary, A. P. (2017). Understanding curcumin-induced modulation of protein aggregation. *Int. J. Biol. Macromol.* 100, 89–96. doi: 10.1016/j.ijbiomac.2016.06.053
- Arosio, P., Michaels, T. C., Linse, S., Månsson, C., Emanuelsson, C., Presto, J., et al. (2016). Kinetic analysis reveals the diversity of microscopic mechanisms through which molecular chaperones suppress amyloid formation. *Nat. Commun.* 7:10948.
- Burmman, B. M., Gerez, J. A., Matečko-Burmman, I., Campioni, S., Kumari, P., Ghosh, D., et al. (2020). Regulation of α -synuclein by chaperones in mammalian cells. *Nature* 577, 127–132. doi: 10.1038/s41586-019-1808-9
- Cheruvu, H., Allen-Baume, V. L., Kad, N. M., and Mason, J. M. (2015). Intracellular screening of a peptide library to derive a potent peptide inhibitor of alpha-synuclein aggregation. *J. Biol. Chem.* 290, 7426–7435. doi: 10.1074/jbc.m114.620484
- Dalvit, C., Pevarello, P., Tatò, M., Veronesi, M., Vulpetti, A., and Sundström, M. (2000). Identification of compounds with binding affinity to proteins via magnetization transfer from bulk water*. *J. Biomol. NMR* 18, 65–68.
- Daturpalli, S., Waudby, C. A., Meehan, S., and Jackson, S. E. (2013). Hsp90 inhibits α -synuclein aggregation by interacting with soluble oligomers. *J. Mol. Biol.* 425, 4614–4628. doi: 10.1016/j.jmb.2013.08.006
- Dehay, B., Bourdenx, M., Gorry, P., Przedborski, S., Vila, M., Hunot, S., et al. (2015). Targeting α -synuclein for treatment of Parkinson's disease: mechanistic and therapeutic considerations. *Lancet Neurol.* 14, 855–866. doi: 10.1016/S1474-4422(15)00006-X
- Ehrnhöfer, D. E., Bieschke, J., Boeddrich, A., Herbst, M., Masino, L., Lurz, R., et al. (2008). EGCG redirects amyloidogenic polypeptides into unstructured, off-pathway oligomers. *Nat. Struct. Mol. Biol.* 15, 558–566. doi: 10.1038/nsmb.1437
- Fares, M. B., Ait-Bouziad, N., Dikiy, I., Mbefo, M. K., Jovicic, A., Kiely, A., et al. (2014). The novel Parkinson's disease linked mutation G51D attenuates in vitro aggregation and membrane binding of alpha-synuclein, and enhances its secretion and nuclear localization in cells. *Hum. Mol. Genet.* 23, 4491–4509. doi: 10.1093/hmg/ddu165
- Fields, C. R., Bengoa-Vergniory, N., and Wade-Martins, R. (2019). Targeting alpha-synuclein as a therapy for Parkinson's disease. *Front. Mol. Neurosci.* 12:299. doi: 10.3389/fnmol.2019.00299
- Fosgerau, K., and Hoffmann, T. (2015). Peptide therapeutics: current status and future directions. *Drug Discov. Today* 20, 122–128. doi: 10.1016/j.drudis.2014.10.003
- Goedert, M. (1999). Filamentous nerve cell inclusions in neurodegenerative diseases: tauopathies and alpha-synucleinopathies. *Philos. Trans. R Soc. Lond. B Biol. Sci.* 354, 1101–1118. doi: 10.1098/rstb.1999.0466
- Hasegawa, M., Nonaka, T., and Masuda-Suzukake, M. (2017). Prion-like mechanisms and potential therapeutic targets in neurodegenerative disorders. *Pharmacol. Ther.* 172, 22–33. doi: 10.1016/j.pharmthera.2016.11.010
- Huggins, K. N., Bisaglia, M., Bubacco, L., Taterek-Nossol, M., Kapurniotu, A., and Andersen, N. H. (2011). Designed hairpin peptides interfere with amyloidogenesis pathways: fibril formation and cytotoxicity inhibition, interception of the preamyloid state. *Biochemistry* 50, 8202–8212. doi: 10.1021/bi200760h
- Kim, Y. S., Lim, D., Kim, J. Y., Kang, S. J., Kim, Y. H., and Im, H. (2009). Beta-Sheet-breaking peptides inhibit the fibrillation of human alpha-synuclein. *Biochem. Biophys. Res. Commun.* 387, 682–687. doi: 10.1016/j.bbrc.2009.07.083
- Lee, J. S., and Lee, S.-J. (2016). Mechanism of anti- α -synuclein immunotherapy. *J. Mov. Disord.* 9, 14–19. doi: 10.14802/jmd.15059
- Levin, J., Schmidt, F., Boehm, C., Prix, C., Bötzel, K., Ryazanov, S., et al. (2014). The oligomer modulator anle138b inhibits disease progression in a Parkinson mouse model even with treatment started after disease onset. *Acta Neuropathol.* 127, 779–780. doi: 10.1007/s00401-014-1265-3
- Li, Y., Zhao, C., Luo, F., Liu, Z., Gui, X., Luo, Z., et al. (2018). Amyloid fibril structure of alpha-synuclein determined by cryo-electron microscopy. *Cell Res.* 28, 897–903. doi: 10.1038/s41422-018-0075-x
- Liu, Y., Graetz, M., Ho, L., and Pukala, T. L. (2015). Ion mobility—mass spectrometry-based screening for inhibition of α -synuclein aggregation. *Eur. J. Mass Spectrom.* 21, 255–264. doi: 10.1255/ejms.1359
- Madine, J., Doig, A. J., and Middleton, D. A. (2008). Design of an N-methylated peptide inhibitor of alpha-synuclein aggregation guided by solid-state NMR. *J. Am. Chem. Soc.* 130, 7873–7881. doi: 10.1021/ja075356q
- Marvian, A. T., Koss, D. J., Aliakbari, F., Morshedi, D., and Outeiro, T. F. (2019). In vitro models of synucleinopathies: informing on molecular mechanisms and protective strategies. *J. Neurochem.* 150, 535–565. doi: 10.1111/jnc.14707
- Mason, J. M. (2010). Design and development of peptides and peptide mimetics as antagonists for therapeutic intervention. *Future Med. Chem.* 2, 1813–1822. doi: 10.4155/fmc.10.259
- Mason, J. M., and Fairlie, D. P. (2015). Toward peptide-based inhibitors as therapies for Parkinson's disease. *Future Med. Chem.* 7, 2103–2105. doi: 10.4155/fmc.15.139
- Meade, R. M., Fairlie, D. P., and Mason, J. M. (2019). Alpha-synuclein structure and Parkinson's disease—lessons and emerging principles. *Mol. Neurodegener.* 14:29.
- Meng, X., Munishkina, L. A., Fink, A. L., and Uversky, V. N. (2009). Molecular mechanisms underlying the flavonoid-induced inhibition of alpha-synuclein fibrillation. *Biochemistry* 48, 8206–8224. doi: 10.1021/bi900506b
- Olsen, J. V., Macek, B., Lange, O., Makarov, A., Horning, S., and Mann, M. (2007). Higher-energy C-trap dissociation for peptide modification analysis. *Nat. Methods* 4:709. doi: 10.1038/nmeth1060
- Pasanen, P., Myllykangas, L., Siitonen, M., Raunio, A., Kaakkola, S., Lyytinen, J., et al. (2014). A novel α -synuclein mutation A53E associated with atypical multiple system atrophy and Parkinson's disease-type pathology. *Neurobiol. Aging* 35, e1–e5.
- Peña-Díaz, S., Pujols, J., Conde-Giménez, M., Čarija, A., Dalfó, E., García, J., et al. (2019). ZPD-2, a small compound that inhibits α -synuclein amyloid aggregation and its seeded polymerization. *Front. Mol. Neurosci.* 12:306. doi: 10.3389/fnmol.2019.00306
- Perni, M., Galvagnion, C., Maltsev, A., Meisl, G., Müller, M. B. D., Challa, P. K., et al. (2017). A natural product inhibits the initiation of α -synuclein aggregation and suppresses its toxicity. *Proc. Natl. Acad. Sci. U.S.A.* 114, E1009–E1017.
- Pujols, J., Peña-Díaz, S., Lázaro, D. F., Peccati, F., Pinheiro, F., González, D., et al. (2018). Small molecule inhibits α -synuclein aggregation, disrupts amyloid fibrils, and prevents degeneration of dopaminergic neurons. *Proc. Natl. Acad. Sci. U.S.A.* 115, 10481–10486. doi: 10.1073/pnas.1804198115
- Rekas, A., Knott, R. B., Sokolova, A., Barnham, K. J., Perez, K. A., Masters, C. L., et al. (2010). The structure of dopamine induced α -synuclein oligomers. *Eur. Biophys. J.* 39, 1407–1419.
- Ruggeri, F. S., Flagmeier, P., Kumita, J. R., Meisl, G., Chirgadze, D. Y., Bongiovanni, M. N., et al. (2020). The influence of pathogenic mutations in α -synuclein on biophysical and structural characteristics of amyloid fibrils. *ACS Nano* 14, 5213–5222. doi: 10.1021/acsnano.9b09676
- Schonhoft, J. D., Monteiro, C., Plate, L., Eisele, Y. S., Kelly, J. M., Boland, D., et al. (2017). Peptide probes detect misfolded transthyretin oligomers in plasma of hereditary amyloidosis patients. *Sci. Transl. Med.* 9:eam7621. doi: 10.1126/scitranslmed.aam7621
- Singh, S. K., Dutta, A., and Modi, G. (2017). α -Synuclein aggregation modulation: an emerging approach for the treatment of Parkinson's disease. *Future Med. Chem.* 9, 1039–1053. doi: 10.4155/fmc-2017-0016

SUPPLEMENTARY MATERIAL

The Supplementary Material for this article can be found online at: <https://www.frontiersin.org/articles/10.3389/fnmol.2020.561462/full#supplementary-material>

- Stefanis, L., Emmanouilidou, E., Pantazopoulou, M., Kirik, D., Vekrellis, K., and Tofaris, G. K. (2019). How is alpha-synuclein cleared from the cell? *J. Neurochem.* 150, 577–590. doi: 10.1111/jnc.14704
- Takahashi, R., Ono, K., Takamura, Y., Mizuguchi, M., Ikeda, T., Nishijo, H., et al. (2015). Phenolic compounds prevent the oligomerization of α -synuclein and reduce synaptic toxicity. *J. Neurochem.* 134, 943–955. doi: 10.1111/jnc.13180
- Tatenhorst, L., Eckermann, K., Dambeck, V., Fonseca-Ornelas, L., Walle, H., Lopes Da Fonseca, T., et al. (2016). Fasudil attenuates aggregation of α -synuclein in models of Parkinson's disease. *Acta Neuropathol. Commun.* 4:39.
- Vaikath, N. N., Hmila, I., Gupta, V., Erskine, D., Ingelsson, M., and El-Agnaf, O. M. A. (2019). Antibodies against alpha-synuclein: tools and therapies. *J. Neurochem.* 150, 612–625. doi: 10.1111/jnc.14713
- Woods, L. A., Radford, S. E., and Ashcroft, A. E. (2013). Advances in ion mobility spectrometry-mass spectrometry reveal key insights into amyloid assembly. *Biochim. Biophys. Acta* 1834, 1257–1268. doi: 10.1016/j.bbapap.2012.10.002
- Yang, H., and Zubarev, R. A. (2010). Mass spectrometric analysis of asparagine deamidation and aspartate isomerization in polypeptides. *Electrophoresis* 31, 1764–1772. doi: 10.1002/elps.201000027
- Young, L. M., Saunders, J. C., Mahood, R. A., Revell, C. H., Foster, R. J., Tu, L.-H., et al. (2015). Screening and classifying small-molecule inhibitors of amyloid formation using ion mobility spectrometry-mass spectrometry. *Nat. Chem.* 7, 73–81. doi: 10.1038/nchem.2129

Conflict of Interest: The authors declare that the research was conducted in the absence of any commercial or financial relationships that could be construed as a potential conflict of interest.

Copyright © 2020 Torpey, Meade, Mistry, Mason and Madine. This is an open-access article distributed under the terms of the Creative Commons Attribution License (CC BY). The use, distribution or reproduction in other forums is permitted, provided the original author(s) and the copyright owner(s) are credited and that the original publication in this journal is cited, in accordance with accepted academic practice. No use, distribution or reproduction is permitted which does not comply with these terms.



Comparison of Common and Disease-Specific Post-translational Modifications of Pathological Tau Associated With a Wide Range of Tauopathies

Fuyuki Kametani^{1*}, Mari Yoshida², Tomoyasu Matsubara³, Shigeo Murayama², Yuko Saito⁴, Ito Kawakami¹, Mitsumoto Onaya⁵, Hidetomo Tanaka⁶, Akiyoshi Kakita⁶, Andrew C. Robinson⁷, David M. A. Mann⁷ and Masato Hasegawa^{1*}

¹ Department of Brain and Neuroscience, Tokyo Metropolitan Institute of Medical Science, Tokyo, Japan, ² Institute for Medical Science of Aging, Aichi Medical University, Aichi, Japan, ³ Department of Neuropathology, Tokyo Metropolitan Institute of Gerontology, Tokyo, Japan, ⁴ Department of Pathology and Laboratory Medicine, National Center Hospital, National Center of Neurology and Psychiatry, Tokyo, Japan, ⁵ Department of Psychiatry, National Hospital Organization Shimofusa Psychiatric Medical Center, Chiba, Japan, ⁶ Department of Pathology, Brain Research Institute, Niigata University, Niigata, Japan, ⁷ Division of Neuroscience & Experimental Psychology, Faculty of Biology, Medicine and Health, School of Biological Sciences, The University of Manchester, Salford, United Kingdom

OPEN ACCESS

Edited by:

Wolfgang Hoyer,
Heinrich Heine University
of Düsseldorf, Germany

Reviewed by:

Dagmar Ehrnhöfer,
AbbVie, Germany
Todd Cohen,
University of North Carolina at Chapel
Hill, United States

*Correspondence:

Fuyuki Kametani
kametani-fy@igakuken.or.jp
Masato Hasegawa
hasegawa-ms@igakuken.or.jp

Specialty section:

This article was submitted to
Neurodegeneration,
a section of the journal
Frontiers in Neuroscience

Received: 10 July 2020

Accepted: 28 September 2020

Published: 04 November 2020

Citation:

Kametani F, Yoshida M, Matsubara T, Murayama S, Saito Y, Kawakami I, Onaya M, Tanaka H, Kakita A, Robinson AC, Mann DMA and Hasegawa M (2020) Comparison of Common and Disease-Specific Post-translational Modifications of Pathological Tau Associated With a Wide Range of Tauopathies. *Front. Neurosci.* 14:581936. doi: 10.3389/fnins.2020.581936

Tauopathies are the most common type of neurodegenerative proteinopathy, being characterized by cytoplasmic aggregates of hyperphosphorylated tau protein. The formation and morphologies of these tau inclusions, the distribution of the lesions and related metabolic changes in cytoplasm differ among different tauopathies. The aim of this study was to examine whether there are differences in the post-translational modifications (PTMs) in the pathological tau proteins. We analyzed sarkosyl-insoluble pathological tau proteins prepared from brains of patients with Alzheimer's disease, Pick's disease, progressive supranuclear palsy, corticobasal degeneration, globular glial tauopathy, and frontotemporal dementia and parkinsonisms linked to chromosome 17 with tau inclusions using liquid chromatography mass spectrometry. In pathological tau proteins associated with a wide range of tauopathies, 170 PTMs in total were identified including new PTMs. Among them, common PTMs were localized in the N- and C-terminal flanking regions of the microtubule binding repeats and PTMs, which were considered to be disease-specific, were found in microtubule binding repeats forming filament core. These suggested that the differences in PTMs reflected the differences in tau filament core structures in each disease.

Keywords: tauopathy, tau, post-translational modifications, amyloid, fibril structure, cryo-EM, ubiquitination, phosphorylation

INTRODUCTION

Neurodegenerative tauopathies are characterized by cytoplasmic aggregates of hyperphosphorylated tau protein (Goedert et al., 1992; Buee et al., 2000; Lee et al., 2001). Among them, Alzheimer's disease (AD), chronic traumatic encephalopathy (CTE), Pick's disease (PiD), progressive supranuclear palsy (PSP), corticobasal degeneration (CBD), globular glial tauopathy

(GGT), and argyrophilic grain disease (AGD) are sporadic tauopathies, while frontotemporal dementia and parkinsonisms linked to chromosome 17 with tau inclusions (FTDP-17T) is a familial disease caused by abnormalities in the tau gene, *MAPT* (Iwatsubo et al., 1994; Spillantini et al., 1997, 1998; Hutton et al., 1998; Poorkaj et al., 1998; Buee and Delacourte, 1999; Goedert and Hasegawa, 1999; Lee et al., 2001; Kovacs, 2015). Although the morphologies of tau inclusions and the distribution of the lesions differ, these diseases are neuropathologically defined by the characteristic tau pathologies observed in nerve cells and/or glial cells, and the formation of these tau aggregates and related metabolic changes in the cytoplasm are believed to be the cause of neurodegeneration (Goedert et al., 1992; Buee et al., 2000; Lee et al., 2001).

Expression of the *MAPT* gene is developmentally regulated by means of alternative splicing of the exons. In adult human brain, six tau isoforms with either three or four microtubule-binding repeats (3R or 4R) are expressed (Goedert et al., 1989). In AD brains, both 3R and 4R tau isoforms are accumulated in a hyperphosphorylated state as pathological inclusions called neurofibrillary tangles and neuropil threads, mainly in neuronal cells (Goedert, 1993; Goedert et al., 1996; Serrano-Pozo et al., 2011; Iqbal et al., 2016). Ultrastructurally, a unique twisted paired helical filaments (PHFs) or related straight filaments (SFs) with a diameter of 10–20 nm and periodicities periodicity of 80 nm are observed (Crowther and Wischik, 1985; Wischik et al., 1988a,b; Crowther et al., 1989; Goedert et al., 1989; Greenberg and Davies, 1990; Lee et al., 1991). On the other hand, in PiD, only 3R tau isoforms selectively accumulate in neuronal cells with SF morphology (15–18 nm), although some exceptions have been reported (Falcon et al., 2018). In PSP, CBD, GGT, and AGD, 4R tau isoforms selectively accumulate in neuronal and glial cells, and the filaments in each disease have unique filamentous morphologies, such as SFs (13–14 nm) in PSP and wide, twisted filaments (20 nm) in CBD (Iwatsubo et al., 1994; Spillantini et al., 1997; Hutton et al., 1998; Poorkaj et al., 1998; Buee and Delacourte, 1999; Goedert and Hasegawa, 1999; Lee et al., 2001; Kovacs, 2015). Furthermore, it has been reported that CBD and PSP can be distinguished biochemically based on the characteristics of the C-terminal fragments (Arai et al., 2004) and the band patterns of protease-resistant fragments (Taniguchi-Watanabe et al., 2016), even though they are both 4R tauopathies.

The discovery of *MAPT* mutations in FTDP-17T established that abnormalities in tau expression and function can cause tau accumulation and neurodegeneration. The clinico-pathological phenotypes of the disease vary, but there is a strong correlation between the locations of the mutations and the neuropathology of the tau proteins (morphology of inclusions, isoform composition, and distributions). For example, PiD-like pathologies have been reported in patients with some mutations in exon 9. PSP- or CBD-like pathologies have been reported in patients with mutations that increase the splicing of exon 10 inclusions, resulting in an increased expression ratio of 4R tau isoforms. On the other hand, cases with intron 10 mutations develop a unique pathology, distinct from other sporadic 4R tauopathies (Spillantini et al., 1996; Reed et al., 1997; Bugiani et al., 1999; Spina et al., 2008; Tacik et al., 2017; Erro et al., 2019).

We have been investigating the sarkosyl-insoluble pathological tau proteins prepared from brains of patients with AD, PiD, CBD, PSP, or and FTDP-17T (intron 10 + 16), and we previously reported that the carboxyl-terminal region of tau (residues 243–406), which constitutes the trypsin-resistant core units of tau aggregates, shows different banding patterns among the diseases (Taniguchi-Watanabe et al., 2016). Furthermore, we determined the sequences and lengths of the tau regions involved in the assembly of the tau filaments in these diseases (Taniguchi-Watanabe et al., 2016). Recent cryo-EM structural analyses of tau filaments isolated from AD, PiD, and CBD brains revealed that the structures or folding of tau proteins in the filaments differs among the diseases. These findings support the idea that the pathogenesis and progression of these tauopathies are closely associated with the formation of disease-specific tau strains or folded conformers, and with cell-to-cell transmission of the pathological proteins (Goedert et al., 2018; Fitzpatrick and Saibil, 2019; Hasegawa, 2019). Furthermore, it has been pointed out that post-translational modifications (PTMs) may also play a role. Therefore, in this study, we have analyzed and compared the PTMs in the pathological tau proteins prepared from a wide range of tauopathies (AD, PSP, CBD, GGT, PiD, and FTDP-17T with MAPT intron 10 mutation) in order to establish whether the PTMs show disease-specificity.

MATERIALS AND METHODS

Brain Tissues, Preparation of Insoluble Tau, and Immunohistochemistry

The cases selected for this study [three AD, three FTDP-17T (intron 10 + 16), three PSP, three CBD, three GGT, and three PiD cases] are listed in **Table 1**.

Sarkosyl-insoluble tau was prepared as previously described (Zhang et al., 2020); this method was developed and afforded highly purified pathological tau proteins. Briefly, 0.5 g tissues were homogenized in 20 volumes (v/w) of extraction buffer, brought to 2% sarkosyl, and incubated for 30 min. The supernatant after a 10 min spin at 20,000 g, was centrifuged at 168,000 × g for 20 min. The pellet was resuspended in a small amount of extraction buffer and centrifuged at 9,500 g for 10 min. The supernatant was diluted threefold in 50 mM Tris-HCl, pH 7.5, containing 0.15 M NaCl, 10% sucrose and 0.2% sarkosyl, and spun at 168,000 g for 20 min.

For immunoblotting, the sarkosyl-insoluble pellet was resuspended in SDS sample buffer and the aliquots were subjected to SDS-PAGE on 4–20% polyacrylamide gradient gel. Immunoblotting was performed with anti-tau C-terminus antibody T46 as described elsewhere (Taniguchi-Watanabe et al., 2016).

For immunohistochemistry, brain tissues were fixed by in 10% buffered formalin and embedded in paraffin, then 8-micron-thick sections were prepared and immunostained with a monoclonal antibody AT8 (Invitrogen).

TABLE 1 | Description of the cases used PTMs analysis.

Case No.	Age at death	Gender	Brain weight	pmi	Brain region	Neuropathological diagnosis
AD1	85	M	1146	8 h	Parietal	AD
AD2	94	F	983	11 h	Parietal	AD
AD3	61	M	nd	nd	Frontal	AD
FTDP-17T1	55	M	1240	nd	Frontal	MAPT +16
FTDP-17T2	53	M	1240	nd	Frontal	MAPT +16
FTDP-17T3	65	F	1040	nd	Frontal	MAPT +16
CBD1	73	M	1200	3 h	Frontal	CBD
CBD2	74	F	899	nd	Frontal	CBD
CBD3	74	F	nd	nd	Frontal	CBD
GGT1	74	M	1222	10 h	Frontal	GGT
GGT2	77	F	1110	2 h	Frontal	GGT
GGT3	76	F	nd	nd	Frontal	GGT
PSP1	63	M	1435	2 h	Frontal	PSP
PSP2	85	M	850	1 h	Frontal	PSP
PSP3	82	M	1280	nd	Frontal	PSP
PiD1	62	F	928	nd	Frontal	Pick
PiD2	56	M	1150	nd	Frontal	Pick
PiD3	nd	nd	nd	nd	Frontal	Pick

LC-MS/MS Analysis of Sarkosyl-Insoluble Tau

Sarkosyl-insoluble fractions containing 500~5000 ng of tau were treated with 70% formic acid for 1 h at room temp, then diluted in water and dried up. For trypsin digestion, 50 mM triethylammonium bicarbonate and 1 µg of Trypsin/Lys-C Mix (Promega) were added. Each mixture was incubated at 37°C for 20 h. After tryptic digestion, 2 µL of 100 mM DTT was added to the mixture, and incubation was continued at 100°C for 5 min. Then the sample was dried and stored at -80°C until assay.

Each sample was resuspended in 0.1% formic acid and introduced into a nano-flow HPLC system, EASY-nLC 1200 (Thermo Fisher Scientific Inc., Waltham, MA, United States). A packed nano-capillary column NTCC-360/75-3-123 (0.075 mm I.D. × 125 mm L, particle diameter 3 µm, Nikkyo Technos Co., Ltd., Tokyo, Japan) was used at a flow rate of 300 nl/min with a 2–80% linear gradient of acetonitrile for 80 min. Eluted peptides were directly detected with an ion trap mass spectrometer, Q-Exactive HF (Thermo Fisher Scientific Inc., Waltham, MA, United States). For ionization, a spray voltage of 2.0 kV and a capillary temperature of 250°C were used. The mass acquisition method consisted of one full MS survey scan with an Orbitrap resolution of 60,000, followed by an MS/MS scan of the most abundant precursor ions from the survey scan with an Orbitrap resolution of 15,000. Dynamic exclusion for the MS/MS was set to 30 s. The MS scan range of 350–1800 m/z was employed in the positive ion mode, followed by data-dependent MS/MS using the HCD operating mode on for the top 15 ions in order of abundance. The data were analyzed with Proteome Discoverer (Thermo Fisher Scientific Inc., Waltham, MA, United States), Mascot software (Matrix Science Inc., Boston, MA, United States) and Scaffold software (Proteome Software, Inc., Oregon, OR, United States). Swissprot

and GenBank databases were used. Mass spectrometry data are obtained from jPOST (Japan Proteome Standard Repository), which is certificated member of ProteomeXchange Consortium. ID number is PXD020371.

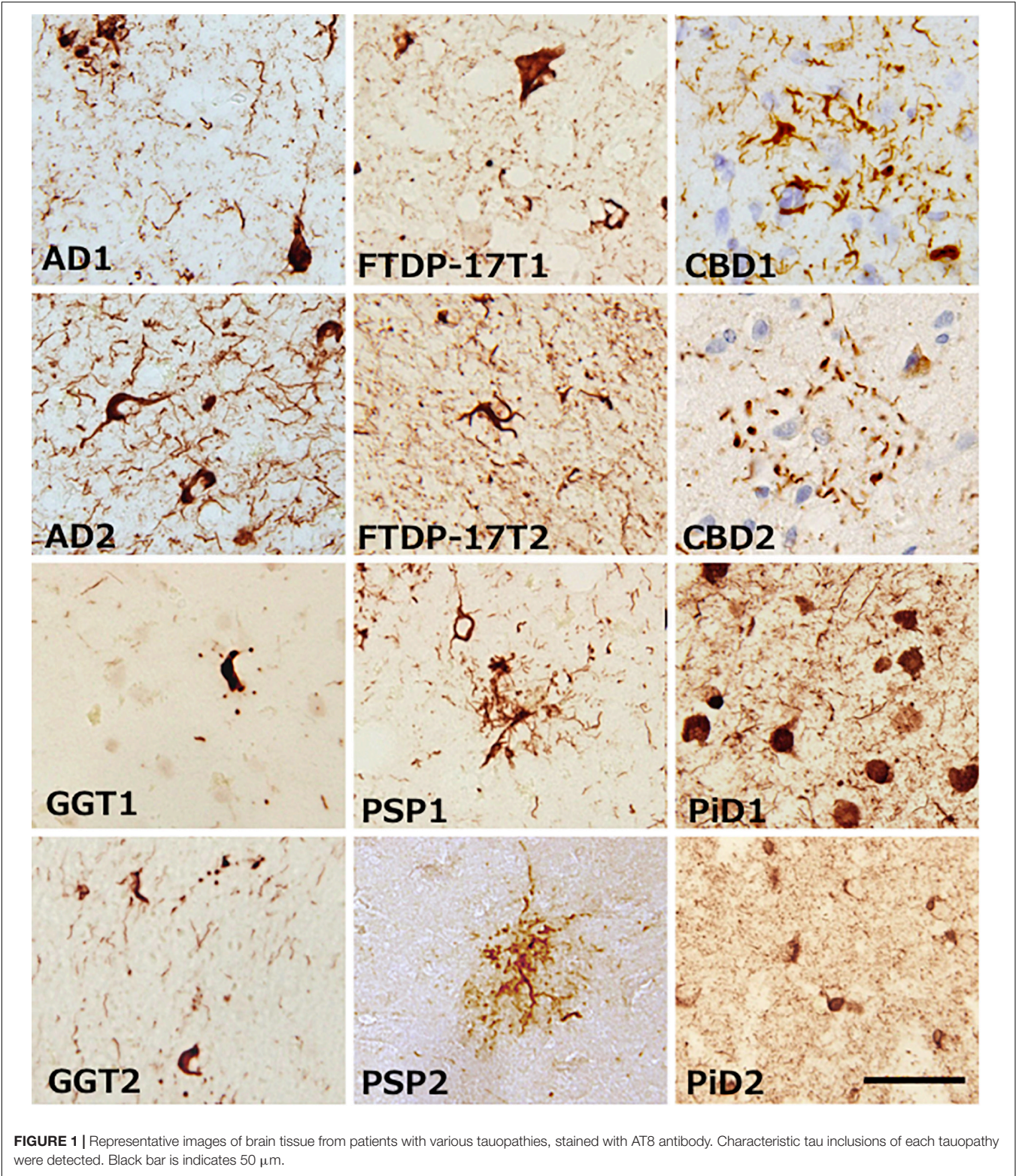
RESULTS AND DISCUSSION

PTMs on Tau From Tauopathy Brains

Alzheimer's disease, FTDP-17T, CBD, GGT, PSP, and PiD were neuropathologically diagnosed and biochemically confirmed by immunoblotting with anti-tau antibodies (in addition, MAPT intron 10 + 16 mutation was identified in the two FTDP-17T cases from Manchester Brain Bank). Two cases of each disease with abundant tau accumulation were selected for this analysis. Representative image of AT8 immunostaining of these cases are shown in **Figure 1**. The characteristic tau inclusions were detected in these diseases (for example, neurofibrillary tangles in AD, coiled bodies and diffuse tangles in FTDP-17T, tufted astrocytes in PSP, astrocytic plaques in CBD, globular glial inclusions in GGT, and Pick bodies in PiD) (**Figure 1**). Pathological tau proteins in the sarkosyl-insoluble fractions prepared from these cases were analyzed by SDS-PAGE and immunoblotting with anti-tau C-terminus antibody (T46). As shown in **Figure 2** and **Supplementary Figure 1**, characteristic hyper-phosphorylated full-length triplet tau bands at 60, 64, and 68 kDa were observed in AD (Hasegawa, 2016, 2019). In contrast, only the upper doublet tau bands at 64 and 68 kDa were detected in the 4R tauopathies FTDP-17T (+16), CBD, GGT, and PSP, while only the lower tau doublet bands at 60 and 64 kDa were detected in PiD (Hasegawa, 2016, 2019). In addition to these full-length tau bands, many C-terminal tau fragments (CTFs) and smears were detected in all these tauopathies (**Figure 2** and **Supplementary Figure 1**). The characteristic bands of CBD and PSP CTFs at 37 kDa CTFs and ~33 kDa CTFs (Arai et al., 2004) were observed in both of the CBD case and both of the PSP cases in this study, respectively. The two FTDP-17T (+16) cases also showed a CBD-tau banding pattern, while the two GGT cases showed a PSP-tau banding pattern (**Figure 2** and **Supplementary Figure 1**). These results are consistent with previous observations, and confirmed the strong link between neuropathological diagnosis and biochemical characterization. After denaturation of the sarkosyl-insoluble tau by formic acid treatment, the pathological tau were digested with trypsin and the tryptic peptides were analyzed by LC-MS/MS. Identified tau peptides (FDR: 0.38%) with or without PTMs are listed in the **Supplementary Table 1**. The recovery of the identified tau-derived peptides in each case was 70–90% and was summarized in **Supplementary Table 2**.

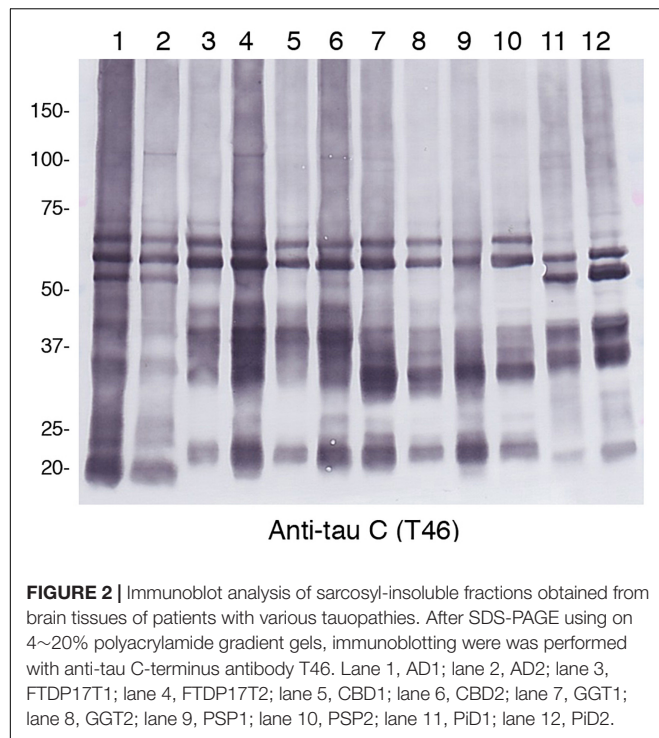
Common PTMs Localized in the N-terminal, Middle- and C-terminal Regions

The PTMs in each case were summarized in **Table 2** (partial excerpt) and **Supplementary Table 3** (all details). In these table, the total number of peptides containing each amino acid residue



and the number of peptides modified with the residues are shown, and the ratios thereof (frequency of modification) are shown in the color-coding defined at the bottom of the table. The gray area in PiD is a region of amino acid residues that does not exist.

As shown in **Table 2** and **Supplementary Table 3**, 170 PTMs in total were identified in the sarkosyl-insoluble tau prepared from these tauopathies. Overall, the phosphorylation sites were focused in the 181–238 and 396–422 regions of the



tau, corresponding N- and C-terminal flanking regions of the microtubule binding repeats. In contrast, ubiquitination sites seemed to be focused in the 254–281 and 369–395. In each tauopathy, when PTMs two or more cases are picked up, those were deamination at 6Gln, 255Asn, 265Asn, 359Asn, 368Asn, and 424Gln, oxidation at 11Met, 31Met, 250Met, 299His, and 419Met, and phosphorylation at 181Thr, 185Ser, 199pSer, 202Ser, 212Thr, 217Thr, 231Thr, 235Ser, 237Ser, 238Ser, 396Ser, 400Ser, 403Thr, 404Ser, and 422Ser were listed. These PTMs were localized in the N-terminal region, middle region (181–238) and the C-terminal region. As for Met, Asn, and Gln, oxidation and deamidation can rarely occur during experimental manipulation. Therefore, it cannot be denied that artificial modification may be included in these amino acid residues.

We previously reported that the carboxyl-terminal region (residues 243–406) of tau including the MT-binding repeat regions form the protease-resistant core units of the tau filaments, and we identified the N-terminal sequences and the trypsin-resistant regions of tau (Taniguchi-Watanabe et al., 2016). We further suggested that the assembly of these specific tau regions might be involved in the pathogenesis and progression of these distinct disease phenotypes (Taniguchi-Watanabe et al., 2016). Recent cryo-EM analyses have revealed that the R3–R4 repeat and 12 residues after the R4 repeat region in AD, the R2–R4 repeat and 12 residues after the R4 repeat region in CBD, and the R1, R3–R4 repeat and 12 residues after R4 repeat region in PiD form the cores of the tau filaments (Fitzpatrick et al., 2017; Falcon et al., 2018; Fitzpatrick and Saibil, 2019; Zhang et al., 2020), in accordance with our previous reports (Taniguchi-Watanabe et al., 2016; Hasegawa, 2019). Overall, the results indicate that most of the common PTMs detected in this study exist outside the core

structures of the tau filaments, suggesting that these regions may not be involved in the strain-dependent tau filament formation.

Characteristic Ubiquitination Sites on Tau in Each Disease

Ubiquitination occurs mainly in the region of 254–281. Furthermore, characteristic ubiquitination of disease was observed in the fibril core region. So far, the core regions revealed by cryoEM are 304–380 in AD, 274–380 in CBD, and 254–378 in PiD, which correspond to the portion between the broken lines in **Supplementary Table 3** (all details). We identified ubiquitination sites characteristic of each disease in the regions forming the fibril cores, as shown in **Table 2** and **Supplementary Table 3**. These included ubiquitination at 311Lys and 317Lys in the R3 region in AD, and ubiquitination at 343Lys, 353Lys, 369Lys, and 375Lys in the R4 and 12 residues after the R4 region in CBD. These ubiquitinated Lys corresponded to the dense part outside the tau fibril core in the data obtained by cryoEM, and it was considered that polyubiquitin chains exist in this part (Arakhamia et al., 2020; Zhang et al., 2020). Similar results have been reported elsewhere (Arakhamia et al., 2020). Similarly, in FTDP-17T, ubiquitination at 343Lys, 353Lys, 369Lys, and 370Lys in the R4 and 12 residues after the R4 region were observed. This pattern to be similar to that in CBD-tau, suggesting that the folding of tau in FTDP-17T (+16) cases seem to be similar to that in CBD. Ubiquitination at 267Lys, 274Lys, 280Lys, and 281 Lys in the R1–R2 region is characteristic of tau prepared from GGT. In PSP cases, no ubiquitination was found in the R2–4 and 12 residues after R4 region. In PiD cases, ubiquitination at 343Lys and 353Lys were found.

Based on the idea that the R2–R4 and 12 residues after R4 region are closely involved in the tau filament core formation, it seems likely that tau in GGT and PSP may have a distinct core structure different from that in AD, CBD, FTDP-17T, and PiD. It also seems likely that PTMs such as ubiquitination of tau protofilaments would affect the assembly of these protofilaments themselves (Arakhamia et al., 2020).

Other Characteristic PTMs

Phosphorylation at 262Ser residue has been reported in various tauopathies but it was not detected in PiD using a specific monoclonal antibody (Arai et al., 2004). We have confirmed this by means of MS/MS analyses of tau prepared from various tauopathies. Furthermore, we have shown in this study phosphorylation at 356Ser residue was detected in various tauopathies, but not in AD. According to cryoEM analysis, 262Ser residues in PiD and 356Ser residue in AD are located in the center of the bent structure and are difficult to access from outside. Therefore, these PTMs are likely to have occurred after fibril formation and it is considered that phosphorylation is unlikely to occur in PiD and AD, respectively. If an antibody specific for phosphorylated Ser356 residue could be raised, it might be useful tool for distinguishing the AD-tau pathology from the other tauopathies.

Extensive deamidation of Asn279 has been detected with specific antibodies in AD, but not in other 4R tauopathies

TABLE 2 | Summarized PTMs in tauopathies. In this table, the total number of peptides containing each amino acid residue and the number of peptides modified with the residues are shown, and the ratios thereof (frequency of modification) are shown in the color-coding defined at the bottom of the table. The gray area in PID is a region of amino acid residues that does not exist.

Summarized PTMs in tauopathies (modified peptide number / idetified peptides number)																		
	AD1	AD2	AD3	FTDP17T1	FTDP17T2	FTDP17T3	CBD1	CBD2	CBD3	GGT1	GGT2	GGT3	PSP1	PSP2	PSP3	PID1	PID2	PID3
6Gln deamidation	1/45	2/50	4/104	3/35	4/50	2/27	0/15	2/34	1/32	2/33	0/14	2/29	0/16	1/23	1/12	4/49	5/60	0/32
11Met oxidation	7/45	15/50	41/104	6/35	20/50	6/27	3/15	13/34	7/32	6/33	2/14	11/29	1/16	9/23	2/12	13/49	18/60	10/32
31Met oxidation	0/11	2/19	49/98	4/24	8/32	8/36	2/15	9/33	9/38	6/23	2/7	5/29	0/13	2/10	4/13	4/25	5/27	4/21
181Thr phosphorylation	15/22	13/22	62/88	2/29	20/36	19/31	14/22	27/41	30/51	20/27	7/17	16/29	10/21	11/17	6/10	47/67	62/83	25/37
185Ser phosphorylation	1/22	0/22	12/88	1/29	2/36	4/31	1/22	5/41	9/51	5/27	0/17	2/29	0/21	1/17	0/10	12/67	27/83	4/37
199Ser phosphorylation	1/3	0/2	5/11	1/7	5/10	1/3	3/6	5/9	4/11	4/7	1/2	1/5	0/4	1/3	1/3	2/5	5/9	1/4
202Ser phosphorylation	1/3	1/2	3/11	3/7	3/10	0/3	3/6	2/9	2/11	3/7	0/2	2/5	2/4	2/3	0/3	1/5	5/9	1/4
217Thr phosphorylation	21/28	17/22	28/41	8/18	17/26	12/19	14/21	19/37	10/21	12/25	1/9	10/23	5/13	10/19	2/5	14/32	18/27	7/15
231Thr phosphorylation	24/29	23/23	70/73	32/32	36/38	34/37	8/11	36/44	38/42	39/39	19/19	35/35	21/21	20/20	11/11	55/55	62/85	28/28
235Ser phosphorylation	14/22	7/18	42/61	12/28	20/32	18/30	8/8	22/39	19/36	18/35	9/17	14/30	10/17	7/16	7/9	21/47	42/79	15/26
237Ser phosphorylation	4/22	3/18	14/61	4/28	4/32	3/30	3/8	12/39	9/36	2/35	0/17	3/30	2/17	2/16	0/9	8/47	11/79	2/26
238Ser phosphorylation	5/22	7/18	21/61	6/28	10/32	8/30	4/8	16/39	11/36	6/35	1/17	5/30	3/17	1/16	0/9	15/47	17/79	4/26
240Lys ubiquitination	1/22	0/18	0/61	0/28	1/32	1/30	0/8	1/39	0/36	1/35	0/17	0/30	0/17	0/16	0/9	0/47	2/79	0/26
244Gln deamidation	1/64	0/69	4/108	3/29	6/49	1/31	3/34	8/60	5/42	9/39	1/20	22/69	2/20	11/50	2/15	9/88	7/85	2/36
250Met oxidation	20/64	26/69	41/108	10/29	17/49	9/31	15/34	27/60	11/42	7/39	8/20	24/69	3/20	23/50	3/15	28/88	22/85	14/36
254Lys ubiquitination	2/64	3/69	4/108	1/29	1/49	0/31	1/34	1/60	1/52	3/39	0/20	5/69	1/20	0/50	0/15	0/88	0/85	0/36
255Asn deamidation	8/11	12/15	14/21	2/3	2/3	5/7	4/5	20/25	9/12	8/11	2/2	13/19	0/1	14/14	2/2	2/2	1/1	0/1
257Lys ubiquitination	1/11	1/15	2/21	0/3	1/3	1/7	0/5	1/25	0/12	0/11	0/2	0/19	0/1	0/14	0/2	0/2	0/1	0/1
257Lys acetylation	0/11	0/15	0/21	0/3	0/3	0/7	0/5	0/25	0/12	0/11	0/2	0/19	0/1	0/14	0/2	1/2	1/1	1/1
259Lys ubiquitination	0/1	2/2	4/5	0/1	-	3/3	-	2/3	0/1	1/2	0/1	1/1	-	0/1	-	-	0/1	0/1
259Lys acetylation	0/1	0/2	0/5	1/1	-	0/3	-	0/3	1/1	0/2	1/1	0/1	-	0/1	-	-	1/1	1/1
262Ser phosphorylation	2/18	6/32	17/74	4/29	8/26	6/34	4/15	8/20	8/36	7/29	2/18	8/38	3/16	0/7	3/14	0/12	0/13	0/14
263Thr phosphorylation	6/18	6/32	3/74	6/29	0/26	3/34	4/15	2/20	2/36	2/29	0/18	0/38	0/16	2/7	1/14	1/12	0/13	0/14
265Asn deamidation	14/18	24/32	52/74	20/29	16/26	22/34	10/15	17/20	25/36	21/29	10/18	28/38	12/16	5/7	11/14	3/12	2/13	3/14
267Lys ubiquitination	2/18	8/32	11/74	2/29	6/26	5/34	0/15	0/20	2/36	8/29	2/18	7/38	0/16	0/7	0/14	0/12	0/13	1/14
267Lys acetylation	0/18	0/32	1/74	1/29	0/26	0/34	0/15	1/20	1/36	1/29	1/18	0/38	0/16	0/7	0/14	0/12	0/13	0/14
274Lys ubiquitination	1/5	0/11	0/18	0/8	0/6	0/5	-	0/6	0/5	2/14	0/4	0/11	-	-	-	0/1	0/1	0/1
274Lys acetylation	0/5	0/11	0/18	1/8	0/6	0/5	-	1/6	1/5	1/14	0/4	2/11	-	-	-	0/1	0/1	0/1
279Asn deamidation	4/4	2/2	4/4	2/5	1/2	0/2	-	1/4	0/3	0/7	0/2	1/5	0/1	0/2	0/1	This gray area does not exist in PID.		
280Lys ubiquitination	0/4	0/2	0/4	0/5	0/2	0/2	-	0/4	0/3	2/7	0/2	0/5	0/1	0/2	0/1			
280Lys acetylation	0/4	0/2	0/4	1/5	1/2	0/2	-	0/4	0/3	1/7	0/2	2/5	0/1	0/2	0/1			
281Lys ubiquitination	0/3	0/4	1/10	1/11	0/4	3/5	0/2	0/8	0/6	3/11	2/7	3/7	0/1	0/3	0/2			
281Lys acetylation	0/3	0/4	0/10	2/11	1/4	0/5	2/2	3/8	4/6	2/11	2/7	0/7	1/1	1/3	1/2			
299His oxidation	0/12	2/28	5/96	5/67	13/129	5/26	0/6	5/17	6/40	9/62	3/32	8/245	2/132	3/12	1/11			
307Gln deamidation	0/17	2/28	7/96	2/67	7/129	2/26	0/6	2/17	3/40	4/62	2/32	5/245	5/134	3/12	0/11			
311Lys ubiquitination	0/17	5/59	19/203	0/67	0/129	0/26	0/6	0/17	0/40	0/62	0/32	0/245	0/134	0/12	0/11			
311Lys acetylation	0/17	1/59	5/203	0/67	0/129	0/26	0/6	0/17	0/40	0/62	1/32	0/245	0/134	0/12	0/11			
317Lys ubiquitination	1/17	7/59	24/203	0/67	0/129	0/26	0/6	0/17	0/40	0/62	0/32	0/245	0/134	0/12	0/11	0/71	0/90	0/27
343Lys ubiquitination	-	-	2/2	2/2	2/3	2/2	-	1/1	1/1	-	-	-	-	-	-	1/2	1/1	-
353Lys ubiquitination	-	0/13	0/4	-	1/2	2/2	0/1	1/3	2/5	0/2	0/1	1/1	-	-	0/1	0/5	0/4	1/4
353Lys acetylation	-	1/1	2/4	-	1/2	0/2	0/1	2/3	2/5	1/2	0/1	1/1	-	-	1/1	4/5	1/4	3/4
356Ser phosphorylation	0/16	0/35	1/135	3/39	7/50	4/45	2/13	4/36	6/54	2/43	2/28	2/57	2/30	2/16	1/18	3/71	3/72	1/35
359Asn deamidation	1/14	4/35	3/135	4/39	3/50	4/45	1/13	1/36	4/54	5/43	2/28	1/57	1/30	0/16	1/18	5/71	5/72	2/35
362His oxidation	0/14	3/35	7/135	1/39	4/50	1/45	0/13	1/36	4/54	1/43	2/28	4/57	2/30	1/16	1/18	6/71	7/72	2/35
368Asn deamidation	1/14	4/35	6/135	20/39	28/50	25/45	4/13	13/36	19/54	9/43	5/28	9/57	9/30	4/16	5/18	9/71	11/72	3/35
369Lys ubiquitination	0/14	0/35	0/135	1/39	5/50	3/45	1/14	1/36	3/54	0/43	0/28	0/57	0/30	0/16	0/18	0/71	0/72	0/35
375Lys ubiquitination	-	0/2	2/5	1/2	1/1	0/1	-	1/3	0/1	-	-	-	-	-	-	0/1	-	-
395Lys ubiquitination	0/8	1/33	10/104	0/23	2/43	2/25	0/24	1/33	0/34	0/35	0/6	0/39	0/19	0/15	0/14	0/53	1/48	0/23
396Ser phosphorylation	8/16	29/37	90/109	16/26	32/47	17/28	20/27	27/37	23/29	28/36	4/7	28/36	13/18	16/26	9/13	38/49	37/46	14/19
400Ser phosphorylation	4/16	19/37	60/109	7/26	17/43	5/28	14/27	16/37	12/29	24/36	2/7	23/36	11/18	14/26	3/13	27/49	28/46	6/19
403Thr phosphorylation	0/16	3/37	22/109	4/26	6/47	5/28	1/27	6/37	1/29	4/38	1/7	11/36	3/18	3/26	2/13	8/49	5/46	4/19
404Ser phosphorylation	8/16	24/37	53/109	15/26	29/47	15/28	21/27	25/37	15/29	23/36	0/7	12/36	9/18	16/26	9/13	24/49	20/46	6/19
407His oxidation	1/5	16/23	20/129	0/29	0/38	0/33	0/15	2/55	0/23	0/36	0/1	0/27	0/10	0/22	0/2	0/26	0/56	0/11
407His phosphorylation	0/5	0/23	20/129	0/29	1/38	0/33	1/15	6/55	0/23	1/36	0/1	3/27	0/10	3/22	0/2	4/26	1/56	0/11
419Met oxidation	0/5	3/8	48/129	3/29	6/38	1/33	1/16	12/55	1/23	1/30	0/1	5/27	0/10	3/22	0/2	1/26	9/56	0/11
422Ser phosphorylation	1/5	0/8	31/129	4/29	6/38	5/33	4/16	15/55	2/23	5/30	0/1	7/27	2/10	5/22	0/2	4/26	15/56	3/11
424Gln deamidation	1/5	4/8	40/129	5/29	6/38	10/33	2/16	5/55	7/23	8/30	0/1	8/27	5/10	3/22	1/2	7/26	15/56	4/11

Frequencies of PTM peptides				
	0-30	-30	-200	-300
phosphorylation				
deamidation				
ubiquitination				
acetylation				
oxidation				
- : not detected				

(Dan et al., 2013). This finding was also partially confirmed in this study. 279Asn was deamidated in all peptides including 279Asn in three cases of AD. Deamidation of 279Asn was detected in two cases of FTDP-17T, one case of CBD, and one case of GGT, but the ratio of the deamidated peptide was 45, 25, and 20%, which is quite different from the case of AD. In AD-tau, Asn279 is located in the outside the core of tau filaments, but it is inside the core in CBD (Fitzpatrick et al., 2017; Arakhamia et al., 2020; Zhang et al., 2020). It may reflect some structural difference in the pathological tau, causing Asn279 to be exposed away from the core region.

Phosphorylation of 217Thr has recently been reported to be a biomarker of AD (Barthelemy et al., 2020; Janelidze et al., 2020; Palmqvist et al., 2020). The average appearance rates of phosphorylated peptides at 217Threonine residue were AD, 73%; FTDP-17T, 58%; CBD, 55%; GGT, 34%; PSP, 44%; PiD, 53% (Table 2 and Supplementary Table 3). AD is clearly high and can be distinguished from other tauopathy. This is consistent with the recent report. No clear distinction could be made regarding the phosphorylation of 181T (Table 2 and Supplementary Table 3).

Furthermore, the average appearance rates of phosphorylation of 231Thr were 80–100% in all tauopathy (Table 2 and Supplementary Table 3). This means that almost all 231Thr residues are phosphorylated. Recently, phosphorylated tau profiles in soluble brain fractions in AD have been reported (Dujardin et al., 2020; Horie et al., 2020). In one report, Thr111, Ser113, Thr153, Thr181, Ser199, Ser202, Thr205, Thr217, Thr231, Ser262, and Ser396, and in the other, Thr181, Ser198, Ser199, Ser202, Thr217, Thr231, Ser262, Ser400, Thr403, Ser404 were phosphorylated, but in our analysis, all of these sites except Thr153 and Ser205 were phosphorylated (Table 2 and Supplementary Table 3). Furthermore, in insoluble brain fractions in AD, phosphorylation occupancies of the highest hyperphosphorylation rates (Thr181, Ser202, Thr217, and Thr231) were 28, 51, 31, and 82%, respectively (Horie et al., 2020). In our analysis, phosphorylation is progressing at these sites, and the frequencies of the phosphorylated peptides were 66% at Thr181, 37% at Ser202, 74% at Thr217, and 93% at Thr231, and the results were almost the same high value. This tendency is also seen in other tauopathy and is not considered to be a characteristic of AD alone.

Methylation and Acetylation at Lys Residues

Lysine methylation is present at multiple sites in soluble tau isolated from cognitively normal elderly cases at locations that only partially overlapped with the distributions reported for cognitively normal middle-aged and AD cohorts, suggesting that lysine methylation may be a physiological PTM of tau protein that changes qualitatively with aging and disease (Huseby et al., 2019). Lys methylations were detected at a very small number of Lys residues in contrast to previous findings. In comparison, acetylation at Lys residues was detected in the area forming the tau fibril core (Table 2 and Supplementary Table 3). In the cases of PiD, 257Lys, 259Lys, 311Lys, and 353Lys residues were characteristically acetylated. In diseases other than

PSP and PiD, the ubiquitination sites also overlap in the area forming the tau fibril core (Table 2 and Supplementary Table 3). Although ubiquitination is inhibited when acetylation occurs at Lys residue, it is unclear whether there is a regulatory relationship between the two.

Newly Identified PTMs in Tau

In this analysis, we found some new PTMs on tau in various tauopathies. Oxidation at 299His and 362His was detected in all the diseases examined. Oxidation at 329His and 330His was detected in FTDP-17T, CBD, and PiD, while oxidation at 407His was detected in AD and CBD. Furthermore, phosphorylation at 407His was detected in all the tauopathies. MS/MS spectra of the identified His phosphorylation peptide was shown as Supplementary Figure 2. It has been reported that phosphorylation of histidine residue is rare in signal transduction systems (Fuhs and Hunter, 2017). In this case, it is located in a region where many Ser/Thr sites are heavily phosphorylated, so it is possible that the 407His is simply phosphorylated concomitantly with Ser/Thr residues, and may not have a physiological role.

Relationship Between PTMs and Tau Filament Structures

Post-translational modifications in tau fibrils may be involved in the stability of the fibrils. PSP tau fibrils are more susceptible to enzymatic digestion than other tau fibrils in other tauopathies (Taniguchi-Watanabe et al., 2016). This is because tau fibrils of PSP have fewer PTMs than other tauopathies (Table 2 and Supplementary Table 3), which may allow digestive enzymes can to directly access the fibril core.

The use of high-performance mass spectrometers is likely to enable the detection of more minor PTMs, but it is questionable whether they are all pathophysiologically important. It may be more useful to identify PTMs common to all diseases, or disease-specific PTMs. As described above, such PTMs are likely to be closely related to the characteristic tau fibril structure in each disease. It is also likely that PTMs such as ubiquitination of tau protofilaments affect the assembly of these protofilaments themselves. Nevertheless, it is reasonable to consider that most of the PTMs occur after assembly or protofilament formation of tau, because it is unlikely that specific lysine residues on unfolded tau would be ubiquitinated by different ligases in the different diseases. It remains unclear whether PTMs affect the filament formation and contribute to form the unique structures, or whether the PTMs occur after the unique structures have been formed. Further analyses are needed to clarify resolve this question. In either case, it can be considered that the differences in PTMs reflects the differences in filament core structures.

DATA AVAILABILITY STATEMENT

The datasets presented in this study can be found in online repositories. The names of the repository/repositories and accession number(s) can be found in the article/Supplementary Material.

ETHICS STATEMENT

The studies involving human participants were reviewed and approved by the research ethics committee of Tokyo Metropolitan Institute of Medical Science. The patients/participants provided their written informed consent to participate in this study.

AUTHOR CONTRIBUTIONS

MY, TM, SM, YS, IK, MO, HT, AK, AR, DM, and HM identified patients and performed the neuropathology. FK and MH carried out the biochemical analysis and the mass spectrometry analysis. All authors contributed to writing the manuscript.

FUNDING

This research was (partially) supported by the Strategic Research Program for Brain Sciences (JP18ek0109391 and JP18dm020719,

to MH) and the Japan Brain Bank Network (SM, MY, and YS) funded by the Strategic Research Program for Brain Science, from Japan Agency for Medical Research and Development (AMED). The work of Manchester Brain Bank is supported by Alzheimer's Research UK and Alzheimer's Society through the Brains for Dementia Research (BDR) program.

ACKNOWLEDGMENTS

We thank Y. Iwasaki, H. Miyahara, A. Akagi, Y. Riku, and T. Ando (Institute for Medical Science of Aging, Aichi Medical University) for various assistants.

SUPPLEMENTARY MATERIAL

The Supplementary Material for this article can be found online at: <https://www.frontiersin.org/articles/10.3389/fnins.2020.581936/full#supplementary-material>

REFERENCES

- Arai, T., Ikeda, K., Akiyama, H., Nonaka, T., Hasegawa, M., Ishiguro, K., et al. (2004). Identification of amino-terminally cleaved tau fragments that distinguish progressive supranuclear palsy from corticobasal degeneration. *Ann. Neurol.* 55, 72–79. doi: 10.1002/ana.10793
- Arakhamia, T., Lee, C. E., Carlomagno, Y., Duong, D. M., Kundinger, S. R., Wang, K., et al. (2020). Posttranslational modifications mediate the structural diversity of Tauopathy strains. *Cell* 180, 633–644e612.
- Barthelemy, N. R., Horie, K., Sato, C., and Bateman, R. J. (2020). Blood plasma phosphorylated-tau isoforms track CNS change in Alzheimer's disease. *J. Exp. Med.* 217:e20200861.
- Buee, L., Bussiere, T., Buee-Scherrer, V., Delacourte, A., and Hof, P. R. (2000). Tau protein isoforms, phosphorylation and role in neurodegenerative disorders. *Brain Res. Brain Res. Rev.* 33, 95–130. doi: 10.1016/S0165-0173(00)00019-9
- Buee, L., and Delacourte, A. (1999). Comparative biochemistry of tau in progressive supranuclear palsy, corticobasal degeneration, FTDP-17 and Pick's disease. *Brain Pathol.* 9, 681–693. doi: 10.1111/j.1750-3639.1999.tb00550.x
- Bugiani, O., Murrell, J. R., Giaccone, G., Hasegawa, M., Ghigo, G., Tabaton, M., et al. (1999). Frontotemporal dementia and corticobasal degeneration in a family with a P301S mutation in tau. *J. Neuropathol. Exp. Neurol.* 58, 667–677. doi: 10.1097/00005072-199906000-00011
- Crowther, R. A., and Wischik, C. M. (1985). Image reconstruction of the Alzheimer paired helical filament. *EMBO J.* 4, 3661–3665. doi: 10.1002/j.1460-2075.1985.tb04132.x
- Crowther, T., Goedert, M., and Wischik, C. M. (1989). The repeat region of microtubule-associated protein tau forms part of the core of the paired helical filament of Alzheimer's disease. *Ann. Med.* 21, 127–132. doi: 10.3109/07853898909149199
- Dan, A., Takahashi, M., Masuda-Suzukake, M., Kametani, F., Nonaka, T., Kondo, H., et al. (2013). Extensive deamidation at asparagine residue 279 accounts for weak immunoreactivity of tau with RD4 antibody in Alzheimer's disease brain. *Acta Neuropathol. Commun.* 1:54. doi: 10.1186/2051-5960-1-54
- Dujardin, S., Commins, C., Lathuiliere, A., Beerepoot, P., Fernandes, A. R., Kamath, T. V., et al. (2020). Tau molecular diversity contributes to clinical heterogeneity in Alzheimer's disease. *Nat. Med.* 26, 1256–1263.
- Erro, M. E., Zelaya, M. V., Mendioroz, M., Larumbe, R., Ortega-Cubero, S., Lanciego, J. L., et al. (2019). Globular glial tauopathy caused by MAPT P301T mutation: clinical and neuropathological findings. *J. Neurol.* 266, 2396–2405. doi: 10.1007/s00415-019-09414-w
- Falcon, B., Zhang, W., Murzin, A. G., Murshudov, G., Garringer, H. J., Vidal, R., et al. (2018). Structures of filaments from Pick's disease reveal a novel tau protein fold. *Nature* 561, 137–140. doi: 10.1038/s41586-018-0454-y
- Fitzpatrick, A. W., and Saibil, H. R. (2019). Cryo-EM of amyloid fibrils and cellular aggregates. *Curr. Opin. Struct. Biol.* 58, 34–42. doi: 10.1016/j.sbi.2019.05.003
- Fitzpatrick, A. W. P., Falcon, B., He, S., Murzin, A. G., Murshudov, G., Garringer, H. J., et al. (2017). Cryo-EM structures of tau filaments from Alzheimer's disease. *Nature* 547, 185–190.
- Fuhs, S. R., and Hunter, T. (2017). pHisphorylation: the emergence of histidine phosphorylation as a reversible regulatory modification. *Curr. Opin. Cell Biol.* 45, 8–16. doi: 10.1016/j.jceb.2016.12.010
- Goedert, M. (1993). Tau protein and the neurofibrillary pathology of Alzheimer's disease. *Trends Neurosci.* 16, 460–465. doi: 10.1016/0166-2236(93)90078-z
- Goedert, M., Falcon, B., Zhang, W., Ghetti, B., and Scheres, S. H. W. (2018). Distinct conformers of assembled tau in Alzheimer's and Pick's diseases. *Cold Spring Harb. Symp. Quant. Biol.* 83, 163–171. doi: 10.1101/sqb.2018.83.037580
- Goedert, M., and Hasegawa, M. (1999). The tauopathies: toward an experimental animal model. *Am. J. Pathol.* 154, 1–6.
- Goedert, M., Spillantini, M. G., Cairns, N. J., and Crowther, R. A. (1992). Tau proteins of Alzheimer paired helical filaments: abnormal phosphorylation of all six brain isoforms. *Neuron* 8, 159–168. doi: 10.1016/0896-6273(92)90117-v
- Goedert, M., Spillantini, M. G., Hasegawa, M., Jakes, R., Crowther, R. A., and Klug, A. (1996). Molecular dissection of the neurofibrillary lesions of Alzheimer's disease. *Cold Spring Harb. Symp. Quant. Biol.* 61, 565–573.
- Goedert, M., Spillantini, M. G., Jakes, R., Rutherford, D., and Crowther, R. A. (1989). Multiple isoforms of human microtubule-associated protein tau: sequences and localization in neurofibrillary tangles of Alzheimer's disease. *Neuron* 3, 519–526. doi: 10.1016/0896-6273(89)90210-9
- Greenberg, S. G., and Davies, P. (1990). A preparation of Alzheimer paired helical filaments that displays distinct tau proteins by polyacrylamide gel electrophoresis. *Proc. Natl. Acad. Sci. U.S.A.* 87, 5827–5831. doi: 10.1073/pnas.87.15.5827
- Hasegawa, M. (2016). Molecular mechanisms in the pathogenesis of Alzheimer's disease and tauopathies-prion-like seeded aggregation and phosphorylation. *Biomolecules* 6:24. doi: 10.3390/biom6020024
- Hasegawa, M. (2019). Structure of NFT: biochemical approach. *Adv. Exp. Med. Biol.* 1184, 23–34. doi: 10.1007/978-981-32-9358-8_2
- Horie, K., Barthelemy, N. R., Mallipeddi, N., Li, Y., Franklin, E. E., Perrin, R. J., et al. (2020). Regional correlation of biochemical measures of amyloid and tau phosphorylation in the brain. *Acta Neuropathol. Commun.* 8:149.

- Huseby, C. J., Hoffman, C. N., Cooper, G. L., Cocuron, J. C., Alonso, A. P., Thomas, S. N., et al. (2019). Quantification of Tau protein lysine methylation in aging and Alzheimer's disease. *J. Alzheimers Dis.* 71, 979–991. doi: 10.3233/jad-190604
- Hutton, M., Lendon, C. L., Rizzu, P., Baker, M., Froelich, S., Houlden, H., et al. (1998). Association of missense and 5'-splice-site mutations in tau with the inherited dementia FTDP-17. *Nature* 393, 702–705.
- Iqbal, K., Liu, F., and Gong, C. X. (2016). Tau and neurodegenerative disease: the story so far. *Nat. Rev. Neurol.* 12, 15–27. doi: 10.1038/nrneurol.2015.225
- Iwatsubo, T., Hasegawa, M., and Ihara, Y. (1994). Neuronal and glial tau-positive inclusions in diverse neurologic diseases share common phosphorylation characteristics. *Acta Neuropathol.* 88, 129–136. doi: 10.1007/s004010050140
- Janelidze, S., Stomrud, E., Smith, R., Palmqvist, S., Mattsson, N., Airey, D. C., et al. (2020). Cerebrospinal fluid p-tau217 performs better than p-tau181 as a biomarker of Alzheimer's disease. *Nat. Commun.* 11:1683.
- Kovacs, G. G. (2015). Invited review: neuropathology of tauopathies: principles and practice. *Neuropathol. Appl. Neurobiol.* 41, 3–23. doi: 10.1111/nan.12208
- Lee, V. M., Balin, B. J., Otvos, L. Jr., and Trojanowski, J. Q. (1991). A68: a major subunit of paired helical filaments and derivatized forms of normal Tau. *Science* 251, 675–678. doi: 10.1126/science.1899488
- Lee, V. M., Goedert, M., and Trojanowski, J. Q. (2001). Neurodegenerative tauopathies. *Annu. Rev. Neurosci.* 24, 1121–1159. doi: 10.1146/annurev.neuro.24.1.1121
- Palmqvist, S., Janelidze, S., Quiroz, Y. T., Zetterberg, H., Lopera, F., Stomrud, E., et al. (2020). Discriminative accuracy of plasma phospho-tau217 for Alzheimer disease vs other neurodegenerative disorders. *JAMA* 324, 772–781. doi: 10.1001/jama.2020.12134
- Poorkaj, P., Bird, T. D., Wijsman, E., Nemens, E., Garruto, R. M., Anderson, L., et al. (1998). Tau is a candidate gene for chromosome 17 frontotemporal dementia. *Ann. Neurol.* 43, 815–825. doi: 10.1002/ana.410430617
- Reed, L. A., Grabowski, T. J., Schmidt, M. L., Morris, J. C., Goate, A., Solodkin, A., et al. (1997). Autosomal dominant dementia with widespread neurofibrillary tangles. *Ann. Neurol.* 42, 564–572. doi: 10.1002/ana.410420406
- Serrano-Pozo, A., Frosch, M. P., Masliah, E., and Hyman, B. T. (2011). Neuropathological alterations in Alzheimer disease. *Cold Spring Harb. Perspect. Med.* 1:a006189. doi: 10.1101/cshperspect.a006189
- Spillantini, M. G., Crowther, R. A., and Goedert, M. (1996). Comparison of the neurofibrillary pathology in Alzheimer's disease and familial presenile dementia with tangles. *Acta Neuropathol.* 92, 42–48. doi: 10.1007/s004010050487
- Spillantini, M. G., Goedert, M., Crowther, R. A., Murrell, J. R., Farlow, M. R., and Ghetti, B. (1997). Familial multiple system tauopathy with presenile dementia: a disease with abundant neuronal and glial tau filaments. *Proc. Natl. Acad. Sci. U.S.A.* 94, 4113–4118. doi: 10.1073/pnas.94.8.4113
- Spillantini, M. G., Murrell, J. R., Goedert, M., Farlow, M. R., Klug, A., and Ghetti, B. (1998). Mutation in the tau gene in familial multiple system tauopathy with presenile dementia. *Proc. Natl. Acad. Sci. U.S.A.* 95, 7737–7741. doi: 10.1073/pnas.95.13.7737
- Spina, S., Farlow, M. R., Unverzagt, F. W., Kareken, D. A., Murrell, J. R., Fraser, G., et al. (2008). The tauopathy associated with mutation +3 in intron 10 of Tau: characterization of the MSTD family. *Brain* 131, 72–89. doi: 10.1093/brain/awm280
- Tacik, P., Sanchez-Contreras, M., Deture, M., Murray, M. E., Rademakers, R., Ross, O. A., et al. (2017). Clinicopathologic heterogeneity in frontotemporal dementia and parkinsonism linked to chromosome 17 (FTDP-17) due to microtubule-associated protein tau (MAPT) p.P301L mutation, including a patient with globular glial tauopathy. *Neuropathol. Appl. Neurobiol.* 43, 200–214. doi: 10.1111/nan.12367
- Taniguchi-Watanabe, S., Arai, T., Kametani, F., Nonaka, T., Masuda-Suzukake, M., Tarutani, A., et al. (2016). Biochemical classification of tauopathies by immunoblot, protein sequence and mass spectrometric analyses of sarkosyl-insoluble and trypsin-resistant tau. *Acta Neuropathol.* 131, 267–280. doi: 10.1007/s00401-015-1503-3
- Wischnik, C. M., Novak, M., Edwards, P. C., Klug, A., Tichelaar, W., and Crowther, R. A. (1988a). Structural characterization of the core of the paired helical filament of Alzheimer disease. *Proc. Natl. Acad. Sci. U.S.A.* 85, 4884–4888. doi: 10.1073/pnas.85.13.4884
- Wischnik, C. M., Novak, M., Thogersen, H. C., Edwards, P. C., Runswick, M. J., Jakes, R., et al. (1988b). Isolation of a fragment of tau derived from the core of the paired helical filament of Alzheimer disease. *Proc. Natl. Acad. Sci. U.S.A.* 85, 4506–4510. doi: 10.1073/pnas.85.12.4506
- Zhang, W., Tarutani, A., Newell, K. L., Murzin, A. G., Matsubara, T., Falcon, B., et al. (2020). Novel tau filament fold in corticobasal degeneration. *Nature* 580, 283–287. doi: 10.1038/s41586-020-2043-0

Conflict of Interest: The authors declare that the research was conducted in the absence of any commercial or financial relationships that could be construed as a potential conflict of interest.

Copyright © 2020 Kametani, Yoshida, Matsubara, Murayama, Saito, Kawakami, Onaya, Tanaka, Kakita, Robinson, Mann and Hasegawa. This is an open-access article distributed under the terms of the Creative Commons Attribution License (CC BY). The use, distribution or reproduction in other forums is permitted, provided the original author(s) and the copyright owner(s) are credited and that the original publication in this journal is cited, in accordance with accepted academic practice. No use, distribution or reproduction is permitted which does not comply with these terms.



Looking Beyond the Core: The Role of Flanking Regions in the Aggregation of Amyloidogenic Peptides and Proteins

Sabine M. Ulamec, David J. Brockwell and Sheena E. Radford*

Astbury Centre for Structural Molecular Biology, School of Molecular and Cellular Biology, Faculty of Biological Sciences, University of Leeds, Leeds, United Kingdom

OPEN ACCESS

Edited by:

Wolfgang Hoyer,
Heinrich Heine University Düsseldorf,
Germany

Reviewed by:

Anita L. Manogaran,
Marquette University, United States
Fuyuki Kametani,
Tokyo Metropolitan Institute
of Medical Science, Japan

*Correspondence:

Sheena E. Radford
S.E.Radford@leeds.ac.uk

Specialty section:

This article was submitted to
Neurodegeneration,
a section of the journal
Frontiers in Neuroscience

Received: 28 September 2020

Accepted: 02 November 2020

Published: 01 December 2020

Citation:

Ulamec SM, Brockwell DJ and
Radford SE (2020) Looking Beyond
the Core: The Role of Flanking
Regions in the Aggregation
of Amyloidogenic Peptides
and Proteins.
Front. Neurosci. 14:611285.
doi: 10.3389/fnins.2020.611285

Amyloid proteins are involved in many neurodegenerative disorders such as Alzheimer's disease [Tau, Amyloid β (A β)], Parkinson's disease [alpha-synuclein (α Syn)], and amyotrophic lateral sclerosis (TDP-43). Driven by the early observation of the presence of ordered structure within amyloid fibrils and the potential to develop inhibitors of their formation, a major goal of the amyloid field has been to elucidate the structure of the amyloid fold at atomic resolution. This has now been achieved for a wide variety of sequences using solid-state NMR, microcrystallography, X-ray fiber diffraction and cryo-electron microscopy. These studies, together with *in silico* methods able to predict aggregation-prone regions (APRs) in protein sequences, have provided a wealth of information about the ordered fibril cores that comprise the amyloid fold. Structural and kinetic analyses have also shown that amyloidogenic proteins often contain less well-ordered sequences outside of the amyloid core (termed here as flanking regions) that modulate function, toxicity and/or aggregation rates. These flanking regions, which often form a dynamically disordered "fuzzy coat" around the fibril core, have been shown to play key parts in the physiological roles of functional amyloids, including the binding of RNA and in phase separation. They are also the mediators of chaperone binding and membrane binding/disruption in toxic amyloid assemblies. Here, we review the role of flanking regions in different proteins spanning both functional amyloid and amyloid in disease, in the context of their role in aggregation, toxicity and cellular (dys)function. Understanding the properties of these regions could provide new opportunities to target disease-related aggregation without disturbing critical biological functions.

Keywords: flanking region, amyloid, synuclein, fuzzy coat, aggregation, Tau, TDP-43, Orb2

INTRODUCTION

In the 60 years since the first atomic structure of the protein myoglobin was solved using X-ray diffraction of protein crystals (Kendrew et al., 1960), the field of structural biology has been dominated by the study of globular proteins with a well-defined tertiary structure, with more than 160,000 unique structures solved to date using crystallography, NMR or cryoEM (Geraets et al., 2020). Despite this feat, more than 50% of the proteins in eukaryotes are now known to have at least one long (>30 residues) sequence that is intrinsically disordered [intrinsically disordered regions

(IDRs)] and also 12% of eukaryotic proteins are completely intrinsically disordered [intrinsically disordered proteins (IDPs)] (Dunker et al., 2000; Ward et al., 2004; Tompa, 2009). IDRs and IDPs are enriched in/for proteins with important regulatory or signaling functions (Ward et al., 2004; Tompa et al., 2006; Coletta et al., 2010) demonstrating the crucial role of non-globular protein structures for biological processes.

Amyloid proteins, some of which are involved in neurodegenerative disorders such as Alzheimer's disease, Parkinson's disease, amyotrophic lateral sclerosis, and Huntington disease (Iadanza et al., 2018a; Benson et al., in press) are commonly IDPs or are proteins that contain IDRs. These diseases share a common fundamental etiology: aberrant self-assembly of their amyloid precursor proteins to form toxic oligomers and highly ordered fibrils with a cross β -sheet structure (Gallardo et al., 2020b; Ullamec and Radford, 2020). A combination of biochemical and biophysical approaches, including limited proteolysis, hydrogen exchange (HX), solution NMR, solid state NMR (ssNMR), cryoEM and EPR have shown that the structured cross- β amyloid core commonly involves only a portion of the amyloid precursor sequence, whilst regions flanking the fibril core (commonly the N- and/or C-terminal regions of the sequence), are flexible and thus are either "invisible" in the structures determined or give rise to only low resolution density in EM images (Gallardo et al., 2020b). Consequently, the high resolution cryoEM and ssNMR structures of fibril architectures determined over the last ~ 5 years, have necessarily focused on the conformations and interactions within fibril cores (Gallardo et al., 2020b), whilst the more dynamic flanking regions remain elusive. The structured cores of amyloid fibrils usually contain short peptide sequences, some with high aggregation propensity, shown to be necessary and sufficient for fibril formation (Giasson et al., 2001; Thompson et al., 2006) and reviewed in Eisenberg and Sawaya (2017). Despite the importance of these sequences for the formation and stability of the amyloid fold, several studies have shown that modifying or changing (e.g., by deletion, mutation, or post-translational modification) the regions that flank the amyloid core can affect the fibril growth kinetics (Johnson et al., 2009; Benilova et al., 2014; Doherty et al., 2020), fibril morphology (Guerrero-Ferreira et al., 2020; Scheres et al., 2020) and the formation of crucial contacts with interaction partners (Gao et al., 2015; Burmann et al., 2020; **Figure 1**). Additionally, the presence of so called "gatekeeper" residues, which surround aggregation-prone regions (APRs) to mitigate their aggregation propensity (Reumers et al., 2009) further underlines the important role of residues not directly involved in forming the amyloid core in the process of aggregation and in the functional consequences of the fibril structure formed. The aim of this review is to highlight the importance of the dynamically disordered flanking regions in amyloid sequences, focusing on their roles in fibril formation, cytotoxicity, and other physiological functions. While more than 50 proteins are known to form amyloid associated with disease (Iadanza et al., 2018a; Benson et al., in press), here we focus on α Syn, TDP-43, A β , Tau, β 2m, Orb2, and PrP as exemplars of IDPs, natively folded proteins, prions, and functional and disease related proteins.

FLANKING REGIONS – WHAT ARE THEY AND WHY ARE THEY IMPORTANT?

Decades of studies of protein folding have led to insights into the roles of individual amino acids in a protein sequence in the search for the native fold (they are kinetically important) and in stabilizing the final folded state (they are thermodynamically important) (Rumbley et al., 2001; Baldwin et al., 2011). In addition, some residues may be conserved because they are important in chaperone binding or in the destabilization of incorrect folds (so-called negative design) (Richardson and Richardson, 2002; Berezovsky et al., 2007). By contrast with our the wealth of knowledge about protein folding, predicting which residues in an amyloid precursor sequence could be kinetically important in driving or controlling the rate or mechanism of amyloid fibril formation; which form the stable fibril core; and which may be innocuous passengers during self-assembly, but may play a role in the fibrillar state, is immensely complex. This is a fundamentally important question, since it is now widely appreciated that, by contrast with protein folding wherein the same globular structure is (usually) adopted by a protein sequence independent of mutation or changes in the solution conditions, amyloid fibril formation is under kinetic control, with the structure of the fibril product being determined by the assembly pathway taken (**Figure 1**). The result is a rugged energy landscape, which can result in potentially many different fibril structures for the same (or very similar) protein sequences (known as fibril polymorphism) (Fitzpatrick et al., 2017; Close et al., 2018; Kollmer et al., 2019; Guerrero-Ferreira et al., 2020). Recent advances in computational methods have provided a suite of algorithms able to define the most aggregation prone region of a protein sequence (Fernandez-Escamilla et al., 2004; Sormanni et al., 2015; Ebo et al., 2020; **Figure 2A**). These regions are commonly found in the amyloid fibril core, stabilizing the final fibril structure, without necessarily playing a role in the kinetics of amyloid formation. Other residues in amyloidogenic peptides and proteins which flank the APRs, can play kinetic and/or thermodynamic roles in amyloid assembly. Changes in these sequences (mutation or post-translational modification) can dramatically alter the rates of fibril formation and the structures of the fibrils formed, without the sequence necessarily forming part of the stable fibril core. As more fibril structures are solved of full-length protein sequences (rather than short peptide fragments), it is becoming clear that the amyloid core can involve only a minor part of the protein sequence, with substantial regions of the polypeptide chain remaining dynamically disordered in the fibril structure (**Figure 2A**). Such regions which flank the amyloid core can play functional roles (binding ligands and receptors for functional amyloid), or perturbing proteostasis (for amyloid fibrils associated with disease) (**Figures 2B–D**).

In this review we focus on the roles of regions that flank the APRs and/or fibril cores in amyloid formation. We differentiate between (i) sequences that flank the APRs determined by *in silico* techniques, (ii) sequences that flank the structured cross- β fibril core based on recent cryoEM and NMR structures of fibrils,

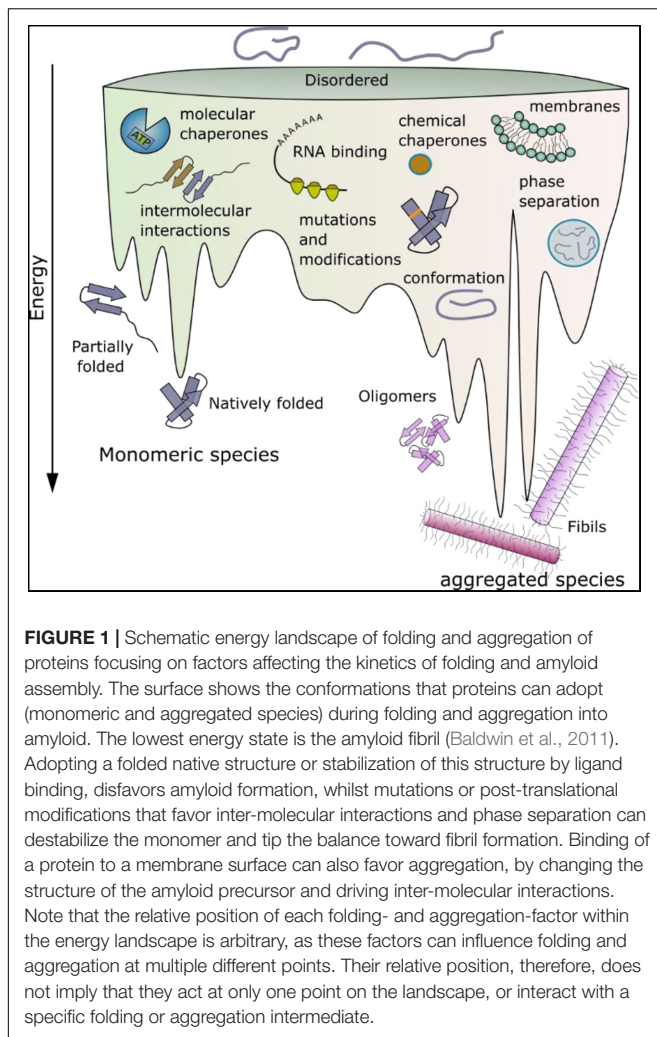


FIGURE 1 | Schematic energy landscape of folding and aggregation of proteins focusing on factors affecting the kinetics of folding and amyloid assembly. The surface shows the conformations that proteins can adopt (monomeric and aggregated species) during folding and aggregation into amyloid. The lowest energy state is the amyloid fibril (Baldwin et al., 2011). Adopting a folded native structure or stabilization of this structure by ligand binding, disfavors amyloid formation, whilst mutations or post-translational modifications that favor inter-molecular interactions and phase separation can destabilize the monomer and tip the balance toward fibril formation. Binding of a protein to a membrane surface can also favor aggregation, by changing the structure of the amyloid precursor and driving inter-molecular interactions. Note that the relative position of each folding- and aggregation-factor within the energy landscape is arbitrary, as these factors can influence folding and aggregation at multiple different points. Their relative position, therefore, does not imply that they act at only one point on the landscape, or interact with a specific folding or aggregation intermediate.

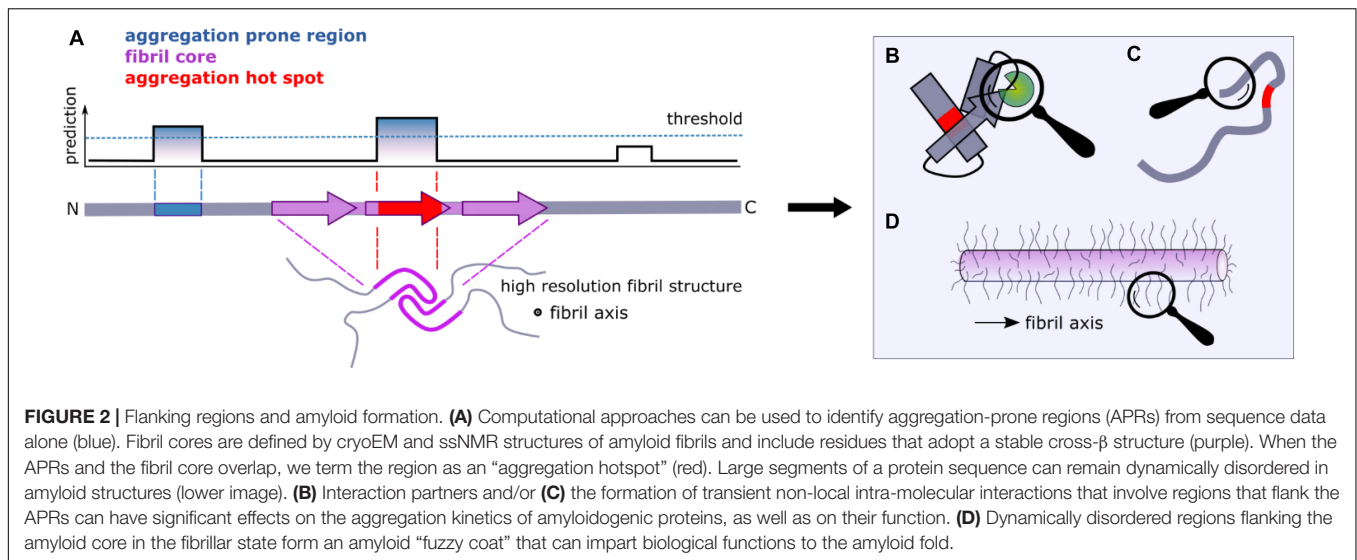
and (iii) sequences that flank coincident APRs and fibril cores (producing an “aggregation hotspot”) (Figure 2). In 2005 used a similar approach where they differentiated between regions that are predicted to be most important for promoting amyloid growth and experimentally determined sensitive regions Dobson and coworkers (Pawar et al., 2005). It is important to note that different flanking regions can be identified in the same protein using these definitions. For example, the use of different algorithms [e.g., CamSol or TANGO (Figure 3)] as well as posttranslational modifications, might result in different flanking regions for the same protein primary sequence. Similarly, on a structural level, as polymorphs for the same protein have different residues involved in their cores, each will have a different flanking region (Figure 3).

IDENTIFICATION OF SEQUENCES INVOLVED IN FORMING AMYLOID

Prior to the development of high-resolution structural methods capable of solving amyloid structures in atomic detail, lower

resolution techniques were employed to provide information about the sequences that drive aggregation. These include analysis of the ability of arrays of peptide fragments from different amyloid precursor sequences to form cross- β amyloid-like structures in isolation (Tenidis et al., 2000; von Bergen et al., 2000; Jones et al., 2003a; Ivanova et al., 2004; Nelson et al., 2005), scanning mutagenesis of a sequence followed by analysis of fibril formation using aggregation assays (e.g., Thioflavin T fluorescence) (Williams et al., 2006; Platt et al., 2008), and determination of the sequences that form the stable amyloid core, e.g., using protease digestion followed by mass spectrometry (Miake et al., 2002; Myers et al., 2006; Kushnir et al., 2020) or HX monitored by $^1\text{H-NMR}$ (Hoshino et al., 2002; Cho et al., 2011; Strohäker et al., 2019). These experimental approaches have been complemented by the development of *in silico* tools (Ebo et al., 2020; Santos et al., 2020), able to identify APRs by calculation of β -sheet propensity (using TANGO) (Fernandez-Escamilla et al., 2004) or solubility (CamSol) (Sormanni et al., 2015) (see Santos et al., 2020 for a recent review of these and other approaches). Most, but not all APRs are found in the fibril core. Residues that are found in fibril cores determined by cryoEM or ssNMR and in the APRs identified using computational methods described above are here defined as “aggregation hotspots” (Figure 3). They often contain motifs crucial for fibril formation [e.g., the Non-Amyloid β -Component (NAC) region of αSyn , the $^{22}\text{NFGAIL}^{27}$ sequence from human islet amyloid polypeptide (IAPP), $^{15}\text{KLVFF}^{20}$ for A β and $^{306}\text{VQIVYK}^{311}$ from Tau].

Huge strides have been made in amyloid fibril structure elucidation in the last decade using X-ray diffraction of microcrystals (usually of short, 6–15 residue peptides) (Rodriguez et al., 2015; Guenther et al., 2018), and, more recently, using ssNMR and cryoEM of amyloid fibrils formed *in vitro* and *ex vivo* from full-length proteins. These studies have shown that the same sequence can produce fibrils with remarkably different quaternary, tertiary and even secondary structural elements (Gallardo et al., 2020b). For example, more than six different amyloid fibril structures of the 140 residue protein, α -synuclein (αSyn) have been solved to date using cryoEM or ssNMR (Table 1; Guerrero-Ferreira et al., 2020; Schweighauser et al., 2020). Notably, while the fibril cores in all of these structures contain the NAC region known to be necessary and sufficient for amyloid formation (Giasson et al., 2001), the length and location of the sequence involved in the remaining portions of structured amyloid core (or conversely the residues involved in unresolved, dynamically disordered regions) varies depending on the morphology of the amyloid fibril formed (Figure 3; Guerrero-Ferreira et al., 2019, 2020; Schweighauser et al., 2020). Thus, between 50% and 70% of the 140 residues of this protein are *not* involved in the cross- β amyloid core. A second striking example is the two fibril structures formed from antibody light chains (LCs) that were extracted from two patients with systemic LC amyloidosis (involving different LC sequences). These studies revealed that these proteins with the same initial immunoglobulin (Ig)-containing native structure (Huang et al., 1996; Swuec et al., 2019), form completely different amyloid fibril architectures, with residues 16–23 and 86–93



(Radamaker et al., 2019), or residues 1–37 and 66–105 forming the core (Swuec et al., 2019).

In general, *in silico*-identified APRs (which may differ slightly when using different algorithms) are shorter in length compared with the experimentally determined fibril core using cryoEM or ssNMR (Figure 3). It should be noted that *in silico* methods also identify APRs that can reside outside the structured amyloid core, and so form the flanking region of aggregation hotspots (Figure 2A). A particularly striking example of this is seen in the functional amyloid Orb2, associated with long term memory formation and storage (Keleman et al., 2007; Majumdar et al., 2012; Khan et al., 2015; Hervas et al., 2020), where there is no overlap of sequence between residues in the experimentally derived fibril core and those in APRs identified using *in silico* methods (Figure 3F). This clearly demonstrates the division of sequence motifs into those which may be kinetically important, those which are thermodynamically important, and some which play neither or both roles.

Similar to the diversity of amyloid flanking regions, it can also be difficult to parse structured and unstructured regions. For the functional amyloid protein Sup35, for example, which is involved in controlling translation in yeast (Lyke et al., 2019), site-directed mutagenesis and fluorescence labeling suggested that the amyloid core comprises amino acids 21–121, flanked by a structurally heterogeneous “transition zone” (residues 1–20 and 122–158), and a very flexible C-terminal region formed by residues 159–250 (Krishnan and Lindquist, 2005). Another example of different residual mobility of flanking regions was seen by performing immunogold labeling and transmission EM, force-volume measurements using atomic force microscopy (AFM) and solution NMR experiments on Tau filaments (Sillen et al., 2005; Wegmann et al., 2013). These experiments suggested that the flanking regions of Tau form a “two layered polyelectrolyte brush” surrounding the fibril core: a dense and mechanically more rigid layer (residues ~173–243) and an N-terminal, less dense and more dynamic layer (residues ~1–172). The increased exposure to solvent renders longer unstructured regions, such

as those in Tau and α Syn sensitive to environmental conditions: Tau amyloid fibrils exhibit a 50% reduction in the rigidity of flanking regions upon increasing KCl concentration from 50 mM to 200 mM and show increased affinity (70% higher adhesion) to negatively charged membranes when lowering the pH from 7.4 to 4.5 (Wegmann et al., 2013). These changes may be relevant during lysosomal degradation (Wang et al., 2009). Finally, while not part of the structured β -sheet rich fibril core, some sequences in the flanking regions can nonetheless form secondary structure as shown using ssNMR for the 17 amino acid long N-terminal region (residues 4–11) of exon 1 of huntingtin. In this case, the region flanking the aggregation-prone expanded polyQ region adopts a solvent exposed and dynamic α -helical structure (Sivanandam et al., 2011).

ROLE OF FLANKING REGIONS AND AGGREGATION HOTSPOTS IN FIBRIL FORMATION

Flanking regions have been shown to play roles in modulating the rates and mechanisms of aggregation (Benilova et al., 2014; Doherty et al., 2020). For example, point mutations linked with early onset familial Parkinson’s disease (Mehra et al., 2019) and ALS (Prasad et al., 2019) or post-translational modifications (including phosphorylation, acetylation, sumoylation, methylation, ubiquitination, glycosylation, and truncations that alter aggregation kinetics) are often remote from the APRs within these protein sequences (Figures 3A,B). These regions also bind to other molecules such as chaperones, nucleic acids, and membranes, and hence, can play functionally important roles (Table 1). Consequently, these regions re-sculpt the aggregation energy landscape (Figure 1) enhancing [or in some cases suppressing (Jonsson et al., 2012)] aggregation and its associated cytotoxicity, and can alter the function of the native amyloid precursor. It is thus crucial to analyze these regions when assessing amyloid formation mechanisms, rather than

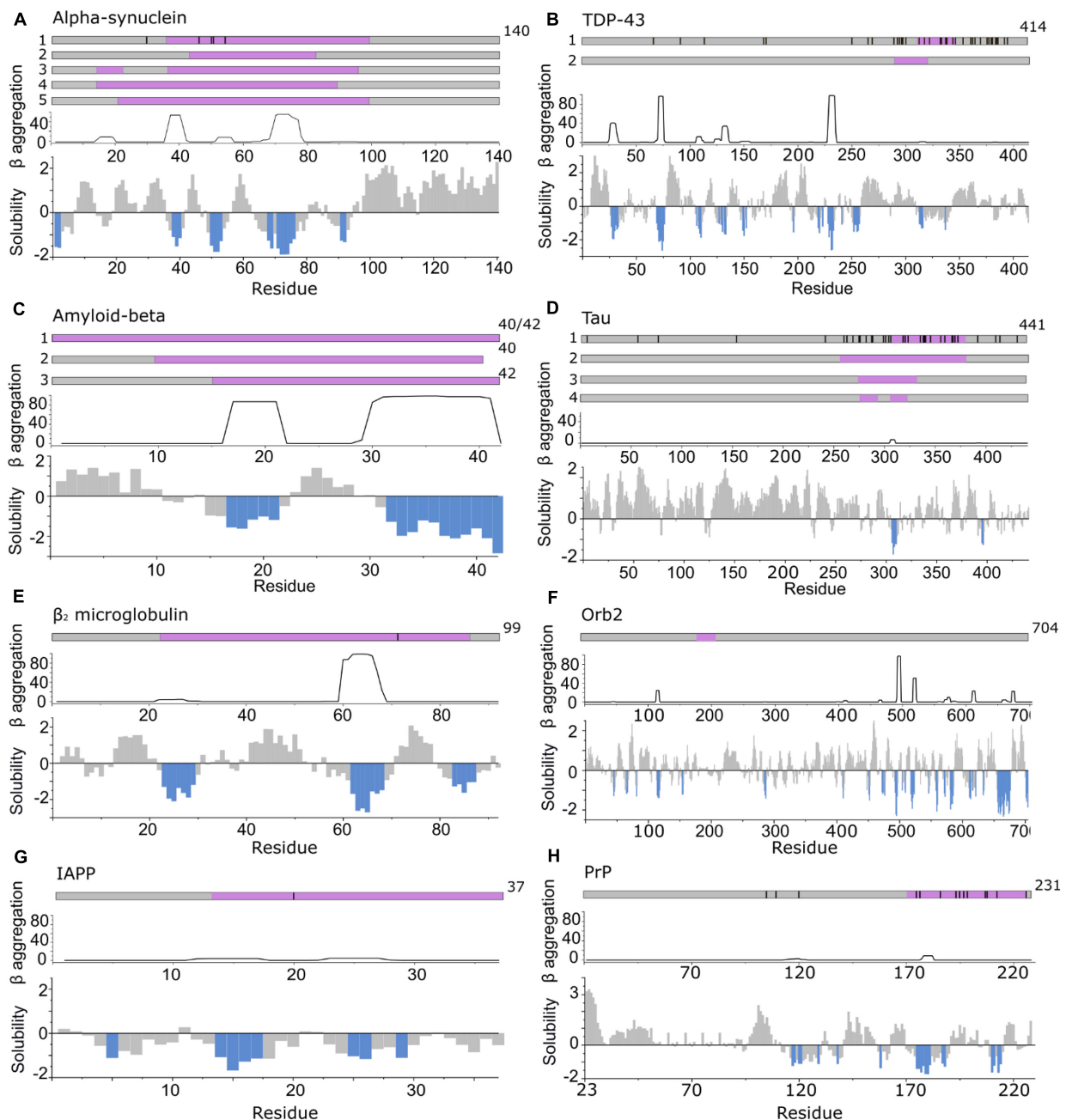



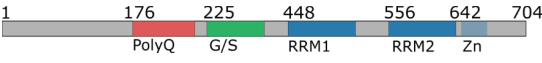

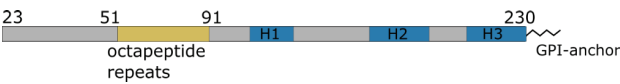
FIGURE 3 | APRs comprise only a small part of the amyloid core. **Top in A–H:** location of fibril cores of α Syn, TDP-43, A β , Tau, β_2 m, Orb2B, IAPP, and PrP defined by recent cryoEM or ssNMR fibril structures (purple). The positions of familial disease mutations are highlighted where appropriate as black lines. **Bottom in A–H:** regions with low solubility predicted by CamSol (below -1 is aggregation promoting highlighted in blue) (Sormanni et al., 2015) and the β -aggregation potential of each sequence predicted using TANGO (Fernandez-Escamilla et al., 2004). **(A)** α Syn including polymorph 1a (1) (Guerrero-Ferreira et al., 2018; Li B. et al., 2018; Li Y. et al., 2018) (core residues 37–99), 1b (2) (Li B. et al., 2018) (core residues 43–83), 2a and b (3) (Guerrero-Ferreira et al., 2019) (core residues 14–24, 36–96) and the MSA *ex vivo* structures including residues 14–94 (for PF-IA and PF-IIA) (4) or residues 21–99 (for PF-IB and PF-IIB) (5) in the fibril core (Schweighauser et al., 2020). **(B)** TDP-43 cryoEM structure solved from C-terminal segments forming a dagger shaped core (1) (residues 312–346) or R-shaped core (2) (residues 288–319) (Cao et al., 2019). **(C)** A β structures solved (1) for A β_{42} (Gremer et al., 2017) and A β_{40} in which all residues comprise the core (Lu et al., 2013; Kollmer et al., 2019) (2) fibrils in which the core is formed by residues 10–40 for A β_{40} (including polymorphs 2A and 3Q) (Petkova et al., 2002; Paravastu et al., 2008) and (3) for A β_{42} (core formed by residues 15–42) (Colvin et al., 2016; Wälti et al., 2016). **(D)** Tau fibril structures PHF and SF from Alzheimer disease patients (1) (Fitzpatrick et al., 2017) (core residues 306–378), NPF and WPF from Pick's Disease (2) (Falcon et al., 2018) (core residues 254–378) and heparin induced structures 4R-s and 3R formed *in vitro* (3) (core residues 272–330) and 4R-t and 4R-j (4) (core residues 274–292, 304–321, respectively) (Zhang et al., 2019). **(E)** The β_2 m fibril core involves residues 22–85 (Iadanza et al., 2018b; Gallardo et al., 2020a). **(F)** The Orb2B fibril core consists of residues 176–206 (Hervas et al., 2020). **(G)** Human IAPP forms fibrils with residues 13–37 (Röder et al., 2020), 14–37 (Cao et al., 2020), or 13–37 (Gallardo et al., 2020a), with its early onset S20G variant adopting fibrils with two- and three filaments involving residues 15–37 in the core (Gallardo et al., 2020a). **(H)** PrP fibrils form fibril core with residues 170–229 revealed using cryoEM (Wang et al., 2020).

TABLE 1 | Summary of the functional roles of different regions of the amyloid proteins shown in **Figure 3**.

Protein	Residues/region	(Dys-)function	References
α Syn			
	1–14	Membrane insertion	Cholak et al., 2020
	1–25	Initial membrane binding	Fusco et al., 2014
	Extreme N-terminus and region around Y39	Chaperone binding	Burmann et al., 2020
	36–42 + 45–57	Involved in liposome clustering	Doherty et al., 2020
	36–42 + 45–57	Forms intra- and intermolecular interactions important for fibril formation	Doherty et al., 2020
	37–54	Forms β -hairpin crucial for nucleation/oligomerization processes	Mirecka et al., 2014
	C-terminal region (91–140)	Protects protein from aggregation by shielding NAC region and/or β -hairpin C-terminal truncation (109–140) results in faster aggregation	Hoyer et al., 2004; Hong et al., 2011; Yu et al., 2015; Stephens et al., 2019
	C-terminal region (residues 110–140)	Binding to chaperone-like protein SERF accelerates aggregation	Falsone et al., 2012
	C-terminal region (residue 125–129)	Dopamine binding drives off-pathway oligomer formation	Herrera et al., 2008
TDP-43			
	3–183	Interactions initiate homodimerization important for polymerization dependent splicing activity	Shiina et al., 2010; Afroz et al., 2017
	1–10 (especially Arg6, Val7, Thr8, and Glu9)	Mediates full-length TDP-43 oligomerization important for splicing activity and key to initiate aggregate formation	Zhang et al., 2013
	RRM1 (104–176), especially residue I107, D105, L111, W113, Q134, G146, F147, F149, R171, K176, N179 [RRM2 (192–262)]	Binds TG-rich DNA and UG-rich RNA for function (e.g., splicing, translation control, transport). RRM2 shows lower binding affinity.	Lukavsky et al., 2013; Kuo et al., 2014
	RRM1 (residue F147 and F149) and residue 208–441	Prevents aggregation by enhancing solubility when bound to single stranded RNA/DNA	Huang et al., 2013
	RRM1 (residue F147 and F149) and 321–366	Autoregulation of own protein expression by binding to its mRNA	Ayala et al., 2011
	Residue 320–340, especially W334, W385, and W412	Involved in liquid-liquid phase separation	Conicella et al., 2016; Sun and Chakrabarty, 2017; Li H.R. et al., 2018
$A\beta$			
	N-terminal domain (residues 1–17)	Binding to cystatin C (cysteine protease inhibitor)	Sastre et al., 2004
	$A\beta_{40}$: central region (residues 25–29); part of the structured fibril core but solvent accessible	Disaggregase activity when binding Lipocalin-type Prostaglandin D synthase (L-PGDS)	Kannaian et al., 2019
Tau			
	1–202	Binding to plasma membrane	Brandt et al., 1995
	N-terminal domain (1–150) interacts with proline rich domain (151–244)	Dimerization (head to tail), suggested to be the natural form for function and toxicity	Rosenberg et al., 2008
	Residue 1–117 and 118–402	Electrostatic interactions between these regions drive phase separation	Boyko et al., 2019

(Continued)

TABLE 1 | Continued

Protein	Residues/region	(Dys-)function	References
β_2m	114–193 (P-rich domain) and 198–278 (microtubule-binding domain)	Actin binding and promoting F-actin bundling and G-actin assembling	He et al., 2009
	N-terminal domain, proline-rich region and MBD	Chaperone binding	Mok et al., 2018
	Proline rich domain, MBD	Interaction and polymerization of tubulin	Barbier et al., 2019; Chen et al., 2019; McKibben and Rhoades, 2019
	Proline rich domain and C-terminal domain	Main locations of phosphorylation sites, but can be found throughout the whole sequence	Liu et al., 2007
	MBD (295–305)	β -hairpin formation that protects the aggregation prone 306–311 region	Chen et al., 2019
	MBD (residue 275–280 and 306–311) and other regions	Heparin binding drives aggregation; MBD shows highest affinity to heparin	Sibille et al., 2006
			
β_2m	Residue 1–6	Stabilization of native structure; accelerates aggregation when deleted	Esposito et al., 2000
	A and G strand (I7A, V9A, and V93A)	Mutations drive fibril growth by destabilizing local tertiary structure and increasing dynamics	Jones et al., 2003b
	A, B, E, F strand (6–11, 21–28, 64–70, 79–83)	Interaction with chaperone α B-crystalline preventing oligomerization and fibril formation	Esposito et al., 2013
			
Orb2B	RNA binding domain	Interaction with RNA facilitates long term memory formation	Krüttner et al., 2012
			
IAPP	1–19	Membrane binding and disruption	Brender et al., 2008
	1–17 and/or 30–37	Liquid-liquid phase separation	Pytowski et al., 2020
			
PrP	N-terminal region (residues 23–90)	Interaction with Tau	Han et al., 2006
	N-terminal region (residue 23–89)	Interaction with α Syn fibrils facilitating α Syn cell-to-cell spreading	Aulić et al., 2017
	Residues 95–110	Receptor binding site for A β 42-oligomers	Laurén et al., 2009
	Hydrophobic region (residue 111–134)	Hydrophobically driven binding/insertion with anionic membranes, this interaction is important for (murine) PrP to gain C-terminal Proteinase K resistance and convert it to PrP ^{Sc}	Wang et al., 2010b
	Octapeptide region in N-terminal domain	Increased numbers of octapeptides that bind Ca ²⁺ promotes fibril formation and disease development	Goldfarb et al., 1991

Each protein sequence is coloured, highlighting regions with different functional activity or those which have been mapped biochemically. RRM, RNA recognition motif; MBD, microtubule binding domain.

focusing solely on short peptide sequences that constitute the APRs. The latter approach, however, can be incredibly fruitful, leading to novel anti-microbial agents (Khodaparast et al., 2018)

and potential cancer treatments (Gallardo et al., 2016). The latter study showed that a *de novo* designed peptide, vascin, based on an amyloidogenic fragment of vascular endothelial

growth factor receptor 2 (VEGFR2) knocked down VEGFR2 as a consequence of VEGFR2-dependent fibril growth (Gallardo et al., 2016). Importantly, aggregation kinetics can be either slowed or accelerated depending on the protein and/or the precise modification of the flanking sequences. This is particularly apposite for IDPs, as the shallow, but rough, energy landscapes of these proteins renders their conformational ensemble sensitive to changes in their sequence and environment. This can result in APRs or binding motifs being exposed or sequestered, which in turn can accelerate, slow or prevent aggregation for the same protein sequence relative to a reference condition. Changes in pH, ionic strength and even being in a different cellular environment (e.g., oligodendrocytes vs neurons) can thus have a significant effect on fibril formation as shown for α Syn (Peng et al., 2018; Stephens et al., 2019). Indeed, far from being passive bystanders, flanking regions may be as important in defining the physiological role and amyloid disease etiology as the canonical APRs themselves (Figure 4). Here we highlight examples where flanking regions are involved in promoting or disfavoring aggregation to draw an overview of the significance of sequence and interaction partners of amyloidogenic proteins and peptides for fibril formation.

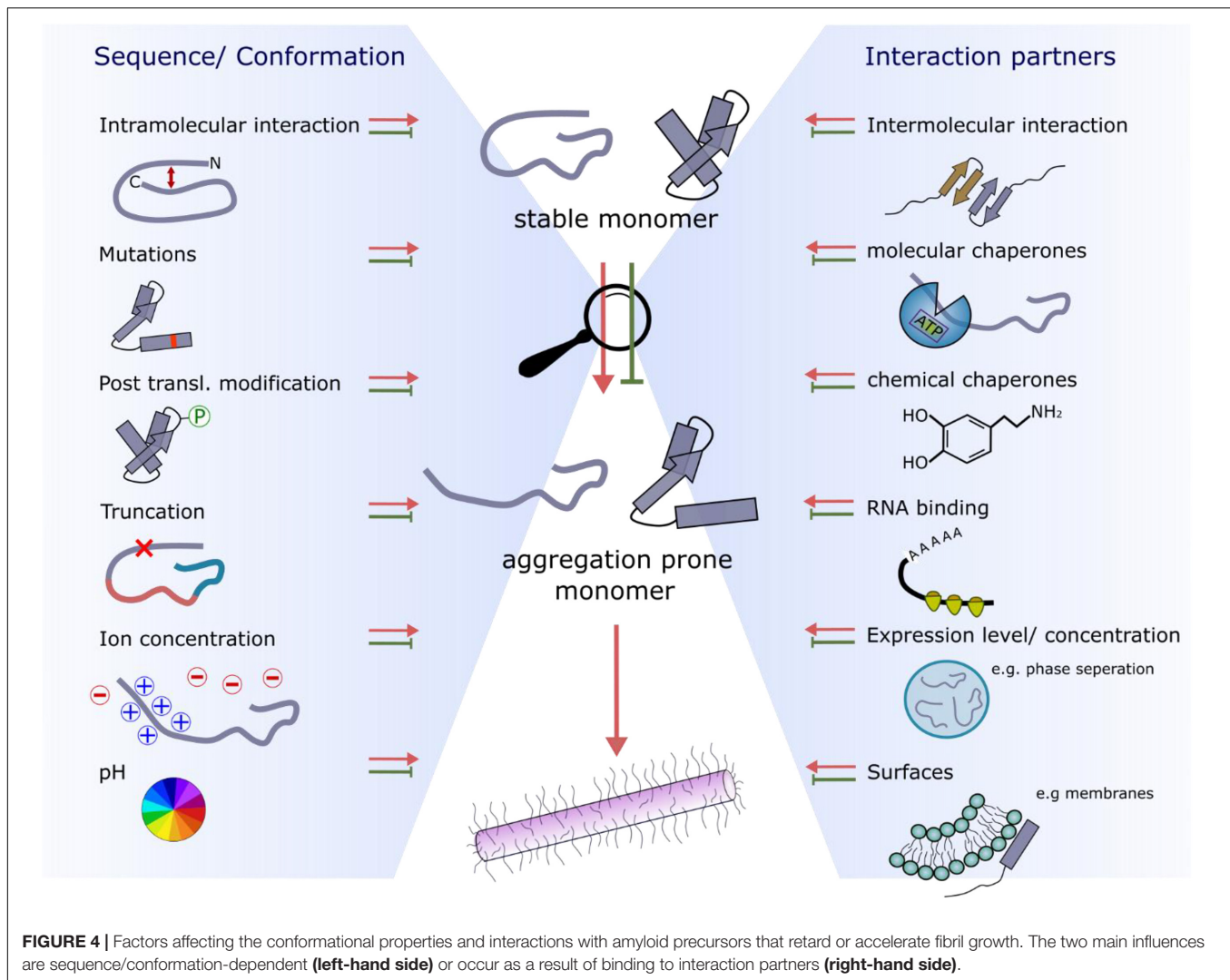
Flanking Regions That Protect Against Aggregation

A protein concentration higher than the critical amyloid concentration (Xue et al., 2008), and (sometimes) the presence of surfaces that can act as nucleation sites are required to overcome the energy barrier needed to form amyloid structures (Buell, 2017). Such surfaces include membranes, other proteins, or the air-water interface [so-called heterogeneous primary nucleation (Buell, 2017; Figure 4)] or the amyloid fibril surface itself (secondary nucleation) (Linse, 2017). In the crowded cell, there is a fine-balance of expressing sufficient protein to maintain function, but avoiding high expression levels to disfavor aggregation. This strategy was described as “life on the edge” by Dobson and co-workers (Tartaglia et al., 2007). Interestingly, more recent work has shown that regions surrounding an aggregation hotspot can play a role in maintaining the correct balance between expression level and aggregation potential, such that aggregation is disfavored, whilst the function of the native protein is maintained. A particularly clear example is the TAR DNA-binding protein 43 (TDP-43). The formation of a negative feedback loop involving the RNA-recognition motif 1 (RRM1, especially residues F147 and F149) and the fibril core-forming C-terminal region [residues 321–366 (Figure 3B)] self-regulates protein expression via a mechanism in which TDP-43 binds its own mRNA leading to decreased protein expression (Ayala et al., 2011; Table 1). Single stranded RNA (ssRNA) or DNA (ssDNA) binding to the flanking regions of TDP-43 also functions as a protective mechanism against amyloid formation by increasing the solubility of TDP-43 (Huang et al., 2013). In addition to translational control, the flanking regions of TDP-43 have also been found to affect its aggregation kinetics directly. For example, cells overexpressing Δ 1–10 TDP-43 do not form cellular inclusions, by contrast with cells producing the

full-length protein (Zhang et al., 2013). Another example where flanking regions protect from aggregation is the homo-tetrameric protein transthyretin (TTR), which is expressed in the liver and cerebrospinal fluid and is associated with amyloidosis. For this protein, the gatekeeper residue K35 [located just at the edge of the fibril core of a recently solved cryoEM structure (Schmidt et al., 2019)] protects the full-length protein from fibril formation (Sant’Anna et al., 2014).

Flanking regions can also limit fibril formation by binding to chaperones, which stabilize and protect the native state of the protein (Wentink et al., 2019; Figure 4). Using *in vitro* and in cell NMR Burmann et al. (2020) recently showed that α Syn is bound to an array of molecular chaperones. Some of these are physiologically relevant (e.g., hsc70, hsp90) whereas others are not (e.g., the periplasmic bacterial chaperones Skp and SurA). Similarly, the ATP-independent nascent polypeptide associated complex (NAC) has been shown to bind to the flanking regions of α Syn and ataxin 3 and retard their aggregation (Martin et al., 2018; Shen et al., 2019). Despite their diversity, all six chaperones in the study by Burmann et al. (2020) were found to bind the N-terminal 10 residues of α Syn and a segment around residue Y39 (Table 1). Inhibition of chaperones Hsc70 and Hsp90 in mammalian cells resulted in the re-localization of α Syn from the cytosol to the mitochondria, amplified fibril growth and increased membrane binding, which has been shown to be the toxic form of α Syn in yeast (Newberry et al., 2020). Interestingly, phosphorylation of Y39, which is associated with α Syn-dependent neurodegeneration (Brahmachari et al., 2016), decreased the interaction with chaperones. Enhancing the concentration of various heat shock proteins thus disfavors α Syn aggregation, potentially providing a therapeutic approach to treat α Syn-aggregation and its associated cytotoxicity (Jones et al., 2014). Similar aggregation-suppressive effects have been reported for other chaperone:protein pairs: β_2 -microglobulin (β_2 m) interacts with α B-crystallin mainly via its flanking regions [residues 6–11, 21–28, 9–83 (Figure 3E and Table 1)] and some residues within the APR (residues 64–70) (Esposito et al., 2013); the N-terminal domain of Tau (residues ~1–40) (as well as the proline-rich region and repetition motifs [residues ~160–370 (Figure 3D and Table 1)] binds to the chaperone DnaJA2 (Mok et al., 2018) and the N-terminal 17 residue flanking region of the huntingtin protein forms a complex with the molecular chaperones Hsc70 (Monsellier et al., 2015) or TriC (Tam et al., 2009) reducing its aggregation. This might be explained by the fact that chaperones bind to flanking regions preventing the formation of crucial conformations/interactions required for amyloid formation. For instance, the exon 1 domain of huntingtin has been shown to initiate aggregation by dimerization of its N-terminal 17 residues (Kelley et al., 2009) which is inhibited by chaperone binding to this sequence (Tam et al., 2009; Monsellier et al., 2015).

By contrast with the chaperones discussed above, other chaperone-like proteins have been shown to accelerate aggregation. For example, the binding of the human protein SERF (or MOAG-4, the SERF homolog in *Caenorhabditis elegans*) has been shown to accelerate aggregation of polyglutamine peptides, huntingtin, A β and α Syn *in vitro* and *in vivo* (van



Ham et al., 2010; Falsone et al., 2012; Meinen et al., 2019). Although the binding site on SERF for all of these amyloidogenic proteins has yet to be identified, α Syn was shown to bind via its C-terminal region (residues 110–140) (Falsone et al., 2012). In other cases, binding of small molecules [chemical chaperones (**Figure 4**)] has been shown to accelerate or to retard the rate of aggregation and/or the morphology of the fibrils formed. For example, the glycosaminoglycan heparin, has been shown to induce the aggregation of Tau, resulting in fibrils with a different structure from Tau fibrils extracted from the brains of patients with Alzheimer's, Pick's or other Tau-associated neurodegenerative disorders (Zhang et al., 2019; Scheres et al., 2020; **Figure 3D**). NMR studies revealed multiple binding sites on Tau for heparin, with binding affinities ranging from 10 μ M to the mM range. The tightest binding is observed within the microtubule binding domain (MBD) (residues 275–280 or 306–311), again highlighting that binding outside the APR modulates aggregation (Sibille et al., 2006). As a final example, the small molecule dopamine binds the C-terminal region of α Syn (residues 125–129), driving

off-pathway oligomer formation that does not result in fibril growth (Herrera et al., 2008).

Flanking Regions That Accelerate Aggregation

As several amyloidogenic proteins are IDPs, transient intra- or inter-molecular interactions mediated by flanking regions can play an important role in defining the overall aggregation propensity of a protein sequence by altering the solvent accessibility of key APRs (**Figure 4**). For example, paramagnetic relaxation enhancement (PRE) NMR and computational modeling experiments revealed that the flexible negatively charged C-terminal region of α Syn (residues 96–140) forms intra- and inter-molecular interactions with the positively charged N-terminal region of the protein, which protect the aggregation-prone NAC region (Hong et al., 2011; Janowska et al., 2015; Yu et al., 2015; Stephens et al., 2019; **Table 1**). Conditions that disfavor these transient interactions [e.g., high cation concentration (Nath et al., 2011), low pH (Hoyer et al., 2002)

or familial Parkinson's disease mutations (Ranjan and Kumar, 2017)] result in perturbation of the protective long-range contacts and accelerate aggregation (reviewed by Stephens et al., 2019). Likewise, truncation of the protective C-terminal region of α Syn, as found in Lewy bodies in disease-associated brains (Muntané et al., 2012), causes more rapid fibril formation, potentially rationalizing the role of truncation of these regions in the development of disease (Hoyer et al., 2004). Similarly, for TTR the C and D strands (not part of the aggregation hotspot) are involved in the interchain contacts that lead to aggregation (Kelly and Lansbury, 1994; Palaninathan et al., 2008). Also, many disease associated mutations of TTR (e.g., V30M and L55P) are located within the C and D strand region (Murakami et al., 1992; Lashuel et al., 1999).

More recently, studies analyzing the aggregation kinetics of N-terminal deletion variants of α Syn have shown that specific regions of the protein are also required for the aggregation of full-length α Syn, building on an array of previous data that suggested an importance of the N-terminal region of the protein for its function (membrane binding) (Fusco et al., 2016; Cholak et al., 2020) and its aggregation (Kessler et al., 2003; Terada et al., 2018). Perhaps most remarkably, based on prediction of aggregation-prone and insoluble regions (Figure 3A) discrete sequences were identified that form a range of precise interactions with residues in the NAC and C-terminal regions, protecting the protein from aggregation (Doherty et al., 2020). Deleting residues 38–61 (that encapsulates a region (residues 47–56) shown by Eisenberg and Sawaya (2017), to form fibrils in isolation and named the pre-NAC region (Rodríguez et al., 2015), or deleting/replacing an even shorter peptide [named P1, residues 36–42] or P1P2 (residues 36–57) results in significantly slower fibril growth compared with the wild-type protein both *in vitro* and in *C. elegans* models (Doherty et al., 2020). The reduced aggregation rate may be a consequence of preventing the formation of inter-molecular contacts between regions of the IDP that form a transient β -hairpin structure (strand 1: residue 37–43 and strand 2: residue 48–54) previously postulated based on Thioflavin T assays and molecular dynamics simulations to drive aggregation (Mirecka et al., 2014; Yu et al., 2015). In accord with this hypothesis, binding of a nanobody known as a β -wrapin to this motif prevents aggregation *in vitro* and in *Drosophila* (Mirecka et al., 2014; Agerschou et al., 2019). Similarly, a specific short aggregation-modulating peptide sequence that lies outside its APRs has been observed for another IDP, Tau, but here the formation of a β -hairpin structure involving residues 295–311 protects the aggregation hotspot [residues 306–311 (Figure 3D)] by using the flanking region 295–300 as a protective shield. Familial point mutations or alternative splicing can result in weakening of this secondary structural element, exposing the APR and promoting aggregation (Chen et al., 2019). Finally, for apolipoprotein apoA-I, involved in systemic amyloidosis, the aggregation hotspot (residues 14–22) is protected by a helix bundle formed at the N-terminus of the protein. Familial amyloidosis associated with disease-promoting mutations (such as G26R, W50R, F71Y, or L170P), all of which are located in regions flanking the amyloid hotspot, induce conformational changes that result in exposure of residues

14–22 and lead to amyloid formation (Adachi et al., 2014; Das et al., 2016).

The aggregation of globular proteins can also be affected by their flanking regions. One well-understood example is β_2 -microglobulin (β_2 m, a 99-residue protein with an Ig fold when natively folded) which is associated with the disease dialysis-related amyloidosis (DRA) (Gejyo et al., 1986). Approximately 30% of the molecules in fibrils of DRA patients is comprised of an N-terminally truncated variant missing the N-terminal six residues (Esposito et al., 2000). This deletion variant which is significantly more aggregation-prone than the full-length protein, is destabilized in its native state, and exhibits increased dynamics that facilitates amyloid formation (Chiti et al., 2001; Jahn et al., 2006; Eichner et al., 2011; Karamanos et al., 2019). An *in vitro* study that introduced point mutations into different β -strands of β_2 m further showed the importance of A- (residues 6–11) and G-strands (residues 91–94), both distant to the aggregation hotspot (Figure 3E). Amino acid substitutions in these strands (I7A, V9A, or V93A) induced aggregation by destabilizing the monomeric structure specifically in these regions, while similar mutations elsewhere in the sequence caused similar loss of thermodynamic stability, yet did not drive aggregation (Jones et al., 2003b). Hence local, rather than global, stability, is important in tailoring the aggregation of natively folded proteins, potentially because of the specific effects this has on fulfilling the aggregation-potential of a sequence's APRs (Langenberg et al., 2020). In a similar vein, a rare mutation in β_2 m has recently been discovered in a French family that results in a different amyloid disease in which the variant protein (D76N) forms fibrils that deposit in the viscera without loss of renal function (Valleix et al., 2012). Importantly, the substituted amino acid (D76N) lies in a solvent exposed loop distant to the single APR in the protein (Figure 3E).

Other globular proteins have also been found to have flanking regions that are critically important for aggregation, including polyglutamine expansion (polyQ) proteins such as ataxin-3 (Saunders and Bottomley, 2009). This ~40 kDa protein has a structured N-terminal protease domain (the Josephin domain) followed by an IDR which contains two (or sometimes three) ubiquitin interacting motifs (UIMs) and an expanded polyQ tract (Paulson, 2012). The aggregation mechanism of ataxin 3 *in vitro* has been shown to involve two kinetically resolved stages. In the first phase, the aggregation-prone Josephin domain self-associates into worm-like fibrils (that lack the cross- β structure of amyloid), with the slow formation of amyloid involving the polyQ tract occurring in a second phase (Ellisdon et al., 2006). Like all polyQ proteins, aggregation of ataxin 3 is critically dependent on the length of the polyQ tract. Importantly, the presence of a long (disease-causing) polyglutamine tract changes the conformational dynamics of the Josephin domain, exposing the aggregation-prone N-terminal region and allowing self-association that results in aggregation (Gales et al., 2005; Scarff et al., 2015). Akin to the results for the mutation causing β_2 m aggregation discussed above, the polyQ tract is believed to diminish the stability of neighboring domains in ataxin 3, creating a local denaturing environment (Ignatova and Gierasch, 2006). The longer the

polyQ sequence, the greater its effect in accelerating aggregation (Scarff et al., 2015).

In addition to intra- and inter-molecular homotypic association, interactions of flanking regions with other molecules/surfaces (heterotypic interactions) can also affect the kinetics of fibril formation (Sarell et al., 2013; **Figure 4**). For several amyloidogenic proteins, including IAPP, A $\beta_{40/42}$ and α Syn, aggregation is accelerated in the presence of membranes (Terakawa et al., 2018). For example, the N-terminal region of α Syn binds to lipid bilayers (forming an α -helical structure) that leads to extensive surface-induced fibril growth (Fusco et al., 2014; Doherty et al., 2020; **Table 1**). For IAPP, the N-terminal 19 residues (which flank the core region of amyloid involving residues ~15–37) bind to membranes and also become helical (Brender et al., 2008). Studies on an N-terminal fragment of IAPP involving residues 1–19 showed that membrane binding and disruption of the bilayer occur independently of fibril formation (Brender et al., 2008). Tau has also been shown to bind membranes, having functional as well as pathogenic effects where the lipid bilayer facilitates protein-protein interactions driving aggregation (Elbaum-Garfinkle et al., 2010). Another example where binding to membranes initiates a critical process can be found for PrP, a GPI anchor protein, as binding and insertion into lipid membranes (in the presence of RNA) initiates the conformational transition to a highly aggregation-prone form of PrP (Wang et al., 2010a). In addition, binding of PrP to anionic phospholipids is mediated by a flanking region outside of the fibril core and comprises the contiguous positively charged (residues 100–110) and “hydrophobic domain” regions (residues 111–134) (Wang et al., 2010b). Surface-induced aggregation is also important in the growing field of nanotechnology where nanoparticles coated with sugars, lipids or proteins, are widely used in drug delivery or diagnostics. These surfaces can also enhance protein aggregation. For example, β_2 m has been shown to aggregate more rapidly in the presence of copolymer particles, cerium oxide particles, quantum dots, and carbon nanotubes in a manner that is dependent on the surface area and surface modification (Linse et al., 2007). Fibril formation of IAPP is also enhanced in the presence of chiral silica nanoribbons (Faridi et al., 2018).

Fibril formation of one protein can also be affected by interactions with other amyloidogenic proteins. For example, α Syn aggregation is enhanced in the presence of Tau, which is biologically relevant since these two proteins are observed to co-aggregate in inclusions in brains from patients with Dementia with Lewy Bodies (DLB) (Colom-Cadena et al., 2013). Similarly, CsgA, a bacterial functional amyloid, also accelerates α Syn aggregation, possibly explaining clinical and epidemiological data that show an accumulation of aggregated α Syn first being found in olfactory epithelium or gastrointestinal tract, before spreading to the brain (Sampson et al., 2020). Aggregation assays with a C-terminally truncated variant of α Syn using PRE NMR experiments revealed that the C-terminal region of α Syn interacts with Tau (Dasari et al., 2019; Lu et al., 2020; **Table 1**). This region is also involved in ion binding, most importantly Ca²⁺, which drives fibril formation probably by changing the conformational dynamics of α Syn to a more extended form

(Han et al., 2018). *In vivo* assays have shown that the native prion protein (PrP^C) or protease-resistant isoform (PrP^{Sc}) bind Tau with their N-terminal disordered segment (residue 23–90) (Han et al., 2006), and also bind to A β oligomers and α Syn fibrils, facilitating cell surface binding and cell-to-cell spreading (Laurén et al., 2009; Aulić et al., 2017). Additionally, single molecule Förster resonance energy transfer experiments (FRET) measuring the conformational ensemble of Tau have shown that heparin induces conformational changes that could be important in promoting amyloid formation (Elbaum-Garfinkle and Rhoades, 2012). These involve a loss of long-range contacts of the N- and C-terminal regions and a compaction of the aggregation-prone MBD (Elbaum-Garfinkle and Rhoades, 2012).

Finally, post-translational modifications including phosphorylation, ubiquitinylation or acetylation are important regulatory modifications of amyloidogenic proteins that influence cellular mechanisms, such as protein degradation, signaling or protein-protein interactions, and also lead to misfolding and aggregation (**Figure 4**). Examples include the 441-residue protein Tau, in which 85 residues have been identified as phosphorylation sites mainly located in the aggregation hotspot that flanks the proline rich and C-terminal domains. Hyperphosphorylation of Tau is believed to trigger its dissociation from microtubules and to drive amyloid formation (Liu et al., 2007). However, recent studies on the four repeat region (K18) of Tau suggest an inhibitory effect of phosphorylation on fibril formation (Haj-Yahya et al., 2020). Finally, the protein huntingtin contains three lysines (K6, K9, K15) in its N-terminal 17-residue region which are often ubiquitinylated or SUMOylated, reducing toxicity by protease degradation or monomer stabilization, respectively (Ehrnhoefer et al., 2011).

Roles of Flanking Regions in Protein Function

As proteins associated with amyloidosis have functional roles in their soluble states, aggregation can lead to a loss of function, as well as a gain of toxic function. For example, Tau (**Table 1**) is known to be present in six different isoforms in the central nervous system formed by alternative splicing processes. This results in deletions in the N-terminal region (45–103) or one of the four repeat regions, R2 (residues 275–305) (Himmler et al., 1989). The expression and translation levels of these isoforms are correlated with different developmental stages (Kosik et al., 1989), pointing to discrete functional roles of each. Indeed, Tau's main function is to bind microtubules with its aggregation-prone MBD (residues 244–371) which induces assembly of microtubules. Although the MBD is primarily responsible for microtubule binding, its N-terminal and C-terminal flanking regions have been shown to modulate the conformation and accessibility of the MBD as part of its functional activity (Goode et al., 2000; Barbier et al., 2019). Further, the proline rich region (residues 151–243) (**Table 1**) also contributes to tubulin binding and its polymerization into microtubules (McKibben and Rhoades, 2019). Other amyloidogenic proteins such as α Syn are also considered to be microtubule-associated proteins (MAP). In

this case much less is known, with current research suggesting a microtubule-polymerizing activity when α Syn binds tubulin via its C-terminal region (Alim et al., 2004), or supporting microtubule association and dynamics by binding probably via its N-terminal- and NAC-regions adopting a helical conformation (Cartelli et al., 2016). Oligomeric α Syn on the other hand has been shown to inhibit tubulin polymerization, resulting in cell death (Chen et al., 2007).

α Syn not only interacts with tubulin, but it also binds to many different proteins and molecules that are important for function (e.g., interaction with receptors to increase the neuronal levels of dopamine or inhibiting SNARE complex formation) and toxicity (e.g., the binding of α Syn to Parkin contributes to the pathophysiology of Parkinson's disease) (Emamzadeh, 2016). The aggregation-prone NAC region of α Syn itself has been implicated in its function [e.g., binding to the dopamine receptor in neurons, regulating dopamine concentration (Lee et al., 2001)]. The ability of α Syn to bind to membranes is key to its physiological function of remodeling membrane vesicles within the presynaptic termini (Diao et al., 2013). *In vitro* NMR studies of α Syn:liposome interactions revealed that the N-terminal 25 residues trigger the interaction with the membrane by acting as an anchor motif, initializing binding of the whole N-terminal and NAC region (membrane sensor region, residues 26–98) with the formation of α -helical structure throughout this region (Fusco et al., 2014). Residues 26–98 are believed to modulate the affinity of α Syn for membranes and are crucial for its function in clustering synaptic vesicles (Fusco et al., 2016). Deleting or replacing residues 36–57 (the P1 and P2 regions discussed above), which flank the aggregation hotspot, showed an inhibition of the membrane remodeling activity, supporting a role of these flanking regions in liposome fusion (Doherty et al., 2020). A study from Cholak et al. (2020) suggests that the very N-terminal region (residues 1–14) of α Syn inserts into membranes to initiate membrane binding, with N-terminal acetylation of α Syn enhancing the lifetime of the membrane-bound state. In accord with the functional importance of these regions, α Syn shows higher sequence similarity to its two known homologs (β Syn and γ Syn) in the N-terminal region compared with the C-terminal region (90% and 77% sequence identity in the N-terminal region and 36% and 1% sequence identity in the C-terminal region between α Syn and β Syn and α Syn and γ Syn, respectively) (George, 2001). Membrane binding is not only involved in α Syn function, but it also represents a risk factor for α Syn aggregation and cytotoxicity, as association with membranes accelerates α Syn fibril formation (Galvagnion et al., 2016; Fusco et al., 2017). Binding to lipid bilayers via its N-terminal helical region has been suggested to be the pathological conformation of α Syn in yeast, causing slower cell growth and cell death (Newberry et al., 2020). Similarly, binding to mitochondrial membranes resulted in cytotoxicity due to enhanced formation of mitochondrial reactive oxygen species (ROS) and reduced ATP levels (Vicario et al., 2018; Ganjam et al., 2019).

The functional amyloid Orb2B is involved in forming long term memories (Keleman et al., 2007; Majumdar et al., 2012; Khan et al., 2015) by affecting translation within neurons (Krüttner et al., 2012) via its RNA binding domain (RBD). The

RBD flanks a glutamine-rich region that drives the formation of fibrils whose formation activates translation (Hervas et al., 2020). TDP-43 is involved in maintaining mRNA stability, maturation and transport via specific RNA-recognition motifs (residues 104–262) (Prasad et al., 2019). For splicing, TDP-43 functions as a dimer stabilized by inter-molecular interactions in the N-terminal region, especially the N-terminal 10 residues (Shiina et al., 2010; Zhang et al., 2013; Afroz et al., 2017). These intermolecular interactions are also involved in initiating aggregation (Zhang et al., 2013), providing a further example of the tug-of-war between sequences involved in function that also enhance aggregation. TDP-43 also exhibits reversible liquid-liquid phase separation, a reversible process of demixing fluids into two distinct liquid-phases [reviewed by Alberti et al. (2019) and de Oliveira et al. (2019)] important for the formation of stress granules that store mRNA:protein complexes under cellular stress (e.g., oxidative or thermal stress) (McDonald et al., 2011; Sun and Chakrabartty, 2017). This function is mediated by the C-terminal prion-like domain of TDP-43 (Table 1). Substitution and deletion variants identified Trp334, Trp385, and Trp412 as important drivers of phase separation (Li H.R. et al., 2018). These residues flank the aggregation hotspot of TDP-43 [residues 288–346 (Figure 3B)] and only Trp334 is part of the fibril core in the dagger shaped polymorph (Cao et al., 2019). TDP-43 liquid droplets remain stable for only a short period of time (timescale of hours) before transforming into irreversible aggregates (Conicella et al., 2016). Using PRE NMR experiments, Conicella et al. (2016) identified residues 321–340 as those responsible for the crucial interactions for phase separation, by forming inter-molecular helix-helix self-assemblies that are disrupted by the ALS-associated mutations (A321G, Q331K, and M337V). Tau also undergoes liquid-liquid phase separation prior to the formation of gel-like and then amyloid-like aggregates (Wegmann et al., 2018). A detailed study of deletion variants revealed that electrostatic interactions between the N-terminal region (residues 1–117) and parts of the C-terminal domain (residues 118–402) drive phase separation [whereas residues in the microtubule binding region are thought to be important for amyloid formation (Elbaum-Garfinkle and Rhoades, 2012)]. Deleting either one of the former regions ablated droplet formation (Boyko et al., 2019). Other amyloid-associated proteins also undergo phase separation, at least *in vitro* (Elbaum-Garfinkle, 2019). For example, liquid-liquid phase separation of IAPP is catalyzed by the air-water-interface (Pytowski et al., 2020). Interestingly, Comparison with the non-fibrillogenic rat IAPP revealed that phase separation does not require the presence of the highly amyloidogenic region (residue 20–29), but hydrogelation and aggregation do (Pytowski et al., 2020). The prion-like functional amyloid Sup35 also undergoes phase separation, generating protein-specific environmental responses. In this protein, the N-terminal prion domain, as well as the flanking M-domain, have a benign role: promoting reversible phase separation and gelation in a pH dependent manner (Franzmann et al., 2018). Finally, α Syn has also been shown to form phase separated droplets which precede aggregation into amyloid *in vitro* and in cells (Ray et al., 2020) The cellular

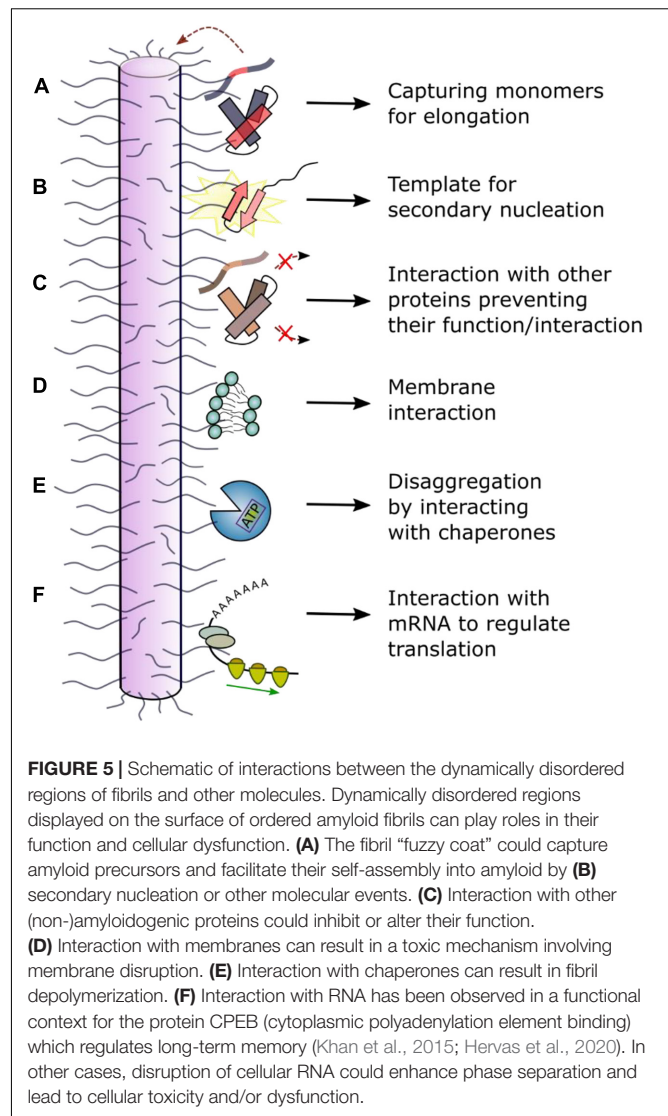
droplets later transform into perinuclear aggresomes, with the familial mutations and phosphorylation of Y39 as discussed above promoting liquid-liquid phase separation, as well as aggregation into amyloid.

REGIONS FLANKING THE STRUCTURED CORE OF AMYLOID FIBRILS: THE IMPORTANCE OF THE INVISIBLE FLANKING REGIONS

The biophysical and biochemical properties of each amyloid fibril polymorph and their effect on cells can differ dramatically. As amyloid formation is under kinetic control, changes in the protein sequence and/or the assembly conditions (*in vitro* or in cells) can affect the structure of the fibrils formed. Accordingly, different fibril structures for Tau isoforms have been observed to form in different amyloid diseases (Scheres et al., 2020). Interestingly, for α Syn amyloid, heterogeneity is also observed for fibrils from patients with Parkinson's disease or Multiple system atrophy [detected using ssNMR and differences in the fluorescence emission spectra of extrinsic fluorophores (Strohäker et al., 2019)]. The ability to discriminate polymorphs by comparison of fluorescence emission spectra of some extrinsic fluorophores (e.g., Thioflavin T or Congo Red) when intercalated into cross- β fibril structures has been noted previously (reviewed by Bhattacharya and Mukhopadhyay, 2016). The differential binding affinity for some antibodies to oligomers and mature fibrils also highlights the structural conversion that has to occur for amyloid fibrils to form. For example, the A β ₄₂ antibody anti-Trx(A β 15)₄ recognizes a structural epitope of oligomers and fibrils but not of the monomer, with the same selectivity for other amyloidogenic proteins (Moretto et al., 2007). Consequently, it is perhaps not surprising that fibrils with different structures may induce different effects *in vivo*. Ferrari et al. (2020), for example, used a pull-down approach with FLAG-tagged Tau to show that different aggregation stages (monomer, oligomer, fibril) have altered reactivity with its cellular environment due to large conformational changes that occur when this natively unfolded protein self-assembles into a β -sheet rich fibrillary protein state. Given that the “fuzzy coat” of disordered peptide regions that flank the cores of amyloid fibrils can vary between fibril polymorphs (Gallardo et al., 2020b), the effect of these dynamic regions on the function, toxicity and further amplification of the fibrils themselves may also vary, perhaps rationalizing the epigenetic difference in disease development in individuals expressing the same aggregation-prone proteins. Below we discuss the importance of these structurally “invisible” flanking regions in amyloid formation and the cellular consequences of these regions in amyloid deposition (Figure 5).

Fibril Elongation, Secondary Nucleation and Seeding

The extent of protein incorporation into insoluble fibrils is controlled by processes such as seeding (fragments broken off from fibrils, creating new fibril ends), elongation (the



addition of monomers or oligomers onto fibril seeds) and secondary nucleation (creation of new nucleation sites on pre-existing fibril surfaces) (Michaels et al., 2018; Shvadchak et al., 2018; Scheidt et al., 2019). These kinetic events that drive amyloid formation could depend on the monomeric amyloid precursor, the structured amyloid core and the nature of the fibril “fuzzy coat.” For example, the flanking regions may be involved in the prion-like ability of α Syn to spread and seed further fibril growth (summarized by Longhena et al., 2017) as secretion of α Syn into the extracellular space occurs in association with membrane vesicles for which binding of the N-terminal region of α Syn is crucial (Emmanouilidou et al., 2010). The elongation rate may be accelerated as the large volume “fuzzy coat” may form transient interactions, “capturing” incoming monomeric protein molecules (Tompä, 2009; Figure 5A). This model is supported by the example of the human Prion Protein (PrP), in which increased numbers of an octapeptide Cu²⁺-binding motif in the N-terminal IDR

(which flanks the folded C-terminal prion domain) promotes fibril formation and disease development (Goldfarb et al., 1991). Additionally, the fibril surface might have a key role in surface-induced secondary nucleation (**Figure 5B**). This is because the surfaces of all but one (Gremer et al., 2017) amyloid fibril structures solved to date are decorated by potentially large region of dynamically disordered protein flanking regions. Secondary nucleation for α Syn and other amyloid proteins, including A β and IAPP, is strongly dependent on pH (Gaspar et al., 2017). This could be explained by fact that the pH affects the dynamics of the solvent exposed flanking regions, as well as the charge along the ordered fibril core (Wegmann et al., 2013). The importance of flanking regions for these processes is illustrated by co-incubation of α Syn and β Syn. NMR analysis of the fibrils formed show increased dynamics in the N-terminal region compared with pure α Syn fibrils, whilst the core structure is unchanged. These co-incubated fibrils exhibited a reduced seeding capacity (Yang et al., 2019). However, the precise molecular mechanism(s) of the elongation and secondary nucleation processes, and how they alter with changes in sequence and fibril structure is not currently understood in detail.

Interaction With Other Amyloidogenic Proteins

Amyloid fibrils can interact with other amyloidogenic precursors and alter their amyloid potential (**Figure 5C**). α Syn fibrils, for instance, have been shown to bind Tau monomers via the α Syn acidic C-terminal region which is dynamically disordered in all fibril structures determined to date (Guerrero-Ferreira et al., 2020; Schweighauser et al., 2020). Since binding of Tau stabilizes microtubules, α Syn fibrils indirectly affect microtubule stability by removing Tau from microtubule surfaces resulting in neuronal dysfunction (Oikawa et al., 2016). Interaction of α Syn fibrils with Tau monomers further induces a conformational change in Tau, promoting its subsequent assembly into Tau amyloid structures (Oikawa et al., 2016). As reviewed by Luo et al. (2016), A β interacts with at least 10 other disease-related amyloidogenic proteins (e.g., IAPP, Tau, α Syn). For example, aggregation of A $\beta_{40/42}$ is inhibited by cystatin C (Sastre et al., 2004), a protein which also colocalizes with A $\beta_{40/42}$ in brain amyloid deposits. ELISA assays with an antibody targeting the N-terminal end of A β (residues 1–17) defined the binding site to be the first 17 residues, since binding was abolished in the presence of the antibody (Sastre et al., 2004). A $\beta_{40/42}$ aggregation is also inhibited in the presence of TTR tetramers. NMR experiments revealed the interaction site to be between the thyroxine binding pocket of the TTR tetramer and A β residues 18–21 (Li et al., 2013). Finally, amyloid proteins have been observed to interact with other proteins in the context of cross-seeding. For example, pre-formed fibrils of IAPP have been shown to cross-seed A β_{40} monomers, accelerating fibril growth (Moreno-Gonzalez et al., 2017). The exact binding site is not known, but the two proteins have been shown to co-localize in disease (Moreno-Gonzalez et al., 2017).

Membrane Binding

Although many studies have shown that oligomers can be cytotoxic and possibly a major culprit of amyloid diseases (Fändrich, 2012; Verma et al., 2015; Fusco et al., 2017; Karamanos et al., 2019), the surface-induced fibril growth process on membranes (Engel et al., 2008; Qiang et al., 2015) and the interaction of mature fibrils with membranes (**Figure 5D**) have both been shown to disrupt cellular function and homeostasis (Martins et al., 2008; Xue et al., 2009; Pieri et al., 2012). *In vitro* experiments on α Syn have shown that its kinetics of aggregation are strongly affected by the presence of liposomes, highlighting the important role of lipid bilayers for fibril formation (Galvagnion et al., 2015). α Syn fibrils (and oligomers) bind negative, but not neutrally charged, liposomes (Grey et al., 2011; Pieri et al., 2012), pointing to an interaction with the N-terminal positively charged flanking region, which is dynamically disordered in the fibrillar state, similar to the interaction that is observed in the monomeric state. Striking work from B  uerlein et al. (2017) used cryo-electron tomography *in situ* to show that polyQ fibrils (from huntingtin-exon 1) interact with membranes of the endoplasmic reticulum, changing the dynamics and structural organization of the organelle. These studies also showed that the sides of the fibril, as well as fibril ends, interact with membranes, although which regions of the fibril are involved in the interaction (the core or dynamic sequences) is not currently known. Similar vesicle membrane disruption was observed *in vitro* for β_2 m fibrils, with the majority of fibrils binding via their ends (Milanesi et al., 2012). Interestingly, the most severe membrane damage was observed for membranes containing the lipid BMP [bis(monoacylglycero)phosphate] which is enriched in lysosomal membranes, rationalizing the role of this organelle in the etiology of many amyloid diseases (Goodchild et al., 2014).

Interaction With Chaperones

Amyloid fibrils have been shown to interact with chaperones in different contexts (**Figure 5E**) of which neuroprotection is one of the foremost (Kannaian et al., 2019). Chaperone binding functions as an inhibitor for primary nucleation (when binding monomers), as well as for secondary nucleation and elongation, and some chaperone systems can even induce disaggregation of fibrils in the presence of ATP (Kannaian et al., 2019). Chaperones such as α B-crystallin have been shown to bind along the length of the fibril surface, perturbing secondary nucleation and elongation for both A β_{40} /A β_{42} and α Syn (Waudby et al., 2010; Shammas et al., 2011). However, despite the authors revealing fascinating images of the chaperone *in situ* using immunogold labeling and immunoelectron microscopy, the exact binding site could not be determined due to the low resolution of this technique. In the case of Hsp27, which binds on the surface of α Syn fibrils causing decreased cytotoxicity and inhibited elongation, total internal reflection fluorescence (TIRF)-based imaging suggested that Hsp27 preferentially binds to hydrophobic patches along the fibril surface (Cox et al., 2018). These hydrophobic motifs involved in the interaction could involve the dynamic regions [residues 1–6 or 36–42 (**Figure 3A**)] as well as the fibril core

itself. A higher resolution analysis, e.g., using HX methods, or more directly using ssNMR, is required to identify the exact chaperone binding sites.

Given the high thermodynamic stability of fibrils, it is perhaps a remarkable feat that chaperones can induce their depolymerization. For α Syn fibrils, for example, Bukau and coworkers have shown that the human chaperone Hsc70, specifically in complex with DNAJB1 (Hsp40 family) and Apg2 is a hsp110 family member (but not other co-chaperones from these families), induces ATP-dependent fibril fragmentation and depolymerization (Gao et al., 2015). Experiments using deletion variants allowed the interaction site of the fibrils with the chaperones to be identified, involving residues 1–30 and 111–140: the flanking regions of the α Syn amyloid core. A similar disaggregase activity has been observed for the Lipocalin-type Prostaglandin D synthase (L-PGDS) and A β ₄₀ fibrils (Kannaian et al., 2019). L-PGDS binds to the central region of the A β ₄₀ sequence (G25–G29). As this sequence forms a bend connecting two β -strands (Petkova et al., 2002) it is part of the structured fibril core (**Figure 3C**), yet is solvent accessible. L-PGDS fulfils its chaperone activity without ATP consumption or any co-chaperones. Also, the protease HTRA1^{S328A} can act as a chaperone and disassemble pre-formed 4R Tau filaments (Poepsel et al., 2015). Such observations may provide exciting new strategies to reduce the fibril load in amyloid diseases involving intracellular amyloid deposition.

Interaction With RNA

Several amyloidogenic proteins and prions have been identified in the context of RNA-modulating functions (Nizhnikov et al., 2016). Usually, as in the case of TDP-43, the native monomeric protein is involved in binding the RNA (see above). However, fibrils can also interact with RNA, as shown for the functional amyloid CPEB, that is involved in long term memory formation (Keleman et al., 2007; Majumdar et al., 2012; Khan et al., 2015). A study on the *Drosophila melanogaster* CPEB homolog, Orb2B, demonstrated that RNA binding to the monomeric protein represses protein translation of some genes, whilst binding to oligomeric states and fibrils activates protein production by stabilizing and elongating the poly(A) tail of mRNA in neurons in complex with other proteins (e.g., CG4612) (Khan et al., 2015; Hervas et al., 2020; **Figure 5F**). Translation activation changes the synthesis of specific synaptic proteins involved in memory formation. A high resolution cryoEM fibril structure demonstrated that only a small part of the Orb2 sequence (residues 176–206) forms the fibril core (**Figure 3F**). The RNA-recognition motif and protein interaction domain are located in the long flanking regions of this 704 residue protein (Hervas et al., 2020).

DISCUSSION

In this review we have discussed the roles of regions that flank the APR sequences in monomeric amyloid precursors, and the role of the dynamically disordered regions that flank the structured core of amyloid fibrils in the interaction with other molecules

and how this impacts cellular (dys)function. The importance of APRs is well recognized and their prediction using various computational tools is now straightforward. How the sequences that flank the APRs affect the kinetics and mechanisms of fibril growth, the structures of fibrils that ultimately form, and the extent and chemical identity of the dynamically disordered “fuzzy coat” regions of fibrils is still not well understood. This understanding is important as flanking regions play vital roles in the formation and interaction of amyloid with the cell and hence in disease.

In several native amyloid precursors, whether initially disordered or structured, regions surrounding the APRs or aggregation hotspot have been shown to be crucial for modulating amyloid formation. Intrinsic interactions in IDPs, including the APR flanking regions, can either promote or disfavor aggregation, by altering the conformational landscape of the IDP and “switching” amyloid formation on or off, as clearly shown for α Syn, A β , and Tau (Elbaum-Garfinkle and Rhoades, 2012; Stephens et al., 2019; Doherty et al., 2020). Also, for initially natively folded proteins, such as β 2m, regions that flank the APRs often stabilize the native conformation. Mutations or truncations in these regions can consequently release the aggregation potential of the APR by locally destabilizing the protein fold leading to fibril formation (Langenberg et al., 2020). Advanced biophysical methods, such as NMR PRE experiments and single molecule FRET analysis can be used to identify transient long-range interactions in IDPs and IDRs in all-residue, if not all-atom, detail. Complemented by molecular dynamics simulations and experiments using deletion or substitution variants, these approaches have helped to identify the role of these “master controller” (Doherty et al., 2020) motifs for amyloid formation and provide targets to develop new strategies to combat amyloid formation and disease (Mirecka et al., 2014; Agerschou et al., 2019; Chen et al., 2019).

In addition to homotypic intra- and inter-molecular events, interactions with other molecules can be vital for amyloid function and pathology. Determining the interaction site of an amyloidogenic protein, or an amyloid fibril, with other molecules can be challenging, given the dynamic nature of the proteins involved. However, NMR experiments using PREs or chemical shifts, or binding assays with deletion variants can enable the identification of the residues that are involved in these binding processes. Such experiments can be used to clarify whether the aggregation hotspot or its flanking regions are required for the interaction, and potentially provide an evolutionary explanation for the development of such high-risk sequences.

Proteins undergo dramatic conformational changes on the pathway from initial precursor to amyloid states. More focus on these structural changes and which parts of the protein sequence drive these transformations might further demonstrate a crucial role of flanking regions in the amyloid cascade. Flanking regions of the fibril core are relatively straightforward to identify (e.g., using HX or protease protection experiments) but are especially hard to analyze structurally since their dynamic properties displayed on a static high molecular weight fibrillar particle provide significant experimental and computational challenges.

All high-resolution structural information on amyloid fibrils formed from intact proteins [rather than short peptides and peptide fragments (Guenther et al., 2018; Rodriguez et al., 2015)] has been gained using ssNMR or cryoEM (Fitzpatrick and Saibil, 2019; Gallardo et al., 2020b; Guerrero-Ferreira et al., 2020; Scheres et al., 2020). These techniques, however, cannot provide atomic resolution information about the structure of the flexible regions which can comprise the large majority of the protein sequence in some amyloid states (Figure 3; Gallardo et al., 2020b). Nevertheless, some studies have shown the importance of the amyloid “fuzzy coat” for interactions with other amyloid precursors, cellular membranes, RNA and chaperones (Figures 4, 5). Assays with protease-treated fibrils, where the “fuzzy coat” is shaved off, would allow a better understanding of which part of the fibril is involved in the binding process and how the cellular consequences of fibril formation depend on the dynamically disordered regions displayed on the cross- β amyloid fold.

Fibril polymorphism has been shown to be responsible for the development of different diseases caused by the same protein [e.g., α Syn causing Parkinson’s disease or Multiple System Atrophy or Dementia with Lewy Bodies (Shahnawaz et al., 2020) or Tau causing Alzheimer’s disease, Pick’s disease, chronic traumatic encephalitis, and corticobasal degeneration (Fitzpatrick et al., 2017; Falcon et al., 2018; Scheres et al., 2020)]. Polymorphs, so far, have been defined by a fibril possessing a different core: but the flanking regions to the core could also be different in fibrils with the same (or similar) core structures. This adds a further, currently unexplored, dimension to amyloid polymorphism and its consequences for disease, since the dynamically disordered regions could have different interactions with cellular components (Wegmann et al., 2013). A more detailed analysis of the extent of conformational fluctuation of these amyloid flanking regions, for instance using EPR, cross-linking, or other techniques able to tackle dynamic heterogeneity, in the future might reveal “polymorphism” in the “fuzzy coat” and how this is related to the development of disease.

It should not be forgotten that flanking regions can have very different lengths. In the case of $A\beta_{40/42}$, (nearly) the whole protein forms the fibril core (Figure 3C) (Lu et al., 2013; Gremer et al., 2017), whilst in other proteins, e.g., Orb2, flanking regions >500 residues in length are observed (Figure 3F; Hervas et al., 2020). Tompa (2009)

hypothesized that the longer the dynamically disordered region, the more likely it can interact with other molecules by a “fly fishing mechanism.” This might explain why functional amyloid fibrils such as Orb2 have long flanking regions able to interact with other proteins, RNA or surfaces, whilst pathological amyloid fibrils, the sequences of which have not evolved for functional reasons, may present shorter flanking regions.

CONCLUSION

In summary, this review highlights the crucial role of regions that flank the APRs in amyloidogenic protein sequences and the dynamic regions that flank the amyloid fibril core for function, fibril formation and cellular dysfunction for a few example proteins. While beautiful fibril structures are now emerging from cryoEM and ssNMR studies, the often poorly visible, but functionally important flanking regions must not be forgotten. Focusing more on these regions with a broad range of biophysical and cellular techniques might help to gain a better understanding of the molecular mechanism of fibril formation and to identify new targets for drug development that do not involve the ordered amyloid core and the aggregation hotspots.

AUTHOR CONTRIBUTIONS

SMU, DJB, and SER wrote the manuscript. All authors contributed to the article and approved the submitted version.

FUNDING

We acknowledge, with thanks, funding from the Wellcome Trust [SU (215062/Z/18/Z) and SR (204963)].

ACKNOWLEDGMENTS

We thank members of the Radford and Brockwell Amyloid group and our collaborators for many helpful and stimulating discussions. We are also grateful to David Klebl for critically reading this review and providing many helpful comments.

REFERENCES

- Adachi, E., Kosaka, A., Tsuji, K., Mizuguchi, C., Kawashima, H., Shigenaga, A., et al. (2014). The extreme N-terminal region of human apolipoprotein A-I has a strong propensity to form amyloid fibrils. *FEBS Lett.* 588, 389–394. doi: 10.1016/j.febslet.2013.11.031
- Afroz, T., Hock, E.-M., Ernst, P., Foglieni, C., Jambeau, M., Gillespie, L. A., et al. (2017). Functional and dynamic polymerization of the ALS-linked protein TDP-43 antagonizes its pathologic aggregation. *Nat. Commun.* 8, 1–15. doi: 10.1038/s41467-017-00062-0
- Agerschou, E. D., Flagmeier, P., Saridakis, T., Galvagnion, C., Komnig, D., Heid, L., et al. (2019). An engineered monomer binding-protein for α -synuclein efficiently inhibits the proliferation of amyloid fibrils. *eLife* 8:e46112. doi: 10.7554/eLife.46112
- Alberti, S., Gladfelter, A., and Mittag, T. (2019). Considerations and challenges in studying liquid-liquid phase separation and biomolecular condensates. *Cell* 176, 419–434. doi: 10.1016/j.cell.2018.12.035
- Alim, M. A., Ma, Q.-L., Takeda, K., Aizawa, T., Matsubara, M., Nakamura, M., et al. (2004). Demonstration of a role for α -synuclein as a functional microtubule-associated protein. *J. Alzheimer’s Dis.* 6, 435–442. doi: 10.3233/JAD-2004-6412
- Aulić, S., Masperone, L., Narkiewicz, J., Isopi, E., Bistaffa, E., Ambrosetti, E., et al. (2017). α -Synuclein amyloids hijack prion protein to gain cell entry, facilitate cell-to-cell spreading and block prion replication. *Sci. Rep.* 7, 1–12. doi: 10.1038/s41598-017-10236-x

- Ayala, Y. M., De Conti, L., Avendaño-Vázquez, S. E., Dhir, A., Romano, M., D'ambrogio, A., et al. (2011). TDP-43 regulates its mRNA levels through a negative feedback loop. *EMBO J.* 30, 277–288. doi: 10.1038/emboj.2010.310
- Baldwin, A. J., Knowles, T. P., Tartaglia, G. G., Fitzpatrick, A. W., Devlin, G. L., Shammas, S. L., et al. (2011). Metastability of native proteins and the phenomenon of amyloid formation. *J. Am. Chem. Soc.* 133, 14160–14163. doi: 10.1021/ja2017703
- Barbier, P., Zejneli, O., Martinho, M., Lasorsa, A., Belle, V., Smet-Nocca, C., et al. (2019). Role of Tau as a microtubule associated protein: structural and functional aspects. *Front. Aging Neurosci.* 11:204. doi: 10.3389/fnagi.2019.00204
- Bäuerlein, F. J., Saha, I., Mishra, A., Kalemánov, M., Martínez-Sánchez, A., Klein, R., et al. (2017). In situ architecture and cellular interactions of PolyQ inclusions. *Cell* 171, 179–187. doi: 10.1016/j.cell.2017.08.009
- Benilova, I., Gallardo, R., Ungureanu, A.-A., Cano, V. C., Snellinx, A., Ramakers, M., et al. (2014). The Alzheimer disease protective mutation A2T modulates kinetic and thermodynamic properties of amyloid- β (A β) aggregation. *J. Biol. Chem.* 289, 30977–30989. doi: 10.1074/jbc.M114.599027
- Benson, M. D., Buxbaum, J. N., Eisenberg, D. S., Merlini, G., Saraiva, M. J., Sekijima, Y., et al. (in press). Amyloid nomenclature 2020: update and recommendations by the international society of amyloidosis (ISA) nomenclature committee. *Amyloid* 1–6. doi: 10.1080/13506129.2020.1835263
- Berezovsky, I. N., Zeldovich, K. B., and Shakhnovich, E. I. (2007). Positive and negative design in stability and thermal adaptation of natural proteins. *PLoS Comput. Biol.* 3:e52. doi: 10.1371/journal.pcbi.0030052
- Bhattacharya, M., and Mukhopadhyay, S. (2016). “Studying protein misfolding and aggregation by fluorescence spectroscopy,” in *Reviews in Fluorescence 2015*, ed. C. Geddes (Cham: Springer), 1–27. doi: 10.1007/978-3-319-24609-3_1
- Boyko, S., Qi, X., Chen, T.-H., Surewicz, K., and Surewicz, W. K. (2019). Liquid–liquid phase separation of tau protein: the crucial role of electrostatic interactions. *J. Biol. Chem.* 294, 11054–11059. doi: 10.1074/jbc.AC119.009198
- Brahmachari, S., Ge, P., Lee, S. H., Kim, D., Karuppagounder, S. S., Kumar, M., et al. (2016). Activation of tyrosine kinase c-Abl contributes to α -synuclein-induced neurodegeneration. *J. Clin. Invest.* 126, 2970–2988. doi: 10.1172/JCI85456
- Brandt, R., Léger, J., and Lee, G. (1995). Interaction of tau with the neural plasma membrane mediated by tau's amino-terminal projection domain. *J. Cell Biol.* 131, 1327–1340. doi: 10.1083/jcb.131.5.1327
- Brender, J. R., Lee, E. L., Cavitt, M. A., Gafni, A., Steel, D. G., and Ramamoorthy, A. (2008). Amyloid fiber formation and membrane disruption are separate processes localized in two distinct regions of IAPP, the type-2 diabetes-related peptide. *J. Am. Chem. Soc.* 130, 6424–6429. doi: 10.1021/ja710484d
- Buell, A. K. (2017). The nucleation of protein aggregates—from crystals to amyloid fibrils. *Int. Rev. Cell Mol. Biol.* 329, 187–226. doi: 10.1016/bbs.ircmb.2016.08.014
- Burmán, B. M., Gerez, J. A., Matečko-Burmann, I., Campioni, S., Kumari, P., Ghosh, D., et al. (2020). Regulation of α -synuclein by chaperones in mammalian cells. *Nature* 577, 127–132. doi: 10.1038/s41586-019-1808-9
- Cao, Q., Boyer, D. R., Sawaya, M. R., Ge, P., and Eisenberg, D. S. (2019). Cryo-EM structures of four polymorphic TDP-43 amyloid cores. *Nat. Struct. Mol. Biol.* 26, 619–627. doi: 10.1038/s41594-019-0248-4
- Cao, Q., Boyer, D. R., Sawaya, M. R., Ge, P., and Eisenberg, D. S. (2020). Cryo-EM structure and inhibitor design of human IAPP (amylin) fibrils. *Nat. Struct. Mol. Biol.* 27, 653–659. doi: 10.1038/s41594-020-0435-3
- Cartelli, D., Aliverti, A., Barbiroli, A., Santambrogio, C., Ragg, E. M., Casagrande, F. V., et al. (2016). α -Synuclein is a novel microtubule dynamase. *Sci. Rep.* 6, 1–13. doi: 10.1038/srep33289
- Chen, D., Drombosky, K. W., Hou, Z., Sari, L., Kashmer, O. M., Ryder, B. D., et al. (2019). Tau local structure shields an amyloid-forming motif and controls aggregation propensity. *Nat. Commun.* 10, 1–14. doi: 10.1038/s41467-019-10355-1
- Chen, L., Jin, J., Davis, J., Zhou, Y., Wang, Y., Liu, J., et al. (2007). Oligomeric α -synuclein inhibits tubulin polymerization. *Biochem. Biophys. Res. Commun.* 356, 548–553. doi: 10.1016/j.bbrc.2007.02.163
- Chiti, F., De Lorenzi, E., Grossi, S., Mangione, P., Giorgetti, S., Caccialanza, G., et al. (2001). A partially structured species of β 2-microglobulin is significantly populated under physiological conditions and involved in fibrillogenesis. *J. Biol. Chem.* 276, 46714–46721. doi: 10.1074/jbc.M107040200
- Cho, M. K., Kim, H. Y., Fernandez, C. O., Becker, S., and Zweckstetter, M. (2011). Conserved core of amyloid fibrils of wild type and A30P mutant α -synuclein. *Protein Sci.* 20, 387–395. doi: 10.1002/pro.570
- Cholak, E., Bugge, K., Khondker, A., Gauger, K., Pedraz-Cuesta, E., Pedersen, M. E., et al. (2020). Avidity within the N-terminal anchor drives α -synuclein membrane interaction and insertion. *FEBS J.* 34, 7462–7482. doi: 10.1096/fj.202000107R
- Close, W., Neumann, M., Schmidt, A., Hora, M., Annamalai, K., Schmidt, M., et al. (2018). Physical basis of amyloid fibril polymorphism. *Nat. Commun.* 9, 1–7. doi: 10.1038/s41467-018-03164-5
- Coletta, A., Pinney, J. W., Solís, D. Y. W., Marsh, J., Pettifer, S. R., and Attwood, T. K. (2010). Low-complexity regions within protein sequences have position-dependent roles. *BMC Syst. Biol.* 4:43. doi: 10.1186/1752-0509-4-43
- Colom-Cadena, M., Gelpi, E., Charif, S., Belbin, O., Blesa, R., Martí, M. J., et al. (2013). Confluence of α -synuclein, tau, and β -amyloid pathologies in dementia with Lewy bodies. *J. Neuropathol. Exp. Neurol.* 72, 1203–1212. doi: 10.1097/NEN.0000000000000018
- Colvin, M. T., Silvers, R., Ni, Q. Z., Can, T. V., Sergeyev, I., Rosay, M., et al. (2016). Atomic resolution structure of monomeric A β 42 amyloid fibrils. *J. Am. Chem. Soc.* 138, 9663–9674. doi: 10.1021/jacs.6b05129
- Conicella, A. E., Zerze, G. H., Mittal, J., and Fawzi, N. L. (2016). ALS mutations disrupt phase separation mediated by α -helical structure in the TDP-43 low-complexity C-terminal domain. *Structure* 24, 1537–1549. doi: 10.1016/j.str.2016.07.007
- Cox, D., Whiten, D. R., Brown, J. W., Horrocks, M. H., San Gil, R., Dobson, C. M., et al. (2018). The small heat shock protein Hsp27 binds α -synuclein fibrils, preventing elongation and cytotoxicity. *J. Biol. Chem.* 293, 4486–4497. doi: 10.1074/jbc.M117.813865
- Das, M., Wilson, C. J., Mei, X., Wales, T. E., Engen, J. R., and Gursky, O. (2016). Structural stability and local dynamics in disease-causing mutants of human apolipoprotein AI: what makes the protein amyloidogenic? *J. Mol. Biol.* 428, 449–462. doi: 10.1016/j.jmb.2015.10.029
- Dasari, A. K., Kaye, R., Wi, S., and Lim, K. H. (2019). Tau interacts with the C-terminal region of α -synuclein, promoting formation of toxic aggregates with distinct molecular conformations. *Biochemistry* 58, 2814–2821. doi: 10.1021/acs.biochem.9b00215
- de Oliveira, G. A., Cordeiro, Y., Silva, J. L., and Vieira, T. C. (2019). Liquid–liquid phase transitions and amyloid aggregation in proteins related to cancer and neurodegenerative diseases. *Adv. Protein Chem. Struct. Biol.* 118, 289–331. doi: 10.1016/bbs.apcsb.2019.08.002
- Diao, J., Burré, J., Vivona, S., Cipriano, D. J., Sharma, M., Kyoung, M., et al. (2013). Native α -synuclein induces clustering of synaptic-vesicle mimics via binding to phospholipids and synaptobrevin-2/VAMP2. *eLife* 2:e00592. doi: 10.7554/eLife.00592
- Doherty, C. P., Ullamec, S. M., Maya-Martinez, R., Good, S. C., Makepeace, J., Khan, G. N., et al. (2020). A short motif in the N-terminal region of α -synuclein is critical for both aggregation and function. *Nat. Struct. Mol. Biol.* 27, 249–259. doi: 10.1038/s41594-020-0384-x
- Dunker, A. K., Romero, P., Obradovic, Z., Garner, E. C., and Brown, C. J. (2000). Intrinsic protein disorder in complete genomes. *Genome Inform.* 11, 161–171. doi: 10.11234/gi1990.11.161
- Ebo, J. S., Guthertz, N., Radford, S. E., and Brockwell, D. J. (2020). Using protein engineering to understand and modulate aggregation. *Curr. Opin. Struct. Biol.* 60, 157–166. doi: 10.1016/j.sbi.2020.01.005
- Ehrnhoefer, D. E., Sutton, L., and Hayden, M. R. (2011). Small changes, big impact: posttranslational modifications and function of huntingtin in Huntington disease. *Neuroscientist* 17, 475–492. doi: 10.1177/1073858410390378
- Eichner, T., Kalverda, A. P., Thompson, G. S., Homans, S. W., and Radford, S. E. (2011). Conformational conversion during amyloid formation at atomic resolution. *Mol. Cell* 41, 161–172. doi: 10.1016/j.molcel.2010.11.028
- Eisenberg, D. S., and Sawaya, M. R. (2017). Structural studies of amyloid proteins at the molecular level. *Annu. Rev. Biochem.* 86, 69–95. doi: 10.1146/annurev-biochem-061516-045104

- Elbaum-Garfinkle, S. (2019). Matter over mind: liquid phase separation and neurodegeneration. *J. Biol. Chem.* 294, 7160–7168. doi: 10.1074/jbc.REV118.001188
- Elbaum-Garfinkle, S., Ramlall, T., and Rhoades, E. (2010). The role of the lipid bilayer in tau aggregation. *Biophys. J.* 98, 2722–2730. doi: 10.1016/j.bpj.2010.03.013
- Elbaum-Garfinkle, S., and Rhoades, E. (2012). Identification of an aggregation-prone structure of tau. *J. Am. Chem. Soc.* 134, 16607–16613. doi: 10.1021/ja305206m
- Ellisdon, A. M., Thomas, B., and Bottomley, S. P. (2006). The two-stage pathway of ataxin-3 fibrillogenesis involves a polyglutamine-independent step. *J. Biol. Chem.* 281, 16888–16896. doi: 10.1074/jbc.M601470200
- Emamzadeh, F. N. (2016). Alpha-synuclein structure, functions, and interactions. *J. Res. Med. Sci.* 21:29. doi: 10.4103/1735-1995.181989
- Emmanouilidou, E., Melachroinou, K., Roumeliotis, T., Garbis, S. D., Ntzouni, M., Margaritis, L. H., et al. (2010). Cell-produced α -synuclein is secreted in a calcium-dependent manner by exosomes and impacts neuronal survival. *J. Neurosci.* 30, 6838–6851. doi: 10.1523/JNEUROSCI.5699-09.2010
- Engel, M. F., Khemtémourian, L., Kleijer, C. C., Meeldijk, H. J., Jacobs, J., Verkleij, A. J., et al. (2008). Membrane damage by human islet amyloid polypeptide through fibril growth at the membrane. *Proc. Natl. Acad. Sci. U.S.A.* 105, 6033–6038. doi: 10.1073/pnas.0708354105
- Esposito, G., Garvey, M., Alverdi, V., Pettitrossi, F., Corazza, A., Fogolari, F., et al. (2013). Monitoring the interaction between β 2-Microglobulin and the molecular chaperone α B-crystallin by NMR and mass spectrometry α B-crystallin dissociates β 2-microglobulin oligomers. *J. Biol. Chem.* 288, 17844–17858. doi: 10.1074/jbc.M112.448639
- Esposito, G., Michelutti, R., Verdone, G., Viglino, P., Hernandez, H., Robinson, C., et al. (2000). Removal of the N-terminal hexapeptide from human β 2-microglobulin facilitates protein aggregation and fibril formation. *Protein Sci.* 9, 831–845. doi: 10.1110/ps.9.5.831
- Falcon, B., Zhang, W., Murzin, A. G., Murshudov, G., Garringer, H. J., Vidal, R., et al. (2018). Structures of filaments from Pick's disease reveal a novel tau protein fold. *Nature* 561, 137–140. doi: 10.1038/s41586-018-0454-y
- Falsone, S. F., Meyer, N. H., Schrank, E., Leitinger, G., Pham, C. L., Fodero-Tavoletti, M. T., et al. (2012). SERF protein is a direct modifier of amyloid fiber assembly. *Cell Reports* 2, 358–371. doi: 10.1016/j.celrep.2012.06.012
- Fändrich, M. (2012). Oligomeric intermediates in amyloid formation: structure determination and mechanisms of toxicity. *J. Mol. Biol.* 421, 427–440. doi: 10.1016/j.jmb.2012.01.006
- Faridi, A., Sun, Y., Okazaki, Y., Peng, G., Gao, J., Kakinien, A., et al. (2018). Mitigating human IAPP amyloidogenesis in vivo with chiral silica nanoribbons. *Small* 14:1802825. doi: 10.1002/smll.201802825
- Fernandez-Escamilla, A.-M., Rousseau, F., Schymkowitz, J., and Serrano, L. (2004). Prediction of sequence-dependent and mutational effects on the aggregation of peptides and proteins. *Nat. Biotechnol.* 22, 1302–1306. doi: 10.1038/nbt1012
- Ferrari, L., Stucchi, R., Konstantoulea, K., van de Kamp, G., Kos, R., Geerts, W. J., et al. (2020). Arginine π -stacking drives binding to fibrils of the Alzheimer protein Tau. *Nat. Commun.* 11, 1–13. doi: 10.1038/s41467-019-13745-7
- Fitzpatrick, A. W., Falcon, B., He, S., Murzin, A. G., Murshudov, G., Garringer, H. J., et al. (2017). Cryo-EM structures of tau filaments from Alzheimer's disease. *Nature* 547, 185–190. doi: 10.1038/nature23002
- Fitzpatrick, A. W., and Saibil, H. R. (2019). Cryo-EM of amyloid fibrils and cellular aggregates. *Curr. Opin. Struct. Biol.* 58, 34–42. doi: 10.1016/j.sbi.2019.05.003
- Franzmann, T. M., Jahnel, M., Pozniakovsky, A., Mahamid, J., Holehouse, A. S., Nüsse, E., et al. (2018). Phase separation of a yeast prion protein promotes cellular fitness. *Science* 359:eaao5654. doi: 10.1126/science.aao5654
- Fusco, G., Chen, S. W., Williamson, P. T., Cascella, R., Perni, M., Jarvis, J. A., et al. (2017). Structural basis of membrane disruption and cellular toxicity by α -synuclein oligomers. *Science* 358, 1440–1443. doi: 10.1126/science.aan6160
- Fusco, G., De Simone, A., Gopinath, T., Vostrikov, V., Vendruscolo, M., Dobson, C. M., et al. (2014). Direct observation of the three regions in α -synuclein that determine its membrane-bound behaviour. *Nat. Commun.* 5, 1–8. doi: 10.1038/ncomms4827
- Fusco, G., Pape, T., Stephens, A. D., Mahou, P., Costa, A. R., Kaminski, C. F., et al. (2016). Structural basis of synaptic vesicle assembly promoted by α -synuclein. *Nat. Commun.* 7, 1–12. doi: 10.1038/ncomms12563
- Gales, L., Cortes, L., Almeida, C., Melo, C. V., do Carmo Costa, M., Maciel, P., et al. (2005). Towards a structural understanding of the fibrillization pathway in Machado-Joseph's disease: trapping early oligomers of non-expanded ataxin-3. *J. Mol. Biol.* 353, 642–654. doi: 10.1016/j.jmb.2005.08.061
- Gallardo, R., Iadanza, M. G., Xu, Y., Heath, G. R., Foster, R., Radford, S. E., et al. (2020a). Fibril structures of diabetes-related amylin variants reveal a basis for surface-templated assembly. *Nat. Struct. Mol. Biol.* 27, 1048–1056. doi: 10.1038/s41594-020-0496-3
- Gallardo, R., Ramakers, M., De Smet, F., Claes, F., Khodaparast, L., Khodaparast, L., et al. (2016). De novo design of a biologically active amyloid. *Science* 354:aah4949. doi: 10.1126/science.aah4949
- Gallardo, R., Ranson, N. A., and Radford, S. E. (2020b). Amyloid structures: much more than just a cross- β fold. *Curr. Opin. Struct. Biol.* 60, 7–16. doi: 10.1016/j.sbi.2019.09.001
- Galvagnion, C., Brown, J. W., Ouberaï, M. M., Flagmeier, P., Vendruscolo, M., Buell, A. K., et al. (2016). Chemical properties of lipids strongly affect the kinetics of the membrane-induced aggregation of α -synuclein. *Proc. Natl. Acad. Sci. U.S.A.* 113, 7065–7070. doi: 10.1073/pnas.1601899113
- Galvagnion, C., Buell, A. K., Meisl, G., Michaels, T. C., Vendruscolo, M., Knowles, T. P., et al. (2015). Lipid vesicles trigger α -synuclein aggregation by stimulating primary nucleation. *Nat. Chem. Biol.* 11, 229–234. doi: 10.1038/nchembio.1750
- Ganjam, G. K., Bolte, K., Matschke, L. A., Neitemeier, S., Dolga, A. M., Höllerhage, M., et al. (2019). Mitochondrial damage by α -synuclein causes cell death in human dopaminergic neurons. *Cell Death Dis.* 10, 1–16. doi: 10.1038/s41419-019-2091-2
- Gao, X., Carroni, M., Nussbaum-Krammer, C., Mogk, A., Nillegoda, N. B., Szlachcic, A., et al. (2015). Human Hsp70 disaggregase reverses Parkinson's-linked α -synuclein amyloid fibrils. *Mol. Cell* 59, 781–793. doi: 10.1016/j.molcel.2015.07.012
- Gaspar, R., Meisl, G., Buell, A. K., Young, L., Kaminski, C. F., Knowles, T. P., et al. (2017). Secondary nucleation of monomers on fibril surface dominates α -synuclein aggregation and provides autocatalytic amyloid amplification. *Q. Rev. Biophys.* 50:e6. doi: 10.1017/S0033583516000172
- Gejyo, F., Odani, S., Yamada, T., Honma, N., Saito, H., Suzuki, Y., et al. (1986). β 2-microglobulin: a new form of amyloid protein associated with chronic hemodialysis. *Kidney Int.* 30, 385–390. doi: 10.1038/ki.1986.196
- George, J.-M. (2001). The synucleins. *Genome Biol.* 3:e3002. doi: 10.1186/gb-2001-3-1-reviews3002
- Geraets, J. A., Pothula, K. R., and Schröder, G. F. (2020). Integrating cryo-EM and NMR data. *Curr. Opin. Struct. Biol.* 61, 173–181. doi: 10.1016/j.sbi.2020.01.008
- Giasson, B. I., Murray, I. V., Trojanowski, J. Q., and Lee, V. M.-Y. (2001). A hydrophobic stretch of 12 amino acid residues in the middle of α -synuclein is essential for filament assembly. *J. Biol. Chem.* 276, 2380–2386. doi: 10.1074/jbc.M008919200
- Goldfarb, L. G., Brown, P., McCombie, W. R., Goldgaber, D., Swergold, G. D., Wills, P. R., et al. (1991). Transmissible familial Creutzfeldt-Jakob disease associated with five, seven, and eight extra octapeptide coding repeats in the PRNP gene. *Proc. Natl. Acad. Sci. U.S.A.* 88, 10926–10930. doi: 10.1073/pnas.88.23.10926
- Goodchild, S. C., Sheynis, T., Thompson, R., Tipping, K. W., Xue, W.-F., Ranson, N. A., et al. (2014). β 2-Microglobulin amyloid fibril-induced membrane disruption is enhanced by endosomal lipids and acidic pH. *PLoS One* 9:e104492. doi: 10.1371/journal.pone.0104492
- Goode, B. L., Chau, M., Denis, P. E., and Feinstein, S. C. (2000). Structural and functional differences between 3-repeat and 4-repeat tau isoforms implications for normal tau function and the onset of neurodegenerative disease. *J. Biol. Chem.* 275, 38182–38189. doi: 10.1074/jbc.M007489200
- Gremer, L., Schölzel, D., Schenk, C., Reinartz, E., Labahn, J., Ravelli, R. B., et al. (2017). Fibril structure of amyloid- β (1–42) by cryo-electron microscopy. *Science* 358, 116–119. doi: 10.1126/science.aao2825
- Grey, M., Linse, S., Nilsson, H., Brundin, P., and Sparr, E. (2011). Membrane interaction of α -synuclein in different aggregation states. *J. Parkinsons Dis.* 1, 359–371. doi: 10.3233/JPD-2011-11067
- Guenther, E. L., Cao, Q., Trinh, H., Lu, J., Sawaya, M. R., Cascio, D., et al. (2018). Atomic structures of TDP-43 LCD segments and insights into reversible or pathogenic aggregation. *Nat. Struct. Mol. Biol.* 25, 463–471. doi: 10.1038/s41594-018-0064-2

- Guerrero-Ferreira, R., Kovacic, L., Ni, D., and Stahlberg, H. (2020). New insights on the structure of alpha-synuclein fibrils using cryo-electron microscopy. *Curr. Opin. Neurobiol.* 61, 89–95. doi: 10.1016/j.conb.2020.01.014
- Guerrero-Ferreira, R., Taylor, N. M., Arteni, A.-A., Kumari, P., Mona, D., Ringler, P., et al. (2019). Two new polymorphic structures of human full-length alpha-synuclein fibrils solved by cryo-electron microscopy. *eLife* 8:e48907. doi: 10.7554/eLife.48907
- Guerrero-Ferreira, R., Taylor, N. M., Mona, D., Ringler, P., Lauer, M. E., Riek, R., et al. (2018). Cryo-EM structure of alpha-synuclein fibrils. *eLife* 7:e36402. doi: 10.7554/eLife.36402
- Haj-Yahya, M., Gopinath, P., Rajasekhar, K., Mirbaha, H., Diamond, M. I., and Lashuel, H. A. (2020). Site-specific hyperphosphorylation inhibits, rather than promotes, Tau fibrillization, seeding capacity, and its microtubule binding. *Angew. Chem.* 132, 4088–4096. doi: 10.1002/ange.201913001
- Han, J., Zhang, J., Yao, H., Wang, X., Li, F., Chen, L., et al. (2006). Study on interaction between microtubule associated protein tau and prion protein. *Sci. China Life Sci.* 49, 473–479. doi: 10.1007/s11427-006-2019-9
- Han, J. Y., Choi, T. S., and Kim, H. I. (2018). Molecular role of Ca²⁺ and hard divalent metal cations on accelerated fibrillation and interfibrillar aggregation of α -Synuclein. *Sci. Rep.* 8, 1–11. doi: 10.1038/s41598-018-20320-5
- He, H. J., Wang, X. S., Pan, R., Wang, D. L., Liu, M. N., and He, R. Q. (2009). The proline-rich domain of tau plays a role in interactions with actin. *BMC Cell Biol.* 10:81. doi: 10.1186/1471-2121-10-81
- Herrera, F. E., Chesi, A., Paleologou, K. E., Schmid, A., Munoz, A., Vendruscolo, M., et al. (2008). Inhibition of α -synuclein fibrillization by dopamine is mediated by interactions with five C-terminal residues and with E83 in the NAC region. *PLoS One* 3:e3394. doi: 10.1371/journal.pone.0003394
- Hervas, R., Rau, M. J., Park, Y., Zhang, W., Murzin, A. G., Fitzpatrick, J. A., et al. (2020). Cryo-EM structure of a neuronal functional amyloid implicated in memory persistence in *Drosophila*. *Science* 367, 1230–1234. doi: 10.1126/science.aba3526
- Himmler, A., Drechsel, D., Kirschner, M. W., and Martin, D. (1989). Tau consists of a set of proteins with repeated C-terminal microtubule-binding domains and variable N-terminal domains. *Mol. Cell. Biol.* 9, 1381–1388. doi: 10.1128/MCB.9.4.1381
- Hong, D.-P., Xiong, W., Chang, J.-Y., and Jiang, C. (2011). The role of the C-terminus of human α -synuclein: intra-disulfide bonds between the C-terminus and other regions stabilize non-fibrillar monomeric isomers. *FEBS Lett.* 585, 561–566. doi: 10.1016/j.febslet.2011.01.009
- Hoshino, M., Katou, H., Hagihara, Y., Hasegawa, K., Naiki, H., and Goto, Y. (2002). Mapping the core of the β 2-microglobulin amyloid fibril by H/D exchange. *Nat. Struct. Biol.* 9, 332–336. doi: 10.1038/nsb792
- Hoyer, W., Antony, T., Cherny, D., Heim, G., Jovin, T. M., and Subramaniam, V. (2002). Dependence of α -synuclein aggregate morphology on solution conditions. *J. Mol. Biol.* 322, 383–393. doi: 10.1016/S0022-2836(02)00775-1
- Hoyer, W., Cherny, D., Subramaniam, V., and Jovin, T. M. (2004). Impact of the acidic C-terminal region comprising amino acids 109–140 on α -synuclein aggregation in vitro. *Biochemistry* 43, 16233–16242. doi: 10.1021/bi048453u
- Huang, D.-B., Ainsworth, C. F., Stevens, F. J., and Schiffer, M. (1996). Three quaternary structures for a single protein. *Proc. Natl. Acad. Sci. U.S.A.* 93, 7017–7021. doi: 10.1073/pnas.93.14.7017
- Huang, Y.-C., Lin, K.-F., He, R.-Y., Tu, P.-H., Koubek, J., Hsu, Y.-C., et al. (2013). Inhibition of TDP-43 aggregation by nucleic acid binding. *PLoS One* 8:e64002. doi: 10.1371/journal.pone.0064002
- Iadanza, M. G., Jackson, M. P., Hewitt, E. W., Ranson, N. A., and Radford, S. E. (2018a). A new era for understanding amyloid structures and disease. *Nat. Rev. Mol. Cell Biol.* 19, 755–773. doi: 10.1038/s41580-018-0060-8
- Iadanza, M. G., Silvers, R., Boardman, J., Smith, H. I., Karamanos, T. K., Debelouchina, G. T., et al. (2018b). The structure of a β 2-microglobulin fibril suggests a molecular basis for its amyloid polymorphism. *Nat. Commun.* 9, 1–10. doi: 10.1038/s41467-018-06761-6
- Ignatova, Z., and Gierasch, L. M. (2006). Extended polyglutamine tracts cause aggregation and structural perturbation of an adjacent β barrel protein. *J. Biol. Chem.* 281, 12959–12967. doi: 10.1074/jbc.M511523200
- Ivanova, M. I., Sawaya, M. R., Gingery, M., Attinger, A., and Eisenberg, D. (2004). An amyloid-forming segment of β 2-microglobulin suggests a molecular model for the fibril. *Proc. Natl. Acad. Sci. U.S.A.* 101, 10584–10589. doi: 10.1073/pnas.0403756101
- Jahn, T. R., Parker, M. J., Homans, S. W., and Radford, S. E. (2006). Amyloid formation under physiological conditions proceeds via a native-like folding intermediate. *Nat. Struct. Mol. Biol.* 13, 195–201. doi: 10.1038/nsmb1058
- Janowska, M. K., Wu, K.-P., and Baum, J. (2015). Unveiling transient protein-protein interactions that modulate inhibition of alpha-synuclein aggregation by beta-synuclein, a pre-synaptic protein that co-localizes with alpha-synuclein. *Sci. Rep.* 5, 15164–15174. doi: 10.1038/srep15164
- Johnson, B. S., Snead, D., Lee, J. J., McCaffery, J. M., Shorter, J., and Gitler, A. D. (2009). TDP-43 is intrinsically aggregation-prone, and amyotrophic lateral sclerosis-linked mutations accelerate aggregation and increase toxicity. *J. Biol. Chem.* 284, 20329–20339. doi: 10.1074/jbc.M109.010264
- Jones, D. R., Moussaud, S., and McLean, P. (2014). Targeting heat shock proteins to modulate α -synuclein toxicity. *Ther. Adv. Neurol. Disord.* 7, 33–51. doi: 10.1177/1756285613493469
- Jones, S., Manning, J., Kad, N. M., and Radford, S. E. (2003a). Amyloid-forming peptides from β 2-microglobulin—insights into the mechanism of fibril formation in vitro. *J. Mol. Biol.* 325, 249–257. doi: 10.1016/S0022-2836(02)01227-5
- Jones, S., Smith, D. P., and Radford, S. E. (2003b). Role of the N and C-terminal strands of beta 2-microglobulin in amyloid formation at neutral pH. *J. Mol. Biol.* 330, 935–941. doi: 10.1016/S0022-2836(03)00688-0
- Jonsson, T., Atwal, J. K., Steinberg, S., Snaedal, J., Jonsson, P. V., Bjornsson, S., et al. (2012). A mutation in APP protects against Alzheimer's disease and age-related cognitive decline. *Nature* 488, 96–99. doi: 10.1038/nature11283
- Kannaian, B., Sharma, B., Phillips, M., Chowdhury, A., Manimekalai, M. S., Adav, S. S., et al. (2019). Abundant neuroprotective chaperone Lipocalin-type prostaglandin D synthase (L-PGDS) disassembles the Amyloid- β fibrils. *Sci. Rep.* 9, 1–17. doi: 10.1038/s41598-019-48819-5
- Karamanos, T. K., Jackson, M. P., Calabrese, A. N., Goodchild, S. C., Cawood, E. E., Thompson, G. S., et al. (2019). Structural mapping of oligomeric intermediates in an amyloid assembly pathway. *eLife* 8:e46574. doi: 10.7554/eLife.46574
- Keleman, K., Krüttner, S., Alenius, M., and Dickson, B. J. (2007). Function of the *Drosophila* CPEB protein Orb2 in long-term courtship memory. *Nat. Neurosci.* 10, 1587–1593. doi: 10.1038/nn1996
- Kelley, N. W., Huang, X., Tam, S., Spiess, C., Frydman, J., and Pande, V. S. (2009). The predicted structure of the headpiece of the Huntingtin protein and its implications on Huntingtin aggregation. *J. Mol. Biol.* 388, 919–927. doi: 10.1016/j.jmb.2009.01.032
- Kelly, J. W., and Lansbury, P. T. (1994). A chemical approach to elucidate mechanism of transthyretin and β -protein amyloid fibril formation. *Amyloid* 1, 186–205. doi: 10.3109/13506129409148451
- Kendrew, J. C., Dickerson, R. E., Strandberg, B. E., Hart, R. G., Davies, D. R., Phillips, D. C., et al. (1960). Structure of myoglobin: a three-dimensional Fourier synthesis at 2 Å resolution. *Nature* 185, 422–427.
- Kessler, J. C., Rochet, J.-C., and Lansbury, P. T. (2003). The N-terminal repeat domain of α -synuclein inhibits β -sheet and amyloid fibril formation. *Biochemistry* 42, 672–678. doi: 10.1021/bi020429y
- Khan, M. R., Li, L., Pérez-Sánchez, C., Saraf, A., Florens, L., Slaughter, B. D., et al. (2015). Amyloidogenic oligomerization transforms *Drosophila* Orb2 from a translation repressor to an activator. *Cell* 163, 1468–1483. doi: 10.1016/j.cell.2015.11.020
- Khodaparast, L., Khodaparast, L., Gallardo, R., Louros, N. N., Michiels, E., Ramakrishnan, R., et al. (2018). Aggregating sequences that occur in many proteins constitute weak spots of bacterial proteostasis. *Nat. Commun.* 9, 1–15. doi: 10.1038/s41467-018-03131-0
- Kollmer, M., Close, W., Funk, L., Rasmussen, J., Bsoul, A., Schierhorn, A., et al. (2019). Cryo-EM structure and polymorphism of A β amyloid fibrils purified from Alzheimer's brain tissue. *Nat. Commun.* 10, 1–8. doi: 10.1038/s41467-019-12683-8
- Kosik, K. S., Orecchio, L. D., Bakalis, S., and Neve, R. L. (1989). Developmentally regulated expression of specific tau sequences. *Neuron* 2, 1389–1397. doi: 10.1016/0896-6273(89)90077-9
- Krishnan, R., and Lindquist, S. L. (2005). Structural insights into a yeast prion illuminate nucleation and strain diversity. *Nature* 435, 765–772. doi: 10.1038/nature03679

- Krüttner, S., Stepien, B., Noordermeer, J. N., Mommaas, M. A., Mechtler, K., Dickson, B. J., et al. (2012). Drosophila CPEB Orb2A mediates memory independent of its RNA-binding domain. *Neuron* 76, 383–395. doi: 10.1016/j.neuron.2012.08.028
- Kuo, P.-H., Chiang, C.-H., Wang, Y.-T., Doudeva, L. G., and Yuan, H. S. (2014). The crystal structure of TDP-43 RRM1-DNA complex reveals the specific recognition for UG- and TG-rich nucleic acids. *Nucleic Acids Res.* 42, 4712–4722. doi: 10.1093/nar/gkt1407
- Kushnirov, V. V., Dergalev, A. A., and Alexandrov, A. I. (2020). Proteinase K resistant cores of prions and amyloids. *Prion* 14, 11–19. doi: 10.1080/19336896.2019.1704612
- Langenberg, T., Gallardo, R., van der Kant, R., Louros, N., Michiels, E., Duran-Romana, R., et al. (2020). Thermodynamic and evolutionary coupling between the native and amyloid state of globular proteins. *Cell Reports* 31, 107512–107534. doi: 10.1016/j.celrep.2020.03.076
- Lashuel, H. A., Wurth, C., Woo, L., and Kelly, J. W. (1999). The most pathogenic transthyretin variant, L55P, forms amyloid fibrils under acidic conditions and protofibrils under physiological conditions. *Biochemistry* 38, 13560–13573. doi: 10.1021/bi991021c
- Laurén, J., Gimbel, D. A., Nygaard, H. B., Gilbert, J. W., and Strittmatter, S. M. (2009). Cellular prion protein mediates impairment of synaptic plasticity by amyloid- β oligomers. *Nature* 457, 1128–1132. doi: 10.1038/nature07761
- Lee, F. J., Liu, F., Pristupa, Z. B., and Niznik, H. B. (2001). Direct binding and functional coupling of α -synuclein to the dopamine transporters accelerate dopamine-induced apoptosis. *FEBS J.* 15, 916–926. doi: 10.1096/fsb2f000334com
- Li, B., Ge, P., Murray, K. A., Sheth, P., Zhang, M., Nair, G., et al. (2018). Cryo-EM of full-length α -synuclein reveals fibril polymorphs with a common structural kernel. *Nat. Commun.* 9, 1–10. doi: 10.1038/s41467-018-05971-2
- Li, H.-R., Chiang, W.-C., Chou, P.-C., Wang, W.-J., and Huang, J.-R. (2018). TAR DNA-binding protein 43 (TDP-43) liquid–liquid phase separation is mediated by just a few aromatic residues. *J. Biol. Chem.* 293, 6090–6098. doi: 10.1074/jbc.AC117.001037
- Li, X., Zhang, X., Ladiwala, A. R. A., Du, D., Yadav, J. K., Tessier, P. M., et al. (2013). Mechanisms of transthyretin inhibition of β -amyloid aggregation in vitro. *J. Neurosci.* 33, 19423–19433. doi: 10.1523/JNEUROSCI.2561-13.2013
- Li, Y., Zhao, C., Luo, F., Liu, Z., Gui, X., Luo, Z., et al. (2018). Amyloid fibril structure of α -synuclein determined by cryo-electron microscopy. *Cell Res.* 28, 897–903. doi: 10.1038/s41422-018-0075-x
- Linse, S. (2017). Monomer-dependent secondary nucleation in amyloid formation. *Biophys. Rev.* 9, 329–338. doi: 10.1007/s12551-017-0289-z
- Linse, S., Cabaleiro-Lago, C., Xue, W.-F., Lynch, I., Lindman, S., Thulin, E., et al. (2007). Nucleation of protein fibrillation by nanoparticles. *Proc. Natl. Acad. Sci. U.S.A.* 104, 8691–8696. doi: 10.1073/pnas.0701250104
- Liu, F., Li, B., Tung, E. J., Grundke-Iqbal, I., Iqbal, K., and Gong, C. X. (2007). Site-specific effects of tau phosphorylation on its microtubule assembly activity and self-aggregation. *Eur. J. Neurosci.* 26, 3429–3436. doi: 10.1111/j.1460-9568.2007.05955.x
- Longhena, F., Faustini, G., Missale, C., Pizzi, M., Spano, P., and Bellucci, A. (2017). The contribution of α -synuclein spreading to Parkinson's disease synaptopathy. *Neural Plast.* 2017, 1–15. doi: 10.1155/2017/5012129
- Lu, J., Zhang, S., Ma, X., Jia, C., Liu, Z., Huang, C., et al. (2020). Structural basis of the interplay between α -synuclein and Tau in regulating pathological amyloid aggregation. *J. Biol. Chem.* 295, 7470–7480. doi: 10.1074/jbc.RA119.012284
- Lu, J.-X., Qiang, W., Yau, W.-M., Schwieters, C. D., Meredith, S. C., and Tycko, R. (2013). Molecular structure of β -amyloid fibrils in Alzheimer's disease brain tissue. *Cell* 154, 1257–1268. doi: 10.1016/j.cell.2013.08.035
- Lukavsky, P. J., Daujotyte, D., Tollervey, J. R., Ule, J., Stuani, C., Buratti, E., et al. (2013). Molecular basis of UG-rich RNA recognition by the human splicing factor TDP-43. *Nat. Struct. Mol. Biol.* 20, 1443–1449. doi: 10.1038/nsmb.2698
- Luo, J., Wärmländer, S. K., Gräslund, A., and Abrahams, J. P. (2016). Cross-interactions between the Alzheimer disease amyloid- β peptide and other amyloid proteins: a further aspect of the amyloid cascade hypothesis. *J. Biol. Chem.* 291, 16485–16493. doi: 10.1074/jbc.R116.714576
- Lyke, D. R., Dorweiler, J. E., and Manogaran, A. L. (2019). The three faces of Sup35. *Yeast* 36, 465–472. doi: 10.1002/yea.3392
- Majumdar, A., Cesario, W. C., White-Grindley, E., Jiang, H., Ren, F., Li, L., et al. (2012). Critical role of amyloid-like oligomers of Drosophila Orb2 in the persistence of memory. *Cell* 148, 515–529. doi: 10.1016/j.cell.2012.01.004
- Martin, E. M., Jackson, M. P., Gamberdinger, M., Gense, K., Karamonos, T. K., Humes, J. R., et al. (2018). Conformational flexibility within the nascent polypeptide-associated complex enables its interactions with structurally diverse client proteins. *J. Biol. Chem.* 293, 8554–8568. doi: 10.1074/jbc.RA117.001568
- Martins, I. C., Kuperstein, I., Wilkinson, H., Maes, E., Vanbrabant, M., Jonckheere, W., et al. (2008). Lipids revert inert A β amyloid fibrils to neurotoxic protofibrils that affect learning in mice. *EMBO J.* 27, 224–233. doi: 10.1038/sj.emboj.7601953
- McDonald, K. K., Aulas, A., Destroismaisons, L., Pickles, S., Bealec, E., Camu, W., et al. (2011). TAR DNA-binding protein 43 (TDP-43) regulates stress granule dynamics via differential regulation of G3BP and TIA-1. *Hum. Mol. Genet.* 20, 1400–1410. doi: 10.1093/hmg/ddr021
- McKibben, K. M., and Rhoades, E. (2019). Independent tubulin binding and polymerization by the proline-rich region of Tau is regulated by Tau's N-terminal domain. *J. Biol. Chem.* 294, 19381–19394. doi: 10.1074/jbc.RA119.010172
- Mehra, S., Sahay, S., and Maji, S. K. (2019). α -Synuclein misfolding and aggregation: implications in Parkinson's disease pathogenesis. *BBA Proteins Proteom.* 1867, 890–908. doi: 10.1016/j.bbapap.2019.03.001
- Meinen, B. A., Gadkari, V. V., Stull, F., Ruotolo, B. T., and Bardwell, J. C. (2019). SERF engages in a fuzzy complex that accelerates primary nucleation of amyloid proteins. *Proc. Natl. Acad. Sci. U.S.A.* 116, 23040–23049. doi: 10.1073/pnas.1913316116
- Miake, H., Mizusawa, H., Iwatsubo, T., and Hasegawa, M. (2002). Biochemical characterization of the core structure of α -synuclein filaments. *J. Biol. Chem.* 277, 19213–19219. doi: 10.1074/jbc.M110551200
- Michaels, T. C., Šarić, A., Habchi, J., Chia, S., Meisl, G., Vendruscolo, M., et al. (2018). Chemical kinetics for bridging molecular mechanisms and macroscopic measurements of amyloid fibril formation. *Annu. Rev. Phys.* 69, 273–298. doi: 10.1146/annurev-physchem-050317-021322
- Milanesi, L., Sheynis, T., Xue, W.-F., Orlova, E. V., Hellewell, A. L., Jelinek, R., et al. (2012). Direct three-dimensional visualization of membrane disruption by amyloid fibrils. *Proc. Natl. Acad. Sci. U.S.A.* 109, 20455–20460. doi: 10.1073/pnas.1206325109
- Mirecka, E. A., Shaykhalishahi, H., Gauhar, A., Akgül, Ş., Lecher, J., Willbold, D., et al. (2014). Sequestration of a β -Hairpin for Control of α -Synuclein Aggregation. *Angew. Chem. Int.* 53, 4227–4230. doi: 10.1002/anie.201309001
- Mok, S.-A., Condello, C., Freilich, R., Gillies, A., Arhar, T., Oroz, J., et al. (2018). Mapping interactions with the chaperone network reveals factors that protect against tau aggregation. *Nat. Struct. Mol. Biol.* 25, 384–393. doi: 10.1038/s41594-018-0057-1
- Monsellier, E., Redeker, V., Ruiz-Arlandis, G., Bousset, L., and Melki, R. (2015). Molecular interaction between the chaperone Hsc70 and the N-terminal flank of huntingtin exon 1 modulates aggregation. *J. Biol. Chem.* 290, 2560–2576. doi: 10.1074/jbc.M114.603332
- Moreno-Gonzalez, I., Edwards, I. I. G., Salvadores, N., Shah Nawaz, M., Diaz-Espinoza, R., and Soto, C. (2017). Molecular interaction between type 2 diabetes and Alzheimer's disease through cross-seeding of protein misfolding. *Mol. Psychiatry* 22, 1327–1334. doi: 10.1038/mp.2016.230
- Moretto, N., Bolchi, A., Rivetti, C., Imbimbo, B. P., Villetti, G., Pietrini, V., et al. (2007). Conformation-sensitive antibodies against Alzheimer amyloid- β by immunization with a thioredoxin-constrained B-cell epitope peptide. *J. Biol. Chem.* 282, 11436–11445. doi: 10.1074/jbc.M609690200
- Muntané, G., Ferrer, I., and Martínez-Vicente, M. (2012). α -Synuclein phosphorylation and truncation are normal events in the adult human brain. *Neuroscience* 200, 106–119. doi: 10.1016/j.neuroscience.2011.10.042
- Murakami, T., Atsumi, T., Maeda, S., Tanase, S., Ishikawa, K., Mita, S., et al. (1992). A novel transthyretin mutation at position 30 (Leu for Val) associated with familial amyloidotic polyneuropathy. *Biochem. Biophys. Res. Commun.* 187, 397–403. doi: 10.1016/S0006-291X(05)81506-2
- Myers, S. L., Thomson, N. H., Radford, S. E., and Ashcroft, A. E. (2006). Investigating the structural properties of amyloid-like fibrils formed in vitro from β 2-microglobulin using limited proteolysis and electrospray ionisation

- mass spectrometry. *Rapid Comm. Mass Spec.* 20, 1628–1636. doi: 10.1002/rcm.2482
- Nath, S., Goodwin, J., Engelborghs, Y., and Pountney, D. (2011). Raised calcium promotes α -synuclein aggregate formation. *Mol. Cell. Neurosci.* 46, 516–526. doi: 10.1016/j.mcn.2010.12.004
- Nelson, R., Sawaya, M. R., Balbirnie, M., Madsen, A. Ø, Riekel, C., Grothe, R., et al. (2005). Structure of the cross- β spine of amyloid-like fibrils. *Nature* 435, 773–778. doi: 10.1038/nature03680
- Newberry, R. W., Leong, J. T., Chow, E. D., Kampmann, M., and DeGrado, W. F. (2020). Deep mutational scanning reveals the structural basis for α -synuclein activity. *Nat. Chem. Biol.* 9, 1–7. doi: 10.1038/s41589-020-0480-6
- Nizhnikov, A. A., Antonets, K. S., Bondarev, S. A., Inge-Vechtomov, S. G., and Derkatch, I. L. (2016). Prions, amyloids, and RNA: pieces of a puzzle. *Prion* 10, 182–206. doi: 10.1080/19336896.2016.1181253
- Oikawa, T., Nonaka, T., Terada, M., Tamaoka, A., Hisanaga, S.-I., and Hasegawa, M. (2016). α -Synuclein fibrils exhibit gain of toxic function, promoting tau aggregation and inhibiting microtubule assembly. *J. Biol. Chem.* 291, 15046–15056. doi: 10.1074/jbc.M116.736355
- Palaninathan, S. K., Mohamedmohaideen, N. N., Snee, W. C., Kelly, J. W., and Sacchettini, J. C. (2008). Structural insight into pH-induced conformational changes within the native human transthyretin tetramer. *J. Mol. Biol.* 382, 1157–1167. doi: 10.1016/j.jmb.2008.07.029
- Paravastu, A. K., Leapman, R. D., Yau, W.-M., and Tycko, R. (2008). Molecular structural basis for polymorphism in Alzheimer's β -amyloid fibrils. *Proc. Natl. Acad. Sci. U.S.A.* 105, 18349–18354. doi: 10.1073/pnas.0806270105
- Paulson, H. (2012). Machado-Joseph disease/spinocerebellar ataxia type 3. *Handb. Clin. Neurol.* 103, 437–449. doi: 10.1016/B978-0-444-51892-7.00027-9
- Pawar, A. P., Dubay, K. F., Zurdo, J., Chiti, F., Vendruscolo, M., and Dobson, C. M. (2005). Prediction of “aggregation-prone” and “aggregation-susceptible” regions in proteins associated with neurodegenerative diseases. *J. Mol. Biol.* 350, 379–392. doi: 10.1016/j.jmb.2005.04.016
- Peng, C., Gathagan, R. J., Covell, D. J., Medellin, C., Stieber, A., Robinson, J. L., et al. (2018). Cellular milieu impacts distinct pathological α -synuclein strains in α -synucleinopathies. *Nature* 557, 558–563. doi: 10.1038/s41586-018-0104-4
- Petkova, A. T., Ishii, Y., Balbach, J. J., Antzutkin, O. N., Leapman, R. D., Delaglio, F., et al. (2002). A structural model for Alzheimer's β -amyloid fibrils based on experimental constraints from solid state NMR. *Proc. Natl. Acad. Sci. U.S.A.* 99, 16742–16747. doi: 10.1073/pnas.262663499
- Pieri, L., Madiona, K., Bousset, L., and Melki, R. (2012). Fibrillar α -synuclein and huntingtin exon 1 assemblies are toxic to the cells. *Biophys. J.* 102, 2894–2905. doi: 10.1016/j.bpj.2012.04.050
- Platt, G. W., Routledge, K. E., Homans, S. W., and Radford, S. E. (2008). Fibril growth kinetics reveal a region of β 2-microglobulin important for nucleation and elongation of aggregation. *J. Mol. Biol.* 378, 251–263. doi: 10.1016/j.jmb.2008.01.092
- Poepsel, S., Sprengel, A., Sacca, B., Kaschani, F., Kaiser, M., Gatsogiannis, C., et al. (2015). Determinants of amyloid fibril degradation by the PDZ protease HTRA1. *Nat. Chem. Biol.* 11, 862–869. doi: 10.1038/nchembio.1931
- Prasad, A., Bharathi, V., Sivalingam, V., Girdhar, A., and Patel, B. K. (2019). Molecular mechanisms of TDP-43 misfolding and pathology in amyotrophic lateral sclerosis. *Front. Mol. Neurosci.* 12:25. doi: 10.3389/fnmol.2019.00025
- Pytowski, L., Lee, C. F., Foley, A. C., Vaux, D. J., and Jean, L. (2020). Liquid–liquid phase separation of type II diabetes-associated IAPP initiates hydrogelation and aggregation. *Proc. Natl. Acad. Sci. U.S.A.* 117, 12050–12061. doi: 10.1073/pnas.1916716117
- Qiang, W., Yau, W.-M., and Schulte, J. (2015). Fibrillation of β amyloid peptides in the presence of phospholipid bilayers and the consequent membrane disruption. *Biochim. Biophys. Acta Biomembr.* 1848, 266–276. doi: 10.1016/j.bbmem.2014.04.011
- Radamaker, L., Lin, Y.-H., Annamalai, K., Huhn, S., Hegenbart, U., Schönland, S. O., et al. (2019). Cryo-EM structure of a light chain-derived amyloid fibril from a patient with systemic AL amyloidosis. *Nat. Commun.* 10, 1–8. doi: 10.1038/s41467-019-09032-0
- Ranjan, P., and Kumar, A. (2017). Perturbation in long-range contacts modulates the kinetics of amyloid formation in α -synuclein familial mutants. *ACS Chem. Neurosci.* 8, 2235–2246. doi: 10.1021/acscchemneuro.7b00149
- Ray, S., Singh, N., Kumar, R., Patel, K., Pandey, S., Datta, D., et al. (2020). α -Synuclein aggregation nucleates through liquid–liquid phase separation. *Nat. Chem.* 12, 705–716. doi: 10.1038/s41557-020-0465-9
- Reumers, J., MaurerStroh, S., Schymkowitz, J., and Rousseau, F. (2009). Protein sequences encode safeguards against aggregation. *Hum. Mutat.* 30, 431–437. doi: 10.1002/humu.20905
- Richardson, J. S., and Richardson, D. C. (2002). Natural β -sheet proteins use negative design to avoid edge-to-edge aggregation. *Proc. Natl. Acad. Sci. U.S.A.* 99, 2754–2759. doi: 10.1073/pnas.052706099
- Röder, C., Kupreichyk, T., Gremer, L., Schäfer, L. U., Pothula, K. R., Ravelli, R. B., et al. (2020). Cryo-EM structure of islet amyloid polypeptide fibrils reveals similarities with amyloid- β fibrils. *Nat. Struct. Mol. Biol.* 27, 660–667. doi: 10.1038/s41594-020-0442-4
- Rodriguez, J. A., Ivanova, M. I., Sawaya, M. R., Cascio, D., Reyes, F. E., Shi, D., et al. (2015). Structure of the toxic core of α -synuclein from invisible crystals. *Nature* 525, 486–490. doi: 10.1038/nature15368
- Rosenberg, K. J., Ross, J. L., Feinstein, H. E., Feinstein, S. C., and Israelachvili, J. (2008). Complementary dimerization of microtubule-associated tau protein: implications for microtubule bundling and tau-mediated pathogenesis. *Proc. Natl. Acad. Sci. U.S.A.* 105, 7445–7450. doi: 10.1073/pnas.0802036105
- Rumbley, J., Hoang, L., Mayne, L., and Englander, S. W. (2001). An amino acid code for protein folding. *Proc. Natl. Acad. Sci. U.S.A.* 98, 105–112. doi: 10.1073/pnas.98.1.105
- Sampson, T. R., Challis, C., Jain, N., Moiseyenko, A., Ladinsky, M. S., Shastri, G. G., et al. (2020). A gut bacterial amyloid promotes α -synuclein aggregation and motor impairment in mice. *eLife* 9:e53111. doi: 10.7554/eLife.53111
- Sant'Anna, R., Braga, C., Varejão, N., Pimenta, K. M., Graña-Montes, R., Alves, A., et al. (2014). The importance of a gatekeeper residue on the aggregation of transthyretin implications for transthyretin-related amyloidoses. *J. Biol. Chem.* 289, 28324–28337. doi: 10.1074/jbc.M114.563981
- Santos, J., Pujols, J., Pallarès, I., Iglesias, V., and Ventura, S. (2020). Computational prediction of protein aggregation: advances in proteomics, conformation-specific algorithms and biotechnological applications. *Comput. Struct. Biotechnol.* 18, 1403–1413. doi: 10.1016/j.csbj.2020.05.026
- Sarell, C. J., Stockley, P. G., and Radford, S. E. (2013). Assessing the causes and consequences of co-polymerization in amyloid formation. *Prion* 7, 359–368. doi: 10.4161/pri.26415
- Sastre, M., Calero, M., Pawlik, M., Mathews, P. M., Kumar, A., Danilov, V., et al. (2004). Binding of cystatin C to Alzheimer's amyloid β inhibits in vitro amyloid fibril formation. *Neurobiol. Aging* 25, 1033–1043. doi: 10.1016/j.neurobiolaging.2003.11.006
- Saunders, H. M., and Bottomley, S. P. (2009). Multi-domain misfolding: understanding the aggregation pathway of polyglutamine proteins. *Protein Eng. Des. Sel.* 22, 447–451. doi: 10.1093/protein/gzp033
- Scarff, C. A., Almeida, B., Fraga, J., Macedo-Ribeiro, S., Radford, S. E., and Ashcroft, A. E. (2015). Examination of ataxin-3 (atx-3) aggregation by structural mass spectrometry techniques: a rationale for expedited aggregation upon polyglutamine (polyQ) expansion. *Mol. Cell. Proteomics* 14, 1241–1253. doi: 10.1074/mcp.M114.044610
- Scheidt, T., Łapińska, U., Kumita, J. R., Whiten, D. R., Klenerman, D., Wilson, M. R., et al. (2019). Secondary nucleation and elongation occur at different sites on Alzheimer's amyloid- β aggregates. *Sci. Adv.* 5:eau3112. doi: 10.1126/sciadv.aau3112
- Scheres, S. H., Zhang, W., Falcon, B., and Goedert, M. (2020). Cryo-EM structures of tau filaments. *Curr. Opin. Struct. Biol.* 64, 17–25. doi: 10.1016/j.sbi.2020.05.011
- Schmidt, M., Wiese, S., Adak, V., Engler, J., Agarwal, S., Fritz, G., et al. (2019). Cryo-EM structure of a transthyretin-derived amyloid fibril from a patient with hereditary ATTR amyloidosis. *Nat. Commun.* 10, 1–9. doi: 10.1038/s41467-019-13038-z
- Schweighauser, M., Shi, Y., Tarutani, A., Kametani, F., Murzin, A. G., Ghetti, B., et al. (2020). Structures of α -synuclein filaments from multiple system atrophy. *Nature* 585, 464–469. doi: 10.1038/s41586-020-2317-6
- Shahnawaz, M., Mukherjee, A., Pritzkow, S., Mendez, N., Rabadia, P., Liu, X., et al. (2020). Discriminating α -synuclein strains in Parkinson's disease and multiple system atrophy. *Nature* 578, 273–277. doi: 10.1038/s41586-020-1984-7

- Shammas, S. L., Waudby, C. A., Wang, S., Buell, A. K., Knowles, T. P., Ecroyd, H., et al. (2011). Binding of the molecular chaperone α B-crystallin to A β amyloid fibrils inhibits fibril elongation. *Biophys. J.* 101, 1681–1689. doi: 10.1016/j.bpj.2011.07.056
- Shen, K., Gamberdinger, M., Chan, R., Gense, K., Martin, E. M., Sachs, N., et al. (2019). Dual role of ribosome-binding domain of NAC as a potent suppressor of protein aggregation and aging-related proteinopathies. *Mol. Cell* 74, 729–741. doi: 10.1016/j.molcel.2019.03.012
- Shiina, Y., Arima, K., Tabunoki, H., and Satoh, J.-I. (2010). TDP-43 dimerizes in human cells in culture. *Cell. Mol. Neurobiol.* 30, 641–652. doi: 10.1007/s10571-009-9489-9
- Shvadchak, V. V., Afitska, K., and Yushchenko, D. A. (2018). Inhibition of α -Synuclein amyloid fibril elongation by blocking fibril ends. *Angew. Chem. Int.* 57, 5690–5694. doi: 10.1002/anie.201801071
- Sibille, N., Sillen, A., Leroy, A., Wieruszeski, J.-M., Mulloy, B., Landrieu, I., et al. (2006). Structural impact of heparin binding to full-length Tau as studied by NMR spectroscopy. *Biochemistry* 45, 12560–12572. doi: 10.1021/bi060964o
- Sillen, A., Leroy, A., Wieruszeski, J. M., Loyens, A., Beauvillain, J. C., Bué, L., et al. (2005). Regions of tau implicated in the paired helical fragment core as defined by NMR. *ChemBiochem* 6, 1849–1856. doi: 10.1002/cbic.200400452
- Sivanandam, V., Jayaraman, M., Hoop, C. L., Kodali, R., Wetzel, R., and van der Wel, P. C. (2011). The aggregation-enhancing huntingtin N-terminus is helical in amyloid fibrils. *J. Am. Chem. Soc.* 133, 4558–4566. doi: 10.1021/ja110715f
- Sormanni, P., Aprile, F. A., and Vendruscolo, M. (2015). The CamSol method of rational design of protein mutants with enhanced solubility. *J. Mol. Biol.* 427, 478–490. doi: 10.1016/j.jmb.2014.09.026
- Stephens, A. D., Zacharopoulou, M., and Schierle, G. S. K. (2019). The cellular environment affects monomeric α -synuclein structure. *Trends Biochem. Sci.* 44, 453–466. doi: 10.1016/j.tibs.2018.11.005
- Strohäker, T., Jung, B. C., Liou, S.-H., Fernandez, C. O., Riedel, D., Becker, S., et al. (2019). Structural heterogeneity of α -synuclein fibrils amplified from patient brain extracts. *Nat. Commun.* 10, 1–12. doi: 10.1038/s41467-019-13564-w
- Sun, Y., and Chakrabartty, A. (2017). Phase to phase with TDP-43. *Biochemistry* 56, 809–823. doi: 10.1021/acs.biochem.6b01088
- Swuec, P., Lavatelli, F., Tasaki, M., Paissoni, C., Rognoni, P., Maritan, M., et al. (2019). Cryo-EM structure of cardiac amyloid fibrils from an immunoglobulin light chain AL amyloidosis patient. *Nat. Commun.* 10, 1–9. doi: 10.1038/s41467-019-09133-w
- Tam, S., Spiess, C., Auyeung, W., Joachimiak, L., Chen, B., Poirier, M. A., et al. (2009). The chaperonin TRiC blocks a huntingtin sequence element that promotes the conformational switch to aggregation. *Nat. Struct. Mol. Biol.* 16, 1279–1287. doi: 10.1038/nsmb.1700
- Tartaglia, G. G., Pechmann, S., Dobson, C. M., and Vendruscolo, M. (2007). Life on the edge: a link between gene expression levels and aggregation rates of human proteins. *Trends Biochem. Sci.* 32, 204–206. doi: 10.1016/j.tibs.2007.03.005
- Tenidis, K., Waldner, M., Bernhagen, J., Fischle, W., Bergmann, M., Weber, M., et al. (2000). Identification of a penta- and hexapeptide of islet amyloid polypeptide (IAPP) with amyloidogenic and cytotoxic properties. *J. Mol. Biol.* 295, 1055–1071. doi: 10.1006/jmbi.1999.3422
- Terada, M., Suzuki, G., Nonaka, T., Kametani, F., Tamaoka, A., and Hasegawa, M. (2018). The effect of truncation on prion-like properties of α -synuclein. *J. Biol. Chem.* 293, 13910–13920. doi: 10.1074/jbc.RA118.001862
- Terakawa, M. S., Lin, Y., Kinoshita, M., Kanemura, S., Itoh, D., Sugiki, T., et al. (2018). Impact of membrane curvature on amyloid aggregation. *Biochem. Biophys. Acta. Biomembr.* 1860, 1741–1764. doi: 10.1016/j.bbamem.2018.04.012
- Thompson, M. J., Sievers, S. A., Karanicolas, J., Ivanova, M. I., Baker, D., and Eisenberg, D. (2006). The 3D profile method for identifying fibril-forming segments of proteins. *Proc. Natl. Acad. Sci. U.S.A.* 103, 4074–4078. doi: 10.1073/pnas.0511295103
- Tompa, P. (2009). Structural disorder in amyloid fibrils: its implication in dynamic interactions of proteins. *FEBS J.* 276, 5406–5415. doi: 10.1111/j.1742-4658.2009.07250.x
- Tompa, P., Dosztányi, Z., and Simon, I. (2006). Prevalent structural disorder in *E. coli* and *S. cerevisiae* proteomes. *J. Proteome Res.* 5, 1996–2000. doi: 10.1021/pr0600881
- Ulamiec, S. M., and Radford, S. E. (2020). Spot the difference: function versus toxicity in amyloid fibrils. *Trends Biochem. Sci.* 45, 635–636. doi: 10.1016/j.tibs.2020.04.007
- Valleix, S., Gillmore, J. D., Bridoux, F., Mangione, P. P., Dogan, A., Nedelec, B., et al. (2012). Hereditary systemic amyloidosis due to Asp76Asn variant β 2-microglobulin. *N. Engl. J. Med.* 366, 2276–2283. doi: 10.1056/NEJMoa1201356
- van Ham, T. J., Holmberg, M. A., van der Goot, A. T., Teuling, E., Garcia-Arencibia, M., Kim, H.-E., et al. (2010). Identification of MOAG-4/SERF as a regulator of age-related proteotoxicity. *Cell* 142, 601–612. doi: 10.1016/j.cell.2010.07.020
- Verma, M., Vats, A., and Taneja, V. (2015). Toxic species in amyloid disorders: oligomers or mature fibrils. *Ann. Indian Acad. Neurol.* 18, 138–145. doi: 10.4103/0972-2327.144284
- Vicario, M., Cieri, D., Brini, M., and Cali, T. (2018). The close encounter between α -synuclein and mitochondria. *Front. Neurosci.* 12:388. doi: 10.3389/fnins.2018.00388
- von Bergen, M., Friedhoff, P., Biernat, J., Heberle, J., Mandelkow, E.-M., and Mandelkow, E. (2000). Assembly of τ protein into Alzheimer paired helical filaments depends on a local sequence motif (306VQIVYK311) forming β structure. *Proc. Natl. Acad. Sci. U.S.A.* 97, 5129–5134. doi: 10.1073/pnas.97.10.5129
- Wälti, M. A., Ravotti, F., Arai, H., Glabe, C. G., Wall, J. S., Böckmann, A., et al. (2016). Atomic-resolution structure of a disease-relevant A β (1–42) amyloid fibril. *Proc. Natl. Acad. Sci. U.S.A.* 113, E4976–E4984. doi: 10.1073/pnas.1600749113
- Wang, F., Wang, X., Yuan, C.-G., and Ma, J. (2010a). Generating a prion with bacterially expressed recombinant prion protein. *Science* 327, 1132–1135. doi: 10.1126/science.1183748
- Wang, F., Yin, S., Wang, X., Zha, L., Sy, M.-S., and Ma, J. (2010b). Role of the highly conserved middle region of prion protein (PrP) in PrP-lipid interaction. *Biochemistry* 49, 8169–8176. doi: 10.1021/bi101146v
- Wang, L.-Q., Zhao, K., Yuan, H.-Y., Wang, Q., Guan, Z., Tao, J., et al. (2020). Cryo-EM structure of an amyloid fibril formed by full-length human prion protein. *Nat. Struct. Mol. Biol.* 27, 1–5. doi: 10.1038/s41594-020-0441-5
- Wang, Y., Martinez-Vicente, M., Krüger, U., Kaushik, S., Wong, E., Mandelkow, E.-M., et al. (2009). Tau fragmentation, aggregation and clearance: the dual role of lysosomal processing. *Hum. Mol. Genet.* 18, 4153–4170. doi: 10.1093/hmg/ddp367
- Ward, J. J., Sodhi, J. S., McGuffin, L. J., Buxton, B. F., and Jones, D. T. (2004). Prediction and functional analysis of native disorder in proteins from the three kingdoms of life. *J. Mol. Biol.* 337, 635–645. doi: 10.1016/j.jmb.2004.02.002
- Waudby, C. A., Knowles, T. P., Devlin, G. L., Skepper, J. N., Ecroyd, H., Carver, J. A., et al. (2010). The interaction of α B-crystallin with mature α -synuclein amyloid fibrils inhibits their elongation. *Biophys. J.* 98, 843–851. doi: 10.1016/j.bpj.2009.10.056
- Wegmann, S., Eftekhazadeh, B., Tepper, K., Zoltowska, K. M., Bennett, R. E., Dujardin, S., et al. (2018). Tau protein liquid-liquid phase separation can initiate tau aggregation. *EMBO J.* 37:e98049. doi: 10.15252/embj.201798049
- Wegmann, S., Medalsy, I. D., Mandelkow, E., and Müller, D. J. (2013). The fuzzy coat of pathological human Tau fibrils is a two-layered polyelectrolyte brush. *Proc. Natl. Acad. Sci. U.S.A.* 110, E313–E321. doi: 10.1073/pnas.1212100110
- Wentink, A., Nussbaum-Krammer, C., and Bukau, B. (2019). Modulation of amyloid states by molecular chaperones. *Cold Spring Harb. Perspect. Biol.* 11:a033969. doi: 10.1101/cshperspect.a033969
- Williams, A. D., Shivaprasad, S., and Wetzel, R. (2006). Alanine scanning mutagenesis of A β (1–40) amyloid fibril stability. *J. Mol. Biol.* 357, 1283–1294. doi: 10.1016/j.jmb.2006.01.041
- Xue, W.-F., Hellewell, A. L., Gosal, W. S., Homans, S. W., Hewitt, E. W., and Radford, S. E. (2009). Fibril fragmentation enhances amyloid cytotoxicity. *J. Biol. Chem.* 284, 34272–34282. doi: 10.1074/jbc.M109.049809
- Xue, W.-F., Homans, S. W., and Radford, S. E. (2008). Systematic analysis of nucleation-dependent polymerization reveals new insights into the mechanism of amyloid self-assembly. *Proc. Natl. Acad. Sci. U.S.A.* 105, 8926–8931. doi: 10.1073/pnas.0711664105
- Yang, X., Williams, J. K., Yan, R., Mouradian, M. M., and Baum, J. (2019). Increased dynamics of α -synuclein fibrils by β -synuclein leads to reduced seeding and cytotoxicity. *Sci. Rep.* 9, 1–13. doi: 10.1038/s41598-019-54063-8

- Yu, H., Han, W., Ma, W., and Schulten, K. (2015). Transient β -hairpin formation in α -synuclein monomer revealed by coarse-grained molecular dynamics simulation. *J. Chem. Phys.* 143:243142. doi: 10.1063/1.4936910
- Zhang, W., Falcon, B., Murzin, A. G., Fan, J., Crowther, R. A., Goedert, M., et al. (2019). Heparin-induced tau filaments are polymorphic and differ from those in Alzheimer's and Pick's diseases. *eLife* 8:e43584. doi: 10.7554/eLife.43584
- Zhang, Y.-J., Caulfield, T., Xu, Y.-F., Gendron, T. F., Hubbard, J., Stetler, C., et al. (2013). The dual functions of the extreme N-terminus of TDP-43 in regulating its biological activity and inclusion formation. *Hum. Mol. Genet.* 22, 3112–3122. doi: 10.1093/hmg/ddt166

Conflict of Interest: The authors declare that the research was conducted in the absence of any commercial or financial relationships that could be construed as a potential conflict of interest.

Copyright © 2020 Ułamec, Brockwell and Radford. This is an open-access article distributed under the terms of the Creative Commons Attribution License (CC BY). The use, distribution or reproduction in other forums is permitted, provided the original author(s) and the copyright owner(s) are credited and that the original publication in this journal is cited, in accordance with accepted academic practice. No use, distribution or reproduction is permitted which does not comply with these terms.



Natural Compounds as Inhibitors of A β Peptide Aggregation: Chemical Requirements and Molecular Mechanisms

Katiuscia Pagano, Simona Tomaselli, Henriette Molinari and Laura Ragona*

NMR Laboratory, Istituto di Scienze e Tecnologie Chimiche (SCITEC), Consiglio Nazionale delle Ricerche – CNR, Milan, Italy

OPEN ACCESS

Edited by:

Wolfgang Hoyer,
Heinrich Heine University
of Düsseldorf, Germany

Reviewed by:

Giuseppe Melacini,
McMaster University, Canada
Cristina Airolidi,
Università di Milano-Bicocca, Italy

*Correspondence:

Laura Ragona
laura.ragona@scitec.cnr.it

Specialty section:

This article was submitted to
Neurodegeneration,
a section of the journal
Frontiers in Neuroscience

Received: 20 October 2020

Accepted: 04 December 2020

Published: 22 December 2020

Citation:

Pagano K, Tomaselli S, Molinari H
and Ragona L (2020) Natural
Compounds as Inhibitors of A β
Peptide Aggregation: Chemical
Requirements and Molecular
Mechanisms.
Front. Neurosci. 14:619667.
doi: 10.3389/fnins.2020.619667

Alzheimer's disease (AD) is one of the most common neurodegenerative disorders, with no cure and preventive therapy. Misfolding and extracellular aggregation of Amyloid- β (A β) peptides are recognized as the main cause of AD progression, leading to the formation of toxic A β oligomers and to the deposition of β -amyloid plaques in the brain, representing the hallmarks of AD. Given the urgent need to provide alternative therapies, natural products serve as vital resources for novel drugs. In recent years, several natural compounds with different chemical structures, such as polyphenols, alkaloids, terpenes, flavonoids, tannins, saponins and vitamins from plants have received attention for their role against the neurodegenerative pathological processes. However, only for a small subset of them experimental evidences are provided on their mechanism of action. This review focuses on those natural compounds shown to interfere with A β aggregation by direct interaction with A β peptide and whose inhibitory mechanism has been investigated by means of biophysical and structural biology experimental approaches. In few cases, the combination of approaches offering a macroscopic characterization of the oligomers, such as TEM, AFM, fluorescence, together with high-resolution methods could shed light on the complex mechanism of inhibition. In particular, solution NMR spectroscopy, through peptide-based and ligand-based observation, was successfully employed to investigate the interactions of the natural compounds with both soluble NMR-visible (monomer and low molecular weight oligomers) and NMR-invisible (high molecular weight oligomers and protofibrils) species. The molecular determinants of the interaction of promising natural compounds are here compared to infer the chemical requirements of the inhibitors and the common mechanisms of inhibition. Most of the data converge to indicate that the A β regions relevant to perturb the aggregation cascade and regulate the toxicity of the stabilized oligomers, are the N-term and β 1 region. The ability of the natural aggregation inhibitors to cross the brain blood barrier, together with the tactics to improve their low bioavailability are discussed. The analysis of the data ensemble can provide a rationale for the selection of natural compounds as molecular scaffolds for the design of new therapeutic strategies against the progression of early and late stages of AD.

Keywords: NMR, amyloid- β protein, protein ligand interactions, self-association, natural compound, Alzheimer

INTRODUCTION

Alzheimer disease (AD) is the main cause of neurodegenerative dementia (Selkoe, 2002b; Lopez and Kuller, 2019). Since the first descriptions of pre-senile dementia by Alois Alzheimer in 1907 (Alzheimer, 1907), the formation of extracellular senile plaques and intraneuronal fibrillary tangles have been regarded as the hallmarks of the neuropathology, as the behavioral symptoms of AD correlate with their accumulation (Selkoe, 1991; Armstrong, 2009; Bloom, 2014). The soluble species of these structures are amyloid- β (A β) peptides for plaques and tau protein for tangles. A β peptides are proteolytic fragments of the transmembrane amyloid precursor protein, whereas tau is a brain-specific, axon-enriched microtubule-associated protein (Black et al., 1996; Haass et al., 2012). The mechanism of Alzheimer onset and progression is complex and still not fully understood. Recent discoveries have revealed pathways that connect A β to tau in seminal steps of AD pathogenesis (Gotz et al., 2001; Lewis et al., 2001; Hurtado et al., 2010; Zempel et al., 2013). A β is upstream of tau in AD pathogenesis and triggers the conversion of tau from a normal to a toxic state, but there is also evidence that toxic tau enhances A β toxicity *via* a feedback loop (Leroy et al., 2012). Yet, substantial genetic evidences identify the misfolding and the extracellular aggregation of A β , mostly A β 1–40 (A β 40) and A β 1–42 (A β 42), as the main cause of AD progression (Hardy and Higgins, 1992; Hardy and Selkoe, 2002; Benilova et al., 2012; Selkoe and Hardy, 2016). The inhibition of A β self-assembly is therefore a promising therapeutic approach for the treatment of AD (Estrada and Soto, 2007).

The multistep mechanism of A β monomers association is depicted in **Figure 1**.

Monomeric A β does not possess cellular toxicity under physiologically relevant concentrations, while soluble oligomers, which show very high heterogeneity in terms of size and structure, have been shown to exhibit substantial neurotoxicity (Knowles et al., 2014; Cremades and Dobson, 2018).

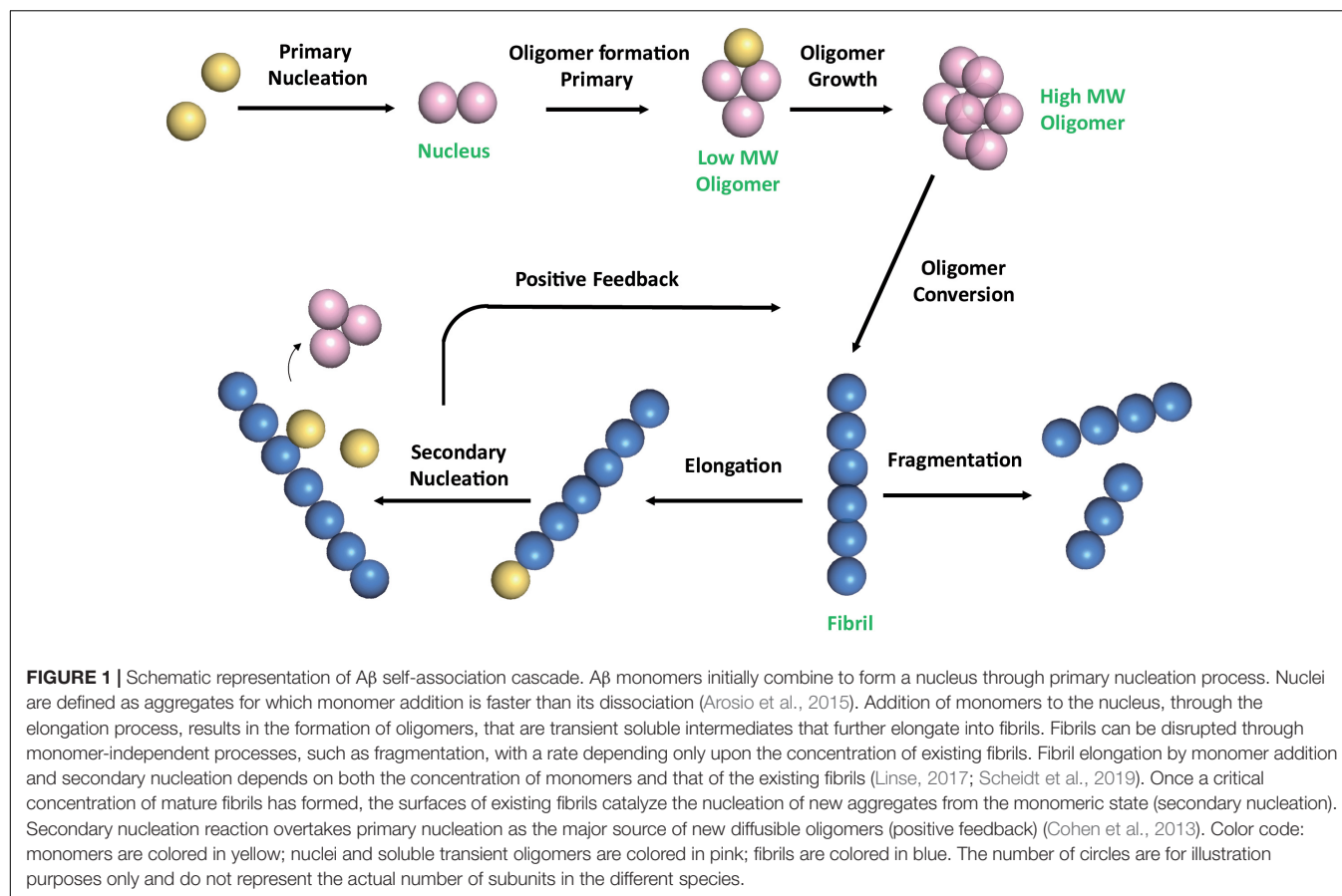
In the past, several compounds have been developed to reduce or prevent A β oligomerization and to destabilize disease relevant A β aggregates, however most of these molecules have shown serious side effects and poor permeability through the blood-brain barrier (BBB), the highly specialized endothelial cell membrane lining cerebral microvessels, which regulates the entry of plasma components into the central nervous system and ensures the export of potentially neurotoxic molecules from the brain to the blood (Abbott et al., 2010; Zenaro et al., 2017). Natural products, with their unique structural diversity, have come to focus as important sources of bioactive chemical domains, with minimal side effects and increased BBB permeability (Bui and Nguyen, 2017). A huge number of natural compounds have shown interesting beneficial effects on the onset and progression of different neurodegenerative diseases. Some classes, as tetracyclines and polyphenols, have the capability to interfere with the aggregation of several unrelated amyloidogenic proteins, such as α -synuclein (associated to Parkinson's disease), islet amyloid polypeptide (IAPP, associated to type-2 diabetes), and it is likely they share partially overlapping mechanisms of action (Andrich and Bieschke, 2015; Giorgetti et al., 2018;

Martinez et al., 2020). Several *in vitro* and *in vivo* studies have proven the therapeutic potential of a wide range of natural compounds against AD progression, however only a small subset of them have been shown to be efficient in preclinical and clinical studies (Andrade et al., 2019). A further critical issue remains the scarcity of reported experimental evidences on their mechanism of action. Some natural compounds have been proposed to attenuate the accumulation of A β peptide either by affecting several signaling cascades *via* the modulation of oxidative stress or by direct interaction with A β peptide and its self-assembled species (Sadhukhan et al., 2018).

In this review, we focus on the natural compounds able to bind monomeric, oligomeric or fibrillar A β species, as deduced from biophysical and/or structural biology approaches. The identification of the key chemical features of the inhibitors and the inhibiting mechanisms are reviewed to highlight the critical features to be addressed in targeting the toxic oligomeric species. The issue of natural compounds low bioavailability is examined and the most important tactics to overcome these limitations and allow successful conversion into therapeutics are discussed.

Natural Compounds With Inhibitory Effects on A β Peptide Aggregation Pathways

A rich and important literature (Ma et al., 2020; Muscat et al., 2020b; Stefanescu et al., 2020) reports both experimental and computational studies, focused on the effects of natural compounds on different self-aggregated A β species. We have reviewed here those studies in which the proposed molecular mechanism of action is supported by a combination of biophysical approaches and experimental structural data. Most of the available data are based on optical spectroscopies, including circular dichroism (CD) and multiple types of fluorescence measurements, useful to estimate the progression of fibrillization, together with the beta content and hydrophobicity of the A β assemblies. In particular the use of dyes, such as thioflavin T (ThT), whose fluorescence intensity increases upon binding to the fibrils, is a popular method to detect amyloid fibrils formation. Dynamic light scattering (DLS), size exclusion chromatography (SEC), Transmission Electron Microscopy (TEM), Atomic Force Microscopy (AFM), provide important information on the size and the morphology of the aggregated species stabilized in the presence of the natural compounds. Conformation-specific antibodies, that recognize the different structural features of amyloidogenic oligomers and fibrils (Kayed et al., 2007; Perchiacca et al., 2012), are very informative to monitor/assess oligomer remodeling induced by natural compounds. High-resolution structural information on amyloid fibrils has only become available in recent years through progress in solid state NMR (ssNMR), cryo-electron microscopy (cryo-EM), and X-ray microcrystallography techniques (Chiti and Dobson, 2017). In particular cryo-EM approaches achieved atomic resolution structures of amyloid fibrils (Antequera et al., 2020; Ciudad et al., 2020). The resolution power of solution NMR spectroscopy contributed significantly to the definition of the molecular mechanism of action of



aggregation inhibitors from natural sources. Indeed, NMR can highlight both Aβ residues involved in the interactions, as well as small molecule chemical groups stabilizing the binding. Thus, peptide-based and ligand-based NMR observation can be fruitfully employed to investigate the interactions of the natural compounds with NMR-visible or NMR-invisible Aβ species, respectively. Among ligand-based NMR approaches, saturation transfer difference (STD) experiment is a well-established homonuclear NMR technique that permits detection of transient binding of small molecule ligands to macromolecular receptors, such as Aβ oligomers, and to identify binding epitopes on the small ligand (Biet and Peters, 2001; Meyer and Peters, 2003). Among peptide-based NMR approaches, a very simple and widely employed experiment is ^1H - ^{15}N Heteronuclear Single Quantum Coherence (^1H - ^{15}N HSQC). It detects ^1H signals that are directly bound to the ^{15}N atoms, thus providing a fingerprint of the amide-NH backbone atoms, when a ^{15}N labeled Aβ sample is available. This experiment is particularly suitable to investigate interactions, as it allows to map peptide residues involved in the binding sites and/or to identify conformational rearrangements, through the measure of changes in chemical shifts, linewidths and/or resonance intensities, upon ligand addition. The dark-state exchange saturation transfer experiment (DEST), has been developed to characterize, at atomic resolution, the interaction between an NMR-visible free peptide species, transiently bound to

an NMR-invisible very high-molecular-weight macromolecular entity (Fawzi et al., 2011). Specifically, DEST NMR methods allowed to expand the knowledge of the determinants of the interaction between Aβ monomers with the NMR-invisible Aβ assemblies and with models of cellular membranes (Ahmed et al., 2019). Finally, simple ^1H NMR approaches, exploiting the time-dependent decrease of NMR peak intensities, can be employed to derive the Aβ aggregation kinetics (Liu et al., 2012; Pagano et al., 2019). Docking and MD studies have been reported for the majority of the compounds, however a comparative analysis of the results is difficult, as simulations were run starting from different monomeric, oligomeric, fibrillar structural models.

The review summarizes results on natural compounds tested on both Aβ40 and Aβ42 isoforms, as they represent the two major components of the amyloid deposits in the brain (Haass and Selkoe, 1993). The longer Aβ42 is considered the most pathogenic, in view of its greater tendency to aggregate and form toxic oligomers (Hou et al., 2004; Qiu et al., 2015). However, Aβ40 is more abundant than Aβ42 (9:1) in the biological fluids (Qiu et al., 2015). In addition, Aβ40 was found in the amyloid deposits of patients affected by cerebral amyloid pathology, which is considered an early step in AD pathogenesis (Garcia-Vinuales et al., 2020; Greenberg et al., 2020), suggesting that both isoforms must be taken in consideration in search of neuroprotective agents.

For each natural compound with A β aggregation inhibitory properties, the main biophysical data available in the literature are reported in the following paragraphs and summarized in **Table 1**.

Brazilin, is a natural compound extracted from *Caesalpinia sappan*.

Biochemical, biophysical, cell biological and molecular simulation methods were applied to investigate Brazilin inhibitory effects on A β 42 fibrillogenesis and cytotoxicity (Du et al., 2015). TEM data indicated that Brazilin inhibited fibril formation in favor of granular aggregates at Brazilin: A β ratio of 10. Brazilin induced aggregates were investigated by SEC revealing two elution peaks, one corresponding to large soluble aggregates with MW above 75KDa and one corresponding to monomeric A β 42. CD spectra of A β 42 detected the presence of β -sheet structures either in the presence and absence of brazilin, however, assays in the presence of antibodies demonstrated that A β 42 aggregates modulated by brazilin were structurally distinct from the toxic oligomers. Time-dependent dot blot assays, carried out using antibodies A11 (specific for toxic on-pathway A β oligomers), and 6E10 (recognizing A β independently of its conformations), showed that, in the presence of brazilin, A11-immunoreactive oligomers were efficiently suppressed, while 6E10 antibody detected both brazilin-treated and untreated A β 42.

Lactate dehydrogenase (LDH) cytotoxicity assays were further carried out using SH-SY5Y cell line, a human derived neuroblastoma cell line presenting many of the biochemical and functional features of human neurons, widely used as a human neuronal cell model in the cytotoxicity studies of AD. Co-incubation of A β 42 monomers and brazilin decreased the A β 42-induced cell death in a dose-dependent manner, as evidenced by the decrease of LDH release. Molecular simulations, employing A β 17–42 pentamer as starting state, indicated that brazilin could inhibit A β 42 fibrillogenesis by directly binding to A β 42 species *via* hydrophobic interactions and hydrogen bonding, and further remodeled mature fibrils by disrupting the intermolecular salt bridge D23-K28 *via* hydrogen bonding. A β residue mainly involved in interaction were L17, F19, F20, and K28 (Du et al., 2015).

Curcumin (Cur), is a polyphenol extracted from rhizome of the Turmeric/*Curcuma longa* plant.

Curcumin was reported to dose-dependently inhibit the formation of A β fibrils from A β 40 and A β 42 and their extensions, as well as to destabilize preformed fibrils (Hamaguchi et al., 2010). At variance, other authors suggested, on the basis of Western blot, TEM and fluorescence data, that curcumin promotes fibrillization by shifting A β 42 fibrillation pathway away from prefibrillar aggregates (Necula et al., 2007; Caesar et al., 2012). Masuda et al. (2011) investigated the binding of curcumin to fibril structures by ssNMR employing selectively ^{13}C labeled A β 42 residues at the N-terminal and in the 17–21 region. 2D ^{13}C – ^{13}C correlation experiments indicated that residues V12 and L17–A21 were mainly involved in the interaction with curcumin. The relevance of the paper is related to the demonstration that the polyphenol interacts with A β 42 fibrils. Dot blot assays with the A11 antibody showed that Cur inhibited

the formation of high molecular weight A β oligomers (Necula et al., 2007). Along the same line, Fu et al. (2014) demonstrated by AFM that when Cur was co-incubated at a 1:1 molar ratio with A β peptide, the oligomers height were capped at ~ 2.5 nm, thus indicating that Cur stabilizes the low molecular weight oligomers (with heights measured by AFM of ~ 1.0 – 2.5 nm) rather than high molecular oligomers (height 3–5 nm) additionally observed in its absence.

Curcumin was also shown to bind monomeric species and/or low MW oligomers. 2D ^1H – ^{15}N HSQC NMR studies indicated that A β 42 residues involved in the interaction are A5, S8, G9, K16, K17, D23, and I31 (Ono JBC 2012). Similar regions (E3, F4, R5, Q15, K16, L17, F20) were mapped by Fu et al. (2014).

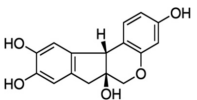
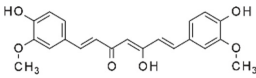
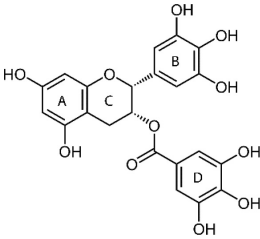
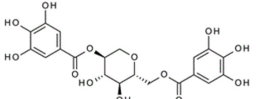
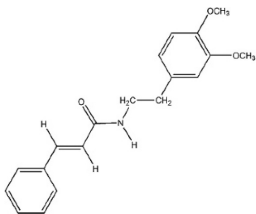
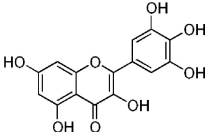
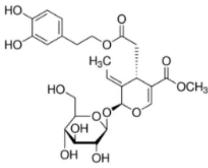
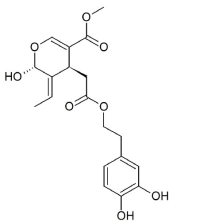
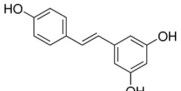
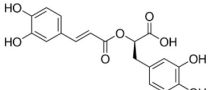
Epigallocatechin gallate (EGCG), is extracted from green tea.

Solution NMR studies indicate that EGCG is able to bind weakly to A β monomers while it displays higher affinity toward oligomers (Kd is one order of magnitude lower for oligomers with respect to monomers). ^1H – ^{15}N HSQC spectra showed a dose-dependent change in A β 40 chemical shifts upon EGCG addition, suggesting that EGCG interacts with monomers. The most pronounced chemical shift changes were observed for residues within the two β -strands seen in the A β 40 protofibrils. However, the chemical shift projection analyses pointed out that EGCG binding to monomer is most likely nonspecific (Ahmed et al., 2017).

DLS changes observed upon EGCG addition to A β 40 peptide are consistent with the ability of EGCG to stabilize A β 40 oligomers starting from either monomers or soluble high molecular weight protofibrils (Bieschke et al., 2010; Ahmed et al., 2017). Electron microscopy (EM) images indicated that, after EGCG addition, the protofibrils are remodeled into smaller spherical oligomers. DLS and EM evidenced the EGCG-induced morphological remodeling, while a combination of several cutting-edge NMR approaches were employed to investigate the same remodeling mechanism at a per-residue level. Specifically, EGCG induced a net inhibition of direct A β 40 monomer–protofibril contacts in the β 1 strand, while a net induction of more engaged direct A β 40 monomer–protofibrils contacts was observed for the N-terminal segment. The dual effect displayed by EGCG explains the remodeling of mature amyloid assemblies into smaller, non-toxic aggregates without the release of transient A β monomers. As a result EGCG stabilizes seeding-incompetent, off-pathway oligomers (Ahmed et al., 2017 and references therein; Ehrnhoefer et al., 2008; Ahmed et al., 2019), interfering with secondary nucleation events known to generate toxic A β assemblies (Ahmed et al., 2017).

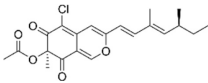
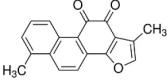
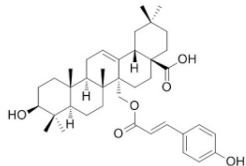
The comparative analysis of A β soluble assemblies (A β n) prepared in the absence or presence of a set of catechins including EGCG, epigallocatechin (EGC) and epicatechin (EC), allowed to correlate cellular toxicity with the unique molecular signatures of A β n induced by the different natural compounds (Ahmed et al., 2019), indicating that A β n toxicity is regulated by the solvent exposure of hydrophobic surfaces. The interactions of selected A β assemblies with membrane biomimetics (SUVs composed of a mixture of DOPE: DOPS: DOPC lipids) were further characterized through TEM and NMR approaches proposing a

TABLE 1 | Natural compounds with antiaggregation effects on A β peptide: chemical structure and summary of the methods employed to describe the inhibitory action.

Natural product	Chemical structure	Methods	References
Brazilin		TEM, SEC, MD, CD antibody recognition	Du et al., 2015
Curcumin		NMR EM dot-blot, immunoblot Docking/MD SS-NMR	Fu et al., 2014 Andrich et al., 2017 Muscat et al., 2020a Masuda et al., 2011
Epigallocatechin gallate		NMR, DLS, fluorescence, EM, wide-angle X-ray diffraction	Ehrnhoefer et al., 2008; Ahmed et al., 2017, 2019
Ginnalin A		AFM, SPR, fluorescence, CD, MD	Fan et al., 2020
Wgx-50		AFM, docking, MD	Tang et al., 2013; Fan et al., 2015
Myricetin		ThT fluorescence, TEM, PICUP, NMR	Ono et al., 2012
Oleuropein		MS, NMR	Galanakis et al., 2011
Oleuropein aglycone		ThT and intrinsic fluorescence, DLS, SDS-PAGE, TEM Docking/MD	Leri et al., 2019 Muscat et al., 2020a
Resveratrol		SPR, TEM, AFM, ThT fluorescence, NMR	Fu et al., 2014
Rosmarinic acid		NMR Docking and MD	Airoldi et al., 2013 Khan et al., 2019; Muscat et al., 2020b

(Continued)

TABLE 1 | Continued

Natural product	Chemical structure	Methods	References
Sclerotiorin		NMR	Wiglenda et al., 2020
Tanshinone		ThT fluorescence, AFM MD	Wang et al., 2013; Dong et al., 2017
Uncarinic acid C		ThT fluorescence, HPLC sedimentation assay, NMR	Murakami et al., 2018

model for oligomer toxicity (Ahmed et al., 2019) (see later, section “Identification of A β Regions Affected by Natural Compounds and Oligomer Remodeling Mechanisms”).

Ginnalin A (GA), is isolated from the red maple. GA addition to A β 42 lowers the ThT fluorescence intensity at the plateau and lengthens the lag phase of the aggregation in a dose-dependent manner. Surface plasmon resonance (SPR) experiments demonstrate that GA binds to A β 42 monomers and/or pentamers (Fan et al., 2020). AFM data confirmed that co-incubation of A β 42 with GA drastically altered the A β 42 aggregation kinetics and protofibrils were absent even after 6 h co-incubation, while irregular amorphous aggregates, instead of mature fibrils, were observed after 24 h. The capability of GA to disintegrate preformed fibrils was further tested by AFM, showing that preformed fibrils could be efficiently disaggregated into many small and amorphous aggregates depending on GA/A β 42 ratio, with the size of the amorphous aggregates decreasing with the increase of GA concentration. Time-lapse CD, performed without and with GA addition to A β 42, indicated that the random coil/ α -helix to β -sheet conformational conversion, a crucial step in fibrillogenesis, was inhibited in a concentration-dependent manner. Further data on the interaction GA/A β 42 at a per-residue level were based on MD simulations suggesting that GA would target monomers residues 17–21, 35, 38, reported to be essential for β -sheet formation and stabilization (Hoyer et al., 2008; Ahmed et al., 2010). The authors propose that GA can target A β 42 fibrillogenesis *via* different mechanisms, namely by binding to monomers at the early nucleation phase, preventing A β –A β associations, and at the later growth phase. Pre-incubation of A β 42 solution with GA give rise to oligomers that do not interact or do not perturb the integrity of cellular membranes, as deduced from toxicity tests on SH-SY5Y cells.

Wgx50, is a natural compound extracted from Sichuan pepper (*Zanthoxylum bungeanum*) that is able to inhibit A β -induced neuronal apoptosis, reduce neuronal calcium toxicity, decrease the accumulation of A β oligomers in the cerebral cortex, and improve the cognitive abilities of mice (Tang et al., 2013, 2014;

Guo et al., 2014; Shi et al., 2016). AFM investigation showed that wxg-50 can directly inhibit A β oligomers. Tang et al. (2013) demonstrated that when A β 42 peptide was co-incubated with wxg-50, no high density plaques and fibrils were observed, oligomers disassembled and only a few fibrils remained, suggesting that wxg-50 could prevent A β fibrils growth.

The binding of wxg-50 on A β fibrils was investigated by docking and MD simulations. The small molecule was docked on Ab17–42 pentameric U-shaped fibril (Fan et al., 2015), and the analysis of the following MD simulations highlighted three possible stable binding sites. Two sites interested the two hydrophobic grooves on the surface of A β protofibril at the level of residues F20 and V18 for the first one, and residues I31 and M35 for the second one. The binding on these two sites made no significant changes in A β structures, but they corresponded to regions responsible for the intermolecular protein-protein assembly of amyloid (Nasica-Labouze et al., 2015). In the third binding site, wxg-50 was packed against the side chains of I32 and L34 in the interior of the protofibril, and caused destabilization of the structure, disrupted the D23–K28 salt bridges, and partially opened the tightly compacted two β -sheets.

Myricetin (Myr), is a flavonol found in many foods of vegetal origin, including tea, onions, cocoa and red wine. Myr was shown to prevent the growth of A β 40 and A β 42 amyloid aggregates *in vitro* and to destabilize preformed fibrils, as demonstrated by ThT fluorescence and TEM analysis (Ono et al., 2003, 2004, 2005). Myr can block A β 40 and A β 42 oligomerization, as shown by photochemical cross-linking method (PICUP) (Ono et al., 2012). NMR studies demonstrated that Myr is able to bind A β 42 monomers, promoting significant chemical shift perturbations of ^1H - ^{15}N HSQC spectra at the level of R5, V12, H13, K16–D23, I31, and I32. Interestingly, the authors observed the selective broadening of few amide peaks (R5, V12, K16, and V18), suggesting a stronger binding in this region. MTT, LTP, and LTD assays established that the phenol remodeled A β oligomer induced lower cellular and synaptic toxicities (Ono et al., 2012).

Oleuropein (OE) and Oleuropein aglycone (OleA). OE is a polyphenol extracted from the fruits and leaves of *Olea europaea* L. endowed with a wide range of beneficial pharmacological

effects, such as antioxidant, anti-inflammatory, antiatherogenic, antibacterial, and anticancer properties (Bazoti et al., 2008 and references therein). Mass spectrometry (MS) experiments showed that OE interacts non-covalently with A β , targeting the A β amino acid segment F4–K28 (Bazoti et al., 2008). NMR titration experiments demonstrated the ability of OE to interact with A β 40 monomer and/or low MW oligomers, with the region H14–F20 identified as the binding epitopes (Galanakis et al., 2011), in agreement with MS results.

Oleuropein aglicone (OleA) is an OE derivative, devoid of the glucose moiety. OleA is the most abundant and typical phenolic components of extra virgin olive oil. Recent data indicated that OleA interferes *in vitro* with the aggregation pathway of amyloidogenic peptides and proteins, including amylin, tau protein, transthyretin (Leri et al., 2016), β 2-microglobulin, α -synuclein, and A β 42 peptide (Leri et al., 2019 and references therein). ThT, DLS, SDS-PAGE, TEM analysis suggested that OleA favors the growth of minute protofibrils, inhibiting their further development along the fibrillation pathway (Daccache et al., 2011; Leri et al., 2019). Intrinsic fluorescence quenching experiments of A β 42 Tyr10, in the presence of acrylamide, demonstrated that OleA binds and stabilizes solvent-exposed oligomeric intermediates, delaying fibril formation. Amyloid assemblies grown in the presence of OleA were unable to bind the cell membrane at the GM1 level, as indicated by FRET efficiency, thus exhibiting low cytotoxicity (Leri et al., 2019). Altogether the data highlight the ability of OleA to induce specific and essential changes in the monomeric peptide or oligomeric assemblies to redirect the aggregation process toward off-pathway and harmless final products.

Docking of OleA to the S-shaped fibril (Fandrich et al., 2018), followed by 150 ns MD simulations, suggested that OleA localizes between adjacent receptor chains, mostly interacting with V18–V24 and N27–I31. The type of established interaction reduces the percentual content of beta sheets, the order parameter value and the inter-chain interaction area if compared to the wild type structure, thus inducing a considerable destabilizing effect on the whole amyloid fibril (Muscat et al., 2020a).

Resveratrol (RES) is a natural non-flavonoid polyphenolic molecule found in many fruits, vegetables, tea, and wine (Berman et al., 2017). RES, thanks to its numerous therapeutic effects, has been studied as therapeutic agent for cardiovascular disease, obesity, diabetes, and for neurological disorders, including Alzheimer's diseases (Tellone et al., 2015; Martin, 2017; Rauf et al., 2018). SPR analysis demonstrated that RES can directly bind to both monomeric and fibrillar A β 40 and A β 42 peptides (Ge et al., 2012). Solution NMR data confirmed the affinity of RES for monomeric species and /or small oligomers.

RES can dose-dependently inhibit A β 42 fibril formation, as demonstrated by TEM. The co-incubation of A β 42 with RES leads to the formation of oligomers, suggesting that RES does not inhibit A β 42 oligomer formation (Feng et al., 2009). Fu et al. (2014) demonstrated by single touch AFM that, when the peptide was co-incubated with RES, low MW oligomers (20 kDa, tetramer) were stabilized. The remodeled RES-capped oligomers showed a reduced cell toxicity, as deduced by MTT assay (Feng et al., 2009; Fu et al., 2014).

The analysis of ^1H - ^{15}N HSQC experiments, showed that resveratrol binds to the peptide N-terminus, as discussed in details in section "Identification of A β Regions Affected by Natural Compounds and Oligomer Remodeling Mechanisms."

Rosmarinic acid (RA) is a phenolic compound present in several plants of the *Lamiaceae* family.

ThT fluorescence and EM studies indicated that RA dose-dependently inhibited fibril formation of A β 40 and A β 42 and destabilized pre-formed fibril (Ono et al., 2004). TEM images indicated the ability of RA in inhibiting A β 42 fibril formation (Sun et al., 2019).

Solution NMR studies highlighted the ability of RA to bind A β 42 oligomers (Airoldi et al., 2013). STD and trNOESY NMR experiments indicated that RA aromatic groups have the highest involvement in the interaction with the oligomers.

Further data on the interaction A β 40/RA were based on docking studies. The models obtained using Autodock starting from the ssNMR structure of A β 40 [PDB ID: 2m4j (Lu et al., 2013)] showed that the complex is stabilized by seven hydrogen bonds involving OH group of dihydroxyphenyl with H13 and L17 and OH group of 2-propenyl with G37. RA interactions thus mask hydrophobic residues of the peptide, thus preventing aggregation (Khan et al., 2019).

Docking of RA to the S-shaped fibril (Fandrich et al., 2018), followed by 150 ns MD simulations suggested that RA mostly interacts with the chain edge, establishing interactions with residues E11–H14 and I32–L34, without inducing remarkable protein conformational changes (Muscat et al., 2020a).

Tanshinones are lipophilic compounds extracted from the roots of *Salvia miltiorrhiza* Bunge. Tanshinone I (TS1) and tanshinone IIA (TS2) are the two most abundant components in the SMB herb. ThT and AFM data clearly demonstrated that they both inhibited amyloid formation at the early lag phase and at the later growth phase (Wang et al., 2013), with TS1 showing better inhibitory potency than TS2. Cell-toxicity experiments reported on a significant level of tanshinone-induced protection of cultured SH-SY5Y cells, indicating that tanshinones are effective inhibitors of A β -induced *in vitro* toxicity. Alternative modes of interactions have been proposed, based on simulations employing different fibril models as starting states (Wang et al., 2013; Dong et al., 2017). Most recent MD simulations in explicit solvent, using a combination of secondary structural analysis, MM-PBSA binding energy calculations, and radial distribution functions computations, indicated that the charged residues within the disordered N-terminus tail of A β 40 and A β 42 are the preferred targets of tanshinones (Dong et al., 2017). According to the simulations, TS molecules favor a disaggregation mechanism driven by the interaction between TS and the N-terminal region of A β 42 fibril, with a shift of the β 1 region and a consequent fibril twist around its fibril axis. As a result, the β -sheet content is reduced and the stability of A β 42 fibril decreased, hampering the lateral association of A β aggregates, inhibiting fibril growth.

Sclerotiorin (SCL) is a chlorine-containing azaphilone-type natural product, that was first isolated in 1940 from *Penicillium sclerotiorum* (Curtin and Reilly, 1940).

Several experimental assays (such as filter retardation assays, EM, CD, ANS) demonstrated unequivocally that SCL perturbs early events in the fibrillar assembly process, leading to the stabilization of small structures with low β -sheet content and a low propensity to form fibrillar aggregates (Wiglenda et al., 2020). Specifically, immunoblot assay and EM indicated that SCL stabilizes A β 42 oligomers migrating at 70–500 KDa. NMR studies showed that SCL addition to A β peptide prevents the broadening, due to aggregation, of ^1H 1D and ^1H - ^{15}N HSQC spectral resonances, holding A β 42 peptides in a soluble state. At variance, A β 42 resonances of untreated samples broaden as a function of time, as a consequence of the formation of high MW NMR invisible species. In line with the reported results, residue level analysis through ^1H - ^{15}N HSQC spectra did not show any chemical shift perturbation, indicating that SCL targets NMR invisible A β species, namely high molecular weight oligomers.

WaterLOGSY experiments assessed the interaction between SCL and A β 42 peptides. In these NMR experiments, the bulk water magnetization is excited and transferred during the NOESY mixing time to the bound ligand *via* different mechanisms. In the WaterLOGSY experiment positive effects were detected only at SCL:A β 42 of 10 indicating that SCL weakly interacts with A β 42 molecules in solution. Ion mobility-mass spectrometry (IM-MS) experiments were further employed to separate A β 42 species based on differences in their overall size, as well as their charge. IM-MS further provides an absolute rotationally averaged collision-cross section (CCS), which allows the prediction of secondary structural changes within aggregating systems. The results indicated that SCL binding leads to conformational compaction at least in a small fraction of A β 42 monomers, which influences their conversion rate into aggregation-competent β -sheet-rich fibrils. The authors propose two potential mechanisms of interaction based on direct association of the hydrophobic diene side chain of SCL with the central or the C-terminal hydrophobic regions of A β 42 peptides, thus facilitating β -sheet formation and promoting the intermolecular association of monomers. Alternatively, the SCL oxygenated bicyclic ring system could form covalent bonds with polar amino acids in the peptide, such as K16 or K28 that are important for the formation of a stable, aggregation-competent b-hairpin structure. IM-MS data provide support to this second hypothesis. The data indicate that SCL binding leads to oligomers remodeling and stabilization of small structures with low β -sheet content, that are up-taken in mammalian cells to a lower extent and exhibit reduced toxicity.

Uncarinic acids are triterpenoids derived from a Japanese medicinal herb *Uncaria rhynchophylla*. A combination of ThT fluorescence experiments and sedimentation assay using HPLC indicated that they inhibit the nucleation phase of A β 42 aggregation (Murakami et al., 2018). Solution NMR studies suggested that Uncarinic acid C can bind A β 42 monomeric species or low molecular-weight oligomers (dimers, trimers, etc.), making contacts with residues R5, H13-L17. Ion mobility-mass spectrometry evidenced the ability of triterpenoids to form a salt bridge between their carboxy group and K16 and K28. The results highlighted the relevant role of carboxy groups whose

direct interaction with monomers, dimers and trimers suppressed further oligomerization (Murakami et al., 2018).

Ligand-Epitopes Involved in the Interaction With A β

Small molecules from natural sources, effective in inhibiting A β aggregation, belong to different classes of chemical compounds, although polyphenols appear to be the most represented class (see **Table 1**). They can affect one or multiple aggregation stages by directly interacting with A β peptide through non-covalent and/or covalent interactions (Ma et al., 2020). Polyphenols ability to hamper A β aggregation has been attributed to the combined action of the phenolic moieties, that can π - π stack or interact hydrophobically with A β aromatic residues and insert into the space of A β aggregates, and/or interact *via* hydrogen bonding through phenolic hydroxyl groups (Fan et al., 2020 and references therein). We focus here on those reports dealing with NMR experiments dedicated to prove the binding epitopes of the natural compound.

Ligand-based NMR spectroscopy, especially STD approaches, were able to dissect the specific ligand binding epitopes for the interaction with amyloid peptides and to select the major components of a natural product interacting with peptide oligomers (Airoldi et al., 2013; Sironi et al., 2014).

In the case of EGCG, NMR approaches demonstrated that the flavan-3-ol unit of catechins is essential for interaction (Sironi et al., 2014) and the epitope mapping, derived from 1D STD, combined with transfer NOESY analyses, revealed that EGCG rings A and D (see **Table 1**) provide the primary contact sites with A β 40 oligomers, while rings B and D undergo significant reorientation, with respect to the plane defined by A and C rings, upon interaction with A β 40 assemblies (Ahmed et al., 2017).

A combination of NMR and synthetic approaches allowed dissecting the differential contribution to A β 42 recognition and binding of the aromatic entities of rosmarinic acid (Airoldi et al., 2013) and chlorogenic acid extracted from coffee (Ciaramelli et al., 2018). NMR approaches have also been extensively employed to investigate the recognition mechanism of flavonoids, widely available in natural foods, for A β 42 oligomers (Guzzi et al., 2017). Quercetin has been identified, on the basis of the STD NMR data, as the best binder, whereby its aromatic A ring represented the region mostly involved in the interaction.

Many polyphenols share a catechol moiety, which plays a role in A β interaction. Indeed, it was demonstrated that the inhibiting activity increased depending on the number of catechol moieties (Tsunoda et al., 2018). When the catechol belongs to a flavonoid, the inhibiting activity has been also related to the formation of Michael adducts with the side chains of K16 and K28 through flavonoid autooxidation (Murakami and Irie, 2019).

A combination of biophysical and docking method additionally identified a guaiacol moiety as an important requirement for the antiaggregating activity of natural based polyphenols (Tomaselli et al., 2019).

Structural planarity is a further feature shared by many inhibitors. Planar molecules are able to establish π - π stacking

with A β aromatic residues, thus destabilizing the intermolecular region in A β 42 aggregates (Murakami and Irie, 2019). Curcumin, tanshinone, and uncarinic acid C share this feature.

Uncarinic acid C belongs to another class of inhibitors, namely sterols. In addition to their interference through the planar hydrophobic structure, it has been proposed that the carboxylic acid group has an important role for the inhibitory activity, as it can establish a salt bridge with K16 and K28 side chains (Bittner, 2006; Murakami et al., 2018), thus hampering further elongation.

The variety of chemical structures observed across the discussed inhibitors underlines once more the importance of natural products as a rich source of bioactive chemical domains, relevant in the discovery and development of new drugs regulating amyloidogenesis.

Identification of A β Regions Affected by Natural Compounds and Oligomer Remodeling Mechanisms

The comparative evaluation of the kind and toxicity of the A β oligomeric species stabilized in the presence of the small molecules, represents a further issue to be considered in ranking the behavior of natural compounds.

Natural compounds can affect amyloid aggregation pathways, targeting different steps of the amyloid aggregation cascade (Figure 1; Ahmed and Melacini, 2018; Wiglenda et al., 2020). The inhibitors action have been attributed to (a) the inhibition of monomers association leading to small aggregates; (b) remodeling of A β oligomers producing off-pathway seeding incompetent species; (c) inhibition of secondary nucleation (Ahmed and Melacini, 2018). Although many natural compounds have been reported to accomplish their action through multiple molecular mechanisms (Fan et al., 2020), the driving mechanism depends on the relative affinities of the inhibitors for A β species. For instance, in the case of EGCG, the mechanism of amyloid inhibition is driven by the preferential binding to A β oligomers (Ahmed et al., 2017; Ahmed and Melacini, 2018).

Soluble oligomers have been recognized as the most neurotoxic species (Klein et al., 2001; Knowles et al., 2014), thus making the targeting of these disease relevant species a valuable therapeutic solution. Many natural compounds can bind oligomers and stabilize off-pathway species. The therapeutical relevance of these interactions can be evaluated testing the cytotoxicity of the resulting oligomers. Indeed, it is widely reported that amyloid aggregate cytotoxicity requires the primary interaction with the cell membrane (Campioni et al., 2010; Benilova et al., 2012) and the poor cytotoxicity is mainly a consequence of their inability to penetrate it (Kayed et al., 2004).

A β soluble oligomers, displaying a very high heterogeneity in size distribution, have been classified in two main groups: low and high molecular weight oligomers, named LMW and HMW, respectively (Fu et al., 2014). A β 42 low MW oligomers (~20 kDa), are essentially composed of tetramers, with smaller amounts of dimers and hexamers. High MW oligomers (~54–60 kDa or higher) appear to be more toxic *in vitro* and *in vivo* compared to A β 42 monomers, low MW oligomers,

and fibrils (Lesne et al., 2006; Frydman-Marom et al., 2009). Natural compounds were shown to interact with both LMW and HMW oligomers. The residue level description of the interactions between natural compounds with LMW oligomers, that are NMR-visible species, can be based on the chemical shift mapping derived from ^1H - ^{15}N HSQC spectra analysis. The NMR characterization of the interactions with soluble HMW oligomers (NMR invisible species) is more challenging and need dark state saturation transfer approaches.

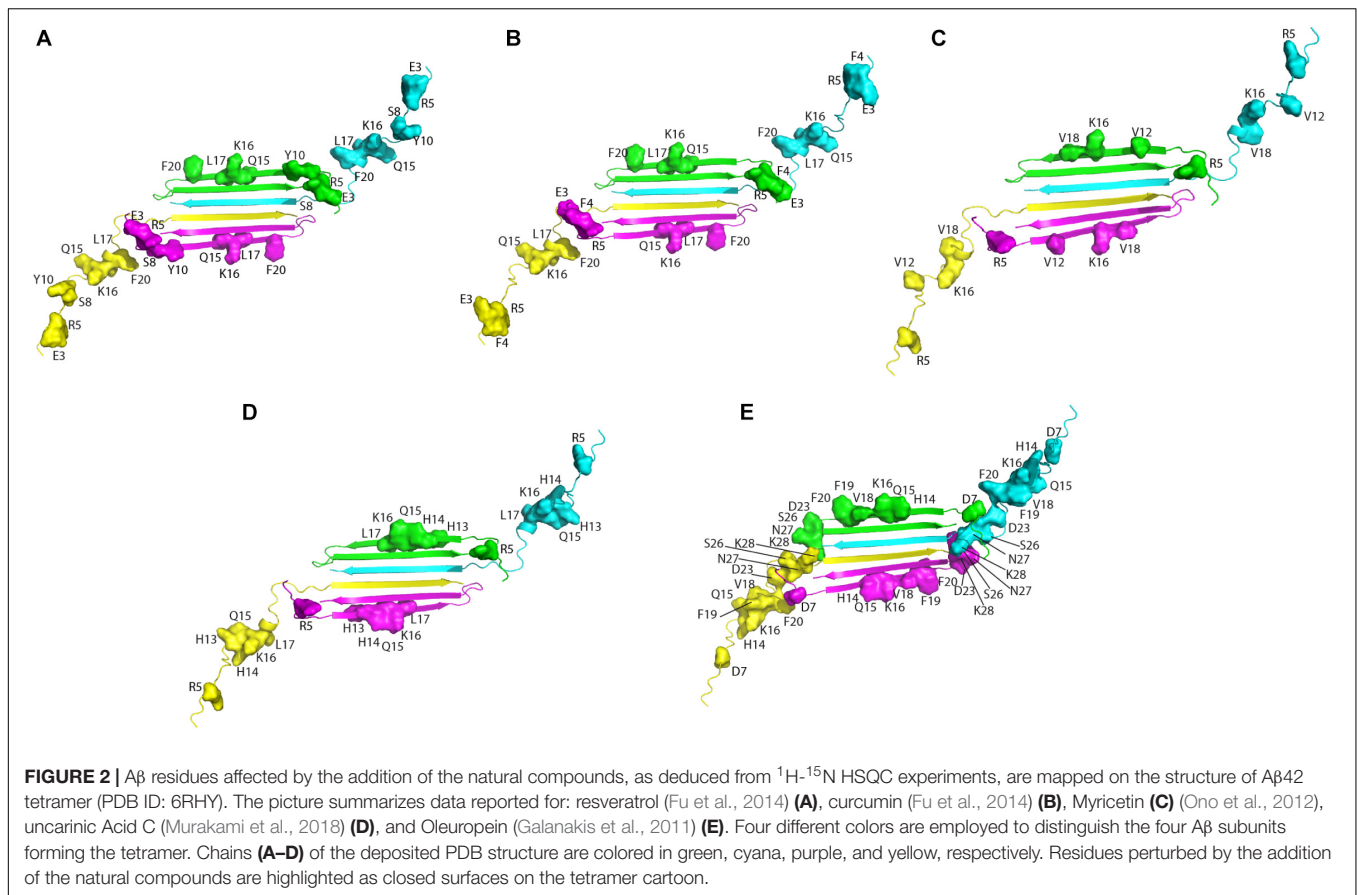
A few natural compounds, namely resveratrol, curcumin, myricitin, Uncarinic Acid C, and oleuropein have been reported to bind monomers or low molecular weight oligomers. Specifically, Fu et al. (2014) demonstrated that resveratrol interacts with A β 42 low molecular weight oligomers (~20 kDa, tetramer). Residue level NMR analysis through ^1H - ^{15}N HSQC experiments indicated that the largest chemical shift changes were observed for residues at the N-terminus and middle region of the A β 42 sequence (E3, R5, S8, Y10, Q15, K16, L17, F20), while the hydrophobic C-terminal residues were substantially unperturbed. A similar pattern of perturbations (E3, F4, R5, Q15, K16, L17, F20) was observed in the presence of curcumin, which is also able to make direct interaction with A β peptide and stabilize A β species endowed with lower cytotoxicity (Fu et al., 2014). The binding of both molecules predominantly occurred at the positions of polar residues, belonging to N-terminal region, which are surface exposed and water accessible, as probed by ^1H - ^{15}N HSQC-NOESY, which measures exchange between the backbone amide protons and water (Fu et al., 2014).

Myricitin can bind A β 42 monomers and or/LMW oligomers as evidenced by marked chemical shift perturbations and amide resonances line broadening for R5, V12, K16, and V18 (Ono et al., 2012).

The sterol Uncarinic Acid C was shown to interact with the A β 42 monomer or LMW oligomers (dimers, trimers, etc.) (Murakami et al., 2018) with R5 and the segment H13-L17 being the most perturbed.

NMR and MS studies showed that oleuropein interacts, non-covalently, in a 1:2 stoichiometry with A β 40. Enzymatic cleavage of the A β :OE complex prior to ESI-MS analysis, indicated that OE interacts with A β regions F4–E11, V12–E22, and F17–K28 (Bazoti et al., 2008). NMR titration studies demonstrated that OE interacts with monomer or low MW oligomers, based on the observation of ^1H and ^{15}N chemical shift perturbation of selected residues (D7, H14, Q15, K16, V18, F19, F20, D23, S26, N27, K28) in ^1H - ^{15}N HSQC spectra of the NMR-visible species (Galanakis et al., 2011).

Altogether, solution NMR data on the interaction of natural compounds with low molecular weight oligomers highlight a common perturbed region located at the N-terminal and β 1 strand. It is interesting to map the residues on the recently published solution NMR structure of the A β 42 oligomer (tetramer) formed in a membrane-mimicking environment (Ciudad et al., 2020). This is the first atomic view of A β 42 oligomers based on experimental data which is greatly helpful to decipher the mechanisms of pathogenesis and design therapeutics (Darling and Shorter, 2020). The tetramer comprises a β -sheet core made of six β -strands, connected by only two



β-turns, leaving two short and two long, flexible N-termini. Notably, residues relevant for the interaction of the natural compounds, as deduced from NMR interaction studies, are all located in highly accessible regions, at the two long flexible N-termini and at the edge of the β-sheet core (Figure 2).

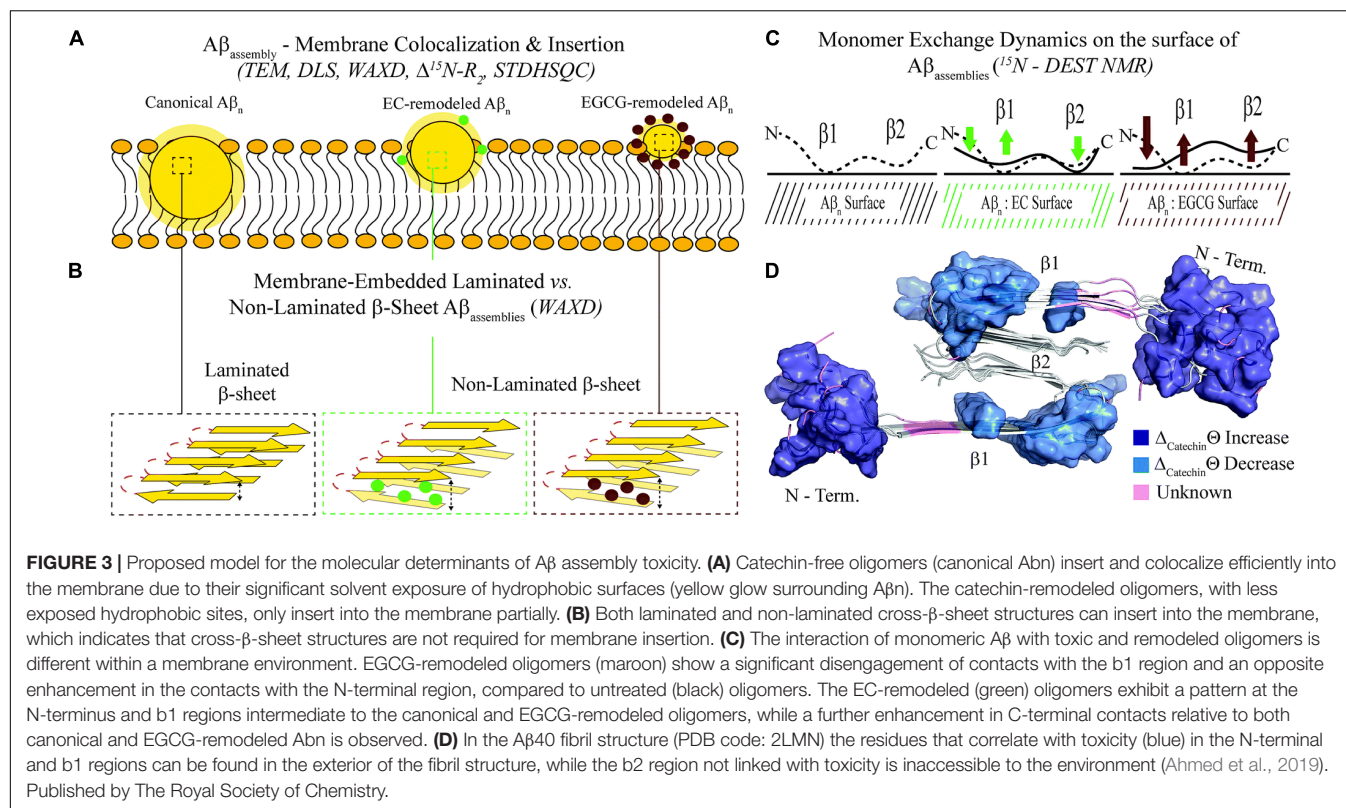
The authors propose, based on MD simulations that the N-termini of the Aβ₄₂ tetramers and octamers, with all their charged residues, are required to traverse through the hydrophobic core of the bilayer, leading to the formation of lipid-stabilized pores. The relevance of the N-terminal tail for membrane interaction and the associated oligomer toxicity has been previously highlighted by many studies (Benilova et al., 2012; Murray et al., 2017; Ahmed et al., 2019). On the basis of the comparative analysis of data reported in the literature (Figure 2), it can be proposed that the binding of the small molecules to Aβ could shield the peptide loci relevant for membrane perturbation/penetration, preventing oligomer insertion. This hypothesis could be reasonable within the framework of the alternative mechanisms of oligomers/membrane interaction up to now proposed, where oligomers (i) bind to membranes inducing local perturbations; (ii) form pore structures, destabilizing cellular ionic homeostasis or (iii) bind to membrane receptors (Um et al., 2012; Jang et al., 2013; Sciacca et al., 2018; Pagano et al., 2019).

An unprecedented contribution to the comprehension of oligomer remodeling induced by natural compounds and of

the molecular determinants of oligomer toxicity is offered by the research work of Melacini's group, based on a combination of several cutting-edge NMR approaches, including ^{15}N dark-state exchange saturation transfer, ^{15}N transverse relaxation (^{15}N R₂), ^1H based 2D saturation transfer difference (STDHSQC) experiments, with complementary techniques such as DLS, fluorescence, EM and wide-angle X-ray diffraction (WAXD) (Ahmed et al., 2017, 2019; Martinez et al., 2020).

The authors were able to show that EGCG remodels oligomers by weakening the monomer-protofibril contacts for the β1 strand peptide region (Q15–E22), which are critical for self-association, thus preventing further monomer addition and stabilizing smaller aggregates. At the same time, EGCG enhances monomer-protofibril interactions at the charged N-terminal region, which is important for the binding to lipid membranes.

The breakthrough of the research is the provision, for the first time, of a structure-toxicity relationship. The authors demonstrated that toxicity of the oligomers remodeled by different catechins scales proportionally to the enhanced solvent exposure of hydrophobic surfaces (Figure 3A). The combination of TEM, WAXD and ^{15}N -based NMR experiments revealed key differences in the recognition of Aβ monomers within a membrane environment by the less toxic EGCG-remodeled Aβ and the more toxic canonical oligomer (Figures 3B–D). The integrated analyses of the data, through agglomerative clustering and Single Value Decomposition, allowed the authors to identify



a cluster of molecular attributes unique to toxic oligomers, including surface hydrophobicity, oligomer size, shielding of the N-terminus and exposure of the β 1 region to monomers. Interestingly, both N-terminus and β 1-turn regions, which were identified as toxicity determinants of A β oligomers, are found in the A β fibril external regions, thus modulating the contacts and the subsequent insertion of A β oligomers into the membranes (Ahmed et al., 2019).

Interestingly, a good agreement is observed among the peptide loci proposed as toxicity determinants (Ahmed et al., 2019), with those deduced from the interaction studies of natural compounds with monomers and/or low molecular weight oligomers (Figure 2).

Ability of Inhibitors to Cross Blood Brain Barrier and Strategies to Improve Their Bioavailability

In a therapeutic perspective, the most promising natural compounds are those that reach the brain tissue in a concentration sufficient to obtain beneficial effects. To this aim, two main factors must be taken in consideration: (i) the ability of the small molecule to cross the BBB; (ii) the compound bioavailability.

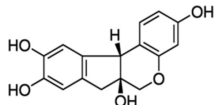
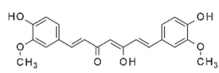
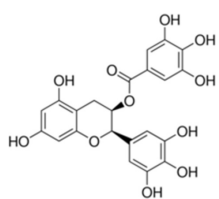
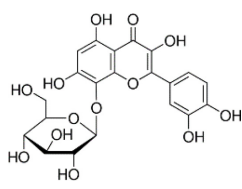
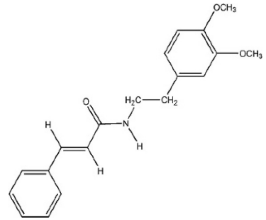
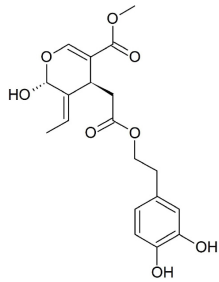
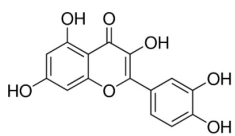
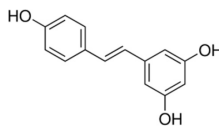
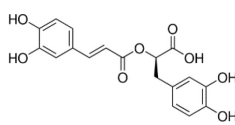
Most of the natural compounds discussed in this review have been characterized for their ability to cross the BBB (Table 2 and references therein). *In vitro* assays were employed for some molecules based on two model systems. The first is a BBB cellular kit, consisting of co-cultures of endothelial cells, pericytes, and

astrocytes (Pervin et al., 2017). The second is a “parallel artificial membrane permeability assay” (PAMPA), which determines the permeability of substances from a donor compartment, through a membrane into an acceptor compartment (Simon et al., 2020). Some natural compounds were instead tested *in vivo*, administering the compounds to mice through intraperitoneal or intra venous injection, and by oral administration. The subsequent analysis of brain tissues homogenates through chromatographic methods, allowed to quantify small molecule concentrations in the brain. In some instances, the efficiency of the compounds to cross BBB was only evaluated on the basis of behavioral tests in animals.

The majority of the molecules tested *in vivo* could cross the BBB, as expected on the basis of their low molecular weight (<500 Da) (Ramalho et al., 2020). The comparative analysis of the concentrations detected in the brain is difficult and is hampered by the different methods and/or units employed by the authors. However, most of the authors underlined that the concentrations reaching the brain were not sufficient to obtain beneficial therapeutic effects.

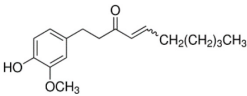
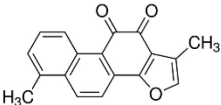
It is worth mentioning here that avoiding the BBB is the conception of a new potential strategy to treat AD, namely to design nanocarriers able to promote the so-called “sink-effect” (Matsuoka et al., 2003; Zhang and Lee, 2011; Tosi et al., 2019). The core of sink-effect hypothesis is based on the idea that brain and plasma A β pools are in equilibrium through the BBB and that the peripheral sequestration of A β may shift this equilibrium toward the peripheral blood circulation, eventually drawing out the excess from the brain and/or from the brain

TABLE 2 | Ability of natural compounds with antiaggregation effects on A β peptide to cross BBB.

Natural product	Chemical structure	BBB crossing (detected concentration)	Methods	References
Brazilin (MW = 286.28)		Low concentrations of free compound reach the brain (0.2543 \pm 0.015 μ g/ml) Need of drug delivery systems	<i>in vivo</i> Intravenous injection Chromatography of brain homogenate	Andrich and Bieschke, 2015
Curcumin (MW = 368.38)		Low concentrations of the free compound reach the brain (4.04 \pm 0.22 μ g/ml) Need of drug delivery systems	<i>in vivo</i> Intravenous injection HPLC analysis of brain homogenate	Fischer et al., 2011
Epigallocatechin gallate (MW = 458.37)		Yes (Permeability coefficient: 9.31 \pm 0.32 10^{-6} cm/s)	BBB cellular kit	Pervin et al., 2017
Gossypin (MW = 480.38)		Quantitative data reported only in the presence of liposomes (concentration not reported)	<i>in vivo</i> Oral administration HPLC analysis of brain homogenate	Fischer et al., 2010
Wgx-50 (MW = 311.38)		Yes (concentration not reported)	<i>in vivo</i> Oral administration LC-MS/MS analysis of brain homogenate	Tang et al., 2013
Oleuropein aglycone (MW = 540.51)		Yes	<i>in vivo</i> Oral administration; behavioral tests in animals	Henriquez et al., 2020a
Quercetin (MW = 302.24)		Low concentrations of free compound reach the brain (12 nmol/g tissue) Need of drug delivery systems	<i>in vivo</i> Oral administration HPLC after solvent extraction	Guzzi et al., 2017; Henriquez et al., 2020b,c
Resveratrol (MW = 228.24)		Low concentrations of free compound reach the brain (406.36 \pm 21.2 ng/g tissue) Need of drug delivery systems	<i>in vivo</i> Intraperitoneal injection HPLC analysis of brain homogenate	Weiner and Selkoe, 2002
Rosmarinic acid (MW = 360.31)		No	<i>in vivo</i> Oral administration HPLC analysis of brain homogenate <i>in vitro</i> BBB cellular kit	Mori et al., 2002

(Continued)

TABLE 2 | Continued

Natural product	Chemical structure	BBB crossing (detected concentration)	Methods	References
6-Shogaol (MW = 276.37)		Yes (Permeability: $8.9 \pm 1.09 \times 10^{-6}$ cm/s)	<i>in vivo</i> Oral administration behavioral tests in mice; <i>in vitro</i> (PAMPA-BBB model)	Selkoe, 2002c; Simon et al., 2020
Tanshinone (MW = 276.29)		Yes (concentration not reported)	<i>in vivo</i> Intraperitoneal injection Coronally sectioned brain Immunostained	Selkoe, 2002b; Selkoe and Schenk, 2003

vessels. Results are reported supporting the hypothesis that A β oligomers spontaneously cross the BBB. Once reached the apical compartment, they are “stolen” by specifically tailored liposomes or polymeric NP decorated with anti-A β antibodies, thus shifting the equilibrium of the peptide from the brain to the peripheral circulation (Mancini et al., 2016; Carradori et al., 2018).

In any therapeutical approach, it is however clear that the main limiting factor is the low bioavailability of the natural compounds, due to their chemical instability, rapid metabolism, and clearance from blood circulation (Wang et al., 1997; Craft et al., 2002; Shen and Ji, 2012; Liu et al., 2016).

A few strategies have been employed to overcome these limitations and develop neuroprotective drugs, efficiently inhibiting A β oligomerization. The first consists in embedding the natural compounds in carriers to enhance bioavailability and direct their distribution toward brain tissue (Ramalho et al., 2020). The investigated drug delivery systems include polymer-based and lipid-based nanoparticles, together with microemulsions and nanoemulsions. The choice of the best nanosystem depends on the physicochemical properties of the drug to be delivered and the drug delivery system properties, i.e., nanoparticle BBB crossing, clearance and induced toxicity (Saraiva et al., 2016; Patra et al., 2018). As an example, in the case of curcumin, which displays low water solubility, a rapid systemic elimination (Yang et al., 2007) and is scarcely capable to penetrate the BBB (Barbara et al., 2017), many drug delivery systems and formulations were investigated including liposomes, solid lipid microparticles, cyclodextrins, and nanoparticles using both natural or synthetic polymers (Barbara et al., 2017; Del Prado-Audelo et al., 2019). These formulations showed enhanced therapeutic properties compared to the free curcumin. Similar approaches were employed for quercetin and resveratrol (Ramalho et al., 2020). It is however, important to note that the prediction of the behavior of NPs *in vivo* still remains a subject of debate, and the “pros and cons” of a variety of NP are still being defined (Ordóñez-Gutiérrez and Wadosell, 2020; Ramalho et al., 2020).

An alternative strategy to enhance bioavailability is the synthesis of natural compounds derivatives. Chemical modifications have been successfully introduced in curcumin to remove labile moieties and improve the water solubility in physiological conditions, preserving the ability to bind A β oligomers and plaques (Airoldi et al., 2011). The chemical conjugation of the active natural compounds with a prodrug

moiety that do not inactivate its inhibitory properties and effectively improve the molecule pharmacokinetic is a promising strategy applied for quercetin (Guzzi et al., 2017) and silybin (García-Vinuales et al., 2020). In particular, glycoconjugation of silybin with trehalose resulted in a significant increase of the bioavailability, with improved solubility and half-life in blood serum. NMR studies further demonstrated that the interaction of the glycoconjugated-silybin with A β oligomers is mainly mediated by silybin, indicating that the threoside moiety does not interfere with silybin interactions (García-Vinuales et al., 2020). In this respect, NMR STD approaches provide important information to guide the effective choice of the prodrug and the linker for chemical conjugation.

Despite the attempted strategies, the bioavailability is still a major problem for the conversion of natural compounds into therapeutics and further innovative scientific and technological efforts are needed in this direction.

CONCLUSION

Inhibiting the toxic aggregation of amyloidogenic A β peptides has been shown to be an attractive approach to fight against AD. Natural compounds that can act as modulators of amyloidogenic aggregation have been widely studied and a number of polyphenolic and non-polyphenolic inhibitors were shown to have powerful effects against protein aggregation through stabilizing monomers, inhibiting nucleation, disaggregating amyloid fibrils, and leading to off-pathway non-toxic oligomeric species.

The main goal of the research in the field, however, remains the identification of the molecular mechanism of natural compound action. An emerging concept that reconciles the large body of literature on the differing mechanisms of amyloid oligomer toxicity, is that toxicity is a pervasive property arising from the exposure of “toxic surfaces” shared by multiple soluble A β assemblies produced by the nucleation-dependent aggregation process (Selkoe, 2002a; Benilova et al., 2012).

Recent advancements in solution NMR, including methods to access the equilibria between NMR visible monomers and soluble high MW NMR invisible oligomers, such as DEST, combined to competitive ANS fluorescence and morphological DLS and EM data, allowed to propose the molecular determinants of A β assembly toxicity (Ahmed et al., 2019). Toxicity is regulated

by the solvent exposure of hydrophobic surfaces. Changes in the accessibility of the hydrophobic β 1-turn region and charged N-terminus to monomer/membrane recognition, have been shown to be the determinants of the induced toxicity (Ahmed et al., 2019). Most of the data reported in the literature converge to indicate these same regions as the preferred binding sites of natural compounds establishing interactions with NMR visible low molecular weight A β species. Interestingly N-term and β 1 stretches are found in the external regions in both A β fibril structure and in the recently published tetramer structure (Ciudad et al., 2020). The structural data of the oligomeric species (Ciudad et al., 2020) together with those on structure-toxicity relationships (Ahmed et al., 2019) indicate, for the first time, that the critical features of the up to now elusive oligomeric species, responsible for AD pathology, are finally coming to light, thus making the design of effective AD inhibitors a realistic option.

Furthermore, some natural compounds, such as EGCG have been shown to interact with many amyloidogenic proteins, such as A β , α Syn, islet amyloid polypeptide (IAPP), huntingtin, tau, and immunoglobulin light chains, revealing that they act on aggregation through a similar mechanism (Andrich and Bieschke, 2015; Martinez et al., 2020). In addition to EGCG, also OleA and quercetin have been classified as potent polyphenols sharing common amyloid targets, namely A β , tau and α -Syn (Henriquez et al., 2020a). These observations strongly suggest

that the structural knowledge of the mechanism of action of these natural compounds should be exploited as a starting point to design and develop therapeutic solutions for the prevention and treatment of different neurodegenerative diseases.

AUTHOR CONTRIBUTIONS

All authors contributed to conceiving the idea of this review, reviewed the literature, contributed to the writing and editing of this manuscript, and given approval to the final version of the manuscript.

ACKNOWLEDGMENTS

HM and LR gratefully acknowledge Fondazione Antonio De Marco (Italy) for technical support. Fulvia Greco is acknowledged for help in manuscript editing. The project was developed within the frame of sPATIALS3 project, financed by the European Regional Development Fund under the ROP of the Lombardy Region ERDF 2014–2020, Axis I “Strengthen technological research, development and innovation”—Action 1.b.1.3 “Support for co-operative R&D activities to develop new sustainable technologies, products and services”—Call Hub.

REFERENCES

- Abbott, N. J., Patabendige, A. A., Dolman, D. E., Yusof, S. R., and Begley, D. J. (2010). Structure and function of the blood-brain barrier. *Neurobiol. Dis.* 37, 13–25. doi: 10.1016/j.nbd.2009.07.030
- Ahmed, M., Davis, J., Aucoin, D., Sato, T., Ahuja, S., Aimoto, S., et al. (2010). Structural conversion of neurotoxic amyloid-beta(1-42) oligomers to fibrils. *Nat. Struct. Mol. Biol.* 17, 561–567. doi: 10.1038/nsmb.1799
- Ahmed, R., Akcan, M., Khondker, A., Rheinstadter, M. C., Bozelli, J. C. Jr., Epan, R. M., et al. (2019). Atomic resolution map of the soluble amyloid beta assembly toxic surfaces. *Chem. Sci.* 10, 6072–6082. doi: 10.1039/c9sc01331h
- Ahmed, R., and Melacini, G. (2018). A solution NMR toolset to probe the molecular mechanisms of amyloid inhibitors. *Chem. Commun. (Camb.)* 54, 4644–4652. doi: 10.1039/c8cc01380b
- Ahmed, R., VanSchouwen, B., Jafari, N., Ni, X., Ortega, J., and Melacini, G. (2017). Molecular mechanism for the (-)-epigallocatechin gallate-induced toxic to nontoxic remodeling of abeta oligomers. *J. Am. Chem. Soc.* 139, 13720–13734. doi: 10.1021/jacs.7b05012
- Airoldi, C., Sironi, E., Dias, C., Marcelo, F., Martins, A., Rauter, A. P., et al. (2013). Natural compounds against Alzheimer's disease: molecular recognition of Abeta1-42 peptide by *Salvia sclareoides* extract and its major component, rosmarinic acid, as investigated by NMR. *Chem. Asian J.* 8, 596–602. doi: 10.1002/asia.201201063
- Airoldi, C., Zona, C., Sironi, E., Colombo, L., Messa, M., Aurilia, D., et al. (2011). Curcumin derivatives as new ligands of Abeta peptides. *J. Biotechnol.* 156, 317–324. doi: 10.1016/j.jbiotec.2011.07.021
- Alzheimer, A. (1907). On a peculiar disease of the cerebral cortex. *Allgem. Zeitsch. Psych. Psych. Gerich. Med.* 64, 146–148.
- Andrade, S., Ramalho, M. J., Loureiro, J. A., and Pereira, M. D. C. (2019). Natural compounds for Alzheimer's disease therapy: a systematic review of preclinical and clinical studies. *Int. J. Mol. Sci.* 20, 2313. doi: 10.3390/ijms20092313
- Andrich, K., and Bieschke, J. (2015). The effect of (-)-epigallocatechin-(3)-gallate on amyloidogenic proteins suggests a common mechanism. *Adv. Exp. Med. Biol.* 863, 139–161. doi: 10.1007/978-3-319-18365-7_7
- Andrich, K., Hegenbart, U., Kimmich, C., Kedia, N., Bergen, H. R. III, Schonland, S., et al. (2017). Aggregation of full-length immunoglobulin light chains from systemic light chain amyloidosis (AL) patients is remodeled by epigallocatechin-3-gallate. *J. Biol. Chem.* 292, 2328–2344. doi: 10.1074/jbc.M116.750323
- Antequera, M. A., Saez, B. C., Ciudad, S. M., Garcia, B. M., Moyano, V. B., Rodriguez, C. P., et al. (2020). [Epidemiology, treatment and mortality in infection by carbapenemase-producing *Enterobacteriaceae*: retrospective study]. *Rev. Chilena Infectol.* 37, 295–303. doi: 10.4067/s0716-10182020000300295
- Armstrong, R. A. (2009). The molecular biology of senile plaques and neurofibrillary tangles in Alzheimer's disease. *Folia Neuropathol.* 47, 289–299.
- Arosio, P., Knowles, T. P., and Linse, S. (2015). On the lag phase in amyloid fibril formation. *Phys. Chem. Chem. Phys.* 17, 7606–7618. doi: 10.1039/c4cp05563b
- Barbara, R., Belletti, D., Pederzoli, F., Masoni, M., Keller, J., Ballestrazzi, A., et al. (2017). Novel curcumin loaded nanoparticles engineered for blood-brain barrier crossing and able to disrupt abeta aggregates. *Int. J. Pharm.* 526, 413–424. doi: 10.1016/j.ijpharm.2017.05.015
- Bazoti, F. N., Bergquist, J., Markides, K., and Tsarabopoulos, A. (2008). Localization of the noncovalent binding site between amyloid-beta-peptide and oleuropein using electrospray ionization FT-ICR mass spectrometry. *J. Am. Soc. Mass Spectrom.* 19, 1078–1085. doi: 10.1016/j.jasms.2008.03.011
- Benilova, I., Karran, E., and De Strooper, B. (2012). The toxic abeta oligomer and Alzheimer's disease: an emperor in need of clothes. *Nat. Neurosci.* 15, 349–357. doi: 10.1038/nn.3028
- Berman, A. Y., Motechin, R. A., Wiesenfeld, M. Y., and Holz, M. K. (2017). The therapeutic potential of resveratrol: a review of clinical trials. *NPJ Precis Oncol.* 1, 35. doi: 10.1038/s41698-017-0038-6
- Bieschke, J., Russ, J., Friedrich, R. P., Ehrnhoefer, D. E., Wobst, H., Neugebauer, K., et al. (2010). EGCG remodels mature alpha-synuclein and amyloid-beta fibrils and reduces cellular toxicity. *Proc. Natl. Acad. Sci. U.S.A.* 107, 7710–7715. doi: 10.1073/pnas.0910723107
- Biet, T., and Peters, T. (2001). Molecular recognition of UDP-Gal by beta-1,4-galactosyltransferase T1. *Angew Chem. Int. Ed. Engl.* 40, 4189–4192. doi: 10.1002/1521-3773(20011119)40:22<4189::AID-ANIE4189>3.0.CO;2-A
- Bittner, S. (2006). When quinones meet amino acids: chemical, physical and biological consequences. *Amino Acids* 30, 205–224. doi: 10.1007/s00726-005-0298-2

- Black, M. M., Slaughter, T., Moshiah, S., Obrocka, M., and Fischer, I. (1996). Tau is enriched on dynamic microtubules in the distal region of growing axons. *J. Neurosci.* 16, 3601–3619.
- Bloom, G. S. (2014). Amyloid-beta and tau: the trigger and bullet in Alzheimer disease pathogenesis. *JAMA Neurol.* 71, 505–508. doi: 10.1001/jamaneurol.2013.5847
- Bui, T. T., and Nguyen, T. H. (2017). Natural product for the treatment of Alzheimer's disease. *J. Basic Clin. Physiol. Pharmacol.* 28, 413–423. doi: 10.1515/jbcp-2016-0147
- Caesar, I., Jonson, M., Nilsson, K. P., Thor, S., and Hammarstrom, P. (2012). Curcumin promotes A-beta fibrillation and reduces neurotoxicity in transgenic *Drosophila*. *PLoS One* 7:e31424. doi: 10.1371/journal.pone.0031424
- Campioni, S., Mannini, B., Zampagni, M., Pensalfini, A., Parrini, C., Evangelisti, E., et al. (2010). A causative link between the structure of aberrant protein oligomers and their toxicity. *Nat. Chem. Biol.* 6, 140–147. doi: 10.1038/nchembio.283
- Carradori, D., Balducci, C., Re, F., Brambilla, D., Le Droumaguet, B., Flores, O., et al. (2018). Antibody-functionalized polymer nanoparticle leading to memory recovery in Alzheimer's disease-like transgenic mouse model. *Nanomedicine* 14, 609–618. doi: 10.1016/j.nano.2017.12.006
- Chiti, F., and Dobson, C. M. (2017). Protein misfolding, amyloid formation, and human disease: a summary of progress over the last decade. *Annu. Rev. Biochem.* 86, 27–68. doi: 10.1146/annurev-biochem-061516-045115
- Ciaramelli, C., Palmioli, A., De Luigi, A., Colombo, L., Sala, G., Riva, C., et al. (2018). NMR-driven identification of anti-amyloidogenic compounds in green and roasted coffee extracts. *Food Chem.* 252, 171–180. doi: 10.1016/j.foodchem.2018.01.075
- Ciudad, S., Puig, E., Botzanowski, T., Meigooni, M., Arango, A. S., Do, J., et al. (2020). Abeta(1-42) tetramer and octamer structures reveal edge conductivity pores as a mechanism for membrane damage. *Nat. Commun.* 11:3014. doi: 10.1038/s41467-020-16566-1
- Cohen, S. I., Linse, S., Luheshi, L. M., Hellstrand, E., White, D. A., Rajah, L., et al. (2013). Proliferation of amyloid-beta42 aggregates occurs through a secondary nucleation mechanism. *Proc. Natl. Acad. Sci. U.S.A.* 110, 9758–9763. doi: 10.1073/pnas.1218402110
- Craft, D. L., Wein, L. M., and Selkoe, D. J. (2002). A mathematical model of the impact of novel treatments on the A beta burden in the Alzheimer's brain, CSF and plasma. *Bull. Math. Biol.* 64, 1011–1031. doi: 10.1006/bulm.2002.0304
- Cremades, N., and Dobson, C. M. (2018). The contribution of biophysical and structural studies of protein self-assembly to the design of therapeutic strategies for amyloid diseases. *Neurobiol. Dis.* 109(Pt B), 178–190. doi: 10.1016/j.nbd.2017.07.009
- Curtin, T. P., and Reilly, J. (1940). Sclerotiorine, C(20)H(20)O(5)Cl, a chlorine-containing metabolic product of *Penicillium sclerotiorum* van Beyma. *Biochem. J.* 34, 1411–1421. doi: 10.1042/bj0341418
- Daccache, A., Lion, C., Sibille, N., Gerard, M., Slomianny, C., Lippens, G., et al. (2011). Oleuropein and derivatives from olives as Tau aggregation inhibitors. *Neurochem. Int.* 58, 700–707. doi: 10.1016/j.neuint.2011.02.010
- Darling, A. L., and Shorter, J. (2020). Atomic Structures of amyloid-beta oligomers illuminate a neurotoxic mechanism. *Trends Neurosci.* 43, 740–743. doi: 10.1016/j.tins.2020.07.006
- Del Prado-Audelo, M. L., Caballero-Floran, I. H., Meza-Toledo, J. A., Mendoza-Munoz, N., Gonzalez-Torres, M., Floran, B., et al. (2019). Formulations of curcumin nanoparticles for brain diseases. *Biomolecules* 9:56. doi: 10.3390/biom9020056
- Dong, M., Zhao, W., Hu, D., Ai, H., and Kang, B. (2017). N-terminus binding preference for either tanshinone or analogue in both inhibition of amyloid aggregation and disaggregation of preformed amyloid fibrils-toward introducing a kind of novel anti-alzheimer compounds. *ACS Chem. Neurosci.* 8, 1577–1588. doi: 10.1021/acschemneuro.7b00080
- Du, W. J., Guo, J. J., Gao, M. T., Hu, S. Q., Dong, X. Y., Han, Y. F., et al. (2015). Brazilin inhibits amyloid beta-protein fibrillogenesis, remodels amyloid fibrils and reduces amyloid cytotoxicity. *Sci. Rep.* 5:7992. doi: 10.1038/srep07992
- Ehrnhoefer, D. E., Bieschke, J., Boeddrich, A., Herbst, M., Masino, L., Lurz, R., et al. (2008). EGCG redirects amyloidogenic polypeptides into unstructured, off-pathway oligomers. *Nat. Struct. Mol. Biol.* 15, 558–566. doi: 10.1038/nsmb.1437
- Estrada, L. D., and Soto, C. (2007). Disrupting beta-amyloid aggregation for Alzheimer disease treatment. *Curr. Top. Med. Chem.* 7, 115–126. doi: 10.2174/156802607779318262
- Fan, H. M., Gu, R. X., Wang, Y. J., Pi, Y. L., Zhang, Y. H., Xu, Q., et al. (2015). Destabilization of Alzheimer's Abeta42 protofibrils with a novel drug candidate wxg-50 by molecular dynamics simulations. *J. Phys. Chem. B* 119, 11196–11202. doi: 10.1021/acs.jpcc.5b03116
- Fan, Q., Liu, Y., Wang, X., Zhang, Z., Fu, Y., Liu, L., et al. (2020). Ginnalin A inhibits aggregation, reverses fibrillogenesis, and alleviates cytotoxicity of amyloid beta(1-42). *ACS Chem. Neurosci.* 11, 638–647. doi: 10.1021/acschemneuro.9b00673
- Fandrich, M., Nystrom, S., Nilsson, K. P. R., Bockmann, A., LeVine, H. III, and Hammarstrom, P. (2018). Amyloid fibril polymorphism: a challenge for molecular imaging and therapy. *J. Intern. Med.* 283, 218–237. doi: 10.1111/joim.12732
- Fawzi, N. L., Ying, J., Ghirlando, R., Torchia, D. A., and Clore, G. M. (2011). Atomic-resolution dynamics on the surface of amyloid-beta protofibrils probed by solution NMR. *Nature* 480, 268–272. doi: 10.1038/nature10577
- Feng, Y., Wang, X. P., Yang, S. G., Wang, Y. J., Zhang, X., Du, X. T., et al. (2009). Resveratrol inhibits beta-amyloid oligomeric cytotoxicity but does not prevent oligomer formation. *Neurotoxicology* 30, 986–995. doi: 10.1016/j.neuro.2009.08.013
- Fischer, J. J., Dalhoff, C., Schrey, A. K., Graebner, O. Y., Michaelis, S., Andrich, K., et al. (2011). Dasatinib, imatinib and staurosporine capture compounds – Complementary tools for the profiling of kinases by Capture Compound Mass Spectrometry (CCMS). *J. Proteomics* 75, 160–168. doi: 10.1016/j.jprot.2011.05.035
- Fischer, J. J., Graebner Baessler, O. Y., Dalhoff, C., Michaelis, S., Schrey, A. K., Ungewiss, J., et al. (2010). Comprehensive identification of staurosporine-binding kinases in the hepatocyte cell line HepG2 using Capture Compound Mass Spectrometry (CCMS). *J. Proteome Res.* 9, 806–817. doi: 10.1021/pr9007333
- Frydman-Marom, A., Rechter, M., Shefler, I., Bram, Y., Shalev, D. E., and Gazit, E. (2009). Cognitive-performance recovery of Alzheimer's disease model mice by modulation of early soluble amyloid assemblies. *Angew Chem. Int. Ed. Engl.* 48, 1981–1986. doi: 10.1002/anie.200802123
- Fu, Z., Aucoin, D., Ahmed, M., Ziliox, M., Van Nostrand, W. E., and Smith, S. O. (2014). Capping of abeta42 oligomers by small molecule inhibitors. *Biochemistry* 53, 7893–7903. doi: 10.1021/bi500910b
- Galanakis, P. A., Bazoti, F. N., Bergquist, J., Markides, K., Spyroulias, G. A., and Tsaropoulos, A. (2011). Study of the interaction between the amyloid beta peptide (1-40) and antioxidant compounds by nuclear magnetic resonance spectroscopy. *Biopolymers* 96, 316–327. doi: 10.1002/bip.21558
- Garcia-Vinuales, S., Ahmed, R., Sciacca, M. F. M., Lanza, V., Giuffrida, M. L., Zimbone, S., et al. (2020). Trehalose conjugates of silybin as prodrugs for targeting toxic abeta aggregates. *ACS Chem. Neurosci.* 11, 2566–2576. doi: 10.1021/acschemneuro.0c00232
- Ge, J. F., Qiao, J. P., Qi, C. C., Wang, C. W., and Zhou, J. N. (2012). The binding of resveratrol to monomer and fibril amyloid beta. *Neurochem. Int.* 61, 1192–1201. doi: 10.1016/j.neuint.2012.08.012
- Giorgetti, S., Greco, C., Tortora, P., and Aprile, F. A. (2018). Targeting amyloid aggregation: an overview of strategies and mechanisms. *Int. J. Mol. Sci.* 19:2677. doi: 10.3390/ijms19092677
- Gotz, J., Chen, F., van Dorpe, J., and Nitsch, R. M. (2001). Formation of neurofibrillary tangles in P301 tau transgenic mice induced by Abeta 42 fibrils. *Science* 293, 1491–1495. doi: 10.1126/science.1062097
- Greenberg, S. M., Bacskai, B. J., Hernandez-Guillamon, M., Pruzin, J., Sperling, R., and van Veluw, S. J. (2020). Cerebral amyloid angiopathy and Alzheimer disease – one peptide, two pathways. *Nat. Rev. Neurol.* 16, 30–42. doi: 10.1038/s41582-019-0281-2
- Guo, Y., Shi, S., Tang, M., Liang, D., Xu, W., Wang, L., et al. (2014). The suppressive effects of gx-50 on Abeta-induced chemotactic migration of microglia. *Int. Immunopharmacol.* 19, 283–289. doi: 10.1016/j.intimp.2014.01.025
- Guzzi, C., Colombo, L., Luigi, A., Salmons, M., Nicotra, F., and Airolidi, C. (2017). Flavonoids and their glycosides as anti-amyloidogenic compounds: abeta1-42 interaction studies to gain new insights into their potential for alzheimer's disease prevention and therapy. *Chem. Asian J.* 12, 67–75. doi: 10.1002/asia.201601291

- Haass, C., Kaether, C., Thinakaran, G., and Sisodia, S. (2012). Trafficking and proteolytic processing of APP. *Cold Spring Harb. Perspect. Med.* 2:a006270. doi: 10.1101/cshperspect.a006270
- Haass, C., and Selkoe, D. J. (1993). Cellular processing of beta-amyloid precursor protein and the genesis of amyloid beta-peptide. *Cell* 75, 1039–1042. doi: 10.1016/0092-8674(93)90312-e
- Hamaguchi, T., Ono, K., and Yamada, M. (2010). REVIEW: curcumin and Alzheimer's disease. *CNS Neurosci. Ther.* 16, 285–297. doi: 10.1111/j.1755-5949.2010.00147.x
- Hardy, J., and Selkoe, D. J. (2002). The amyloid hypothesis of Alzheimer's disease: progress and problems on the road to therapeutics. *Science* 297, 353–356. doi: 10.1126/science.1072994
- Hardy, J. A., and Higgins, G. A. (1992). Alzheimer's disease: the amyloid cascade hypothesis. *Science* 256, 184–185. doi: 10.1126/science.1566067
- Henriquez, G., Gomez, A., Guerrero, E., and Narayan, M. (2020a). Potential Role of natural polyphenols against protein aggregation toxicity: In Vitro, In Vivo, and clinical studies. *ACS Chem. Neurosci.* 11, 2915–2934. doi: 10.1021/acscchemneuro.0c00381
- Henriquez, G., Mendez, L., Schmid, A. N., Guerrero, E. D., Collins, S. A., Castaneda, E., et al. (2020b). Testing amyloid cross-toxicity in the vertebrate brain. *ACS Omega* 5, 15586–15591. doi: 10.1021/acscomega.0c01819
- Henriquez, G., Mendez, L., Varela-Ramirez, A., Guerrero, E., and Narayan, M. (2020c). Neuroprotective effect of Brazilin on amyloid beta (25-35)-induced pathology in a human neuroblastoma model. *ACS Omega* 5, 13785–13792. doi: 10.1021/acscomega.0c00396
- Hou, L., Shao, H., Zhang, Y., Li, H., Menon, N. K., Neuhaus, E. B., et al. (2004). Solution NMR studies of the A beta(1-40) and A beta(1-42) peptides establish that the Met35 oxidation state affects the mechanism of amyloid formation. *J. Am. Chem. Soc.* 126, 1992–2005. doi: 10.1021/ja036813f
- Hoyer, W., Gronwall, C., Jonsson, A., Stahl, S., and Hard, T. (2008). Stabilization of a beta-hairpin in monomeric Alzheimer's amyloid-beta peptide inhibits amyloid formation. *Proc. Natl. Acad. Sci. U.S.A.* 105, 5099–5104. doi: 10.1073/pnas.0711731105
- Hurtado, D. E., Molina-Porcel, L., Iba, M., Aboagye, A. K., Paul, S. M., Trojanowski, J. Q., et al. (2010). A beta accelerates the spatiotemporal progression of tau pathology and augments tau amyloidosis in an Alzheimer mouse model. *Am. J. Pathol.* 177, 1977–1988. doi: 10.2353/ajpath.2010.100346
- Jang, H., Connolly, L., Arce, F. T., Ramachandran, S., Kagan, B. L., Lal, R., et al. (2013). Mechanisms for the insertion of toxic, fibril-like beta-amyloid oligomers into the membrane. *J. Chem. Theory Comput.* 9, 822–833. doi: 10.1021/ct300916f
- Kayed, R., Head, E., Sarsoza, F., Saing, T., Cotman, C. W., Necula, M., et al. (2007). Fibril specific, conformation dependent antibodies recognize a generic epitope common to amyloid fibrils and fibrillar oligomers that is absent in prefibrillar oligomers. *Mol. Neurodegener.* 2:18. doi: 10.1186/1750-1326-2-18
- Kayed, R., Sokolov, Y., Edmonds, B., McIntire, T. M., Milton, S. C., Hall, J. E., et al. (2004). Permeabilization of lipid bilayers is a common conformation-dependent activity of soluble amyloid oligomers in protein misfolding diseases. *J. Biol. Chem.* 279, 46363–46366. doi: 10.1074/jbc.C400262020
- Khan, R. H., Siddiqi, M. K., Uversky, V. N., and Salahuddin, P. (2019). Molecular docking of Abeta1-40 peptide and its Iowa D23N mutant using small molecule inhibitors: possible mechanisms of Abeta-peptide inhibition. *Int. J. Biol. Macromol.* 127, 250–270. doi: 10.1016/j.ijbiomac.2018.12.271
- Klein, W. L., Kraft, G. A., and Finch, C. E. (2001). Targeting small Abeta oligomers: the solution to an Alzheimer's disease conundrum? *Trends Neurosci.* 24, 219–224. doi: 10.1016/s0166-2236(00)01749-5
- Knowles, T. P., Vendruscolo, M., and Dobson, C. M. (2014). The amyloid state and its association with protein misfolding diseases. *Nat. Rev. Mol. Cell Biol.* 15, 384–396. doi: 10.1038/nrm3810
- Leri, M., Natalello, A., Bruzzone, E., Stefani, M., and Bucciantini, M. (2019). Oleuropein aglycone and hydroxytyrosol interfere differently with toxic Abeta1-42 aggregation. *Food Chem. Toxicol.* 129, 1–12. doi: 10.1016/j.fct.2019.04.015
- Leri, M., Nosi, D., Natalello, A., Porcari, R., Ramazzotti, M., Chiti, F., et al. (2016). The polyphenol Oleuropein aglycone hinders the growth of toxic transthyretin amyloid assemblies. *J. Nutr. Biochem.* 30, 153–166. doi: 10.1016/j.jnutbio.2015.12.009
- Leroy, K., Ando, K., Laporte, V., Dedecker, R., Suain, V., Authélet, M., et al. (2012). Lack of tau proteins rescues neuronal cell death and decreases amyloidogenic processing of APP in APP/PS1 mice. *Am. J. Pathol.* 181, 1928–1940. doi: 10.1016/j.ajpath.2012.08.012
- Lesne, S., Koh, M. T., Kotilinek, L., Kaye, R., Glabe, C. G., Yang, A., et al. (2006). A specific amyloid-beta protein assembly in the brain impairs memory. *Nature* 440, 352–357. doi: 10.1038/nature04533
- Lewis, J., Dickson, D. W., Lin, W. L., Chisholm, L., Corral, A., Jones, G., et al. (2001). Enhanced neurofibrillary degeneration in transgenic mice expressing mutant tau and APP. *Science* 293, 1487–1491. doi: 10.1126/science.1058189
- Linse, S. (2017). Monomer-dependent secondary nucleation in amyloid formation. *Biophys. Rev.* 9, 329–338. doi: 10.1007/s12551-017-0289-z
- Liu, G., Gaines, J. C., Robbins, K. J., and Lazo, N. D. (2012). Kinetic profile of amyloid formation in the presence of an aromatic inhibitor by nuclear magnetic resonance. *ACS Med. Chem. Lett.* 3, 856–859. doi: 10.1021/ml300147m
- Liu, W., Zhai, Y., Heng, X., Che, F. Y., Chen, W., Sun, D., et al. (2016). Oral bioavailability of curcumin: problems and advancements. *J. Drug Target* 24, 694–702. doi: 10.3109/1061186X.2016.1157883
- Lopez, O. L., and Kuller, L. H. (2019). Epidemiology of aging and associated cognitive disorders: Prevalence and incidence of Alzheimer's disease and other dementias. *Handb. Clin. Neurol.* 167, 139–148. doi: 10.1016/B978-0-12-804766-8.00009-1
- Lu, J. X., Qiang, W., Yau, W. M., Schwieters, C. D., Meredith, S. C., and Tycko, R. (2013). Molecular structure of beta-amyloid fibrils in Alzheimer's disease brain tissue. *Cell* 154, 1257–1268. doi: 10.1016/j.cell.2013.08.035
- Ma, L., Yang, C., Zheng, J., Chen, Y., Xiao, Y., and Huang, K. (2020). Non-polyphenolic natural inhibitors of amyloid aggregation. *Eur. J. Med. Chem.* 192:112197. doi: 10.1016/j.ejmech.2020.112197
- Mancini, S., Minniti, S., Gregori, M., Sancini, G., Cagnotto, A., Couraud, P. O., et al. (2016). The hunt for brain Abeta oligomers by peripherally circulating multi-functional nanoparticles: Potential therapeutic approach for Alzheimer disease. *Nanomedicine* 12, 43–52. doi: 10.1016/j.nano.2015.09.003
- Martin, I. (2017). Resveratrol for Alzheimer's disease? *Sci. Transl. Med.* 9:eam6055. doi: 10.1126/scitranslmed.aam6055
- Martinez, P. K., Ahmed, R., and Melacini, G. (2020). Catechins as Tools to understand the molecular basis of neurodegeneration. *Molecules* 25:3571. doi: 10.3390/molecules25163571
- Masuda, Y., Fukuchi, M., Yatagawa, T., Tada, M., Takeda, K., Irie, K., et al. (2011). Solid-state NMR analysis of interaction sites of curcumin and 42-residue amyloid beta-protein fibrils. *Bioorg. Med. Chem.* 19, 5967–5974. doi: 10.1016/j.bmc.2011.08.052
- Matsuoka, Y., Saito, M., LaFrancois, J., Saito, M., Gaynor, K., Olm, V., et al. (2003). Novel therapeutic approach for the treatment of Alzheimer's disease by peripheral administration of agents with an affinity to beta-amyloid. *J. Neurosci.* 23, 29–33.
- Meyer, B., and Peters, T. (2003). NMR spectroscopy techniques for screening and identifying ligand binding to protein receptors. *Angew Chem. Int. Ed. Engl.* 42, 864–890. doi: 10.1002/anie.200390233
- Mori, C., Spooner, E. T., Wisniewski, K. E., Wisniewski, T. M., Yamaguchi, H., Saido, T. C., et al. (2002). Intraneuronal Abeta42 accumulation in Down syndrome brain. *Amyloid* 9, 88–102.
- Murakami, K., and Irie, K. (2019). Three structural features of functional food components and herbal medicine with amyloid beta42 anti-aggregation properties. *Molecules* 24:125. doi: 10.3390/molecules2411125
- Murakami, K., Yoshioka, T., Horii, S., Hanaki, M., Midorikawa, S., Taniwaki, S., et al. (2018). Role of the carboxy groups of triterpenoids in their inhibition of the nucleation of amyloid beta42 required for forming toxic oligomers. *Chem. Commun. (Camb.)* 54, 6272–6275. doi: 10.1039/c8cc03230k
- Murray, B., Sharma, B., and Belfort, G. (2017). N-Terminal Hypothesis for Alzheimer's Disease. *ACS Chem. Neurosci.* 8, 432–434. doi: 10.1021/acscchemneuro.7b00037
- Muscat, S., Pallante, L., Stojceski, F., Danani, A., Grasso, G., and Deriu, M. A. (2020a). The Impact of natural compounds on S-shaped Abeta42 fibril: from molecular docking to biophysical characterization. *Int. J. Mol. Sci.* 21:2017. doi: 10.3390/ijms21062017
- Muscat, S., Stojceski, F., and Danani, A. (2020b). Elucidating the effect of static electric field on amyloid beta 1-42 supramolecular assembly. *J. Mol. Graph. Model.* 96:107535. doi: 10.1016/j.jmgm.2020.107535

- Nasica-Labouze, J., Nguyen, P. H., Sterpone, F., Berthoumieu, O., Buchete, N. V., Cote, S., et al. (2015). Amyloid beta protein and Alzheimer's Disease: when computer simulations complement experimental studies. *Chem. Rev.* 115, 3518–3563. doi: 10.1021/cr500638n
- Necula, M., Kaye, D., Milton, S., and Glabe, C. G. (2007). Small molecule inhibitors of aggregation indicate that amyloid beta oligomerization and fibrillization pathways are independent and distinct. *J. Biol. Chem.* 282, 10311–10324. doi: 10.1074/jbc.M608207200
- Ono, K., Hasegawa, K., Naiki, H., and Yamada, M. (2004). Curcumin has potent anti-amyloidogenic effects for Alzheimer's beta-amyloid fibrils in vitro. *J. Neurosci. Res.* 75, 742–750. doi: 10.1002/jnr.20025
- Ono, K., Hirohata, M., and Yamada, M. (2005). Ferulic acid destabilizes preformed beta-amyloid fibrils in vitro. *Biochem. Biophys. Res. Commun.* 336, 444–449. doi: 10.1016/j.bbrc.2005.08.148
- Ono, K., Li, L., Takamura, Y., Yoshiike, Y., Zhu, L., Han, F., et al. (2012). Phenolic compounds prevent amyloid beta-protein oligomerization and synaptic dysfunction by site-specific binding. *J. Biol. Chem.* 287, 14631–14643. doi: 10.1074/jbc.M111.325456
- Ono, K., Yoshiike, Y., Takashima, A., Hasegawa, K., Naiki, H., and Yamada, M. (2003). Potent anti-amyloidogenic and fibril-destabilizing effects of polyphenols in vitro: implications for the prevention and therapeutics of Alzheimer's disease. *J. Neurochem.* 87, 172–181. doi: 10.1046/j.1471-4159.2003.01976.x
- Ordóñez-Gutiérrez, L., and Wandosell, F. (2020). Nanoliposomes as a therapeutic tool for Alzheimer's disease. *Front. Synaptic Neurosci.* 12:20. doi: 10.3389/fnsyn.2020.00020
- Pagano, K., Galante, D., D'Arrigo, C., Corsaro, A., Nizzari, M., Florio, T., et al. (2019). Effects of prion protein on Abeta42 and pyroglutamate-modified Abeta42Epsilon3-42 oligomerization and toxicity. *Mol. Neurobiol.* 56, 1957–1971. doi: 10.1007/s12035-018-1202-x
- Patra, J. K., Das, G., Fraceto, L. F., Campos, E. V. R., Rodriguez-Torres, M. D. P., Acosta-Torres, L. S., et al. (2018). Nano based drug delivery systems: recent developments and future prospects. *J. Nanobiotechnol.* 16:71. doi: 10.1186/s12951-018-0392-8
- Perchiasci, J. M., Ladiwala, A. R., Bhattacharya, M., and Tessier, P. M. (2012). Structure-based design of conformation- and sequence-specific antibodies against amyloid beta. *Proc. Natl. Acad. Sci. U.S.A.* 109, 84–89. doi: 10.1073/pnas.1111232108
- Pervin, M., Unno, K., Nakagawa, A., Takahashi, Y., Iguchi, K., Yamamoto, H., et al. (2017). Blood brain barrier permeability of (-)-epigallocatechin gallate, its proliferation-enhancing activity of human neuroblastoma SH-SY5Y cells, and its preventive effect on age-related cognitive dysfunction in mice. *Biochem. Biophys. Res. Rep.* 9, 180–186. doi: 10.1016/j.bbrep.2016.12.012
- Qiu, T., Liu, Q., Chen, Y. X., Zhao, Y. F., and Li, Y. M. (2015). Abeta42 and Abeta40: similarities and differences. *J. Pept. Sci.* 21, 522–529. doi: 10.1002/psc.2789
- Ramallo, M. J., Andrade, S., Loureiro, J. A., and do Carmo Pereira, M. (2020). Nanotechnology to improve the Alzheimer's disease therapy with natural compounds. *Drug Deliv. Transl. Res.* 10, 380–402. doi: 10.1007/s13346-019-00694-3
- Rauf, A., Imran, M., Butt, M. S., Nadeem, M., Peters, D. G., and Mubarak, M. S. (2018). Resveratrol as an anti-cancer agent: a review. *Crit. Rev. Food Sci. Nutr.* 58, 1428–1447. doi: 10.1080/10408398.2016.1263597
- Sadhukhan, P., Saha, S., Dutta, S., Mahalanobish, S., and Sil, P. C. (2018). Nutraceuticals: an emerging therapeutic approach against the pathogenesis of Alzheimer's disease. *Pharmacol. Res.* 129, 100–114. doi: 10.1016/j.phrs.2017.11.028
- Saraiva, C., Praca, C., Ferreira, R., Santos, T., Ferreira, L., and Bernardino, L. (2016). Nanoparticle-mediated brain drug delivery: overcoming blood-brain barrier to treat neurodegenerative diseases. *J. Control Release* 235, 34–47. doi: 10.1016/j.jconrel.2016.05.044
- Scheidt, T., Lapinska, U., Kumita, J. R., Whiten, D. R., Klenerman, D., Wilson, M. R., et al. (2019). Secondary nucleation and elongation occur at different sites on Alzheimer's amyloid-beta aggregates. *Sci. Adv.* 5:eau3112. doi: 10.1126/sciadv.aau3112
- Sciacca, M. F. M., Monaco, I., La Rosa, C., and Milardi, D. (2018). The active role of Ca(2+) ions in Abeta-mediated membrane damage. *Chem. Commun. (Camb.)* 54, 3629–3631. doi: 10.1039/c8cc01132j
- Selkoe, D. (2002a). Alzheimer's disease: conversation with an expert. *Harv. Health Lett.* 27:5.
- Selkoe, D. J. (1991). The molecular pathology of Alzheimer's disease. *Neuron* 6, 487–498. doi: 10.1016/0896-6273(91)90052-2
- Selkoe, D. J. (2002b). Alzheimer's disease is a synaptic failure. *Science* 298, 789–791. doi: 10.1126/science.1074069
- Selkoe, D. J. (2002c). Deciphering the genesis and fate of amyloid beta-protein yields novel therapies for Alzheimer disease. *J. Clin. Invest.* 110, 1375–1381. doi: 10.1172/JCI16783
- Selkoe, D. J., and Hardy, J. (2016). The amyloid hypothesis of Alzheimer's disease at 25 years. *EMBO Mol. Med.* 8, 595–608. doi: 10.15252/emmm.201606210
- Selkoe, D. J., and Schenk, D. (2003). Alzheimer's disease: molecular understanding predicts amyloid-based therapeutics. *Annu. Rev. Pharmacol. Toxicol.* 43, 545–584. doi: 10.1146/annurev.pharmtox.43.100901.140248
- Shen, L., and Ji, H. F. (2012). The pharmacology of curcumin: is it the degradation products? *Trends Mol. Med.* 18, 138–144. doi: 10.1016/j.molmed.2012.01.004
- Shi, S., Liang, D., Chen, Y., Xie, Y., Wang, Y., Wang, L., et al. (2016). Gx-50 reduces beta-amyloid-induced TNF-alpha, IL-1beta, NO, and PGE2 expression and inhibits NF-kappaB signaling in a mouse model of Alzheimer's disease. *Eur. J. Immunol.* 46, 665–676. doi: 10.1002/eji.201545855
- Simon, A., Darcsi, A., Kery, A., and Riethmuller, E. (2020). Blood-brain barrier permeability study of ginger constituents. *J. Pharm. Biomed. Anal.* 177:112820. doi: 10.1016/j.jpba.2019.112820
- Sironi, E., Colombo, L., Lompo, A., Messa, M., Bonanomi, M., Regonesi, M. E., et al. (2014). Natural compounds against neurodegenerative diseases: molecular characterization of the interaction of catechins from green tea with Abeta1-42, PrP106-126, and ataxin-3 oligomers. *Chemistry* 20, 13793–13800. doi: 10.1002/chem.201403188
- Stefanescu, R., Stanciu, G. D., Luca, A., Paduraru, L., and Tamba, B. I. (2020). Secondary metabolites from plants possessing inhibitory properties against beta-amyloid aggregation as revealed by thioflavin-T assay and correlations with investigations on transgenic mouse models of Alzheimer's disease. *Biomolecules* 10:870. doi: 10.3390/biom10060870
- Sun, J. Y., Jiang, G. D., and Shigemori, H. (2019). Inhibitory Activity on amyloid aggregation of rosmarinic acid and its substructures from isodon japonicus. *Nat. Product Commun.* 14:5. doi: 10.1177/1934578X19843039
- Tang, M., Shi, S., Guo, Y., Xu, W., Wang, L., Chen, Y., et al. (2014). GSK-3/CREB pathway involved in the gx-50's effect on Alzheimer's disease. *Neuropharmacology* 81, 256–266. doi: 10.1016/j.neuropharm.2014.02.008
- Tang, M., Wang, Z., Zhou, Y., Xu, W., Li, S., Wang, L., et al. (2013). A novel drug candidate for Alzheimer's disease treatment: gx-50 derived from Zanthoxylum bungeanum. *J. Alzheimers Dis.* 34, 203–213. doi: 10.3233/JAD-121831
- Tellone, E., Galtieri, A., Russo, A., Giardina, B., and Ficarra, S. (2015). Resveratrol: a focus on several neurodegenerative diseases. *Oxid. Med. Cell. Longev.* 2015:392169. doi: 10.1155/2015/392169
- Tomaselli, S., La Vitola, P., Pagano, K., Brandi, E., Santamaria, G., Galante, D., et al. (2019). Biophysical and in vivo studies identify a new natural-based polyphenol, counteracting abeta oligomerization in vitro and abeta oligomer-mediated memory impairment and neuroinflammation in an acute mouse model of Alzheimer's disease. *ACS Chem. Neurosci.* 10, 4462–4475. doi: 10.1021/acschemneuro.9b00241
- Tosi, G., Pederzoli, F., Belletti, D., Vandelli, M. A., Forni, F., Duskey, J. T., et al. (2019). Nanomedicine in Alzheimer's disease: amyloid beta targeting strategy. *Prog. Brain Res.* 245, 57–88. doi: 10.1016/bs.pbr.2019.03.001
- Tsunoda, T., Takase, M., and Shigemori, H. (2018). Structure-activity relationship of clovamide and its related compounds for the inhibition of amyloid beta aggregation. *Bioorg. Med. Chem.* 26, 3202–3209. doi: 10.1016/j.bmc.2018.04.044
- Um, J. W., Nygaard, H. B., Heiss, J. K., Kostylev, M. A., Stagi, M., Vortmeyer, A., et al. (2012). Alzheimer amyloid-beta oligomer bound to postsynaptic prion protein activates Fyn to impair neurons. *Nat. Neurosci.* 15, 1227–1235. doi: 10.1038/nn.3178
- Wang, Q., Yu, X., Patal, K., Hu, R., Chuang, S., Zhang, G., et al. (2013). Tanshinones inhibit amyloid aggregation by amyloid-beta peptide, disaggregate amyloid fibrils, and protect cultured cells. *ACS Chem. Neurosci.* 4, 1004–1015. doi: 10.1021/cn400051e
- Wang, Y. J., Pan, M. H., Cheng, A. L., Lin, L. I., Ho, Y. S., Hsieh, C. Y., et al. (1997). Stability of curcumin in buffer solutions and characterization of its degradation

- products. *J. Pharm. Biomed. Anal.* 15, 1867–1876. doi: 10.1016/s0731-7085(96)02024-9
- Weiner, H. L., and Selkoe, D. J. (2002). Inflammation and therapeutic vaccination in CNS diseases. *Nature* 420, 879–884. doi: 10.1038/nature01325
- Wiglenda, T., Groenke, N., Hoffmann, W., Manz, C., Diez, L., Buntru, A., et al. (2020). Sclerotiorin stabilizes the assembly of nonfibrillar Aβ₄₂ oligomers with low toxicity, seeding activity, and beta-sheet content. *J. Mol. Biol.* 432, 2080–2098. doi: 10.1016/j.jmb.2020.01.033
- Yang, K. Y., Lin, L. C., Tseng, T. Y., Wang, S. C., and Tsai, T. H. (2007). Oral bioavailability of curcumin in rat and the herbal analysis from *Curcuma longa* by LC-MS/MS. *J. Chromatogr. B Analyt. Technol. Biomed. Life Sci.* 853, 183–189. doi: 10.1016/j.jchromb.2007.03.010
- Zempel, H., Luedtke, J., Kumar, Y., Biernat, J., Dawson, H., Mandelkow, E., et al. (2013). Amyloid-beta oligomers induce synaptic damage via Tau-dependent microtubule severing by TLL6 and spastin. *EMBO J.* 32, 2920–2937. doi: 10.1038/emboj.2013.207
- Zenaro, E., Piacentino, G., and Constantin, G. (2017). The blood-brain barrier in Alzheimer's disease. *Neurobiol. Dis.* 107, 41–56. doi: 10.1016/j.nbd.2016.07.007
- Zhang, Y., and Lee, D. H. (2011). Sink hypothesis and therapeutic strategies for attenuating Aβ levels. *Neuroscientist* 17, 163–173. doi: 10.1177/1073858410381532
- Conflict of Interest:** The authors declare that the research was conducted in the absence of any commercial or financial relationships that could be construed as a potential conflict of interest.

Copyright © 2020 Pagano, Tomaselli, Molinari and Ragona. This is an open-access article distributed under the terms of the Creative Commons Attribution License (CC BY). The use, distribution or reproduction in other forums is permitted, provided the original author(s) and the copyright owner(s) are credited and that the original publication in this journal is cited, in accordance with accepted academic practice. No use, distribution or reproduction is permitted which does not comply with these terms.



Novel Phosphorylation-State Specific Antibodies Reveal Differential Deposition of Ser26 Phosphorylated A β Species in a Mouse Model of Alzheimer's Disease

Sathish Kumar^{1*}, Akshay Kapadia¹, Sandra Theil¹, Pranav Joshi¹, Florian Riffel¹, Michael T. Heneka^{2,3} and Jochen Walter^{1*}

¹Department of Neurology, University of Bonn Medical Center, Bonn, Germany, ²Department of Neurodegenerative Diseases and Geropsychiatry, Neurology, University of Bonn Medical Center, Bonn, Germany, ³German Center for Neurodegenerative Diseases (DZNE), Bonn, Germany

OPEN ACCESS

Edited by:

Wolfgang Hoyer,
Heinrich Heine University of
Düsseldorf, Germany

Reviewed by:

Wayne Carter,
University of Nottingham,
United Kingdom
Tadafumi Hashimoto,
The University of Tokyo, Japan

*Correspondence:

Sathish Kumar
sathish.kumar@ukbonn.de
Jochen Walter
jochen.walter@ukbonn.de

Received: 20 October 2020

Accepted: 15 December 2020

Published: 15 January 2021

Citation:

Kumar S, Kapadia A, Theil S, Joshi P, Riffel F, Heneka MT and Walter J (2021) Novel Phosphorylation-State Specific Antibodies Reveal Differential Deposition of Ser26 Phosphorylated A β Species in a Mouse Model of Alzheimer's Disease. *Front. Mol. Neurosci.* 13:619639. doi: 10.3389/fnmol.2020.619639

Aggregation and deposition of amyloid- β (A β) peptides in extracellular plaques and in the cerebral vasculature are prominent neuropathological features of Alzheimer's disease (AD) and closely associated with the pathogenesis of AD. Amyloid plaques in the brains of most AD patients and transgenic mouse models exhibit heterogeneity in the composition of A β deposits, due to the occurrence of elongated, truncated, and post-translationally modified A β peptides. Importantly, changes in the deposition of these different A β variants are associated with the clinical disease progression and considered to mark sequential phases of plaque and cerebral amyloid angiopathy (CAA) maturation at distinct stages of AD. We recently showed that A β phosphorylated at serine residue 26 (pSer26A β) has peculiar characteristics in aggregation, deposition, and neurotoxicity. In the current study, we developed and thoroughly validated novel monoclonal and polyclonal antibodies that recognize A β depending on the phosphorylation-state of Ser26. Our results demonstrate that selected phosphorylation state-specific antibodies were able to recognize Ser26 phosphorylated and non-phosphorylated A β with high specificity in enzyme-linked immunosorbent assay (ELISA) and Western Blotting (WB) assays. Furthermore, immunofluorescence analyses with these antibodies demonstrated the occurrence of pSer26A β in transgenic mouse brains that show differential deposition as compared to non-phosphorylated A β (npA β) or other modified A β species. Notably, pSer26A β species were faintly detected in extracellular A β plaques but most prominently found intraneuronally and in cerebral blood vessels. In conclusion, we developed new antibodies to specifically differentiate A β peptides depending on the phosphorylation state of Ser26, which are applicable in ELISA, WB, and immunofluorescence staining of mouse brain tissues. These site- and phosphorylation state-specific A β antibodies represent novel tools to examine phosphorylated A β species to further understand and dissect the complexity in the age-related and spatio-temporal deposition of different A β variants in transgenic mouse models and human AD brains.

Keywords: Alzheimer's disease, amyloid- β peptide, cerebral amyloid angiopathy, post-translational modification, modified amyloid- β , phosphorylation, monoclonal antibody, mouse models

INTRODUCTION

Alzheimer's disease (AD) is the most common form of dementia worldwide (Alzheimer's Association, 2020). The two primary pathological hallmarks of the AD brain are abnormal extracellular deposits of amyloid- β (A β) peptide and intracellular neurofibrillary tangles (NFTs) of tau protein (Selkoe and Hardy, 2016; Goedert, 2018; DeTure and Dickson, 2019; Jellinger, 2020). The aggregation and deposition of A β peptides in the form of amyloid plaques is a critical early step in the disease process that is hypothesized to trigger a complex pathological cascade that ultimately leads to the development of clinical dementia (Duyckaerts et al., 2009; Braak et al., 2011; Calderon-Garcidueñas and Duyckaerts, 2017; Davidson et al., 2018). The critical role of A β in the pathogenesis of AD is strongly supported by the identification of early-onset familial AD (FAD)-causing mutations within the genes encoding either the amyloid precursor protein (APP) itself or presenilin 1 and 2 (PS1 and PS2) that commonly alter the production of A β peptides in quantitative and qualitative ways (Bateman et al., 2011; Benilova et al., 2012; Katsnelson et al., 2016; De Strooper and Karran, 2016). Strikingly, mutations identified in the APP either within or close to the A β region affect A β production or alter A β aggregation properties, and thereby promote the formation of toxic A β aggregates (Grant et al., 2007; Hunter and Brayne, 2018). Further, there is strong evidence that the genetic risk for AD that has been associated with polymorphisms in both Apolipoprotein E (ApoE) and Clusterin (CLU) is at least partly attributable to effects of these proteins on A β deposition (Ray et al., 1998; Tanzi, 2012; Bettens et al., 2013; Karch et al., 2014; Tcw and Goate, 2017; Belloy et al., 2019). Collectively, these genetic studies indicate that the accumulation and aggregation of A β can be a trigger in the pathogenesis of AD-related dementia.

Amyloid deposits in the parenchyma and vasculature consist mainly of A β peptides with 38–43 amino acids (A β 38, A β 40, A β 42, and A β 43; Masters et al., 1985; Glenner and Wong, 2012; Moro et al., 2012). Consistent with an increased propensity to form aggregates (Harper and Lansbury, 1997; Rochet and Lansbury, 2000; Lansbury and Lashuel, 2006; Grant et al., 2007; Teplow, 2012), A β 42 is the predominant species found initially in amyloid plaques in the parenchyma (Iwatsubo et al., 1996; Mann and Iwatsubo, 1996). In addition to these well-known amino acid length variants, several additional N- and C-terminally truncated or elongated A β variants have been described (Saido et al., 1996; Russo et al., 1997; Tekirian et al., 1998; Geddes et al., 1999; Saito et al., 2011; Schönherr et al., 2016; Becker-Pauly and Pietrzik, 2017; Dunys et al., 2018; Walter et al., 2019). Further heterogeneity in A β species comes from several post-translational modifications that are also found in characteristic A β deposits in parenchymal extracellular plaques and cerebral amyloid angiopathy (CAA; Saido et al., 1995; Shimizu et al., 2000; Milton, 2001, 2005; Miravalle et al., 2005; Schilling et al., 2008; Wirths et al., 2010; Kumar et al., 2011, 2016; Kummer et al., 2011; Frost et al., 2013). These truncated, elongated, and post-translationally modified A β peptides have peculiar characteristics in aggregation behavior, deposition, and biostability (Kumar and Walter, 2011; Bayer and Wirths, 2014;

Thal et al., 2015; Barykin et al., 2017; Roher et al., 2017; Wirths and Zampar, 2019).

The phosphorylation at Serine residue 8 promotes aggregation, increases neurotoxicity and affects stability and proteolytic degradation of A β (Kumar et al., 2011, 2012; Rezaei-Ghaleh et al., 2016a,b). By using phosphorylation-state specific monoclonal antibodies (mAbs), we showed that phosphorylated Ser8-A β (pSer8A β) accumulates early inside of brain neurons of transgenic APP/PS1 knock-in mice, and is also a prominent component of extracellular plaques during aging (Kumar et al., 2013). The presence of pSer8A β was also demonstrated in the brains of human sporadic AD, FAD, CAA, Down syndrome (DS) cases, non-human primates, canines, and a variety of transgenic mouse models (Kumar et al., 2011, 2018, 2020; Rijal Upadhyaya et al., 2014; Ashby et al., 2015; Gerth et al., 2018). A β can also undergo phosphorylation at serine residue 26, which strongly affects its conformation, aggregation, neurotoxicity, and deposition (Milton, 2001; Kumar et al., 2016). Importantly, Ser26-phosphorylated A β (pSer26A β) species assemble into specific oligomeric forms that do not proceed further into larger fibrillar aggregates (Rezaei-Ghaleh et al., 2014, 2016b). pSer26A β occurs *in vivo* in transgenic mouse models of AD and in human AD brains, showing contrasting distribution as compared to non-phosphorylated A β (npA β) peptides. Furthermore, phosphorylation of A β at Ser26 strongly promotes the formation and stabilization of low molecular weight soluble A β oligomers with increased toxicity on human neurons (Kumar et al., 2016).

In the current study, we developed and thoroughly validated novel site- and phosphorylation-state Ser26-A β specific antibodies. Our results show that selected phosphorylation state-specific antibodies recognize Ser26-phosphorylated and non-phosphorylated A β with high specificity in enzyme-linked immunosorbent assay (ELISA), Western Blotting (WB), and immunofluorescence staining. Our study reveals the selective accumulation of pSer26A β species in cerebral blood vessels and intraneuronal deposits in transgenic mouse brains.

MATERIALS AND METHODS

Reagents and Antibodies

Synthetic non-modified and post-translationally modified A β 1–40 and A β 1–42 peptides were purchased from Peptide Specialty Laboratory (Germany). Methanol was from Sigma. Precast 4–12% NuPAGE Bis-Tris mini gels and prestained protein molecular weight markers were from Life technologies. Nitrocellulose membranes were from Schleicher and Schuell (Germany). WB detection reagents were from GE Healthcare (UK) or LiCOR Biosciences. Protease and phosphatase inhibitors were from Roche Laboratories (Germany). BCATM protein assay kit was from Thermo Fisher Scientific (USA). Mouse monoclonal A β antibodies 6E10 and 4G8 were purchased from Covance Laboratories (USA), and 82E1 antibody was from IBL Corporation (Japan). Development and application of rat monoclonal 7H3D6 antibody were described previously (Kumar et al., 2013). The anti-mouse, anti-rabbit secondary antibodies conjugated to horseradish peroxidase were from Sigma-Aldrich (Germany), and anti-rat secondary antibodies

were from Rockland immunochemical (Gilbertsville, PA, USA). Anti-mouse, anti-rabbit, anti-rat 488, 594, and 647 secondary fluorescent antibodies were from Thermo Fisher Scientific. IRDye800CW and IRDye680RD were from LI-COR Biotechnology. The dilutions of each antibody stock are mentioned in the appropriate “Materials and Methods” section or figure legends.

Generation of Phosphorylation-State Specific Antibodies

Phosphorylation-state specific antibodies were generated by immunizing mice or rabbits with synthetic monomeric A β 20–34 peptides with Ser-26 in phosphorylated (antigen sequence: FAEDVG(p)SNKGAIIGC) or non-phosphorylated state (antigen sequence: FAEDVGSNKGAIIGC) conjugated with keyhole limpet hemocyanin (KLH) as an immunogen. Hybridoma cell clones were generated and antibodies were characterized for their specificity against pSer26A β and npA β peptides by indirect ELISA and WB. By protein G affinity chromatography, we purified the antibodies from conditioned media of hybridoma cell lines. Rabbit polyclonal phosphorylation state-specific antibodies were purified from the serum by double-affinity purification using pSer26A β and npA β peptide. The specificity of the purified antibodies was characterized by ELISA and WB.

Preparation of A β Aggregates

Aggregated A β 1–40 variants of npA β and pSer26A β peptides were prepared by dissolving the respective synthetic peptides (100 μ M) in phosphate-buffered saline (PBS) and incubation at 37°C with stirring. Unaggregated A β was obtained immediately after suspending the peptides in PBS and stored after flash freezing in liquid nitrogen until further use. Aggregated A β was collected at different incubation times and also flash-frozen for further use. SDS–PAGE, Native–PAGE, WB, and Thioflavin T (ThT) fluorescence assays were carried out to confirm the unaggregated (0 h) and aggregated (12, 24, 48, 72, and 96 h) state of A β as previously described (Kumar et al., 2011, 2012). Fluorescence intensity was determined using a Varian Cary Eclipse fluorescence spectrophotometer. Excitation and emission wavelengths were set at 446 and 482 nm, respectively. The fluorescence intensity was measured three times for each sample and then the three readings were averaged.

Western Immunoblotting

Synthetic peptides or brain extracts were separated on 4–12% NuPAGE gels and transferred to 0.45 μ m nitrocellulose membranes. The membranes were blocked and incubated sequentially with the indicated primary and secondary antibodies and then developed by enhanced chemiluminescence using ECL imager (BioRad Inc.) or LiCOR Imaging. Quantification was performed by densitometric analysis using Quantity One software (BioRad Inc.).

ELISA Assays

Monomeric npA β and pSer26A β peptides were used as antigens for coating using PBS, pH 7.4, as coating buffer. For the antibody titer evaluation, 1 μ g/ml A β working stock solution was prepared

in PBS and kept on ice. Hundred microliter of antigen solution (npA β and pSer26A β) was added per well and incubated at 4°C for 16 h. After incubation, residual liquid from the plate was removed by gently tapping the plates. Two-hundred microliter blocking buffer (1 mg/ml BSA) was added per well and incubated at 25°C for 2 h, and wells dried again. To measure the antibody titer, 5H11C10 antibody (1 mg/ml) and SA6193 antibody were serially diluted to 1:10, 1:30, 1:90, 1:270, 1:810, 1:2,430, 1:7,290 in coating buffer, added respectively to the wells and incubated at 25°C for 2 h. After the incubation, the wells were washed with 200 μ l of PBS, thrice, and finally, the residual liquid was removed by gentle tapping. Hundred microliter diluted secondary antibodies (Dilution: 1:2,500; anti-mouse IgG-HRP conjugate or anti-rabbit IgG-HRP conjugate) was added to each well respectively and incubated at 25°C for 2 h. After incubation, the wells were washed thoroughly as mentioned above. One-hundred microliters of 3,3',5,5'-tetramethylbenzidine (TMB) substrate was added to each well and the plate incubated at 25°C until sufficient blue color developed. Hundred microliter of stop solution (4 M H₂SO₄) was added to each well and plates were read at a Tecan plate reader at a wavelength of 450 nm and background measurement at 620 nm. Multiple readings were recorded for a single well and averaged. In each experiment, reading for a single sample was recorded in technical triplicates. Data were averaged and plotted as the mean of the readings along with standard deviation ($n = 3$).

For the detection of different concentrations of npA β and pSer26A β peptides by ELISA with 5H11C10 and SA6193 antibodies, Working stock solutions of 2.5, 1.0, 0.5, 0.25, 0.1, 0.05, 0.025 ng/ μ l were prepared and 100 μ l of stock solutions were added per well to achieve final concentrations of 250, 100, 50, 25, 10, 5, 2.5 ng/per well. One-hundred microliters of 5H11C10 and SA6193 antibody solutions (Dilution: 1:250, in blocking buffer) was added to each well. Further incubation steps and measurements were performed as mentioned above.

Protein Extraction and Immunohistochemistry

For biochemical analysis of pSer26A β and npA β variants, full-length APP (Fl-APP), and APP C-terminal fragments (APP-CTFs), whole-brain homogenates from APP/PS1 Δ E9 (Tg) and non-transgenic (WT) mice were prepared as described previously (Kumar et al., 2011). APP/PS1 Δ E9 mice were obtained from the Jackson Laboratories (strain # 005864; Jankowsky et al., 2004). Mice were housed under standard conditions at 22°C and a 12 h–12 h light-dark cycle with free access to food and water. Animal care and handling was performed according to the Declaration of Helsinki and approved by the local ethical committees (LANUV NRW). Briefly, for sequential A β extraction, brain tissue was homogenized with a douncer followed by sonication in RIPA buffer containing protease and phosphatase inhibitors. Homogenates were cleared by centrifugation at 14,000 g for 30 min at 4°C. After centrifugation, the resulting supernatant containing water-soluble proteins was aliquoted, saved at –80°C for further usage and the pellet was re-homogenized in 2% SDS in 50 mM Tris buffer (pH 7.3) supplemented with protease and

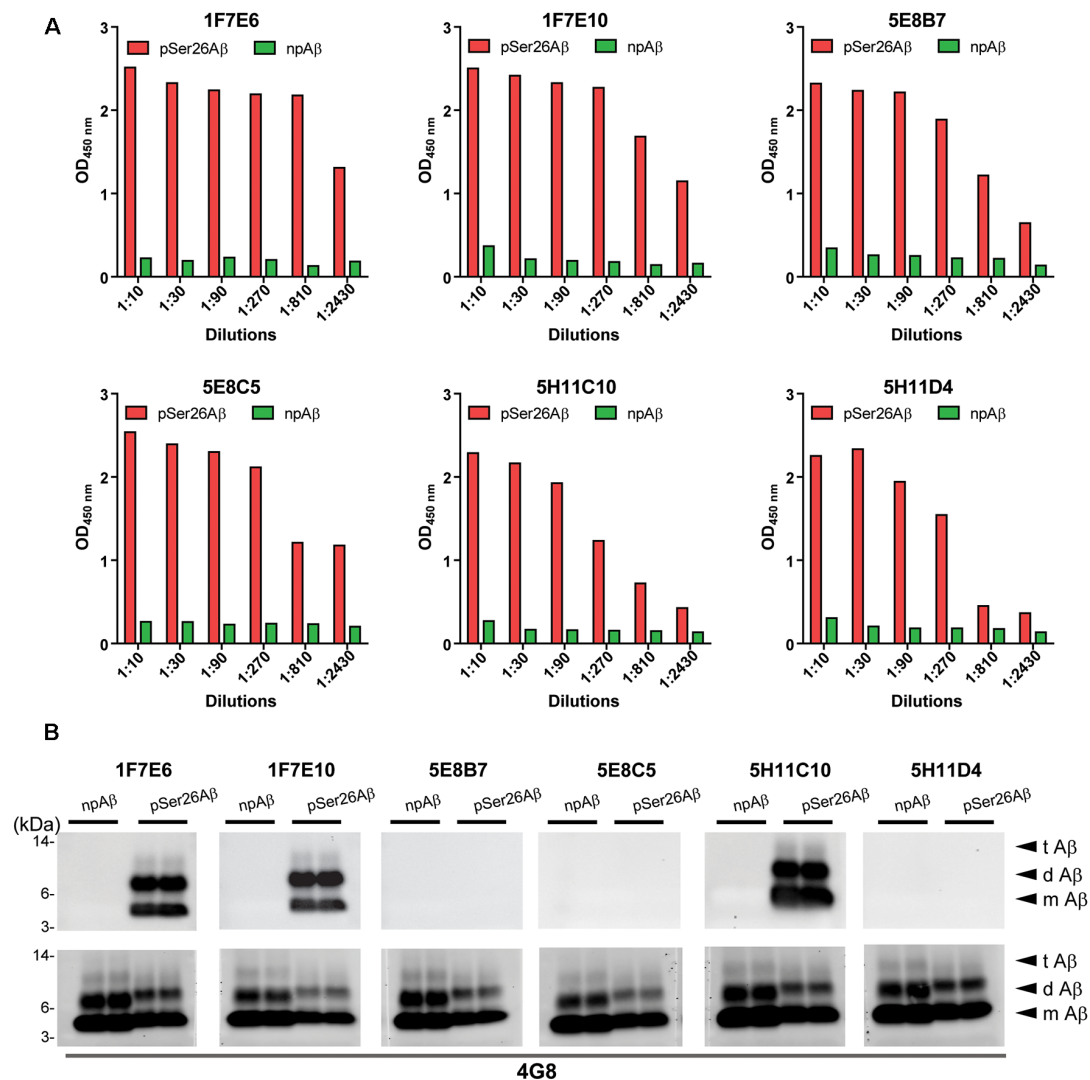


FIGURE 1 | Screening hybridomas secreting anti-pSer26A β monoclonal antibodies. **(A)** Enzyme-linked immunosorbent assay (ELISA) assay of hybridoma supernatants with synthetic pSer26A β and npA β peptides demonstrate specific reactivity against the pSer26A β peptides even at higher dilutions. Six hybridoma clones demonstrate a positive reaction to the pSer26A β peptide. **(B)** Western Blotting (WB) analysis of synthetic npA β and pSer26A β peptides (200 ng) with hybridoma supernatants shows the specific detection of monomeric (m A β), dimeric (d A β), and trimeric (t A β) species of pSer26A β by three hybridoma clones. 5H11C10 demonstrates the highest reactivity. Reprobing of the blot with generic A β antibody 4G8 was used to detect both npA β and pSer26A β peptide variants.

phosphatase inhibitors followed by sonication and centrifuged as described above. The resultant supernatant SDS extract was aliquoted and stored at -80°C .

Immunofluorescence analyses of mouse brains were performed on 20 μm sagittal paraformaldehyde (PFA) fixed sections as described previously (Kumar et al., 2013, 2016). For immunofluorescence staining, the brain tissue sections were washed twice with $1\times$ PBS and then subjected to antigen retrieval methods using reveal decloaker (Biocare Medical #RV1000) followed by permeabilization by using 0.25% triton x-100 in PBS for 30 min. Non-specific binding sites were blocked by treatment with 5% normal horse serum with 2.5% bovine serum albumin in PBS, before the

addition of the primary antibodies. Mouse on Mouse (M.O.M) blocking reagent (Vector Laboratories, MKB-2213) was used for primary antibodies generated in mouse or rat (dilutions: 1:250). The primary antibodies were incubated overnight in a humid chamber at 4°C followed by incubation with an appropriate fluorescently tagged secondary antibody. After incubation, tissue sections were mounted onto slides by using VECTASHIELD Antifade mounting medium with 4',6-Diamidino-2'-phenylindole dihydrochloride (DAPI). The z-stack images ($10\times$ magnification, $2,048 \times 2,048$ resolution, steps = 49, and size = 2) were acquired by using the Visitron VisiScope spinning disk confocal microscope at $10\times$ magnification.

RESULTS

Screening of Anti-pSer26A β Monoclonal Antibodies

Hybridoma culture supernatants were screened for pSer26A β specific antibodies by indirect ELISA using synthetic pSer26A β and npA β peptides. A total of six hybridoma clones showed a positive reaction with the pSer26A β peptide (**Figure 1A**). Then, WB was employed to further validate the monoclonal antibodies. npA β and pSer26A β peptides were electrophoresed and immunoblotted with hybridoma supernatants. The results showed that only three hybridoma clones among six that were positive in ELISA detect pSer26A β peptides by WB (**Figure 1B**). All three clones were highly specific for Ser26-phosphorylated A β and recognized monomeric, dimeric, and trimeric species of the pSer26A β peptide. **Table 1** summarizes the class, and subclass of the hybridoma clones, demonstrating that the antibodies all belong to IgG1 (5E8B7, 5E8C5, 5H11C10, 5H11D4) or IgG2a (1F7E6 and 1F7E10), subclass with kappa light chain (**Table 1**).

Purification and Titer of Purified pSer26A β mAb 5H11C10

As 5H11C10 has the highest reactivity and titer among all of the clones in WB, this mAb was purified by fast protein liquid chromatography (FPLC) using protein G Sepharose columns. SDS-PAGE analysis shows two bands in lanes 4, 5, and 6 with a molecular weight of 50 and 25 kDa, which correspond to the molecular weights of IgG heavy chain and light chain (**Supplementary Figure 1**). Indirect ELISA analysis showed that the titer in hybridoma supernatants against pSer26A β was 2.04×10^7 (**Figure 2A**), and purified antibody titer was 1.28×10^6 (**Figure 2B**). WB and ELISA analysis with purified 5H11C10 antibody also demonstrated this antibody to be highly specific for pSer26A β peptide (**Figures 2C,D** and **Supplementary Figures 2A, 3A**). In addition to monomeric and dimeric pSer26A β , the 5H11C10 antibody also detected aggregated forms in a phosphorylation state-dependent manner (**Figure 2E** and **Supplementary Figure 4**). WB analysis revealed that antibody 5H11C10 also does not recognize the aggregates of non-phosphorylated A β when compared to the phosphorylation state-independent monoclonal antibody 82E1 (**Supplementary Figure 4**). Importantly, antibody 5H11C10 specifically detects A β variants phosphorylated at Ser26 residue and did not cross-react with other truncated and/or post-translationally modified variants of A β variants not phosphorylated at Ser26 residue (**Figure 2F** and **Supplementary Figure 3B**).

Generation and Characterization of Non-phosphorylated Ser26A β Specific Antibodies

To facilitate specific detection of non-phosphorylated Ser26A β (npA β) and to allow co-staining with the mouse monoclonal antibody 5H11C10, we also generated polyclonal antibodies from rabbits. Antibody SA6193 obtained from immunizations of rabbits with npA β showed very high specificity for A β not phosphorylated at Ser-26 in both WB (**Figure 3A**

TABLE 1 | Ig classes and subclasses, and titer of monoclonal antibodies against pSer26A β .

Hybridoma	Class and subclass	Titer of supernatant of cell culture medium
1F7E6	IgG2a, k	> 1:2,430 (pSer26A β); 0 (npA β)
1F7E10	IgG2a, k	> 1:2,430 (pSer26A β); > 1:10 (npA β)
5E8B7	IgG1, k	> 1:2,430 (pSer26A β); > 1:10 (npA β)
5E8C5	IgG1, k	> 1:2,430 (pSer26A β); 0 (npA β)
5H11C10	IgG1, k	> 1:2,430 (pSer26A β); 0 (npA β)
5H11D4	IgG1, k	> 1:2,430 (pSer26A β); > 1:10 (npA β)

Starting dilution: 1:10. The titer is the highest dilution with P/N (Positive/Negative) ≥ 2.1 .

and **Supplementary Figure 3**) and ELISA (**Figure 3B**). Western immunoblot analysis and ELISA of the different concentrations of npA β and pSer26A β peptides showed that purified SA6193 antibody was highly specific for A β peptides not phosphorylated at Ser26 (**Figures 3C,D** and **Supplementary Figure 2B**). This antibody also specifically detected A β aggregates with Ser-26 in a non-phosphorylated state (**Figure 3E**). Notably, SA6193 antibody detects all of the tested non-modified (A β 1–40 or A β 1–42), truncated (A β 3–40 or A β 3–42) and modified A β 40 or A β 42 variants that carry post-translational modifications in their N-terminal regions, including pSer8A β , nitrated and pyroglutamate A β , but does not cross-react with A β variants that are phosphorylated at Ser26 residue (**Figure 3F** and **Supplementary Figure 3B**). Together, these data demonstrate that the rabbit polyclonal antibody SA6193 is highly specific for A β variants not phosphorylated at Ser26 residue.

Phosphorylation State-Specific Antibodies Demonstrate the Presence of pSer26A β Peptides in Transgenic Mouse Models of AD

We took advantage of these antibodies to characterize the deposition of pSer26A β and npA β in transgenic mouse brains. WB analysis of brain extracts from APP/PS1 Δ E9 transgenic mice with 5H11C10 and SA6193 antibodies showed the presence of pSer26A β and npA β peptides in SDS-soluble fractions (predominantly containing intracellular and membrane-associated A β) at 12 months of age (**Figures 4A,B**). A β reactivity was not detected in non-transgenic mouse brains with both antibodies. Furthermore, both antibodies did not show any reactivity against full-length APP or its C-terminal fragments in brain extracts of transgenic mice, suggesting selective phosphorylation of Ser26 after the generation of A β . In contrast, other commonly used monoclonal antibodies 6E10 or 4G8 also recognized the full-length APP or the APP-CTF (**Figures 4C,D**). Furthermore, immunofluorescence staining with the phosphorylation state-specific antibodies demonstrates the deposition of pSer26A β aggregates in the APP/PS1 Δ E9 transgenic mouse brains (**Figures 4E,F**). pSer26A β species were faintly detected in A β plaques (**Figures 4E,F**; arrowheads). Interestingly, immunostaining revealed deposition of pSer26A β the cerebral vasculature (**Figures 4E,F**; arrows) and intraneuronally (**Figures 4E,F**; asterisks). Additional immunofluorescence staining with 5H11C10 together with

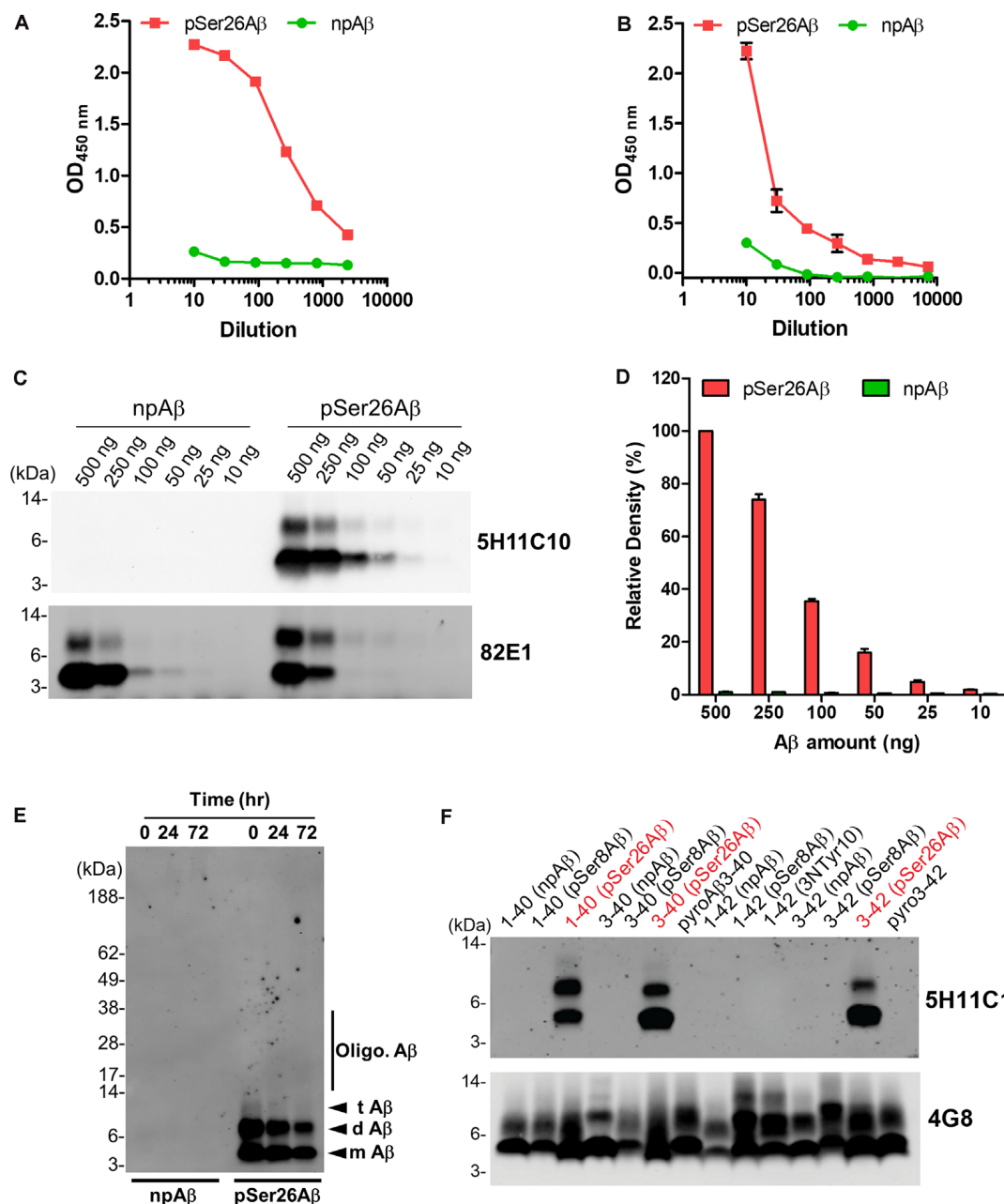


FIGURE 2 | Analysis of pSer26Aβ mAb 5H11C10. **(A,B)** Titer determination by indirect ELISA of hybridoma supernatants before **(A)** and after affinity purification **(B)**. **(C)** WB analysis of different amounts of npAβ and pSer26Aβ peptides with 5H11C10 antibody (concentration: 1 μg/ml) or generic 82E1 antibody. The 5H11C10 antibody selectively recognizes as low as 25 ng of pSer26Aβ in WB and ELISA (**Supplementary Figures 2A, 3A**). **(D)** Densitometric quantification of the 5H11C10 antibody reactivity against various quantities of the pSer26Aβ peptide. Values indicate mean ± SD (*n* = 3). **(E)** Preparations of unaggregated (0 h) and aggregated (24 and 72 h) npAβ and pSer26Aβ peptides were electrophoresed and immunoblotted with 5H11C10 antibody. The 5H11C10 antibody specifically detects pSer26Aβ in both unaggregated and aggregated state (**Supplementary Figure 4**). m Aβ-monomeric Aβ; d Aβ-dimeric Aβ; t Aβ-trimeric Aβ; Oligo. Aβ-Oligomeric Aβ **(F)** Variety of non-modified, truncated, and post-translationally modified Aβ40 and Aβ42 variants were electrophoresed and immunoblotted using 5H11C10 antibody. 5H11C10 antibody specifically detects Aβ variants phosphorylated at Ser26 (written in red), whereas other modified and non-modified variants are not detected.

generic Aβ antibodies further confirms the intraneuronal accumulation as well as pronounced deposition of pSer26Aβ in the blood vessels in APP/PS1ΔE9 transgenic mouse brains (**Supplementary Figure 5**). Detection of pSer26Aβ by the

antibody 5H11C10 was efficiently blocked by pre-adsorption with synthetic pSer26Aβ, further demonstrating the specificity of this antibody in the detection of pSer26Aβ deposits (**Supplementary Figure 6**).

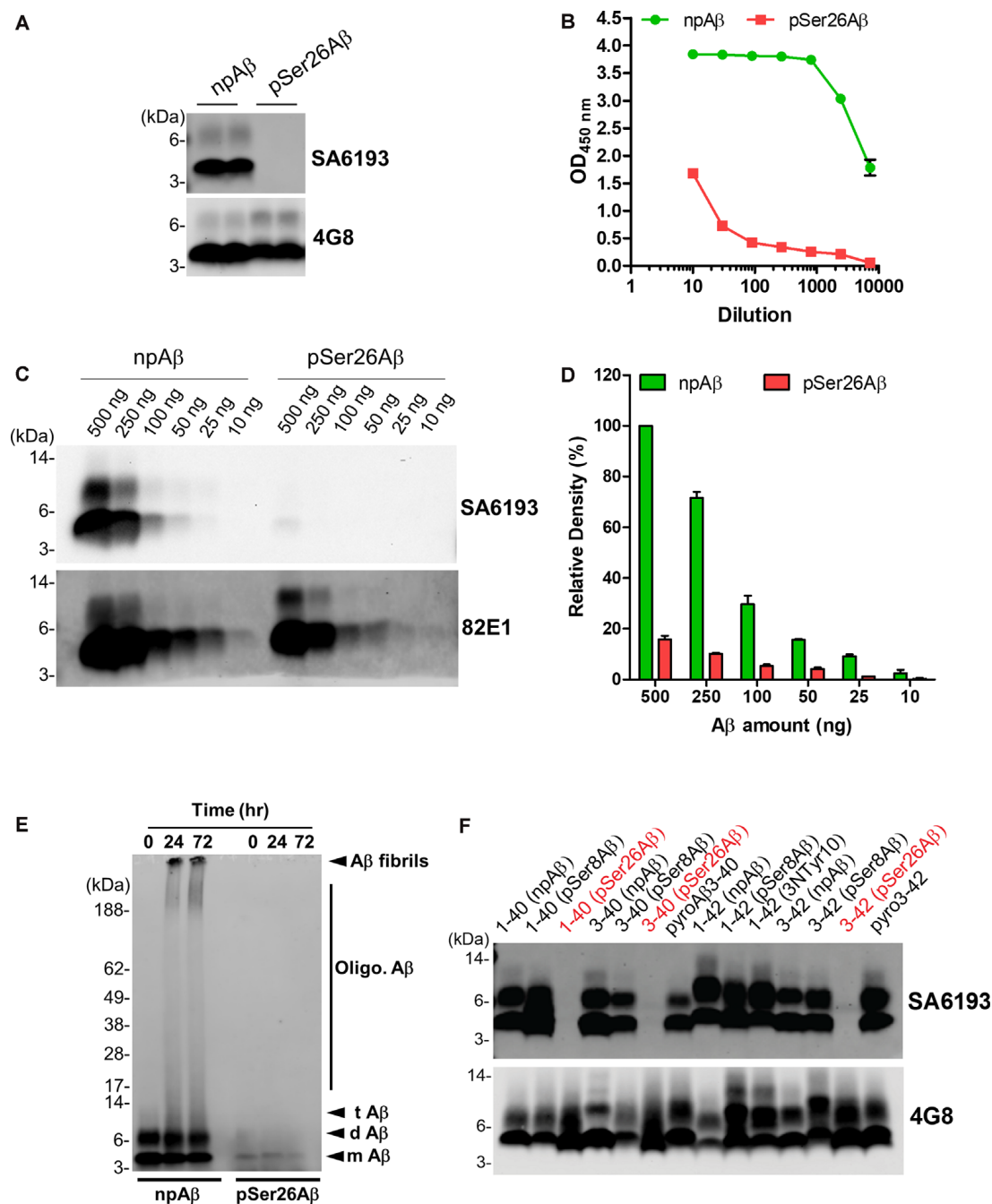


FIGURE 3 | Characterization of the non-phosphorylated Ser26Aβ specific polyclonal SA6193 antibody. **(A)** WB analysis of synthetic npAβ and pSer26Aβ peptides (200 ng) with rabbit sera shows the specific detection of npAβ by SA6193 rabbit polyclonal antibody. Reprobing of the blot with generic 82E1 antibody shows the presence of both npAβ and pSer26Aβ variants. **(B)** Purified SA6193 antibody binding assessed by serial dilution of antibody on ELISA plates that were coated with npAβ and pSer26Aβ antigen. **(C)** WB analysis of different quantities of npAβ and pSer26Aβ peptides with SA6193 antibody or 82E1 antibody. The SA6193 antibody selectively recognizes npAβ monomers and dimers. SA6193 antibody selectively detects npAβ as low as 25 ng in WB **(C)** and ELISA **(Supplementary Figure 2B)**. The membrane immunoprobed with 82E1 antibody shows the presence of both Aβ variants. **(D)** Densitometry quantification of the SA6193 antibody shows the reactivity against various quantities of the npAβ peptide. Values indicate mean \pm SD ($n = 3$). **(E)** Preparations of unaggregated (0 h) and aggregated (24 and 72 h) npAβ and pSer26Aβ peptides were electrophoresed and immunoblotted with SA6193 antibody. The SA6193 antibody specifically detects npAβ in both unaggregated and aggregated state **(Supplementary Figure 4)**. m Aβ-monomeric Aβ; d Aβ-dimeric Aβ; t Aβ-trimeric Aβ; Oligo. Aβ-Oligomeric Aβ **(F)** Variety of non-modified, truncated, and post-translationally modified Aβ40 and Aβ42 variants were electrophoresed and immunoblotted with SA6193 antibody. SA6193 antibody does not cross-react with Aβ variants that are phosphorylated at Ser26 residue but detects all of the tested non-modified (Aβ1–40 or Aβ1–42), truncated (Aβ3–40 or Aβ3–42) and modified Aβ40 and Aβ42 variants that carry other PTMs in their N-terminal regions, including phosphorylated Ser8-Aβ, nitrated and pyroglutamate Aβ **(Supplementary Figure 3)**.

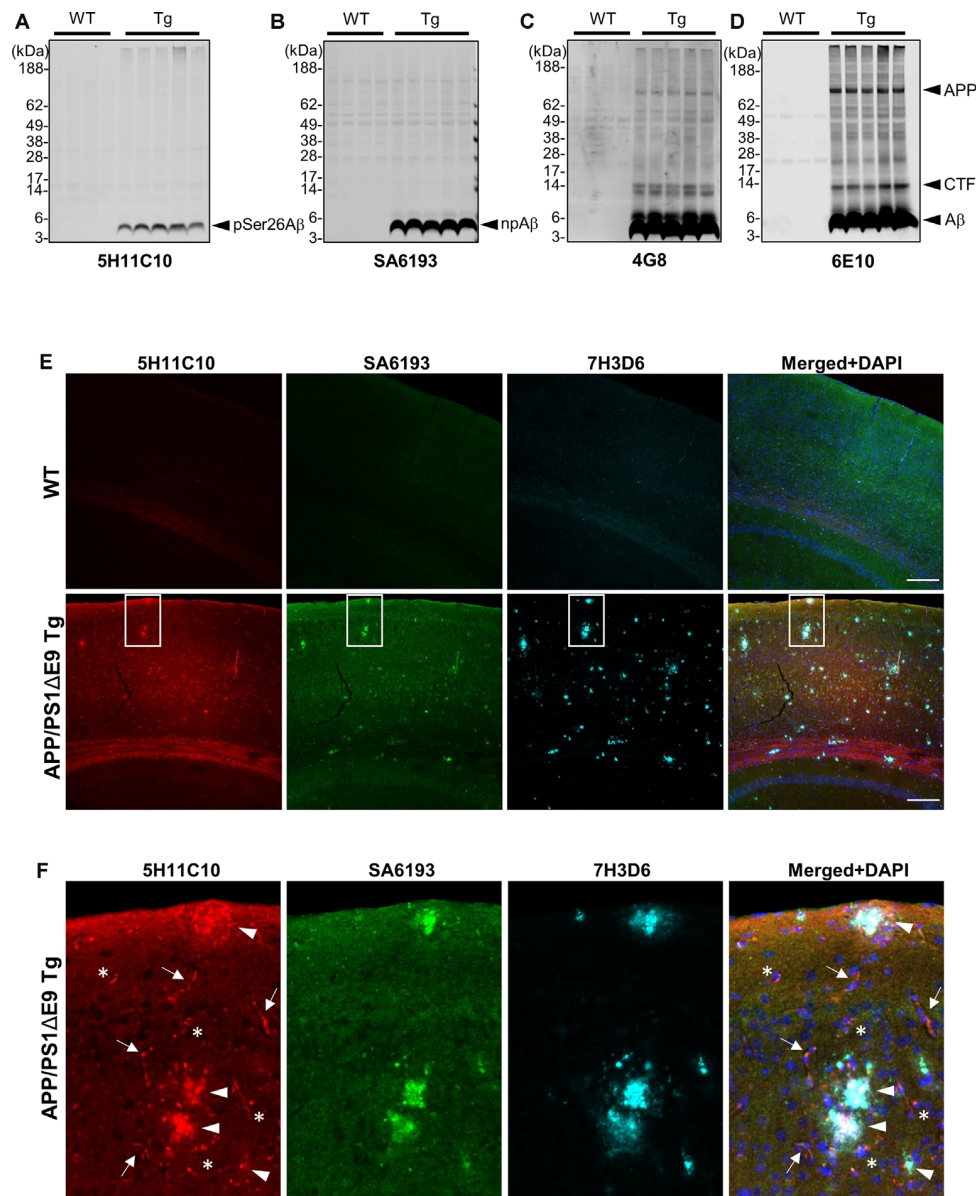


FIGURE 4 | Biochemical and immunofluorescence analysis of pSer26Aβ in transgenic mouse brain. **(A–D)** WB analysis of SDS fractions of 12-months-old APP/PS1ΔE9 transgenic (Tg) and non-Tg (WT) mouse brain homogenates with 5H11C10 **(A)** and SA6193 **(B)** antibodies shows the specific detection of pSer26Aβ and npAβ peptides *in vivo*. In contrast to 4G8 **(C)** and 6E10 **(D)** antibodies, the 5H11C10 and SA6193 antibodies show no reactivity against full-length APP and APP-CTFs in transgenic mouse brain extracts, further demonstrating the specificity of these antibodies for the respective Aβ peptides with phosphorylated or unphosphorylated Ser26. **(E, F)** Immunofluorescence analysis of 12-month-old non-transgenic and APP/PS1ΔE9 transgenic mouse brain tissues with 5H11C10 and SA6193 antibodies. Representative images showing intraneuronal deposits **(F; indicated by asterisks)**, extracellular amyloid plaques **(F; indicated by arrowheads)**, and vascular deposition **(F; indicated by arrows)** of pSer26Aβ peptides. White boxes indicate the area in each image that is shown at higher magnification in enlarged images in panel **(F)**. Rat monoclonal 7H3D6 antibody, which is highly specific for N-terminally unmodified Aβ, demonstrates abundant staining of extracellular amyloid plaques, indicating the presence of N-terminally unmodified Aβ species starting from amino acid Asp1 predominantly in extracellular amyloid plaques **(Supplementary Figure 5)**. Scale bar: 200 μm.

DISCUSSION

Here, we developed and validated novel site- and phosphorylation state-specific Ser26Aβ antibodies. The pSer26Aβ-specific mAb 5H11C10 demonstrates that pSer26Aβ is particularly accumulated in vessels and intraneuronal deposits

that also contain npAβ, but much less in extracellular plaques as compared to unphosphorylated or otherwise modified Aβ species in the brain of APP/PS1ΔE9 transgenic mice.

The amyloid cascade hypothesis describes that the accumulation and aggregation of Aβ peptides into oligomeric or fibrillar structures is initiating the disease process and triggers

a complex pathological cascade that ultimately leads to the development of clinical dementia (Braak and Braak, 1991; Thal et al., 2006; Haass and Selkoe, 2007; Walsh and Selkoe, 2007; Braak et al., 2011; Benilova et al., 2012; Viola and Klein, 2015; Katsnelson et al., 2016; Selkoe and Hardy, 2016; De Strooper and Karran, 2016; DeTure and Dickson, 2019; Jellinger, 2020). The accumulation of age-dependent post-translational modifications in A β may be contributing factors to aggregation and toxicity, and thus to the pathogenesis of AD (Thal et al., 2015; Barykin et al., 2017; Roher et al., 2017; Schaffert and Carter, 2020). Various modified A β species are detected in the brains of human AD patients, DS cases, transgenic AD mouse and natural animal species that develop A β related pathology (Saido et al., 1995, 1996; Iwatsubo et al., 1996; Russo et al., 1997; Tekirian et al., 1998; Fonseca et al., 1999; Shimizu et al., 2000; Schilling et al., 2008; Wirths et al., 2010; Saito et al., 2011; Frost et al., 2013; Kumar et al., 2013, 2016, 2020). Some of the modified species are also observed intraneuronally, years before plaque development, NFT formation, and synaptic loss (Wirths et al., 2004, 2010; Bayer and Wirths, 2010; Jawhar et al., 2011; Li et al., 2018). Post-translational modifications could accelerate the oligomerization and fibrillization of A β and thereby increase synaptic impairment and neurotoxicity, and the deposition in AD characteristic lesions. The differential deposition of modified A β variants is also associated with different stages of AD pathogenesis (Rijal Upadhya et al., 2014; Gerth et al., 2018).

Phosphorylation of A β has been identified at the two serine residues within the A β 1–40/42 peptide, Ser-8 and Ser-26 (Milton, 2001, 2005; Kumar and Walter, 2011; Kumar et al., 2011, 2016). Phosphorylation of A β alters its conformation, aggregation, stability, neurotoxicity, proteolytic degradation and deposition (Kumar et al., 2011, 2012; Rijal Upadhya et al., 2014; Ashby et al., 2015; Rezaei-Ghaleh et al., 2016a,b). Immunohistochemical and immunofluorescence stainings demonstrated the occurrence of pSer8A β and pSer26A β *in vivo* in the brains of human AD patients (Rijal Upadhya et al., 2014; Ashby et al., 2015; Gerth et al., 2018), DS cases (Kumar et al., 2020), non-human primates and canines (Kumar et al., 2018). Notably, the detection of pSer8A β , together with pyroglutamate modified A β in brain sections or brain homogenates has been recently explored to establish a staging system for AD pathology based on the sequential deposition of these modified A β variants during the pathogenesis of AD (Rijal Upadhya et al., 2014; Thal et al., 2015, 2019; Gerth et al., 2018). Notably, the biochemical detection of phosphorylated A β species in human brains was associated with the symptomatic phase, implying that the accumulation of phosphorylated A β correlates with *in vitro* and *in vivo* studies that have demonstrated accelerated aggregation and increased neurotoxicity of phosphorylated A β peptides (Kumar et al., 2011, 2016). Thus, changes in the biochemical or biophysical properties of A β induced by phosphorylation may represent critical events in the pathogenesis of AD.

Site- and phosphorylation state-specific antibodies serve as important tools to investigate the spatial and temporal distribution of protein modifications in tissues or cells, and to examine their biological function (Mandell, 2003; Goto and

Inagaki, 2007, 2014; Kumar et al., 2013). Our previous study demonstrated that phosphorylation at Ser-26 results in the formation of low and intermediate molecular weight soluble oligomers that remain as non-fibrillar assemblies and do not produce high molecular weight A β oligomers or fibrils (Kumar et al., 2016). These aggregation characteristics are reminiscent of findings on Osaka (A β E22 Δ) or Dutch (A β E22Q) mutant A β variants that also exhibit enhanced oligomerization without fibrillization (Watson et al., 1999; Baumketner et al., 2008; Fawzi et al., 2008; Tomiyama et al., 2008; Kamp et al., 2014). These A β species also are detected intracellularly and in the vasculature with limited deposition in extracellular plaques (Herzig et al., 2001; Davis et al., 2004; Tomiyama et al., 2010; Kulic et al., 2012), very similar to the behavior of pSer26A β peptides. The amino acid residue Glu22 and Ser26 are located close to or within the β -turn motif, which plays a crucial role in A β monomer folding and oligomerization. Especially, the formation of the turn/bend-like structure from Gly25 to Gly29 is important for fibrillization of A β and is one of the earliest events in A β self-association. Ser26 is located at the center of the turn motif and we demonstrated that phosphorylation at Ser26 interferes with the formation of a fibril-specific salt-bridge between amino acid residues Asp23 and Lys28 (Rezaei-Ghaleh et al., 2014). The introduction of a negatively charged phosphate group at Ser26 may additionally cause intermolecular repulsive interactions that prevent or destabilize fibrillar conformations and thereby promote the formation of soluble non-fibrillar A β oligomers. Thus, oligomers formed by pSer26A β might not be incorporated in fibrillary assemblies found in extracellular plaques, but accumulate inside of neurons or the vasculature, and it will be interesting to further analyze the specific role of this A β species in AD pathogenesis.

Dysregulation of post-translational modifications is associated with age-related processes and contributes to age-related diseases including AD. Thus, the site- and phosphorylation-state specific antibodies against amino acid Ser26 of the A β peptide described here could facilitate investigations on the role of pSer26A β in the complex pathobiology of AD.

DATA AVAILABILITY STATEMENT

The original contributions presented in the study are included in the article/**Supplementary Materials**, further inquiries can be directed to the corresponding author/s.

ETHICS STATEMENT

The animal care and handling was performed according to the Declaration of Helsinki and approved by the local ethical committees (LANUV NRW).

AUTHOR CONTRIBUTIONS

SK and JW conceived the study, acquired funding, and wrote the manuscript. SK, AK, ST, PJ, and FR performed experiments and

analyzed data. MTH provided mouse brain tissues. All authors contributed to the article and approved the submitted version.

FUNDING

We acknowledge Deutsche Forschungsgemeinschaft [grant #WA1477/6-3 (JW)] and the Alzheimer Forschungs Initiative e.V. [grants #12854 and #17011 (SK)] for research funding.

REFERENCES

- Alzheimer's Association. (2020). 2020 Alzheimer's disease facts and figures. *Alzheimers Dement.* 16, 391–460. doi: 10.1002/alz.12068
- Ashby, E. L., Miners, J. S., Kumar, S., Walter, J., Love, S., and Kehoe, P. G. (2015). Investigation of A β phosphorylated at serine 8 (pA β) in Alzheimer's disease, dementia with lewy bodies and vascular dementia. *Neuropathol. Appl. Neurobiol.* 41, 428–444. doi: 10.1111/nan.12212
- Barykin, E. P., Mitkevich, V. A., Kozin, S. A., and Makarov, A. A. (2017). Amyloid β modification: a key to the sporadic Alzheimer's disease? *Front. Genet.* 8:58. doi: 10.3389/fgene.2017.00058
- Bateman, R. J., Aisen, P. S., De Strooper, B., Fox, N. C., Lemere, C. A., Ringman, J. M., et al. (2011). Autosomal-dominant Alzheimer's disease: a review and proposal for the prevention of Alzheimer's disease. *Alzheimers Res. Ther.* 3:1. doi: 10.1186/alzrt59
- Baumketner, A., Krone, M. G., and Shea, J.-E. (2008). Role of the familial Dutch mutation E22Q in the folding and aggregation of the 15–28 fragment of the Alzheimer amyloid- β protein. *Proc. Natl. Acad. Sci. U S A* 105, 6027–6032. doi: 10.1073/pnas.0708193105
- Bayer, T. A., and Wirths, O. (2010). Intracellular accumulation of amyloid- β —a predictor for synaptic dysfunction and neuron loss in Alzheimer's disease. *Front. Aging Neurosci.* 2:8. doi: 10.3389/fnagi.2010.00008
- Bayer, T. A., and Wirths, O. (2014). Focusing the amyloid cascade hypothesis on N-truncated A β peptides as drug targets against Alzheimer's disease. *Acta Neuropathol.* 127, 787–801. doi: 10.1007/s00401-014-1287-x
- Becker-Pauly, C., and Pietrzik, C. U. (2017). The metalloprotease meprin β is an alternative β -secretase of APP. *Front. Mol. Neurosci.* 9:159. doi: 10.3389/fnmol.2016.00159
- Belloy, M. E., Napolioni, V., and Greicius, M. D. (2019). A quarter century of APOE and Alzheimer's disease: progress to date and the path forward. *Neuron* 101, 820–838. doi: 10.1016/j.neuron.2019.01.056
- Benilova, I., Karran, E., and De Strooper, B. (2012). The toxic A β oligomer and Alzheimer's disease: an emperor in need of clothes. *Nat. Neurosci.* 15, 349–357. doi: 10.1038/nn.3028
- Bettens, K., Sleegers, K., and van Broeckhoven, C. (2013). Genetic insights in Alzheimer's disease. *Lancet Neurol.* 12, 92–104. doi: 10.1016/S1474-4422(12)70259-4
- Braak, H., and Braak, E. (1991). Neuropathological staging of Alzheimer-related changes. *Acta Neuropathol.* 82, 239–259. doi: 10.1007/BF00308809
- Braak, H., Thal, D. R., Ghebremedhin, E., and Del Tredici, K. (2011). Stages of the pathologic process in Alzheimer disease: age categories from 1 to 100 years. *J. Neuropathol. Exp. Neurol.* 70, 960–969. doi: 10.1097/NEN.0b013e318232a379
- Calderon-Garcidueñas, A. L., and Duyckaerts, C. (2017). Alzheimer disease. *Handb. Clin. Neurol.* 145, 325–337. doi: 10.1016/B978-0-12-802395-2.00023-7
- Davidson, Y. S., Robinson, A., Prasher, V. P., and Mann, D. M. A. (2018). The age of onset and evolution of braak tangle stage and thal amyloid pathology of Alzheimer's disease in individuals with down syndrome. *Acta Neuropathol. Commun.* 6:56. doi: 10.1186/s40478-018-0559-4
- Davis, J., Xu, F., Deane, R., Romanov, G., Previti, M. L., Zeigler, K., et al. (2004). Early-onset and robust cerebral microvascular accumulation of amyloid beta-protein in transgenic mice expressing low levels of a vasculotropic Dutch/Iowa mutant form of amyloid beta-protein precursor. *J. Biol. Chem.* 279, 20296–20306. doi: 10.1074/jbc.M312946200

ACKNOWLEDGMENTS

We thank the Microscopy Core Facility of the Medical Faculty at the University of Bonn for providing their help and services.

SUPPLEMENTARY MATERIAL

The Supplementary Material for this article can be found online at: <https://www.frontiersin.org/articles/10.3389/fnmol.2020.619639/full#supplementary-material>.

- DeTure, M. A., and Dickson, D. W. (2019). The neuropathological diagnosis of Alzheimer's disease. *Mol. Neurodegener.* 14:32. doi: 10.1186/s13024-019-0333-5
- Dunys, J., Valverde, A., and Checler, F. (2018). Are N- and C-terminally truncated A β species key pathological triggers in Alzheimer's disease? *J. Biol. Chem.* 293, 15419–15428. doi: 10.1074/jbc.R118.003999
- Duyckaerts, C., Delatour, B., and Potier, M.-C. (2009). Classification and basic pathology of Alzheimer disease. *Acta Neuropathol.* 118, 5–36. doi: 10.1007/s00401-009-0532-1
- Fawzi, N. L., Kohlstedt, K. L., Okabe, Y., and Head-Gordon, T. (2008). Protofibril assemblies of the arctic, Dutch and Flemish mutants of the Alzheimer's A β 1–40 peptide. *Biophys. J.* 94, 2007–2016. doi: 10.1529/biophysj.107.121467
- Fonseca, M. I., Head, E., Velazquez, P., Cotman, C. W., and Tenner, A. J. (1999). The presence of isoaspartic acid in β -amyloid plaques indicates plaque age. *Exp. Neurol.* 157, 277–288. doi: 10.1006/exnr.1999.7058
- Frost, J. L., Le, K. X., Cynis, H., Ekpo, E., Kleinschmidt, M., Palmour, R. M., et al. (2013). Pyroglutamate-3 amyloid- β deposition in the brains of humans, non-human primates, canines and Alzheimer disease-like transgenic mouse models. *Am. J. Pathol.* 183, 369–381. doi: 10.1016/j.ajpath.2013.05.005
- Geddes, J. W., Tekirian, T. L., and Mattson, M. P. (1999). N-terminus truncated beta-amyloid peptides and C-terminus truncated secreted forms of amyloid precursor protein: distinct roles in the pathogenesis of Alzheimer's disease. *Neurobiol. Aging* 20, 75–79. doi: 10.1016/s0197-4580(99)00012-3
- Gerth, J., Kumar, S., Rijal Upadhaya, A., Ghebremedhin, E., von Arnim, C. A. F., Thal, D. R., et al. (2018). Modified amyloid variants in pathological subgroups of β -amyloidosis. *Ann. Clin. Transl. Neurol.* 5, 815–831. doi: 10.1002/acn3.577
- Glennier, G. G., and Wong, C. W. (2012). Alzheimer's disease: initial report of the purification and characterization of a novel cerebrovascular amyloid protein. 1984. *Biochem. Biophys. Res. Commun.* 425, 534–539. doi: 10.1016/j.bbrc.2012.08.020
- Goedert, M. (2018). Tau filaments in neurodegenerative diseases. *FEBS Lett.* 592, 2383–2391. doi: 10.1002/1873-3468.13108
- Goto, H., and Inagaki, M. (2007). Production of a site- and phosphorylation state-specific antibody. *Nat. Protoc.* 2, 2574–2581. doi: 10.1038/nprot.2007.374
- Goto, H., and Inagaki, M. (2014). Method for the generation of antibodies specific for site and posttranslational modifications. *Methods Mol. Biol.* 1131, 21–31. doi: 10.1007/978-1-62703-992-5_2
- Grant, M. A., Lazo, N. D., Lomakin, A., Condron, M. M., Arai, H., Yamin, G., et al. (2007). Familial Alzheimer's disease mutations alter the stability of the amyloid beta-protein monomer folding nucleus. *Proc. Natl. Acad. Sci. U S A* 104, 16522–16527. doi: 10.1073/pnas.0705197104
- Haass, C., and Selkoe, D. J. (2007). Soluble protein oligomers in neurodegeneration: lessons from the Alzheimer's amyloid β -peptide. *Nat. Rev. Mol. Cell Biol.* 8, 101–112. doi: 10.1038/nrm2101
- Harper, J. D., and Lansbury, P. T. Jr. (1997). Models of amyloid seeding in Alzheimer's disease and scrapie: mechanistic truths and physiological consequences of the time-dependent solubility of amyloid proteins. *Annu. Rev. Biochem.* 66, 385–407. doi: 10.1146/annurev.biochem.66.1.385
- Herzig, M. C., Winkler, D. T., Walker, L. C., and Jucker, M. (2001). Transgenic mouse models of cerebral amyloid angiopathy. *Adv. Exp. Med. Biol.* 487, 123–128. doi: 10.1007/978-1-4615-1249-3_10
- Hunter, S., and Brayne, C. (2018). Understanding the roles of mutations in the amyloid precursor protein in Alzheimer disease. *Mol. Psychiatry* 23, 81–93. doi: 10.1038/mp.2017.218

- Iwatsubo, T., Saido, T. C., Mann, D. M., Lee, V. M., and Trojanowski, J. Q. (1996). Full-length amyloid- β (1-42(43)) and amino-terminally modified and truncated amyloid- β 42(43) deposit in diffuse plaques. *Am. J. Pathol.* 149, 1823–1830.
- Jankowsky, J. L., Fadale, D. J., Anderson, J., Xu, G. M., Gonzales, V., Jenkins, N. A., et al. (2004). Mutant presenilins specifically elevate the levels of the 42 residue β -amyloid peptide *in vivo*: evidence for augmentation of a 42-specific gamma secretase. *Hum. Mol. Genet.* 13, 159–170. doi: 10.1093/hmg/ddh019
- Jawhar, S., Wirths, O., and Bayer, T. A. (2011). Pyroglutamate amyloid- β (A β): a hatchet man in Alzheimer disease. *J. Biol. Chem.* 286, 38825–38832. doi: 10.1074/jbc.R111.288308
- Jellinger, K. A. (2020). Neuropathological assessment of the Alzheimer spectrum. *J. Neural. Transm.* 127, 1229–1256. doi: 10.1007/s00702-020-02232-9
- Kamp, J. A., Moursel, L. G., Haan, J., Terwindt, G. M., Lesnik Oberstein, S. A. M. J., van Duinen, S. G., et al. (2014). Amyloid β in hereditary cerebral hemorrhage with amyloidosis-Dutch type. *Rev. Neurosci.* 25, 641–651. doi: 10.1515/revneuro-2014-0008
- Karch, C. M., Cruchaga, C., and Goate, A. M. (2014). Alzheimer's disease genetics: from the bench to the clinic. *Neuron* 83, 11–26. doi: 10.1016/j.neuron.2014.05.041
- Katsnelson, A., De Strooper, B., and Zoghbi, H. Y. (2016). Neurodegeneration: from cellular concepts to clinical applications. *Sci. Transl. Med.* 8:364ps18. doi: 10.1126/scitranslmed.aal2074
- Kulic, L., McAfoose, J., Welt, T., Tackenberg, C., Späni, C., Wirth, F., et al. (2012). Early accumulation of intracellular fibrillar oligomers and late congophilic amyloid angiopathy in mice expressing the Osaka intra-A β APP mutation. *Transl. Psychiatry* 2:e183. doi: 10.1038/tp.2012.109
- Kumar, S., Frost, J. L., Cotman, C. W., Head, E., Palmour, R., Lemere, C. A., et al. (2018). Deposition of phosphorylated amyloid- β in brains of aged nonhuman primates and canines. *Brain Pathol.* 28, 427–430. doi: 10.1111/bpa.12573
- Kumar, S., Lemere, C. A., and Walter, J. (2020). Phosphorylated A β peptides in human down syndrome brain and different Alzheimer's-like mouse models. *Acta Neuropathol. Commun.* 8:118. doi: 10.1186/s40478-020-00959-w
- Kumar, S., Rezaei-Ghaleh, N., Terwel, D., Thal, D. R., Richard, M., Hoch, M., et al. (2011). Extracellular phosphorylation of the amyloid β -peptide promotes formation of toxic aggregates during the pathogenesis of Alzheimer's disease. *EMBO J.* 30, 2255–2265. doi: 10.1038/emboj.2011.138
- Kumar, S., Singh, S., Hinze, D., Josten, M., Sahl, H.-G., Siepmann, M., et al. (2012). Phosphorylation of amyloid- β peptide at serine 8 attenuates its clearance via insulin-degrading and angiotensin-converting enzymes. *J. Biol. Chem.* 287, 8641–8651. doi: 10.1074/jbc.M111.279133
- Kumar, S., and Walter, J. (2011). Phosphorylation of amyloid beta (A β) peptides—a trigger for formation of toxic aggregates in Alzheimer's disease. *Aging* 3, 803–812. doi: 10.18632/aging.100362
- Kumar, S., Wirths, O., Stüber, K., Wunderlich, P., Koch, P., Theil, S., et al. (2016). Phosphorylation of the amyloid β -peptide at Ser26 stabilizes oligomeric assembly and increases neurotoxicity. *Acta Neuropathol.* 131, 525–537. doi: 10.1007/s00401-016-1546-0
- Kumar, S., Wirths, O., Theil, S., Gerth, J., Bayer, T. A., and Walter, J. (2013). Early intraneuronal accumulation and increased aggregation of phosphorylated A β in a mouse model of Alzheimer's disease. *Acta Neuropathol.* 125, 699–709. doi: 10.1007/s00401-013-1107-8
- Kummer, M. P., Hermes, M., Delekarte, A., Hammerschmidt, T., Kumar, S., Terwel, D., et al. (2011). Nitration of tyrosine 10 critically enhances amyloid β aggregation and plaque formation. *Neuron* 71, 833–844. doi: 10.1016/j.neuron.2011.07.001
- Lansbury, P. T., and Lashuel, H. A. (2006). A century-old debate on protein aggregation and neurodegeneration enters the clinic. *Nature* 443, 774–779. doi: 10.1038/nature05290
- Li, S., Jin, M., Liu, L., Dang, Y., Ostaszewski, B. L., and Selkoe, D. J. (2018). Decoding the synaptic dysfunction of bioactive human AD brain soluble A β to inspire novel therapeutic avenues for Alzheimer's disease. *Acta Neuropathol. Commun.* 6:121. doi: 10.1186/s40478-018-0626-x
- Mandell, J. W. (2003). Phosphorylation state-specific antibodies: applications in investigative and diagnostic pathology. *Am. J. Pathol.* 163, 1687–1698. doi: 10.1016/S0002-9440(10)63525-0
- Mann, D. M., and Iwatsubo, T. (1996). Diffuse plaques in the cerebellum and corpus striatum in down's syndrome contain amyloid β protein (A β) only in the form of A β 42 (43). *Neurodegeneration* 5, 115–120. doi: 10.1006/neur.1996.0017
- Masters, C. L., Simms, G., Weinman, N. A., Multhaup, G., McDonald, B. L., and Beyreuther, K. (1985). Amyloid plaque core protein in Alzheimer disease and down syndrome. *Proc. Natl. Acad. Sci. U S A* 82, 4245–4249. doi: 10.1073/pnas.82.12.4245
- Milton, N. G. (2001). Phosphorylation of amyloid- β at the serine 26 residue by human cdc2 kinase. *Neuroreport* 12, 3839–3844. doi: 10.1097/00001756-200112040-00047
- Milton, N. G. N. (2005). Phosphorylated amyloid- β : the toxic intermediate in Alzheimer's disease neurodegeneration. *Subcell. Biochem.* 38, 381–402. doi: 10.1007/0-387-23226-5_20
- Miravalle, L., Calero, M., Takao, M., Roher, A. E., Ghetti, B., and Vidal, R. (2005). Amino-terminally truncated A β peptide species are the main component of cotton wool plaques. *Biochemistry* 44, 10810–10821. doi: 10.1021/bi0508237
- Moro, M. L., Giaccone, G., Lombardi, R., Indaco, A., Uggetti, A., Morbin, M., et al. (2012). APP mutations in the A β coding region are associated with abundant cerebral deposition of A β 38. *Acta Neuropathol.* 124, 809–821. doi: 10.1007/s00401-012-1061-x
- Ray, W. J., Ashall, F., and Goate, A. M. (1998). Molecular pathogenesis of sporadic and familial forms of Alzheimer's disease. *Mol. Med. Today* 4, 151–157. doi: 10.1016/s1357-4310(98)01229-5
- Rezaei-Ghaleh, N., Amininasab, M., Giller, K., Kumar, S., Stundl, A., Schneider, A., et al. (2014). Turn plasticity distinguishes different modes of amyloid- β aggregation. *J. Am. Chem. Soc.* 136, 4913–4919. doi: 10.1021/ja411707y
- Rezaei-Ghaleh, N., Amininasab, M., Kumar, S., Walter, J., and Zweckstetter, M. (2016a). Phosphorylation modifies the molecular stability of β -amyloid deposits. *Nat. Commun.* 7:11359. doi: 10.1038/ncomms11359
- Rezaei-Ghaleh, N., Kumar, S., Walter, J., and Zweckstetter, M. (2016b). Phosphorylation interferes with maturation of amyloid- β fibrillar structure in the N terminus. *J. Biol. Chem.* 291, 16059–16067. doi: 10.1074/jbc.M116.728956
- Rijal Upadhyaya, A., Kosterin, I., Kumar, S., von Arnim, C. A. F., Yamaguchi, H., Fändrich, M., et al. (2014). Biochemical stages of amyloid- β peptide aggregation and accumulation in the human brain and their association with symptomatic and pathologically preclinical Alzheimer's disease. *Brain* 137, 887–903. doi: 10.1093/brain/awt362
- Rochet, J. C., and Lansbury, P. T. Jr. (2000). Amyloid fibrillogenesis: themes and variations. *Curr. Opin. Struct. Biol.* 10, 60–68. doi: 10.1016/s0959-440x(99)00049-4
- Roher, A. E., Kokjohn, T. A., Clarke, S. G., Sierks, M. R., Maarouf, C. L., Serrano, G. E., et al. (2017). APP/A β structural diversity and Alzheimer's disease pathogenesis. *Neurochem. Int.* 110, 1–13. doi: 10.1016/j.neuint.2017.08.007
- Russo, C., Saido, T. C., DeBusk, L. M., Tabaton, M., Gambetti, P., and Teller, J. K. (1997). Heterogeneity of water-soluble amyloid β -peptide in Alzheimer's disease and down's syndrome brains. *FEBS Lett.* 409, 411–416. doi: 10.1016/s0014-5793(97)00564-4
- Saido, T. C., Iwatsubo, T., Mann, D. M., Shimada, H., Ihara, Y., and Kawashima, S. (1995). Dominant and differential deposition of distinct β -amyloid peptide species, A β N3(pE), in senile plaques. *Neuron* 14, 457–466. doi: 10.1016/0896-6273(95)90301-1
- Saido, T. C., Yamao-Harigaya, W., Iwatsubo, T., and Kawashima, S. (1996). Amino- and carboxyl-terminal heterogeneity of beta-amyloid peptides deposited in human brain. *Neurosci. Lett.* 215, 173–176. doi: 10.1016/0304-3940(96)12970-0
- Saito, T., Suemoto, T., Brouwers, N., Slegers, K., Funamoto, S., Mihira, N., et al. (2011). Potent amyloidogenicity and pathogenicity of A β 43. *Nat. Neurosci.* 14, 1023–1032. doi: 10.1038/nn.2858
- Schaffert, L.-N., and Carter, W. G. (2020). Do post-translational modifications influence protein aggregation in neurodegenerative diseases: a systematic review. *Brain Sci.* 10:232. doi: 10.3390/brainsci10040232
- Schilling, S., Zeitschel, U., Hoffmann, T., Heiser, U., Francke, M., Kehlen, A., et al. (2008). Glutaminyl cyclase inhibition attenuates pyroglutamate A β and Alzheimer's disease-like pathology. *Nat. Med.* 14, 1106–1111. doi: 10.1038/nm.1872
- Schönherr, C., Bien, J., Isbert, S., Wichert, R., Prox, J., Altmeppen, H., et al. (2016). Generation of aggregation prone N-terminally truncated amyloid β peptides

- by meprin β depends on the sequence specificity at the cleavage site. *Mol. Neurodegener.* 11:19. doi: 10.1186/s13024-016-0084-5
- Selkoe, D. J., and Hardy, J. (2016). The amyloid hypothesis of Alzheimer's disease at 25 years. *EMBO Mol. Med.* 8, 595–608. doi: 10.15252/emmm.201606210
- Shimizu, T., Watanabe, A., Ogawara, M., Mori, H., and Shirasawa, T. (2000). Isoaspartate formation and neurodegeneration in Alzheimer's disease. *Arch. Biochem. Biophys.* 381, 225–234. doi: 10.1006/abbi.2000.1955
- De Strooper, B., and Karran, E. (2016). The cellular phase of Alzheimer's disease. *Cell* 164, 603–615. doi: 10.1016/j.cell.2015.12.056
- Tanzi, R. E. (2012). The genetics of Alzheimer disease. *Cold Spring Harb. Perspect. Med.* 2:a006296. doi: 10.1101/cshperspect.a006296
- Tcw, J., and Goate, A. M. (2017). Genetics of β -amyloid precursor protein in Alzheimer's disease. *Cold Spring Harb. Perspect. Med.* 7:a024539. doi: 10.1101/cshperspect.a024539
- Tekirian, T. L., Saido, T. C., Markesbery, W. R., Russell, M. J., Wekstein, D. R., Patel, E., et al. (1998). N-terminal heterogeneity of parenchymal and cerebrovascular A β deposits. *J. Neuropathol. Exp. Neurol.* 57, 76–94. doi: 10.1097/00005072-199801000-00009
- Teplow, D. B. (2012). Molecular biology of neurodegenerative diseases. Preface. *Prog. Mol. Biol. Transl. Sci.* 107, xiii–xiv. doi: 10.1016/B978-0-12-385883-2.00014-X
- Thal, D. R., Capetillo-Zarate, E., Del Tredici, K., and Braak, H. (2006). The development of amyloid β protein deposits in the aged brain. *Sci. Aging Knowledge Environ.* 2006:re1. doi: 10.1126/sageke.2006.6.re1
- Thal, D. R., Ronisz, A., Tousseyn, T., Rijal Upadhaya, A., Balakrishnan, K., Vandenberghe, R., et al. (2019). Different aspects of Alzheimer's disease-related amyloid β -peptide pathology and their relationship to amyloid positron emission tomography imaging and dementia. *Acta Neuropathol. Commun.* 7:178. doi: 10.1186/s40478-019-0837-9
- Thal, D. R., Walter, J., Saido, T. C., and Fandrich, M. (2015). Neuropathology and biochemistry of A β and its aggregates in Alzheimer's disease. *Acta Neuropathol.* 129, 167–182. doi: 10.1007/s00401-014-1375-y
- Tomiyama, T., Matsuyama, S., Iso, H., Umeda, T., Takuma, H., Ohnishi, K., et al. (2010). A mouse model of amyloid beta oligomers: their contribution to synaptic alteration, abnormal tau phosphorylation, glial activation and neuronal loss *in vivo*. *J. Neurosci.* 30, 4845–4856. doi: 10.1523/JNEUROSCI.5825-09.2010
- Tomiyama, T., Nagata, T., Shimada, H., Teraoka, R., Fukushima, A., Kanemitsu, H., et al. (2008). A new amyloid beta variant favoring oligomerization in Alzheimer's-type dementia. *Ann. Neurol.* 63, 377–387. doi: 10.1002/ana.21321
- Viola, K. L., and Klein, W. L. (2015). Amyloid β oligomers in Alzheimer's disease pathogenesis, treatment and diagnosis. *Acta Neuropathol.* 129, 183–206. doi: 10.1007/s00401-015-1386-3
- Walsh, D. M., and Selkoe, D. J. (2007). A β oligomers—a decade of discovery. *J. Neurochem.* 101, 1172–1184. doi: 10.1111/j.1471-4159.2006.04426.x
- Walter, S., Jumpertz, T., Hüttenrauch, M., Ogorek, I., Gerber, H., Storck, S. E., et al. (2019). The metalloprotease ADAMTS4 generates N-truncated A β 4-x species and marks oligodendrocytes as a source of amyloidogenic peptides in Alzheimer's disease. *Acta Neuropathol.* 137, 239–257. doi: 10.1007/s00401-018-1929-5
- Watson, D. J., Selkoe, D. J., and Teplow, D. B. (1999). Effects of the amyloid precursor protein Glu693–Gln 'Dutch' mutation on the production and stability of amyloid β -protein. *Biochem. J.* 340, 703–709.
- Wirths, O., and Zampar, S. (2019). Emerging roles of N- and C-terminally truncated A β species in Alzheimer's disease. *Expert Opin. Ther. Targets* 23, 991–1004. doi: 10.1080/14728222.2019.1702972
- Wirths, O., Erck, C., Martens, H., Harmeier, A., Geumann, C., Jawhar, S., et al. (2010). Identification of low molecular weight pyroglutamate A β oligomers in Alzheimer disease: a novel tool for therapy and diagnosis. *J. Biol. Chem.* 285, 41517–41524. doi: 10.1074/jbc.M110.178707
- Wirths, O., Multhaup, G., and Bayer, T. A. (2004). A modified β -amyloid hypothesis: intraneuronal accumulation of the β -amyloid peptide—the first step of a fatal cascade. *J. Neurochem.* 91, 513–520. doi: 10.1111/j.1471-4159.2004.02737.x

Conflict of Interest: The authors declare that the research was conducted in the absence of any commercial or financial relationships that could be construed as a potential conflict of interest.

Copyright © 2021 Kumar, Kapadia, Theil, Joshi, Riffel, Heneka and Walter. This is an open-access article distributed under the terms of the Creative Commons Attribution License (CC BY). The use, distribution or reproduction in other forums is permitted, provided the original author(s) and the copyright owner(s) are credited and that the original publication in this journal is cited, in accordance with accepted academic practice. No use, distribution or reproduction is permitted which does not comply with these terms.



Prediction of Transmembrane Regions, Cholesterol, and Ganglioside Binding Sites in Amyloid-Forming Proteins Indicate Potential for Amyloid Pore Formation

Katja Venko^{1*}, Marjana Novič¹, Veronika Stoka² and Eva Žerovnik^{2*}

¹ Theory Department, National Institute of Chemistry, Ljubljana, Slovenia, ² Department of Biochemistry and Molecular and Structural Biology, Jožef Stefan Institute, Ljubljana, Slovenia

OPEN ACCESS

Edited by:

Jinghui Luo,
Paul Scherrer Institut
(PSI), Switzerland

Reviewed by:

Alex Peralvarez-Marín,
Autonomous University of
Barcelona, Spain
Joost Schymkowitz,
VIB & KU Leuven Center for Brain &
Disease Research, Belgium

*Correspondence:

Eva Žerovnik
eva.zerovnik@ijs.si
Katja Venko
katja.venko@ki.si

Received: 20 October 2020

Accepted: 12 January 2021

Published: 10 February 2021

Citation:

Venko K, Novič M, Stoka V and
Žerovnik E (2021) Prediction of
Transmembrane Regions, Cholesterol,
and Ganglioside Binding Sites in
Amyloid-Forming Proteins Indicate
Potential for Amyloid Pore Formation.
Front. Mol. Neurosci. 14:619496.
doi: 10.3389/fnmol.2021.619496

Besides amyloid fibrils, amyloid pores (APs) represent another mechanism of amyloid induced toxicity. Since hypothesis put forward by Arispe and colleagues in 1993 that amyloid-beta makes ion-conducting channels and that Alzheimer's disease may be due to the toxic effect of these channels, many studies have confirmed that APs are formed by prefibrillar oligomers of amyloidogenic proteins and are a common source of cytotoxicity. The mechanism of pore formation is still not well-understood and the structure and imaging of APs in living cells remains an open issue. To get closer to understand AP formation we used predictive methods to assess the propensity of a set of 30 amyloid-forming proteins (AFPs) to form transmembrane channels. A range of amino-acid sequence tools were applied to predict AP domains of AFPs, and provided context on future experiments that are needed in order to contribute toward a deeper understanding of amyloid toxicity. In a set of 30 AFPs we predicted their amyloidogenic propensity, presence of transmembrane (TM) regions, and cholesterol (CBM) and ganglioside binding motifs (GBM), to which the oligomers likely bind. Noteworthy, all pathological AFPs share the presence of TM, CBM, and GBM regions, whereas the functional amyloids seem to show just one of these regions. For comparative purposes, we also analyzed a few examples of amyloid proteins that behave as biologically non-relevant AFPs. Based on the known experimental data on the β -amyloid and α -synuclein pore formation, we suggest that many AFPs have the potential for pore formation. Oligomerization and α -TM helix to β -TM strands transition on lipid rafts seem to be the common key events.

Keywords: amyloid-forming proteins, amyloidogenic regions, transmembrane regions, amino-acid sequence predictors, cholesterol and ganglioside binding motifs, amyloid pore

INTRODUCTION

It is widely accepted and inherited cases confirm a notion that the major part of the pathology of neurodegenerative diseases is due to aberrant processes of protein misfolding and formation of amyloid fibrils by the amyloidogenic proteins concerned: α -synuclein in Parkinson's disease, β -amyloid (A β) in Alzheimer's disease, SOD1 and TDP-43 in amyotrophic lateral sclerosis, etc.

Dobson (2002) discovered that these conformational transitions are not reserved to amyloidogenic proteins, but that under certain conditions all proteins can be converted into amyloid fibrils, even the very stable and α -helical myoglobin (Fandrich et al., 2001). However, the tendency to misfold and aggregate to amyloid at physiological pH and temperature is not the same for all proteins; certain proteins or their parts—after cleavage—are more susceptible to the formation of amyloid fibrils. Amyloidogenic proteins do not have common sequence motifs, but by comparing the protein sequences it can be predicted that some parts are hot spots that form a cross- β spine of amyloid-like fibrils (Nelson et al., 2005). The peptides, which are as short as hexapeptides, can form amyloid fibrils (Tenidis et al., 2000). From the molecular forces that determine the cross- β structure of the amyloid, the main chain hydrogen bonds, but also aromatic repetitive patterns (Gazit, 2007) seem to be of great importance, the latter probably undergoing Π stacking (Gazit, 2002, 2007; Reymer et al., 2014). The secondary structure in the native fold protein is important, but not directly correlated with the secondary structure of the amyloid fibrils. The over-prediction of α -helices compared to the X-ray structure derived α -helices indicates the propensity of α to β transition in the intermediate (Morillas et al., 2001), partially unfolded state and, for intrinsically disordered proteins, partially folded state.

The transition to amyloid fibrils is a reaction consisting of a lag, growth and plateau phases. The most common mechanism is nucleation via an oligomeric nucleus and the other spectrum is downhill polymerization (Žerovnik et al., 2011; Dovidchenko et al., 2014). In due course of amyloid fibrils formation the prefibrillar oligomers of different shapes can be formed; from rings as found at A β (Oxana, 2019), to globules, spheres, or stars. Some of these prefibrillar oligomers are on-pathway and determine the nucleus that assigns the lag phase, some are off-pathway. Some are benign some are toxic differing by subtle changes in conformation (Capitini et al., 2018; Sengupta and Udgaonkar, 2018). The toxic prefibrillar oligomers (Bucciantini et al., 2002; Leri et al., 2016) are thought to make pores into membranes, similar to antimicrobial peptides or bacterial toxins (Anderluh and Žerovnik, 2012; Last and Miranker, 2013). The “channel hypothesis” of AD is not new. It is based on electrophysiological measurements by the group of Arispe et al. (1993a,b); Arispe et al. (2014), Kawahara et al. (2000), and Diaz et al. (2009). Later, the same concept was increased to other amyloid proteins, among them α -synuclein (α -syn), by Lashuel et al. (2002) and Lashuel and Lansbury (2006). Amyloid pore (AP) formation (Kawahara et al., 2011; Di Scala et al., 2016; Kandel et al., 2017) is still not fully understood and has not been directly proven in living cells until recently (Jamasbi et al., 2018). Various *in vitro* studies on membrane vesicles, artificial lipid bilayers, and neuronal cell cultures were performed for A β and α -syn (Kawahara et al., 2000; Tsigelny et al., 2012; Chen et al., 2016; Di Scala et al., 2016; Kandel et al., 2017; Hannestad et al., 2020; Perissinotto et al., 2020). Recent, still *in vitro* study revealed the imaging of how α -syn forms the AP in membrane

predominantly composed of anionic phospholipids, alike those making mitochondrial membranes. Since the interaction of neuronal α -syn with lipid membranes appears crucial in the context of Parkinson's disease, authors tried to explain the roles of different lipids in pathogenic protein aggregation and membrane disruption (Hannestad et al., 2020). Perissinotto et al. (2020) showed that metals (iron in particular) influence interaction of α -syn with lipid rafts. Kaye et al. (2020) has written a review on existence of endogenous oligomeric and multimeric species in α -synucleopathies. The association of α -syn with plasma membrane of hippocampal neurons was demonstrated to induce the formation of pore-like structures (Li et al., 2020). The analysis of Lee et al. (2017) has shown structure and conductance of oligomeric A β pores in a natural lipid membrane, which closely mimics the *in vivo* cellular environment. Recent studies also include interaction of A β with cellular membranes (Bode et al., 2017) and animal models (Julien et al., 2018), both confirming the hypothesis of membrane perforation. For example, in *C. elegans* the membrane repair response was turned on when A β was fed to animals (Julien et al., 2018).

Moreover, in last years the researchers have elucidated the X-ray crystallographic structures of oligomers derived from A β , α -synuclein, and β 2-microglobulin (Kreutzer and Nowick, 2018). Out of these three amyloidogenic peptides/proteins, the A β β -hairpin mimics have provided the most insight into amyloid oligomers. Study has revealed a new mode of self-assembly, where three A β β -hairpin mimics assemble to form a triangular trimer which can pack together with other triangular trimers to form higher-order oligomers (hexamers and dodecamers). These higher-order oligomers can form annular pore-like assemblies and exhibit toxicity toward neuronally derived cells (Kreutzer and Nowick, 2018). Specific pore-forming β -barrel oligomers of A β 42 in DPC micelle conditions were reported also by Serra-Batiste et al. (2016). Recently, another atomic level structures of β -sheet pore-forming A β (1-42) oligomers were obtained by nuclear magnetic resonance (NMR) and mass spectrometry (MS), and a mechanism for membrane disruption based on electrophysiology and simulation studies in membranes was provided (Ciudad et al., 2020). These structural findings are significant and address the gap in understanding the molecular basis of amyloid diseases.

Various methods have been developed to calculate the propensity to form amyloid fibrils, such as AGGRESCAN, AGGRESCAN3D, TANGO, WALTZ, etc. The method AGGRESCAN3D (Pujols et al., 2018) takes into account the tertiary structure of proteins apart from their sequence. The overview of the available programs is described in the review paper of Pallarés and Ventura (2019). A preliminary screening of amyloidogenic sequence fragments can be performed with the RFamy predictor (<http://server.malab.cn/RFamyloid>) (Niu et al., 2018) and the AmyPro database (<https://amypro.net>) (Varadi et al., 2018). This database includes pathogenic amyloids as well as prions and functional amyloids, and allows users to screen their sequences against the entire collection of validated amyloidogenic sequence fragments. Further, AmyPred2 (Tsolis et al., 2013) (<http://aias.biol.uoa.gr/AMYPRED2>) shows a CONSENSUS result of many methods. Previously, this program

Abbreviations: AP, amyloid pore; APFs, amyloid-forming proteins; CBM, cholesterol binding motif; GBM, ganglioside binding motif; TM, transmembrane.

was successfully used to predict amyloid-prone regions in human stefin B wild-type and proline mutants (Hasanbasic et al., 2019). In this study a set of 30 potentially AFPs was selected and the amyloid-fibril propensity was calculated using various tools (Table 1).

In the interaction of prefibrillar oligomers with phospholipid membranes, the lipid rafts, i.e., the microdomains of membranes rich in gangliosides and cholesterol, play an important role (Jang et al., 2009, 2013; Di Scala et al., 2016; Kandel et al., 2019). There are some parallels to the entry of virus particles (Yahi and Fantini, 2014). For example, the spike protein of the coronavirus SARS-CoV-2 in the S2-part has a motif that binds to lipid rafts and thus enables the S1-part to attach and interact with the ACE2-receptor (Fantini et al., 2020). Of interest, the SARS coronavirus (SARS CoV-1) protein E (E for envelope) was shown to form cation-selective membrane channels (Wilson et al., 2004; Verdiá-Báguena et al., 2012). The SARS-CoV-2 protein E thus likely functions as a “viroporin,” but also may have an important function in the infection process and subsequent inflammation (Pacheco et al., 2015).

Therefore, the main focus of our study was to determine in the set of 30 AFPs the domains that could be crucial for AP formation [TM regions, ganglioside (GBM) and cholesterol binding motifs (CBM)]. In this regard, several publicly available tools were used to assess whether the proteins under investigation have TM regions, either α -helices or β -strands. Detailed description and list of these tools are available in section Materials and Methods and Supplementary Table 1. Indeed, we were able to determine possible TM regions in some of the amyloidogenic proteins involved in neurodegenerative pathology. For others, we suspect that they can still form TM channels when in the oligomeric state. Further on, in the same set of sequences we looked for the motifs that represent signatures for the binding to gangliosides and cholesterol, GBM and CBM, respectively. Lipid rafts are rich in cholesterol and gangliosides (Figure 1) (Sezgin et al., 2017), and both are the sites where membrane interaction often begins; as seen in viruses (Wilson et al., 2004; Verdiá-Báguena et al., 2012) or in the direct pore formation through APs (Di Scala et al., 2016). The association of oligomeric α -synuclein with plasma membrane of hippocampal neurons was demonstrated to induce the formation of pore-like structures (Li et al., 2020). Furthermore, the results of Pacheco et al. (2015) go in line with the data of β -amyloid, another experimentally confirmed amyloidogenic pore forming peptide (Sepúlveda et al., 2014). Models of rather mobile A β channels have been proposed already in 2007 by the Nussinov group, who used molecular dynamics simulations (Jang et al., 2007, 2009, 2016; Capone et al., 2012). The simulations indicated that β -sheet channels might break into loosely associated mobile β -sheet subunits. The preferred channel sizes (16- to 24-mer) were compatible with electron microscopy/atomic force microscopy-derived dimensions (Jang et al., 2009).

Further *in vitro* experiments have shown that AP formation involves both membrane lipids, ganglioside and cholesterol, that physically interact with amyloid proteins through specific structural motifs (GBM and CBM) (Jang et al., 2007, 2009, 2013; Di Scala et al., 2016; Dong et al., 2017). Mutation or

deletion of these motifs abolished pore formation in α -synuclein (Parkinson's disease) and A β (Alzheimer's disease). Moreover, both peptides did no longer form Ca²⁺-permeable pores in the presence of drugs that target either cholesterol or ganglioside or both membrane lipids, indicating that gangliosides and cholesterol cooperate to favor the formation of AP through a common molecular mechanism (Di Scala et al., 2016). Figure 2 highlights the α -synuclein and β -amyloid domains that were confirmed by *in vitro* experiments to be involved in AP formation. Based on studies of how the β -amyloid tetramer and α -synuclein octamer insert into membranes (Tsigelny et al., 2012; Ciudad et al., 2020) we propose a possible common mechanism of membrane AP formation for other AFPs (Figure 3).

MATERIALS AND METHODS

The data set for this *in silico* experiment was generated by an extensive literature search for human proteins with a known amyloidogenic mode of action. A total of 30 proteins were selected for this study. The amino acid sequences of these proteins were compiled from UniProtKB database (<https://www.uniprot.org/>). The list of proteins and UniProtKB codes are shown in Table 1. The detailed protein descriptions and amino acid sequence representation and results of TM regions predictions, amyloidogenic regions, GBM and CBM regions are available in Supplementary Tables 1, 5).

Prediction of Amyloidogenic Sequence Fragments and Propensity to Form Amyloid

Using the AmyPro database, we screened selected amino acid sequences against the entire collection of validated amyloidogenic sequence fragments to predict amyloidogenic regions within proteins (Varadi et al., 2018) (<https://amypro.net>). The database is publicly accessible and provides the boundaries of experimentally validated amyloidogenic sequence regions. Additional data are available, such as the functional relevance of the proteins and their amyloid state, experimental techniques used in the amyloid state studies, and relevant data transferred from the UniProt database.

Furthermore, the consensus method for the prediction of the amyloid propensity AmylPred2 (Tsolis et al., 2013) (<http://aias.biol.uoa.gr/AMYLpred2>), was implemented in our data set. The FASTA format of the sequences was used as input. The consensus of different methods specifically developed for the prediction of features related to the formation of amyloid fibrils was generated for each protein. In this work a consensus of at least four methods was used.

RFamyloid is a platform for protein sequence analysis based on machine learning approaches (Niu et al., 2018) (<http://server.malab.cn/RFamyloid>). With the RFamy classifier we estimated the propensity for amyloid based on the input of selected amino acid sequences in FASTA format. The predictions are based on the training set of original protein sequences from the Uniprot and AmyPro data sets and the technique of random forest

TABLE 1 | The list of 30 studied amyloid-forming proteins.

ID	Protein name	UniProtKB ID	Amyloid category	RFAmy probability ^a	Amyloidogenic regions AmyPRO database ^b and AmyLPred2 ^c
1	β-amyloid	P05067	Pathological	0.731	11–42 ^b , 16–21 ^c , 30–42 ^c
2	α-synuclein	P37840	Pathological	0.783	35–81 ^b , 36–42 ^c , 52–65 ^c
3	Prion protein	P04156	Pathological	0.849	84–125 ^{b,c} , 148–171 ^{b,c} , 194–216 ^{b,c} , 223–231 ^b
4	Tau protein	P10636	Pathological	0.842	275–280 ^{b,c} , 302–329 ^b , 369–370 ^c , 373–373 ^c , 397–402 ^c
5	β-2 microglobulin	P61769	Pathological	0.788	21–41 ^{b,c} , 54–71 ^{b,c} , 83–89 ^{b,c} , 91–96 ^b
6	Cystatin C	P01034	Pathological	0.848	47–51 ^{b,c} , 56–65 ^{b,c} , 95–104 ^{b,c}
7	Transthyretin	P02766	Pathological	0.864	10–20 ^{b,c} , 26–34 ^c , 91–96 ^{b,c} , 105–115 ^{b,c} , 119–124 ^{b,c}
8	Lysozyme C	P61626	Pathological	0.783	5–14 ^b , 25–34 ^{b,c} , 56–61 ^{b,c} , 76–84 ^c , 107–112 ^c
9	IAPP-amylin	P10997	Pathological	0.807	11–37 ^b , 13–24 ^c
10	Calcitonin	P01258	Pathological	0.704	6–11 ^{b,c} , 15–20 ^b
11	Prolactin	P01236	Pathological	0.785	7–34 ^b , 21–31 ^c , 43–57 ^b , 80–89 ^c , 95–101 ^c , 130–137 ^c , 167–174 ^c , 187–195 ^c
12	Insulin	P01308	Pathological	0.733	13–18 ^{b,c} , 18–25 ^c , 32–38 ^{b,c} , 44–48 ^c
13	TDP-43	Q13148	Pathological	0.775	26–33 ^c , 55–60 ^c , 69–76 ^c , 105–111 ^c , 123–135 ^c , 148–153 ^c , 216–221 ^c , 225–234 ^c , 247–256 ^c , 381–407 ^b
14	Superoxide dismutase 1	P00441	Pathological	0.761	4–7 ^c , 12–23 ^b , 101–107 ^{b,c} , 112–120 ^c , 147–153 ^{b,c}
15	Stefin B (cystatin B)	P04080	Pathological	0.780	39–59 ^{b,c} , 64–71 ^{b,c} , 80–87 ^b , 95–98 ^b
16	α-crystallin B chain	P02511	Pathological	0.701	26–29 ^c , 70–84 ^c , 91–98 ^c
17	α-1-antichymo-trypsin	P01011	Pathological	0.068	31–42 ^c , 50–66 ^c , 179–192 ^c , 216–228 ^c , 238–243 ^c , 250–255 ^c , 287–290 ^c , 304–308 ^c , 333–340 ^c , 355–364 ^c , 366–369 ^c , 376–382 ^c , 384–392 ^c
18	Stefin A (cystatin A)	P01040	Biologically non-relevant	0.806	46–57 ^c , 65–70 ^c , 81–85 ^c
19	Myoglobin	P02144	Biologically non-relevant	0.816	2–30 ^{b,c} , 68–73 ^c , 102–119 ^{b,c}
20	α-phosphatidyl inositol 3-kinase	P27986	Biologically non-relevant	0.841	23–28 ^b , 38–44 ^c , 74–79 ^c
21	Cathelicidin	P49913	Pathological	0.844	5–6 ^c
22	Secretin	P09683	Negative control	0.859	21–26 ^c
23	Corticoliberin	P06850	Functional	0.334	1–40 ^{b,c}
24	GIP—gastric inhibitory polypeptide	P09681	Functional	0.864	1–43 ^b , 23–28 ^c
25	Urocortin	P55089	Functional	0.839	1–40 ^{b,c}
26	α-crystallin A chain	P02489	Pathological	0.783	66–80 ^b , 23–27 ^c , 37–45 ^c , 50–56 ^c , 70–78 ^c
27	Obestatin	Q9UBU3	Functional	0.689	1–23 ^b
28	Glucagon	P01275	Functional	0.699	1–10 ^b , 22–27 ^c
29	Defensin-6	Q01524	Functional	0.713	1–32 ^b , 21–31 ^c
30	β-endorphin	P01189	Functional	0.704	1–31 ^b , 14–23 ^c

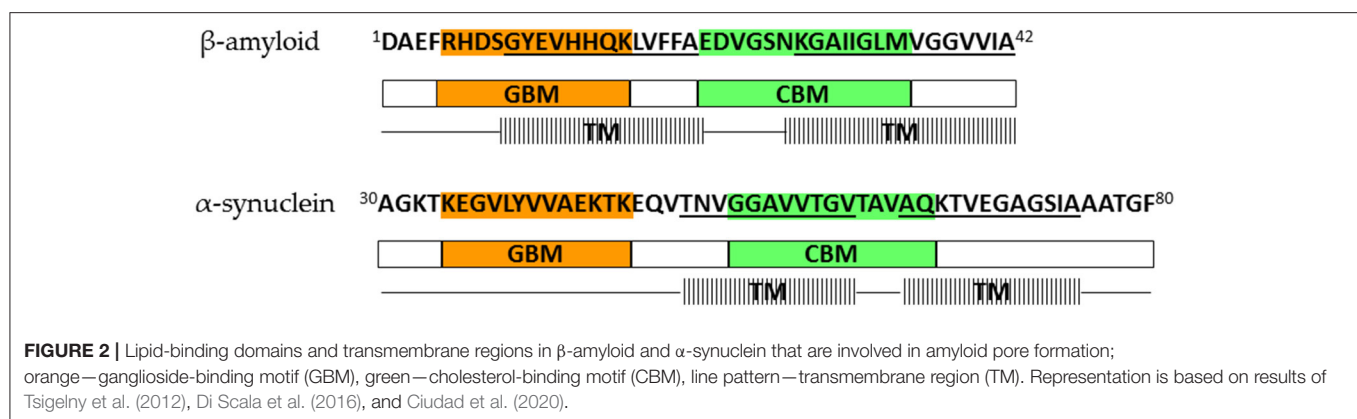
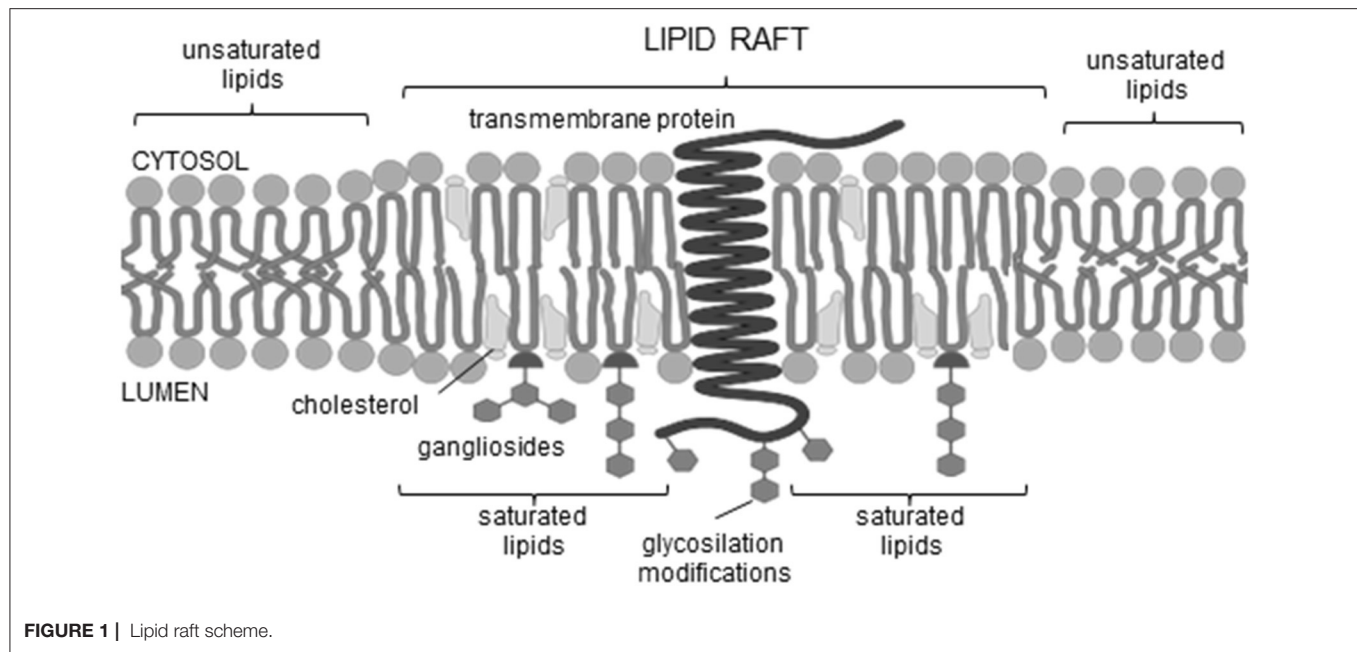
^aRFAmy predictor (<http://server.malab.cn/RFAmyloid/>).^bAmyPRO database (<https://amypro.net/>).^cAmyLPred2 predictor (<http://aias.biol.uoa.gr/AMYPRED2/>).

for the classification of protein sequences (≤ 0.5 non-amyloid, > 0.5 amyloid).

Prediction of TM Regions

Several programs are available for the prediction of TM segments of proteins, either α-helices or β-strands. In this study different

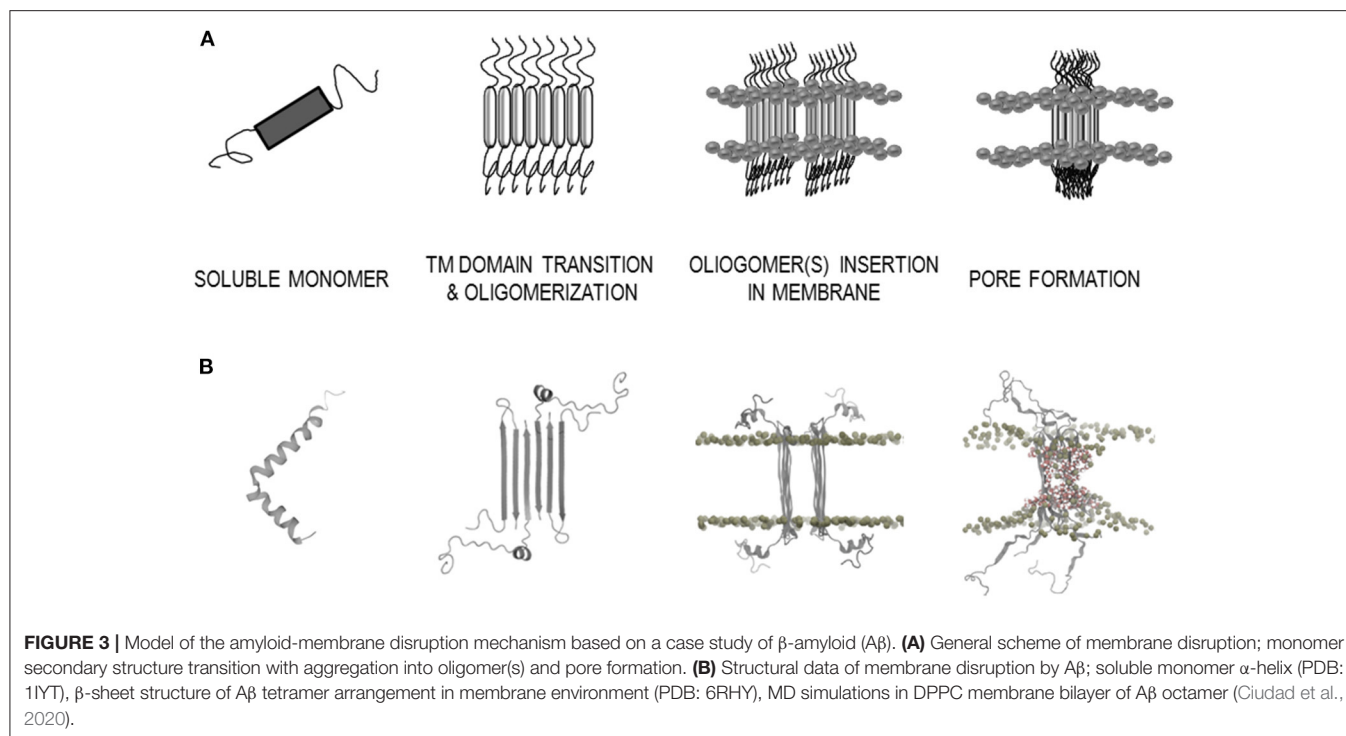
predictors were used, which are listed in **Supplementary Table 2**. All predictors are freely available online. PredαTM and PredβTM (Roy Choudhury and Novič, 2015) were developed in our laboratory and show reliable performance with reasonable predictions of α-helices or β-strands when compared to other predictors used. Reports of the benchmark analyzed are available



in studies by Venko et al. (2017) and Roy Choudhury and Novič (2015). The Pred α TM and Pred β TM are two-layer predictors; the first layer is a classifier of TM segments, while the second layer is an adjustment of the border amino acids of the TM segments, based on the propensity of border amino acids in structurally solved TM proteins available in the PDB database (Roy Choudhury and Novič, 2009). The initial classifier for predicting α -helix TM segments was based on the artificial neural network algorithm (Pasquier et al., 1999), later both classifiers were upgraded by using the support vector machine algorithm (Venko et al., 2017). Algorithms Pred α TM and Pred β TM are using the sliding window approach (20 and 10 amino acids for α -helix and β -strand, respectively) and each segment is classified by the pre-developed SVM classifier as either transmembrane or non-transmembrane (Roy Choudhury and Novič, 2012).

By concept, α - or β -TM regions are segments of predominantly hydrophobic residues, which are energetically suitable for the hydrophobic membrane environment and

have aromatic/charged residues at the membrane-water interface (terminal positions of the TM regions). In general, the identification of α - or β -TM regions can be approached by two different concepts: pattern-based or homology-based. By first, TM features are predicted based on algorithms using hydrophobicity scales or sequence similarity, by second, the prediction is based on algorithms that make a comparison with existing data from homologs. Therefore, in the first case the applicability for homologs and non-homologs is theoretically the same, while in the second case the probability of the prediction depends on the homology rate or is biased with it (Venko et al., 2017). Since all TM proteins with currently known high-resolution structures are strictly homomers and no mix assemblies of both TM segments have yet been determined, the predictors for each TM unit have been separated and developed separately to achieve a better precision in the predictions of the TM regions. Both types of predictors use different computational methods, which can generally be categorized into three classes:



physico-chemical methods [PRED-TMR (Pasquier et al., 1999), BOMP (Berven et al., 2004)], statistical methods [TMpred (Hofmann and Stoffel, 1993)], and machine learning methods [HMMTOP (Tusnady and Simon, 2001), TMMHMM (Krogh et al., 2001), MEMSAT-SVM (Nugent and Jones, 2009), Pred α TM (Roy Choudhury and Novic, 2015), OCTOPUS (Viklund and Elofsson, 2008), B2TMPRED (Jacoboni et al., 2001), PRED-TMBB (Bagos et al., 2004), Pred β TM (Roy Choudhury and Novic, 2015), TBBpred (Natt et al., 2004), BOCTOPUS2 (Hayat et al., 2016), PureseqTM (Wang et al., 2019), MPEx (Snider et al., 2009), ABTMpro (Cheng et al., 2005)]. In addition, it is proposed to apply a consensus approach for relevant predictions based on the analysis of the results of various currently available predictors. This type of consensus approach is already included in predictors such as CCTOP (Dobson et al., 2015), TOPCONS (Tsirigos et al., 2015) and ConBBPred (Bagos et al., 2005). Machine learning methods are regarding various performance analyses recognized as the most advanced and accurate (Roy Choudhury and Novic, 2015; Venko et al., 2017). Most often they are based on learning algorithms such as Support Vector Machines, Hidden Markov Models and Neural Networks. Interfacial hydropathy profile with White-Wimley scale was defined in MPEx (Snider et al., 2009). Further on, an FFPred3 (Cozzetto et al., 2016) server was used for feature-based function prediction and then a search for any membrane gene ontology domains was performed.

Protein Sequence Screening for Cholesterol and Ganglioside Binding Motifs

All protein sequences were manually screened for the presence of CBM and GBM, as suggested by Fantini and colleagues (Fantini

and Barrantes, 2013; Yahi and Fantini, 2014; Fantini et al., 2020). Cholesterol interacts with membrane lipids and proteins at the molecular/atomic scale, thus the consensus cholesterol binding motifs CRAC and/or CARC were characterized (Fantini and Barrantes, 2013). The CRAC domain is generally referred as Cholesterol Recognition/interaction Amino acid Consensus sequence present in the TM segment. This is motif of mandatory amino acid residues (L/V)-X1-5-(Y)-X1-5-(K/R). The CARC domain is similar to the CRAC sequence, but exhibits the opposite orientation (K/R)-X1-5-(Y/F)-X1-5-(L/V) from the N-term to the C-term (an inverted CRAC domain) (Fantini and Barrantes, 2013). Aside, a possible universal GBM is a variation of motifs consisting of a triad of mandatory amino acid residues such as (K/R)-Xn-(F/Y/W)-Xn-(K/R). While the Xn are intercalating segments of usually four to five residues, which can contain any amino acid, but often glycine (G), proline (P), and/or serine (S) residues (Yahi and Fantini, 2014).

RESULTS

P propensity of 30 Proteins to Form Amyloid

Table 1 lists 30 human AFPs that we have selected for analysis based on experimental evidence that 29 of them form amyloid aggregates. We also included secretin as a putative negative control, since it was experimentally shown not to form amyloid, however, by predictive methods it proved to be highly amyloidogenic (**Table 1**, **Supplementary Table 5**). The functional category for each of the studied proteins is also shown in **Table 1**. Particularly, in addition to the 19 pathological AFPs, we also included three biologically non-relevant, seven functional amyloids and one negative control. However, for

amyloidogenic protein cathelicidin the contrasting results among different sources were reported.

The chosen AFPs were examined for their propensity to form amyloid using the RFamy predictor and for possible amyloidogenic sequence fragments using the AmyPro database and the AmylPred2 predictor. The results are shown in **Table 1**. A detailed graphical sequence representation is available in **Supplementary Table 5**, where the AmyPro amyloidogenic validated sequence fragments are marked. The RFamy program classified 28 proteins as amyloids (probability >0.5). Using the AmyPRO database, the amyloidogenic sequence fragments were determined for 25 of the selected proteins; whereas for myoglobin and α -phosphatidyl inositol 3-kinase, homologous sequences from other species represented in the AmyPRO database were used. The only exceptions were stefin A, α -crystallin B chain, α -1-antichymotrypsin, cathelicidin, and secretin. For the above cases, it was crucial to use AmylPred2 (Tsolis et al., 2013) a consensus approach to predict amyloidogenic sequence fragments.

An interesting observation was made for α -1-antichymotrypsin since on one side, this protein was found in the amyloid plaques from the hippocampus of Alzheimer disease brains (Shoji et al., 1991; Padmanabhan et al., 2006; Tyagi et al., 2013) and known to promote A β deposition in plaques (Ma et al., 1994; Eriksson et al., 1995; Nilsson et al., 2001), thus confirming its pathological role. On the other side, we found a sequence homology with urocortin, a functional amyloid (Maji et al., 2009). Moreover, the antibacterial peptide cathelicidin was reported to act as immunomodulator that can contribute to the development of autoimmune diseases (Kahlenberg and Kaplan, 2013) and promote inflammation (Takahashi et al., 2018). On the other side, it exhibits a protective role as an inhibitor of amyloid self-assembly of A β (De Lorenzi et al., 2017) and islet amyloid polypeptide (IAPP) (Armiento et al., 2020).

Probability of Forming Transmembrane Secondary Structures

Potential TM regions, either α -helices or β -strands have been predicted from amino acid sequences of the 305 proteins. Interestingly, for almost all AFPs at least one α - or β -TM region was determined. **Table 2** shows the regions that can form TM α -helices or β -strands. The results of the predictions for each TM predictor are shown in **Supplementary Table 3**. **Table 2** lists only α - or β -TM regions that meet the following criteria: they are predicted with at least two or more TM predictors, or the predicted TM region characterizes the same residues and secondary structures as in experimentally solved 3D structure of the soluble native form. In **Supplementary Table 3** we have highlighted the regions which may form TM α -helices (gray color) and the regions which may form TM β -strands (yellow color).

For the majority of proteins, β -TM secondary structures were more likely, but the ATMBpro predictor favored α -helices in all cases. Compared to other TM predictors, the ATMBpro tool is more restrictive in predicting whether a protein has the potential to be TM or not, since only three of 30 proteins have a high probability of being TM proteins (>0.5), seven have a

medium probability (≥ 0.1 and ≤ 0.5) and the rest have a very low probability (<0.1). Interesting are also the predictions of the MEMSAT-SVM predictor, which for 17 proteins emphasizes the α -TM regions as pore-lining helices. In general, only one α -TM region is predicted for the majority of proteins, while β -TM regions are predicted more frequently, usually up to three or even more regions per protein (**Table 2**, **Supplementary Tables 3, 5**). Furthermore, the interfacial hydropathy profiles of all analyzed proteins are represented in **Supplementary Table 4**. Noteworthy, the results of FFPred3 search for membrane feature-based functions showed some membrane gene ontology domains in almost all analyzed proteins (**Supplementary Table 6**).

Cholesterol and Ganglioside Binding Motifs

For almost all 30 analyzed proteins cholesterol and ganglioside binding motifs were detected. In **Table 3** the sequences of CBM and GBM according to codes [(L or V)-(1–5 residues)-(Y)-(1–5 residues)-(K or R)], [(K or R)-(1–5 residues)-(Y or F)-(1–5 residues)-(L or V)] (Fantini and Barrantes, 2013), and [(K or R)-(4–6 residues)-(F or Y or W)-(4–6 residues)-(K or R)] (Yahi and Fantini, 2014; Fantini et al., 2020) are listed. Moreover, on a schematic representation of each protein sequence, the GBM and CBM motifs are highlighted in orange and green colors, respectively (**Supplementary Table 5**).

Further on, the representative TM regions which include a CBM are underlined in **Table 2**. Namely, all 19 pathological AFPs were determined to possess at least one TM region, which fulfilled the criteria of including all three regions (TM, CBM, and GBM), while on the contrary; the functional AFPs and negative control do not satisfy above mentioned criteria (**Table 4**). Among the biologically non-relevant proteins α -phosphatidylinositol 3-kinase and stefin A possess TM regions with the fulfilled criteria (TM, CBM, and GBM), while myoglobin does not show TM regions, which would fulfill TM-CBM-GBM criteria.

DISCUSSION

In accordance with the proposal of Dobson (2002) and Chiti and Dobson (2017) that any protein under proper conditions can transform into amyloid state, we determined the propensity to form amyloids for all 30 AFPs (**Table 1**). However, the kinetics of amyloid fibril formation is dictated by stability of the protein and its tendency to form folding intermediates (Dobson, 2017) as seen for example in the case of stefin B against stefin A (Jenko et al., 2004).

Similarly, it is believed that most if not all amyloid proteins can form oligomers, which exert toxicity via membrane binding and perforation (Bucciantini et al., 2002; Stefani and Dobson, 2003). The channel theory of Alzheimer's disease (AD) was proposed in 1993 by Arispe et al. (1993a,b), who stated that β -amyloid (A β) peptide perforates the plasma membrane, leading to the entry of Ca²⁺ ions and downstream signaling, which eventually causes cytotoxicity (Pacheco et al., 2015; Di Scala et al., 2016). Not long ago, the structure of the A β oligomer that could perforate the plasma membrane was proposed based on molecular dynamics and solid state NMR (Ciudad et al., 2020), which contributes to a better understanding of the possible mechanism of toxicity in

TABLE 2 | Transmembrane α -helix and β -strand predictions for the set of 30 amyloid-forming proteins; in italics are TM regions with CBM.

ID	Protein name	TM regions		ATMBpro probability	
		α -helix	β -strand	TM protein	α -helix / β -strand TM protein
1	β -amyloid	23–38*	10–21, 30–40	0.831	0.808/0.023
2	α -synuclein	61–76*	33–42, 55–66, 72–82	0.132	0.096/0.036
3	Prion protein	90–109, 198–216*	/	0.896	0.883/0.013
4	Tau protein	/	13–21, 324–334, 359–368, 371–380	0.044	0.040/0.004
5	β -2 microglobulin	/	50–56, 60–70	0.270	0.242/0.029
6	Cystatin C	95–112	41–49, 59–66	0.980	0.964/0.016
7	Transthyretin	104–119*	26–35, 65–81, 88–97, 105–111, 114–122	0.001	0.001/0.000
8	lysozyme C	20–35*	11–21, 34–42, 51–60	0.017	0.015/0.001
9	IAPP-amylin	13–28*	7–16	0.034	0.027/0.007
10	Calcitonin	/	4–12	0.015	0.012/0.003
11	Prolactin	/	81–91, 95–104, 162–171	0.415	0.413/0.002
12	Insulin	/	31–39	0.057	0.049/0.008
13	TDP-43	385–400*	25–34, 54–63, 67–76, 147–155, 225–233, 264–274, 342–351	0.377	0.369/0.008
14	Superoxide dismutase 1	/	42–48	0.004	0.004/0.000
15	Stefin B (cystatin B)	/	35–43, 49–58, 65–72	0.004	0.003/0.002
16	α -crystallin B chain	/	25–34, 75–83, 114–123	0.010	0.010/0.000
17	α -1-antichymotrypsin	50–68*, 376–392*	31–37, 55–65, 73–83, 180–195, 217–230, 240–249	0.171	0.029/0.000
18	Stefin A (cystatin A)	/	36–46, 53–59, 65–73	0.002	0.001/0.001
19	Myoglobin	/	9–18, 29–37, 65–77	0.001	0.001/0.000
20	α -phosphatidylinositol 3-kinase	/	8–14, 38–44, 74–83	0.043	0.025/0.018
21	Cathelicidin	/	1–9, 19–26	0.003	0.003/0.000
22	Secretin	/	6–13, 19–27	0.151	0.137/0.014
23	Corticoliberin	/	9–16	0.078	0.067/0.011
24	GIP—gastric inhibitory polypeptide	/	22–30	0.022	0.021/0.014
25	Urocortin	6–21*	9–16	0.186	0.186/0.046
26	α -crystallin A chain	/	86–93	0.017	0.017/0.000
27	Obestatin	/	6–11	0.054	0.029/0.025
28	Glucagon	/	/	0.015	0.009/0.006
29	Defensin-6	/	/	0.006	0.006/0.000
30	β -endorphin	/	14–20	0.037	0.024/0.013

*Pore-lining helix estimation by MEMSAT-SVM predictor. Bold values indicates core amino acids residues in motif.

AD (Press-Sandler and Miller, 2018). Meanwhile, Lashuel et al. (2002) and Lashuel and Lansbury (2006) describe that APs are formed by many amyloidogenic proteins and are a common source of amyloid-induced toxicity. The mechanism of their formation is still not well-understood and the imaging of pores in living cells remains an open issue. However, not so recent ago APs by A β were confirmed in living cells (Bode et al., 2017) and the membrane repair response was induced by A β in *C. elegans* model (Julien et al., 2018).

In order to get a deeper understanding of amyloid membrane interaction, we used different bioinformatics and machine learning tools to predict amyloidogenic (Table 1) and TM regions (Table 2, Supplementary Table 3) in a set of 30 selected proteins, all associated with protein misfolding and aggregation into amyloid fibrils (Sawaya et al., 2007). Since machine learning approaches are best suited to solve problems in the absence of

general theories (i.e., large amounts of data with noisy patterns), they are ideal for usage in the case of protein complexity. According to the results of the α -TM region predictions the Memsat-SVM predictor is one of the most sensitive, since this predictor is the only one that predicts α -TM regions in 25 proteins. However, Memsat-SVM predictor in benchmark analyses in deed performed as one of the best TM predictors. In particular performs well at predicting the correct number of TM helices (95% accuracy) and also has a balanced number of over- and under predictions, which is favorable to avoid bias toward either type of prediction, and suggests good sensitivity while avoiding over predicting helices. By statistical parameters has very low rate of false positives (4%), for in comparison to others predictors, which have in general rate of false positives >10% (Nugent and Jones, 2009; Venko et al., 2017). The TMpred and TMHMM predictors estimated α -TM regions in about one third

TABLE 3 | Presence of potential cholesterol and ganglioside binding motifs.

ID	Protein name	Cholesterol binding motif (L/V)-X ₁₋₅ -(Y)-X ₁₋₅ -(K/R) (K/R)-X ₁₋₅ -(Y/F)-X ₁₋₅ -(L/V)		Ganglioside binding motif (K/R)-X _n -(F/Y/W)-X _n -(K/R)	
1	β-amyloid A	5–12 16–24 22–35	RNDSGYEV KLVF ^a EDV ^a EDVGSNKGAIIGLM ^{a,b*}	5–16	RHDSGYEVHHQK
2	α-synuclein	34–41 53–65	KEGVL ^b YV ^b GGAVVTGVTAVAQ ^{a,b*}	34–46	KEGVL ^b YV ^b AEKTK
3	Prion protein	129–139 183–196 191–203	RENMHRYPNQV RESQAYYQ ^b RGSSMV RGSSMVL ^b FSSPPV ^a	3–15 183–194	RPKPGGWNTGGSR RESQAYYQ ^b RGSS
4	Tau protein	5–10 327–334 434–441	RQEFV LTFRENAK ^b KLDFKDRV	322–334	KETHKLT ^b FRENAK
5	β-2 microglobulin	19–27 58–65 75–82	KSNFLNCYV KDWSFYLL ^b KDEYACRV	58–68	KDWSFYLLYYT
6	Cystatin C	25–31 31–36 36–47 84–94	RALDFAV VGEYNK KASNDMYHSRAL ^b KAFCSFQIYAV	23–46	RRALDFAVGEYNK
7	Transthyretin	30–35 71–80 103–110	VH ^b VRK ^b VEIDTKYYWK ^b RRYTIAL ^{a,b}	35–48	KAADDTWEPFASGK
8	Lysozyme C	1–8 14–25 31–41 119–130	KVF ^b ERCEL RLGMDGYRGISL ^{a,b} LAKWESGYNTR ^{a,b} RDVRQYVQGC ^b GV	21–33 107–119	RGISLANW ^b MCLAK RAWAWR ^b NRCQNR
9	IAPP-amylin	11–17	RLANFLV ^{a,b}	1–11	KNTAF ^b CATQR
10	Calcitonin	9–18	LGTYTQDFNK ^b	18–28	KFTFPQTAIR
11	Prolactin	16–23 77–84 88–98 164–172	RDLFDRV KDFLSLIV ^b RSWNEPLYHLV ^b RLSAYYNLL ^b	88–102 164–177	RSWNEPLYHLVTEVR RLSAYYNLLHCLR
12	Insulin	33–43	VEALYLVCGER ^b	43–50	RGFFYTPK
13	TDP-43	74–82 145–150 151–159 208–216 226–231	VWNYPKDNK ^b KGF ^b GFV ^b RFTEYETQV ^b REFSQYGDV ^b RAFAFV ^b	151–160 208–219	RFTEYETQVK REFSQYGDVMDV
14	Superoxide dismutase 1	14–23 42–47	VQGIINFEQK LHGFRV ^b	23–36	KESNGP ^b VKVWGSIK
15	Stefin B (cystatin B)	33–37 39–47 48–56 80–89	KKFPV ^b KAVSFKSQV ^b VAGTNYFIK ^b LSNYQTNK	30–39 78–91	KENK ^b KFPVFK KPLT ^b LSNYQTNKAK
16	α-crystallin B chain	22–32 44–50 72–79 82–89	RLFDQFFGEHL ^b LSPFYLR KDRFSVNL ^b KHFSPEEL ^b	11–22 69–82	RRPFF ^b FHSPSR RLEKDRFSVNL ^b DKV
17	α-1-antichymotrypsin	156–166 183–193 226–231 295–303 367–377	LINDYVKNGTR VLN ^b YIFFK ^b LTIPYFR ^b RDY ^b NLNDIL RTIVRFNRPFL	154–166	KKLINDYVKNGTR

(Continued)

TABLE 3 | Continued

ID	Protein name	Cholesterol binding motif (L/V)-X ₁₋₅ -(Y)-X ₁₋₅ -(K/R) (K/R)-X ₁₋₅ -(Y/F)-X ₁₋₅ -(L/V)		Ganglioside binding motif (K/R)-X _n -(F/Y/W)-X _n -(K/R)	
18	Stefin A (cystatin A)	30–38	KTNETYKL ^b	30–44	KTNETYGLAVQK
		38–47	KLEAVQYKTQV ^b	58–71	RAGDNKYMHLKVFK
		48–56	VAGTNYIYK ^b		
		58–67	RAGDNKYMHL ^b		
		68–73	KVFKSL ^b		
19	Myoglobin	81–89	VLTYQVQDK		
		43–50	KFDKFKHL	43–51	KFDKFKHLK
		136–141	LELFRK		
		141–151	KDMASNYKEL		
20	α -phosphatidylinositol 3-kinase	13–20	LYDYKKER ^b	11–20	RALDYKKER
		68–76	RGDFPGTYV ^b	68–81	RGDRPGTYVEYIGR
		76–81	VEYIGR ^b		
21	Cathelicidin	14–23	KIGKEFKRIV ^b	14–25	KIGKEFKRIVQR
		25–34	RIKDFLRNLV ^b		
22	Secretin	/		/	
23	Corticoliberin	/		/	
24	GLP—gastric inhibitory polypeptide	16–27	KIHQQDFVNWLL ^b	/	
25	Urocortin	34–40	RIIFDSV	/	
26	α -crystallin A chain	12–22	RTLGPFPYSRL	66–79	RSDRDKFVFLDVK
		50–57	RQSLFRTV	89–100	KVQDDFVEIHGK
		79–86	KHFSPEDL ^b	104–116	RQDDHGYISREFHR
27	Obestatin	/		/	
28	Glucagon	18–26	RAQDFVQWL	/	
29	Defensin-6	/		/	
30	β -endorphin	/		/	

^aIn α -TM region.^bIn β -TM region.^{*}Experimentally defined. Bold values indicates > 0.15.

of proteins, while the remaining α -TM predictors estimated α -TM regions in only three of the 30 AFPs. Such a difference in the sensitivity of α -TM regions predictors is somewhat surprising, since most predictors for α -TM regions in benchmark analysis showed very high ($\geq 90\%$) sensitivities (Venko et al., 2017). Anyhow, since of the amphipathic nature of the β -TM regions, the hydrophobicity alone is an inefficient differentiating factor, so in advanced β -TM predictors the inclusion of non-linear statistics and evolutionary profiles was added to optimize predictions (Bagos et al., 2005). The recent benchmark analysis for β -TM predictors presented in Venko et al. (2017) shows that the Pred β TM predictor based on machine-learning methodology currently outperforms all state-of-art β -TM region prediction methods. Indeed, in 27 proteins β -strand TM regions were predicted with the Pred β TM predictor. Some predictors were less sensitive (PRED-TMBB, B2TmPred, MEPx-BB), while the remaining predictors did not predict any β -TM regions. This fact is consisted with the estimated sensitivity of the separate β -TM predictors in the study by Roy Choudhury and Novič (2015). In general, the comparison between amyloidogenicity and TM potential is evident for 21 AFPs. As shown in Table 2,

at least one or more TM regions in each protein were predicted by several TM region predictors. However, the estimation with the ABTMpro predictor shows that most of them have a very low TM probability score. It is interesting that those ones which appear in amyloid or neurodegenerative diseases (such as A β , cystatin C and prion) have a high probability of behaving as TM proteins (Di Scala et al., 2016; Kandel et al., 2017). However, in most AFPs sequences both TM secondary structures α -helices and β -strands were predicted, thus it is hard to decide, which one is the preferred one in AP formation. Tsigelny et al. (2012) in their study of α -synuclein membrane interaction provided reasonable explanation of this ambiguity and pointed out that during membrane binding and TM transition both secondary structures possibly occur. Their computational analysis of α -synuclein TM scores predicted that the region including residues 64–79 resembles a TM helix, since this region contains a significant number of hydrophobic residues that could play a critical role during the process of membrane penetration. Further analysis shows that α -synuclein α -helical conformer penetrates the membrane and undergoes change in the secondary structure with portions of the α -helices

TABLE 4 | Representation of 30 amyloid-forming proteins (AFPs) according to amyloid category and fulfilled criteria of including all three domains (transmembrane, cholesterol, and ganglioside binding regions).

Amyloid category	No. of AFPs	No. of AFPs fulfilled TM-CBM-GBM criteria
Pathological	19	19
Functional	7	0
Biologically non-relevant	3	2
Negative control	1	0

converting into π -helices and eventually extending into β -strands (Sepúlveda et al., 2014).

For the 42 amino acids long β -amyloid ($A\beta$) they have recently by using a combination of molecular dynamics calculations and solid state NMR measurements determined the structure of the pore-forming oligomers in lipid environment [tetramers/octamers, PDB: 6RHY (Ciudad et al., 2020)] (Figure 3B). Using several TM predictors, we showed that for the $A\beta$ peptide, both types of TM regions are possible (Table 2, Supplementary Table 3). Although the ATMBpro predictor seems to prefer the α -helix structure, Ciudad et al. (2020) showed in their semi-empirical study that β -strand structures might be involved in the oligomerization and pore formation by $A\beta$. The two regions (G9-A21 and K28-A42) were confirmed as TM segments and both in formation of β -strands (Ciudad et al., 2020). Thus, predictors defined the second β -strand segment (A30-V40) correctly, while the first segment was determined by B2TMPred (Y10-A21) and partly with PRED-TMBB (F4-H14) predictor.

The architecture of the $A\beta$ tetramer [PDB: 6RHY (Ciudad et al., 2020)], which could form pores in membranes, showed that the secondary structure in the oligomer differs from that present in the soluble monomers. Two α -helices were determined in the monomer [PDB: 1IYT (Crescenzi et al., 2002)], while antiparallel β -strands are present in the tetramer. This seems to be consistent with α to β secondary structure transition on the membrane. Indeed, it is known that many amyloidogenic proteins transform into β -sheet conformation before aggregating into amyloid fibrils. This type of oligomers with higher β -structure of Hyp was shown to be more toxic (Evangelisti et al., 2016). It is possible that α -helical parts on the lipid rafts, rich in gangliosides, undergo a secondary structure transition from α to β . It is remarkable that possible ganglioside binding sites can be detected for 25 analyzed AFPs (Table 3, Supplementary Table 5). For example, comparing human stefins B and A, such a site is found at the end of the α -helical part of stefin B (K30-K39), whereas in stefin A it prolongs up to residue 44 (K30-K44) (which is an overpredicted α -helix (Žerovnik et al., 1999). Both proteins also demonstrate another potential ganglioside binding site from residues K56-R68 (stefin B) and R58-K71 (stefin A), which resides in the third β -strand of native soluble form [PDB: 1DVD, (Žerovnik et al., 2011)]. The importance of cholesterol and ganglioside-binding domains in AP formation was experimentally shown

in study of Di Scala et al. (2016). Mutation or deletion of these motifs in α -synuclein and $A\beta$ abolished pore formation. Therefore, in our study another remarkable property of AFPs was observed, namely, that also the cholesterol binding domains in TM regions were found in 25 AFPs (Table 3). In general the CRAC and/or CARC domains were detected in TM regions, but occasionally some mispredicted unrealistic cholesterol binding domains outside TM regions were also observed. This is in accordance with observations of Fantini and Barrantes (2013).

The schematic mechanism of $A\beta$ pore formation based on the possible tetramer structure (Ciudad et al., 2020) is depicted in Figure 3B. Derived from the case of $A\beta$ we propose a more general mechanism (Figure 3A). This may apply to most amyloidogenic proteins, including cystatin C and the stefins A and B, which are involved in the typical amyloid disease; the hereditary amyloid angiopathy (cystatin C) or in a progressive myoclonal epileptic syndrome EPM1 with features of neurodegeneration (stefin B) and are non-physiological (such as stefin A) serving as model proteins in our previous work on protein aggregation to amyloid fibrils (stefins A and B) (Žerovnik et al., 1999, 2010; Anderluh and Žerovnik, 2012). In Parkinson's disease, the calcium-permeable pores formed by small oligomers of α -synuclein are thought the primary pathological species (Sepúlveda et al., 2014; Di Scala et al., 2016; Press-Sandler and Miller, 2018; Li et al., 2020). Our predictions for α -synuclein (residues 30–80) are in concordance with previously experimentally confirmed AP domains (Figure 2) (Sepúlveda et al., 2014). For the islet amyloid polypeptide and calcitonin experiments have also been conducted, which further confirm our assumption that many amyloidogenic proteins have potential to induce toxicity via pore formation (Press-Sandler and Miller, 2018). The islet amyloid polypeptide (IAPP or amylin) is a highly amyloidogenic peptide, and it has been hypothesized that transient membrane-bound α -helical structures of human IAPP are precursors of the amyloid deposits formation. The high-resolution structure of rat IAPP in the membrane-mimicking detergent micelles composed of dodecylphosphocholine was solved and α -TM region (A5-S23) was characterized (Nanga et al., 2009). The characterized regions are almost identical to our TM predicted regions; α -helix (A13-S28) or β -strand (C7-L16). While the MD simulations of possible structures of "amylin membrane channels" in various lipid bilayers using relatively large sizes of oligomers (12–36-mers) have been investigated and demonstrate the β -strands interfacing with the pore (Press-Sandler and Miller, 2018). The amphipathic α -helix was also experimentally determined in the membrane environment for the hormone calcitonin (T6-Y22) (Motta et al., 1991) and (S5-L19) (Hashimoto et al., 1999). The characterized regions are consistent with our TM predicted region for β -strand (L4-L12).

Furthermore, by using molecular dynamics and other computational methods the toxicity mechanism of transactive response DNA-binding protein 43 (TDP-43), which has the prion-like C-terminal domain (residues 258–414) and is believed to be a major component of neuronal inclusion bodies in amyotrophic lateral sclerosis, was studied. By the unbiased atomic-detailed molecular dynamics simulations, the C-terminal fragments of TDP-43 were observed to aggregate

and form disordered-toroidal pores in a lipid bilayer (Chen et al., 2016). Apart, the interaction of tau protein with membranes was recently investigated experimentally, in aim to characterize the effect of the tau-membrane interactions on the function, aggregation, and toxicity of tau in neuronal cultures. Although, the atomic structures of tau oligomers are unknown and currently it seems that the lack of the structure might delay the future studies on tau oligomers on membrane surfaces (Press-Sandler and Miller, 2018). Interestingly, the only relevant region predicted in tau protein is β -TM region (324–334) and is located in exon 10, which contains the microtubule-binding region and is only expressed in 4-repeat (4R) tau isoforms, while 3-repeat (3R) tau isoforms are produced without exon 10 (Kametani and Hasegawa, 2018). The rest of the proteins that were analyzed in our study, up to our knowledge, do not have experimentally solved 3D structures of their oligomers in membrane environments.

It is worth to highlight a comparison of amyloidogenic peptides with the antimicrobial ones. Although they do not share common sequences, typical secondary structures, or the same biological activity, both exhibit membrane-disruption ability to induce cytotoxicity (Zhang et al., 2014). The interactions with membranes may be on the surface or within the cell membrane. Consequently, membrane interactions may affect the structure of the amyloid species and at the same time, the structure of the membrane that leads to cytotoxicity. Despite the existence of different membrane disruption mechanisms, the formation of TM pores appears to be a generic mechanism applicable to both antimicrobial and amyloidogenic membrane interacting peptides (Zhang et al., 2014; Press-Sandler and Miller, 2018). A comparison of different computationally modeled and experimental observed amyloid channels reveals several common features in channel structure and activity. Amyloid membranes channels preferably contain a U-shaped β -strand—turn- β -strand conformation (Zhang et al., 2014). In general, three models for the mechanism of membrane interaction/perforation by amyloid or antimicrobial peptides have been proposed: pore model, carpeting model, and detergent-like model (Zhang et al., 2014; Press-Sandler and Miller, 2018). However, the understanding of the molecular mechanisms of amyloidogenic proteins interaction with membranes remains a challenge to both experimental and computational studies.

CONCLUSIONS

Even though all proteins may under certain conditions form amyloid state (according to Dobson, 2002), they differ in the propensity and likelihood to form such a state, depending on thermodynamic and kinetic factors and environment, such as temperature, pH, reactive oxidative species—i.e., free radicals (ROS) and the crowding milieu. In our analysis we cannot predict all these factors but get by using various predictive methods a number expressing the propensity to transform into amyloid state (Table 1). From the functional point of view,

among the 30 analyzed amyloid forming proteins (AFPs), we can differentiate those, which are a hallmark of disease and are termed “pathological” (19 cases), those that are biologically non-relevant (3), those that are “functional” (7) and a putative negative control (Table 1). The results of our study confirm a common feature of AFPs to possess regions of TM segments, either α -TM helices or β -TM strands, as proposed by several TM predictors (Table 2). Moreover, interactions of amyloidogenic proteins with membranes via lipid rafts rich in gangliosides and cholesterol are indicated (Table 3), as the predictions confirm such binding sites in all of the 19 pathological AFPs, while they are not fully present in functional amyloids (Table 4). Based on the membrane interaction and structural data of a generic oligomer type of an AFP (A β) leading to AP (Tsigelny et al., 2012; Ciudad et al., 2020), we suggest, that such mechanism of induced toxicity via AP formation could be indeed a generic property (Bucciantini et al., 2002). Since Ciudad et al. (2020) emphasize that toxicity arises from the hydrophilic residues located on the edges of the β -sheets, which lead to the formation of lipid-stabilized pores, the oligomerization and the α -TM helix or β -TM strand transition on the membrane surface (on lipid rafts) seem to be the common key events. Hopefully, in the near future stable TM regions that were defined in this study will be further confirmed experimentally for several amyloidogenic proteins. Thus, potentially, all AFPs can under certain circumstances form APs and become toxic. It depends, where and how this happens and if it leads to pathology or is transient, perhaps signaling proteotoxic stress to cells (Protter and Parker, 2016).

DATA AVAILABILITY STATEMENT

The original contributions presented in the study are included in the article/Supplementary Materials, further inquiries can be directed to the corresponding authors.

AUTHOR CONTRIBUTIONS

EŽ, VS, and MN: conceptualization. KV and VS: methodology and analysis. KV: software and visualization. KV, VS, and EŽ: investigation. KV and EŽ: writing—original draft preparation. MN and VS: writing—review and editing. VS: supervision. MN: project administration. MN and EŽ: funding acquisition. All authors have read and agreed to the published version of the manuscript.

FUNDING

This research was funded by Slovenian Research Agency, ARRS program grant P1-0017 (led by MN) and P1-0140 (led by prof. B. Turk).

SUPPLEMENTARY MATERIAL

The Supplementary Material for this article can be found online at: <https://www.frontiersin.org/articles/10.3389/fnmol.2021.619496/full#supplementary-material>

REFERENCES

- Anderluh, G., and Žerovnik, E. (2012). Pore formation by human stefin B in its native and oligomeric states and the consequent amyloid induced toxicity. *Front. Mol. Neurosci.* 5:85. doi: 10.3389/fnmol.2012.00085
- Arispe, N., Pollard, H. B., and Rojas, E. (1993b). Giant multilevel cation channels formed by Alzheimer disease amyloid beta-protein [A beta P-(1-40)] in bilayer membranes. *Proc. Natl. Acad. Sci. U.S.A.* 90, 10573–10577. doi: 10.1073/pnas.90.22.10573
- Arispe, N., Rojas, E., and Pollard, H. B. (1993a). Alzheimer disease amyloid beta protein forms calcium channels in bilayer membranes: blockade by tromethamine and aluminum. *Proc. Natl. Acad. Sci. U.S.A.* 90, 567–571. doi: 10.1073/pnas.90.2.567
- Arispe, N., Williams, M. R., Rivera, I., Lin, H. P., Cauvi, D. M., and De Maio, A. (2014). Calcium channel blockers used as anti-hypertension agents affect the toxicity of Aβ peptides on neurons. *Biophys. J.* 106:295a. doi: 10.1016/j.bpj.2013.11.1721
- Armiento, V., Hille, K., Naltsas, D., Lin, J. S., Barron, A. E., and Kapurniotu, A. (2020). The human host-defense peptide cathelicidin LL-37 is a nanomolar inhibitor of amyloid self-assembly of islet amyloid polypeptide (IAPP). *Angew. Chem. Int. Ed. Engl.* 59, 12837–12841. doi: 10.1002/anie.202000148
- Bagos, P. G., Liakopoulos, T. D., and Hamodrakas, S. J. (2005). Evaluation of methods for predicting the topology of beta-barrel outer membrane proteins and a consensus prediction method. *BMC Bioinform.* 6:7. doi: 10.1186/1471-2105-6-7
- Bagos, P. G., Liakopoulos, T. D., Spyropoulos, I. C., and Hamodrakas, S. J. (2004). A Hidden Markov Model method, capable of predicting and discriminating beta-barrel outer membrane proteins. *BMC Bioinform.* 5:29. doi: 10.1186/1471-2105-5-29
- Berven, F. S., Flikka, K., Jensen, H. B., and Eidhammer, I. (2004). BOMP: a program to predict integral beta-barrel outer membrane proteins encoded within genomes of Gram-negative bacteria. *Nucleic Acids Res.* 32, W394–399. doi: 10.1093/nar/gkh351
- Bode, D. C., Baker, M. D., and Viles, J. H. (2017). Ion channel formation by amyloid-beta 42 oligomers but not amyloid-beta 40 in cellular membranes. *J. Biol. Chem.* 292, 1404–1413. doi: 10.1074/jbc.M116.762526
- Bucciantini, M., Giannoni, E., Chiti, F., Baroni, F., Formigli, L., Zurdo, J., et al. (2002). Inherent toxicity of aggregates implies a common mechanism for protein misfolding diseases. *Nature* 416, 507–511. doi: 10.1038/416507a
- Capitini, C., Patel, J. R., Natalello, A., D'Andrea, C., Relini, A., Jarvis, J. A., et al. (2018). Structural differences between toxic and nontoxic Hyp F-N oligomers. *Chem. Commun.* 54, 8637–8640. doi: 10.1039/C8CC03446J
- Capone, R., Jang, H., Kotler, S. A., Connelly, L., Arce, F. T., Ramachandran, S., et al. (2012). All-d-enantiomer of β-amyloid peptide forms ion channels in lipid bilayers. *J. Chem. Theory Comput.* 8, 1143–1152. doi: 10.1021/ct200885r
- Chen, C. H., Khan, A., Huang, J. J. T., and Ulmschneider, M. B. (2016). Mechanisms of membrane pore formation by amyloidogenic peptides in amyotrophic lateral sclerosis. *Chem. Eur. J.* 22, 9958–9961. doi: 10.1002/chem.201601765
- Cheng, J., Randall, A., Sweredoski, M., and Baldi, P. (2005). SCRATCH: a protein structure and structural feature prediction server. *Nucleic Acids Res.* 33, w72–76. doi: 10.1093/nar/gki396
- Chiti, F., and Dobson, C. M. (2017). Protein misfolding, amyloid formation, and human disease: a summary of progress over the last decade. *Ann. Rev. Biochem.* 86, 27–68. doi: 10.1146/annurev-biochem-061516-045115
- Ciudad, S., Puig, E., Botzanowski, T., Meigooni, M., Arango, A. S., Do, J., et al. (2020). Aβ(1-42) tetramer and octamer structures reveal edge conductivity pores as a mechanism for membrane damage. *Nat. Commun.* 11:3014. doi: 10.1038/s41467-020-16566-1
- Cozzetto, D., Minneci, F., Currant, H., and Jones, D. T. (2016). FFPred 3: feature-based function prediction for all Gene Ontology domains. *Sci. Rep.* 6:31865. doi: 10.1038/srep31865
- Crescenzi, O., Tomaselli, S., Guerrini, R., Salvadori, S., D'Ursi, A. M., Temussi, P. A., et al. (2002). Solution structure of the Alzheimer amyloid beta-peptide (1-42) in a polar microenvironment. Similarity with a virus fusion domain. *Eur. J. Biochem.* 269, 5642–5648. doi: 10.1046/j.1432-1033.2002.03271.x
- De Lorenzi, E., Chiari, M., Colombo, R., Cretich, M., Sola, L., Vanna, R., et al. (2017). Evidence that the human innate immune peptide LL-37 may be a binding partner of Amyloid-β and inhibitor of fibril assembly. *J. Alzheimers Dis.* 59, 1213–1226. doi: 10.3233/JAD-170223
- Di Scala, C., Yahi, N., Boutemeur, S., Flores, A., Rodriguez, L., Chahinian, H., et al. (2016). Common molecular mechanism of amyloid pore formation by Alzheimer's beta-amyloid peptide and alpha-synuclein. *Sci. Rep.* 6:28781. doi: 10.1038/srep28781
- Diaz, J. C., Simakova, O., Jacobson, K. A., Arispe, N., and Pollard, H. B. (2009). Small molecule blockers of the Alzheimer Aβ calcium channel potentially protect neurons from Aβ cytotoxicity. *Proc. Natl. Acad. Sci. U.S.A.* 106, 3348–3353. doi: 10.1073/pnas.0813355106
- Dobson, C. M. (2002). Protein-misfolding diseases: getting out of shape. *Nature* 418, 729–730. doi: 10.1038/418729a
- Dobson, C. M. (2017). The amyloid phenomenon and its links with human disease. *Cold Spring Harb. Perspect. Biol.* 9:a023648. doi: 10.1101/cshperspect.a023648
- Dobson, L., Reményi, I., and Tusnády, G. E. (2015). CCTOP: A Consensus Constrained TOPology prediction web server. *Nucleic Acids Res.* 43, W408–W412. doi: 10.1093/nar/gkv451
- Dong, X., Sun, Y., Wei, G., Nussinov, R., and Ma, B. (2017). Binding of protofibrillar Abeta trimers to lipid bilayer surface enhances Abeta structural stability and causes membrane thinning. *Phys. Chem. Chem. Phys.* 19, 27556–27569. doi: 10.1039/C7CP05959K
- Dovidchenko, N. V., Leonova, E. I., and Galzitskaya, O. V. (2014). Mechanisms of amyloid fibril formation. *Biochemistry* 79, 1515–1527. doi: 10.1134/S0006297914130057
- Eriksson, S., Janciauskiene, S., and Lannfelt, L. (1995). Alpha 1-antichymotrypsin regulates Alzheimer beta-amyloid peptide fibril formation. *Proc. Natl. Acad. Sci. U.S.A.* 92, 2313–2317. doi: 10.1073/pnas.92.6.2313
- Evangelisti, E., Cascella, R., Becatti, M., Marrazza, G., Dobson, C. M., Chiti, F., et al. (2016). Binding affinity of amyloid oligomers to cellular membranes is a generic indicator of cellular dysfunction in protein misfolding diseases. *Sci. Rep.* 6:32721. doi: 10.1038/srep32721
- Fandrich, M., Fletcher, M. A., and Dobson, C. M. (2001). Amyloid fibrils from muscle myoglobin. *Nature* 410, 165–166. doi: 10.1038/35065514
- Fantini, J., and Barrantes, F. J. (2013). How cholesterol interacts with membrane proteins: an exploration of cholesterol-binding sites including CRAC, CARC, and tilted domains. *Front. Physiol.* 4:31. doi: 10.3389/fphys.2013.00031
- Fantini, J., Di Scala, C., Chahinian, H., and Yahi, N. (2020). Structural and molecular modelling studies reveal a new mechanism of action of chloroquine and hydroxychloroquine against SARS-CoV-2 infection. *Int. J. Antimicrob. Agents* 55:105960. doi: 10.1016/j.ijantimicag.2020.105960
- Gazit, E. (2002). A possible role for pi-stacking in the self-assembly of amyloid fibrils. *FASEB J.* 16, 77–83. doi: 10.1096/fj.01-0442hyp
- Gazit, E. (2007). Self assembly of short aromatic peptides into amyloid fibrils and related nanostructures. *Prion* 1, 32–35. doi: 10.4161/pri.1.1.4095
- Hannestad, J. K., Rocha, S., Agnarsson, B., Vladimir, P., Zhdanov, V. P., Wittung-Stafshede, P., et al. (2020). Single-vesicle imaging reveals lipid-selective and stepwise membrane disruption by monomeric α-synuclein. *Proc. Natl. Acad. Sci. U.S.A.* 117, 14178–14186. doi: 10.1073/pnas.1914670117
- Hasanbasic, S., Taler-Vercic, A., Puizdar, V., Stoka, V., Tusek Znidaric, M., Vilfan, A., et al. (2019). Prolines affect the nucleation phase of amyloid fibrillation reaction; Mutational analysis of human stefin B. *ACS Chem. Neurosci.* 10, 2730–2740. doi: 10.1021/acschemneuro.8b00621
- Hashimoto, Y., Toma, K., Nishikido, J., Yamamoto, K., Haneda, K., Inazu, T., et al. (1999). Effects of glycosylation on the structure and dynamics of eel calcitonin in micelles and lipid bilayers determined by nuclear magnetic resonance spectroscopy. *Biochemistry* 38, 8377–8384. doi: 10.1021/bi983018j
- Hayat, S., Peters, C., Shu, N., Tsigirgos, K. D., and Elofsson (2016). A. Inclusion of dyad-repeat pattern improves topology prediction of transmembrane β-barrel proteins. *Bioinformatics* 32, 1571–1573. doi: 10.1093/bioinformatics/btw025
- Hofmann, K., and Stoffel, W. (1993). TMbase - a database of membrane spanning proteins segments. *Biol. Chem. Hoppe Seyler* 374:166.
- Jacoboni, I., Martelli, P. L., Fariselli, P., De Pinto, V., and Casadio, R. (2001). Prediction of the transmembrane regions of beta barrel membrane proteins with a neural network based predictor. *Prot. Sci.* 10, 779–787. doi: 10.1110/ps.37201
- Jamasbi, E., Hossain, M. A., Tan, M., Separovic, F., and Ciccotosto, G. D. (2018). Fluorescence imaging of the interaction of amyloid beta 40 peptides with

- live cells and model membrane. *Biochim. Biophys. Acta Biomembr.* 1860, 1609–1615. doi: 10.1016/j.bbmem.2018.01.024
- Jang, H., Arce, F. T., Capone, R., Ramachandran, S., Lal, R., and Nussinov, R. (2009). Misfolded amyloid ion channels present mobile β -sheet subunits in contrast to conventional ion channels. *Biophys. J.* 97, 3029–3037. doi: 10.1016/j.bpj.2009.09.014
- Jang, H., Arce, F. T., Lee, J., Alan, L., Gillman, A. L., Ramachandran, S., et al. (2016). Computational methods for structural and functional studies of Alzheimer's amyloid ion channels. *Methods Mol. Biol.* 1345, 251–268. doi: 10.1007/978-1-4939-2978-8_16
- Jang, H., Connelly, L., Arce, F. T., Ramachandran, S., Bruce, L., Kagan, B. L., et al. (2013). Mechanisms for the insertion of toxic, fibril-like β -amyloid oligomers into the membrane. *J. Chem. Theory Comput.* 9, 822–833. doi: 10.1021/ct300916f
- Jang, H., Zheng, J., and Nussinov, R. (2007). Models of β -amyloid ion channels in the membrane suggest that channel formation in the bilayer is a dynamic process. *Biophys. J.* 93, 1938–1949. doi: 10.1529/biophysj.107.110148
- Jenko, S., Skarabot, M., Kenig, M., Guncar, G., Musevic, I., Turk, D., et al. (2004). Different propensity to form amyloid fibrils by two homologous proteins—Human stefins A and B: searching for an explanation. *Proteins* 55, 417–425. doi: 10.1002/prot.20041
- Julien, C., Tomberlin, C., Roberts, C. M., Akram, A., Stein, G. H., Silverman, M. A., et al. (2018). In vivo induction of membrane damage by β -amyloid peptide oligomers. *Acta Neuropathol. Commun.* 6:131. doi: 10.1186/s40478-018-0634-x
- Kahlenberg, J. M., and Kaplan, M. J. (2013). Little peptide, big effects: the role of LL-37 in inflammation and autoimmune disease. *J. Immunol.* 191, 4895–4901. doi: 10.4049/jimmunol.1302005
- Kametani, F., and Hasegawa, M. (2018). Reconsideration of amyloid hypothesis and tau hypothesis in Alzheimer's disease. *Front. Neurosci.* 12:25. doi: 10.3389/fnins.2018.00025
- Kandel, N., Matos, J. O., and Tatulian, S. A. (2019). Structure of amyloid β 25–35 in lipid environment and cholesterol dependent membrane pore formation. *Sci. Rep.* 9:2689. doi: 10.1038/s41598-019-38749-7
- Kandel, N., Zheng, T., Huo, Q., and Tatulian, S. A. (2017). Membrane binding and pore formation by a cytotoxic fragment of amyloid β peptide. *J. Phys. Chem. B* 121, 10293–10305. doi: 10.1021/acs.jpcc.7b07002
- Kawahara, M., Kuroda, Y., Arispe, N., and Rojas, E. (2000). Alzheimer's beta-amyloid, human islet amylin, and prion protein fragment evoke intracellular free calcium elevations by a common mechanism in a hypothalamic GnRH neuronal cell line. *J. Biol. Chem.* 275, 14077–14083. doi: 10.1074/jbc.275.19.14077
- Kawahara, M., Ohtsuka, I., Yokoyama, S., Kato-Negishi, M., and Sadakane, Y. (2011). Membrane incorporation, channel formation, and disruption of calcium homeostasis by Alzheimer's β -amyloid protein. *Internatl. J. Alzheimer's Dis.* 2011:304583. doi: 10.4061/2011/304583
- Kayed, R., Dettmer, U., and Lesne, S. E. (2020). Soluble endogenous oligomeric alpha-synuclein species in neurodegenerative diseases: expression, spreading, and cross-talk. *J. Parkinsons Dis.* 10, 791–818. doi: 10.3233/JPD-201965
- Kreutzter, A. G., and Nowick, J. S. (2018). Elucidating the structures of amyloid oligomers with macrocyclic β -hairpin peptides: insights into Alzheimer's disease and other amyloid diseases. *Acc. Chem. Res.* 51, 706–718. doi: 10.1021/acs.accounts.7b00554
- Krogh, A., Larsson, B., von Heijne, G., and Sonnhammer, E. L. L. (2001). Predicting transmembrane protein topology with a hidden Markov model: application to complete genomes. *J. Mol. Biol.* 305, 567–580. doi: 10.1006/jmbi.2000.4315
- Lashuel, H. A., Hartley, D., Petre, B. M., Walz, T., Peter, T., and Lansbury, P. T. (2002). Neurodegenerative disease: amyloid pores from pathogenic mutations affiliations. *Nature* 418:291. doi: 10.1038/418291a
- Lashuel, H. A., and Lansbury, P. T. (2006). Are amyloid diseases caused by protein aggregates that mimic bacterial pore-forming toxins? *Q. Rev. Biophys.* 39, 167–201. doi: 10.1017/S0033583506004422
- Last, N. B., and Miranker, A. D. (2013). Common mechanism unites membrane poration by amyloid and antimicrobial peptides. *Proc. Natl. Acad. Sci. U.S.A.* 110, 6382–6387. doi: 10.1073/pnas.1219059110
- Lee, J., Kim, Y. H., Arce, F. T., Gillman, A. L., Jang, H., Kagan, B. L., et al. (2017). Amyloid beta ion channels in a membrane comprising brain total lipid extracts. *ACS Chem. Neurosci.* 8, 1348–1357. doi: 10.1021/acscchemneuro.7b00006
- Leri, M., Bemporad, F., Oropesa-Nunez, R., Canale, C., Calamai, M., Nosi, D., et al. (2016). Molecular insights into cell toxicity of a novel familial amyloidogenic variant of beta 2-microglobulin. *J. Cell. Mol. Med.* 20, 1443–1456. doi: 10.1111/jcmm.12833
- Li, S., Yuan, L., Dai, G., Chen, R. A., Liu, D. X., and Fung, T. S. (2020). Regulation of the ER stress response by the ion channel activity of the infectious bronchitis Coronavirus envelope protein modulates virion release, apoptosis, viral fitness, and pathogenesis. *Front. Microbiol.* 10:3022. doi: 10.3389/fmicb.2019.03022
- Ma, J., Yee, A., Brewer, B. H., Jr., Das, S., and Potter, H. (1994). Amyloid-associated proteins α 1-antichymotrypsin and apolipoprotein E promote assembly of Alzheimer β -protein into filaments. *Nature* 372, 92–94. doi: 10.1038/372092a0
- Maji, S. K., Perrin, M. H., Sawaya, M. R., Jessberger, S., Vadodaria, K., Rissman, R. A., et al. (2009). Functional amyloids as natural storage of peptide hormones in pituitary secretory granules. *Science* 325, 328–332. doi: 10.1126/science.1173155
- Morillas, M., Vanik, D. L., and Surewicz, W. K. (2001). On the mechanism of α -helix to β -sheet transition in the recombinant prion protein. *Biochemistry* 40, 6982–6987. doi: 10.1021/bi010232q
- Motta, A., Pastore, A., Goud, N. A., and Castiglione Morelli, M. A. (1991). Solution conformation of salmon calcitonin in sodium dodecyl sulfate micelles as determined by two-dimensional NMR and distance geometry calculations. *Biochemistry* 30, 10444–10450. doi: 10.1021/bi00107a012
- Nanga, R. P. R., Brender, J. R., Xu, J., Hartman, K., Subramanian, V., and Ramamoorthy, A. (2009). Three-dimensional structure and orientation of rat islet amyloid polypeptide protein in a membrane environment by solution NMR spectroscopy. *J. Am. Chem. Soc.* 131, 8252–8261. doi: 10.1021/ja9010095
- Natt, N. K., Kaur, H., and Raghava, G. P. S. (2004). Prediction of Transmembrane regions of beta-barrel proteins using ANN and SVM based method. *Prot. Struct. Funct. Bioinform.* 56, 11–18. doi: 10.1002/prot.20092
- Nelson, R., Sawaya, M. R., Balbirnie, M. (2005). Structure of the cross-beta spine of amyloid-like fibrils. *Nature* 435, 773–778. doi: 10.1038/nature03680
- Nilsson, L. N., Bales, K. R., DiCarlo, G., Gordon, M. N., Morgan, D., Paul, S. M., et al. (2001). Alpha-1-antichymotrypsin promotes beta-sheet amyloid plaque deposition in a transgenic mouse model of Alzheimer's disease. *J. Neurosci.* 21, 1444–1451. doi: 10.1523/JNEUROSCI.21-05-01444.2001
- Niu, M., Li, Y., Wang, C., and Han, K. (2018). RFAMyloid: A web server for predicting amyloid proteins. *Int. J. Mol. Sci.* 19:2071. doi: 10.3390/ijms19072071
- Nugent, T., and Jones, D. T. (2009). Transmembrane protein topology prediction using support vector machines. *BMC Bioinform.* 10:159. doi: 10.1186/1471-2105-10-159
- Oxana, G. (2019). New mechanism of amyloid fibril formation. *Current Prot. Pept. Sci.* 20, 630–640. doi: 10.2174/1389203720666190125160937
- Pacheco, C. R., Morales, C. N., Ramírez, A. E., Muñoz, F. J., Gallegos, S. S., Caviedes, P. A., et al. (2015). Extracellular α -synuclein alters synaptic transmission in brain neurons by perforating the neuronal plasma membrane. *J. Neurochem.* 132, 731–741. doi: 10.1111/jnc.13060
- Padmanabhan, J., Levy, M., Dickson, D. W., and Potter, H. (2006). Alpha1-antichymotrypsin, an inflammatory protein overexpressed in Alzheimer's disease brain, induces tau phosphorylation in neurons. *Brain* 129, 3020–3034. doi: 10.1093/brain/awl255
- Pallarés, I., and Ventura, S. (2019). Advances in the prediction of protein aggregation propensity. *Curr. Med. Chem.* 26, 3911–3920. doi: 10.2174/0929867324666170705121754
- Pasquier, C., Promponas, V. J., Palaos, G. A., and Hamodrakas, J. S. (1999). A novel method for predicting transmembrane segments in proteins based on a statistical analysis of the SwissProt database: the PRED-TMR algorithm. *Protein Eng.* 12, 381–385. doi: 10.1093/protein/12.5.381
- Perissinotto, F., Stani, C., De Cecco, E., Vaccari, L., Rondelli, V., Posocco, P., et al. (2020). Iron-mediated interaction of alpha synuclein with lipid raft model membranes. *Nanoscale* 12, 7631–7640. doi: 10.1039/D0NR00287A
- Press-Sandler, O., and Miller, Y. (2018). Molecular mechanisms of membrane-associated amyloid aggregation: computational perspective and challenges. *BBA Biomem.* 1860, 1889–1905. doi: 10.1016/j.bbmem.2018.03.014
- Protter, D. S. W., and Parker, R. (2016). Principles and properties of stress granules. *Trends Cell Biol.* 26, 668–679. doi: 10.1016/j.tcb.2016.05.004
- Pujols, J., Peña-Díaz, S., and Ventura, S. (2018). AGGRESCAN3D: Toward the prediction of the aggregation propensities of protein

- structures. *Methods Mol. Biol.* 1762, 427–443. doi: 10.1007/978-1-4939-7756-7_21
- Reymer, A., Frederick, K. K., Rocha, S., Beke-Somfai, T., Kitts, C. C., Lindquist, S., et al. (2014). Orientation of aromatic residues in amyloid cores: structural insights into prion fiber diversity. *Proc. Natl. Acad. Sci. U.S.A.* 111, 17158–17163. doi: 10.1073/pnas.1415663111
- Roy Choudhury, A., and Novič, M. (2009). Data-driven model for the prediction of protein transmembrane regions. *SAR QSAR Environ. Res.* 20, 741–754. doi: 10.1080/10629360903438602
- Roy Choudhury, A., and Novič, M. (2012). Amino acid distribution in transmembrane regions: a statistical analysis and comparison with globular proteins. *Int. J. Chem. Model.* 4, 205–219.
- Roy Choudhury, A., and Novič, M. (2015). PredβTM: A novel β-transmembrane region prediction algorithm. *PLoS ONE* 10:e0145564. doi: 10.1371/journal.pone.0145564
- Sawaya, M. R., Sambashivan, S., Nelson, R., Ivanova, M. I., Sievers, S. A., Apostol, M. I., et al. (2007). Atomic structures of amyloid cross-beta spines reveal varied steric zippers. *Nature* 447, 453–457. doi: 10.1038/nature05695
- Sengupta, I., and Udgaonkar, J. B. (2018). Structural mechanisms of oligomer and amyloid fibril formation by the prion protein. *Chem. Commun.* 54, 6230–6242. doi: 10.1039/C8CC03053G
- Sepúlveda, F. J., Fierro, H., Fernandez, E., Castillo, C., Peoples, R. W., Opazo, C., et al. (2014). Nature of the neurotoxic membrane actions of amyloid-β on hippocampal neurons in Alzheimer's disease. *Neurobiol. Aging* 35, 472–481. doi: 10.1016/j.neurobiolaging.2013.08.035
- Serra-Batiste, M., Ninot-Pedrosa, M., Bayoumi, M., Gairí, M., Maglia, G., and Carulla, N. (2016). Aβ42 assembles into specific β-barrel pore-forming oligomers in membrane-mimicking environments. *Proc. Natl. Acad. Sci. U.S.A.* 113, 10866–10871. doi: 10.1073/pnas.1605104113
- Sezgin, E., Levental, I., Mayor, S., and Eggeling, C. (2017). The mystery of membrane organization: composition, regulation and roles of lipid rafts. *Nat. Rev. Mol. Cell. Biol.* 18, 361–374. doi: 10.1038/nrm.2017.16
- Shoji, M., Hirai, S., Yamaguchi, H., Harigaya, Y., Ishiguro, K., and Matsubara, E. (1991). Alpha 1-antichymotrypsin is present in diffuse senile plaques. A comparative study of beta-protein and alpha 1-antichymotrypsin immunostaining in the Alzheimer brain. *Am. J. Pathol.* 138, 247–257.
- Snider, C., Jayasinghe, S., Hristova, K., and White, S. H. (2009). MPEx: a tool for exploring membrane proteins. *Protein Sci.* 18, 2624–2628. doi: 10.1002/pro.256
- Stefani, M., and Dobson, C. M. (2003). Protein aggregation and aggregate toxicity: new insights into protein folding, misfolding diseases and biological evolution. *J. Mol. Med.* 81, 678–699. doi: 10.1007/s00109-003-0464-5
- Takahashi, T., Kulkarni, N. N., Lee, E. Y., Zhang, L. J., Wong, G. C. L., and Gallo, R. L. (2018). Cathelicidin promotes inflammation by enabling binding of self-RNA to cell surface scavenger receptors. *Sci. Rep.* 8:4032. doi: 10.1038/s41598-018-22409-3
- Tenidis, K., Waldner, M., Bernhagen, J., Fischle, W., Bergmann, M., Weber, M., et al. (2000). Identification of a penta- and hexapeptide of islet amyloid polypeptide (IAPP) with amyloidogenic and cytotoxic properties. *J. Mol. Biol.* 295, 1055–1071. doi: 10.1006/jmbi.1999.3422
- Tsigelny, I. F., Sharikov, Y., Wrasidlo, W., Gonzalez, T., Desplats, P. A., Crews, L., et al. (2012). Role of α-synuclein penetration into the membrane in the mechanisms of oligomer pore formation. *FEBS J.* 279, 1000–1013. doi: 10.1111/j.1742-4658.2012.08489.x
- Tsirigos, K. D., Peters, C., Shu, N., Käll, L., and Elofsson, A. (2015). The TOPCONS web server for combined membrane protein topology and signal peptide prediction. *Nucleic Acids Res.* 43, W401–W407. doi: 10.1093/nar/gkv485
- Tsolis, A. C., Papandreou, N. C., Iconomidou, V. A., and Hamodrakas, S. J. (2013). A consensus method for the prediction of 'aggregation-prone' peptides in globular proteins. *PLoS ONE* 8:e54175. doi: 10.1371/journal.pone.0054175
- Tusnádý, G. E., and Simon, I. (2001). The HMMTOP transmembrane topology prediction server. *Bioinformatics* 17, 849–850. doi: 10.1093/bioinformatics/17.9.849
- Tyagi, E., Fiorelli, T., Norden, M., and Padmanabhan, J. (2013). Alpha 1-Antichymotrypsin, an inflammatory protein overexpressed in the brains of patients with Alzheimer's disease, induces Tau hyperphosphorylation through c-Jun N-Terminal kinase activation. *Int. J. Alzheimers Dis.* 2013:606083. doi: 10.1155/2013/606083
- Varadi, M., De Baets, G., Vranken, W. F., Tompa, P., and Pancsa, R. (2018). AmyPro: a database of proteins with validated amyloidogenic regions. *Nucleic Acids Res.* 46, D387–D392. doi: 10.1093/nar/gkx950
- Venko, K., Roy Choudhury, A., and Novič, M. (2017). Computational approaches for revealing the structure of membrane transporters: Case study on bilitranslocase. *Comp. Struct. Biotechnol. J.* 15, 232–242. doi: 10.1016/j.csbj.2017.01.008
- Verdiá-Báguena, C., Nieto-Torres, J. L., Alcaraz, A., De Diego, M. L., Torres, J., Aguilera, V. M., et al. (2012). Coronavirus E protein forms ion channels with functionally and structurally involved membrane lipids. *Virology* 432, 485–494. doi: 10.1016/j.virol.2012.07.005
- Viklund, H., and Elofsson, A. (2008). Improving topology prediction by two-track ANN-based preference scores and an extended topological grammar. *Bioinformatics* 24, 1662–1668. doi: 10.1093/bioinformatics/btn221
- Wang, Q., Ni, C. M., Li, Z., Li, X. F., Han, R. M., Zhao, F., et al. (2019). PureseqTM: efficient and accurate prediction of transmembrane topology from amino acid sequence only. *bioRxiv [Preprint]*. doi: 10.1101/627307
- Wilson, L., McKinlay, C., Gage, P., and Ewart, G. (2004). SARS coronavirus E protein forms cation-selective ion channels. *Virology* 330, 322–331. doi: 10.1016/j.virol.2004.09.033
- Yahi, N., and Fantini, J. (2014). Deciphering the glycolipid code of Alzheimer's and Parkinson's amyloid proteins allowed the creation of a universal ganglioside-binding peptide. *PLoS ONE* 9:e104751. doi: 10.1371/journal.pone.0104751
- Žerovnik, E., Staniforth, R. A., and Turk, D. (2010). Amyloid fibril formation by human stefins: Structure, mechanism & putative functions. *Biochimie* 92, 1597–1607. doi: 10.1016/j.biochi.2010.05.012
- Žerovnik, E., Stoka, V., Mirtic, A., Guncar, G., Grdadolnik, J., Staniforth, R., et al. (2011). Mechanisms of amyloid fibril formation - focus on domain-swapping. *FEBS J.* 278, 2263–2282. doi: 10.1111/j.1742-4658.2011.08149.x
- Žerovnik, E., Virden, R., Jerala, R., Kroon-Zitko, L., Turk, V., and Waltho, J. P. (1999). Differences in the effects of TFE on the folding pathways of human stefins A and B. *Prot. Struct. Funct. Bioinform.* 36, 205–216. doi: 10.1002/(SICI)1097-0134(19990801)36:2<205::AID-PROT6>3.0.CO;2-4
- Zhang, M., Zhao, J., and Zheng, J. (2014). Molecular understanding of a potential functional link between antimicrobial and amyloid peptides. *Soft Matter*. 10, 7425–7451. doi: 10.1039/C4SM00907J

Conflict of Interest: The authors declare that the research was conducted in the absence of any commercial or financial relationships that could be construed as a potential conflict of interest.

Copyright © 2021 Venko, Novič, Stoka and Žerovnik. This is an open-access article distributed under the terms of the Creative Commons Attribution License (CC BY). The use, distribution or reproduction in other forums is permitted, provided the original author(s) and the copyright owner(s) are credited and that the original publication in this journal is cited, in accordance with accepted academic practice. No use, distribution or reproduction is permitted which does not comply with these terms.



A Novel SOD1 Intermediate Oligomer, Role of Free Thiols and Disulfide Exchange

Bon-Kyung Koo^{1*}, William Munroe^{1†}, Edith B. Gralla¹, Joan Selverstone Valentine^{1*} and Julian P. Whitelegge^{1,2*}

¹ Department of Chemistry and Biochemistry, University of California, Los Angeles, Los Angeles, CA, United States, ² The Pasarow Mass Spectrometry Laboratory, David Geffen School of Medicine, NPI-Semel Institute for Neuroscience and Human Behavior, University of California, Los Angeles, Los Angeles, CA, United States

OPEN ACCESS

Edited by:

Cláudio M. Gomes,
University of Lisbon, Portugal

Reviewed by:

Bryan Shaw,
Baylor University, United States
Jens Danielsson,
Stockholm University, Sweden

*Correspondence:

Bon-Kyung Koo
bonkbong9@gmail.com
Joan Selverstone Valentine
jafselverstone@gmail.com
Julian P. Whitelegge
jpw@chem.ucla.edu

† Present address:

William Munroe,
Department of Chemistry, California
State University, Camarillo, CA,
United States

Specialty section:

This article was submitted to
Neurodegeneration,
a section of the journal
Frontiers in Neuroscience

Received: 19 October 2020

Accepted: 24 December 2020

Published: 18 February 2021

Citation:

Koo B-K, Munroe W, Gralla EB,
Valentine JS and Whitelegge JP
(2021) A Novel SOD1 Intermediate
Oligomer, Role of Free Thiols
and Disulfide Exchange.
Front. Neurosci. 14:619279.
doi: 10.3389/fnins.2020.619279

Wild-type human SOD1 forms a highly conserved intra-molecular disulfide bond between C57-C146, and in its native state is greatly stabilized by binding one copper and one zinc atom per monomer rendering the protein dimeric. Loss of copper extinguishes dismutase activity and destabilizes the protein, increasing accessibility of the disulfide with monomerization accompanying disulfide reduction. A further pair of free thiols exist at C6 and C111 distant from metal binding sites, raising the question of their function. Here we investigate their role in misfolding of SOD1 along a pathway that leads to formation of amyloid fibrils. We present the seeding reaction of a mutant SOD1 lacking free sulfhydryl groups (AS-SOD1) to exclude variables caused by these free cysteines. Completely reduced fibril seeds decreasing the kinetic barrier to cleave the highly conserved intramolecular disulfide bond, and accelerating SOD1 reduction and initiation of fibrillation. Presence or absence of the pair of free thiols affects kinetics of fibrillation. Previously, we showed full maturation with both Cu and Zn prevents this behavior while lack of Cu renders sensitivity to fibrillation, with presence of the native disulfide bond modulating this propensity much more strongly than presence of Zn or dimerization. Here we further investigate the role of reduction of the native C57-C146 disulfide bond in fibrillation of wild-type hSOD1, firstly through removal of free thiols by paired mutations C6A, C111S (AS-SOD1), and secondly in seeded fibrillation reactions modulated by reductant tris (2-carboxyethyl) phosphine (TCEP). Fibrillation of AS-SOD1 was dependent upon disulfide reduction and showed classic lag and exponential growth phases compared with wild-type hSOD1 whose fibrillation trajectories were typically somewhat perturbed. Electron microscopy showed that AS-SOD1 formed classic fibrils while wild-type fibrillation reactions showed the presence of smaller “sausage-like” oligomers in addition to fibrils, highlighting the potential for mixed disulfides involving C6/C111 to disrupt efficient fibrillation. Seeding by addition of sonicated fibrils lowered the TCEP concentration needed for fibrillation in both wild-type and AS-SOD1 providing evidence for template-driven structural disturbance that elevated susceptibility to reduction and thus propensity to fibrillate.

Keywords: fibrillation, disulfide reduction, fibril seeding, Cu/Zn superoxide dismutase 1, amyotrophic lateral sclerosis, oligomerization, analytical ultracentrifugation

INTRODUCTION

Over 100 different mutations in SOD1 (an abundant copper- and zinc-containing superoxide dismutase 1), the antioxidant enzyme, have been identified to account for fALS (familial amyotrophic lateral sclerosis), a fatal neurodegenerative disorder caused by formation of abnormal protein aggregates in neuronal cells. Detergent-resistant aggregates isolated from the spinal cords of ALS transgenic mice contain full-length apo hSOD1 proteins that acquire toxic properties in the disease mechanism (Shaw et al., 2008), and SOD1 fibrils have been shown to induce cytokine expression in mononuclear cells, thus causing inflammation (Fiala et al., 2010), and to activate microglial cells (Roberts et al., 2013), suggesting that fibrils have toxic properties that may be related to ALS. On the other hand, the Dokholyan group recently found evidence that SOD1 trimer is toxic to the type of neuron affected in ALS (Fay et al., 2016) and that large SOD1 fibrils protect rather than harm neurons (Zhu et al., 2018). However, still the fibrillation mechanism of SOD1 has remained elusive unlike that of other well-studied amyloids, and it is very important to understand the morphological differences and the reducing level of amyloid forming proteins in the cell of protein-misfolding diseases for comprehending of SOD1-fALS etiology.

SOD1 is a 32 kDa homodimer which forms a β -barrel and contains an intramolecular disulfide bond formed by C57 and C146 in addition to 2 reduced C6 and C111 in each 153-residue subunit (Valentine and Hart, 2003; Valentine et al., 2005). Over-expression of mutant SOD1 in neural tissues of fALS transgenic mice and in transfected cultured cells results in aggregation and neurotoxicity linked to inter-molecular disulfide cross-linking of the free cysteines C6 and C111 (Niwa et al., 2007; Cozzolino et al., 2008; Leinartaitė and Johansson, 2013; Toichi et al., 2013). Protein fibrillary aggregation *in vitro* requires a significant conformational conversion of proteins thought to be first to the monomer (also known as “nucleus”), to subsequently form oligomers which is a rate-limiting step of the overall aggregation reaction (LeVine, 1999; Banci et al., 2006). Once the nucleus forms, it functions as “seed” (a structural template) to convert native dimeric proteins into β -sheet-rich monomeric structures and subsequently elongate the protein fibril. This mechanism, which accelerates and even triggers protein aggregation, is called the seeding reaction (Szedberg and Pedersen, 1940; LeVine, 1999; Bouldin et al., 2012). Protein conformational changes, aggregation and amyloid fibril formation can be monitored based on spectroscopic and biophysical methods such as fluorescence spectroscopy, analytical ultracentrifugation, and so on (Doucette et al., 2004; Cristovao et al., 2019).

The AS mutant, C6A/C111S, is a “pseudo-WT” SOD1 in which both free cysteines have been removed by mutation, with the buried Cys6 mutated to alanine and the surface Cys111 changed to serine. AS-SOD1 (mutant SOD1 lacking free sulfhydryl groups C6A/C111S) has a stability similar to that of WT-SOD1 but melts reversibly, while WT-SOD1 melts irreversibly, presumably because of disulfide-induced aggregation following thermal unfolding (Lepock et al., 1990;

Hallewell et al., 1991; Parge et al., 1992; Oztug Durer et al., 2009). Here, we compared the seeding effect in the fibrillations of apo WT-SOD1 and apo AS-SOD1 to exclude variables caused by disulfide cross-linking of the free cysteines and to study the mechanism behind fibrillation lag time. During the lag time of SOD1 fibrillation, the protein undergoes conformational changes from native dimer to monomer which we further investigate by analytical ultracentrifugation. For this conformational conversion, the well conserved intramolecular disulfide bond of SOD1 requires reduction. When 10% of fully reduced fibril seed were added to the SOD1 fibrillation reaction, SOD1 reduction and fibrillation initiation was accelerated. We suggest some chaotropes such as low concentrations of GuHCl accelerated the fibrillation initiation possibly through a similar mechanism. Therefore, the mechanism behind decreasing the lag time is due to disulfide reduction and a conformational change that leads to accelerated initiation of fibrillation.

MATERIALS AND METHODS

SOD1 Expression and Purification

Wild-type SOD1 was expressed in *S. cerevisiae* and purified following the procedures from the published procedures (Wiedau-Pazos et al., 1996; Doucette et al., 2004; Hough et al., 2004). C6A/C111S SOD1 (AS-SOD1) was expressed in *E. coli* and purified using a similar procedure. Purified SOD1 was demetallated by dialysis in a Slide-a-lyzer (Pierce, 10,000 Da. MWCO) against (1) 10 mM EDTA, 100 mM sodium acetate, pH 3.8, (2) 100 mM NaCl, 100 mM sodium acetate, pH 3.8, and (3) 10 mM potassium phosphate, pH 7.0 as the dialysis buffer. Apo-SOD1 was flash-frozen in liquid nitrogen and stored at -20°C prior to use. Metal content of apo and metallated SOD1 was determined by inductive coupled plasma mass spectrometry (ICP-MS, Agilent 7,500 Series). All apo-proteins contained less than 0.1 equivalents of Cu and Zn per dimer.

In vitro Fibril/Fibril Seed Formation

To make fibrils, 40 μM of apo protein was prepared in 10 mM potassium phosphate (KPi), pH 7.0 with 5 mM TCEP and 40 μM of thioflavin-T (TfT) as described (Chattopadhyay et al., 2008). TfT binds to beta sheet-rich structures, such as those in amyloid aggregates, and enhances fluorescence, so it is often used as a diagnostic of amyloid structure (LeVine, 1999). The protein samples were reduced with 5 mM TCEP during fibrillation at 37°C without shaking. To monitor fibril formation, 200 μM of each reaction was in separate wells of a 96 well plate to which a Teflon ball (1/8 in. diameter) had been added. The plate was agitated at 300 rpm (3 mm rotation diameter) in a Fluoroskan plate-reader (Thermo) at 37°C . Fluorescence measurements were recorded every 15 min using at $\lambda_{\text{ex}} = 444 \text{ nm}$ $\lambda_{\text{em}} = 485 \text{ nm}$, with an integration time of 200 ms. All reactions were performed in replicates of 3 or more. Data was fitted to the following equation:

$$F = F_0 + (A + ct)/(1 + \exp[k(t_m - t)]), \quad (1)$$

where lag phase was calculated as $t_m - t$.

Fibril seeds were prepared from fibrils generated as described above. Fibrils extracted from a 96-well microplate were centrifuged in a microcentrifuge tube at $16,800 \times g$ for 15 min. The supernatant was pipetted out, washed with 10 mM potassium phosphate buffer twice and the fibrils were resuspended in the same volume (200 μ L) of 2 M guanidinium hydrochloride, 10 mM potassium phosphate, pH 7, by pipetting up and down and vortexing at medium speeds and incubated at 37°C for 90 min. They were then moved to a glass vial and sonicated for 30 min in a water bath sonicator (Branson Scientific, 100 watts) and centrifuged to remove supernatant (guanidinium hydrochloride) twice and then used within 30 min. Seeding reactions were assembled using 10–20% by volume of fibril seeds prepared by the above protocol, 40 μ M apo SOD1 and 40 μ M ThT in 10 mM potassium phosphate, pH 7.

Iodoacetamide Labeling

Disulfide-intact or disulfide-reduced apo-SOD1 at 3–5 mg/ml was treated with 20 mM IAA at room temperature for 1 h in dark. Excess IAA and TCEP were removed by 3 rounds of centrifugation in 10 mM potassium phosphate, pH 7. The presence of IAA bound to cysteines was checked by ESI-MS.

Proteolysis of Fibrillar and Soluble SOD1

Trypsin (porcine; Promega) proteolysis was in 50 mM NH_4HCO_3 at 37°C for 30 min at 1:30 (wt:wt) enzyme:substrate. SOD1 fibrils were separated from soluble contaminants by ultracentrifugation in an Airfuge (Beckman Coulter) at $125,000 \times g$ for 30 min; then the pellet was washed with 50 mM NH_4HCO_3 . Soluble apo SOD1 was diluted to the same concentration as the fibril with 50 mM NH_4HCO_3 and was digested similarly. After proteolysis, the reaction was quenched by 1 mM PMSF.

SEC-HPLC and ICP-MS

Disulfide-oxidized and -reduced apo-SOD1, which are dimeric and monomeric, respectively, were prepared and performed for SEC-HPLC and high-resolution MS/MS as previously described (Chattopadhyay et al., 2008; Chan et al., 2013). For the ICP-MS, 20 μ L sample was taken and added 50 μ L of nitric acid (Optima grade). Then, it was heated for 2 h at 95°C with opened lid. It was then diluted with 2 mL of 2% nitric acid and added 20 μ L internal standard for ICP-MS. The experiment was performed as previously described (Chattopadhyay et al., 2015).

Analytical Ultracentrifugation

SOD1 samples were examined by sedimentation velocity using a Beckman XL-A analytical ultracentrifuge equipped with the AN-60 rotor (Beckman Instruments). SOD1 samples were loaded into 1.2 cm path length charcoal-filled Epon double sector cells. Measurements were recorded at 280 nm to monitor the behavior of the SOD1 sample at various rotor speeds. For all the measurements, the sedimentation coefficient values were corrected to $S_{20,w}$ (standard solvent conditions in water at 20°C).

Hypothetical sedimentation coefficients for monomeric and dimeric SOD1 were calculated from the molecular weight, partial

specific volume, and approximate axial ratio using the following equation:

$$s = \frac{M^{2/3}(1 - \bar{v}\rho)}{N6\pi\eta \left(\frac{3}{4\pi N}\right)^{1/3} \left(1 + \frac{\delta H}{\bar{v}\rho}\right)^{1/3} (f/f_0)} \quad (2)$$

Where the terms are as follows: s is the sedimentation coefficient in seconds (with S having units of 1×10^{-13} s), M is the macromolecule's molecular weight, \bar{v} is the partial specific volume of the macromolecule, ρ is the solvent density, N is Avogadro's number, η is the solution viscosity in Poise, δH is hydration of the macromolecule in g water per g macromolecule, and f/f_0 is the calculated Perrin factor for the asymmetry of the macromolecule (Szedberg and Pedersen, 1940; Schachman, 1959; Tanford, 1961; Van Holde et al., 1998).

Electron Microscopy

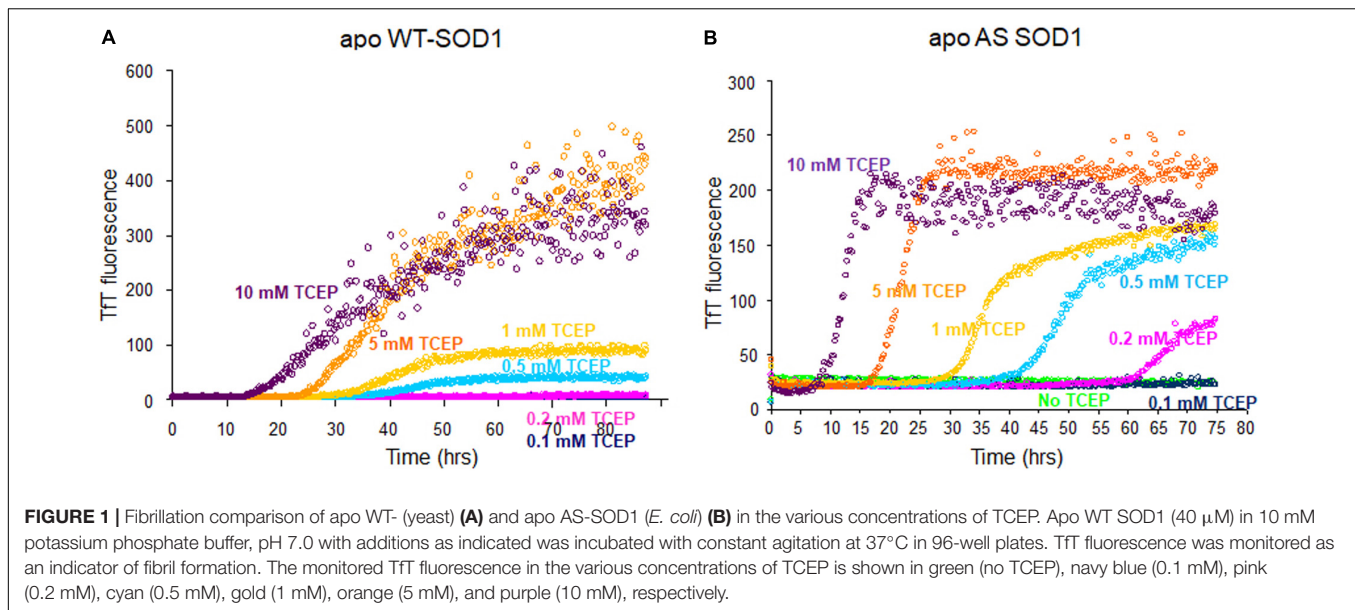
Five microliters of the fibril suspension were deposited on a formavar-coated copper grid (Ted Pella, Inc.). The sample was allowed to adsorb for 5 min, blotted, washed 3 times with 10 mM HEPES, blotted and then stained with freshly filtered 2% uranyl acetate (100 μ M) for 3 min, blotted again. The grids were air-dried for 30 min before insertion into a JEM12000 electron microscope operated at 80 keV. Fibrils were typically visualized at a magnification of 75,000.

RESULTS

Fibrillation of Apo AS-SOD1 Is Dramatically Changed Depending Only on the Reduction of s-s Bond

In addition to Cys-57 and Cys-146, which form the native intramolecular disulfide bond, SOD1 contains 2 reduced cysteine residues, Cys-6 and Cys-111, and during the lag time, we could observe disulfide scrambling between (Cys-111 and Cys-146) or (Cys-6 and Cys-111) (**Supplementary Figure S1**). Consequently, we wanted to compare WT-SOD1 to AS-SOD1, which is mutated C6A and C111S to exclude the effect of disulfide scrambling. Apo AS-SOD1 formed amyloid-like aggregates at neutral pH under reducing conditions as WT. To compare the fibrillation, we used fibrils generated by incubating apo WT^{S-S} or apo AS^{S-S} in the presence of varying concentrations of TCEP (previous lab studies used dithiothreitol).

The fibrillation of apo WT-SOD1 showed more complex behavior than apo AS-SOD1 (compare **Figures 1A,B**) because it has more variables such as disulfide scrambling. In fact, apo AS-SOD1 shows dramatically cleaner Tft fluorescence profiles. Tft fluorescence profiles of WT vs. AS-SOD1 depends on the TCEP concentrations (**Figures 1A,B**). Across the Tft fibrillation experiment, AS had shorter lag times than WT at comparable TCEP concentrations, and the slope of AS was consistently steeper during the growth phase compared with WT. The simplest interpretation is that reduction of the disulfide allows unhindered amyloid growth in AS whereas WT is delayed and slowed down by disulfide scrambling. The free C6 and C111



thiols are clearly un-necessary for fibrillation of AS-SOD1 in the presence of reductant and the process appears more efficient because disulfide scrambling is eliminated in the AS mutant.

Reducing of Disulfide Bond During Lag Time

To compare disulfide bond status around the initiation of fibrillation in different TCEP concentrations (before growth phase has started) we used mass spectrometry after iodoacetamide (IAA) treatment (if the disulfide is intact then the molecule is 112 Da lighter – 2 molecules IAA minus a disulfide). Samples were collected at 47 h in 0.5 mM TCEP, 7.5 h in 5 mM TCEP, and 5 h in 10 mM TCEP after shaking the 96-well plate right before the initiations. In the presence of 0.5 mM TCEP, separate peaks corresponding to apo AS^{SH} (Mw 15,870.53 Da) and apo AS^{S-S} (Mw 15,756.43 Da) were observed with a ratio of approximately 1.8–1. In the 5 mM TCEP, a single peak for the mixture of apo AS^{SH} and apo AS^{S-S} as the ratio of 7.5–1. However, in the 10 mM TCEP, it was a single peak of completely reduced apo AS-SOD1 (**Figure 2**). Fibrillation initiation is slowly started around 47 h if intact disulfide bonds are less than 25% (**Figure 2D**) in case of 0.5 mM TCEP (these ratios assume that disulfide reduction and modification of each thiol with IAA does not change the ionization efficiency).

Previously, we showed that NoCys mutant spontaneously fibrillates with a lag phase of about 10 h (Chattopadhyay et al., 2015), and apo NoCys-SOD1 has been shown to behave structurally and biophysically very close to WT^{2SH} (Furukawa and O'Halloran, 2005; Furukawa et al., 2008). This is comparable to a lag phase of about 15 h for apo WT^{S-S} or about 7 h for apo AS^{S-S} in 10 mM TCEP, the concentration high enough to completely reduce intact disulfide bond (**Figure 2C**). Although AS is completely reduced in 10 mM TCEP, we could see the mass of 15,818 Da, suggesting modification with one thiol-molecule IAA, possibly suggesting that some structural

modification during the lag time renders one thiol somewhat in-accessible to the IAA (**Figures 2C,D**). All these experiments show that the substantial majority of all disulfide bonds is reduced before growth phase of fibrillation commences.

Lowering the Kinetic Barrier by Amyloid Seeds

To examine the seeding effect, fibrils were generated by incubating apo WT^{S-S} or apo AS^{S-S} in 5 mM TCEP. The fibril from apo AS consists completely of AS^{2SH} in the presence of GdmCl, as shown in **Supplementary Figure S2** by denaturation in the presence of IAA and subsequent HPLC-MS. It is mainly AS^{2SH} in the absence of GdmCl also (**Supplementary Figure S2**). When seeds prepared from these fibrils (AS^{2SH}, absence of GdmHCl) were added at 10% to soluble apo WT SOD1^{S-S} and apo AS SOD1^{S-S} in the various concentrations of reducing agents, fibril growth for AS-SOD1 occurred dramatically with a very short lag phase compared to WT-SOD1 (**Figures 3A,B**). Strikingly, we found that addition of 10% seed decreased the necessary TCEP for the fibrillation initiation as well as it decreased the lag time (compare AS vs. WT; **Figures 3A,B**). Unseeded reactions did not fibrillate at 0.1 mM TCEP (**Figure 1**), but seeded reactions showed the fibrillation initiation at 0.1 mM (navy blue) or even in the absence of TCEP in case of apo AS-SOD1 (**Figure 3B**, green).

Comparing the Tft fluorescence at 0.5 mM TCEP of seeded vs. unseeded apo AS-SOD1, the lag time of unseeded fibrillation (compare with **Figure 1**) is around 40 h (navy blue), however, the lag time of 10% seeded fibrillation is shorter than 5 h (red) (**Figure 3C**). LC-MS was performed to examine the disulfide bond status in this seeding reaction. The fibrillated aggregation was initiated at 40 h without seed or 5 h with seed in 0.5 mM TCEP as shown in **Figures 1, 3**, therefore LC-MS was performed for the following reaction mixtures: (1) after 3 h shaking incubation, (2) fibril seed, and (3) 10% seed added reaction

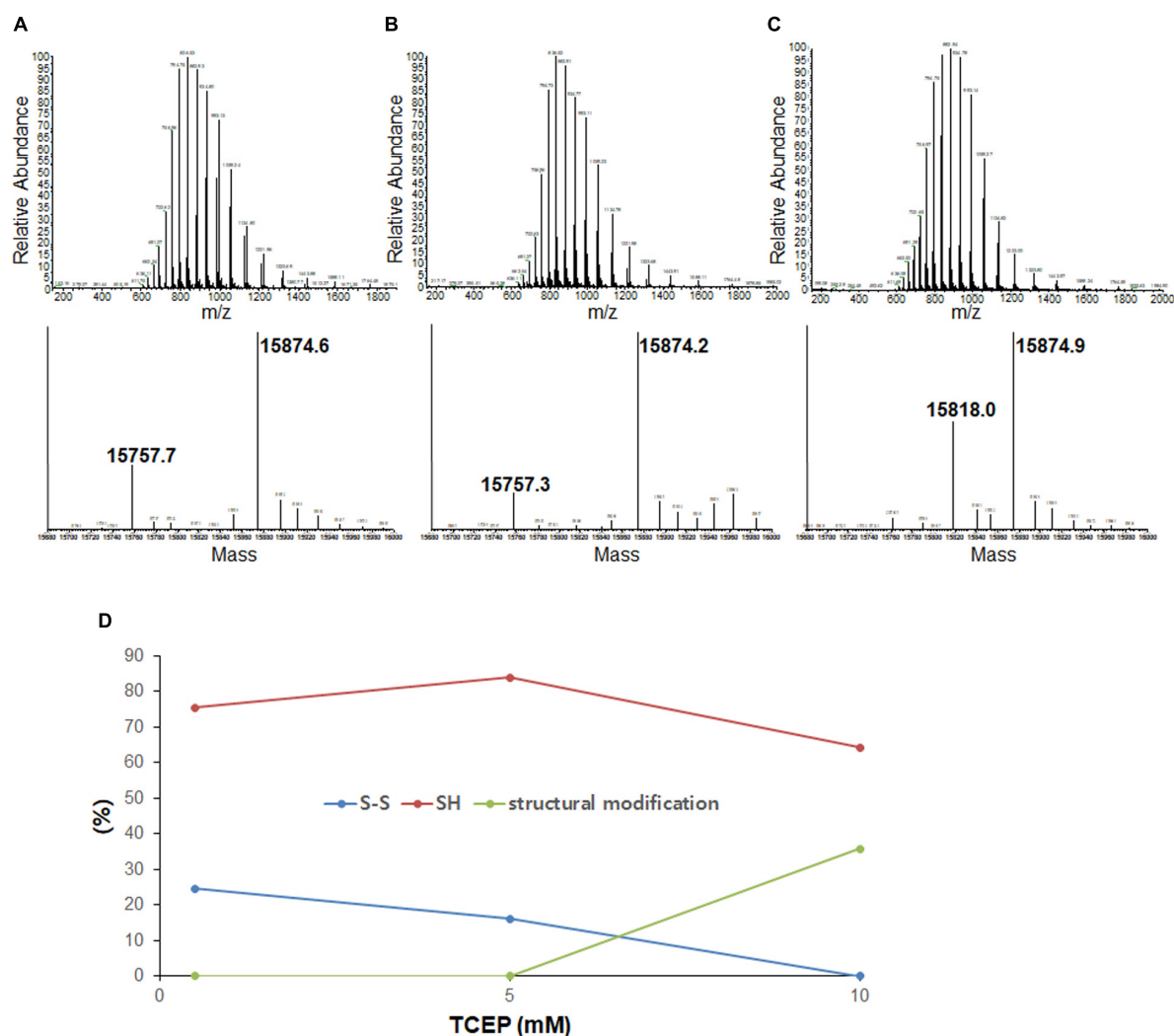


FIGURE 2 | LC-MS of the lag phase of apo AS-SOD1 in 0.5 mM (A), 5 mM (B), and 10 mM (C) TCEP at 47 h (A), 7.5 h (B), and 5.5 h (C), respectively. Molecular weights of AS S-S and AS SH treated with iodoacetamide are about 15756.43 Da and 15870.53 Da based on PeptideMass (http://web.expasy.org/cgi-bin/peptide_mass/peptide-mass.pl). (D) The percentages of the ratio of AS S-S and AS SH are shown in different TCEP concentrations.

mixture after 3 h shaking incubation. We found apo AS-SOD1 in 0.5 mM TCEP is oxidized with intramolecular disulfide bond at the beginning of shaking incubation, but if 10% reduced fibril seed is added, it is also completely reduced rapidly (Figure 3D). Clearly, reduced fibril seed has a powerful ability to initiate fibrillation in the AS mutant.

It Takes Time to Reduce Intact Disulfide Bond During Lag Time in Low TCEP

We wanted to see the disulfide bond status during lag phase as time proceeds in presence of very little amount of reducing agent, so we performed LC-MS for reaction mixtures collected as time courses for apo AS-SOD1 thiol-alkylated by IAA in the low TCEP of 0.5 mM, and displayed the percentage of disulfide status as time passed (Figure 4). During the lag phase of apo AS^{S-S} fibrillation in 0.5 mM TCEP, it takes a long time of about 40 h to reduce

the intact disulfide bond to initiate the fibrillation (Figure 1B, cyan), and the ratio of apo AS^{SH} to apo AS^{S-S} was approximately 1:10.3 at 3, 1:3.8 at 5, 1:4.8 at 10, 1:1.3 at 22, and 1:0.54 at 47 h (these ratios assume the ionization efficiency is unchanged by reduction). The initiation of apo AS-SOD1 is started when intact disulfide bond is reduced more than about 70% (Figures 2D, 4). However, when completely reduced 10% of apo AS-SOD1 fibril seeds were added to 5 mM TCEP fibrillation reaction, it could lower the lag time substantially suggesting lowering the kinetic barrier to onset of fibrillation (Figure 3D).

Amyloid Fibril Images of Apo WT-SOD1 and Apo AS-SOD1

The electron microscopy (EM) confirmed the presence of amyloid fibrils and enabled comparisons of apo WT-SOD1 and apo AS-SOD1 fibrils (Figure 5). Apo AS-SOD1 fibrils

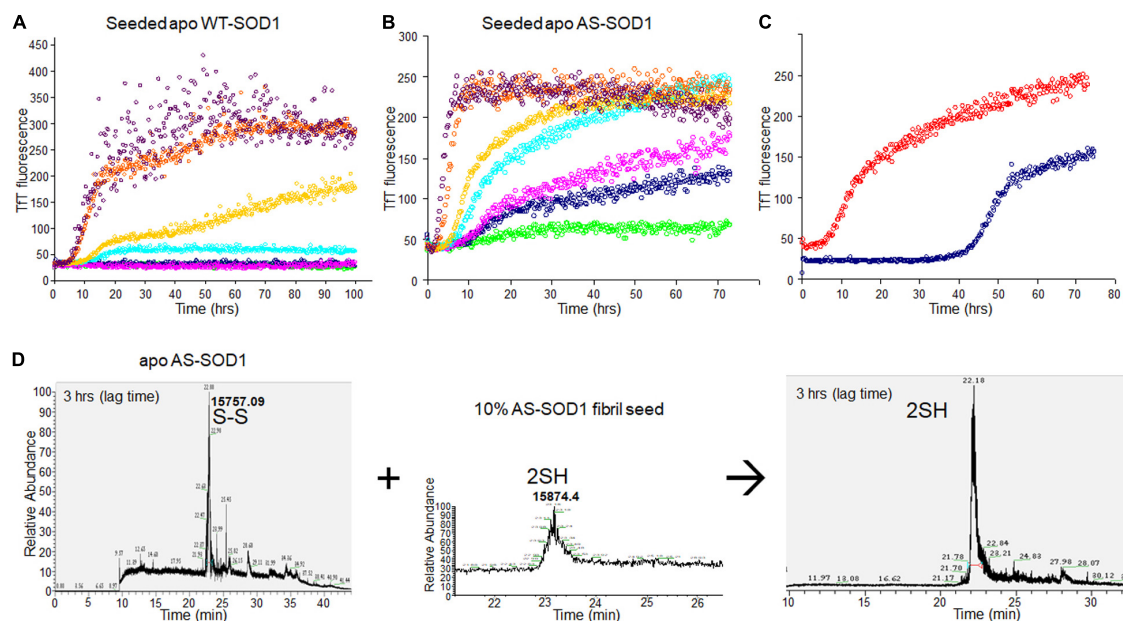


FIGURE 3 | 10% fibril seeds (AS-SOD1, see **Figure 3**) were added to the fibrillation of apo WT-SOD1 (40 μ M) (**A**) and apo AS-SOD1 (40 μ M) (**B**) in the various concentrations of TCEP, in 10 mM potassium phosphate buffer, pH 7.0. TTF fluorescence was monitored as an indicator of fibril formation. The monitored TTF fluorescence in the various concentrations of TCEP is shown in green (no TCEP), navy blue (0.1 mM), pink (0.2 mM), cyan (0.5 mM), gold (1 mM), orange (5 mM), and purple (10 mM), respectively. (**C**) Comparison of unseeded (navy blue) and 10% seeded (red) fibrillation of apo AS-SOD1 in 0.5 mM TCEP. (**D**) 10% fully reduced fibril seeds accelerated SOD1 reduction.

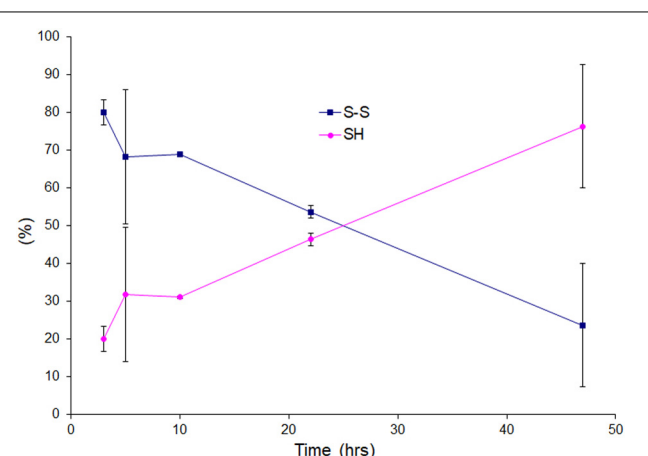


FIGURE 4 | Oxidation and reduction of thiol group of the lag phase of apo AS-SOD1 in 0.5 mM TCEP at 3, 5, 10, 22, and 47 h.

(**Figures 5D–F**) look smoother like classical amyloid. Apo WT-SOD1 fibrils look sparse, and we can see the non-fibrillar intermediates of apo WT-SOD1 looking short with rounded ends (sausage-like) and lacking the dark characteristic of amyloid. Comparison of WT (5 mM TCEP; **Figure 5B**) vs. AS (5 mM TCEP; **Figure 5E**) shows the most dramatically contrasting comparison. Furthermore, WT (0.5 mM TCEP; **Figure 5A**) showing the sausage-like intermediates contrasting with mature amyloid fibrils in a single image is striking. It is also shown

the globular soluble apo WT- or AS-SOD1 in the background as white spots. When 10% fibril seeds were added, it looks like soluble globular SOD1 proteins are budding on the various very short fibril fragments to longer fibril fragments (**Figures 5C,F**). We conclude the AS mutant fibrils move rapidly to form mature amyloid (classical amyloid appearance), whereas WT amyloid formation is disrupted allowing us to see what appear to be novel non-amyloid intermediates more easily.

Conformational Change During Lag Time

To examine how the TCEP treatments affected the SOD1 protein during fibrillization, sedimentation velocity experiments were performed using the soluble supernatant. The observed sedimentation coefficients of SOD1 measured during fibrillation lag time correspond to either monomer (apo AS-SOD1) or a partially denatured monomer (apo WT-SOD1). The reason the lag time of apo WT-SOD1 is longer than apo AS-SOD1 may be due to the fact it is the mixture of monomer and denatured monomer during the lag time of apo WT-SOD1, which requires more time to undergo more complex conformational conversions with four cysteines (**Figure 6A**), whereas apo AS-SOD1 is only monomer (**Figure 6B**).

Guanidine Hydrochloride Behaves Similarly to Amyloid Seeds

At the beginning SOD1 fibril was denatured in GuHCl for making amyloid seeds, but later we found that GuHCl can also affect SOD1 fibrillation at much lower concentrations. At 100 mM

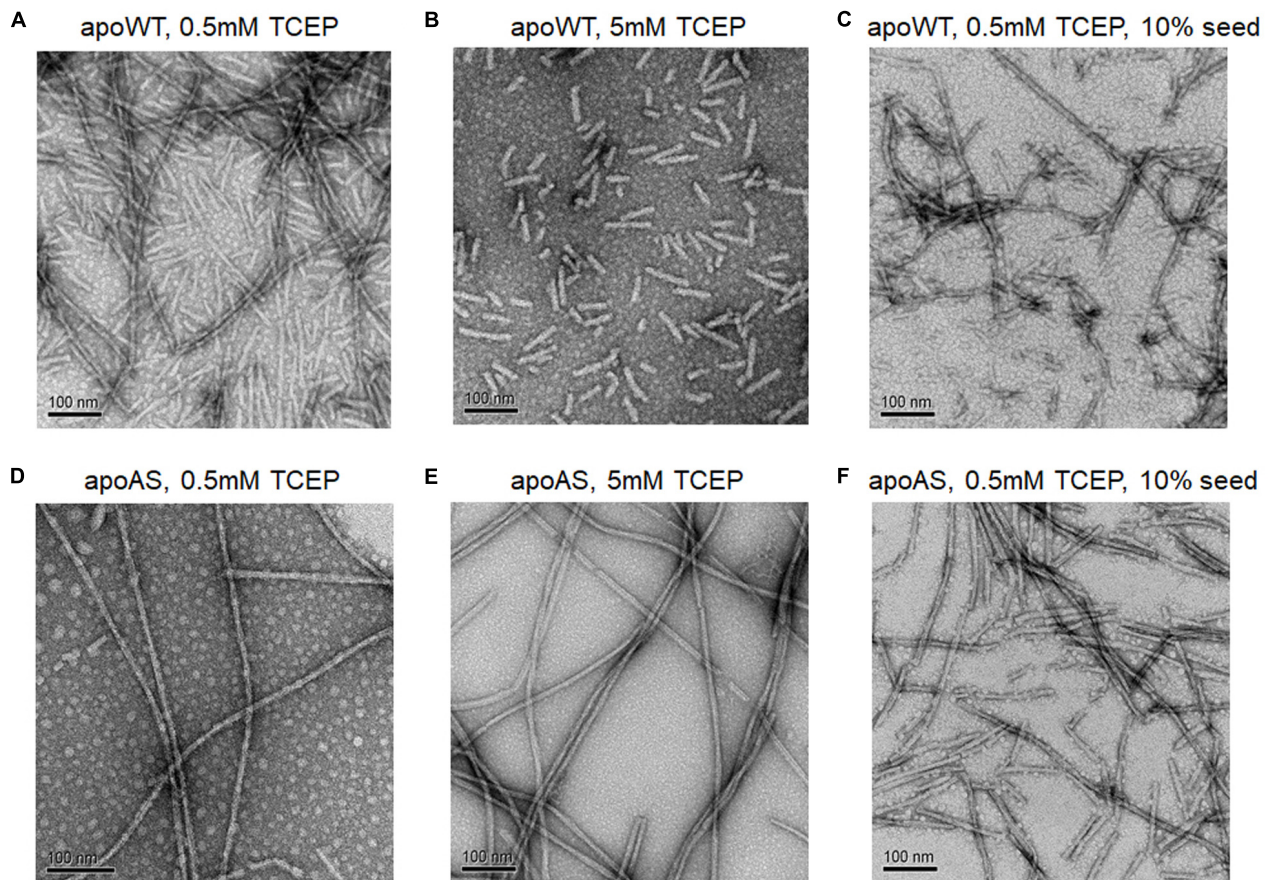


FIGURE 5 | Electron micrographs of SOD1 fibrils. **(A)** apo WT-SOD1 fibrils in the presence of 0.5 mM TCEP **(B)** apo WT-SOD1 fibrils in the presence of 5 mM TCEP **(C)** 10% seeded apo WT-SOD1 fibrils in the presence of 0.5 mM TCEP **(D)** apo AS-SOD1 fibrils in the presence of 0.5 mM TCEP **(E)** apo AS-SOD1 fibrils in the presence of 5 mM TCEP **(F)** 10% seeded apo AS-SOD1 fibrils in the presence of 0.5 mM TCEP.

GuHCl the lag time decreased from about 40 h to about 5 h, like SOD1 fibril seeds in the presence of 0.5 mM TCEP (**Figure 7A**). Even 10 mM (0.5%) GuHCl reduced the lag time to almost half, about 18 h, presumably in a way that is quite distinct from the mechanism of protein denaturation at 6 M. As with 10% seeded apo AS-SOD1 fibrillation, 10% GuHCl also shortened the lag time even at 0.1 mM TCEP (**Figure 7B**). A reasonable comparison of seeding vs. low concentrations of chaotropes such as GuHCl in accelerating the reduction kinetics of SOD1 and promoting protein aggregation and fibrillation *in vivo* will bring us closer to understanding the precise molecular mechanism of fibrillation of SOD1.

DISCUSSION

Previously, our laboratory showed that monomeric apo, disulfide-reduced WT-SOD1, represented as apo WT^{2SH} (the unmodified polypeptide released from the ribosome before it acquires the earliest posttranslational modification), could initiate fibrillation of disulfide-intact forms of the protein (WT^{S-S}), either apo or zinc-bound, at low, sub-stoichiometric

amounts. This activity required the presence of thiols on cysteine residues at both positions 57 and 146, as single mutants apo-C57S or -C146S were unable to initiate fibrillation of apo WT-SOD1, nor were the S-alkylated form of apo, disulfide-reduced WT (Chattopadhyay et al., 2008). In addition to Cys-57 and Cys-146, which form the intramolecular disulfide bond, SOD1 contains 2 reduced cysteine residues, Cys-6 and Cys-111, and it is known that SOD1 undergoes disulfide scrambling with these reduced cysteines (**Supplementary Figure S1**; Leinartaite and Johansson, 2013; Toichi et al., 2013). We chose 0.5 mM TCEP concentration which is low enough to initiate SOD1 fibrillation (**Supplementary Figure S1A**) for cysteine alkylation and tryptic digestion before SOD1 fibrillation, and it is well supported by the mass spectrometry data where alkylation and tryptic digestion of apo SOD1 revealed the presence of peptides representing SOD1 with non-native intramolecular disulfides, including C111-C146 or C6-C111 (**Supplementary Figure S1B**) as presented by Leinartaite (Leinartaite and Johansson, 2013). So, we wanted to compare WT-SOD1 to simpler AS-SOD1 which is mutated C6A and C111S to exclude the effect of disulfide scrambling. In humans the initiating Met residue is removed and the second amino-acid residue is N-acetylated.

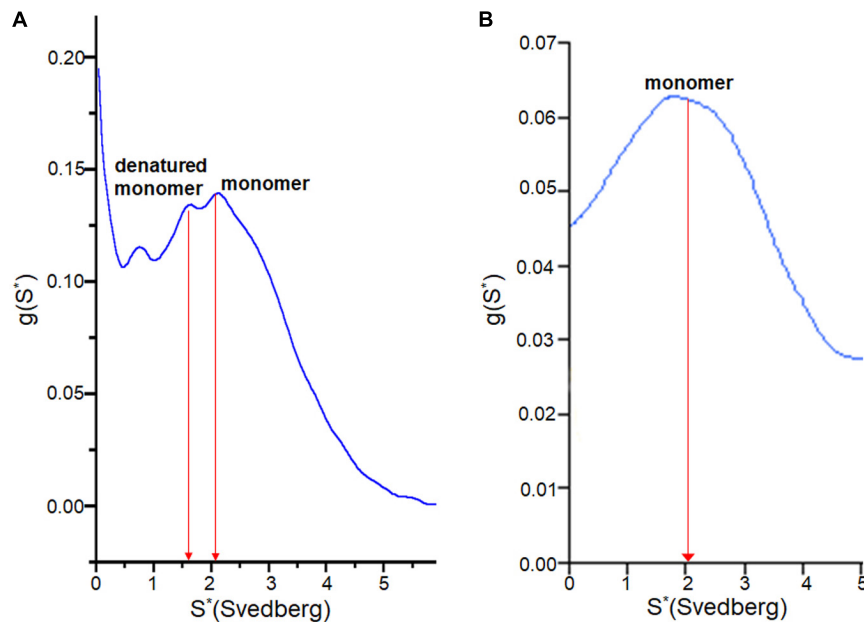


FIGURE 6 | $g(s)$ plot from sedimentation velocity of analytical ultracentrifugation on SOD1. It shows conformational change of apo WT-SOD1 for 10 h incubation **(A)** and apo AS-SOD1 for 12 h incubation **(B)** at 37°C in 5 mM TCEP during lag time of fibrillation. The hydrodynamic property ($S_{20,w}$) of SOD1 is about 2 for the monomer and about 3 for the dimer.

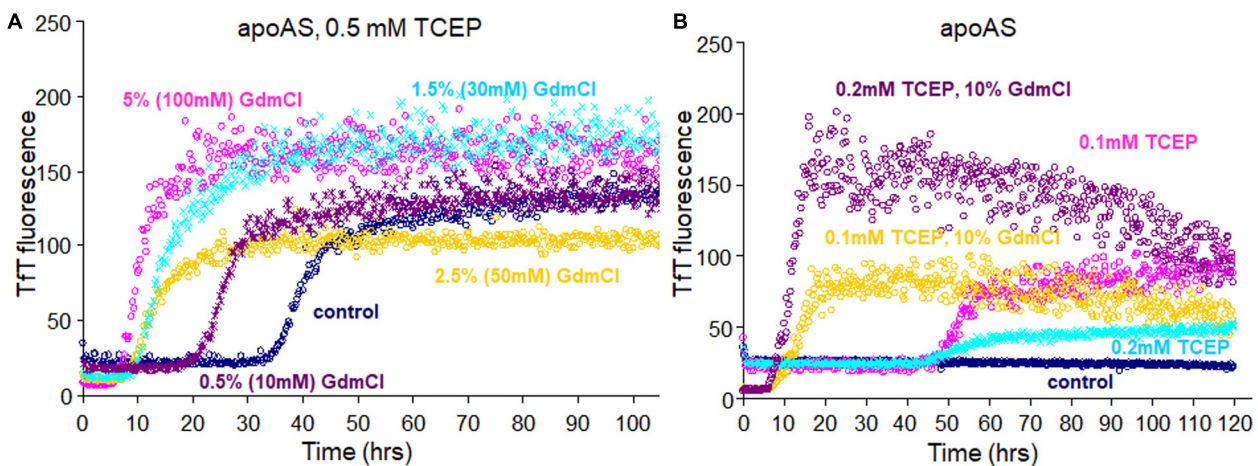


FIGURE 7 | Fibrillation of apo AS-SOD1^{S-S} **(A)** in presence of 0.5 mM TCEP with addition of various concentrations of GuHCl and **(B)** with addition of 10% of GuHCl in 0.1 or 0.2 mM TCEP concentrations.

Since human SOD1 was first sequenced as the protein form it has been traditionally numbered from this Ala residue as A1. A1 has not been found among hSOD1 mutations and N-terminal acetylation apparently does not affect amyloid behavior. We compared the fibrillation of WT-SOD1 from *Saccharomyces cerevisiae* (with N-terminal acetylation) and from *E. coli* (without N-terminal acetylation), and they showed almost identical fibrillation kinetics (data not shown). Consequently, we have used expression in *Saccharomyces cerevisiae* for WT-SOD1 because it is faithful to the acetylated N-terminus of hSOD1 and

in *E. coli* for AS-SOD1 because it is easy to get overexpressed and quickly purified.

We found that the free Cys thiols are unnecessary for fibrillation (in the presence of reductant) as shown in **Figure 1**. Fibrillation of AS-SOD1 shows the initiation point and stationary point clearly better than WT-SOD1. It is initiated faster than WT-SOD1 in mostly reduced condition at 5 or 10 mM TCEP and started to initiate even in very little reduced condition at 0.2 mM TCEP in contrast with WT-SOD1. This indicates that disulfide scrambling may slow down and interfere with

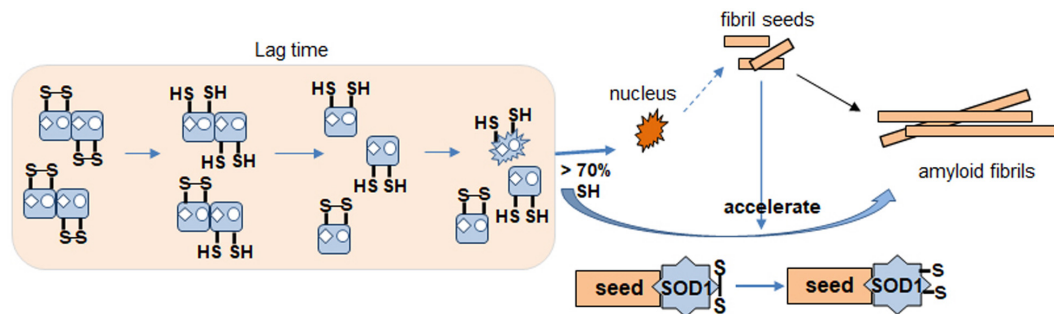


FIGURE 8 | Proposed apo SOD1 fibrillation model. Formation of nucleus for fibrillation involves destabilization of dimer by metal loss. Disulfide reduction and monomerization allow conformational change to a species that is more likely to proceed toward fibrillation and amyloid formation (nucleus). Seed enhances kinetics of this reaction. Disulfide shuffling in WT but not mutant AS interferes with fibrillation causing a delay.

fibrillation, in some ways additional two free thiols in human SOD1 may be one of a range of protective mechanisms to retard the aggregation of SOD1, such as correct metal binding which is critical to prevent misfolding or tryptophan residue 32 in hSOD1 which is investigated as having a modulating role in its ability to propagate and template aggregation (Leal et al., 2015; Crown et al., 2020). This is the notable difference of SOD1 compared to other proteins such as α -synuclein, an intrinsically disordered protein, which are capable of fibrilization (Sarafian et al., 2017).

We varied TCEP concentration to see the effect on lag time of apo AS-SOD1. It was confirmed that the thiol groups of apo AS-SOD1 are more reduced at higher TCEP concentrations (Figure 2). Recently, it is reported that the disulfide bond of apo WT-SOD1 was reduced by 30% in 10 mM TCEP at 37°C, pH 7.4 based on differential scanning calorimetry (DSC) and size-exclusion chromatography (SEC-HPLC) (Abdolvahabi et al., 2016). This was compared with apo AS-SOD1 which was around 70% reduced in 10 mM TCEP at 37°C, pH 7.0 (Figure 2D) probably due to a slightly more favorable configuration. Once formed, the disulfide bond in WT hSOD1 is partially buried near the dimer interface (Banci et al., 2006). In fact, the accessibility of the disulfide bond may be a significant factor controlling the differences in disulfide reactivity of apo vs. holo, WT vs. ALS (or other) mutant hSOD1. The thermodynamic stability of the disulfide in ALS mutants is not consistently lower than WT hSOD1. However, the reduction rate of the disulfide is consistently faster for ALS mutants (Bouldin et al., 2012). Removal of all cysteines in SOD1 prevents formation of any disulfide linked aggregates, and the thiol-disulfide status in SOD1 is important in determining the aggregation state of the protein (Furukawa et al., 2004). Previously we used 5 mM DTT to form SOD1 fibrils, but later we found that DTT caused more oxidation on SOD1 during fibrillation based on MS data (data not shown). TCEP is not a thiol-containing reagent, so it performs no direct disulfide exchange function. TCEP is more powerful an irreversible reducing agent, more hydrophilic, and more resistant to oxidation in air. Since TCEP concentrations affect the lag time, this suggests that reduction of the disulfide bonds must precede fibrillation and it is the rate determining step of the

fibrillation initiation of SOD1. However, complete reduction of intact disulfide bond is not exactly essential for the fibrillation initiation. Fibrillation initiation is slowly started at around 40 h if intact disulfide bonds are less than ~30% in case of 0.5 mM TCEP (Figure 4). A conformational change is observed at higher than 5 mM TCEP (Figures 2C,D).

Misfolding/aggregation of mutant SOD1 is transmissible through a seeding mechanism inside the cell and among cells. Seeded aggregations of SOD1 proteins are a key event to understand progression/propagation of pathological changes in SOD1-related fALS and even sALS cases without mutation in SOD1 (Ogawa and Furukawa, 2014). For other proteins, it is known that the addition of fibril seeds to a solution shortens the lag time of the forming fibrils (Lee et al., 2007). This effect has been termed “nucleation-dependent” by Wood et al. and they explained that the added seeds act as catalytic sites that induce conformational changes in the protein (alpha synuclein) and accelerate fibrillation reaction rates (Wood et al., 1999; Scheibel et al., 2004). We wanted to examine the seed effect on both wild type and the simpler AS mutant of SOD1 fibrillations during the lag phase in detail to exclude the effect of disulfide cross linkage as we described above. Seeds are commonly generated by sonication driven shearing of mature fibrils to generate active ends (Furukawa and O’Halloran, 2005). They are then incubated with soluble protein and Tft fluorescence is monitored as a measure of the rate of fibril growth (Chattopadhyay et al., 2015). The key findings of our study are: (1) mostly reduced amyloid seed lowered the kinetic barrier of SOD1 fibrillation and accelerated amyloid fibrillation. Somehow seeds interact with monomeric apo SOD1 and render the native disulfide bond more exposed raising susceptibility to reduction, via an induced conformational change that improves accessibility to reductant. (2) AS-SOD1 shows kinetics clearly. The lag time of fibrillation is very long in low TCEP concentration (Figure 2, 60 h in 0.2 mM, 40 h in 0.5 mM), which means it takes a long time to reduce intact disulfide bond, but under more strongly reducing conditions such as 5 or 10 mM TCEP, its lag time is comparable to 10–20 h lag time of α -synuclein which does not have a disulfide bond. In 5 mM TCEP, mostly reduced condition, apo AS-SOD1 is monomeric, however, apo WT-SOD1 is a mixture

of native monomer and partially denatured monomer based on sedimentation velocity experiments performed in the analytical ultracentrifuge (**Figure 6**). This indicates that apo WT-SOD1 has larger conformational complexity than AS-SOD1 resulting from disulfide scrambling using the two free thiols in WT-SOD1 that is not possible in AS-SOD1.

Based on our results identifying redox status of apo SOD1, we propose a model for the SOD1 fibrillation pathway (**Figure 8**). During lag time, SOD1 undergoes conformational changes from dimer to monomer, denatured monomer as its disulfide bond status changes. It is the rate determining step of the fibrillation initiation of SOD1, and human SOD1 has several controlling factors of this process like free thiols, metal binding or some specific residue like Trp32. The apo form of disulfide reduced SOD1 initiates to form the amyloid nucleus or seed if disulfide reduced forms are more than 70%. The monomeric nucleus subsequently becomes stabilized by recruitment of additional soluble WT or mutant SOD1 and elongates to form a mature fibril in multiple steps (Chattopadhyay et al., 2015). Seeded growth proceeds this way as well. The intact disulfide bond in SOD1 is buried and hard to break but somehow fibril seed is capable of increasing accessibility in order to break the disulfide faster, presumably by a conformational change.

Some chaotropes like GuHCl increase flexibility of SOD1, as do ALS mutations *in vivo*. It shows that GuHCl at low concentration can also affect the SOD1 fibrillation similar to amyloid seeds (**Figure 7**). Thus, mostly reduced SOD1 fibril seeds (**Supplementary Figure S2**) seem to associate with SOD1 molecules during lag time and act like a chaotropic denaturant. The EM showed immature intermediates of apo WT-SOD1 looking “sausage-like” quite distinguishable from mature fibrils of apo AS-SOD1 (**Figure 5**). It seems that alternative disulfide shuffling delays fibril maturation allowing us to view intermediates in the fibrillation process. Further study to investigate the toxicity of these intermediates compared to mature fibrils will be critical.

If amyloid formation is more efficient when the two free thiols are missing, then why has human SOD1 kept them given evolutionary pressure? One possibility lies in the intermembrane space (IMS) of the mitochondria as part of a quality control mechanism to identify faulty individual mitochondria. SOD1 has to lose its co-factors and structure for passage across the outer mitochondrial membrane and refolding in the IMS requires the chaperone Copper Chaperone for Superoxide dismutase (CCS). The correct disulfide has to be reformed and maybe the two free thiols provide complexity to the system such that elevated levels of activated oxygen (superoxide and hydrogen peroxide) damage the protein before it can fold correctly leaving misfolded (but not amyloid) SOD1 species to subsequently kill that specific mitochondrion.

As we seek to understand intricate details of the fibrillation/amyloid pathway of human SOD1 we are aware that effective therapeutic action may be best in order to avoid this pathway at all. An approach that appears promising involves

stabilization of the dimer even when aberrant metalation is prevalent. Hasnain and co-workers have detailed a class of small molecules that bind Cys111 and shift equilibria away from monomerization and nucleus formation (Capper et al., 2018; Chantadul et al., 2020).

DATA AVAILABILITY STATEMENT

The original contributions presented in the study are included in the article/**Supplementary Material**, further inquiries can be directed to the corresponding author/s.

AUTHOR CONTRIBUTIONS

B-KK was first and major author. WM and EG provided help with some experiments. JV and JW directed research. JW was senior corresponding author. All authors contributed to the article and approved the submitted version.

FUNDING

This work was supported by the program project grant P01 NS049134 from NINDS.

ACKNOWLEDGMENTS

We thank Dr. Mark Arbing for purifying AS SOD1 from *E. coli* and Dr. Martin L Philips for help with the analytical ultracentrifugation experiments and analysis of experimental results. We also thank Dr. Sergey Ryazantsev for help with electron microscopy and analysis the data. We thank Dr. Yuewei Sheng and Dr. Madhuri Chattopadhyay for advising on purification of WT SOD1 and seeding experiments.

SUPPLEMENTARY MATERIAL

The Supplementary Material for this article can be found online at: <https://www.frontiersin.org/articles/10.3389/fnins.2020.619279/full#supplementary-material>

Supplementary Figure 1 | Disulfide scrambling in apo WT-SOD1 (40 μ M) at 0.5 mM TCEP. **(A)** TCEP concentration dependence of fibril formation for apo WT-SOD1. Fibrillation of WT-SOD1 in 10 mM potassium phosphate buffer, pH 7 is stimulated as higher TCEP concentration. TCEP concentrations are: 0 mM TCEP (green), 0.1 mM (navy), 0.2 mM (pink), 0.5 mM (cyan), 1 mM (gold), 5 mM (orange), and 10 mM (purple), respectively. **(B)** HPLC-MS spectrum of DTT reduced and iodoacetamide alkylated apo WT-SOD1 digested with trypsin. Each peak in the spectrum represents a tryptic peptide.

Supplementary Figure 2 | LC-MS of apo AS-SOD1 fibril seeds produced from 5 mM TCEP in the presence of GdmCl **(A)** or no GdmCl **(B)**. Apo AS-SOD1 fibril seeds are completely reduced in the presence of GdmCl. Molecular weight of AS-SOD1: 15756.43, reduced and alkylated with IAA AS-SOD1: 15870.53.

REFERENCES

- Abdolvahabi, A., Shi, Y., Chuprin, A., Rasouli, S., and Shaw, B. F. (2016). Stochastic formation of fibrillar and amorphous superoxide dismutase oligomers linked to amyotrophic lateral sclerosis. *ACS Chem. Neurosci.* 7, 799–810. doi: 10.1021/acschemneuro.6b00048
- Banci, L., Bertini, I., Cantini, F., D'Amelio, N., and Gaggelli, E. (2006). Human SOD1 before harboring the catalytic metal: solution structure of copper-depleted, disulfide-reduced form. *J. Biol. Chem.* 281, 2333–2337. doi: 10.1074/jbc.m506497200
- Bouldin, S. D., Darch, M. A., Hart, P. J., and Outten, C. E. (2012). Redox properties of the disulfide bond of human Cu,Zn superoxide dismutase and the effects of human glutaredoxin 1. *Biochem. J.* 446, 59–67. doi: 10.1042/bj20120075
- Capper, M. J., Wright, G. S. A., Barbieri, L., Luchinat, E., Mercatelli, E., McAlary, L., et al. (2018). The cysteine-reactive small molecule ebbsen facilitates effective SOD1 maturation. *Nat. Commun.* 9:1693.
- Chan, P. K., Chattopadhyay, M., Sharma, S., Souda, P., Gralla, E. B., Borchelt, D. R., et al. (2013). Structural similarity of wild-type and ALS-mutant superoxide dismutase-1 fibrils using limited proteolysis and atomic force microscopy. *Proc. Natl. Acad. Sci. U.S.A.* 110, 10934–10939. doi: 10.1073/pnas.1309613110
- Chantadul, V., Wright, G. S. A., Ampornanai, K., Shahid, M., Antonyuk, S. V., Washbourn, G., et al. (2020). Ebbsen as template for stabilization of A4V mutant dimer for motor neuron disease therapy. *Commun. Biol.* 3:97.
- Chattopadhyay, M., Durazo, A., Sohn, S. H., Strong, C. D., Gralla, E. B., Whitelegge, J. P., et al. (2008). Initiation and elongation in fibrillation of ALS-linked superoxide dismutase. *Proc. Natl. Acad. Sci. U.S.A.* 105, 18663–18668. doi: 10.1073/pnas.0807058105
- Chattopadhyay, M., Nwadiibia, E., Strong, C. D., Gralla, E. B., Valentine, J. S., and Whitelegge, J. P. (2015). The disulfide bond, but not zinc or dimerization, controls initiation and seeded growth in amyotrophic lateral sclerosis-linked Cu,Zn superoxide dismutase (SOD1) fibrillation. *J. Biol. Chem.* 290, 30624–30636. doi: 10.1074/jbc.m115.666503
- Cozzolino, M., Amori, I., Pesaresi, M. G., Ferri, A., Nencini, M., and Carri, M. T. (2008). Cysteine 111 affects aggregation and cytotoxicity of mutant Cu,Zn-superoxide dismutase associated with familial amyotrophic lateral sclerosis. *J. Biol. Chem.* 283, 866–874. doi: 10.1074/jbc.m705657200
- Cristovao, J. S., Henriques, B. J., and Gomes, C. M. (2019). Biophysical and spectroscopic methods for monitoring protein misfolding and amyloid aggregation. *Methods Mol. Biol.* 1873, 3–18. doi: 10.1007/978-1-4939-8820-4_1
- Crown, A., McAlary, L., Fagerli, E., Brown, H., Yerbury, J. J., Galaleldeen, A., et al. (2020). Tryptophan residue 32 in human Cu-Zn superoxide dismutase modulates prion-like propagation and strain selection. *PLoS One* 15:e0227655. doi: 10.1371/journal.pone.0227655
- Doucette, P. A., Whitson, L. J., Cao, X., Schirf, V., Demeler, B., Valentine, J. S., et al. (2004). Dissociation of human copper-zinc superoxide dismutase dimers using chaotrope and reductant. Insights into the molecular basis for dimer stability. *J. Biol. Chem.* 279, 54558–54566. doi: 10.1074/jbc.m409744200
- Fay, J. M., Zhu, C., Proctor, E. A., Tao, Y., Cui, W., Ke, H., et al. (2016). A phosphomimetic mutation stabilizes SOD1 and rescues cell viability in the context of an ALS-associated mutation. *Structure* 24, 1898–1906. doi: 10.1016/j.str.2016.08.011
- Fiala, M., Chattopadhyay, M., La Cava, A., Tse, E., Liu, G., Lourenco, E., et al. (2010). IL-17A is increased in the serum and in spinal cord CD8 and mast cells of ALS patients. *J. Neuroinflammation* 7:76. doi: 10.1186/1742-2094-7-76
- Furukawa, Y., Kaneko, K., Yamanaka, K., O'Halloran, T. V., and Nukina, N. (2008). Complete loss of post-translational modifications triggers fibrillar aggregation of SOD1 in the familial form of amyotrophic lateral sclerosis. *J. Biol. Chem.* 283, 24167–24176. doi: 10.1074/jbc.m802083200
- Furukawa, Y., and O'Halloran, T. V. (2005). Amyotrophic lateral sclerosis mutations have the greatest destabilizing effect on the apo- and reduced form of SOD1, leading to unfolding and oxidative aggregation. *J. Biol. Chem.* 280, 17266–17274. doi: 10.1074/jbc.m500482200
- Furukawa, Y., Torres, A. S., and O'Halloran, T. V. (2004). Oxygen-induced maturation of SOD1: a key role for disulfide formation by the copper chaperone CCS. *EMBO J.* 23, 2872–2881. doi: 10.1038/sj.emboj.7600276
- Hallewell, R. A., Imlay, K. C., Lee, P., Fong, N. M., Gallegos, C., Getzoff, et al. (1991). Thermostabilization of recombinant human and bovine CuZn superoxide dismutases by replacement of free cysteines. *Biochem. Biophys. Res. Commun.* 181, 474–480. doi: 10.1016/s0006-291x(05)81443-3
- Hough, M. A., Grossmann, J. G., Antonyuk, S. V., Strange, R. W., Doucette, P. A., Rodriguez, J. A., et al. (2004). Dimer destabilization in superoxide dismutase may result in disease-causing properties: structures of motor neuron disease mutants. *Proc. Natl. Acad. Sci. U.S.A.* 101, 5976–5981. doi: 10.1073/pnas.0305143101
- Leal, S. S., Cristovao, J. S., Biesemeier, A., Cardoso, I., and Gomes, C. M. (2015). Aberrant zinc binding to immature conformers of metal-free copper-zinc superoxide dismutase triggers amorphous aggregation. *Metallomics* 7, 333–346. doi: 10.1039/c4mt00278d
- Lee, C. C., Nayak, A., Sethuraman, A., Belfort, G., and McRae, G. J. (2007). A three-stage kinetic model of amyloid fibrillation. *Biophys. J.* 92, 3448–3458. doi: 10.1529/biophysj.106.098608
- Leinartaitė, L., and Johansson, A. S. (2013). Disulfide scrambling in superoxide dismutase 1 reduces its cytotoxic effect in cultured cells and promotes protein aggregation. *PLoS One* 8:e78060. doi: 10.1371/journal.pone.0078060
- Lepock, J. R., Frey, H. E., and Hallewell, R. A. (1990). Contribution of conformational stability and reversibility of unfolding to the increased thermostability of human and bovine superoxide dismutase mutated at free cysteines. *J. Biol. Chem.* 265, 21612–21618.
- LeVine, H. III (1999). Quantification of beta-sheet amyloid fibril structures with thioflavin T. *Methods Enzymol.* 309, 274–284. doi: 10.1016/s0076-6879(99)09020-5
- Niwa, J., Yamada, S., Ishigaki, S., Sone, J., Takahashi, M., Katsuno, M., et al. (2007). Disulfide bond mediates aggregation, toxicity, and ubiquitylation of familial amyotrophic lateral sclerosis-linked mutant SOD1. *J. Biol. Chem.* 282, 28087–28095. doi: 10.1074/jbc.m704465200
- Ogawa, M., and Furukawa, Y. (2014). A seeded propagation of Cu, Zn-superoxide dismutase aggregates in amyotrophic lateral sclerosis. *Front. Cell Neurosci.* 8:83. doi: 10.3389/fncel.2014.00083
- Oztug Durer, Z. A., Cohlberg, J. A., Dinh, P., Padua, S., Ehrenclou, K., Downes, S., et al. (2009). Loss of metal ions, disulfide reduction and mutations related to familial ALS promote formation of amyloid-like aggregates from superoxide dismutase. *PLoS One* 4:e5004. doi: 10.1371/journal.pone.0005004
- Parge, H. E., Hallewell, R. A., and Tainer, J. A. (1992). Atomic structures of wild-type and thermostable mutant recombinant human Cu,Zn superoxide dismutase. *Proc. Natl. Acad. Sci. U.S.A.* 89, 6109–6113. doi: 10.1073/pnas.89.13.6109
- Roberts, K., Zeineddine, R., Corcoran, L., Li, W., Campbell, I. L., and Yerbury, J. J. (2013). Extracellular aggregated Cu/Zn superoxide dismutase activates microglia to give a cytotoxic phenotype. *Glia* 61, 409–419. doi: 10.1002/glia.22444
- Sarafian, T. A., Littlejohn, K., Yuan, S., Fernandez, C., Cilluffo, M., Koo, B. K., et al. (2017). Stimulation of synaptoneurosome glutamate release by monomeric and fibrillated alpha-synuclein. *J. Neurosci. Res.* 95, 1871–1887. doi: 10.1002/jnr.24024
- Schachman, H. K. (1959). *Ultracentrifugation in Biochemistry*. New York, NY: Academic Press.
- Scheibel, T., Bloom, J., and Lindquist, S. L. (2004). The elongation of yeast prion fibers involves separable steps of association and conversion. *Proc. Natl. Acad. Sci. U.S.A.* 101, 2287–2292. doi: 10.1073/pnas.0308754101
- Shaw, B. F., Lelie, H. L., Durazo, A., Nersissian, A. M., Xu, G., Chan, P. K., et al. (2008). Detergent-insoluble aggregates associated with amyotrophic lateral sclerosis in transgenic mice contain primarily full-length, unmodified superoxide dismutase-1. *J. Biol. Chem.* 283, 8340–8350. doi: 10.1074/jbc.m707751200
- Szedberg, T., and Pedersen, K. O. (1940). *The Ultracentrifuge*. Oxford: Oxford University Press.
- Tanford, C. (1961). *Physical Chemistry of Macromolecules*. New York, NY: John Wiley & Sons.
- Toichi, K., Yamanaka, K., and Furukawa, Y. (2013). Disulfide scrambling describes the oligomer formation of superoxide dismutase (SOD1) proteins in the familial

- form of amyotrophic lateral sclerosis. *J. Biol. Chem.* 288, 4970–4980. doi: 10.1074/jbc.m112.414235
- Valentine, J. S., Doucette, P. A., and Zittin Potter, S. (2005). Copper-zinc superoxide dismutase and amyotrophic lateral sclerosis. *Annu. Rev. Biochem.* 74, 563–593.
- Valentine, J. S., and Hart, P. J. (2003). Misfolded CuZnSOD and amyotrophic lateral sclerosis. *Proc. Natl. Acad. Sci. U.S.A.* 100, 3617–3622. doi: 10.1073/pnas.0730423100
- Van Holde, K. E., Johnson, W. C., and Ho, P. S. (1998). *Principles of Physical Biochemistry*. New Jersey, NJ: Prentice Hall.
- Wiedau-Pazos, M., Goto, J. J., Rabizadeh, S., Gralla, E. B., Roe, J. A., Lee, M. K., et al. (1996). Altered reactivity of superoxide dismutase in familial amyotrophic lateral sclerosis. *Science* 271, 515–518.
- Wood, S. J., Wypych, J., Steavenson, S., Louis, J. C., Citron, M., and Biere, A. L. (1999). alpha-synuclein fibrillogenesis is nucleation-dependent. Implications for the pathogenesis of Parkinson's disease. *J. Biol. Chem.* 274, 19509–19512. doi: 10.1074/jbc.274.28.19509
- Zhu, C., Beck, M. V., Griffith, J. D., Deshmukh, M., and Dokholyan, N. V. (2018). Large SOD1 aggregates, unlike trimeric SOD1, do not impact cell viability in a model of amyotrophic lateral sclerosis. *Proc. Natl. Acad. Sci. U.S.A.* 115, 4661–4665. doi: 10.1073/pnas.1800187115

Conflict of Interest: The authors declare that the research was conducted in the absence of any commercial or financial relationships that could be construed as a potential conflict of interest.

Copyright © 2021 Koo, Munroe, Gralla, Valentine and Whitelegge. This is an open-access article distributed under the terms of the Creative Commons Attribution License (CC BY). The use, distribution or reproduction in other forums is permitted, provided the original author(s) and the copyright owner(s) are credited and that the original publication in this journal is cited, in accordance with accepted academic practice. No use, distribution or reproduction is permitted which does not comply with these terms.



Rationally Designed Bicyclic Peptides Prevent the Conversion of A β 42 Assemblies Into Fibrillar Structures

Tatsuya Ikenoue¹, Francesco A. Aprile^{1,2}, Pietro Sormanni¹ and Michele Vendruscolo^{1*}

¹ Centre for Misfolding Diseases, Department of Chemistry, University of Cambridge, Cambridge, United Kingdom,

² Department of Chemistry, Molecular Sciences Research Hub, Imperial College London, London, United Kingdom

OPEN ACCESS

Edited by:

Cláudio M. Gomes,
University of Lisbon, Portugal

Reviewed by:

Aphrodite Kapurniotu,
Technical University of Munich,
Germany

Sandra Macedo-Ribeiro,
Universidade do Porto, Portugal

*Correspondence:

Michele Vendruscolo
mv245@cam.ac.uk

Specialty section:

This article was submitted to
Neurodegeneration,
a section of the journal
Frontiers in Neuroscience

Received: 29 October 2020

Accepted: 01 February 2021

Published: 25 February 2021

Citation:

Ikenoue T, Aprile FA, Sormanni P
and Vendruscolo M (2021) Rationally
Designed Bicyclic Peptides Prevent
the Conversion of A β 42 Assemblies
Into Fibrillar Structures.
Front. Neurosci. 15:623097.
doi: 10.3389/fnins.2021.623097

There is great interest in drug discovery programs targeted at the aggregation of the 42-residue form of the amyloid β peptide (A β 42), since this molecular process is closely associated with Alzheimer's disease. The use of bicyclic peptides may offer novel opportunities for the effective modification of A β 42 aggregation and the inhibition of its cytotoxicity, as these compounds combine the molecular recognition ability of antibodies with a relatively small size of about 2 kD. Here, to pursue this approach, we rationally designed a panel of six bicyclic peptides targeting various epitopes along the sequence of A β 42 to scan its most amyloidogenic region (residues 13–42). Our kinetic analysis and structural studies revealed that at sub-stoichiometric concentrations the designed bicyclic peptides induce a delay in the condensation of A β 42 and the subsequent transition to a fibrillar state, while at higher concentrations they inhibit such transition. We thus suggest that designed bicyclic peptides can be employed to inhibit amyloid formation by redirecting the aggregation process toward amorphous assemblies.

Keywords: amyloid—beta, Alzheimer's disease, bicyclic peptides, rational design, protein aggregation

INTRODUCTION

Since the formation of aberrant deposits composed primarily of the A β peptide is a molecular hallmark of Alzheimer's disease (Selkoe and Hardy, 2016; Jack et al., 2018), a major therapeutic strategy for this condition has been based on the discovery of compounds capable of inhibiting A β aggregation (Schenk et al., 1999; Sevigny et al., 2016). However, disease-modifying compounds have not yet become available (Cummings et al., 2020). Major drug discovery efforts have been devoted to the identification of small molecules, which have high brain penetration and low manufacturing costs, but also typically low specificity and high risk of side effects. In parallel, other efforts have been devoted to the development of antibodies, which have the advantage of high specificity, but the disadvantages of high manufacturing costs, difficulty for administration, low permeability, and sometimes poor developability (Sormanni et al., 2018).

Bicyclic peptides have recently been introduced in the drug discovery field as they are thought to enable the combination of the advantages of small molecules with those of antibodies (Driggers et al., 2008; Getz et al., 2011; Angelini et al., 2012; Lian et al., 2014; Quartararo et al., 2014; Bartoloni et al., 2015; Bionda and Fasan, 2015). These molecules consist of polypeptide chains where three cysteine residues spaced within the sequence are chemically linked to a cyclic

compound. This design results in the formation of two macrocyclic rings that serve as binding regions (**Figure 1**). As the topology of bicyclic peptides is restrained, they have a relatively small entropy cost upon binding and thus a good binding affinity and specificity (Angelini et al., 2012; Chen et al., 2014; Bionda and Fasan, 2015). Having a small size of about 2 kDa, at least in principle, they are endowed with multiple advantages over antibodies, including the possibility of simple chemical synthesis, better tissue penetration, higher resistance to protease cleavage and inactivation, and extended half-life *in vivo* (Bock et al., 2013).

Bicyclic peptides against specific targets can be developed in a variety of ways. Phage display, for example, can be used for the isolation of these compounds from large combinatorial libraries (Heinis et al., 2009; Angelini et al., 2012; Baeriswyl and Heinis, 2013). This method, however, may become time-consuming and at times ineffective, in particular when one aims at targeting aggregation-prone antigens or weakly immunogenic epitopes. To overcome these limitations, we have introduced a method for the rational design of antibodies (Aprile et al., 2015, 2017; Sormanni et al., 2015a, 2018) and bicyclic peptides (Ikenoue et al., 2020), which enables the targeting of specific epitopes within intrinsically disordered proteins.

Here, we present an application of this design strategy by generating a panel of bicyclic peptides capable of binding A β 42 and interfering with its aggregation process. A β 42 aggregates through a complex process that involves the combination of different microscopic steps and multiple molecular species (Cohen et al., 2013; Michaels et al., 2018). In this context, it is becoming increasingly recognized that the A β 42 oligomers formed during the aggregation process are highly neurotoxic (Benilova et al., 2012; Mannini et al., 2014). Therefore, therapeutic strategies are being developed to decrease the concentrations of these oligomeric species, for example, by delaying or preventing their formation (Bucciantini et al., 2002; Kaye et al., 2003; Lesne et al., 2006; Haass and Selkoe, 2007; Benilova et al., 2012; Cremades et al., 2012; Cohen et al., 2013; Aprile et al., 2017). In one of such strategies, the amyloid aggregation process is redirected toward off-pathway non-toxic species. The small molecule trodusquemine, for example, can modulate the aggregation process of A β 42 and by redirecting it toward the formation of off-pathway non-toxic aggregates (Limbocker et al., 2019). Furthermore, strategies aimed at reducing the populations of oligomers by speeding up the aggregation process have also been proposed (Bieschke et al., 2011; Civitelli et al., 2016; Sonzini et al., 2017). Along these lines, we show here that our rationally designed bicyclic peptides prevent the conversion of A β 42 assemblies into fibrillar structure.

RESULTS

Rational Design and Synthesis of Bicyclic Peptides Targeting Different A β 42 Epitopes

We employed the cascade method, a computational antibody discovery strategy (Sormanni et al., 2015a, 2018;

Ikenoue et al., 2020), to generate six bicyclic peptides targeting different regions of the amino acid sequence of A β 42 (section “Materials and Methods”). These six peptides (DesBP1–DesBP6) were designed to scan epitopes in the most amyloidogenic region of A β 42 (residues 13–42) (**Figure 1A**) (section “Materials and Methods”). For the cyclization, we incorporated in the designed sequences three cysteine residues separated by two groups of six residues (**Figure 1A**). Because the cyclization achieved via reducible disulfide bonds could be problematic for therapeutic purposes, we then used tris-(bromomethyl)benzene (TBMB), a small bromine-containing organic compound, as a scaffold to anchor each designed peptide (**Figure 1B**). We carried out the reaction in aqueous solvents at 30°C in 1 h, with the threefold rotational symmetry of the TBMB molecule ensuring the formation of a unique structural and spatial isomer. The synthesized bicyclic peptides showed high purity. To assess the solubility of the DesBPs in phosphate buffer, static and dynamic light scattering (DLS) measurements were performed immediately after ultracentrifugation (**Supplementary Figures S1a,b**). The results showed 50 μ M of all the DesBPs remained largely soluble at 5°C, except DesBP4, which formed assemblies of about \sim 140 nm in size (**Supplementary Figure S1d**). Far-UV CD spectra show that DesBP1, DesBP2, DesBP5, and DesBP6 tend to retain structured states (**Supplementary Figure S1c**). AFM images taken after 1 day, however, showed the presence of assemblies in all cases (**Supplementary Figure S1d**).

Characterization of the Effects of the DesBPs on the Aggregation Kinetics of A β 42

In order to investigate the effects of the DesBPs on A β 42 aggregation, we carried out *in vitro* aggregation assays using the fluorescent dye thioflavin T (ThT) as amyloid-sensitive probe. We monitored A β 42 fibril formation at the concentration of 2 μ M in the presence of different molar ratios [A β 42]:[DesBP] (from 0.05 to 16) at 37°C under quiescent conditions, using a highly reproducible aggregation assay previously described (Hellstrand et al., 2010; Ikenoue et al., 2020).

Sub-Stoichiometric Concentrations of DesBPs Delay A β 42 Aggregation and Increase ThT Fluorescence

In the presence of low concentrations of DesBPs, we observed significant changes in the ThT fluorescence intensities in the presence of DesBP1, DesBP2, DesBP5, and DesBP6, both in unseeded (**Figures 2A–C**) and in seeded assays (**Supplementary Figure S2**), but not in the presence of DesBP3 and DesBP4 (**Supplementary Figure S3**), a result likely due to the presence of the solubilizing DED motif on DesBP3 and DesBP4. The DED motif generates an electrostatic repulsion with the ED motif on A β 42, which is likely to interfere with the designed epitope–paratope complementarity (**Figure 1A**). From the analysis of the normalized curves (**Figure 2B**), we obtained the dependence of the half-time of aggregation ($t_{1/2}$) on the concentrations of the DesBPs, which indicate that these bicyclic peptides delay the aggregation process of A β 42 (**Figure 2C**).

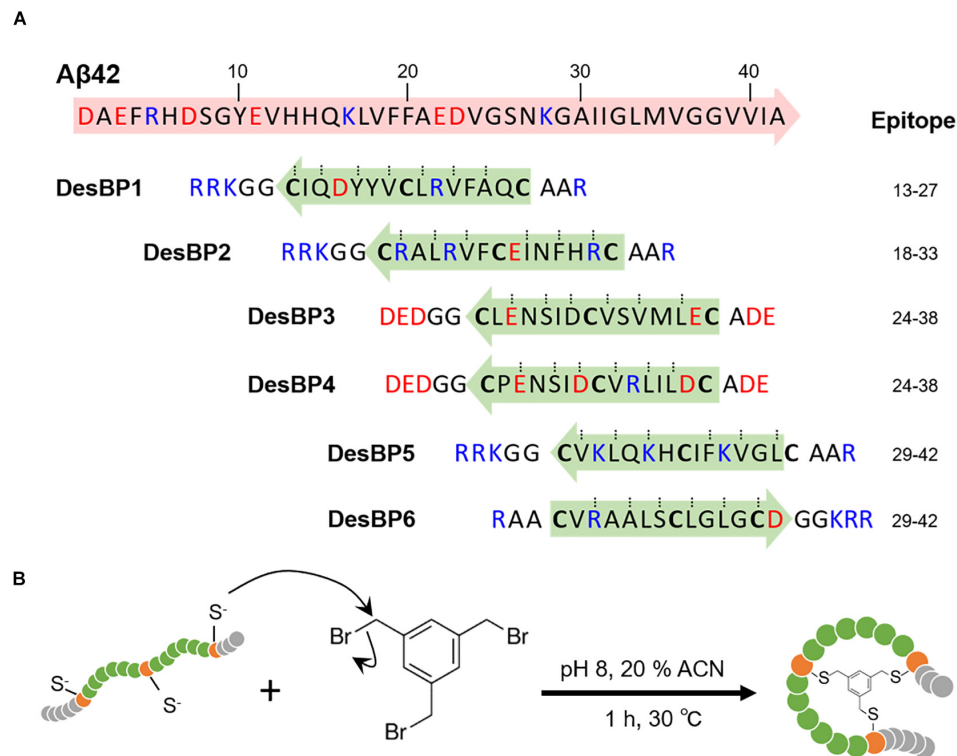


FIGURE 1 | Generation of the rationally designed bicyclic peptides. **(A)** Representation of the six amino acids sequences designed to bind A β 42 (DesBP1–DesBP6). Three cysteine residues are included for cyclization (bold) and the binding site obtained from the cascade procedure (green and blue arrows) is inserted between cysteine residues. Charged residues are added at N- and C-termini to improve solubility and modulate the binding; positive ones (blue) for DesBP1, DesBP2, DesBP5, and DesBP6, and negative ones (red) for DesBP3 and DesBP4 as controls. Dotted lines mark residues predicted to be involved in backbone–backbone hydrogen bonding and arrows denote the N- to C-termini direction. **(B)** Synthesis of the bicyclic peptides. A rationally designed peptide with three cysteine residues is tethered to the trifunctional compound 1,3,5-tris(bromomethyl)benzene (TBMB) in a nucleophilic substitution reaction.

High Concentrations of DesBPs Delay A β 42 Aggregation and Decrease ThT Fluorescence

We then tested the effects of high concentrations (0.25- to 16-fold excess) of the DesBPs on the A β 42 aggregation process (Figure 3). The ThT profiles of DesBP1, DesBP2, DesBP5, and DesBP6 (Figure 3A), but again not of DesBP3 and DesBP4 (Supplementary Figure S3), showed an increase in $t_{1/2}$ (Figure 3B). At the same time, we observed a suppression of the ThT intensity (Figure 3C) as the concentrations of the DesBPs were increased. To investigate this phenomenon, we studied the morphological changes of the aggregates by using the fluorescent probe ANS, which binds to hydrophobic surfaces. The comparison of the ThT and ANS profiles is shown in Figure 3C, and individual ThT and ANS fluorescence profiles at various concentrations of DesBPs are shown in Supplementary Figure S4. We observed that the ANS intensity was increased in a concentration-dependent manner, while the ThT intensity was suppressed (Figure 3C and Supplementary Figure S4), indicating that the DesBPs induced structural changes to more hydrophobic aggregates.

To further characterize the morphology of the aggregates, we used atomic force microscopy (AFM) after each incubation in the absence and in the presence of 0.25 and 16 molar equivalents of the DesBPs (Figure 3D). Representative AFM

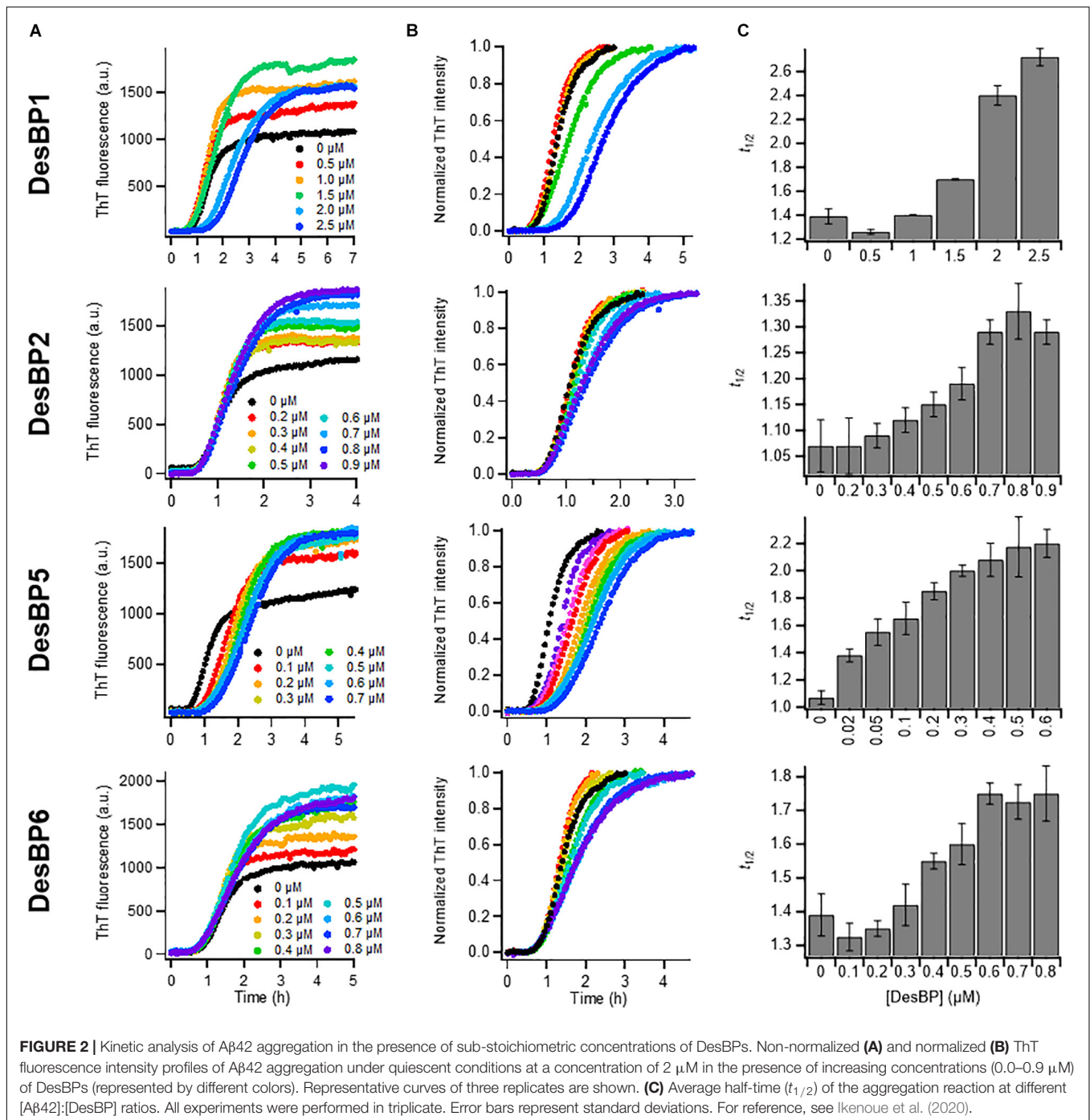
images show a morphological transition from fibrillar to non-fibrillar aggregates, consistent with the increase of ANS fluorescence. These different morphologies are presumably caused by the incorporation of the DesBPs into the A β 42 aggregates. Furthermore, the aggregates did not show seeding ability, apart from those formed in the presence of DesBP6, suggesting that they are not fibrillar (Supplementary Figure S5).

Taken together, our results indicate that these DesBPs extend the lag phase at all concentrations, but appear to exhibit a concentration-dependent mechanism of modulation of A β 42 aggregation. At low concentrations, the DesBPs increase the ThT intensity (Figure 2), while at higher concentrations, they decrease the ThT intensity by redirecting the aggregation process toward non-fibrillar aggregates (Figure 3).

Characterization of the Effects of the DesBPs on the Structures of the Aggregates of A β 42

Sub-stoichiometric Concentrations of DesBPs Delay the Aggregation of A β 42 Into Fibrillar Structures

To investigate the structures of the A β 42 aggregates formed in the presence of the DesBPs, we performed time course DLS measurements to monitor the early stages of aggregation of



10 μ M A β 42 in the presence of 0.25 molar equivalents of DesBP (Figure 4A). The results showed a rapid (within 10 min) appearance of aggregates of about 1.0 μ m in size. The ThT profiles, however, did not show any increase until at least 30 min (Figure 4B), showing that these early aggregates do not yet have a fully ordered fibrillar structure. In addition, the growth in the ANS signal within the initial 30 min suggests the presence of hydrophobic assemblies (Figure 4B). Next, in the presence of 0.25 molar equivalents of the DesBPs, the A β 42

concentration was varied from 2 to 10 μ M in the ThT assays. To confirm that the products were still amyloid fibrils, far-UV CD spectrometry measurements were performed in the case of 10 μ M of A β 42. After a 1-day incubation, the CD spectra showed fibrillar structures, although aggregates in the presence of DesBP2 and DesBP5 showed less β -sheet contents (Figure 4E). The ThT profiles indicate that the aggregation of A β 42 was enhanced in the presence of the DesBPs (Figure 4F), without the formation of significant amounts of off-pathway aggregates (Supplementary

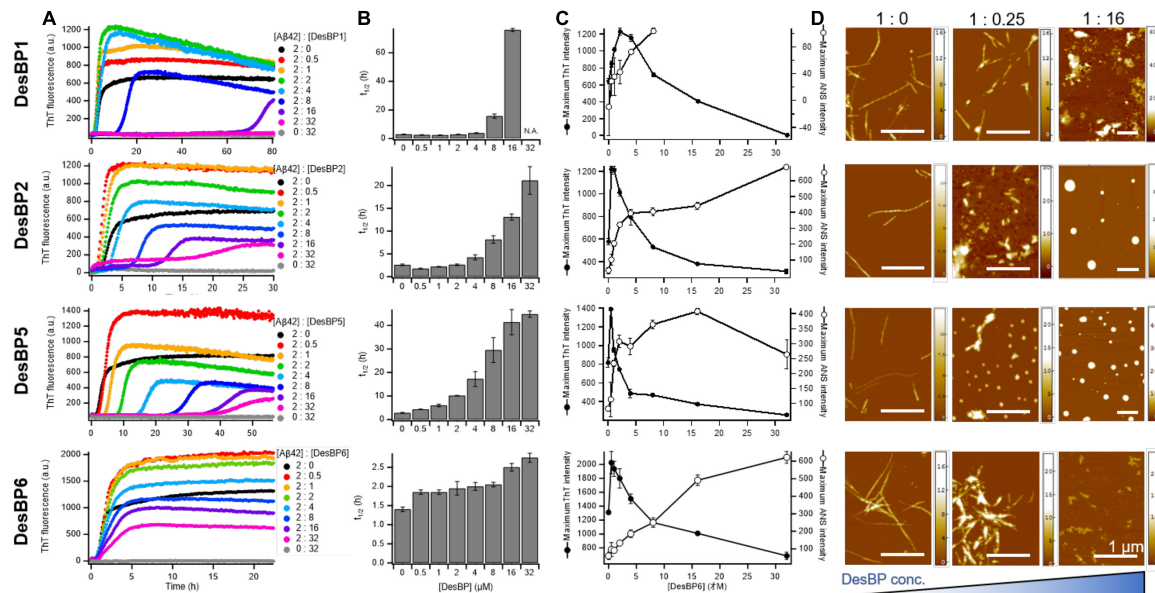


FIGURE 3 | Kinetic analysis and morphological changes of A β 42 aggregation in the presence of high concentrations of DesBPs. **(A)** ThT kinetic profiles of A β 42 aggregation under quiescent conditions at a concentration of 2 μ M in the absence or in the presence of increasing concentrations (0.5–32 μ M) of DesBPs (represented by different colors). Representative profiles of three replicates are shown. **(B)** Average half-time ($t_{1/2}$) of the aggregation at each [A β 42]:[DesBP] ratio. **(C)** Averaged maximum ThT (closed circle) and ANS (opened circle) fluorescence intensity at each [A β 42]:[DesBP] ratio (kinetic profiles are shown in **Supplementary Figure S4**). All aggregation experiments were performed in triplicate. **(D)** Representative AFM images of A β 42 aggregates at the end of the ThT assay (32 h) formed in the presence of 0 (left), 0.25 (middle), and 16 (right) molar equivalents of DesBPs. The scale bar on the AFM images indicates 1 μ m, and the scale on the right represents the height.

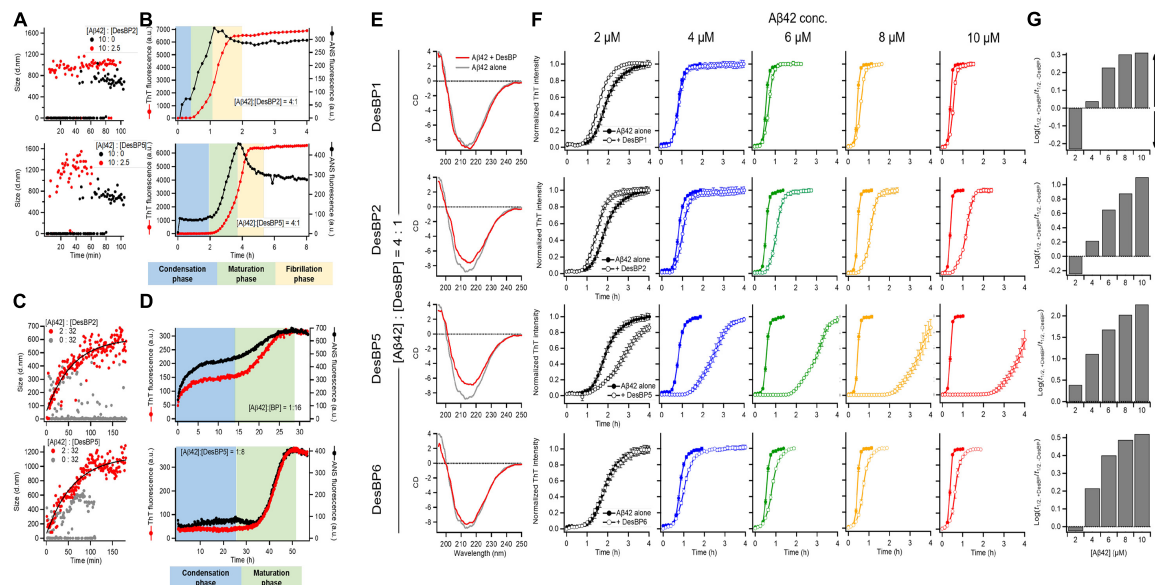


FIGURE 4 | Comparison of the structural properties of A β 42 aggregates at low and high DesBP concentrations. Kinetics of 10 μ M A β 42 aggregation observed by DLS **(A,C)**, ThT and ANS fluorescence **(B,D)** in the presence of 0.25 and 16 molar equivalents of DesBP2 and DesBP5. Blue, green, and yellow regions in **(B)** and **(D)** represent the condensation, maturation, and fibrillation phases in the aggregation process of A β 42, respectively. **(E)** Secondary structure of A β 42 aggregates in the presence of 0.25 molar equivalents DesBPs. Far-UV CD spectra of 10 μ M A β 42 aggregates in the absence (gray) and in the presence (red) of DesBPs. **(F,G)** Kinetics of A β 42 aggregation in the presence of 0.25 molar equivalents DesBPs for increasing concentrations of A β 42 (from 2 to 10 μ M). Normalized ThT profiles **(F)** (non-normalized ThT profiles are shown in **Supplementary Figure S6**), and effects of DesBPs on $t_{1/2}$, the half time of aggregation; the y-axis reports the logarithm of the ratio of $t_{1/2}$ in the presence and absence of a DesBP **(G)**. All experiments were performed in triplicate.

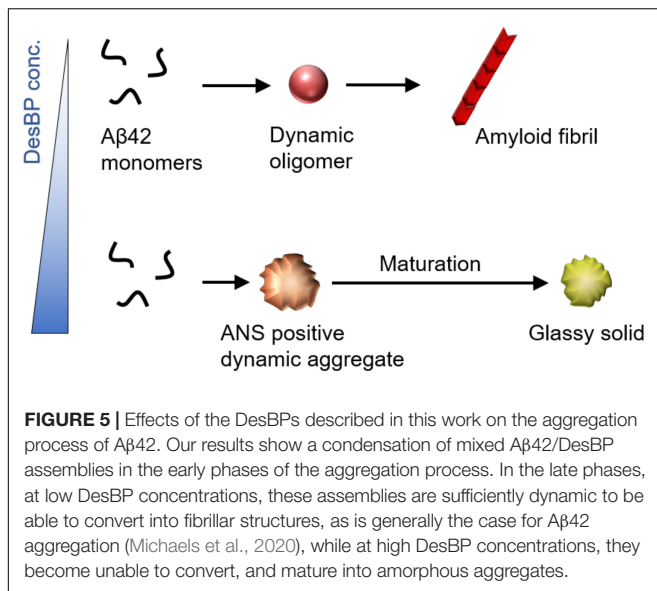


Figure S6). We then evaluated the changes the half-time of aggregation, finding that the $t_{1/2}$ values in the presence of DesBP1, DesBP2, DesBP5, and DesBP6 were increased in a concentration-dependent manner (**Figure 4G**).

High Concentrations of DesBPs Delay Aβ42 Aggregation and Promote the Formation of Amorphous Assemblies

In the presence of 16-fold excess DesBP concentration, for 2 μM Aβ42 concentration, the analysis of DLS (**Figure 4C**), ThT, and ANS (**Figure 4D**) measurements indicated a gradual formation of amorphous assemblies, presumably of mixed Aβ42/DesBP composition, since the intensity of the ThT and ANS decreases by about 20-fold at high DesBP concentration. At high DesBP concentrations, the aggregates appear to be no longer fibrillar, as also shown by the AFM images in **Figure 3** and the seeding experiments in **Supplementary Figure S5**.

Taken together, these results show that DesBPs promote the condensation of Aβ42 monomers into assemblies formed by interacting Aβ42 and DesBP molecules in the early stages of Aβ42 aggregation. The presence of these assemblies delays, or even blocks, the formation of structured aggregates in the late stages.

CONCLUSION

We have described the effects on the aggregation process of Aβ42 of a panel of bicyclic peptides designed to bind different epitopes along the Aβ42 sequence. Our results show that in the early phases of aggregation, there is a condensation of mixed assemblies formed by the Aβ42 and DesBP molecules (**Figure 5**). In the late phases, at low DesBP concentrations, these assemblies tend to convert into fibrillar structures, while at high DesBP concentrations, they mature into amorphous aggregates (**Figure 5**). These results indicate that bicyclic peptides can be

used to remodel the Aβ42 aggregation process by redirecting it toward non-fibrillar species.

MATERIALS AND METHODS

Reagents

All reagents were purchased from Sigma-Aldrich, excluding ThT UltraPure Grade (ThT ≥ 95%), which was purchased from Eurogentec Ltd.

Rational Design of the Bicyclic Peptides

In our rational design strategy, we regard a bicyclic peptide sequence as formed by four regions, which are separated by the three cysteine residues required for bicyclization. In this view, we designed the two central regions to enable the binding to the target epitope, as depicted in **Figure 1B**. By contrast, we retained some motifs (i.e., Ala-Ala at the N-terminus and Gly-Gly at the C-terminus for DesBP1, DesBP2, DesBP5, and DesBP6) of the amino acid sequences of the two terminal regions in order to facilitate the bicyclization reaction. These regions were further endowed with charged residues to enhance the overall solubility of the constructs. We set the length of the binding sites to six or seven residues, following unsuccessful preliminary attempts to carry out the bicyclization reaction with longer sequences, or without the Ala-Ala and Gly-Gly motifs at the termini. The rational design was performed with the cascade method (Sormanni et al., 2015a) (**Figure 1A**). The charged residues at the termini were chosen using the CamSol intrinsic solubility score (Sormanni et al., 2015b).

Recombinant Expression of Aβ42

Aβ42 peptides (MDAEFRHDSGY EVVHHQKLIVFF AEDVGSNKGAIIGLMVGGVVIA), here called Aβ42, were obtained as described previously by recombinant expression in the *Escherichia coli* BL21 Gold (DE3) strain (Stratagene) (Habchi et al., 2017). The purification procedure was carried out by sonication of *E. coli* cells, dissolution of inclusion bodies in 8 M urea, ion exchange in batch mode on diethylaminoethyl cellulose resin, and lyophilization, followed by further purification using a Superdex 75 HR 26/60 column (GE Healthcare). Eluates were analyzed using SDS-polyacrylamide gel electrophoresis (SDS-PAGE) for the presence of protein products. The fractions containing recombinant Aβ42 were combined, frozen using liquid nitrogen, and lyophilized again.

Synthesis of the Bicyclic Peptides

The rationally designed linear peptides were purchased from ChinaPeptides. In order to achieve cyclization, the peptides were dissolved in the reaction buffer (20 mM NH₄HCO₃, 5 mM EDTA, pH 8.0) at 625 μM. One-quarter volume of 5 mM TBMB in 100% acetonitrile was added to obtain a final concentration of 500 μM peptide and 1 mM TBMB and incubated for 1 h at 30°C. The cyclized peptides were purified by reversed-phase chromatography on a C18 column using H₂O/0.08% trifluoroacetic acid (TFA) and acetonitrile/0.08% TFA as solvents,

using a GRACE VYDAC C18 (218TP) column 22×250 mm. The correct mass was then validated by analytical LC/MS (Xevo).

ThT and ANS Fluorescence Aggregation Assay

Solutions of monomeric peptides were prepared by dissolving the lyophilized A β 42 peptide in 6 M GuHCl. The designed bicyclic peptides in their monomeric form were purified from oligomeric species and salt using a Superdex 75 10/300 GL column (GE Healthcare) at a flow rate of 0.5 mL/min, followed by elution in 20 mM sodium phosphate buffer (pH 8) and addition of 200 μ M EDTA. The peptide concentration was determined from the absorbance of the integrated peak area using $\epsilon_{280} = 14951 \text{ mol}^{-1} \text{ cm}^{-1}$. The designed bicyclic peptides were dissolved in water and centrifuged at 20°C for 1 h at 435,000 g before use. The obtained DesAbs in their monomeric forms were diluted with buffer to the desired concentration and supplemented with 20 μ M ThT and 50 μ M ANS from a 1 mM stock. ANS experiments were carried out as described previously (Ikenoue et al., 2020). Seeding experiments were performed in the presence of 10% (v/v) preformed fibrils, as described previously (Ikenoue et al., 2020). Preformed fibrils were prepared by the same procedure used with spontaneous fibril formation. All samples were prepared in low-binding Eppendorf tubes on ice using careful pipetting to avoid introduction of air bubbles. Each sample was then pipetted into multiple wells of a 96-well half-area, low-binding polyethylene glycol coating plate (Corning 3881) with a clear bottom, at 80 μ L per well. Assays were initiated by placing the 96-well plate at 37°C under quiescent conditions in a plate reader (Fluostar Optima; BMG Labtech). The fluorescence was simultaneously measured through the bottom of the plate with excitation filter at 440 nm for ThT and 380 nm for ANS and emission filter at 480 nm.

Static and Dynamic Light Scattering

The light scattering measurements were performed on a Zetasizer Nano S instrument (Malvern Instruments, Malvern, United Kingdom) in backscattering mode at 173°. The instrument was equipped with a light source with a wavelength of 633 nm and a Peltier temperature controller at 25°C. Samples were prepared as described above, and 70 μ L of them was pipetted into disposable plastic micro cuvette.

CD Spectroscopy

Far-UV CD spectra of proteins and peptides in soluble and insoluble states were measured with a J-820 spectropolarimeter (Jasco, Japan) using a cell with a light path of 1 mm at each condition. Individual A β 42 solutions were prepared at 10 μ M for CD measurements. The CD signals between 195 and 250 nm were expressed as mean residue ellipticity $[\theta]$ ($\text{deg cm}^2 \text{ dmol}^{-1}$). Temperature regulation was carried out using a PFD-425S Peltier-unit (Jasco, Japan).

Atomic Force Microscopy

Atomic force microscopy measurements were carried out in air with the sample deposited on functionalized mica. To

functionalize the surface, after cleaving, the bare mica substrate was incubated with a 10 μ L drop of 0.05% (v/v) APTES [(3-aminopropyl)triethoxysilane, Fluka] in Milli-Q water for 1 min at room temperature, rinsed with Milli-Q water, and then dried by the passage of a gentle flow of gaseous nitrogen. The preparation of the mica AFM samples was made at room temperature by deposition of a 10 μ L aliquot of 10 μ M solution for 5 min. Then the samples were rinsed with ultrapure water and dried by a gentle flow of nitrogen.

Atomic force microscopy imaging was carried out in intermittent contact mode on a JPK Nanowizard II AFM recorded with AC mode under ambient conditions using an integral gain of 120 Hz, post-gain of 0.008 Hz, and 0.3 Hz line-rate for $4 \times 4 \mu\text{m}$ images. Images flattening and statistical analysis were performed by SPIP (Image metrology) software.

DATA AVAILABILITY STATEMENT

The original contributions presented in the study are included in the article/**Supplementary Material**. Further inquiries can be directed to the corresponding author/s.

AUTHOR CONTRIBUTIONS

TI, FA, PS, and MV were involved in the design of research. PS designed the peptide. TI performed the experiments. TI, FA, and MV wrote the manuscript. All authors discussed the results and commented on the manuscript.

FUNDING

This work was supported by the Japan Society for the Promotion of Science (JSPS) oversea research fellowships. FA was supported by UK Research and Innovation (Future Leaders Fellowship MR/S033947/1) and the Alzheimer's Society, United Kingdom (317, 511).

SUPPLEMENTARY MATERIAL

The Supplementary Material for this article can be found online at: <https://www.frontiersin.org/articles/10.3389/fnins.2021.623097/full#supplementary-material>

Supplementary Figure 1 | Solubility of the DesBPs in the absence of A β 42 before and after incubation. Static (a) and dynamic (b) light scattering of 50 μ M DesBP monomers solved in phosphate buffer at 5°C. (c) Far-UV CD spectra of 32 μ M DesBP monomers. (d) Representative AFM images of 32 μ M DesBPs after 1 day incubation at 37°C. The scale bar on the AFM images indicates 1 μm , and the scale on the right represents the height.

Supplementary Figure 2 | Seeding experiments of A β 42 amyloid fibrils at sub-stoichiometric concentrations of DesBPs. Non-normalized (a) and normalized ThT kinetic profiles (b) of A β 42 aggregation under quiescent conditions at a concentration of 2 μ M in the absence or in the presence of various concentrations (0.1–0.9 μ M) of DesBPs (represented by different colors). (c) Maximum ThT intensity of the aggregation at each [A β 42]:[DesBP] ratio. All experiments were performed in triplicate.

Supplementary Figure 3 | DesBP3 and DesBP4 do not affect significantly A β 42 aggregation. ThT (**a**) and ANS (**b**) kinetic profiles of A β 42 aggregation under quiescent conditions at a concentration of 2 μ M in the absence or in the presence of various concentration (0.5–32 μ M) of DesBPs (represented by different colors). (**c**) Representative AFM images of A β 42 aggregates in the presence of 16 molar equivalents of DesBPs. The scale bar on the AFM images indicates 1 μ m, and the scale on the right represents the height. All aggregation experiments were performed in triplicate.

Supplementary Figure 4 | Kinetic profile of ThT and ANS fluorescence of A β 42 aggregation at various concentrations of DesBPs. ThT (closed circles) and ANS (opened circles) kinetic profiles of A β 42 aggregation under quiescent conditions at a concentration of 2 μ M in the absence or in the presence of various

concentrations (0.5–32 μ M) of DesBP1, DesBP2, DesBP5, and DesBP6 (represented by different colors). All experiments were performed in triplicate.

Supplementary Figure 5 | Seeded aggregation assay of A β 42 in the presence of high molar equivalents of DesBPs. The aggregates formed in the presence of the DesBPs, with the exception of the case of DesBP6, did not show seeding ability, indicating that they do not have a fibrillar nature. Experiments were performed in triplicate.

Supplementary Figure 6 | Kinetics of A β 42 aggregation in the presence of 0.25 molar equivalents DesBPs. We report the results for increasing concentrations of A β 42, from 2 to 10 μ M. All experiments were performed in triplicate.

REFERENCES

- Angelini, A., Cendron, L., Chen, S., Touati, J., Winter, G., Zanotti, G., et al. (2012). Bicyclic peptide inhibitor reveals large contact interface with a protease target. *ACS Chem. Biol.* 7, 817–821. doi: 10.1021/cb200478t
- Aprile, F. A., Sormanni, P., Perni, M., Arosio, P., Linse, S., Knowles, T. P. J., et al. (2017). Selective targeting of primary and secondary nucleation pathways in abeta42 aggregation using a rational antibody scanning method. *Sci. Adv.* 3:e1700488. doi: 10.1126/sciadv.1700488
- Aprile, F. A., Sormanni, P., and Vendruscolo, M. (2015). A rational design strategy for the selective activity enhancement of a molecular chaperone toward a target substrate. *Biochemistry* 54, 5103–5112. doi: 10.1021/acs.biochem.5b00459
- Baeriswyl, V., and Heinis, C. (2013). Polycyclic peptide therapeutics. *ChemMedChem* 8, 377–384. doi: 10.1002/cmdc.201200513
- Bartoloni, M., Jin, X., Marcaida, M. J., Banha, J., Dibonaventura, I., Bongoni, S., et al. (2015). Bridged bicyclic peptides as potential drug scaffolds: synthesis, structure, protein binding and stability. *Chem. Sci.* 6, 5473–5490. doi: 10.1039/c5sc01699a
- Benilova, I., Karran, E., and De Strooper, B. (2012). The toxic abeta oligomer and Alzheimer's disease: an emperor in need of clothes. *Nat. Neurosci.* 15, 349–357. doi: 10.1038/nn.3028
- Bieschke, J., Herbst, M., Wiglenda, T., Friedrich, R. P., Boeddrich, A., Schiele, F., et al. (2011). Small-molecule conversion of toxic oligomers to nontoxic beta-sheet-rich amyloid fibrils. *Nat. Chem. Biol.* 8, 93–101. doi: 10.1038/nchembio.719
- Bionda, N., and Fasan, R. (2015). Ribosomal synthesis of natural-product-like bicyclic peptides in *escherichia coli*. *Chembiochem* 16, 2011–2016. doi: 10.1002/cbic.201500179
- Bock, J. E., Gavenonis, J., and Kritzer, J. A. (2013). Getting in shape: controlling peptide bioactivity and bioavailability using conformational constraints. *ACS Chem. Biol.* 8, 488–499. doi: 10.1021/cb300515u
- Bucciantini, M., Giannoni, E., Chiti, F., Baroni, F., Formigli, L., Zurdo, J., et al. (2002). Inherent toxicity of aggregates implies a common mechanism for protein misfolding diseases. *Nature* 416, 507–511. doi: 10.1038/416507a
- Chen, S., Bertoldo, D., Angelini, A., Pojer, F., and Heinis, C. (2014). Peptide ligands stabilized by small molecules. *Angew. Chem. Int. Ed. Engl.* 53, 1602–1606. doi: 10.1002/anie.201309459
- Civitelli, L., Sandin, L., Nelson, O., Khattak, S. I., Brorsson, A. C., and Kågedal, K. (2016). The luminescent oligothiophene p-ftaa converts toxic abeta1-42 species into nontoxic amyloid fibers with altered properties. *J. Biol. Chem.* 291, 9233–9243. doi: 10.1074/jbc.m115.696229
- Cohen, S. I. A., Linse, S., Luheshi, L. M., Hellstrand, E., White, D. A., Rajah, L., et al. (2013). Proliferation of amyloid-beta42 aggregates occurs through a secondary nucleation mechanism. *Proc. Natl. Acad. Sci. U.S.A.* 110, 9758–9763. doi: 10.1073/pnas.1218402110
- Cremades, N., Cohen, S. I., Deas, E., Abramov, A. Y., Chen, A. Y., Orte, A., et al. (2012). Direct observation of the interconversion of normal and toxic forms of alpha-synuclein. *Cell* 149, 1048–1059. doi: 10.1016/j.cell.2012.03.037
- Cummings, J., Lee, G., Ritter, A., Sabbagh, M., and Zhong, K. (2020). Alzheimer's disease drug development pipeline: 2020. *Alzheimer's Dement.* 6:e12050.
- Driggers, E. M., Hale, S. P., Lee, J., and Terrett, N. K. (2008). The exploration of macrocycles for drug discovery—an underexploited structural class. *Nat. Rev. Drug Discov.* 7, 608–624. doi: 10.1038/nrd2590
- Getz, J. A., Rice, J. J., and Daugherty, P. S. (2011). Protease-resistant peptide ligands from a knottin scaffold library. *ACS Chem. Biol.* 6, 837–844. doi: 10.1021/cb200039s
- Haass, C., and Selkoe, D. J. (2007). Soluble protein oligomers in neurodegeneration: lessons from the Alzheimer's amyloid beta-peptide. *Nat. Rev. Mol. Cell Biol.* 8, 101–112. doi: 10.1038/nrm2101
- Habchi, J., Chia, S., Limbocker, R., Mannini, B., Ahn, M., Perni, M., et al. (2017). Systematic development of small molecules to inhibit specific microscopic steps of abeta42 aggregation in Alzheimer's disease. *Proc. Natl. Acad. Sci. U.S.A.* 114, E200–E208.
- Heinis, C., Rutherford, T., Freund, S., and Winter, G. (2009). Phage-encoded combinatorial chemical libraries based on bicyclic peptides. *Nat. Chem. Biol.* 5, 502–507. doi: 10.1038/nchembio.184
- Hellstrand, E., Boland, B., Walsh, D. M., and Linse, S. (2010). Amyloid beta-protein aggregation produces highly reproducible kinetic data and occurs by a two-phase process. *ACS Chem. Neurosci.* 1, 13–18. doi: 10.1021/cn900015v
- Ikenoue, T., Aprile, F. A., Sormanni, P., Ruggeri, F. S., Perni, M., Heller, G. T., et al. (2020). A rationally designed bicyclic peptide remodels A β 42 aggregation in vitro and reduces its toxicity in a worm model of Alzheimer's disease. *Sci. Rep.* 10, 1–15.
- Jack, C. R. Jr., Bennett, D. A., Blennow, K., Carrillo, M. C., Dunn, B., Haeberlein, S. B., et al. (2018). NIA-AA research framework: toward a biological definition of Alzheimer's disease. *Alzheimer's Dement.* 14, 535–562. doi: 10.1016/j.jalz.2018.02.018
- Kayed, R., Head, E., Thompson, J. L., McIntire, T. M., Milton, S. C., and Cotman, C. W. (2003). Common structure of soluble amyloid oligomers implies common mechanism of pathogenesis. *Science* 300, 486–489. doi: 10.1126/science.1079469
- Lesne, S., Koh, M. T., Kotilinek, L., Kaye, R., Glabe, C. G., Yang, A., et al. (2006). A specific amyloid-beta protein assembly in the brain impairs memory. *Nature* 440, 352–357. doi: 10.1038/nature04533
- Lian, W., Jiang, B., Qian, Z., and Pei, D. (2014). Cell-permeable bicyclic peptide inhibitors against intracellular proteins. *J. Am. Chem. Soc.* 136, 9830–9833. doi: 10.1021/ja503710n
- Limbocker, R., Chia, S., Ruggeri, F. S., Perni, M., Cascella, R., Heller, G. T., et al. (2019). Trodusquemine enhances A β 42 aggregation but suppresses its toxicity by displacing oligomers from cell membranes. *Nat. Comm.* 10:225.
- Mannini, B., Mulvihill, E., Sgromo, C., Cascella, R., Khodarahmi, R., Ramazzotti, M., et al. (2014). Toxicity of protein oligomers is rationalized by a function combining size and surface hydrophobicity. *ACS Chem. Biol.* 9, 2309–2317. doi: 10.1021/cb500505m
- Michaels, T. C., Šarić, A., Curk, S., Bernfur, K., Arosio, P., Meisl, G., et al. (2020). Dynamics of oligomer populations formed during the aggregation of Alzheimer's A β 42 peptide. *Nat. Chem.* 12, 445–451. doi: 10.1038/s41557-020-0452-1
- Michaels, T. C., Šarić, A., Habchi, J., Chia, S., Meisl, G., Vendruscolo, M., et al. (2018). Chemical kinetics for bridging molecular mechanisms and macroscopic measurements of amyloid fibril formation. *Annu. Rev. Phys. Chem.* 69, 273–298. doi: 10.1146/annurev-physchem-050317-021322
- Quartararo, J. S., Eshelman, M. R., Peraro, L., Yu, H., Baleja, J. D., Lin, Y. S., et al. (2014). A bicyclic peptide scaffold promotes phosphotyrosine mimicry and cellular uptake. *Bioorg. Med. Chem.* 22, 6387–6391. doi: 10.1016/j.bmc.2014.09.050

- Schenk, D., Barbour, R., Dunn, W., Gordon, G., Grajeda, H., Guido, T., et al. (1999). Immunization with amyloid-beta attenuates Alzheimer-disease-like pathology in the pdapp mouse. *Nature* 400, 173–177. doi: 10.1038/22124
- Selkoe, D. J., and Hardy, J. (2016). The amyloid hypothesis of Alzheimer's disease at 25 years. *EMBO Mol. Med.* 8, 595–608.
- Sevigny, J., Chiao, P., Bussière, T., Weinreb, P. H., Williams, L., Maier, M., et al. (2016). The antibody aducanumab reduces A β plaques in Alzheimer's disease. *Nature* 537:50.
- Sonzini, S., Stanyon, H. F., and Scherman, O. A. (2017). Decreasing amyloid toxicity through an increased rate of aggregation. *Phys. Chem. Chem. Phys.* 19, 1458–1465. doi: 10.1039/c6cp06765d
- Sormanni, P., Aprile, F. A., and Vendruscolo, M. (2015a). Rational design of antibodies targeting specific epitopes within intrinsically disordered proteins. *Proc. Natl. Acad. Sci. U.S.A.* 112, 9902–9907. doi: 10.1073/pnas.1422401112
- Sormanni, P., Aprile, F. A., and Vendruscolo, M. (2015b). The camsol method of rational design of protein mutants with enhanced solubility. *J. Mol. Biol.* 427, 478–490. doi: 10.1016/j.jmb.2014.09.026
- Sormanni, P., Aprile, F. A., and Vendruscolo, M. (2018). Third generation antibody discovery methods: In silico rational design. *Chem. Soc. Rev.* 47, 9137–9157.
- Conflict of Interest:** The authors declare that the research was conducted in the absence of any commercial or financial relationships that could be construed as a potential conflict of interest.

Copyright © 2021 Ikenoue, Aprile, Sormanni and Vendruscolo. This is an open-access article distributed under the terms of the Creative Commons Attribution License (CC BY). The use, distribution or reproduction in other forums is permitted, provided the original author(s) and the copyright owner(s) are credited and that the original publication in this journal is cited, in accordance with accepted academic practice. No use, distribution or reproduction is permitted which does not comply with these terms.



Identification of Two Novel Peptides That Inhibit α -Synuclein Toxicity and Aggregation

Blagovesta Popova^{1†}, Dan Wang^{1†}, Abirami Rajavel¹, Karthikeyan Dhamotharan¹, Diana F. Lázaro², Jennifer Gerke¹, Joachim F. Uhrig³, Michael Hoppert⁴, Tiago F. Outeiro^{2,5,6,7} and Gerhard H. Braus^{1*}

¹Department of Molecular Microbiology and Genetics, Institute for Microbiology and Genetics, University of Goettingen, Göttingen, Germany, ²Department of Experimental Neurodegeneration, Center for Biostructural Imaging of Neurodegeneration, University Medical Center Goettingen, Göttingen, Germany, ³Department of Plant Molecular Biology and Physiology, University of Goettingen, Göttingen, Germany, ⁴Department of General Microbiology, Institute of Microbiology and Genetics, University of Goettingen, Göttingen, Germany, ⁵Max Planck Institute for Experimental Medicine, Göttingen, Germany, ⁶Translational and Clinical Research Institute, Faculty of Medical Sciences, Newcastle University, Framlington Place, Newcastle upon Tyne, United Kingdom, ⁷Deutsches Zentrum für Neurodegenerative Erkrankungen (DZNE), Göttingen, Germany

OPEN ACCESS

Edited by:

Wolfgang Hoyer,
Heinrich Heine University of
Düsseldorf, Germany

Reviewed by:

Jody M. Mason,
University of Bath, United Kingdom
Gaia Faustini,
University of Brescia, Italy

*Correspondence:

Gerhard H. Braus
gbraus@gwdg.de

[†]These authors have contributed
equally to this work

Received: 28 January 2021

Accepted: 16 March 2021

Published: 12 April 2021

Citation:

Popova B, Wang D, Rajavel A, Dhamotharan K, Lázaro DF, Gerke J, Uhrig JF, Hoppert M, Outeiro TF and Braus GH (2021) Identification of Two Novel Peptides That Inhibit α -Synuclein Toxicity and Aggregation. *Front. Mol. Neurosci.* 14:659926. doi: 10.3389/fnmol.2021.659926

Aggregation of α -synuclein (α Syn) into proteinaceous deposits is a pathological hallmark of a range of neurodegenerative diseases including Parkinson's disease (PD). Numerous lines of evidence indicate that the accumulation of toxic oligomeric and prefibrillar α Syn species may underpin the cellular toxicity and spread of pathology between cells. Therefore, aggregation of α Syn is considered a priority target for drug development, as aggregation inhibitors are expected to reduce α Syn toxicity and serve as therapeutic agents. Here, we used the budding yeast *S. cerevisiae* as a platform for the identification of short peptides that inhibit α Syn aggregation and toxicity. A library consisting of approximately one million peptide variants was utilized in two high-throughput screening approaches for isolation of library representatives that reduce α Syn-associated toxicity and aggregation. Seven peptides were isolated that were able to suppress specifically α Syn toxicity and aggregation in living cells. Expression of the peptides in yeast reduced the accumulation of α Syn-induced reactive oxygen species and increased cell viability. Next, the peptides were chemically synthesized and probed for their ability to modulate α Syn aggregation *in vitro*. Two synthetic peptides, K84s and K102s, of 25 and 19 amino acids, respectively, significantly inhibited α Syn oligomerization and aggregation at sub-stoichiometric molar ratios. Importantly, K84s reduced α Syn aggregation in human cells. These peptides represent promising α Syn aggregation antagonists for the development of future therapeutic interventions.

Keywords: α -synuclein, Parkinson's disease, protein aggregation, oligomerization, peptide drug discovery, yeast, library screening

INTRODUCTION

Protein misfolding and aggregation is a hallmark event in a growing number of human diseases, including Parkinson's disease (PD). PD is the second most common neurodegenerative disorder, affecting 1–2% of the population over the age of 60. The pathological hallmark of the disease is a massive loss of dopaminergic neurons in the *substantia nigra pars compacta* of the brain (German et al., 1992). PD is characterized by the deposition of the small neuronal protein α -synuclein (α Syn) into intracellular inclusions, known as Lewy bodies (LB; Spillantini et al., 1997). Missense mutations and genomic multiplications of α Syn gene (SNCA) are linked to autosomal dominant familial PD, which marks α Syn as a prime target in PD research (Polymeropoulos et al., 1997; Krüger et al., 1998; Singleton et al., 2003; Chartier-Harlin et al., 2004; Zarranz et al., 2004; Appel-Cresswell et al., 2013; Lesage et al., 2013). The α Syn protein is intrinsically disordered and can self-assemble into oligomeric protofibrils that can further mature into different types of fibrils and aggregates (Breydo et al., 2012). Pathological conditions promote α Syn aggregation, especially in connection with genetic mutations (Conway et al., 1998; Fredenburg et al., 2007), molecular crowding (Shtilerman et al., 2002; Uversky et al., 2002), increased α Syn protein levels (Conway et al., 1998; Breydo et al., 2012), post-translational modifications (Stefanis, 2012; Popova et al., 2015), low pH (Ahmad et al., 2012), or oxidative conditions (Hashimoto et al., 1999). *in vitro* studies suggest that α Syn exists in various conformations and oligomeric states in a dynamic equilibrium, where the monomer can aggregate into small oligomeric species, stabilized by β -sheet interactions, which slowly convert into higher molecular weight insoluble protofibrils and amyloidogenic fibrils, resembling those found in LB (Conway et al., 1998, 2000; Karpinar et al., 2009; Bengoa-Vergniory et al., 2017). The mechanisms promoting pathological protein aggregation are still unknown. There is a substantial and increasing body of evidence implicating accumulation of oligomeric/protofibrillar α Syn species as one major contribution to neurodegeneration (Karpinar et al., 2009; Winner et al., 2011; Bengoa-Vergniory et al., 2017). The mechanism of α Syn oligomer-induced neurotoxicity involves disruption of numerous cellular processes, among them, are increased mitochondrial, lysosomal, and vesicular membrane permeability, autophagic and lysosomal dysfunction, proteasomal effects, endoplasmic reticulum stress and synaptic dysfunction (Bengoa-Vergniory et al., 2017). Several studies demonstrated that certain species of α Syn can seed the aggregation and formation of inclusions both *in vivo* and *in vitro* (Hansen et al., 2011; Luk et al., 2012). Therefore, inhibition of α Syn aggregation is an extremely important target for drug development. Inhibitors that prevent oligomerization and aggregation of the protein are expected to serve as therapeutic medicines that can prevent the propagation of the disease (Dehay et al., 2015).

We and others have demonstrated that complex diseases such as PD can be modeled in a simple eukaryotic organism such as the budding yeast *Saccharomyces cerevisiae* due to the high conservation of biological pathways, affected by protein misfolding and aggregation (Outeiro and Lindquist, 2003;

Cooper et al., 2006; Gitler et al., 2008; Petroi et al., 2012; Lázaro et al., 2014; Kleinknecht et al., 2016; Popova et al., 2021). Strikingly, although there is no SNCA homolog in the yeast genome, the expression of the protein in yeast recapitulates several relevant aspects of PD. Overexpression of α Syn results in growth impairment and accumulation of the protein into cytoplasmic inclusions similar to the pathogenesis of the disease (Outeiro and Lindquist, 2003; Petroi et al., 2012). Therefore, yeast emerges as a powerful platform for primary screening for cytoprotective compounds (Tenreiro et al., 2017).

In this study, we used a peptide library and performed two high-throughput screens to isolate peptides that reduce α Syn-associated toxicity and aggregation. From a pool of one million candidates, we isolated seven candidates that specifically reduce the toxicity and aggregation of human α Syn in yeast. Two peptides with a length of 25 amino acids (K84s) and 19 amino acids (K102s) are effective inhibitors of α Syn oligomerization and fibrilization as determined with Thioflavin-T staining of amyloid fibrils, electron microscopy imaging, and biochemical analysis. Importantly, K84s reduced α Syn aggregation in the human cell.

MATERIALS AND METHODS

Yeast Strains, Transformation and Growth Conditions

Plasmids and *Saccharomyces cerevisiae* strains are listed in **Table 1** and **Table 2**. Yeast plasmids were constructed using GENEART Seamless cloning and assembly kit (Life technologies). All constructs were verified by DNA sequencing. Yeast strains were grown in YPAD (Yeast Extract—Peptone—Dextrose plus Adenine medium) or synthetic complete dropout (SC) medium (Guthrie and Fink, 1990), lacking the respective amino acid for selection, supplemented with 2% glucose, 2% raffinose or 2% galactose. *S. cerevisiae* strains were used for transformations performed by standard lithium acetate procedure (Gietz et al., 1992).

Spotting Assay

For growth test on solid medium, yeast cells were pre-grown in minimal medium containing 2% raffinose lacking the corresponding marker to mid-log phase. Cells were normalized to equal densities, serially diluted 10-fold starting with an OD₆₀₀ of 0.1, and spotted on SC-plates containing either 2% glucose or 2% galactose and lacking in the corresponding marker. The plates were incubated at 30°C for 3 days. Singer ROTOR HDA bench robot (Singer Instruments, UK) was used for robotic pinning from a 96-well liquid cell suspension (source plate) onto multiple solid agar (target) plates using the manufacturer's software.

Growth Analysis in Liquid Culture

Cells were pre-grown in 2% raffinose-containing selective SC medium until logarithmic growth phase and inoculated in 2% galactose-containing SC medium to equal densities of OD₆₀₀ = 0.1. Optical density measurements of 100 μ l cell cultures were performed in quadruplicates in 96-well plates for 24 h using a microplate reader with temperature control and continuous shaking (Infinite M200, Tecan).

TABLE 1 | Plasmids used in this study.

Name	Description	Source
pGADT7	2 μ ; LEU2; ADH1pr; ADH1term; AmpR	Clontech Inc.
pGBKT7	2 μ ; TRP1; ADH1pr; ADH1term; KanR	Clontech Inc.
pME4897	pGBKT7-GAL4-BD-SNCA	This study
pME4898	pGADT7-AD-K50	This study
pME4899	pGADT7-AD-K84	This study
pME4900	pGADT7-AD-K102	This study
pME4901	pGADT7-AD-K89	This study
pME4902	pGADT7-AD-K117	This study
pME4903	pGADT7-AD-K94	This study
pME4904	pGADT7-AD-K97	This study
p425-GPD	2 μ ; LEU2; GPDpr; CYC1term; AmpR	Mumberg et al. (1994)
pME4905	p425-GPD-K50	This study
pME4906	p425-GPD-K84	This study
pME4907	p425-GPD-K94	This study
pME4908	p425-GPD-K89	This study
pME4909	p425-GPD-K97	This study
pME4910	p425-GPD-K102	This study
pME4911	p425-GPD-K117	This study
p424-GAL1	2 μ m; TRP1; GAL1pr; CYC1term; AmpR	Mumberg et al. (1994)
p425-GAL1	2 μ m; LEU2; GAL1pr; CYC1term; AmpR	Mumberg et al. (1994)
p426-GAL1	2 μ m; URA3, GAL1pr; CYC1term; AmpR	Mumberg et al. (1994)
pME3759	p426-GAL1-GFP	Petroi et al. (2012)
pME3772	p426-GAL1-SNCA-mCherry	Petroi et al. (2012)
pRS304	TRP1; GAL1pr; CYC1term; AmpR	Sikorski and Hieter (1989)
pME3597	pRS304-GAL1-SNCA	Shahpasandzadeh et al. (2014)
Addgene 15587	p303-GAL1-FLAG-htt103Q Δ Pro-CFP	Duenwald et al. (2006)
pME4912	pET22b-K50-6xHis	This study
pME4913	pET22b-SNCA	This study

TABLE 2 | Yeast strains used in this study.

Name	Genotype	Source
W303-1A	<i>MATa, ura3-1, trp1-1, leu2-3_112, his3-11, ade2-1, can1-100</i>	EUROSCARF
BY4741	<i>MATa, ura3Δ0, his3Δ 1, leu2Δ0, met15Δ0</i>	EUROSCARF
RH3465	W303 containing GAL1-GFP in <i>ura3</i> locus	Petroi et al. (2012)
RH3468	W303 containing three genomic copies of GAL1-SNCA-GFP in <i>ura3</i> locus	Petroi et al. (2012)
AH109	<i>MATa, trp1-901, leu2-3, 112, ura3-52, his3-200, gal4Δ, gal80Δ, LYS2::GAL1UAS-GAL1TATA-HIS3, GAL2UAS-GAL2TATA-ADE2, URA3 : : MEL1UAS-MEL1TATA-lacZ, MEL1</i>	Clontech Inc.
Y187	<i>MATalpha, ura3-52, his3-200, ade2-101, trp1-901, leu2-3, 112, gal4Δ, met-, gal80Δ, URA3 : GAL1UAS-GAL1 TATA-lacZ, MEL1</i>	Clontech Inc.
RH3788	BY4741 containing GAL1-FLAG-htt103Q Δ Pro-CFP in <i>his3</i> locus	This study
AH109-syn	AH109 containing GAL1-SNCA in <i>trp1</i> locus	This study

Yeast-Two-Hybrid Screen

The library approach of yeast two-hybrid high-throughput screening involves a bait protein being screened against a pool of prey proteins. Yeast clones expressing interacting proteins are selected based on reporter gene activation and the resulting ability to grow on selective media. The yeast strains AH109 (Mat a) and Y187 (Mat α) were used for the Y2H experiments. The strain AH109 was transformed with the *GAL4-BD-SNCA* bait construct (pME4897). The random peptide library (four million primary clones) was obtained from Fritz and Green (Fritz and Green, 1996) and amplified by transformation in *E. coli*. Plasmid was prepared in bulk from a pool of one million individually grown colonies and transformed into Y187 strain (prey constructs). To warrant a sufficiently complete library representation after the transformation of yeast strain Y187, five million individual prey-containing yeast colonies have

been obtained, pooled, and frozen in aliquots. Aliquots were used for mating with a freshly prepared bait yeast strain. The AH109 strain, transformed with the bait construct was inoculated in 50 ml SC-Trp from a fresh single colony overnight. On the next day, one library aliquot was thawed at 37°C for 10 min and mixed with 9 ml YPAD medium to regenerate for 2 h at 30°C. The optical density of both strains was measured at 600 nm after appropriate dilution. 10 OD₆₀₀ units from both strains were pelleted and mixed with 10 ml YPAD containing 20% PEG6000. Mating of the cells was achieved by incubating the flask at 30°C for 6–8 h at 80 rpm on a rotation shaker. After successful mating, the cells were pelleted and resuspended gently in 2 ml SC-Leu-Trp-His liquid medium containing 2% glucose. Mating efficiency was checked by plating of 10 μ l, 20 μ l, and 50 μ l inoculum on SC-Leu-Trp plates (selection for diploids) to obtain >5 million zygotes in each screening

experiment ensuring complete representation of the library. The rest of the cell suspension was used to inoculate 500 ml of SC-Leu-Trp-His Semi-Solid Media (SSM), containing 1% Gelrite, 2% glucose, and supplemented with ampicillin. The SSM containing the diploid cells was then mixed vigorously using a magnetic stirrer, equally distributed among 30 Petri dishes, and incubated at 30°C for 5–10 days. Colonies observed on SC-Leu-Trp-His SSM were collected by transferring 10 μ l of the grown single colony using a pipette into a 96-well plate containing 90 μ l of SC-Leu-Trp-His liquid media. The cells were resuspended by mixing and incubated at 30°C overnight. The 96-well plates were spotted onto solid SC-Leu-Trp agar plates using Singer ROTOR HDA. The agar plates were incubated for 1–2 days at 30°C and served as master plates from which different selection plates for confirmation of interactions were pinned. From every single positive clone from the screen, four technical replicates were pinned from SC-Leu-Trp plates onto agar selection plates with increasing stringency (SC-Leu-Trp-His, SC-Leu-Trp-His + 5 mM 3-AT, SC-Leu-Trp-His + 7.5 mM 3-AT or SC-Leu-Trp-His-Ade). Based on growth on selection plates, positive clones were selected, and cells were grown in 5 ml SC-Leu overnight at 30°C at a rotary shaker to lose the bait plasmid. Prey plasmids were isolated from yeast cells. To achieve maximum yield of prey plasmid recovery, *E. coli* DH5 α cells were transformed with 10 μ l of the plasmid mixture, plasmids were re-isolated and sequenced.

Toxicity-Rescue Screen

The second high-throughput screening approach employed direct isolation of modifiers of α Syn toxicity by co-expressing α Syn gene without a tag along with roughly one million peptides from the PEP1170⁺ library. Yeast strain AH109 was transformed with plasmid pME3597, harboring α Syn encoding gene under *GAL1* promoter. Isolated single colonies were tested for growth by spotting assay. A clone with moderate growth inhibition upon expression of α Syn was mated with the PEP1170⁺ library as described in the Y2H screen procedure. After successful mating, the diploid cells were diluted and plated on 30 large SC-Leu-Trp agar plates (140 mm diameter), supplemented with 2% galactose for induction of α Syn expression. The plates were incubated at 30°C and observed for growth regularly. Colonies that appeared first were streaked on SC-Leu-Trp agar plates, supplemented with 2% glucose. Single colonies were used for prey plasmid rescue as described above and sequenced.

Fluorescence Microscopy and Quantifications

Yeast cells were grown in SC selective medium containing 2% raffinose at 30°C overnight and transferred to 2% galactose containing medium for induction of α Syn-GFP expression for 6 h. Fluorescent images were obtained with Zeiss Observer. Z1 microscope (Zeiss) equipped with a CSU-X1 A1 confocal scanner unit (YOKOGAWA), QuantEM:512SC digital camera (Photometrics), and SlideBook 6.0 software package (Intelligent Imaging Innovations). For quantification of aggregation, at least 200 cells were counted per strain and per experiment. The number of cells presenting inclusions was referred to the total

number of cells counted. The values are the mean of at least four independent experiments.

Flow Cytometry

Cells were grown and protein expression was induced as described above. Yeast cell membrane integrity was analyzed with propidium iodide (PI) staining. Yeast cells were incubated with 12.5 μ g/ml PI for 30 min in dark. Dihydrorhodamine 123 (DHR123) was used as an indicator for intracellular ROS accumulation. Yeast cells, expressing *GAL1*-driven α Syn-mCherry were incubated with DHR123 (Sigma-Aldrich) at a final concentration of 5 μ g/ml for 1.5 h at 30°C. Before flow cytometry measurements, the cells were washed and re-suspended in 50 mM trisodium citrate buffer, pH 7.0. Flow cytometry analysis was performed on a BD FACSCANTO II (Becton Dickinson). Twenty thousand events were counted for each experiment. Data analysis was performed using the BD FACSDIVA software (Becton Dickinson).

Immunoblotting

Yeast cells harboring α Syn-GFP were pre-grown at 30°C in SC selective medium containing 2% raffinose. Cells were transferred to SC medium containing 2% galactose at OD₆₀₀ = 0.1 to induce the *GAL1* promoter for 6 h. Total protein extracts were prepared, and the protein concentrations were determined with a Bradford assay. Forty microgram of each protein were subjected to 12% SDS-polyacrylamide gel electrophoresis and transferred to a nitrocellulose membrane. Membranes were probed with anti- α Syn rabbit antibody (Santa Cruz, USA). GAPDH mouse monoclonal antibody (Thermo Fisher Scientific, USA) was used as a loading control. The use of actin as a loading control was avoided since yeast actin intron contains a cryptic promoter that is normally inactive, however, its deletion can lead to transcriptional interference (Irniger et al., 1992). Pixel density values for Western quantification were obtained from TIFF files generated from digitized X-ray films (KODAK) and analyzed with the ImageJ software (NIH, Bethesda, MD, USA).

Human Recombinant α Syn Expression and Purification

The expression and purification of α Syn were performed as previously described (Miranda et al., 2013). Briefly, *E. coli* BL21 (DE3) cells were transformed with pET22b- α Syn construct, and expression of 500 ml LB culture was induced with isopropyl β -D-1-thiogalactopyranoside (IPTG) with the final concentration of 1 mM at OD = 0.3 at 37°C overnight. Cells were pelleted, frozen at –80°C, and re-suspended in lysis buffer (750 mM NaCl, 10 mM Tris pH 8.0, 1 mM EDTA, 1 mM protease inhibitor mix). Cells were lysed by sonication on ice (five times, 30 s each step, cool down for 1 min after each sonication step), heated at 95°C for 15 min, and then centrifuged at 13,000 rpm at 4°C for 20 min. The supernatant was dialyzed overnight at 4°C against dialysis buffer (50 mM NaCl, 10 mM Tris pH 7.6, 1 mM EDTA). α Syn was purified on two HiTrap Q FF 1 ml anion exchange columns (GE Healthcare) in 25 mM Tris pH 7.7 with a NaCl gradient from 0–600 mM. α Syn fractions were collected as judged by 12% SDS-polyacrylamide gel electrophoresis. α Syn was further

purified by size-exclusion chromatography on a Superdex 75 26/600 prep grade 120 ml column (GE Healthcare) in SEC buffer (100 mM NaCl, 25 mM HEPES, 1 mM DTT, pH 8.0). The purification of α Syn was confirmed by SDS-PAGE and Western blotting analysis, and proteins were stored at -80°C .

Expression and Purification of K50-His6

K50-His6 was found to be insoluble when expressed in *E. coli* BL21 (DE3), which is why hybrid conditions were used for the purification of the protein from bacterial cells. *E. coli* BL21 (DE3) cells were transformed with pET22b-K50-His6 construct, and expression of 100 ml LB culture was induced with isopropyl IPTG with a final concentration of 0.1 mM at OD = 0.2 at 30°C for 4 h. Cells were pelleted and re-suspended in 4 ml resuspension buffer (20 mM Tris pH 8.0). Cells were disrupted by sonication on ice (5 times, 30 s each step, cool down for 1 min after each sonication step), and then centrifuged at 13,000 rpm in 4°C for 10 min. The supernatant was removed and the pellet was re-suspended in 3 ml cold isolation buffer (2 M urea, 20 mM Tris pH 8.0, 500 mM NaCl, 2% Triton-X 100). The sonication and centrifugation steps were repeated as above, the supernatant was collected and supplemented with imidazole to a final concentration of 10 mM. The protein was bound to Ni-NTA beads by agitation for 1.5 h at 4°C . The resin was settled by gravity and the beads were washed with 10 ml washing buffer (20 mM Tris pH 8.0, 10 mM Imidazole) and with 10 ml native washing buffer (50 mM Tris pH 8.0, 300 mM NaCl, 10 mM Imidazole). The protein was eluted with elution buffer (50 mM Tris pH 8.0, 300 mM NaCl, 250 mM Imidazole). The buffer was exchanged using Amicon® Ultra-3K centrifugal filter device with 250 mM NaCl, 20 mM HEPES, pH 8.0.

Ultracentrifugation and Fractionation

The sedimentation assay, extraction of SDS-soluble and insoluble α Syn protein fractions were performed as described (Popova et al., 2018). Equal amounts of yeast cells corresponding to total OD = 10 were collected by centrifugation and resuspended in lysis buffer (50 mM Tris-HCl pH 7.5, 1 mM EDTA, 5 mM DTT, 1 \times protease inhibitor mix (Roche). The cells were lysed by shaking with glass beads at 4°C . The crude lysate was centrifuged for 5 min at 500 g to pellet the cell debris. 200 μl of each cleared lysate was centrifuged at 100,000 g for 30 min. The supernatant was designated as a soluble protein. The pellet was washed 3 times with the lysis buffer, resuspended in 200 μl lysis buffer containing 2% SDS, and incubated on ice for 30 min. The suspension was centrifuged for 30 min at 100,000 g and the supernatant was labeled as SDS-soluble protein fraction. The pellet was washed three times with lysis buffer, resuspended in 200 μl 6 M urea, and designated as SDS-insoluble fraction (pellet). Equal amount from each fraction (20 μl) was analyzed by SDS-PAGE and Western blotting.

Thioflavin T Assay

For the modified Thioflavin T (ThT) assay (Giehm and Otzen, 2010) α Syn was incubated at a final concentration of 30 μM or 50 μM in 25 mM HEPES (pH = 6.5), 100 mM NaCl, 0.002%

SDS, and 100 μM Thioflavin T, either alone or in presence of the peptides at the indicated molar ratios in a final volume of 100 μl per well. The samples were incubated at 37°C for at least 100 h with continuous shaking in a black 96-well plate, pre-loaded with one glass bead per well, and covered with an adhesive plate sealer. Fibril formation was monitored by fluorescence every 2 min, with excitation at 440 nm and emission at 480 nm in a fluorescent plate reader (Tecan Infinite M200). Samples containing the peptides without α Syn were used as negative controls. All experiments were carried out in quadruplicates.

Transmission Electron Microscopy (TEM)

α Syn aggregation products were analyzed by negative staining and transmission electron microscopy according to Hoppert and Holzenburg (Hoppert and Holzenburg, 1998). In brief, a carbon film, evaporated onto a freshly cleaved mica surface, was partially floated off on the surface of a sample droplet for 1 min. The carbon/mica sandwich was removed, allowing the carbon film to fall back into its original position. For washing, the sandwich was transferred to a water drop and treated in the same way for 3 s to remove buffer constituents. Staining of the sample was performed by slowly immersing the sandwich into phosphotungstic acid (pH 7.0, 3%); the carbon film was completely floated off. Electron microscope grids (300 mesh, Plano, Wetzlar, Germany) were used to pick up the floating carbon film. After the grid was removed from the droplet, excess fluid was blotted by touching the grid vertically with a piece of filter paper. After drying, the negative stained samples were imaged using a Jeol EM 1011 transmission electron microscope (Jeol, Echting, Germany), equipped with a Gatan Orius 4 K camera (Gatan, Munich, Germany).

Human Cells

Human neuroglioma cells (H4) were maintained in Opti-MEM I Reduced Serum Medium (Life Technologies-Gibco) supplemented with 10% fetal bovine serum Gold (FBS) (PAA, Cölbe, Germany) at 37°C in an atmosphere of 5% CO_2 . The cells were plated in 12-well plates (Costar, Corning, New York) 24 h before transfection. H4 cells were transfected with FuGENE® six Transfection Reagent (Promega, Madison, WI) according to the manufacturer's instructions with equal amounts of plasmids of SynT and synphilin-1 as previously described (McLean et al., 2001; Lázaro et al., 2014). Twenty-four hours after the transfections, the cells were treated with K84s or K102s peptides at a concentration of 1 μM . 2% Ethanol was used as vehicle control. After 24 h, the cells were subjected to immunocytochemistry to examine α Syn inclusion formation.

Immunocytochemistry

Twenty-four hours after exposition to the peptides, cells were washed with PBS and fixed with 4% paraformaldehyde for 10 min at room temperature. Cells were then permeabilized with 0.5% Triton X-100 (Sigma) for 20 min at room temperature and blocked in 1.5% normal goat serum (PAA)/PBS for 1 h. Cells were incubated overnight with mouse anti- α Syn primary antibody (1:1,000, BD Transduction Laboratories, NJ), and afterward with a secondary antibody (Alexa Fluor 568 donkey anti-mouse IgG)

for 2 h at room temperature. Finally, cells were stained with DAPI (Life Technologies-Invitrogen) (1:5,000 in PBS) for 10 min and maintained in PBS for epifluorescence microscopy.

Quantification of α Syn Inclusions

Transfected cells were scored based on the pattern of α Syn inclusions and classified as presented. Results were expressed as the percentage of the total number of transfected cells, and a minimum of 50 cells was counted *per* condition.

Synthetic Peptides

Custom synthesis and analysis of the FITC-K84s and FITC-K102s was performed by the company ProteoGenix (Schiltigheim, France) (**Supplementary Figure 1**). Ten microliters of sample K102 was injected on an HPLC column (Kromasil 100-5C18, 4.6×250 mm, $5 \mu\text{m}$) using a linear acetonitrile/0.1% (v/v) formic acid in H_2O /0.1% (v/v) formic acid gradient (from 32% to 57% (v/v) acetonitrile/0.1 formic acid in 25 min, plus additional 5 min with 100% (v/v) acetonitrile/0.1 formic acid). 10 μl of sample K84 was injected on a HPLC column (Agela 100-5C18, 4.6×250 mm, $5 \mu\text{m}$) using a linear acetonitrile/0.1% (v/v) formic acid in H_2O /0.1% (v/v) formic acid gradient (from 35% to 60% (v/v) acetonitrile/0.1 formic acid in 25 min, plus additional 5 min with 100% (v/v) acetonitrile/0.1 formic acid). The flow rate was 1 ml/min. Detection was performed at 220 nm.

Peptides K50s, K89s, K94s, and K97s were synthesized by the company GenScript (Leiden, Netherlands) and analyzed at the Service Unit Metabolomics at the Institute of Microbiology and Genetics (University of Göttingen) (**Supplementary Figure 2**). Peptides were dissolved in $\text{AcCN}/\text{H}_2\text{O}$ (2% v/v) and analyzed with a Q ExactiveTM Focus orbitrap mass spectrometer coupled to an UltiMateTM 3000 HPLC (Thermo Fisher Scientific). The pure solvent was used as control. Five microliters of each sample was injected on a HPLC column (AcclaimTM 120, C18, $5 \mu\text{m}$, 120 Å, 4.6×100 mm (Thermo Fisher Scientific)) using a linear acetonitrile/0.1% (v/v) formic acid in H_2O /0.1% (v/v) formic acid gradient (from 5% to 95% (v/v) acetonitrile/0.1 formic acid in 20 min, plus additional 10 min with 95% (v/v) acetonitrile/0.1 formic acid) with a flow rate of 0.8 ml/min at 30°C. The measurements were performed in a mass range of 70–1,050 m/z in positive mode with electrospray ionization (ESI). A CoronaTM VeoTM RS Charged aerosol detector (CAD) (Thermo Fisher Scientific) was used as an additional detector. Data acquisition and analysis were performed with Thermo Scientific XcaliburTM 4.1 (Thermo Fisher Scientific) and with FreeStyleTM 1.6 (Thermo Fisher Scientific) software.

RESULTS

Screening for α Syn Interacting Peptides and for Suppressors of Toxicity

A peptide library consisting of approximately one million peptide variants was utilized for intracellular screening for interaction partners of α Syn using the yeast-two-hybrid (Y2H) method. The peptide library was generated by random insertion of 60 nt

random sequences flanked by *EcoRI* and *XhoI* restriction sites into the scaffold B1 domain (nt 1483 - nt 1857) of protein G from *Staphylococcus aureus* at a site of a loop between two β -sheets (Fritz and Green, 1996). The random sequence may contain stop codons leading to peptides of variable length lacking the C-terminus of the protein GB1 domain. The library may also contain clones with a 61 nt insert that are not in frame with the C-terminal part of the protein GB1 domain resulting in a C-terminal addition of the sequence PSRH* to the random peptide. The small peptides are expressed as a fusion to the B42 transcription activation domain (AD) (“prey”). The “bait” protein α Syn was expressed as a fusion to the *GAL4* DNA-binding domain (BD). The Y2H screen was performed by selection for cellular yeast growth as previously described (James et al., 1996). Productive interaction between the bait and the prey brings the transcription activation and DNA-binding domains together and initiates the expression of two biosynthetic reporter genes (*ADE2* and *HIS3*) that allow growth in the absence of histidine and adenine (**Supplementary Figure 3**). No background yeast growth was observed in the Y2H screening indicating that the GB1 scaffold that is present in all clones is not able to either interact with the bait protein or alter its toxic properties. An optimized interaction-mating protocol was used for improved yield of double transformants to cover efficiently the complexity of the peptide library (Soellick and Uhrig, 2001). Optimization of screening conditions was performed by testing for auto-activation of the bait construct (α Syn) aiming to increase the stringency and avoid false positives. Two rounds of Y2H screenings were independently performed to achieve unbiased results and to increase the chances for the identification of interaction partners. Two-hundred and thirty-four clones were selected that grew on a prototrophic semi-solid growth medium without histidine. These putative interaction partners from the initial Y2H screen were validated for their potential to induce the expression of the reporter genes on selective media in a secondary screen. The clones were inoculated in a liquid selective medium, and 90 clones were selected that showed the most pronounced growth for further validation. Growth assays were performed in an ordered array using an automatic robotic platform on multiple selection plates with increasing stringency, achieved by the addition of different concentration of the histidine analogue 3-AT (3-Amino-1,2,4-triazole), a competitive inhibitor of the enzyme derived of the *HIS3* gene, and double selection in the absence of histidine and adenine (**Supplementary Figure 4A**). Thirty-seven clones were selected based on their growth on selection media, plasmids were rescued and sequenced.

A second alternative and novel screening approach was used to directly select peptides that suppress the toxicity of α Syn (“toxicity-rescue screen”). A constructed yeast strain with moderate growth inhibition upon expression of α Syn (**Supplementary Figure 4B**) was mated with yeasts of the opposite mating type carrying the peptide library. Screening for yeast diploid cells that revealed enhanced growth upon expression of individual library variants was performed on large selection plates, supplemented with galactose for induction of α Syn expression. Colonies that appeared during the first

3 days of growth at 30°C were picked and the corresponding plasmids were isolated and amplified in bacteria. Thirty-one unique individual library representatives were characterized by sequencing.

Seven Peptide Constructs Suppress α Syn Toxicity and Aggregation

The isolated peptide constructs from the Y2H screen and toxicity-rescue screen were individually tested for their ability to suppress α Syn toxicity in yeast. The starting point was an inducible “high-tox” yeast strain that harbors three genomically integrated α Syn-GFP-encoding gene copies resulting in a strong growth retardation phenotype (Petroi et al., 2012), which was transformed individually with the peptide constructs. Spotting tests were performed to determine the effect of different peptide constructs on yeast growth. Seven clones demonstrated reproducible suppression of α Syn toxicity, as shown by the spotting test (Figure 1A). Two of them (K50 and K117) were isolated from the Y2H screen and five peptide constructs (K84, K89, K94, K97, K102) were isolated from the toxicity-rescue screen. There were no identical peptides, isolated from both screens. The toxicity suppression effect was specific for the isolated peptides since growth tests of yeast cells carrying random peptides from the screen as a control revealed no growth enhancement effect (Supplementary Figure 5A). These results suggest that the modulation of α Syn toxicity is attributed to the unique peptide sequences. Next, the peptide-encoding sequences including the flanking scaffold protein sequences but without the bulky activation domain were re-cloned behind the constitutive *GPD* promoter (Table 3). K50 and K117 contain the full-length scaffold protein sequence plus the variable part, whereas the peptides isolated from the toxicity-rescue screen had premature stop codons and were shorter in length. Yeast high-tox strain was re-transformed with the new constructs. Growth assays on solid and in liquid medium revealed similar suppression of α Syn-induced toxicity when the peptides were expressed without the N-terminal activation domain (Figures 1B,C). Expression of the peptide constructs alone did not affect the growth of yeast wild-type cells (Supplementary Figure 5B). Immunoblotting analysis revealed similar steady-state levels of α Syn protein in the presence and absence of the peptide constructs after 6 h induction of protein expression (Figures 1D,E) indicating that the differences in toxicity are not due to changed α Syn protein levels.

We analyzed whether the expression of the peptides affects the aggregate formation of α Syn-GFP. In yeast, the number of cells with aggregates is an established and very sensitive variable that correlates with cytotoxicity (Outeiro and Lindquist, 2003; Petroi et al., 2012). Fluorescent microscopy studies were performed with α Syn high-tox strain in the presence and absence of peptide constructs (Figure 2A). The numbers of cells displaying aggregates were significantly reduced upon co-expression of AD-peptides or peptides without the AD, in comparison to the control (Figures 2B,C). Expression of the peptides might affect also other toxic forms of α Syn that precede aggregation.

To assess, whether the differences in growth and aggregate formation correlate with changes in cytotoxicity, propidium

iodide (PI) staining for membrane permeability was performed as a sensitive method for quantification of yeast viability. Flow cytometry measurements of cells, expressing α Syn and the peptide constructs showed a significantly decreased number of PI-positive cells in comparison to α Syn expression in the absence of peptide expression (Figure 2D). These results correlate with the data from the growth assays and reveal that the expression of the seven peptides significantly reduces α Syn aggregate formation and enhances cell growth and viability.

Peptides Reduce the Accumulation of Reactive Oxygen Species

Oxidative stress is a central event in PD that triggers α Syn misfolding and aggregation (Giasson et al., 2000). We analyzed the effect of peptide expression on the accumulation of reactive oxygen species (ROS) by using the dye Dihydrorhodamine 123 (DHR123). DHR123 accumulates in cells, where it is oxidized by free radicals to the bright green fluorescent product rhodamine 123. Expression of α Syn resulted in a significant increase in the number of cells accumulating ROS in comparison to the wild-type cells, as assessed by flow cytometry. Co-expression of the peptides significantly reduced the number of cells that accumulate ROS (Figure 3). These results indicate that the expression of the seven peptides affects specific molecular pathways that attenuate the accumulation of ROS.

The Peptide-Mediated Suppression of Toxicity Is Specific for α Syn

The specificity of the effect of peptide expression for α Syn was evaluated. The seven peptide constructs were transformed into a yeast disease model of Huntington disease that expresses a toxic polypeptide unrelated to α Syn. Expression of exon one of human huntingtin with 103 glutamine residues (Htt103Q) is toxic to yeast cells and forms aggregates (Duennwald et al., 2006). A yeast strain that expressed the Htt103Q-CFP construct with modest toxicity was constructed. Expression of the peptide constructs did neither suppress toxicity nor aggregate formation (Figure 4). These results indicate that the observed effects of peptide construct expression are specific to α Syn and that there is no indication of overlap with the molecular mechanisms, suppressing the Htt103Q toxicity. Interestingly, expression of K50 and K117 increased the Htt103Q toxicity, indicating distinct pathways involved in general protection from misfolded proteins in yeast. These results support previous findings from genetic screens in yeast that genes suppressing the toxicity of α Syn and Htt103Q do not overlap (Willingham et al., 2003; Cooper et al., 2006).

Expression of K50, K84, and K102 Reduces the Levels of Insoluble α Syn

The solubility of α Syn in cells expressing different peptide constructs was determined to characterize the effect of peptide construct expression on the biochemical nature of α Syn species in yeast cells. Six hours after induction of protein expression crude protein extracts from equal numbers of

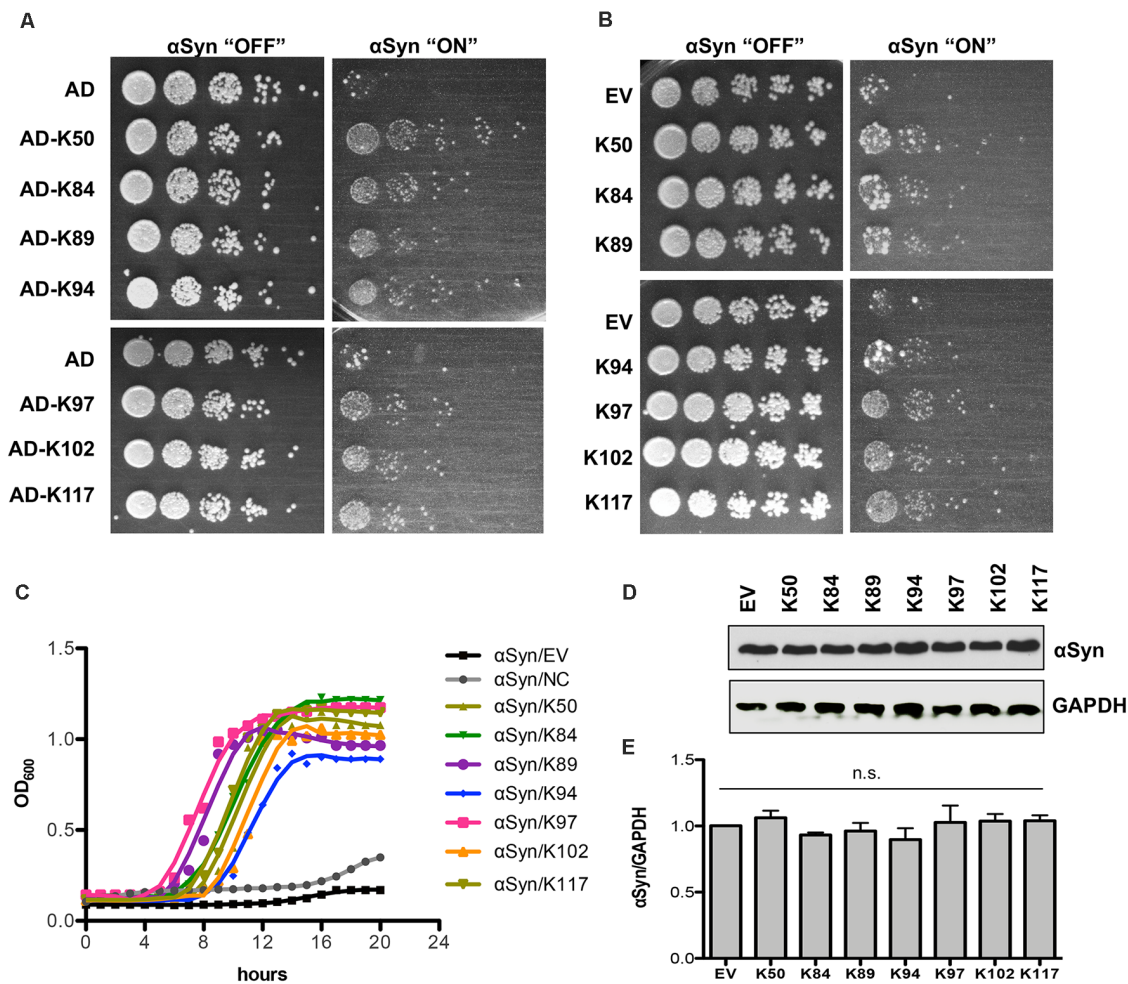


FIGURE 1 | Expression of seven peptide constructs reduces α Syn-induced growth inhibition. **(A)** The yeast strain that harbors three copies of *GAL1*-driven α Syn-GFP-encoding gene (inducible "high-tox" strain RH3468) was transformed with the plasmid constructs, isolated from the screen. The Y2H plasmids contain the peptide-encoding sequence, fused to the B42-activation domain (AD). Yeast cells were spotted in 10-fold dilution on SC-Leu-Ura selective plates containing glucose (control: α Syn "OFF") or galactose (α Syn "ON") for induction of *GAL1* promoter. Plasmid with AD was used as a control. Images of the plates were captured on the third day. **(B)** The peptide-encoding sequences were re-cloned without the N-terminal activation domain and driven by the *GPD* promoter. The yeast high-tox strain was transformed with the corresponding plasmids and spotting assays were performed. Empty vector (EV) was used as a control. **(C)** Growth analyses of yeast cells from **(B)** in galactose-containing medium for 20 h. **(D)** Immunoblotting analysis of protein crude extracts of yeast cells from **(B)** after 6 h induction in galactose-containing medium with an anti- α Syn antibody. Anti-GAPDH antibody was used as a loading control. **(E)** Densitometric analysis of the immunodetection of α Syn-GFP, relative to the loading control GAPDH. n.s.: not significant, ($n = 3$).

TABLE 3 | Amino acid sequences of peptides expressed in yeast.

Peptide construct	Amino acid sequence
K50	MYKLILNGKEFSRPRWARTVWRASMGALAIMLALET TLKG ETTTEAVDAATAEKVFKQYANDNGVDGEWYDDATKTFTVTE
K84	MYKLILNGKEFLWVGCLRGSAGIECVVHGGPPSRH
K89	MYKLILNGKEFVQGLMPRRAAWGGRSSRGRWPSRH
K94	MYKLILNGKEFIARSMGNMRMSERRRG
K97	MYKLILNGKEFLGCLPLSTAPLACWRTG
K102	MYKLILNGKEFLKRWARSTRWGTASCGGS
K117	MYKLILNGKEFGMILRMCWRVQAQMMRVPLCLALET TLKG ETTTEAVDAATAEKVFKQYANDNGVDGEWYDDATKTFTVTE

The sequence of the GB1-scaffold protein is highlighted in red. K50 and K117 were isolated from the Y2H screen. The other peptides were isolated from the toxicity-rescue screen.

cells were prepared. The protein extracts were subjected to fractionation to produce soluble, SDS-soluble, and SDS-insoluble fractions, and equal amounts of the fractions were loaded on

SDS gel (**Figure 5A**). Comparison of the different fractions revealed significant decreases of SDS-insoluble α Syn (pellet) in cells, expressing K50, K84, and K102 compared to controls

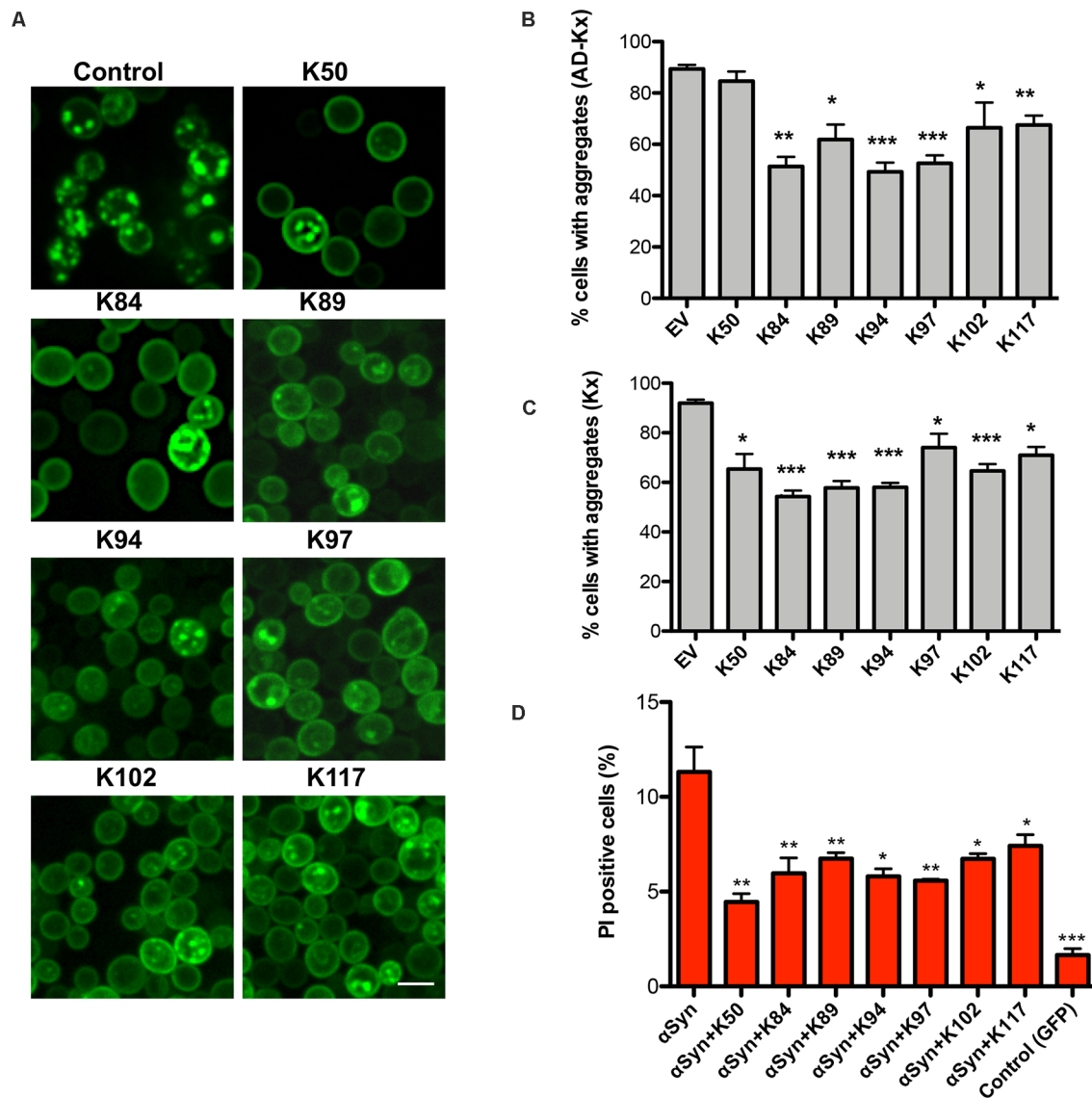


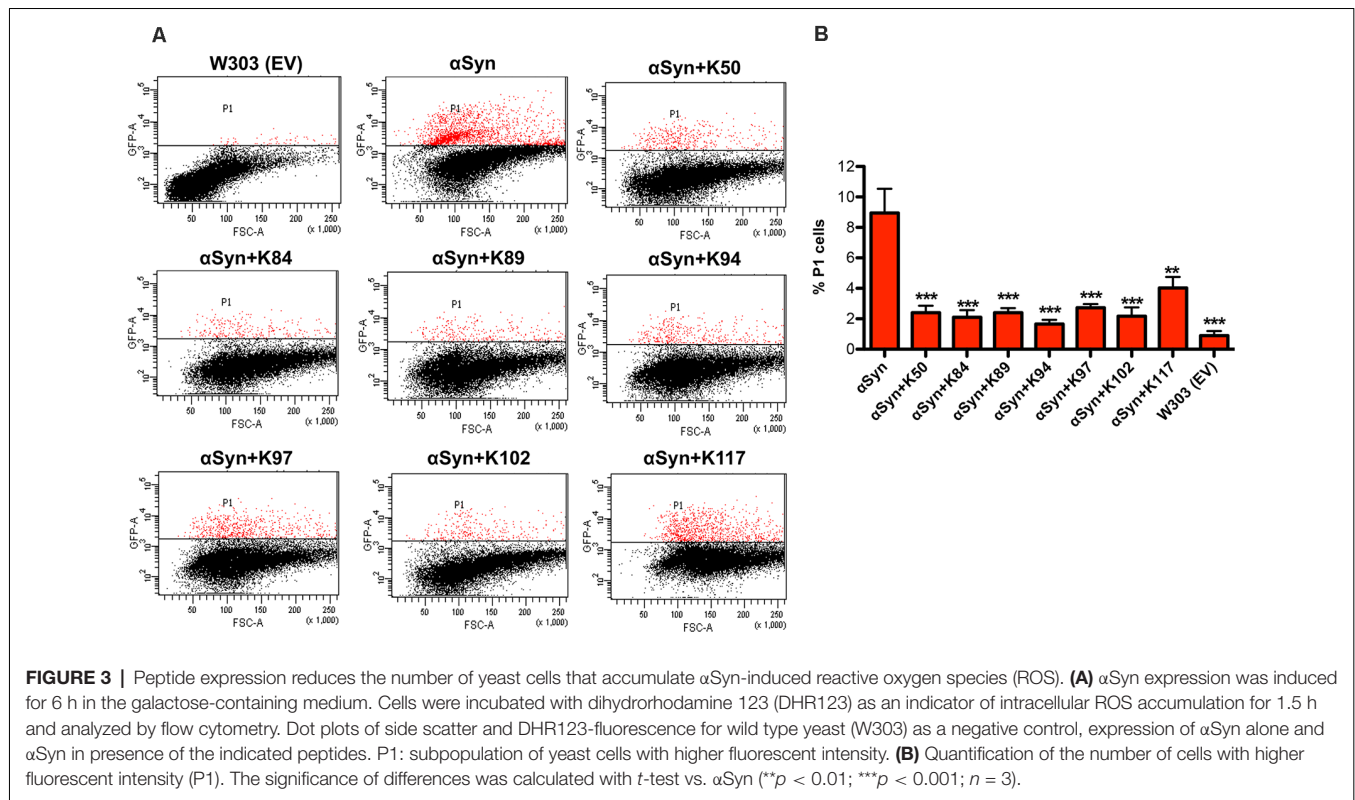
FIGURE 2 | Peptide-mediated reduction of α Syn-GFP aggregation and increased cell viability. **(A)** Life-cell microscopy 6 h after induction of *GAL1*- α Syn-GFP expression in galactose-containing medium. Yeast cells (RH3468) were co-transformed with plasmids harboring the indicated peptide constructs under the constitutive *GPD* promoter or empty vector as a control. Scale bar: 2 μ m. Quantification of the percentage of cells with α Syn aggregates, co-expressing AD-peptide (AD-Kx) **(B)** or the peptides without AD (Kx) **(C)**. Significance of differences was calculated with *t*-test (* p < 0.05; ** p < 0.01; *** p < 0.001; n = 4). **(D)** Propidium iodide (PI) fluorescence intensity of yeast cells, expressing α Syn and indicated peptides after 24 h of induction was assessed by flow cytometry. Quantification of PI-positive cells with higher fluorescent intensities than the background 6 h after induction of α Syn expression. Cells expressing GFP were used as a negative control. Significance of differences was calculated with *t*-test relative to α Syn (* p < 0.05; ** p < 0.01; n = 4).

(Figure 5B). This suggests that K50, K84, and K102 inhibit insoluble α Syn species formation in living cells.

K84s and K102s Peptides Inhibit α Syn Aggregation *In vitro*

The formation of α Syn amyloid fibrils can be reproduced *in vitro* by incubation of recombinant α Syn protein in the presence of Thioflavin-T (ThT), a dye that specifically binds to amyloid fibrils. We compared the aggregation properties of α Syn in the absence and presence of each of the identified synthetic peptides

to determine, whether the peptides directly affect the kinetics of α Syn amyloid formation. Minimal peptide sequences shortened to the variable region were deduced based on secondary structure predictions of the peptides that were expressed in yeast (Table 4). Flanking amino acids were incorporated where they stabilized the secondary structure as predicted with PEP FOLD 3 (Shen et al., 2014) and the peptides were chemically synthesized (denoted as Ks; Supplementary Figure 6). Among the seven isolated peptides, K50 and K117 contain the C-terminal scaffold domain and are longer. K50 was expressed in *E. coli* and purified



as a His-tagged recombinant protein. Attempts to purify soluble K117 in *E. coli* were unsuccessful, hence the peptide was not further used for *in vitro* studies. α Syn recombinant protein was purified as described (Miranda et al., 2013). Fifty micromolar α Syn was incubated with the peptides at molar ratios of 1:0.5 or 1:1, added at time point 0. The kinetics of aggregation was monitored by ThT fluorescence every 15 min for 100 h. The addition of peptides K50 at a molar ratio of 1:0.2 and K84s, K89s, and K102s at a molar ratio of 1:1 reduced the ThT signal by more than 75%, indicating that the peptides were able to inhibit the aggregation of α Syn (Figures 5C–F, Supplementary Figure 7). At increasingly stoichiometric ratios, we observed progressively reduced inhibition consistent with a general dose-dependence. A modest reduction of α Syn aggregation was observed for K97s (Supplementary Figure 7), whereas addition of K50s and K94s had no effect on α Syn aggregation (Supplementary Figure 7). K89s and K102s reduced the lag phase of the aggregation process, while at the same time reducing the maximum ThT fluorescence signal, indicating a reduction in aggregation. These data suggest that the peptides change the fibrilization kinetics and the overall formation of ThT-positive species.

As a second direct qualitative measure for fibril formation, samples used in continuous growth experiments were imaged using transmission electron microscopy (TEM). We analyzed the morphological features of the aggregates at a stoichiometry of 1:1 (1:0.2 for K50) since it was most effective in ThT experiments. α Syn control formed typical long unbranched amyloid fibrils (the fully assembled polymer), formed by two twisted protofibrils (Figures 6A,B), similar to observed structures of α Syn fibrils

(Dearborn et al., 2016; Guerrero-Ferreira et al., 2018). Samples incubated with K50, K84s and K102s were inhibited in fibril formation. Small round globular structures that resemble in morphology observed oligomeric species (Cappai et al., 2005; Pieri et al., 2016), and a few short fibrils could be observed. Aggregation in presence of K89s resulted in the formation of long twisted fibrils. We measured the periodicity of α Syn fibrils formed in the presence and absence of K89s. Based on measurements of straight fibrils outside of crowded regions, the periodicity was found to be significantly increased from 116 ± 8.5 nm for α Syn to 145.5 ± 12.5 nm in presence of K89s (Figures 6B,C). Thus, K89s changed the fibril morphology that might translate into differences in cytotoxicity. Similarly, the C-terminally truncated form of α Syn that shows stronger cytotoxicity (Tanaka et al., 2019) forms twisted fibrils with reduced periodicity (Iyer et al., 2017). The addition of K97s reduced the fibril load and the length of the fibrils. These data corroborate the observed effects of peptides in living cells and indicate direct interference of the peptides with α Syn amyloid formation. The results suggest K84s and K102s synthetic peptides as the most promising inhibitors of α Syn aggregation due to their short length and inhibition propensity.

K50, K84s, K89s, and K102s Act at Early Steps of Aggregation by Modulating the Oligomeric State of α Syn

We investigated whether the inhibition of α Syn aggregation by the peptides is accompanied by modulation of the low molecular weight oligomeric species. Equal amounts of samples

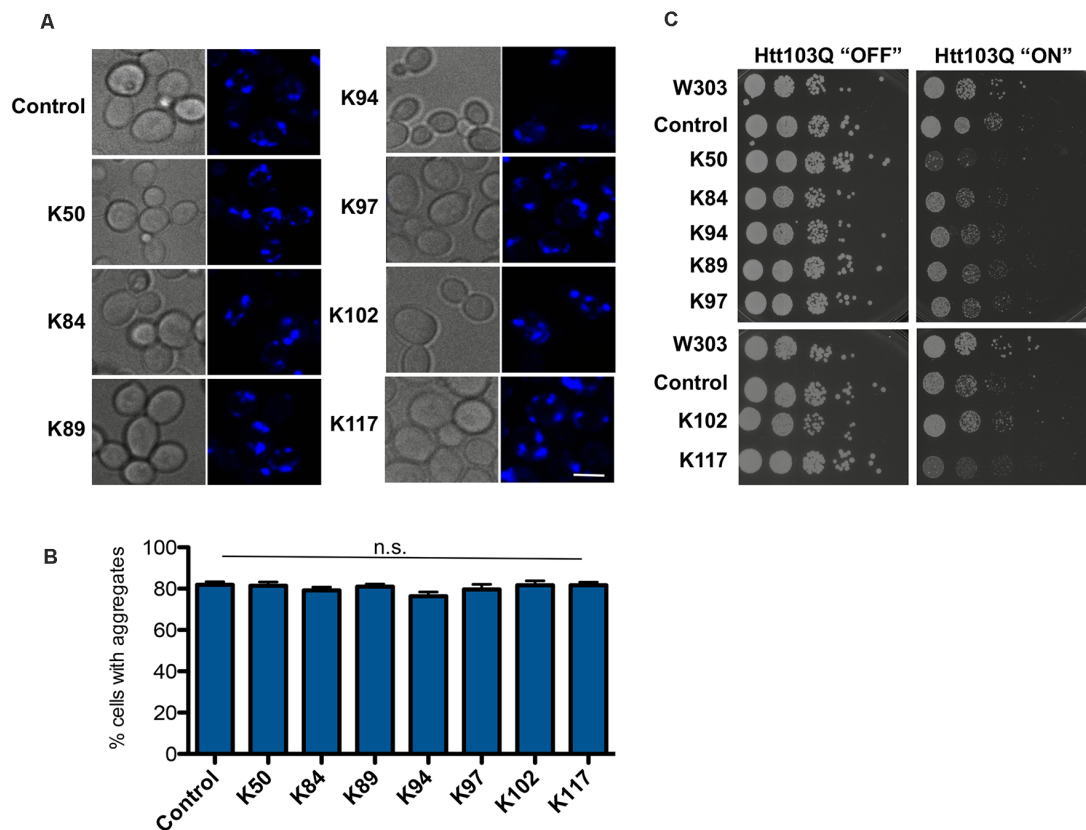


FIGURE 4 | Huntingtin-103Q aggregation and cellular yeast growth phenotypes are independent of the presence of α Syn-specific peptides. **(A)** Life cell microscopy of yeast strain RH3788, co-expressing huntingtin construct with 103 PolyQ repeats (Htt103Q Δ Pro-CFP) and the indicated peptide constructs or empty vector as a control. Yeast cells, pre-grown to mid-log phase, were induced in galactose-containing medium and examined for aggregates at 6 h of induction. Expression of the Htt103Q variant revealed the formation of fluorescent foci. Scale bar: 5 μ m. **(B)** Aggregate quantification of yeast cells, expressing Htt103Q construct. For each strain, the number of cells displaying cytoplasmic foci is presented as a percent of the total number of cells counted. For quantification of aggregation at least 200 cells were counted. **(C)** Yeast cells from **(A)** were spotted in 10-fold dilutions on selection plates containing glucose (Htt103Q "OFF") or galactose (Htt103Q "ON") for induction of *GAL1* promoter. W303—wildtype yeast background strain, transformed with empty vectors. Control: Htt103Q Δ ProCFP strain, transformed with empty vector. n.s.: not significant.

were collected from the endpoint of aggregation reactions and analyzed by SDS-PAGE and immunoblotting (**Figure 7**). α Syn SDS-stable oligomeric species, migrating at 15 kDa, 36 kDa, and 70 kDa were readily detected, corresponding to monomeric and different oligomeric α Syn species. The band intensity of the oligomeric species was evaluated by densitometry and compared to the control, where no peptide was present. A decrease in the accumulation of α Syn oligomeric species was observed with increasing concentration of K84s, K89s, and K50. The addition of K102s almost completely abolished the formation of α Syn oligomers. These results suggest that K50, K84s, K89s significantly suppress the first steps of oligomerization without completely inhibiting it, whereas K102s strongly inhibit the formation of low molecular weight α Syn oligomers.

K84s Reduces the Formation of α Syn Aggregates in Human Cells

Finally, we tested the ability of K84s and K102s to modulate α Syn aggregation in human cells. Human neuroglioma cells (H4)

have been extensively used to model α Syn aggregation. In this model, cells co-expressing a C-terminally modified α Syn (SynT) and synphilin-1, exhibit the formation of α Syn inclusions, as previously described (McLean et al., 2001; Lázaro et al., 2014). We have previously shown that not all α Syn inclusions formed display amyloid-like properties and are Thioflavin positive, as they likely represent different types of protein aggregates (Lázaro et al., 2014). The peptides were labeled with fluorescein (FITC) to follow their internalization into the cells. However, due to the low amounts used in this study, especially for K102, the signal was low. Twenty-four hours after transfection, the cells were incubated with 1 μ M K84s or K102s peptide. α Syn inclusion formation was assessed after 24 h. Treatment with 1 μ M K84s resulted in a significant reduction in the percentage of cells with inclusions (**Figure 8**).

DISCUSSION

The aggregation of α Syn into amyloid fibrils is a major pathogenic process in PD and other synucleinopathies

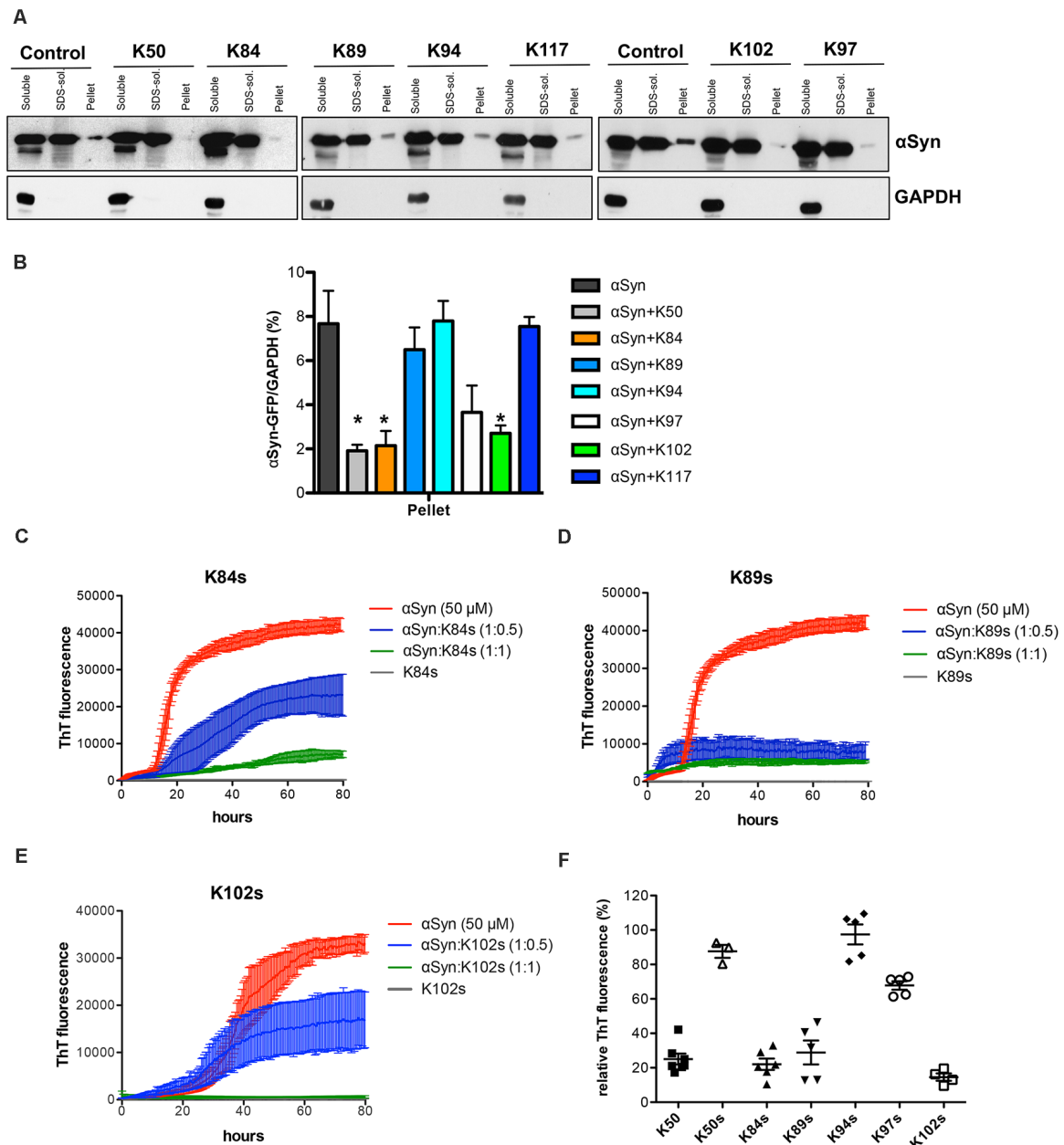


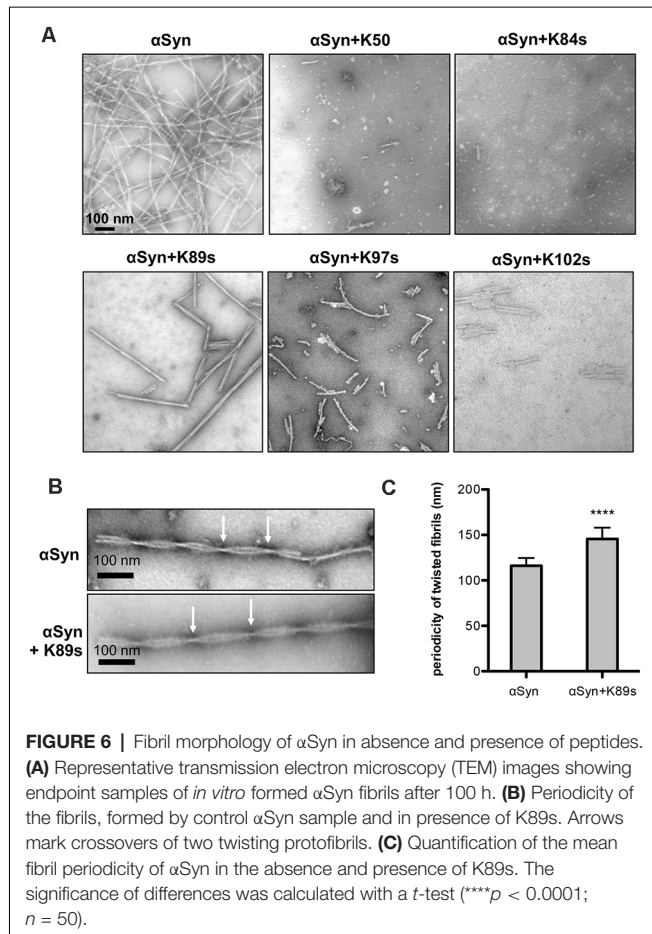
FIGURE 5 | Distribution of α Syn-GFP levels across different solubility fractions. **(A)** Yeast cells, expressing *GAL1*-driven α Syn-GFP from three genomic copies and the indicated peptide constructs or the corresponding empty vector (control) were induced for 6 h in galactose medium. Starting from an equal number of cells, crude protein extracts were prepared and fractionated by ultracentrifugation to produce soluble, SDS-soluble and SDS-insoluble fractions (pellet), revealing the level of insoluble α Syn. Equal amounts from all fractions were analyzed by immunoblotting with anti- α Syn. The membranes were stripped and probed with an anti-GAPDH antibody as a loading control. **(B)** Densitometric analysis of the immunodetection of α Syn-GFP relative to GAPDH loading control. The significance of differences was calculated with *t*-test vs. α Syn ($p < 0.05$; $n = 4$). **(C)** Peptide-mediated effect on the amyloidogenic properties of α Syn *in vitro*. Aggregation kinetics of α Syn in the presence and absence of the synthetic peptides K84s **(C)**, K89s **(D)**, or K102s **(E)** monitored by ThT fluorescence emission. α Syn was incubated at a concentration of 50 μ M in the absence or upon addition of the peptides in the indicated molar ratios at time point 0. The ThT fluorescence emission was recorded every 15 min for 100 h. Incubation of the peptides alone served as a control. Representative curves showing the fluorescent signal over time. **(F)** Quantification of the relative ThT fluorescence signal in presence of the indicated peptides at molar ratio 1:1 (1:0.2 for K50) after 100 h relative to α Syn alone. The data are mean of five independent experiments.

(Lashuel et al., 2013; Villar-Piqué et al., 2015). Accumulating evidence suggests that oligomers/protofibrils exert damaging effects in the affected cells. Membrane damage, mitochondrial

defects, and synaptic dysfunction are some examples of the proposed pathogenic mechanisms (Bengoa-Vergniory et al., 2017). This suggests that inhibition of α Syn oligomerization

TABLE 4 | Amino acid sequences and physicochemical properties of chemically synthesized short peptides.

Synthetic peptide	Amino acid sequence	Length (aa)	Charge	Nature	pI
K50s	FSPRWARTVWRASMGALAIMLALE	24	2	basic	12.2
K84s	FLVWGCLRGSAIGECVWHGGPPSRH	25	3	basic	8.2
K89s	VQGLMPRRAAWGGRSSRGWRPSRH	24	7	basic	13.2
K94s	IARSMGNMRMSERRRG	16	4	basic	12.7
K97s	LGCLPLSTAPLACWRTG	17	1	basic	8.2
K102s	FLKRWARSTRWGTASCGGS	19	4	basic	12.2



and conversion into fibrillar aggregates is a viable strategy for therapeutic intervention in PD. The development of PD therapies that reduce or block α Syn aggregation is a priority goal in Parkinson's research. Such therapies could potentially prevent or delay the onset of PD or slow its progression.

Peptides are very promising candidates for drug development, especially because of their small size, functional diversity, and a high degree of specificity towards a given target. Short peptides are composed of natural amino acids and their degradation is less likely to be toxic in comparison to synthetic small molecules. Moreover, they can be quickly and cheaply synthesized and also can undergo several chemical modifications for tuning of their properties such as membrane permeability or stability. Currently, there are more than 60 FDA-approved peptide drugs on the market, including peptide inhibitors for the treatment

of neurodegenerative diseases (Fosgerau and Hoffmann, 2015; Baig et al., 2018). Most of the attempts to isolate peptides able to inhibit α Syn aggregation utilize semi-rationally designed libraries of peptides spanning parts of the N-terminal domain (1–60), which contains a multi-repeated consensus sequence (KTKEGV) and has an alpha-helical propensity, or the central domain (61–95), known as non-amyloid-beta component (NAC) that is highly hydrophobic and is involved in α Syn aggregation (El-Agnaf et al., 2004; Abe et al., 2007; Cheruvara et al., 2015; Torpey et al., 2020). Yeast was successfully used before only for the selection of candidates from a cyclic octamer peptide library that were able to rescue α Syn toxicity (Kritzer et al., 2009). In this study, we isolated short peptides that inhibit α Syn induced toxicity and aggregation using yeast as a screening platform. For the first time, a random library of short linear peptides was expressed in the PD model and directly screened for toxicity-rescue. This approach has the advantage that the candidates are selected based on the phenotype rather than affinity and toxic sequences are avoided.

We screened a library with a diversity $\sim 1 \times 10^6$ random amino acid sequences with a length of 20 residues, inserted into the B1 domain of protein G from *Staphylococcus aureus* at the site of a loop between two β -sheets as a scaffold. The diversity of the library represents only a small fraction of the formal sequencing space of 20^{20} possible sequences that are beyond a real-life experiment. However, protein interactions are governed frequently by just a few hydrophobic and/or charged residues spaced in the appropriate way that offers a large number of participating peptide sequences with properties suitable for interaction with a target protein. The scaffold stably folds into a 3D structure, which enhances the presentation of the random peptides towards the target protein. Seven peptides could be identified that can diminish α Syn aggregation and toxicity in yeast. Plasmid-borne expression of the peptides rescued the strong growth retardation phenotype of a high-tox yeast strain, expressing α Syn and increased cell viability. Importantly, the expression of the peptides significantly reduced the number of cells with aggregates. This effect was specific for α Syn since peptide expression had no impact on the aggregate formation of Htt103Q, a toxic and aggregation-prone polypeptide involved in Huntington's disease.

Two consecutive optimization steps resulted in the identification of minimal peptide sequences that are still able to inhibit α Syn aggregation: (i) the peptides were expressed without the bulky N-terminal activation domain, keeping the first 11 amino acids from the scaffold protein; (ii) the peptide sequences of K50, K84, K89, K94, K97, and K102 were shortened

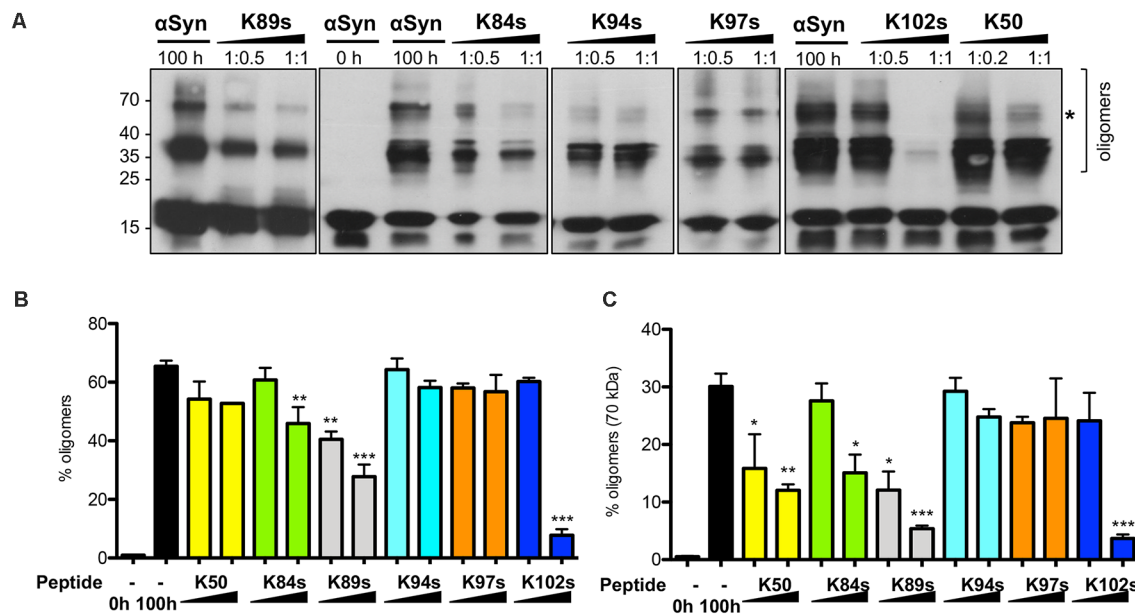


FIGURE 7 | Peptide-mediated reduction in α Syn oligomerization *in vitro*. **(A)** α Syn was incubated in the absence or presence of peptides in the indicated molar ratios. A sample at the initial time point (0 h) served as a control. Equal amounts of samples were collected after 100 h and analyzed by immunoblotting with the anti- α Syn antibody. **(B)** Densitometric analysis of the immunodetection of α Syn oligomeric species. The relative amount of α Syn oligomeric species was normalized to the total immunodetection/well. **(C)** The relative amount of higher molecular weight α Syn oligomeric species (70 kDa band, indicated with *), normalized to the total immunodetection/well. Significance of differences was calculated with *t*-test vs. α Syn without addition of peptides (black bars) (**p* < 0.05; ***p* < 0.01; ****p* < 0.001; *n* = 3).

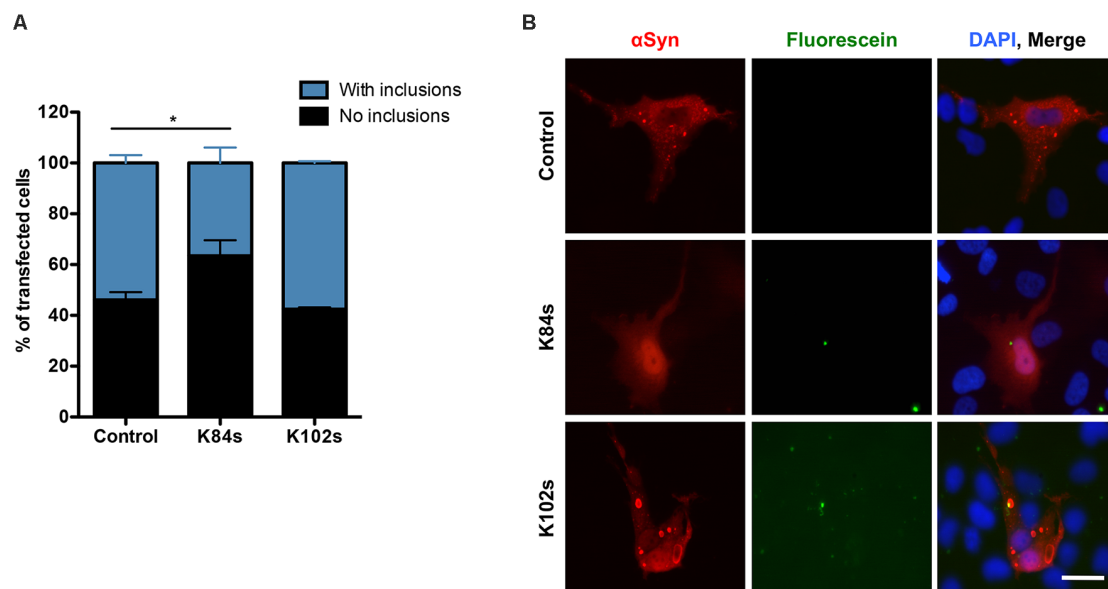


FIGURE 8 | K84s reduces α Syn aggregation in human cells. **(A)** H4 cells were transfected with α Syn and treated with K84s (1 μ M) or K102s (1 μ M). Control: 2% ethanol (vehicle). Significance of differences was calculated with one-side *t*-test (**p* < 0.05; *n* = 3). **(B)** Representative images of transfected cells treated with 1 μ M of K84s and K102s. Scale bar = 30 μ m.

to the variable region and synthetic peptides (denoted with s) with a length between 16 and 25 amino acids were used for *in vitro* aggregation assays. The addition of peptides K50, K84s,

K89s, and K102s reduced α Syn amyloid formation *in vitro* by more than 75%. The ability of the peptides to inhibit α Syn aggregation was confirmed with TEM assays. The addition of

K50 and K84s revealed the formation of oligomeric assemblies of α Syn similar to previously observed (Carija et al., 2019). The activity of the peptides was concentration-dependent and still evident in the sub-stoichiometric ratio of 1:0.5. This suggests that the peptides bind to oligomeric rather than to monomeric α Syn species. The synthetic K50s peptide corresponding to the short variable region of K50 lost the inhibition activity, suggesting changes in the structural properties of the polypeptide.

Oligomers are the intermediate species of the α Syn aggregation process. Their characterization is difficult due to their heterogeneity and variability. *in vitro*, both, on-pathways and off-pathways oligomers have been identified that exhibit different structural properties, suggesting multiple aggregation pathways (Villar-Piqué et al., 2015). Recently, Paslawski et al. reported the formation of two types of α Syn oligomers—one that can be elongated by monomers to form fibrils and a second one that stacks together to form more amorphous structures (Paslawski et al., 2014). The identification and expression of α Syn variants prone to oligomerization, but not fibrillization, suggests that oligomeric species might be the most toxic forms of α Syn (Karpinar et al., 2009; Winner et al., 2011; Rockenstein et al., 2014). Peptides K84s, K89s, and K102s significantly reduced the accumulation of soluble oligomeric species *in vitro*. This was accompanied by reduction of α Syn-induced toxicity by expression of the peptides in yeast cells, as well as reduction of the SDS-insoluble α Syn fraction by expression of K84 and K102 *in vivo*. These data propose K84s and K102s as potent suppressors of toxicity by reducing the load of oligomeric species and inhibiting the aggregation process of α Syn. This might have also important implications for the pathological spreading of the disease in the brain, since oligomeric species are proposed as candidates for mediating the prion-like spreading of α Syn aggregation (Luk et al., 2009, 2012; Hansen et al., 2011). Using fluorescently-labeled peptides, we demonstrated that they can be internalized into human cells. Importantly, peptide K84s reduced α Syn aggregation in human cells, suggesting it might constitute a promising new lead for the development of novel therapeutic strategies for synucleinopathies.

The peptides obtained from the screenings may serve as a starting point to dissect the amino acids involved in interaction and rescue function. One of the next important steps will be the mapping of the interaction sites of the peptides with α Syn for understanding the anti-aggregation mechanism. This may direct the synthesis of shorter peptides or peptidomimetic synthetic molecules that may be suitable as anti- α Syn-aggregation drugs.

DATA AVAILABILITY STATEMENT

The original contributions presented in the study are included in the article/Supplementary Material, further inquiries can be directed to the corresponding author.

AUTHOR CONTRIBUTIONS

Conceived and designed the experiments: BP and GB. Performed the experiments: BP, DW, AR, KD, DL, MH, and JG. Analyzed the data: BP, DW, AR, KD, DL, MH, TO, and GB. Contributed

reagents/materials: JU. Wrote the article: BP and GB. All authors discussed and reviewed the manuscript. All authors contributed to the article and approved the submitted version.

FUNDING

This work was supported by Deutsche Forschungsgemeinschaft (DFG: BR 1502/18-1 to GB). DW was supported by China Scholarship Council (CSC No. 201706760021). TO was supported by the Deutsche Forschungsgemeinschaft (DFG, German Research Foundation) under Germany's Excellence Strategy—EXC 2067/1- 390729940).

ACKNOWLEDGMENTS

We thank Katharina Ziese-Kubon for excellent technical assistance and Cedric Blötz for help with the Y2H screen.

SUPPLEMENTARY MATERIAL

The Supplementary Material for this article can be found online at: <https://www.frontiersin.org/articles/10.3389/fnmol.2021.659926/full#supplementary-material>.

SUPPLEMENTARY FIGURE 1 | Analysis of peptides FITC-K84s and FITC-K102s. The upper panels represent the HPLC chromatograms of the samples. The lower panels represent the mass spectrometry spectrum of the sample peaks, marked with an asterisk in the upper panel.

SUPPLEMENTARY FIGURE 2 | Analysis of peptides K50s, K89s, K94s, and K97s. The peptides were analyzed with LC-MS equipped with a charged aerosol detector (CAD). The upper panel shows the CAD chromatogram of the peptide sample (above) compared to the solvent control (below). Y-axis gives the relative current in %. The lower panel shows the MS spectrum of the peptide peak, marked with an asterisk in the upper panel.

SUPPLEMENTARY FIGURE 3 | Flowchart depicting yeast-two-hybrid (Y2H) screening. Y2H assay is a step-by-step procedure starting from the construction of bait (α Syn), fused to the GAL4 DNA-binding domain (BD) and amplification of the library, where each peptide construct is fused to B42 activation domain (AD). The bait is transformed into AH109 yeast strain that harbors *HIS3* and *ADE2* reporter genes driven by a GAL4 regulatory binding site to select for growth on media lacking histidine and adenine and was mated with the library. Selection for diploids is performed on SC-Leu-Trp medium. Positive clones are selected by their ability to activate the transcription of the reporter genes that enable growth on SC-Leu-Trp-His medium.

SUPPLEMENTARY FIGURE 4 | Exemplary growth assay for selection of library candidates. **(A)** Ninety colonies were picked from the initial selection on SC-Leu-Trp-His semi-solid medium after 6 days of incubation at 30°C. The cells were spotted on SC-Leu-Trp plate, allowed to grow for 2 days, and pinned in four technical replicates onto agar selection plates with increasing stringency. Red boxes indicate clones, selected for plasmid isolation and sequencing. **(B)** Spotting assay of yeast strain expressing GAL1-driven α Syn used for the toxicity-rescue screen. Yeast strain AH109 was transformed with an integrative vector harboring α Syn-encoding gene or empty vector (EV) as a control. Yeast cells were spotted in 10-fold dilution on selective SC-Trp plates, containing 2% glucose or galactose and allowed to grow for 3 days at 30°C.

SUPPLEMENTARY FIGURE 5 | Expression of the peptide constructs does not affect yeast growth. **(A)** Expression of random peptide constructs does not rescue α Syn-induced growth inhibition. A yeast strain that harbors three copies of the GAL1-driven α Syn-GFP-encoding gene was transformed with three random plasmid constructs that contain the peptide-encoding sequence fused to the B42-activation domain (AD), or with a vector with AD. Yeast cells were spotted in 10-fold dilution on SC-Leu-Ura selective plates containing glucose (control: α Syn

"OFF") or galactose (α Syn "ON") for induction of *GAL1* promoter. Yeast wild-type isogenic background strain transformed with AD-vector was used as positive growth control. **(B)** Yeast strain, expressing *GAL1*-driven GFP was transformed with the plasmids, encoding the peptide sequences without the N-terminal AD. Spotting assay was performed as described. Empty vector (EV) was used as a control.

SUPPLEMENTARY FIGURE 6 | Secondary structure predictions of the indicated peptides. PEP FOLD 3 tool was used for predicting peptide structures from amino acid sequences. **(A)** Peptide constructs with N-terminal GB1-scaffold expressed in yeast. K50 and K117 contain also the C-terminal scaffold sequence, as indicated in **Table 3**. **(B)** Predicted structure of the synthetic peptides

REFERENCES

- Abe, K., Kobayashi, N., Sode, K., and Ikebukuro, K. (2007). Peptide ligand screening of α -synuclein aggregation modulators by in silico panning. *BMC Bioinformatics* 8:451. doi: 10.1186/1471-2105-8-451
- Ahmad, B., Chen, Y., and Lapidus, L. J. (2012). Aggregation of α -synuclein is kinetically controlled by intramolecular diffusion. *Proc. Natl. Acad. Sci. U S A* 109, 2336–2341. doi: 10.1073/pnas.1109526109
- Appel-Cresswell, S., Vilarino-Guell, C., Encarnacion, M., Sherman, H., Yu, I., Shah, B., et al. (2013). α -synuclein p.H50Q, a novel pathogenic mutation for Parkinson's disease. *Mov. Disord.* 28, 811–813. doi: 10.1002/mds.25421
- Baig, M. H., Ahmad, K., Saeed, M., Alharbi, A. M., Barreto, G. E., Ashraf, G. M., et al. (2018). Peptide based therapeutics and their use for the treatment of neurodegenerative and other diseases. *Biomed. Pharmacother.* 103, 574–581. doi: 10.1016/j.biopha.2018.04.025
- Bengoia-Vergniory, N., Roberts, R. F., Wade-Martins, R., and Alegre-Abarrategui, J. (2017). α -synuclein oligomers: a new hope. *Acta Neuropathol.* 134, 819–838. doi: 10.1007/s00401-017-1755-1
- Breydo, L., Wu, J. W., and Uversky, V. N. (2012). α -synuclein misfolding and Parkinson's disease. *Biochim. Biophys. Acta* 1822, 261–285. doi: 10.1016/j.bbdis.2011.10.002
- Cappai, R., Leck, S.-L., Tew, D. J., Williamson, N. A., Smith, D. P., Galatis, D., et al. (2005). Dopamine promotes α -synuclein aggregation into SDS-resistant soluble oligomers via a distinct folding pathway. *FASEB J.* 19, 1377–1379. doi: 10.1096/fj.04-3437fje
- Carija, A., Pinheiro, F., Pujols, J., Brás, I. C., Lázaro, D. F., Santambrogio, C., et al. (2019). Biasing the native α -synuclein conformational ensemble towards compact states abolishes aggregation and neurotoxicity. *Redox Biol.* 22:101135. doi: 10.1016/j.redox.2019.101135
- Chartier-Harlin, M. C., Kachergus, J., Roumier, C., Mouroux, V., Douay, X., Lincoln, S., et al. (2004). α -synuclein locus duplication as a cause of familial Parkinson's disease. *Lancet* 364, 1167–1169. doi: 10.1016/S0140-6736(04)17103-1
- Cheruvara, H., Allen-Baume, V. L., Kad, N. M., and Mason, J. M. (2015). Intracellular screening of a peptide library to derive a potent peptide inhibitor of α -synuclein aggregation. *J. Biol. Chem.* 290, 7426–7435. doi: 10.1074/jbc.M114.620484
- Conway, K. A., Harper, J. D., and Lansbury, P. T. (1998). Accelerated *in vitro* fibril formation by a mutant α -synuclein linked to early-onset Parkinson disease. *Nat. Med.* 4, 1318–1320. doi: 10.1038/3311
- Conway, K. A., Lee, S. J., Rochet, J. C., Ding, T. T., Williamson, R. E., and Lansbury, P. T. Jr. (2000). Acceleration of oligomerization, not fibrillization, is a shared property of both α -synuclein mutations linked to early-onset Parkinson's disease: implications for pathogenesis and therapy. *Proc. Natl. Acad. Sci. U S A* 97, 571–576. doi: 10.1073/pnas.97.2.571
- Cooper, A. A., Gitler, A. D., Cashikar, A., Haynes, C. M., Hill, K. J., Bhullar, B., et al. (2006). α -synuclein blocks ER-Golgi traffic and Rab1 rescues neuron loss in Parkinson's models. *Science* 313, 324–328. doi: 10.1126/science.1129462
- Dearborn, A. D., Wall, J. S., Cheng, N., Heymann, J. B., Kajava, A. V., Varkey, J., et al. (2016). α -synuclein amyloid fibrils with two entwined, asymmetrically associated protofibrils. *J. Biol. Chem.* 291, 2310–2318. doi: 10.1074/jbc.M115.698787
- Dehay, B., Bourdenx, M., Gorry, P., Przedborski, S., Vila, M., Hunot, S., et al. (2015). Targeting α -synuclein for treatment of Parkinson's disease: mechanistic and therapeutic considerations. *Lancet Neurol.* 14, 855–866. doi: 10.1016/S1474-4422(15)00006-X
- Duennwald, M. L., Jagdish, S., Muchowski, P. J., and Lindquist, S. (2006). Flanking sequences profoundly alter polyglutamine toxicity in yeast. *Proc. Natl. Acad. Sci. U S A* 103, 11045–11050. doi: 10.1073/pnas.0604547103
- El-Agnaf, O. M. A., Paleologou, K. E., Greer, B., Abogre, A. M., King, J. E., Salem, S. A., et al. (2004). A strategy for designing inhibitors of α -synuclein aggregation and toxicity as a novel treatment for Parkinson's disease and related disorders. *FASEB J.* 18, 1315–1317. doi: 10.1096/fj.03-1346fje
- Fosgerau, K., and Hoffmann, T. (2015). Peptide therapeutics: current status and future directions. *Drug Discov. Today* 20, 122–128. doi: 10.1016/j.drudis.2014.10.003
- Fredenburg, R. A., Rospigliosi, C., Meray, R. K., Kessler, J. C., Lashuel, H. A., Eliez, D., et al. (2007). The impact of the E46K mutation on the properties of α -synuclein in its monomelic and oligomeric states. *Biochemistry* 46, 7107–7118. doi: 10.1021/bi7000246
- Fritz, C., and Green, M. (1996). Methods for selecting a random peptide that binds to a target protein. Patent number WO1996023899A1.
- German, D. C., Manaye, K. F., Sonsalla, P. K., and Brooks, B. A. (1992). Midbrain dopaminergic cell loss in Parkinson's disease and MPTP-induced parkinsonism: sparing of calbindin-D28k-containing cells. *Ann. N Y Acad. Sci.* 648, 42–62. doi: 10.1111/j.1749-6632.1992.tb24523.x
- Giasson, B. I., Duda, J. E., Murray, I. V., Chen, Q., Souza, J. M., Hurtig, H. I., et al. (2000). Oxidative damage linked to neurodegeneration by selective α -synuclein nitration in synucleinopathy lesions. *Science* 290, 985–989. doi: 10.1126/science.290.5493.985
- Giehml, L., and Otzen, D. E. (2010). Strategies to increase the reproducibility of protein fibrillization in plate reader assays. *Anal. Biochem.* 400, 270–281. doi: 10.1016/j.ab.2010.02.001
- Gietz, D., St Jean, A., Woods, R. A., and Schiestl, R. H. (1992). Improved method for high efficiency transformation of intact yeast cells. *Nucleic Acids Res.* 20:1425. doi: 10.1093/nar/20.6.1425
- Gitler, A. D., Bevis, B. J., Shorter, J., Strathearn, K. E., Hamamichi, S., Su, L. J., et al. (2008). The Parkinson's disease protein α -synuclein disrupts cellular Rab homeostasis. *Proc. Natl. Acad. Sci. U S A* 105, 145–150. doi: 10.1073/pnas.0710685105
- Guerrero-Ferreira, R., Taylor, N. M., Mona, D., Ringler, P., Lauer, M. E., Riek, R., et al. (2018). Cryo-EM structure of α -synuclein fibrils. *Elife* 7:e36402. doi: 10.7554/eLife.36402
- Guthrie, C., and Fink, G. Eds. (1990). *Guide to Yeast Genetics and Molecular Biology. Methods in Enzymology*. Vol. 194. United States: Academic Press. pp. 1–933.
- Hansen, C., Angot, E., Bergström, A.-L., Steiner, J. A., Pieri, L., Paul, G., et al. (2011). α -synuclein propagates from mouse brain to grafted dopaminergic neurons and seeds aggregation in cultured human cells. *J. Clin. Invest.* 121, 715–725. doi: 10.1172/JCI43366
- Hashimoto, M., Hsu, L. J., Xia, Y., Takeda, A., Sisk, A., Sundsmo, M., et al. (1999). Oxidative stress induces amyloid-like aggregate formation of NACP/ α -

- synuclein *in vitro*. *Neuroreport* 10, 717–721. doi: 10.1097/00001756-199903170-00011
- Hoppert, M., and Holzenburg, A. (1998). *Electron Microscopy in Microbiology*. Oxford, UK: Bios Scientific Publishers. Available online at: <https://www.amazon.co.uk/Electron-Microscopy-Microbiology-Microscopical-Handbooks/dp/1859960162>. Accessed January 26, 2021.
- Irniger, S., Egli, C., Kuenzler, M., and Braus, G. H. (1992). The yeast actin intron contains a cryptic promoter that can be switched on by preventing transcriptional interference. *Nucleic Acids Res.* 20, 4733–4739. doi: 10.1093/nar/20.18.4733
- Iyer, A., Roeters, S. J., Kogan, V., Woutersen, S., Claessens, M. M. A. E., and Subramaniam, V. (2017). C-terminal truncated α -synuclein fibrils contain strongly twisted β -sheets. *J. Am. Chem. Soc.* 139, 15392–15400. doi: 10.1021/jacs.7b07403
- James, P., Halladay, J., and Craig, E. A. (1996). Genomic libraries and a host strain designed for highly efficient two-hybrid selection in yeast. *Genetics* 144, 1425–1436. doi: 10.1093/genetics/144.4.1425
- Karpinar, D. P., Balija, M. B., Kugler, S., Opazo, F., Rezaei-Ghaleh, N., Wender, N., et al. (2009). Pre-fibrillar α -synuclein variants with impaired β -structure increase neurotoxicity in Parkinson's disease models. *EMBO J.* 28, 3256–3268. doi: 10.1038/emboj.2009.257
- Kleinknecht, A., Popova, B., Lázaro, D. F., Pinho, R., Valerius, O., Outeiro, T. F., et al. (2016). C-terminal tyrosine residue modifications modulate the protective phosphorylation of serine 129 of α -synuclein in a yeast model of Parkinson's disease. *PLoS Genet.* 12:e1006098. doi: 10.1371/journal.pgen.1006098
- Kritzer, J. A., Hamamichi, S., McCaffery, J. M., Santagata, S., Naumann, T. A., Caldwell, K. A., et al. (2009). Rapid selection of cyclic peptides that reduce α -synuclein toxicity in yeast and animal models. *Nat. Chem. Biol.* 5, 655–663. doi: 10.1038/nchembio.193
- Krüger, R., Kuhn, W., Müller, T., Woitalla, D., Graeber, M., Kosel, S., et al. (1998). Ala30Pro mutation in the gene encoding α -synuclein in Parkinson's disease. *Nat. Genet.* 18, 106–108. doi: 10.1038/ng0298-106
- Lashuel, H. A., Overk, C. R., Oueslati, A., and Masliah, E. (2013). The many faces of α -synuclein: from structure and toxicity to therapeutic target. *Nat. Rev. Neurosci.* 14, 38–48. doi: 10.1038/nrn3406
- Lázaro, D. F., Rodrigues, E. F., Langohr, R., Shahpasandzadeh, H., Ribeiro, T., Guerreiro, P., et al. (2014). Systematic comparison of the effects of α -synuclein mutations on its oligomerization and aggregation. *PLoS Genet.* 10:e1004741. doi: 10.1371/journal.pgen.1004741
- Lesage, S., Anheim, M., Letournel, F., Bousset, L., Honore, A., Rozas, N., et al. (2013). G51D α -synuclein mutation causes a novel parkinsonian-pyramidal syndrome. *Ann. Neurol.* 73, 459–471. doi: 10.1002/ana.23894
- Luk, K. C., Kehm, V., Carroll, J., Zhang, B., O'Brien, P., Trojanowski, J. Q., et al. (2012). Pathological α -synuclein transmission initiates Parkinson-like neurodegeneration in nontransgenic mice. *Science* 338, 949–953. doi: 10.1126/science.1227157
- Luk, K. C., Song, C., O'Brien, P., Stieber, A., Branch, J. R., Brunden, K. R., et al. (2009). Exogenous α -synuclein fibrils seed the formation of Lewy body-like intracellular inclusions in cultured cells. *Proc. Natl. Acad. Sci. U S A* 106, 20051–20056. doi: 10.1073/pnas.0908005106
- McLean, P. J., Kawamata, H., Hyman, B. T. (2001). Alpha-synuclein-enhanced green fluorescent protein fusion proteins form proteasome sensitive inclusions in primary neurons. *Neuroscience* 104, 901–912. doi: 10.1016/s0306-4522(01)00113-0
- Miranda, H. V., Xiang, W., de Oliveira, R. M., Simões, T., Pimentel, J., Klucken, J., et al. (2013). Heat-mediated enrichment of α -synuclein from cells and tissue for assessing post-translational modifications. *J. Neurochem.* 126, 673–684. doi: 10.1111/jnc.12251
- Mumberg, D., Müller, R., Funk, M., Müller, R., and Funk, M. (1994). Regulatable promoters of *Saccharomyces cerevisiae*: comparison of transcriptional activity and their use for heterologous expression. *Nucleic Acids Res.* 22, 5767–5768. doi: 10.1093/nar/22.25.5767
- Outeiro, T. F., and Lindquist, S. (2003). Yeast cells provide insight into α -synuclein biology and pathobiology. *Science* 302, 1772–1775. doi: 10.1126/science.1090439
- Paslawski, W., Mysling, S., Thomsen, K., Jørgensen, T. J. D., and Otzen, D. E. (2014). Co-existence of two different α -synuclein oligomers with different core structures determined by hydrogen/deuterium exchange mass spectrometry. *Angew. Chem. Int. Ed. Engl.* 53, 7560–7563. doi: 10.1002/anie.201400491
- Petroi, D., Popova, B., Taheri-Talesh, N., Irniger, S., Shahpasandzadeh, H., Zweckstetter, M., et al. (2012). Aggregate clearance of α -synuclein in *Saccharomyces cerevisiae* depends more on autophagosome and vacuole function than on the proteasome. *J. Biol. Chem.* 287, 27567–27579. doi: 10.1074/jbc.M112.361865
- Pieri, L., Madiona, K., and Melki, R. (2016). Structural and functional properties of prefibrillar α -synuclein oligomers. *Sci. Rep.* 6:24526. doi: 10.1038/srep24526
- Polymeropoulos, M. H., Lavedan, C., Leroy, E., Ide, S. E., Dehejia, A., Dutra, A., et al. (1997). Mutation in the α -synuclein gene identified in families with Parkinson's disease. *Science* 276, 2045–2047. doi: 10.1126/science.276.5321.2045
- Popova, B., Kleinknecht, A., Arendarski, P., Mischke, J., Wang, D., and Braus, G. H. (2018). Sumoylation protects against β -synuclein toxicity in yeast. *Front. Mol. Neurosci.* 11:94. doi: 10.3389/fnmol.2018.00094
- Popova, B., Kleinknecht, A., and Braus, G. H. (2015). Posttranslational modifications and clearing of α -synuclein aggregates in yeast. *Biomolecules* 5, 617–634. doi: 10.3390/biom5020617
- Popova, B., Wang, D., Pätz, C., Akkermann, D., Lázaro, D. F., Galka, D., et al. (2021). DEAD-box RNA helicase Dbp4/DDX10 is an enhancer of α -synuclein toxicity and oligomerization. *PLoS Genet.* 17:e1009407. doi: 10.1371/journal.pgen.1009407
- Rockenstein, E., Nuber, S., Overk, C. R., Ubhi, K., Mante, M., Patrick, C., et al. (2014). Accumulation of oligomer-prone α -synuclein exacerbates synaptic and neuronal degeneration *in vivo*. *Brain* 137, 1496–1513. doi: 10.1093/brain/awu057
- Shahpasandzadeh, H., Popova, B., Kleinknecht, A., Fraser, P. E., Outeiro, T. F., and Braus, G. H. (2014). Interplay between sumoylation and phosphorylation for protection against α -synuclein inclusions. *J. Biol. Chem.* 289, 31224–31240. doi: 10.1074/jbc.M114.559237
- Shen, Y., Maupetit, J., Derreumaux, P., and Tufféry, P. (2014). Improved PEP-FOLD approach for peptide and miniprotein structure prediction. *J. Chem. Theory Comput.* 10, 4745–4758. doi: 10.1021/ct500592m
- Shtilerman, M. D., Ding, T. T., and Lansbury, P. T. (2002). Molecular crowding accelerates fibrillization of α -synuclein: could an increase in the cytoplasmic protein concentration induce Parkinson's disease? *Biochemistry* 41, 3855–3860. doi: 10.1021/bi0120906
- Sikorski, R. S., and Hieter, P. (1989). A system of shuttle vectors and yeast host strains designed for efficient manipulation of DNA in *Saccharomyces cerevisiae*. *Genetics* 122, 19–27. doi: 10.1093/genetics/122.1.19
- Singleton, A. B., Farrer, M., Johnson, J., Singleton, A., Hague, S., Kachergus, J., et al. (2003). α -Synuclein locus triplication causes Parkinson's disease. *Science* 302:841. doi: 10.1126/science.1090278
- Soellick, T. R., and Uhrig, J. F. (2001). Development of an optimized interaction-mating protocol for large-scale yeast two-hybrid analyses. *Genome Biol.* 2:RESEARCH0052. doi: 10.1186/gb-2001-2-12-research0052
- Spillantini, M. G., Schmidt, M. L., Lee, V. M., Trojanowski, J. Q., Jakes, R., and Goedert, M. (1997). α -synuclein in Lewy bodies. *Nature* 388, 839–840. doi: 10.1038/42166
- Stefanis, L. (2012). α -synuclein in Parkinson's disease. *Cold Spring Harb. Perspect. Med.* 2:a009399. doi: 10.1101/cshperspect.a009399
- Tanaka, G., Yamanaka, T., Furukawa, Y., Kajimura, N., Mitsuoka, K., and Nukina, N. (2019). Sequence- and seed-structure-dependent polymorphic fibrils of α -synuclein. *Biochim. Biophys. Acta* 1865, 1410–1420. doi: 10.1016/j.bbdis.2019.02.013
- Tenreiro, S., Franssens, V., Winderickx, J., and Outeiro, T. F. (2017). Yeast models of Parkinson's disease-associated molecular pathologies. *Curr. Opin. Genet. Dev.* 44, 74–83. doi: 10.1016/j.gde.2017.01.013
- Torpey, J. H., Meade, R. M., Mistry, R., Mason, J. M., and Madine, J. (2020). Insights into peptide inhibition of α -synuclein aggregation. *Front. Neurosci.* 14:1082. doi: 10.3389/fnins.2020.561462
- Uversky, V. N., Cooper, E. M., Bower, K. S., Li, J., and Fink, A. L. (2002). Accelerated α -synuclein fibrillation in crowded milieu. *FEBS Lett.* 515, 99–103. doi: 10.1016/s0014-5793(02)02446-8
- Villar-Piqué, A., Lopes da Fonseca, T., and Outeiro, T. F. (2015). Structure, function and toxicity of α -synuclein: the Bermuda triangle

- in synucleinopathies. *J. Neurochem.* 139, 240–255. doi: 10.1111/jnc.13249
- Willingham, S., Outeiro, T. F., DeVit, M. J., Lindquist, S. L., and Muchowski, P. J. (2003). Yeast genes that enhance the toxicity of a mutant huntingtin fragment or α -synuclein. *Science* 302, 1769–1772. doi: 10.1126/science.1090389
- Winner, B., Jappelli, R., Maji, S. K., Desplats, P. A., Boyer, L., Aigner, S., et al. (2011). *in vivo* demonstration that α -synuclein oligomers are toxic. *Proc. Natl. Acad. Sci. U S A* 108, 4194–4199. doi: 10.1073/pnas.1100976108
- Zarranz, J. J., Alegre, J., Gómez-Esteban, J. C., Lezcano, E., Ros, R., Ampuero, I., et al. (2004). The new mutation, E46K, of α -synuclein causes Parkinson and Lewy body dementia. *Ann. Neurol.* 55, 164–173. doi: 10.1002/ana.10795

Conflict of Interest: The authors declare that the research was conducted in the absence of any commercial or financial relationships that could be construed as a potential conflict of interest.

Copyright © 2021 Popova, Wang, Rajavel, Dhamotharan, Lázaro, Gerke, Uhrig, Hoppert, Outeiro and Braus. This is an open-access article distributed under the terms of the Creative Commons Attribution License (CC BY). The use, distribution or reproduction in other forums is permitted, provided the original author(s) and the copyright owner(s) are credited and that the original publication in this journal is cited, in accordance with accepted academic practice. No use, distribution or reproduction is permitted which does not comply with these terms.



Arginine and Arginine-Rich Peptides as Modulators of Protein Aggregation and Cytotoxicity Associated With Alzheimer's Disease

Somayra S. A. Mamsa^{1,2*} and Bruno P. Meloni^{2,3,4}

¹School of Molecular Sciences, Faculty of Science, The University of Western Australia, Perth, WA, Australia, ²Perron Institute for Neurological and Translational Science, QEII Medical Centre, Perth, WA, Australia, ³Centre for Neuromuscular and Neurological Disorders, The University of Western Australia, Crawley, WA, Australia, ⁴Department of Neurology, Sir Charles Gairdner Hospital, QEII Medical Centre, Perth, WA, Australia

OPEN ACCESS

Edited by:

Wolfgang Hoyer,
Heinrich Heine University of
Düsseldorf, Germany

Reviewed by:

Homira Behbahani,
Karolinska Institutet (KI), Sweden
Balaji Krishnan,
University of Texas Medical Branch at
Galveston, United States

*Correspondence:

Somayra S. A. Mamsa
somayra.mamsa@
research.uwa.edu.au

Specialty section:

This article was submitted to
Brain Disease Mechanisms,
a section of the journal
Frontiers in Molecular Neuroscience

Received: 17 August 2021

Accepted: 29 September 2021

Published: 28 October 2021

Citation:

Mamsa SSA and Meloni BP
(2021) Arginine and Arginine-Rich
Peptides as Modulators of Protein
Aggregation and Cytotoxicity
Associated With Alzheimer's Disease.
Front. Mol. Neurosci. 14:759729.
doi: 10.3389/fnmol.2021.759729

A substantial body of evidence indicates cationic, arginine-rich peptides (CARPs) are effective therapeutic compounds for a range of neurodegenerative pathologies, with beneficial effects including the reduction of excitotoxic cell death and mitochondrial dysfunction. CARPs, therefore, represent an emergent class of promising neurotherapeutics with multimodal mechanisms of action. Arginine itself is a known chaotrope, able to prevent misfolding and aggregation of proteins. The putative role of proteopathies in chronic neurodegenerative diseases such as Alzheimer's disease (AD) warrants investigation into whether CARPs could also prevent the aggregation and cytotoxicity of amyloidogenic proteins, particularly amyloid-beta and tau. While monomeric arginine is well-established as an inhibitor of protein aggregation in solution, no studies have comprehensively discussed the anti-aggregatory properties of arginine and CARPs on proteins associated with neurodegenerative disease. Here, we review the structural, physicochemical, and self-associative properties of arginine and the guanidinium moiety, to explore the mechanisms underlying the modulation of protein aggregation by monomeric and multimeric arginine molecules. Arginine-rich peptide-based inhibitors of amyloid-beta and tau aggregation are discussed, as well as further modulatory roles which could reduce proteopathic cytotoxicity, in the context of therapeutic development for AD.

Keywords: arginine, aggregation, Alzheimer's disease, peptides, amyloid-beta (A β), tau & phospho-tau protein

INTRODUCTION

Alzheimer's disease (AD) is a progressive, neurodegenerative disease estimated to affect over 44 million people worldwide, with a devastating impact on patients, their loved ones and caregivers, as well as vast social and economic consequences (Alzheimer's Association, 2021). As the single biggest risk factor for AD is age, the prevalence of AD continues to increase as the average life expectancy rises; by 2050, it is predicted that

over 100 million people worldwide will have the disease (GBD 2016 Dementia Collaborators, 2019). Clinically, AD is characterised by memory loss, impaired cognition, changes in mood, affect and behaviour, and a decline in the ability to carry out everyday tasks. These symptoms arise gradually, developing over the course of several years from mild cognitive impairment to dementia of increasing severity. Due to the progressive and insidious nature of AD, limited availability of tools for definitive diagnosis (Gofton and Weaver, 2006), and a lack of efficacious and disease-modifying therapeutics (Weller and Budson, 2018), AD remains a significant issue in global health.

AD is characterised by the development of proteopathies, specifically cytotoxic aggregates of amyloid-beta and tau. A range of therapeutic approaches for AD-associated proteopathies are therefore in various stages of development, including enzyme inhibitors targeting the production pathway of amyloid-beta (Kumar et al., 2018), gene silencing technologies to limit the expression of pro-aggregatory mutant tau proteins (Miller et al., 2004), kinase inhibitors aimed at preventing the pro-aggregatory hyperphosphorylation of tau, passive and active immunotherapies developed to drive protein clearance, and small molecule inhibitors of protein aggregation. These strategies are comprehensively reviewed in the literature (Hardy and De Strooper, 2017; Congdon and Sigurdsson, 2018; Pedrini et al., 2019). It remains unclear whether the proteopathies observed in AD are causative or consequential with regards to other aspects of AD pathogenesis, such as inflammation, neurovascular dysfunction, and metabolic disorders. Although the precise, mechanistic contributions of protein aggregation to the pathogenesis of AD are still contested, targeting protein aggregation remains a central priority in drug development; the recent approval of the amyloid-beta-lowering human monoclonal antibody Aducanumab by the United States Food and Drug Administration (FDA) represents the first drug to be approved by the FDA for the treatment of AD in 18 years.

Broadly, peptide-based therapeutics represent a particularly desirable class of candidates for pharmacotherapy, as peptides can be designed with high target specificity and bioactivity, and further optimised for increased safety, tolerability, efficacy and stability through sequence and structural modifications (Di, 2015; Räder et al., 2018; Evers et al., 2019). In the case of protein aggregation, the sequence and structural features of target proteins can be used to inform the rational design of peptides for binding and inhibition. Additionally, methods for screening peptide-based compounds are well-developed, including a variety of predictive *in silico* tools for assessing potential interactions between peptides and proteins (D'Annessa et al., 2020). As a general class, peptide-based inhibitors of protein aggregation developed for AD have been reviewed in detail by Goyal et al. (2017), Kumar and Sim (2014), and Funke and Willbold (2012). Despite their advantages, challenges in the development of anti-aggregatory peptides include lack of membrane permeability and difficulty in penetrating the blood-brain barrier. Cationic arginine-rich peptides (CARPs) demonstrate a particular ability to cross cellular membranes

as well as the blood-brain barrier (Mitchell et al., 2000; Schmidt et al., 2010; Allolio et al., 2018), rendering them popular “carrier” molecules for a range of therapeutic “cargo” such as oligonucleotides, peptides and proteins (reviewed by Habault and Poyet, 2019). However, the aggregation-modulating properties of arginine itself may be favourable for peptide drugs targeting proteopathies. Here, we discuss the unique properties of arginine in modulating protein aggregation, as well as arginine-rich peptides, and peptides which have employed arginine as a key residue, in targeting the proteopathies associated with AD.

ARGININE

Structure and Physicochemical Properties of the Arginine Monomer

Arginine is one of two basic amino acids, alongside lysine, which is consistently protonated at physiological pH. The structure of arginine is highly unique; arginine monomers are comprised of a polar, hydrophilic head group conjugated to a hydrophobic body, and an aliphatic side chain capped with a guanidino group. At physiological pH, the carboxyl moiety of arginine is deprotonated, while protonation of both the amino group into an amide and the guanidino group into the cationic guanidinium moiety, confers the overall cationicity of the molecule to a net charge of +1. In proteins, the guanidinium moiety contributes extensively to the intra- and inter-molecular associations of arginine residues by imparting a strong capacity for electrostatic interactions such as hydrogen bonding. The structure of arginine in comparison to lysine is shown in **Figure 1**.

Guanidinium itself is a planar molecule comprised of three amino groups conjugated to a central carbon atom; these three amino groups facilitate the formation of bidentate hydrogen bonds in three directions, enabling arginine to participate in a higher number of electrostatic interactions compared to lysine. Guanidinium also contributes to several distinctive properties of

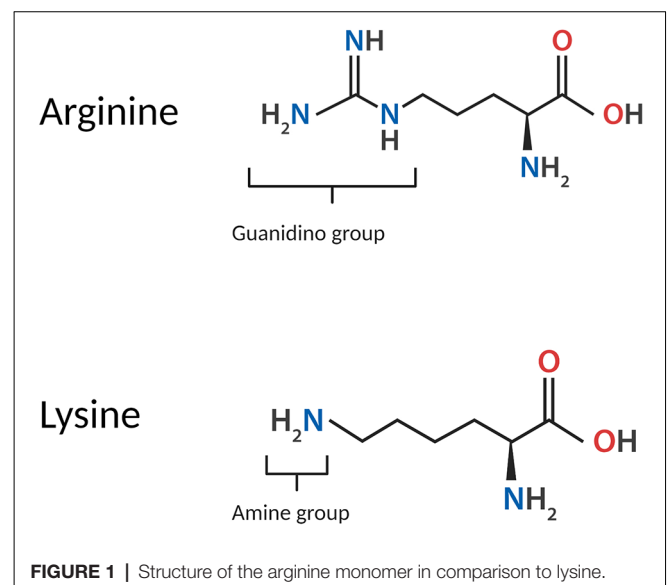


FIGURE 1 | Structure of the arginine monomer in comparison to lysine.

arginine and its behaviour in biological systems. The side chain of arginine is able to remain protonated under all physiological conditions and in even highly basic solutions (Xu et al., 2017), as the guanidinium moiety carries a highly stable, delocalised cationic charge with a pKa of 13.8 (Fitch et al., 2015) owing to resonance stabilisation. Due to its remarkable chemistry and emergent properties, guanidinium has been the subject of extensive study. The high stability of guanidinium is attributed to its Y-conjugated, quasi-aromatic structure with six delocalised pi electrons, which was regarded by Gund (1972) as a novel form of aromaticity. Additionally, the side chain of arginine is conferred partial hydrophobicity by the hydration structure of guanidinium; guanidinium is poorly hydrated above and below its plane, retaining only in-plane hydration (Mason et al., 2003, 2004).

Emergent Properties, Self-association and Clustering

Notably, the guanidinium moiety of arginine imparts a strong tendency for self-association. While it is a basic tenet of physical chemistry that ions with like charges repel each other, guanidinium ions in solution are able to overcome the Coulomb repulsion typically driving this effect and form thermodynamically stable pairs (Vazdar et al., 2018). This behaviour also extends to arginine; Shukla and Trout (2010) observed the tendency of arginine monomers to form clusters in solution, through three dominant modes of self-association: guanidinium-to-guanidinium stacking; bonding of the guanidinium moiety of an arginine monomer to the carboxylate group of another; and bonding of the arginine C-terminus to the N-terminus of an adjacent arginine monomer. The ability of arginine to form stable clusters has largely been attributed to the hydrogen-bonding ability of guanidinium (Li et al., 2010).

Computational simulations have also demonstrated like-charge pairing of di-arginine peptides through the association of their side chains, while the NH⁴⁺-containing side chains of di-lysine peptides do not exhibit any attraction to each other (Vazdar et al., 2018), evidencing the critical role of the guanidinium moiety in arginine-arginine interactions. Longer, poly-arginine peptides are also attracted to each other in solution. The self-association of polyarginine-10 (R10) peptides was demonstrated by Tesei et al. (2017) through computational modelling and experimentally confirmed by small-angle X-ray scattering experiments. The guanidinium cations of arginine side chains throughout R10 were found to associate with the corresponding guanidinium groups on pairing R10 molecules to form like-charge ion pairs, while the guanidinium cation of the ninth residue was also found to bind the negatively charged C-terminus of the adjacent R10 peptide through the formation of an intermolecular salt bridge (Tesei et al., 2017; Vazdar et al., 2018). The latter mechanism functions as an “adhesive patch” between two R10 peptides, a binding motif absent in the interactions between two molecules of the similarly cationic peptide polylysine-10 (K10), which only repels itself in solution (Tesei et al., 2017; Vazdar et al., 2018).

The formation of like-charge guanidinium pairing between arginine residues is also likely to impart stability in the tertiary structure of proteins; a number of biologically occurring protein structures are known to contain arginine residues oriented in close proximity to each other in three-dimensional space, with these steric arrangements enabled by the formation of guanidinium pairs within the structure (Tesei et al., 2017; Vazdar et al., 2018).

At physiological pH, where arginine is protonated, self-association of arginine also facilitates the formation of dynamic arginine clusters bound to protein surfaces. *In silico*, arginine ions bind to the surface of proteins such as lysozyme through interactions mediated by their guanidinium and carboxyl groups; while bound, the remaining guanidinium or carboxyl group of each arginine monomer interacts in a head-to-tail orientation with the carboxyl or guanidinium group of another arginine molecule in solution, which itself is able to interact with another arginine molecule through the same mechanism (Vagenende et al., 2013). Arginine clusters remain bound to proteins for a remarkably long period of time, and are thus considered to “extend” the surface of the protein they are bound to (Vagenende et al., 2013); indeed, experimental results confirm that binding of arginine ions to a protein *in vitro* results in a size increase of the protein detectable by chromatography (Vagenende et al., 2013). Corollary to this, it is expected that clusters of arginine can alter the physicochemical properties of the protein they are bound to, including charge and hydrophobicity, and could therefore alter their properties *in vivo*, such as solubility, stability and activity.

Effects of Arginine on Protein Aggregation

It is well-established that arginine modulates protein aggregation, acting as a molecular cosolvent and “chemical chaperone” in solution (Sharma et al., 2013). Arginine is commonly used as an additive to maintain protein stability in the biopharmaceutical industry and has conventionally been regarded as an aggregation suppressant (Golovanov et al., 2004; Arakawa et al., 2006; Ghosh et al., 2009). Shiraki et al. (2002) evaluated the effects of 15 amino acids on lysozyme under the conditions of thermal unfolding- and dilution-induced, aggregation; among them, arginine was found to be the most effective suppressor of aggregation, increasing protein solubility. Arginine has also proven particularly useful for solubilising membrane proteins otherwise prone to aggregation (Arakawa et al., 2011). Notably, the effects of arginine on proteins in solution are unique even in comparison to guanidine (Arakawa et al., 2007).

A number of experimental and computational studies have aimed to develop a mechanistic understanding of the molecular processes underlying the suppression of protein aggregation by arginine. It was previously reported by Das et al. (2007) that the self-association of arginine gives rise to hydrophobic surfaces through alignment of its methylene groups, which are then driven by the hydrophobic effect to bind the exposed hydrophobic residues of unfolded and intrinsically disordered proteins. Das et al. (2007) pertinently observed that the

amyloid-beta peptide exhibits increased solubility and decreased fibril formation in the presence of arginine, and concluded, from their analyses, that these effects were due to hydrophobic surfaces of arginine clusters masking the pro-aggregatory hydrophobic residues of amyloid-beta monomers, preventing their self-association. However, while arginine does form hydrophobic columns along its crystallographic axis in crystal structures, molecular dynamics simulations subsequently performed by Shukla and Trout (2010) did not support the finding of methylene alignment in solution. While Shukla and Trout indeed confirmed the assembly of supramolecular arginine clusters, observing the formation of dimers and higher order n-mers at physiological pH, no hydrophobic surfaces were formed in these clusters through methylene alignment as proposed by Das et al. (2007).

Furthermore, Shukla and Trout (2010) also observed strong preferential interactions between arginine and the aromatic residues of their model proteins, mediated by cation- π stacking; these observations were consistent with previous results by Arakawa et al. (2007), which demonstrated that while both arginine and guanidine displayed a strong affinity for most protein residues, their affinities were particularly strong for aromatic residues, which are generally hydrophobic. Tsumoto et al. (2004) had also previously observed that the aggregation-suppressive effects of arginine, which could not be explained through either surface tension effects or preferential interactions alone, were substantially mediated through the interactions of arginine guanidinium groups with the side chains of protein tryptophan residues. In the folded state of proteins, hydrophobic residues such as tryptophan are internalised or “buried” from the protein surface, while their externalisation in protein unfolding promotes aggregation; thus, arginine could indeed have a noticeable effect on the aggregation of unfolded or disordered proteins by binding hydrophobic surfaces and preventing their self-association, albeit through different molecular mechanisms than those proposed by Das et al. (2007).

Interestingly, however, Shukla and Trout (2010) reported that interactions between arginine and aromatic residues were insufficient to fully explain the effect of arginine on protein aggregation; in their study, the overall effect on aggregation was disproportionate when considering the relatively low number of aromatic residues comprising their model proteins. This led the authors to consider additional mechanisms, particularly the accumulation of arginine molecules on protein surfaces to form dynamic clusters; it was concluded that these clusters were able to “crowd out” the model proteins, preventing their self-association. Further research led to the classification of arginine as a “neutral crowder” in this context (Baynes et al., 2005). A comparative study by Schneider and Trout (2009) on the effects of arginine hydrochloride and guanidine hydrochloride on the aggregation of bovine serum albumin (BSA), lysozyme and α -chymotrypsinogen revealed that arginine had a unique effect: it was neither attracted to nor repelled from the protein surface. However, Schneider et al. (2011) later described a shift in the preferential interaction of arginine at high concentrations, from neutral to highly excluded, concluding that the “neutral crowder”

effect was not able to completely describe the behaviour of salt forms of arginine such as arginine hydrochloride. Additionally, *in silico* analysis by Li et al. (2010) demonstrated the ability of arginine to solubilise hydrophobic and aromatic moieties by forming a “cage-like” solvation layer around the molecules. The mechanisms of aggregation suppression by arginine are therefore complex, involving not only interactions between arginine and proteins, but interactions between arginine and other arginine molecules; this tendency to form self-associative assemblies is an important factor in the aggregation-modulating effects of arginine.

Continued studies over the past decade, however, have demonstrated the effects of arginine on protein aggregation vary depending on its context and concentration, and are not always suppressive. Arginine potently inhibits the aggregation of lysozyme (Matsuoka et al., 2007; Ito et al., 2011), and porcine and mink growth hormones (Cirkovas and Sereikaite, 2011); monomeric arginine prevents the oligomerisation of insulin (Varughese and Newman, 2012; Březina et al., 2018; Haghighi-Poodeh et al., 2020), and di-arginine peptides exhibit even higher efficacy for suppressing insulin aggregation (Nuhu and Curtis, 2015). At physiological pH, arginine hydrochloride also suppresses the aggregation of immunoglobulin G1 (IgG1), with this effect attributed to the interactions between arginine and hydrophobic IgG1 residues (Fukuda et al., 2014). However, arginine and its derivatives arginine amide and arginine ethylester were found to alter the aggregation pathway of BSA, inducing the formation of larger BSA aggregates (Borzova et al., 2017) rather than inhibiting aggregation *per se*. Additionally, high concentrations of arginine suppress the aggregation of α -lactalbumin, while low concentrations are known to substantially alter its aggregation pathway, resulting in a distinctive aggregate morphology (Smirnova et al., 2013). These varied observations indicate the effects of arginine on protein aggregation are more complex and diverse than previously established. Thus, arginine is perhaps best described as a “complex molecular cosolvent”, and the molecular context of arginine greatly influences the manner in which it modulates the behaviour of proteins in solution.

PROTEOPATHIES ASSOCIATED WITH ALZHEIMER'S DISEASE

Until the 1990s, the dominant theory of AD focused on the “cholinergic hypothesis” which posited the impairment of cholinergic neurotransmission as the primary cause of cognitive decline observed in patients with AD (reviewed by Francis et al., 1999). However, subsequent bodies of evidence have strongly implicated amyloid-beta deposition as a central event in the development of AD, regarded as the “amyloid cascade hypothesis” (first proposed by Hardy and Higgins, 1992; reviewed by Barage and Sonawane, 2015, and more recently by Ricciarelli and Fedele, 2017). The minimal correlation between cerebral amyloid-beta load and the severity of cognitive decline observed in patients with AD (Nelson et al., 2012), however, has led to an increased focus on the role of tauopathy in the pathogenesis of AD. Moreover, the presence of cerebral

amyloid-beta plaques is not always concomitant with impaired cognition (Arboleda-Velasquez et al., 2019). The development of amyloid-beta pathology is therefore considered necessary, yet insufficient, for the progression of AD. Broad evidence from laboratory, preclinical and clinical studies suggests that amyloid-beta aggregation can also drive the progression of tauopathy (reviewed by Stancu et al., 2014; Hanseeuw et al., 2019), which is increasingly believed to play a key role in cognitive decline (Nelson et al., 2012; Di et al., 2016; Digma et al., 2019). The precise, mechanistic roles of these proteopathies in the aetiology and pathogenesis of AD are the subject of extensive research and debate; however, pathogenic protein aggregation remains strongly implicated in the disease (Lovestone and McLoughlin, 2002; Thal and Fändrich, 2015; Jouanne et al., 2017; Gandhi et al., 2019; Johnson et al., 2019). We will briefly outline the characteristics of amyloid-beta and tau and their aggregation pathways.

Amyloid-Beta

Amyloid-beta peptides are 38- to 43-residue peptides resulting from the sequential cleavage of amyloid precursor protein (APP) by the secretase family of enzymes (Crescenzi et al., 2002). APP itself is heterogeneous, ranging from 110 to 140 kDa, with three major isoforms (695, 751, and 770 residues in length) determined by the splicing pattern of its expression product, and is subjected to a range of post-translational modifications including sulfation, phosphorylation, and N- and O-linked glycosylation (Zheng and Koo, 2011). The generation of amyloid-beta results from a cleavage pathway of APP commonly referred to as the amyloidogenic pathway. This begins with the cleavage of APP by beta-secretase (BACE1), generating two fragments: a C-terminal fragment of APP referred to as C99, and a secreted, soluble N-terminal fragment termed sAPP- β . C99 is subsequently bound by the gamma-secretase complex, comprised of four protein subunits: presenilin (PSEN; PSEN1/PSEN2 isoforms), presenilin enhancer (PEN), Nicastrin, and APH-1. Processing of C99 by gamma-secretase results in a series of sequentially shorter cleavage products, until the amyloid-beta peptide is released (O'Brien and Wong, 2011). In the central nervous system, amyloid-beta is predominantly secreted by neurons and astrocytes into the extracellular space of the brain and physiologically cleared by the vascular system and cerebrospinal fluid. In AD, clearance mechanisms for amyloid-beta are impaired, leading to accumulation in the brain parenchyma (Ramanathan et al., 2015). Multiple amyloid-beta isoforms have been observed in the brain tissue of patients with AD, including amyloid-beta₁₋₄₀ (A β 40), amyloid-beta₁₋₄₂ (A β 42), and amyloid-beta₁₋₄₃ (A β 43; Welander et al., 2009); among them, A β 42 is the primary constituent of neuritic plaques observed in end-stage AD (O'Brien and Wong, 2011).

While physiological roles of amyloid-beta peptides have been identified (Pearson and Peers, 2006; Morley et al., 2019), the aggregation of amyloid-beta monomers has causally been associated with neuronal toxicity (Yankner and Lu, 2009; Pauwels et al., 2012; Prasansuklab and Tencomnao, 2013; Carrillo-Mora et al., 2014). Amyloid-beta aggregates occur in a variety of assemblies, from low molecular weight oligomers

(including dimers, trimers, tetramers, and pentamers) to higher molecular weight oligomers (hexamers, nonamers, dodecamers; Wolff et al., 2017), protofibrils, and fibrils, as well as amorphous aggregates (Jiang et al., 2012). *in vitro*, the formation of these aggregate species is affected by various factors including the presence and concentration of specific ions, such as metals, as well as pH and temperature (Valerio et al., 2008; Jiang et al., 2012; Bin et al., 2013; Faller et al., 2013; Bhowmik et al., 2014; Zhao and Ai, 2018). Amyloid-beta aggregation is illustrated in **Figure 2**.

Multiple regions of the amyloid-beta sequence are considered pro-aggregatory. A report by Liu et al. (2004) described six fragments of amyloid-beta₁₋₄₀ (A β 40), formed by residues A β 40₁₋₂₈, A β 40₁₂₋₂₈, A β 40₁₇₋₂₈, A β 40₁₀₋₂₀, A β 40₂₅₋₃₅, and A β 40₁₇₋₄₀, which had a pro-aggregatory effect on the full-length peptide. Hsu et al. (2018) later identified several key residues involved in amyloid-beta aggregation: H14, E22, D23, G33, G37, and G38. Enache et al. (2018) later characterised the influence of key hydrophobic regions, particularly the well-characterised hydrophobic core domain KLVFF, as well as the C-terminal hydrophobic sequence IIGLMVGGVV and a histidine-containing tetrad, VHHQ, on amyloid-beta aggregation through atomic force microscopy and voltammetry. New insights into the aggregation pathway of amyloid-beta were also attained more recently by Nirmalraj et al. (2020) at nanometer resolution. A β 42 was shown to aggregate faster than A β 40 at all stages of assembly. Additionally, the study by Nirmalraj et al. (2020) confirmed that oligomers are not simply an intermediate aggregation species along a linear path to the formation of mature fibrils; oligomers were present even at timepoints where mature fibrils were detected. The pathological effects of different aggregate assemblies have been the subject of extensive research and debate (reviewed by Di Carlo, 2010), however, it is widely accepted that soluble oligomers are a highly cytotoxic species, preceding the development of end-stage neuritic plaques (Resende et al., 2008; Larson and Lesné, 2012; Sengupta et al., 2016; Chen et al., 2017).

Tau

Tau proteins are encoded by the *MAPT* gene on chromosome 7 (Neve et al., 1986); the pre-mRNA product of *MAPT* undergoes a range of alternative splicing events, resulting in transcript variants encoding six protein isoforms found in the central nervous system (D'Souza and Schellenberg, 2000). These isoforms range from 352 to 441 residues in length and are comprised of four distinct functional domains: the N-terminal projection domain (residues 1–165), proline-rich region (PRR; residues 166–242), microtubule-binding domain (MTBD; 243–367), and C-terminal domain (368–441). The N-terminal domain and MTBD are the primary sites affected by alternative splicing, and the resulting isoforms can be categorised by the number of repeat regions comprising the MTBD: 3R (three-repeat) and 4R (four-repeat) tau (D'Souza and Schellenberg, 2000). The absence of an insert, or the presence of one or two inserts, in the N-terminal projection domain also demarcates each of the isoforms as 0N, 1N or 2N, respectively; the six isoforms are thus referred to as 0N3R, 1N3R, 2N3R, 0N4R, 1N4R, and 2N4R, depending on their number of N-terminal

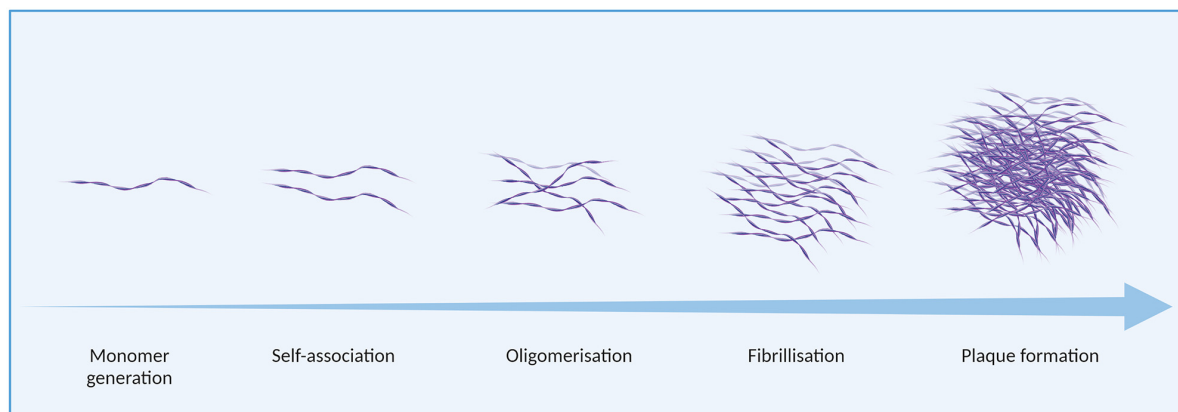


FIGURE 2 | Amyloid-beta aggregation in Alzheimer's disease (AD).

inserts and MTBD repeats. In the adult human brain, 3R and 4R isoforms of tau are present in equal abundance, and tau aggregates found in AD are comprised of both three- and four-repeat isoforms (Kolarova et al., 2012).

Physiologically, tau is involved in the assembly and stabilisation of microtubules (Weingarten et al., 1975), as well as in the regulation of intracellular trafficking (Vershini et al., 2007; Dixit et al., 2008). These activities are regulated by post-translational modifications of the tau protein, which include phosphorylation, glycosylation, deamidation, oxidation, nitration, glycation, and ubiquitination. These modifications to tau and their physiological consequences have previously been reviewed in detail by Avila et al. (2004). Most pertinent to the development of tau aggregates found in AD is tau phosphorylation, which negatively regulates the binding of tau to microtubules and the cellular membrane (Brandt et al., 1995). Tau phosphorylation can occur at any of the multiple serine, threonine and tyrosine residues found on the protein (Williamson et al., 2002; Noble et al., 2013). Phosphorylation of tau induces a conformational change in the protein, reducing its ability to stimulate microtubule assembly (Jameson et al., 1980). In AD, phosphorylation of tau is observed to be over three times higher than in physiological conditions (Köpke et al., 1993). Hyperphosphorylated tau detaches from microtubules, aggregating in the cytosol, as illustrated in **Figure 3**. Tau acetylation, which similarly increases the negative charge of tau, has also been associated with AD (Irwin et al., 2012; Lucke-Wold et al., 2017).

Tau aggregation primarily involves a shift in the conformation of two hexapeptide regions in the protein, VQIVYK and VQIINK (also referred to as PHF6 and PHF6* respectively), from a random coil to a beta sheet structure (von Bergen et al., 2005; Li and Lee, 2006; Eschmann et al., 2015). Oligomers of tau aggregate further to form paired helical filaments (PHFs) and, subsequently, the neurofibrillary tangles (NFTs) observed in end-stage AD. Tau multimers in a variety of conformations including straight filaments, twisted ribbons, and small oligomeric aggregates have also been observed in

the brain tissue of patients with AD (Grundke-Iqbal et al., 1986; Meraz-Ríos et al., 2010). Recent, comprehensive reviews by Niewiadomska et al. (2021) and Shafiei et al. (2017) have established oligomeric assemblies of tau as cytotoxic species.

CATIONIC ARGININE-RICH PEPTIDES AS AGGREGATION INHIBITORS FOR ALZHEIMER'S DISEASE

Inhibitory Peptides for Amyloid-Beta Aggregation

Through phage display, Kawasaki et al. (2010) identified libraries of three- and four-residue peptides capable of inhibiting (A β 42) oligomerisation, and found arginine-containing peptides were enriched in both libraries; arginine comprised two of three, and two-to-three of four, residues in the majority of peptides identified, including RRRR, RRRL, RFRK, RRY, and RPR. Kawasaki et al. (2011) also found that while monomeric arginine and di-arginine were able to bind A β 42, they did not have significant effects on the formation of A β 42 oligomers, leading the authors to conclude that these molecules were too small to effectively inhibit A β 42 oligomerisation. Together with the higher binding affinity and inhibitory effect of SRPGLRR in comparison to the three- and four-residue peptides, Kawasaki et al. (2011) concluded the size of the compound could be an important factor in the development of inhibitory peptides for amyloid-beta aggregation.

Notably, among the arginine-rich peptides screened by Kawasaki et al. (2011), RRRR and RRRL were found to be comparatively weaker, yet still effective, inhibitors of A β 42 oligomerisation than RFRK. While the authors concluded that the higher efficacy of RFRK as an aggregation inhibitor was likely due to the phenylalanine residue of RFRK binding a phenylalanine residue of amyloid-beta, thereby strengthening the interaction between the inhibitor and amyloid-beta, an arginine residue in the second position of either inhibitory peptide

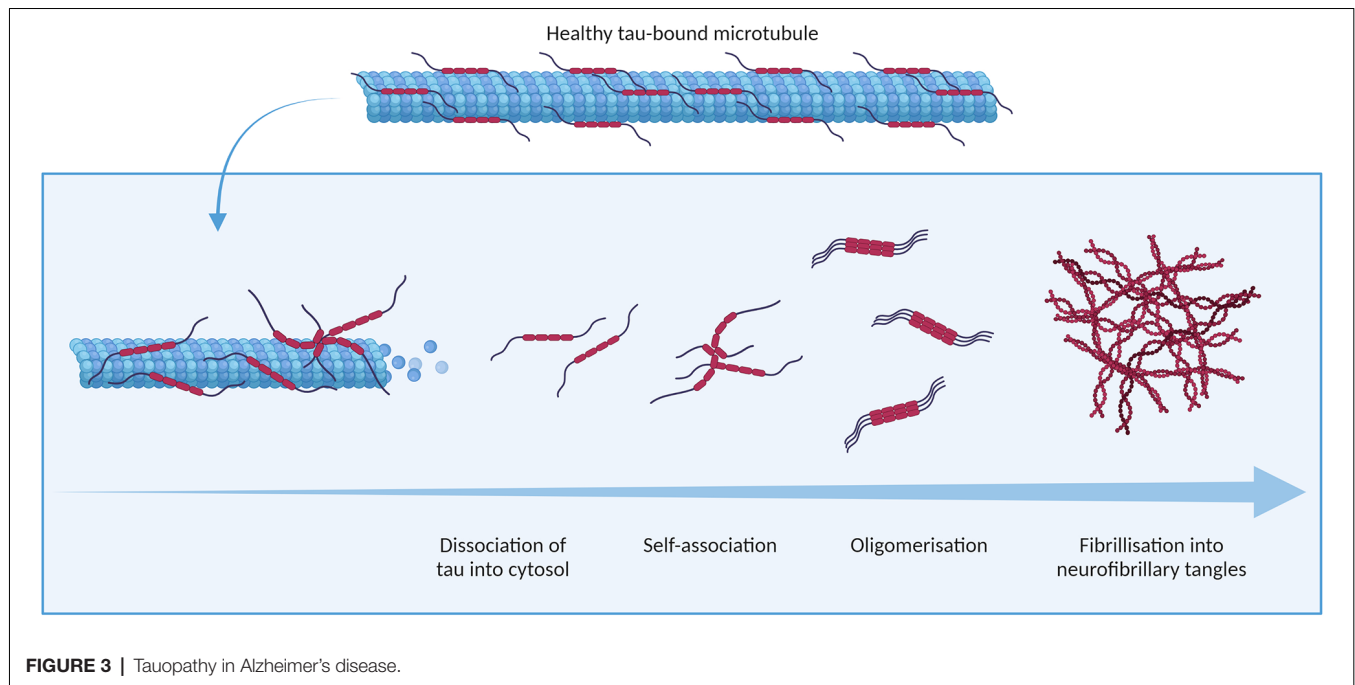


FIGURE 3 | Tauopathy in Alzheimer's disease.

could also bind a phenylalanine residue of A β 42 through its aliphatic side chain, and ability to form cation- π interactions with aromatic residues. It is, therefore, possible that the increased efficacy of RFRK was rather due to the cationicity of the lysine residue in RFRK imparting a stronger capacity for inhibition of A β 42 aggregation than the terminal alanine and leucine residues of RRRA and RRRL, respectively. Regardless, the efficacy of RRRA, RRRL, RFRK, and SRPGLRR as inhibitors of A β 42 oligomerisation led Kawasaki et al. (2011) to consider arginine an important residue for inhibiting A β 42 aggregation.

Further work by Kawasaki and Kamijo (2012) demonstrated that two additional hybrid peptides combining arginine residues with organic moieties, Arg-Arg-7-amino-4-trifluoromethylcoumarin (RR-AFC) and Arg-Arg-thiobenzyl ester (ZRR-SBzl), were also able to inhibit amyloid-beta aggregation. Recent *in silico* characterisation of RR-AFC conducted by Barale et al. (2019) using molecular dynamics simulation indeed evidenced the critical role of arginine residues in the destabilisation of amyloid-beta protofibrils; in particular, the arginine residues of RR-AFC were found to bind amyloid-beta protofibrils through hydrogen bonding *via* their guanidinium moieties.

Many peptide-based candidates rationally designed to inhibit amyloid-beta aggregation have been derived from the sequence of amyloid-beta itself, exploiting its propensity for self-aggregation to facilitate targeted binding (Watanabe et al., 2002; Austen et al., 2008; Viet et al., 2011; Arai et al., 2014; Kino et al., 2015; Kumar et al., 2015; Cheng et al., 2017; Lu et al., 2019; Jokar et al., 2020). The majority of these peptides contain elements derived from amyloidogenic sequences involved in beta-sheet formation (Moss et al., 2003), such as the KLVFF (amyloid-beta_{16–20}) and GGVVIA

(amyloid-beta_{37–42}) motifs, and are thus termed beta-sheet breakers (Soto et al., 1998). The design of these peptides generally includes an amyloid-derived sequence for target binding, conjugated to a flexible hydrophilic or cationic element to disrupt aggregation. One such inhibitor was a KLVFF-derived retro-inverso peptide, RI-OR2 (rGffvlkGr; lower case denoting D-amino acids), which effectively reduced A β 42 aggregation *in vitro* (Parthasarathy et al., 2013). As RI-OR2 was not designed to penetrate the blood-brain barrier, it was subsequently fused to the arginine-rich cell-penetrating TAT peptide resulting in the hybrid peptide, RI-OR2-TAT (Ac-rGffvlkGrrrrqrkkkGy-NH₂; net charge +11.0). Intriguingly, experimental results from Parthasarathy et al. (2013) indicated that RI-OR2-TAT not only had beneficial effects on the aggregation and cytotoxicity of A β 42 aggregation in cell models and in a transgenic mouse model of amyloidogenesis (APP^{Swe}/PS1 Δ E9) *in vivo*, but also demonstrated greater efficacy for inhibiting the aggregation of A β 42 *in vitro* compared to RI-OR2. The inhibitory effects of RI-OR2-TAT on A β 42 aggregation were evident at even the earliest detectable stages of A β 42 oligomerisation. Surface plasmon resonance (SPR) experiments conducted by Parthasarathy et al. (2013) further indicated RI-OR2-TAT had a higher binding affinity for A β 42 than RI-OR2 alone. It is likely that the increased efficacy of RI-OR2-TAT as an inhibitor of A β 42 aggregation was mediated by the arginine content of TAT, specifically through: (a) greater capacity for hydrogen bonding imparted by the arginine residues of the TAT peptide, facilitating a higher number of electrostatic interactions between the inhibitory peptide and A β 42; (b) increased cationic charge of the RI-OR2-TAT peptide conferred by the arginine-rich TAT component, driving further charge-

based repulsion of bound A β 42 monomers; and (c) the increased length of the inhibitory peptide likely causing greater steric and/or electrostatic interference between monomers of A β 42, preventing their self-association. Importantly, these findings suggested that arginine-rich peptides could themselves have a mechanistic role in modulating the development of amyloid-beta aggregates beyond their use as “carrier” peptides alone.

Cheng et al. (2017) later developed a bipartite peptide comprised of polyarginine-8 (R8) conjugated to the sequence of amyloid-beta_{25–35} (RRRRRRRRGSNKGAIIGLM; net charge +9.0) which effectively reduced cerebral accumulation of amyloid-beta and ameliorated cognitive deficits in the *APP/PS1* double transgenic mouse model of AD. The design of the peptide was comprised of the amyloid-beta_{25–35} self-recognition element to facilitate binding to amyloid-beta monomers, with the polyarginine component intended to drive charge-based repulsion of the bound monomers from each other, preventing their ability to aggregate.

More recently, Henning-Knechtel et al. (2020) designed two cell-penetrating peptides comprised of a hydrophobic signal sequence (MLRTKDLIWTFLFGTAVS; NCAM1) conjugated to a polycationic sequence (KKRPKP; PrP_{23–28}) or an amyloid-derived self-recognition motif sequence (KLVFF; A β _{16–20}) via a lysine residue to increase the cationic charge of the peptide. The NCAM1-PrP peptide carried a higher overall charge of +6 compared to the +4 charge of NCAM1-A β , resulting from a higher proportion of cationic residues. While both NCAM1-PrP and NCAM1-A β were found to inhibit the aggregation of A β 42 *in vitro*, NCAM1-PrP achieved effective inhibition at substoichiometric concentrations, while an equimolar concentration of NCAM1-A β to amyloid-beta was required. As amyloid-beta is negatively charged at physiological pH (net charge –2.7), the increased efficacy of NCAM1-PrP as an aggregation inhibitor compared to the KLVFF-containing NCAM1-A β peptide was attributed to its higher proportion of cationic residues, reportedly essential in stabilising the dimers formed between NCAM1-PrP and amyloid-beta. Additionally, although NCAM1 itself was able to bind amyloid-beta, the addition of a polycationic sequence was required to exert a modulatory effect on aggregation, suggesting the overall charge of an inhibitory peptide may be as important for preventing the aggregation of amyloid-beta as structural specificity. Indeed, Henning-Knechtel et al. suggested that the NCAM1-A β peptide could be optimised through further addition of cationic residues, thus it is conceivable that higher arginine content could increase its efficacy. These results also support the idea that electrostatic interactions between an inhibitory peptide and amyloid-beta are sufficient to drive target binding in the absence of amyloid-beta-derived sequence motifs, as was demonstrated by Parthasarathy et al. (2013).

The effects of a short peptide comprised entirely of arginine, polyarginine-9 (R9), were investigated by Fonar et al. (2018) in the triple transgenic (3xTg) mouse model of AD which harbours FAD mutations inducing the development of both amyloid-beta and tau pathology. 3xTg mice treated with R9 displayed a trend toward lower levels of cerebral

amyloid-beta compared to untreated controls, as well as a trend toward reduced levels of oligomeric amyloid-beta in hippocampal lysates, however, these findings did not reach statistical significance. The effects of longer polyarginine peptides on amyloid-beta pathology may be an interesting area for further research; it is possible that increased cationic charge imparted by longer stretches of arginine could impart a greater capacity for electrostatic repulsion of amyloid-beta monomers, thereby inhibiting aggregation. Additionally, D-enantiomeric polyarginine peptides could potentially exert a stronger effect due to the increased proteolytic stability of D-amino acids (Feng and Xu, 2016) in comparison to L-isoforms.

Among the most promising aggregation inhibitors targeting amyloid-beta is the cationic arginine-rich RD2 peptide (ptlthnrrrrr; +6.2 net charge), demonstrated to eliminate amyloid-beta oligomers *in vivo*, and rescue amyloid-beta pathology and cognitive deficits in a transgenic mouse model of AD (Schemmert et al., 2019; Zhang et al., 2019). RD2 is a rationally-optimised derivative of an arginine-rich precursor peptide, D3 (rprrtlhrrnr; +5.2 net charge), which was initially identified through mirror-image phage display (Wiesehan et al., 2003) and also shown to be effective in targeting amyloid-beta (van Groen et al., 2008). A series of C-terminally amidated D3 analogues were developed, outlined in **Table 1**, to identify a candidate for further development (Klein et al., 2017). Notably, increasing the charge of the inhibitory peptide was associated with increased binding affinity to amyloid-beta (Ziehm et al., 2016).

Continued characterisation of D3 analogues indicated RD2 had the most favourable pharmacokinetic profile with regards to half-life and oral bioavailability (Leithold et al., 2016). Indeed, the initial success of RD2 in phase I clinical trials has led to its ongoing development as a potential therapeutic candidate for AD (Elfgen et al., 2021). The molecular mechanisms of both D3 and RD2 were investigated in detail through computational studies and experimental verification by Olubiyi et al. (2014), revealing that both D3 and RD2 bind amyloid-beta with high affinity, and reduce β -sheet formation, largely due to electrostatic interactions between the arginine residues of the inhibitory peptides and key anionic residues (E11, E22 and D23) of amyloid-beta.

Inhibitory Peptides for Tau Aggregation

Peptide-based inhibitors of tau aggregation have focused on the PHF6 and PHF6* regions of the MTBD, which are well-characterised as pro-aggregatory sequences (Li and Lee, 2006; Eschmann et al., 2015). Ralhan et al. (2017) reported inhibition of PHF6 aggregation by the poly-arginine-6 (R6) and R8 peptides, as well as the reversal of PHF6 fibril formation by R6 which acted as a beta-sheet breaker, inducing the disassembly of PH6 fibrils into sparser aggregates. While early peptides targeting the PHF6 region have shown effective inhibition of the isolated hexapeptide *in vitro*, these peptides were unable to prevent the aggregation of full-length tau (Sievers et al., 2011; Zheng et al., 2011; Seidler et al., 2018), which additionally

contains the amyloidogenic PHF6* sequence considered to be a significant driver of tau aggregation. Seidler et al. (2018) subsequently developed new inhibitory peptides through combinatorial mutagenesis of the VQIINKKLD motif. These peptides are comprised of 10 residues, outlined in **Table 2**, and able to prevent aggregation of the full-length tau protein. Importantly, to achieve this, the inclusion of an arginine residue was required at the ninth position in order to prevent self-association of one of the two main interfaces involved in full-length tau aggregation: the KKL region of the tau KVQIINKKLD sequence, termed “interface B”.

Longer polyarginine peptides (R32 to R96) were demonstrated by Nadimidla et al. (2017) to inhibit the aggregation of both PHF6 and the PHF6*-containing amyloidogenic tau fragment GKVQIINKKLDL, as well as aggregation of the full-length mutant tau protein P301L, which is found in human tauopathies (Cosacak et al., 2017). The aggregation of PHF6 and PHF6* peptides was also inhibited, albeit to a lesser degree, by the cationic polymer polyethylenimine (PEI), implicating the positive charge of these compounds as a key factor in suppressing tau aggregation. Tau is aggregated in the presence of heparin *in vitro* to model the proaggregatory role of polyanionic molecules such as heparan sulfate proteoglycans found in NFTs *in vivo* (Fichou et al., 2018; Maïza et al., 2018); it is likely that, in addition to interacting electrostatically with negatively charged stretches

of tau itself, strongly cationic compounds such as polyarginine could inhibit the seeding and nucleation of tau aggregation by complexing with essential polyanionic cofactors involved in the aggregation process. Furthermore, post-translational modifications which increase the negative charge of tau *in vivo*, such as phosphorylation, acetylation and nitration, could potentially increase the affinity of CARPs for tau, and their ability to modulate its aggregation.

Zhang et al. (2020) subsequently reported an arginine-rich, D-enantiomeric peptide termed p-NH (nitmnsrrrrrh; net charge +4.1), discovered through phage display, was able to inhibit tau aggregation *in vitro* and reduce tau^{P301S} levels in transgenic mice. *In vitro*, p-NH was shown to inhibit PHF6 aggregation in a dose-dependent manner; this effect was optimal at an 8-fold molar excess of the peptide over PHF6, but remained effective at equimolar and substoichiometric concentrations. Remarkably, p-NH was also able to reverse aggregation when added to preformed PHF6 fibrils. Importantly, Zhang et al. (2020) reported p-NH was able to interact directly with PHF6 through hydrogen bond formation.

More recently, Aggidis et al. (2021) reported a D-enantiomeric, retro-inverso peptide (rrrrrrrrGpkyk(ac)iqvGr; net charge +11.0) based on the PHF6 sequence, termed RI-AG03, able to prevent tau aggregation. As a retro-inverso peptide, RI-AG03 was optimised for increased proteolytic stability from the AG03 peptide, itself selected from a family of peptides designed to inhibit tau aggregation (Aggidis, 2019)

TABLE 1 | Cationic arginine-rich peptides with modulatory effects on amyloid-beta aggregation.

Peptide	Sequence (Net charge at pH 7)	Effect	Reference
R5	RRRRR (+5.0)	Modulation of Aβ aggregation towards the formation of large, amorphous, non-toxic aggregates	Gibson and Murphy (2005)
KLFF-R5	KLFFRRRRR (+6.0)		
D3	rprrlthnrr (+5.2)	Reduction of Aβ oligomers <i>in vitro</i>	van Groen et al. (2008)
RFRK	RFRK (+3.0)	Inhibition of Aβ aggregation <i>in vitro</i>	Kawasaki et al. (2011)
RRRL	RRRL (+3.0)		
RRRA	RRRA (+3.0)		
SRPGLRR	SRPGLRR (+3.0)		
RR-AFC	RR-7-amino-4-trifluoromethylcoumarin (+3.0)	Inhibition of Aβ aggregation <i>in vitro</i>	Kawasaki and Kamijo (2012)
ZRR-SBzl	RR-thiobenzyl ester (+3.0)		
RI-OR2-TAT	Ac-rGffvIkGrrrrqrkrGy-NH ₂ (+11.0)	Inhibition of Aβ aggregation <i>in vitro</i> , reduced cerebral Aβ load <i>in vivo</i>	Parthasarathy et al. (2013)
15M S.A.	Ac-rklmqptnrrnpt-NH ₂ (+5.0)	Modulation of Aβ aggregation towards the formation of large, amorphous, non-toxic aggregates	Barr et al. (2016)
DB1	rpitrhtdnrr-NH ₂ (+4.1)		
DB2	rpittlqthqnr-NH ₂ (+3.1)		
DB3	rpitrthqnr-NH ₂ (+5.1)		
DB4	rprrlthqnr-NH ₂ (+6.1)	No effect on Aβ aggregation <i>in vitro</i>	
DB5	rpitrqthqnr-NH ₂ (+3.1)	Inhibition of Aβ aggregation <i>in vitro</i>	
DB3DB3	rpitrthqnrppitrthqnr-NH ₂ (+9.2)		
RD2RD2	ptlthnrrrrrrptlthnrrrr (+11.4)	Reduction of Aβ oligomers <i>in vitro</i> and <i>in vivo</i>	Kutzsche et al. (2017)
RD2D3	ptlthnrrrrrrprrlthnrr-NH ₂ (+11.4)		
D3D3	rprrlthnrrrrprrlthnrr-NH ₂ (+11.4)		
R8-Aβ ₂₅₋₃₅	RRRRRRRR-GSNKGAIIGLM (+9.0)	Reduced cerebral Aβ load <i>in vivo</i>	Cheng et al. (2017)
R9	RRRRRRRR (+9.0)	Trend toward reduced Aβ oligomers <i>in vivo</i>	Fonar et al. (2018)
RD2	ptlthnrrrr-NH ₂ (+6.2)	Reduction of Aβ oligomers <i>in vitro</i> and <i>in vivo</i>	Zhang et al. (2019)
NCAM1-PrP	MLRTKDLIWLFFLGTAVS-KKRPKP-NH ₂ (+6.0)	Inhibition of Aβ aggregation <i>in vitro</i>	Henning-Knechtel et al. (2020)
NCAM1-Aβ	MLRTKDLIWLFFLGTAVS-KKLVFF-NH ₂ (+4.0)		

Lowercase letters denote D-enantiomeric residues.

which are summarised in **Table 2**. The majority of the inhibitory peptides developed by Aggidis (2019) significantly reduced the aggregation of recombinant human tau $\Delta 1-250$, which exhibits faster aggregation kinetics than full-length tau protein, in a dose-dependent manner. Importantly, Aggidis (2019) reported that increasing arginine content of the inhibitory peptides, up to five residues, increased tau $\Delta 1-250$ solubility. An interesting observation is that R8 alone was unable to prevent tau $\Delta 1-250$ aggregation, in contrast to prior results indicating the effective inhibition of PHF6 aggregation by R6 and R8 (Ralhan et al., 2017); taken together, these effects are consistent with observations reported by Seidler et al. (2018) that PHF6* aggregation is a significant driver of aggregation in larger tau fragments.

CATIONIC ARGININE-RICH PEPTIDES AS MODULATORS OF PROTEOPATHIC CYTOTOXICITY

As the precise, mechanistic roles of amyloid-beta and tau aggregates in the pathogenesis of AD remain unclear, CARPs could also be beneficial by mitigating the cellular effects of cytotoxic amyloids, rather than preventing the formation of aggregates *per se*. As comprehensively detailed in a review

by Meloni et al. (2020), CARPs have favourable biological effects in models of neuronal injury and disease, such as stroke and traumatic brain injury, through multimodal mechanisms of action. Here, we will discuss how the bioactive properties of CARPs could be beneficial specifically in the context of proteopathic cytotoxicity associated with AD.

Modulation of Cytotoxicity Through Effects on Amyloid Formation

There are multiple potential mechanisms for CARPs to confer cytoprotection against toxic aggregates of amyloid-beta and tau. As described, the predominant approach has focused on inhibiting aggregation; CARPs which have demonstrated the ability to reduce amyloid-beta-induced cytotoxicity *in vitro* by inhibiting aggregation include those developed by Kawasaki et al. (2011), Parthasarathy et al. (2013), Cheng et al. (2017) and Henning-Knechtel et al. (2020). Additionally, Nadimidla et al. (2017), whose work reported inhibition of tau aggregation through high molecular-weight polyarginine peptides, demonstrated increased rates of cell survival in cultures exposed to cytotoxic concentrations of tau when treated with polyarginine peptides.

TABLE 2 | Polyarginine and arginine-rich peptides with modulatory effects on tau aggregation.

Peptide	Sequence (Net charge at pH 7)	Effect	Reference
R6	RRRRRR (+6.0)	Inhibition of tau PHF6 aggregation <i>in vitro</i>	Ralhan et al. (2017)
R8	RRRRRRRR (+9.0)		
R32	R ₃₂ (+32.0)		
R96	R ₉₆ (+96.0)	Inhibition of tau PHF6 and PHF6* aggregation <i>in vitro</i>	Nadimidla et al. (2017)
WINK	DVQWINKKRR (+3.0)		
MINK	DVQMINKKRR (+3.0)		
AG01	Ac-RGVQIINKGR-NH ₂ (+3.0)	Reduction of tau $\Delta 1-250$ aggregation <i>in vitro</i>	Aggidis (2019)
AG02	Ac-RGVQIVYKGR-NH ₂ (+3.0)		
AG02R4	Ac-RRGVQIVYKGRR-NH ₂ (+5.0)		
AG02R5	Ac-RGVQIVYKGRRRR-NH ₂ (+6.0)		
AGR502	Ac-RRRGVQIVYKGR-NH ₂ (+6.0)		
AG02PR5	Ac-RRRGVQIVYKGRRRR-NH ₂ (+8.0)		
AG02R6	Ac-RRRGVQIVYKGRRR-NH ₂ (+7.0)		
AG02R9	Ac-RGVQIVYKGRRRRRRR-NH ₂ (+10.0)		
AG02TAT	Ac-RGVQIVYKGRYGRKKRRQRRR-NH ₂ (+11.0)		
AG02 Δ I	Ac-RGVQK(Ac)VYKGR-NH ₂ (+3.0)		
AG02 Δ V	Ac-RGVQIK(Ac)YKGR-NH ₂ (+3.0)		
AG03	Ac-RGVQIK(Ac)YKPGRRRRRRRR-NH ₂ (+10.0)		
AG03-Cys	Ac-RGVQIK(Ac)YKPGRRRRRRRRC-OH (+9.9)		
AG03M	Ac-RGV(m)QI(m)K(Ac)Y(m)KP(m)GRRRRRRRR-NH ₂ (+10.0)		
FAM-RI-AG03	Ac-k(FAM)rrrrrrrGpkyk(ac)iqvGr-NH ₂ (+10.0)	No significant effect on tau $\Delta 1-250$ aggregation	
Scrambled AG03	Ac-RGQPKIK(Ac)YVGRRRRRRRR-NH ₂ (+10.0)		
R8	RRRRRRRR (+8.0)		
TAT	Ac-YGRKKRRQRRR-NH ₂ (+8.0)	Reduction of tau PHF6 aggregation <i>in vitro</i> and tau aggregation <i>in vivo</i>	Zhang et al. (2020)
p-NH	NITMNSRRRRNH (+4.1)		
RI-AG03	Ac-rrrrrrrGpkyk(ac)iqvGr-NH ₂ (+10.0)	Inhibition of tau PHF6 and tau $\Delta 1-250$ aggregation <i>in vitro</i>	Aggidis et al. (2021)
TAT-7H	YGRKKRRQRRR-HHHHHHH (+8.7)	Inhibition of tau Ser202 and Thr205 phosphorylation	Kondo et al. (2021)

(Ac) and (m) denote residue acetylation and methylation, respectively. Lowercase letters denote D-enantiomeric residues.

However, as the cytotoxicity of amyloid-beta aggregates varies depending on the aggregate conformation, inhibiting aggregation is not the only means of decreasing the concentration of cytotoxic aggregate species. CARPs, through their ability to electrostatically bind monomers of amyloid-beta, may be able to bind and stabilise monomers in conformations favouring non-oligomeric aggregation pathways. Gibson and Murphy (2005) previously reported that polyarginine-5 (R5) and KLVFF-R5 peptides broadly increased the aggregation of amyloid-beta₁₋₄₂ overall, resulting in the formation of larger amyloid-beta₁₋₄₂ aggregates with lower cytotoxicity. Barr et al. (2016) reported that a 15-residue cationic peptide, with 20% of its sequence comprised of arginine residues, reduced the formation of soluble, cytotoxic amyloid-beta₁₋₄₂ oligomers by driving the aggregation pathway toward the formation of larger, amorphous aggregates; these amorphous aggregates were also observed to have lower cytotoxicity than the oligomers formed by amyloid-beta₁₋₄₂ alone. A potential therapeutic mechanism for peptides targeting amyloid-beta could therefore involve the reduction of cytotoxic, soluble oligomeric amyloid-beta species by driving the aggregation pathway toward the formation of non-toxic insoluble aggregate species, rather than aiming to inhibit aggregation.

Potential Indirect Mechanisms of Cytoprotection Against Amyloids

CARPs may be able to prevent the cellular conditions favouring the formation of cytotoxic aggregates. For example, a proteomic study of neuronal cultures treated with the polyarginine-18 peptide (R18) showed overall levels of tau were significantly decreased (MacDougall et al., 2019a, supplementary information), however the mechanisms underlying this effect are unclear. Arginine is also able to scavenge free radicals and mitigate oxidative stress (Wascher et al., 1997; Haklar et al., 1998), an ability that extends to polyarginine peptides (Marshall et al., 2015). Oxidative stress has a synergistic relationship with amyloid-beta pathology (reviewed in detail by Cheignon et al., 2018), as well as tau phosphorylation and polymerisation (reviewed by Zhao and Zhao, 2013). Reducing oxidative stress could potentially therefore aid, indirectly, in preventing the formation of aggregate species. Additionally, as oxidative stress is believed to be one of the main mechanisms through which amyloid-beta and tau aggregates induce toxic effects (Butterfield et al., 2013), there may be a potential role for arginine and CARPs in cytoprotection through the indirect, downstream effects of rescuing oxidative damage, an area which requires further investigation.

CARPs may also be able to prevent the development of tauopathy through inhibition of tau hyperphosphorylation, which is pro-aggregatory. The p-NH peptide developed by Zhang et al. (2020) was reported to significantly reduce tau phosphorylation at Thr181, Ser202, Thr231, Ser396, and Ser404 in the human neuroblastoma N2a cell line. More recently, a CARP developed by Kondo et al. (2021) termed TAT-7H (YGRKKRRQRRR-HHHHHHH; net charge +8.7) was shown to inhibit the phosphorylation of Ser202 and Thr205 in a neuronal

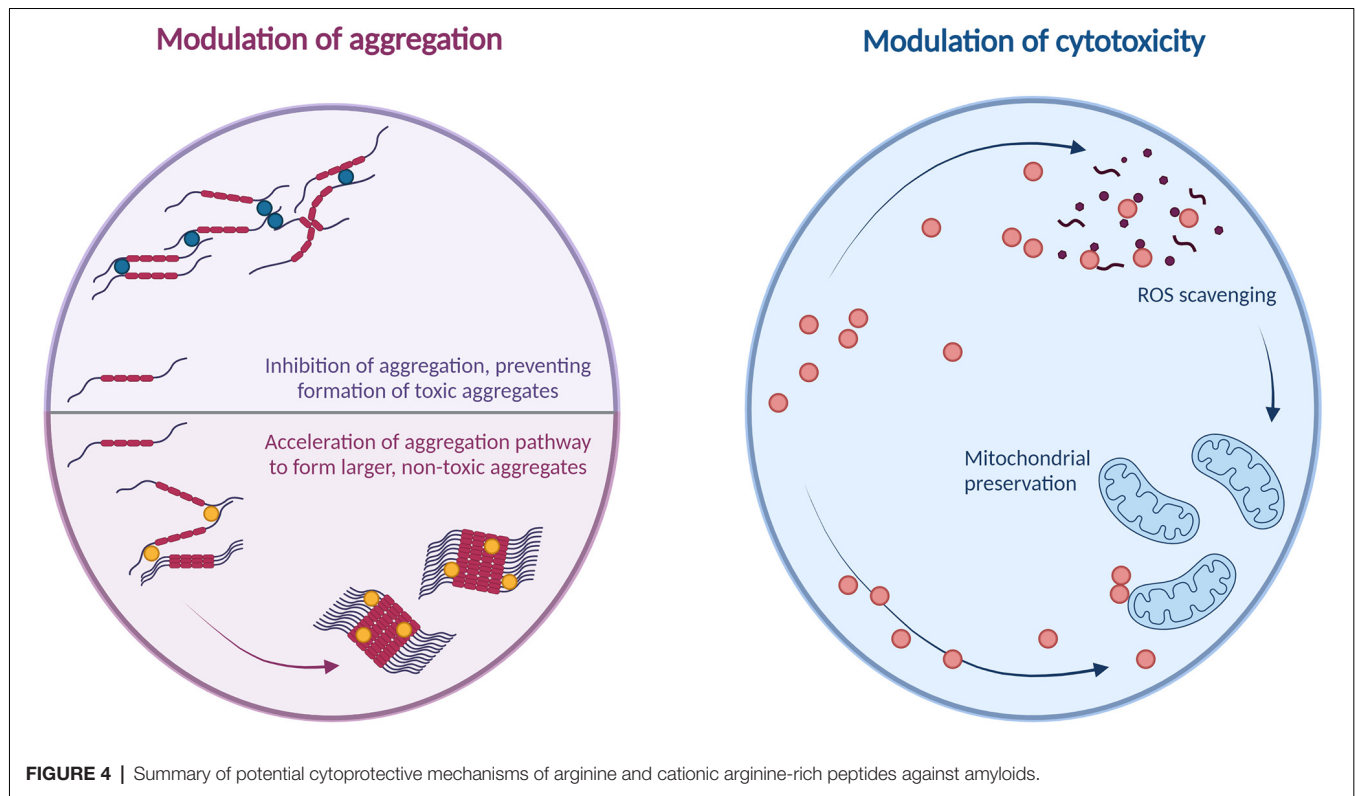
cell line differentiated from human tau^{P301S} double knock-in induced pluripotent stem cells.

Protein aggregates in AD also induce cytotoxicity through mitochondrial damage; tau oligomers are believed to induce mitochondrial damage *via* their detrimental effects on intracellular transport networks (Shafiei et al., 2017), while accumulation of amyloid-beta at the mitochondrial membranes induces mitochondrial damage through mechanisms including aberrant interactions with mitochondrial proteins, generation of reactive oxygen species, and disruption of the electron transport chain (reviewed in detail by Reddy et al., 2010, and Chen and Yan, 2007). The ability of CARPs to preserve mitochondrial function has been discussed at length in a review by MacDougall et al. (2019b); thus, another area for future research would be the potential for CARPs to preserve mitochondrial function and mitigate cytotoxicity in models of amyloid-beta and tau-induced neuronal injury. These mechanisms are summarized in **Figure 4**.

It is also possible that arginine-rich peptides, through their extensive capacity for electrostatic interactions, may be able to bind pre-formed aggregates and prevent their deleterious cellular effects. It was recently discovered that fibrillar formations of tau exhibit an altered interactome than tau monomers and nano-aggregates. Ferrari et al. (2020) demonstrated that tau fibrils preferentially interact with a set of proteins containing disordered stretches significantly enriched for arginine residues, with these aberrant interactions mediated by pi-pi stacking interactions. Crucially, Ferrari et al. (2020) found that the replacement of arginine residues in these interacting proteins with lysine precluded their interactions with tau fibrils. The proteins comprising the altered interactome of tau fibrils were identified as predominantly belonging to three functional clusters: RNA-binding proteins, regulators of protein phosphorylation, and microtubule-associated proteins. It was inferred that these interactions may, in part, be responsible for the cytotoxicity of tau aggregates in AD (Ferrari et al., 2020). It is possible that exogenous arginine-rich compounds may be able to prevent cytotoxicity by competitively binding to tau fibrils through the same mechanism, preventing tau fibrils from associating with these aberrant interactors. Thus, the potential effects of CARPs on the cytotoxicity of preformed tau aggregates presents an interesting area for future research.

POTENTIAL ROLES FOR ARGININE IN OTHER NEURODEGENERATIVE DISEASE-ASSOCIATED PROTEOPATHIES

Monomeric arginine has demonstrated efficacy in preventing the aggregation of alpha-synuclein. While alpha-synuclein aggregation is predominantly associated with Parkinson's disease (reviewed comprehensively by Fields et al., 2019), alpha-synuclein has also been implicated in AD (Kotzbauer et al., 2001; Crews et al., 2009; Twohig and Nielsen, 2019). Arginine was found to inhibit rotenone-induced aggregation of alpha-synuclein *in vitro*, even inhibiting further aggregation even when added past the stage of initial nucleation (Shristi, 2014). The inhibitory effects of arginine on alpha-synuclein



aggregation were further confirmed in detail by Ghosh et al. (2018), who demonstrated arginine-based inhibition of alpha-synuclein aggregation both *in vitro* and *in situ* in live cells. Ghosh et al. (2018) also evidenced the cytoprotective effects of arginine on cultures treated with pre-aggregated alpha-synuclein. Interestingly, the use of lysine, a similarly cationic amino acid, was associated with increased alpha-synuclein aggregation *in vitro*, while guanidinium hydrochloride was associated with decreased viability of cells treated with aggregated alpha-synuclein. These results indicate that while the guanidinium moiety of arginine is essential to its activities, the overall properties of arginine rather than either its general cationicity or the guanidinium moiety in isolation, are key to its anti-aggregatory and cytoprotective effects in the context of alpha-synuclein aggregation.

Recently, the CARP RD2RD2 (ptlhthnrrrrrptlhthnrrrrr; +10.4 charge) was investigated as a potential therapeutic candidate for amyotrophic lateral sclerosis (ALS) in a mouse model of mutant superoxide dismutase 1 (SOD1) expression (Post et al., 2021). Administration of RD2RD2 was associated with reductions in motor deficits and neuroinflammation, although the precise molecular mechanisms underlying these effects remain to be elucidated.

Minakawa and Nagai (2021) recently discussed arginine as a modulator of aggregatory proteins containing polyglutamine (polyQ) stretches, a pathogenic feature of neurodegenerative diseases such as Huntington's disease (HD) and spinocerebellar ataxias (SCAs). Oligomers of polyQ proteins, as well as polyQ

protein monomers which are enriched for beta-sheet structure, have previously been associated with cytotoxicity (Kayed et al., 2003; Miller et al., 2011). When added to polyQ proteins *in vitro*, monomeric arginine was found to prevent the aggregation of polyQ proteins, including the initial transition from alpha-helical to beta-sheet-enriched monomers, subsequent oligomerisation, and the seeding of aggregation by pre-formed aggregates (Minakawa et al., 2020). Arginine, arginine methyl ester and arginine ethyl ester were also shown by Singh et al. (2019) to prevent aggregation of a polyQ-containing Huntington exon 1 protein (mHTTex1) *in vitro*, and rescue motor deficits in a model of HD *in vivo*. Minakawa et al. (2020) also investigated the effects of arginine administration *in vivo* and found motor deficits were rescued in multiple mouse and invertebrate models of SCA. Notably, arginine was able to rescue motor deficits even past the stage of initial symptom onset in a SCA1 mouse model (Minakawa et al., 2020).

Aggregation of an mHTT protein was also suppressed by a hybrid peptide, 8R10Q (RRRRRRRRRQQQQQQQQQ; net charge +8.0) designed by He et al. (2019) through a principle similar to the bipartite peptide designed for amyloid-beta aggregation by Cheng et al. (2017): inclusion of a self-recognition component (a ten-residue stretch of glutamine), conjugated to a polyarginine component to drive charge-based repulsion of bound monomers as well as increase solubility and membrane permeability.

The effects of arginine and its derivatives on polyQ aggregation and cytotoxicity are consistent with the advantages

conferred by the structure and cationicity of arginine in amyloid-beta and tau-targeting peptides, as well as the effects of CARPs including polyarginine peptides on glutamic acid-induced excitotoxicity (reviewed comprehensively by Meloni et al., 2020). By evaluating a set of arginine derivatives with either N- or C-terminal substitutions, Singh et al. (2019) inferred the guanidino group of arginine was essential to its anti-aggregatory effect on a polyQ peptide (polyglutamine-35; Q35) *in vitro*. Citrulline, ornithine and lysine, which lack the guanidino moiety, were unable to prevent Q35 aggregation, while arginine and arginine ethyl ester prevented Q35 aggregation in a dose-dependent manner (Singh et al., 2019).

PEPTIDYLARGININE CITRULLINATION AND ARGININE-RICH THERAPEUTICS

Arginine molecules can be converted to citrulline by arginine deiminase (ADI) through hydrolysis of their guanidinium groups, causing the strongly basic, cationic arginine side chain to be replaced by neutral urea. Whereas ADI converts free arginine molecules, peptidylarginine deiminases (PADs) catalyse the conversion of peptide-bound arginine residues to citrulline residues (Wang and Wang, 2013). Citrullination affects the ability of the residue to form hydrogen bonds, altering its intermolecular interactions.

Increased PAD activity has been associated with AD (Acharya et al., 2012; Wang et al., 2021); in particular, levels of PAD II detected in the hippocampus were found to be significantly higher in AD patients than in controls by Ishigami et al. (2005), concomitant with the presence of citrullinated proteins in AD-affected hippocampi. It is conceivable that higher levels of PAD activity in AD could affect the overall efficacy of CARP therapeutics through citrullination of their arginine residues, however, this remains to be observed. Moreover, understanding of PADs in AD more broadly remains limited. Further research on peptidylarginine citrullination in AD is required to hypothesise the potential effects of PADs on CARPs as therapeutic candidates in this context. Additionally, as current preclinical models of AD are unable to recapitulate all aspects of AD pathogenesis, it is difficult to predict how overexpression of PADs upregulated in human AD might affect CARPs shown to be highly efficacious in animal models, such as RD2.

It is worth noting, however, that PAD activity is tightly controlled by calcium ions (Lamensa and Moscarello, 1993; Sambandam et al., 2004; Mondal and Thompson, 2019), and PAD II is activated through elevated intracellular calcium levels (Slade et al., 2015). CARPs themselves have previously been shown to reduce intracellular calcium influx through multiple mechanisms (Meloni et al., 2015a,b; Edwards et al., 2017), including downregulation of the NMDAR subunit NR2B. Therefore, it is possible that CARPs may be able to prevent excessive activation of PADs in AD through upstream inhibition of calcium influx. In summary, although PADs could theoretically affect the ability of CARPs to exert beneficial effects in AD through citrullination of their arginine residues, it is difficult to predict whether this is likely to occur *in vivo* based on the paucity of evidence; additionally, the putative effects of

CARPs on calcium signalling in states of neurological injury and disease render this a complex area. Regardless, the favourable safety profile of CARPs (Edwards et al., 2020) should allow CARPs to be evaluated at varying dose levels for efficacy in human AD.

CONCLUSION

Arginine has several distinctive properties, largely owing to the unique structure and chemistry of the guanidinium group. While monomeric arginine has long been regarded as a potent inhibitor of protein aggregation, polypeptides enriched for arginine residues also display interesting effects on the formation and cytotoxicity of protein aggregates. Arginine residues have substantial bioactive properties in the context of modulating protein aggregation, and should therefore be given particular consideration in the rational design of amyloid-targeting therapeutic peptides.

The lack of effective therapeutic options for AD presents a significant global health challenge. Peptide drugs are a rapidly growing class of therapeutic candidates, and while their design and optimisation carries a distinct set of challenges, they hold promise in the treatment of AD through their potential advantages of high target specificity and bioactivity. We have identified a number of CARPs which effectively modulate the aggregation pathway of amyloid-beta, as well as potential roles of arginine in peptide-based therapeutic design for targeting tau oligomerisation.

Interestingly, CARPs have also demonstrated significant neuroprotective effects in models of stroke and traumatic brain injury, particularly by targeting excitotoxicity, which is also a pathological feature of AD (reviewed by Wang and Reddy, 2017). The complex and multifactorial nature of AD pathogenesis particularly warrants therapeutic candidates with multiple mechanisms of action. The potential for CARPs to modulate proteopathies associated with AD, therefore, warrant further investigation. CARPs could potentially target the formation and/or deleterious cellular effects of amyloids in AD through diverse roles: decreasing the concentration of soluble, cytotoxic oligomers by either preventing aggregation or driving aggregation toward the formation of non-cytotoxic species; mitigating oxidative stress, which is known to drive the formation of cytotoxic amyloids; and preserving the function of mitochondria, which are a site of cellular damage from amyloids. These possibilities present several lines of inquiry for further research.

AUTHOR CONTRIBUTIONS

SM wrote the manuscript with input from BM. Both authors revised the manuscript and approved the final version.

ACKNOWLEDGEMENTS

We thank Professor Frank Mastaglia for editorial suggestions. Figures throughout the manuscript were created using Biorender (<https://biorender.com>).

REFERENCES

- Acharya, N. K., Nagele, E. P., Han, M., Coretti, N. J., DeMarshall, C., Kosciuk, M. C., et al. (2012). Neuronal PAD4 expression and protein citrullination: possible role in production of autoantibodies associated with neurodegenerative disease. *J. Autoimmun.* 38, 369–380. doi: 10.1016/j.jaut.2012.03.004
- Aggidis, A., Chatterjee, S., Townsend, D., Fullwood, N. J., Ortega, E. R., Tarutani, A., et al. (2021). Peptide-based inhibitors of tau aggregation as a potential therapeutic for Alzheimer's disease and other tauopathies. *bioRxiv* [Preprint]. doi: 10.1101/2021.06.04.447069
- Aggidis, A. (2019). The development of peptide-based inhibitors for Tau aggregation as a potential therapeutic for Alzheimer's disease. Available online at: <https://eprints.lancs.ac.uk/id/eprint/140396/1/2019AggidisPhD.pdf>.
- Allolio, C., Magarkar, A., Jurkiewicz, P., Baxová, K., Javanainen, M., Mason, P. E., et al. (2018). Arginine-rich cell-penetrating peptides induce membrane multilamellarity and subsequently enter via formation of a fusion pore. *Proc. Natl. Acad. Sci.* 115, 11923–11928. doi: 10.1073/pnas.1811520115
- Alzheimer's Association. (2021). Alzheimer's disease facts and figures. *Alzheimers Dement.* 17, 327–406. doi: 10.1002/alz.12328
- Arai, T., Sasaki, D., Araya, T., Sato, T., Sohma, Y., and Kanai, M. A. (2014). A cyclic KLVFF-derived peptide aggregation inhibitor induces the formation of less-toxic off-pathway amyloid- β oligomers. *Chembiochem.* 15, 2577–2583. doi: 10.1002/cbic.201402430
- Arakawa, J., Uegaki, M., and Ishimizu, T. (2011). Effects of L-arginine on solubilization and purification of plant membrane proteins. *Protein Expr. Purif.* 80, 91–96. doi: 10.1016/j.pep.2011.05.014
- Arakawa, T., Ejima, D., Tsumoto, K., Obeyama, N., Tanaka, Y., Kita, Y., et al. (2007). Suppression of protein interactions by arginine: a proposed mechanism of the arginine effects. *Biophys. Chem.* 127, 1–8. doi: 10.1016/j.bpc.2006.12.007
- Arakawa, T., Kita, Y., Ejima, D., Tsumoto, K., and Fukada, H. (2006). Aggregation suppression of proteins by arginine during thermal unfolding. *Protein Pept. Lett.* 13, 921–927. doi: 10.2174/0929866060778256171
- Arboleda-Velasquez, J. F., Lopera, F., O'Hare, M., Delgado-Tirado, S., Marino, C., Chmielewska, N., et al. (2019). Resistance to autosomal dominant Alzheimer's disease in an APOE3 Christchurch homozygote: a case report. *Nat. Med.* 25, 1680–1683. doi: 10.1038/s41591-019-0611-3
- Austen, B. M., Paleologou, K. E., Ali, S. A., Qureshi, M. M., Allsop, D., and El-Agnaf, O. M. (2008). Designing peptide inhibitors for oligomerization and toxicity of Alzheimer's beta-amyloid peptide. *Biochemistry.* 47, 1984–1992. doi: 10.1021/bi701415b
- Avila, J., Lucas, J. J., Perez, M., and Hernandez, F. (2004). Role of tau protein in both physiological and pathological conditions. *Physiol. Rev.* 84, 361–384. doi: 10.1152/physrev.00024.2003
- Barage, S. H., and Sonawane, K. D. (2015). Amyloid cascade hypothesis: pathogenesis and therapeutic strategies in Alzheimer's disease. *Neuropeptides.* 52, 1–18. doi: 10.1016/j.npep.2015.06.008
- Barale, S. S., Parulekar, R. S., Fandilolu, P. M., Dhanavade, M. J., and Sonawane, K. D. (2019). Molecular insights into destabilization of Alzheimer's A β protofibril by arginine containing short peptides: a molecular modeling approach. *ACS Omega* 4, 892–903. doi: 10.1021/acsomega.8b02672
- Barr, R. K., Verdile, G., Wijaya, L. K., Morici, M., Taddei, K., Gupta, V. B., et al. (2016). Validation and characterization of a novel peptide that binds monomeric and aggregated β -Amyloid and inhibits the formation of neurotoxic oligomers. *J. Biol. Chem.* 291, 547–559. doi: 10.1074/jbc.M115.679993
- Baynes, B. M., Wang, D. I., and Trout, B. L. (2005). Role of arginine in the stabilization of proteins against aggregation. *Biochemistry* 44, 4919–4925. doi: 10.1021/bi047528r
- Bhowmik, D., MacLaughlin, C. M., Chandrakesan, M., Ramesh, P., Venkatramani, R., Walker, G. C., et al. (2014). pH changes the aggregation propensity of amyloid- β without altering the monomer conformation. *Phys. Chem. Chem. Phys.* 16, 885–889. doi: 10.1039/c3cp54151g
- Bin, Y., Li, X., He, Y., Chen, S., and Xiang, J. (2013). Amyloid- β peptide (1–42) aggregation induced by copper ions under acidic conditions. *Acta Biochim. Biophys. Sin. (Shanghai)* 45, 570–577. doi: 10.1093/abbs/gmt044
- Borzova, V. A., Markossian, K. A., Klymenov, S. Y., and Kurganov, B. I. (2017). A change in the aggregation pathway of bovine serum albumin in the presence of arginine and its derivatives. *Sci. Rep.* 7:3984. doi: 10.1038/s41598-017-04409-x
- Brandt, R., Léger, J., and Lee, G. (1995). Interaction of tau with the neural plasma membrane mediated by tau's amino-terminal projection domain. *J. Cell Biol.* 131, 1327–1340. doi: 10.1083/jcb.131.5.1327
- Březina, K., Duboué-Dijon, E., Palivec, V., Jiráček, J., Křížek, T., Viola, C. M., et al. (2018). Can arginine inhibit insulin aggregation? a combined protein crystallography, capillary electrophoresis and molecular simulation study. *J. Phys. Chem. B.* 122, 10069–10076. doi: 10.1021/acs.jpbc.8b06557
- Butterfield, D. A., Swomley, A. M., and Sultana, R. (2013). Amyloid β -peptide (1–42)-induced oxidative stress in Alzheimer disease: importance in disease pathogenesis and progression. *Antioxid. Redox. Signal.* 19, 823–835. doi: 10.1089/ars.2012.5027
- Carrillo-Mora, P., Luna, R., and Colín-Barenque, L. (2014). Amyloid beta: multiple mechanisms of toxicity and only some protective effects? *Oxid. Med. Cell Longev.* 2014:795375. doi: 10.1155/2014/795375
- Cheignon, C., Tomas, M., Bonnefont-Rousselot, D., Faller, P., Hureau, C., and Collin, F. (2018). Oxidative stress and the amyloid beta peptide in Alzheimer's disease. *Redox Biol.* 14, 450–464. doi: 10.1016/j.redox.2017.10.014
- Chen, G. F., Xu, T. H., Yan, Y., Zhou, Y. R., Jiang, Y., Melcher, K., et al. (2017). Amyloid beta: structure, biology and structure-based therapeutic development. *Acta Pharmacol. Sin.* 38, 1205–1235. doi: 10.1038/aps.2017.28
- Chen, J. X., and Yan, S. D. (2007). Amyloid-beta-induced mitochondrial dysfunction. *J. Alzheimers Dis.* 12, 177–184. doi: 10.3233/jad-2007-12208
- Cheng, Y. S., Chen, Z. T., Liao, T. Y., Lin, C., Shen, H. C., Wang, Y. H., et al. (2017). An intranasally delivered peptide drug ameliorates cognitive decline in Alzheimer transgenic mice. *EMBO Mol. Med.* 9, 703–715. doi: 10.15252/emmm.201606666
- Cirkovas, A., and Sereikaite, J. (2011). Different effects of (L)-arginine on the heat-induced unfolding and aggregation of proteins. *Biologicals* 39, 181–188. doi: 10.1016/j.biologicals.2011.04.003
- Congdon, E. E., and Sigurdsson, E. M. (2018). Tau-targeting therapies for Alzheimer disease. *Nat. Rev. Neurol.* 14, 399–415. doi: 10.1038/s41582-018-0013-z
- Cosacak, M. I., Bhattarai, P., Bocova, L., Dzewas, T., Mashkaryan, V., Papadimitriou, C., et al. (2017). Human TAUP301L overexpression results in TAU hyperphosphorylation without neurofibrillary tangles in adult zebrafish brain. *Sci. Rep.* 7:12959. doi: 10.1038/s41598-017-13311-5
- Crescenzi, O., Tomaselli, S., Guerrini, R., Salvadori, S., D'Ursi, A. M., Temussi, P. A., et al. (2002). Solution structure of the Alzheimer amyloid beta-peptide (1–42) in an apolar microenvironment. Similarity with a virus fusion domain. *Eur. J. Biochem.* 269, 5642–5648. doi: 10.1046/j.1432-1033.2002.03271.x
- Crews, L., Tsigelny, I., Hashimoto, M., and Masliah, E. (2009). Role of synucleins in Alzheimer's disease. *Neurotox Res.* 16, 306–317. doi: 10.1007/s12640-009-9073-6
- D'Annese, I., Di Leva, F. S., La Teana, A., Novellino, E., Limongelli, V., and Di Marino, D. (2020). Bioinformatics and biosimulations as toolbox for peptides and peptidomimetics design: where are we? *Front. Mol. Biosci.* 7:66. doi: 10.3389/fmolb.2020.00066
- Das, U., Hariprasad, G., Ethayathulla, A. S., Manral, P., Das, T. K., Pasha, S., et al. (2007). Inhibition of protein aggregation: supramolecular assemblies of arginine hold the key. *PLoS One.* 2:e1176. doi: 10.1371/journal.pone.0001176
- Di Carlo, M. (2010). Beta amyloid peptide: from different aggregation forms to the activation of different biochemical pathways. *Eur. Biophys. J.* 39, 877–888. doi: 10.1007/s00249-009-0439-8
- Di, J., Cohen, L. S., Corbo, C. P., Phillips, G. R., El Idrissi, A., and Alonso, A. D. (2016). Abnormal tau induces cognitive impairment through two different mechanisms: synaptic dysfunction and neuronal loss. *Sci. Rep.* 6:20833. doi: 10.1038/srep20833
- Di, L. (2015). Strategic approaches to optimizing peptide ADME properties. *AAPS J.* 17, 134–143. doi: 10.1208/s12248-014-9687-3
- Digma, L. A., Madsen, J. R., Reas, E. T., Dale, A. M., Brewer, J. B., Banks, S. J., et al. (2019). Tau and atrophy: domain-specific relationships with cognition. *Alzheimers Res. Ther.* 11:65. doi: 10.1186/s13195-019-0518-8

- Dixit, R., Ross, J. L., Goldman, Y. E., and Holzbaur, E. L. (2008). Differential regulation of dynein and kinesin motor proteins by tau. *Science* 319, 1086–1089. doi: 10.1126/science.1152993
- D'Souza, I., and Schellenberg, G. D. (2000). Determinants of 4-repeat tau expression. Coordination between enhancing and inhibitory splicing sequences for exon 10 inclusion. *J. Biol. Chem.* 275, 17700–17709. doi: 10.1074/jbc.M909470199
- Edwards, A. B., Anderton, R. S., Knuckey, N. W., and Meloni, B. P. (2017). Characterisation of neuroprotective efficacy of modified poly-arginine-9 (R9) peptides using a neuronal glutamic acid excitotoxicity model. *Mol. Cell Biochem.* 426, 75–85. doi: 10.1007/s11010-016-2882-z
- Edwards, A. B., Mastaglia, F. L., Knuckey, N. W., and Meloni, B. P. (2020). Neuroprotective cationic arginine-rich peptides (CARPs): an assessment of their clinical safety. *Drug Saf.* 43, 957–969. doi: 10.1007/s40264-020-00962-z
- Elfgen, A., Santiago-Schübel, B., Hupert, M., Schemmert, S., Schartmann, E., Tusche, M., et al. (2021). Oral absorption enhancement of the amyloid- β oligomer eliminating compound RD2 by conjugation with folic acid. *Eur. J. Pharm. Sci.* 156:105581. doi: 10.1016/j.ejps.2020.105581
- Enache, T. A., Chiorcea-Paquim, A. M., and Oliveira-Brett, A. M. (2018). Amyloid beta peptide VHHQ, KLVFF and IIGLMVGGVV domains involved in fibrilization: AFM and electrochemical characterization. *Anal. Chem.* 90, 2285–2292. doi: 10.1021/acs.analchem.7b04686
- Eschmann, N. A., Do, T. D., LaPointe, N. E., Shea, J. E., Feinstein, S. C., Bowers, M. T., et al. (2015). Tau aggregation propensity engrained in its solution state. *J. Phys. Chem. B.* 119, 14421–14432. doi: 10.1021/acs.jpcc.5b08092
- Evers, A., Pfeiffer-Marek, S., Bossart, M., Heubel, C., Stock, U., Tiwari, G., et al. (2019). Peptide optimization at the drug discovery-development interface: tailoring of physicochemical properties toward specific formulation requirements. *J. Pharm. Sci.* 108, 1404–1414. doi: 10.1016/j.xphs.2018.11.043
- Faller, P., Hureau, C., and Berthoumieu, O. (2013). Role of metal ions in the self-assembly of the Alzheimer's amyloid- β peptide. *Inorg. Chem.* 52, 12193–12206. doi: 10.1021/ic4003059
- Feng, Z., and Xu, B. (2016). Inspiration from the mirror: D-amino acid containing peptides in biomedical approaches. *Biomol. Concepts* 7, 179–187. doi: 10.1515/bmc-2015-0035
- Ferrari, L., Stucchi, R., Konstantoulea, K., van de Kamp, G., Kos, R., Geerts, W. J. C., et al. (2020). Arginine π -stacking drives binding to fibrils of the Alzheimer protein Tau. *Nat. Commun.* 11:571. doi: 10.1038/s41467-019-13745-7
- Fichou, Y., Lin, Y., Rauch, J. N., Vigers, M., Zeng, Z., Srivastava, M., et al. (2018). Cofactors are essential constituents of stable and seeding-active tau fibrils. *Proc. Natl. Acad. Sci. U S A* 115, 13234–13239. doi: 10.1073/pnas.1810058115
- Fields, C. R., Bengoa-Vergniory, N., and Wade-Martins, R. (2019). Targeting alpha-synuclein as a therapy for Parkinson's disease. *Front. Mol. Neurosci.* 12:299. doi: 10.3389/fnmol.2019.00299
- Fitch, C. A., Platzter, G., Okon, M., Garcia-Moreno, B. E., and McIntosh, L. P. (2015). Arginine: its pKa value revisited. *Protein Sci.* 24, 752–761. doi: 10.1002/pro.2647
- Fonar, G., Polis, B., Meirson, T., Maltsev, A., and Samson, A. O. (2018). Subcutaneous sustained-release of poly-arginine ameliorates cognitive impairment in a transgenic mouse model of Alzheimer's disease. *Adv. Alzheimers Dis.* 7, 153–182. doi: 10.4236/aad.2018.74011
- Francis, P. T., Palmer, A. M., Snape, M., and Wilcock, G. K. (1999). The cholinergic hypothesis of Alzheimer's disease: a review of progress. *J. Neurol. Neurosurg. Psychiatry* 66, 137–147. doi: 10.1136/jnnp.66.2.137
- Fukuda, M., Kameoka, D., Torizawa, T., Saitoh, S., Yasutake, M., Imaeda, Y., et al. (2014). Thermodynamic and fluorescence analyses to determine mechanisms of IgG1 stabilization and destabilization by arginine. *Pharm. Res.* 31, 992–1001. doi: 10.1007/s11095-013-1221-2
- Funke, S. A., and Willbold, D. (2012). Peptides for therapy and diagnosis of Alzheimer's disease. *Curr. Pharm. Des.* 18, 755–767. doi: 10.2174/138161212799277752
- Gandhi, J., Antonelli, A. C., Afridi, A., Vatsia, S., Joshi, G., Romanov, V., et al. (2019). Protein misfolding and aggregation in neurodegenerative diseases: a review of pathogenesis, novel detection strategies and potential therapeutics. *Rev. Neurosci.* 30, 339–358. doi: 10.1515/revneuro-2016-0035
- GBD 2016 Dementia Collaborators. (2019). Global, regional and national burden of Alzheimer's disease and other dementias, 1990–2016: a systematic analysis for the global burden of disease study 2016. *Lancet. Neurol.* 18, 88–106. doi: 10.1016/S1474-4422(18)30403-4
- Ghosh, R., Sharma, S., and Chattopadhyay, K. (2009). Effect of arginine on protein aggregation studied by fluorescence correlation spectroscopy and other biophysical methods. *Biochemistry* 48, 1135–1143. doi: 10.1021/bi802065j
- Ghosh, S., Kundu, A., and Chattopadhyay, K. (2018). Small molecules attenuate the interplay between conformational fluctuations, early oligomerization and amyloidosis of alpha synuclein. *Sci. Rep.* 8:5481. doi: 10.1038/s41598-018-23718-3
- Gibson, T. J., and Murphy, R. M. (2005). Design of peptidyl compounds that affect beta-amyloid aggregation: importance of surface tension and context. *Biochemistry* 44, 8898–8907. doi: 10.1021/bi050225s
- Gofton, T., and Weaver, D. F. (2006). Challenges in the clinical diagnosis of Alzheimer's disease: influence of "family coaching" on the mini-mental state examination. *Am. J. Alzheimers Dis. Other Dement.* 21, 109–112. doi: 10.1177/1533317506002100210
- Golovanov, A. P., Hautbergue, G. M., Wilson, S. A., and Lian, L. Y. (2004). A simple method for improving protein solubility and long-term stability. *J. Am. Chem. Soc.* 126, 8933–8939. doi: 10.1021/ja049297h
- Goyal, D., Shuaib, S., Mann, S., and Goyal, B. (2017). Rationally designed peptides and peptidomimetics as inhibitors of Amyloid- β (A β) aggregation: potential therapeutics of Alzheimer's Disease. *ACS Comb. Sci.* 19, 55–80. doi: 10.1021/acscmb.6b00116
- Grundke-Iqbal, I., Iqbal, K., Tung, Y. C., Quinlan, M., Wisniewski, H. M., and Binder, L. I. (1986). Abnormal phosphorylation of the microtubule-associated protein tau (tau) in Alzheimer cytoskeletal pathology. *Proc. Nat. Acad. Sci. U S A* 83, 4913–4917. doi: 10.1073/pnas.83.13.4913
- Gund, P. (1972). Guanidine, trimethylenemethane and "Y-delocalization." Can acyclic compounds have "aromatic" stability? *J. Chem. Educ.* 49:100. doi: 10.1021/ed049p100
- Habault, J., and Poyet, J. L. (2019). Recent advances in cell penetrating peptide-based anticancer therapies. *Molecules* 24:927. doi: 10.3390/molecules24050927
- Haghighi-Poodeh, S., Kurganov, B., Navidpour, L., Yaghmaei, P., and Ebrahim-Habibi, A. (2020). Characterization of arginine preventive effect on heat-induced aggregation of insulin. *Int. J. Biol. Macromol.* 145, 1039–1048. doi: 10.1016/j.ijbiomac.2019.09.196
- Haklar, G., Ulukaya-Durakba-a, C., Yüksel, M., Dağlı, T., and Yalçın, A. S. (1998). Oxygen radicals and nitric oxide in rat mesenteric ischaemia-reperfusion: modulation by L-arginine and NG-nitro-L-arginine methyl ester. *Clin. Exp. Pharmacol. Physiol.* 25, 908–912. doi: 10.1111/j.1440-1681.1998.tb02342.x
- Hanseu, B. J., Betensky, R. A., Jacobs, H. I. L., Schultz, A. P., Sepulcre, J., Becker, J. A., et al. (2019). Association of amyloid and tau with cognition in preclinical Alzheimer disease: a longitudinal study. *JAMA Neurol.* 76, 915–924. doi: 10.1001/jamaneurol.2019.1424
- Hardy, J., and De Strooper, B. (2017). Alzheimer's disease: where next for anti-amyloid therapies? *Brain* 140, 853–855. doi: 10.1093/brain/awx059
- Hardy, J. A., and Higgins, G. A. (1992). Alzheimer's disease: the amyloid cascade hypothesis. *Science* 256, 184–185. doi: 10.1126/science.1566067
- He, R. Y., Lai, X. M., Sun, C. S., Kung, T., Hong, J., Jheng, Y., et al. (2019). Nanoscopic insights of amphiphilic peptide against the oligomer assembly process to treat Huntington's disease. *Adv. Sci. (Weinh)* 7:1901165. doi: 10.1002/advs.201901165
- Henning-Knechtel, A., Kumar, S., Wallin, C., Krol, S., Warmlander, S. K. T. S., Jarvet, J., et al. (2020). Designed cell-penetrating peptide inhibitors of amyloid-beta aggregation and cytotoxicity. *Cell Rep. Phys. Sci.* 1:100014. doi: 10.1016/j.xcrp.2020.100014
- Hsu, F., Park, G., and Guo, Z. (2018). Key residues for the formation of A β 42 amyloid fibrils. *ACS Omega* 3, 8401–8407. doi: 10.1021/acsomega.8b00887
- Irwin, D. J., Cohen, T. J., Grossman, M., Arnold, S. E., Xie, S. X., Lee, V. M., et al. (2012). Acetylated tau, a novel pathological signature in Alzheimer's disease and other tauopathies. *Brain* 135, 807–818. doi: 10.1093/brain/awx013
- Ishigami, A., Ohsawa, T., Hiratsuka, M., Taguchi, H., Kobayashi, S., Saito, Y., et al. (2005). Abnormal accumulation of citrullinated proteins catalyzed by peptidylarginine deiminase in hippocampal extracts from patients with Alzheimer's disease. *J. Neurosci. Res.* 80, 120–128. doi: 10.1002/jnr.20431

- Ito, L., Shiraki, K., Matsuura, T., Okumura, M., Hasegawa, K., Baba, S., et al. (2011). High-resolution X-ray analysis reveals binding of arginine to aromatic residues of lysozyme surface: implication of suppression of protein aggregation by arginine. *Protein Eng. Des. Sel.* 24, 269–274. doi: 10.1093/protein/gzq101
- Jameson, L., Frey, T., Zeeberg, B., Daldorf, F., and Caplow, M. (1980). Inhibition of microtubule assembly by phosphorylation of microtubule-associated proteins. *Biochemistry* 19, 2472–2479. doi: 10.1021/bi00552a027
- Jiang, D., Rauda, I., Han, S., Chen, S., and Zhou, F. (2012). Aggregation pathways of the amyloid β (1–42) peptide depend on its colloidal stability and ordered β -sheet stacking. *Langmuir* 28, 12711–12721. doi: 10.1021/la3021436
- Johnson, K., Hanseeuw, B. J., Betensky, R. A., Jacobs, H. L., Schlitz, A. P., Sepulcre, J., et al. (2019). Association of amyloid and tau With cognition in preclinical Alzheimer disease: a longitudinal study. *JAMA Neurol.* 76, 915–924. doi: 10.1001/jamaneurol.2019.1424
- Jokar, S., Erfani, M., Bavi, O., Khazaei, S., Sharifzadeh, M., Hajiramezani, M., et al. (2020). Design of peptide-based inhibitor agent against amyloid- β aggregation: Molecular docking, synthesis and in vitro evaluation. *Bioorg Chem.* 102:104050. doi: 10.1016/j.bioorg.2020.104050
- Jouanne, M., Rault, S., and Voisin-Chiret, A. S. (2017). Tau protein aggregation in Alzheimer's disease: An attractive target for the development of novel therapeutic agents. *Eur. J. Med. Chem.* 139, 153–167. doi: 10.1016/j.ejmech.2017.07.070
- Kawasaki, T., and Kamijo, S. (2012). Inhibition of aggregation of amyloid β 42 by arginine-containing small compounds. *Biosci. Biotechnol. Biochem.* 76, 762–766. doi: 10.1271/bbb.110879
- Kawasaki, T., Onodera, K., and Kamijo, S. (2011). Identification of novel short peptide inhibitors of soluble 37/48 kDa oligomers of amyloid β 42. *Biosci. Biotechnol. Biochem.* 75, 1496–1501. doi: 10.1271/bbb.110198
- Kawasaki, T., Onodera, K., and Kamijo, S. (2010). Selection of peptide inhibitors of soluble A β (1–42) oligomer formation by phage display. *Biosci. Biotechnol. Biochem.* 74, 2214–2219. doi: 10.1271/bbb.100388
- Kayed, R., Head, E., Thompson, J. L., McIntire, T. M., Milton, S. C., Cotman, C. W., et al. (2003). Common structure of soluble amyloid oligomers implies common mechanism of pathogenesis. *Science* 300, 486–489. doi: 10.1126/science.1079469
- Kino, R., Araya, T., Arai, T., Sohma, Y., and Kanai, M. (2015). Covalent modifier-type aggregation inhibitor of amyloid- β based on a cyclo-KLVFF motif. *Bioorg. Med. Chem. Lett.* 25, 2972–2975. doi: 10.1016/j.bmcl.2015.05.027
- Klein, A. N., Ziehm, T., van Groen, T., Kadish, I., Elfgen, A., Tusche, M., et al. (2017). Optimization of d-peptides for A β monomer binding specificity enhances their potential to eliminate toxic A β oligomers. *ACS Chem. Neurosci.* 8, 1889–1900. doi: 10.1021/acscchemneuro.7b00045
- Kolarova, M., Garcia-Sierra, F., Bartos, A., Ricny, J., and Ripova, D. (2012). Structure and pathology of tau protein in Alzheimer disease. *Int. J. Alzheimers Dis.* 2012:731526. doi: 10.1155/2012/731526
- Kondo, K., Ikura, T., Tanaka, H., Fujita, K., Takayama, S., Yoshioka, Y., et al. (2021). Hepta-histidine inhibits tau aggregation. *ACS Chem. Neurosci.* 12, 3015–3027. doi: 10.1021/acscchemneuro.1c00164
- Köpke, E., Tung, Y. C., Shaikh, S., Alonso, A. C., Iqbal, K., and Grundke-Iqbal, I. (1993). Microtubule-associated protein tau. abnormal phosphorylation of a non-paired helical filament pool in Alzheimer disease. *J. Biol. Chem.* 268, 24374–24384.
- Kotzbauer, P. T., Trojanowski, J. Q., and Lee, V. M. (2001). Lewy body pathology in Alzheimer's disease. *J. Mol. Neurosci.* 17, 225–232. doi: 10.1385/jmn:17:2:225
- Kumar, D., Ganeshpurkar, A., Kumar, D., Modi, G., Gupta, S. K., and Singh, S. K. (2018). Secretase inhibitors for the treatment of Alzheimer's disease: Long road ahead. *Eur. J. Med. Chem.* 148, 436–452. doi: 10.1016/j.ejmech.2018.02.035
- Kumar, R., Namechi, R., and Sim, V. L. (2015). Structure-based peptide design to modulate amyloid beta aggregation and reduce cytotoxicity. *PLoS One* 10:e0129087. doi: 10.1371/journal.pone.0129087
- Kumar, J., and Sim, V. (2014). D-amino acid-based peptide inhibitors as early or preventative therapy in Alzheimer disease. *Prion* 8, 119–124. doi: 10.4161/pr.28220
- Kutzsche, J., Schemmert, S., Tusche, M., Neddens, J., Rabl, R., Jürgens, D., et al. (2017). Large-scale oral treatment study with the four most promising D3-derivatives for the treatment of Alzheimer's disease. *Molecules* 22:1693. doi: 10.3390/molecules22101693
- Lamensa, J. W., and Moscarello, M. A. (1993). Deimination of human myelin basic protein by a peptidylarginine deiminase from bovine brain. *J. Neurochem.* 61, 987–996. doi: 10.1111/j.1471-4159.1993.tb03612.x
- Larson, M. E., and Lesné, S. E. (2012). Soluble A β oligomer production and toxicity. *J. Neurochem.* 120, 125–139. doi: 10.1111/j.1471-4159.2011.07478.x
- Leithold, L. H., Jiang, N., Post, J., Niemietz, N., Schartmann, E., Ziehm, T., et al. (2016). Pharmacokinetic properties of tandem d-peptides designed for treatment of Alzheimer's disease. *Eur. J. Pharm. Sci.* 89, 31–38. doi: 10.1016/j.ejps.2016.04.016
- Li, J., Garg, M., Shah, D., and Rajagopalan, R. (2010). Solubilization of aromatic and hydrophobic moieties by arginine in aqueous solutions. *J. Chem. Phys.* 133:054902. doi: 10.1063/1.3469790
- Li, W., and Lee, V. M. (2006). Characterization of two VQIXK motifs for tau fibrillization in vitro. *Biochemistry* 45, 15692–15701. doi: 10.1021/bi061422+
- Liu, R., McAllister, C., Lyubchenko, Y., and Sierks, M. R. (2004). Residues 17–20 and 30–35 of beta-amyloid play critical roles in aggregation. *J. Neurosci. Res.* 75, 162–171. doi: 10.1002/jnr.10859
- Lovestone, S., and McLoughlin, D. M. (2002). Protein aggregates and dementia: is there a common toxicity. *J. Neurol. Neurosurg. Psychiatry* 72, 152–161. doi: 10.1136/jnnp.72.2.152
- Lu, J., Cao, Q., Wang, C., Zheng, J., Luo, F., Xie, J., et al. (2019). Structure-Based Peptide Inhibitor Design of Amyloid- β Aggregation. *Front. Mol. Neurosci.* 12:54. doi: 10.3389/fnmol.2019.00054
- Lucke-Wold, B., Seidel, K., Udo, R., Omalu, B., Ornstein, M., Nolan, R., et al. (2017). Role of tau acetylation in Alzheimer's disease and chronic traumatic encephalopathy: the way forward for successful treatment. *J. Neurol. Neurosurg.* 4:140.
- MacDougall, G., Anderton, R. S., Mastaglia, F. L., Knuckey, N. W., and Meloni, B. P. (2019b). Mitochondria and neuroprotection in stroke: Cationic arginine-rich peptides (CARPs) as a novel class of mitochondria-targeted neuroprotective therapeutics. *Neurobiol. Dis.* 121, 17–33. doi: 10.1016/j.nbd.2018.09.010
- MacDougall, G., Anderton, R. S., Mastaglia, F. L., Knuckey, N. W., and Meloni, B. P. (2019a). Proteomic analysis of cortical neuronal cultures treated with poly-arginine peptide-18 (R18) and exposed to glutamic acid excitotoxicity. *Mol. Brain* 12:66. doi: 10.1186/s13041-019-0486-8
- Maiza, A., Chantepie, S., Vera, C., Fife, A., Huynh, M. B., Stettler, O., et al. (2018). The role of heparan sulfates in protein aggregation and their potential impact on neurodegeneration. *FEBS Lett.* 592, 3806–3818. doi: 10.1002/1873-3468.13082
- Marshall, J., Wong, K. Y., Rupasinghe, C. N., Tiwari, R., Zhao, X., Berberoglu, E. D., et al. (2015). Inhibition of N-Methyl-D-aspartate-induced retinal neuronal death by polyarginine peptides is linked to the attenuation of stress-induced hyperpolarization of the inner mitochondrial membrane potential. *J. Biol. Chem.* 290, 22030–22048. doi: 10.1074/jbc.M115.662791
- Mason, P. E., Neilson, G. W., Dempsey, C. E., Barnes, A. C., and Cruickshank, J. M. (2003). The hydration structure of guanidinium and thiocyanate ions: implications for protein stability in aqueous solution. *Proc. Natl. Acad. Sci. U S A* 100, 4557–4561. doi: 10.1073/pnas.0735920100
- Mason, P. E., Neilson, G. W., Enderby, J. E., Sabouni, M. L., Dempsey, C. E., MacKerell, A. D., Jr., et al. (2004). The structure of aqueous guanidinium chloride solutions. *J. Am. Chem. Soc.* 126, 11462–11470. doi: 10.1021/ja040034x
- Matsuoka, T., Tomita, S., Hamada, H., and Shiraki, K. (2007). Amidated amino acids are prominent additives for preventing heat-induced aggregation of lysozyme. *J. Biosci. Bioeng.* 103, 440–443. doi: 10.1263/jbb.103.440
- Meloni, B. P., Milani, D., Edwards, A. B., Anderton, R. S., O'Hare Doig, R. L., Fitzgerald, M., et al. (2015a). Neuroprotective peptides fused to arginine-rich cell penetrating peptides: Neuroprotective mechanism likely mediated by peptide endocytic properties. *Pharmacol. Ther.* 153, 36–54. doi: 10.1016/j.pharmthera.2015.06.002
- Meloni, B. P., Brookes, L. M., Clark, V. W., Cross, J. L., Edwards, A. B., Anderton, R. S., et al. (2015b). Poly-arginine and arginine-rich peptides are neuroprotective in stroke models. *J. Cereb. Blood Flow. Metab.* 35, 993–1004. doi: 10.1038/jcbfm.2015.11

- Meloni, B. P., Mastaglia, F. L., and Knuckey, N. W. (2020). Cationic arginine-rich peptides (CARPs): a novel class of neuroprotective agents with a multimodal mechanism of action. *Front. Neurol.* 11:108. doi: 10.3389/fneur.2020.00108
- Meraz-Ríos, M. A., Lira-De León, K. I., Campos-Peña, V., De Anda-Hernández, M. A., and Mena-López, R. (2010). Tau oligomers and aggregation in Alzheimer's disease. *J. Neurochem.* 112, 1353–1367. doi: 10.1097/JCN.0000000000000616
- Miller, J., Arrasate, M., Brooks, E., Libeu, C. P., Legleiter, J., Hatters, D., et al. (2011). Identifying polyglutamine protein species in situ that best predict neurodegeneration. *Nat. Chem. Biol.* 7, 925–934. doi: 10.1038/nchembio.694
- Miller, V. M., Gouvion, C. M., Davidson, B. L., and Paulson, H. L. (2004). Targeting Alzheimer's disease genes with RNA interference: an efficient strategy for silencing mutant alleles. *Nucleic Acids Res.* 32, 661–668. doi: 10.1093/nar/gkh208
- Minakawa, E. N., and Nagai, Y. (2021). Protein aggregation inhibitors as disease-modifying therapies for polyglutamine diseases. *Front. Neurosci.* 15:621996. doi: 10.3389/fnins.2021.621996
- Minakawa, E. N., Popiel, H. A., Tada, M., Takahashi, T., Yamane, H., Saitoh, Y., et al. (2020). Arginine is a disease modifier for polyQ disease models that stabilizes polyQ protein conformation. *Brain* 143, 1811–1825. doi: 10.1093/brain/awaa115
- Mitchell, D. J., Kim, D. T., Steinman, L., Fathman, C. G., and Rothbard, J. B. (2000). Polyarginine enters cells more efficiently than other polycationic homopolymers. *J. Pept. Res.* 56, 318–325. doi: 10.1034/j.1399-3011.2000.00723.x
- Mondal, S., and Thompson, P. R. (2019). Protein arginine deiminases (PADs): biochemistry and chemical biology of protein citrullination. *Acc. Chem. Res.* 52, 818–832. doi: 10.1021/acs.accounts.9b00024
- Morley, J. E., Farr, S. A., Nguyen, A. D., and Xu, F. (2019). Editorial: what is the physiological function of amyloid-beta protein. *J. Nutr. Health Aging* 23, 225–226. doi: 10.1007/s12603-019-1162-5
- Moss, M. A., Nichols, M. R., Reed, D. K., Hoh, J. H., Rosenberry, T. L. (2003). The peptide KLVFF-K(6) promotes beta-amyloid(1–40) protofibril growth by association but does not alter protofibril effects on cellular reduction of 3- (4,5-dimethylthiazol-2-yl)-2,5-diphenyltetrazolium bromide (MTT). *Mol. Pharmacol.* 64, 1160–1168. doi: 10.1124/mol.64.5.1160
- Nadimida, K., Ismail, T., and Kanapathipillai, M. (2017). Tau peptides and tau mutant protein aggregation inhibition by cationic polyethyleneimine and polyarginine. *Biopolymers* 107:e23024. doi: 10.1002/bip.23024
- Nelson, P. T., Alafuzoff, I., Bigio, E. H., Bouras, C., Braak, H., Cairns, N. J., et al. (2012). Correlation of Alzheimer disease neuropathologic changes with cognitive status: a review of the literature. *J. Neuropathol. Exp. Neurol.* 71, 362–381. doi: 10.1097/NEN.0b013e31825018f7
- Neve, R. L., Harris, P., Kosik, K. S., Kurnit, D. M., and Donlon, T. A. (1986). Identification of cDNA clones for the human microtubule-associated protein tau and chromosomal localization of the genes for tau and microtubule-associated protein 2. *Brain Res.* 387, 271–280. doi: 10.1016/0169-328x(86)90033-1
- Niewiadomska, G., Niewiadomski, W., Steczkowska, M., and Gasiorowska, A. (2021). Tau oligomers neurotoxicity. *Life (Basel)* 11:28. doi: 10.3390/life11010028
- Nirmalraj, P. N., List, J., Battacharya, S., Howe, G., Xu, L., Thompson, D., et al. (2020). Complete aggregation pathway of amyloid β (1–40) and (1–42) resolved on an atomically clean interface. *Sci. Adv.* 6:eaz6014. doi: 10.1126/sciadv.aaz6014
- Noble, W., Hanger, D. P., Miller, C. C., and Lovestone, S. (2013). The importance of tau phosphorylation for neurodegenerative diseases. *Front. Neurol.* 4:83. doi: 10.3389/fneur.2013.00083
- Nuhu, M. M., and Curtis, R. (2015). Arginine dipeptides affect insulin aggregation in a pH- and ionic strength-dependent manner. *Biotechnol. J.* 10, 404–416. doi: 10.1002/biot.201400190
- O'Brien, R. J., and Wong, P. C. (2011). Amyloid precursor protein processing and Alzheimer's disease. *Annu. Rev. Neurosci.* 34, 185–204. doi: 10.1146/annurev-neuro-061010-113613
- Olubiyi, O. O., Frenzel, D., Bartnik, D., Glück, J. M., Brener, O., Nagel-Steger, L., et al. (2014). Amyloid aggregation inhibitory mechanism of arginine-rich D-peptides. *Curr. Med. Chem.* 21, 1448–1457. doi: 10.2174/0929867321666131129122247
- Parthasarathy, V., McClean, P. L., Hölscher, C., Taylor, M., Tinker, C., Jones, G., et al. (2013). A novel retro-inverso peptide inhibitor reduces amyloid deposition, oxidation and inflammation and stimulates neurogenesis in the APPsw/PS1 Δ E9 mouse model of Alzheimer's disease. *PLoS One* 8:e54769. doi: 10.1371/journal.pone.0054769
- Pauwels, K., Williams, T. L., Morris, K. L., Jonckheere, W., Vandersteen, A., Kelly, G., et al. (2012). Structural basis for increased toxicity of pathological a β 42:a β 40 ratios in Alzheimer disease. *J. Biol. Chem.* 287, 5650–5660. doi: 10.1074/jbc.M111.264473
- Pearson, H. A., and Peers, C. (2006). Physiological roles for amyloid beta peptides. *J. Physiol.* 575, 5–10. doi: 10.1113/jphysiol.2006.111203
- Pedrin, S., Morici, M., and Martins, R. N. (2019). “Chapter 14—Current and prospective treatments for Alzheimer's disease (and other neurodegenerative diseases), in *Neurodegeneration and Alzheimer's Disease: The Role of Diabetes, Genetics, Hormones, and Lifestyle*, eds Ralph N. Martins, Charles S. Brennan, W. M. A. D. Binosha Fernando, Margaret A. Brennan, and Stephanie J. Fuller (John Wiley & Sons), 391–442. doi: 10.1002/9781119356752.ch14
- Post, J., Kogel, V., Schaffrath, A., Lohmann, P., Shah, N. J., Langen, K. J., et al. (2021). A novel anti-inflammatory d-peptide inhibits disease phenotype progression in an ALS mouse model. *Molecules* 26:1590. doi: 10.3390/molecules26061590
- Prasansuklab, A., and Tencomnao, T. (2013). Amyloidosis in Alzheimer's disease: the toxicity of amyloid beta (A β), mechanisms of its accumulation and implications of medicinal plants for therapy. *Evid. Based Complement Alternat. Med.* 2013:413808. doi: 10.1155/2013/413808
- Räder, A. F. B., Reichart, F., Weinmüller, M., and Kessler, H. (2018). Improving oral bioavailability of cyclic peptides by N-methylation. *Bioorg. Med. Chem.* 26, 2766–2773. doi: 10.1016/j.bmc.2017.08.031
- Ralhan, K., Guru, K. V., and Gupta, S. (2017). “Arginine-rich β -sheet breaker peptides as potential tau protein aggregation inhibitors,” in *SfN's 47th Annual Meeting, Neuroscience 2017* (Washington, D.C., USA), 11–15. <https://repository.iitgn.ac.in/handle/123456789/3328>.
- Ramanathan, A., Nelson, A. R., Sagare, A. P., and Zlokovic, B. V. (2015). Impaired vascular-mediated clearance of brain amyloid beta in Alzheimer's disease: the role, regulation and restoration of LRP1. *Front. Aging Neurosci.* 7:136. doi: 10.3389/fnagi.2015.00136
- Reddy, P. H., Manczak, M., Mao, P., Calkins, M. J., Reddy, A. P., and Shirendeb, U. (2010). Amyloid-beta and mitochondria in aging and Alzheimer's disease: implications for synaptic damage and cognitive decline. *J. Alzheimers Dis.* 20, S499–S512. doi: 10.3233/JAD-2010-100504
- Resende, R., Ferreira, E., Pereira, C., and Resende de Oliveira, C. (2008). Neurotoxic effect of oligomeric and fibrillar species of amyloid-beta peptide 1–42: involvement of endoplasmic reticulum calcium release in oligomer-induced cell death. *Neuroscience* 155, 725–737. doi: 10.1016/j.neuroscience.2008.06.036
- Ricciarelli, R., and Fedele, E. (2017). The amyloid cascade hypothesis in Alzheimer's disease: it's time to change our mind. *Curr. Neuropharmacol.* 15, 926–935. doi: 10.2174/1570159X15666170116143743
- Sambandam, T., Belousova, M., Accavitti-Loper, M. A., Blanquicett, C., Guercello, V., Rajmakers, R., et al. (2004). Increased peptidylarginine deiminase type II in hypoxic astrocytes. *Biochem. Biophys. Res. Commun.* 325, 1324–1329. doi: 10.1016/j.bbrc.2004.10.173
- Schemmert, S., Scharfmann, E., Zafiu, C., Kass, B., Hartwig, S., Lehr, S., et al. (2019). A β oligomer elimination restores cognition in transgenic Alzheimer's mice with full-blown pathology. *Mol. Neurobiol.* 56, 2211–2223. doi: 10.1007/s12035-018-1209-3
- Schmidt, N., Mishra, A., Lai, G. H., and Wong, G. C. (2010). Arginine-rich cell-penetrating peptides. *FEBS Lett.* 584, 1806–1813. doi: 10.1016/j.febslet.2009.11.046
- Schneider, C., Shukla, D., and Trout, B. L. (2011). Arginine and the hofmeister series: the role of ion-ion interactions in protein aggregation suppression. *J. Phys. Chem. B* 115, 7447–7458. doi: 10.1021/jp111920y
- Schneider, C. P., and Trout, B. L. (2009). Investigation of cosolute-protein preferential interaction coefficients: new insight into the mechanism by which

- arginine inhibits aggregation. *J. Phys. Chem. B* 113, 2050–2058. doi: 10.1021/jp808042w
- Seidler, P. M., Boyer, D. R., Rodriguez, J. A., Sawaya, M. R., Cascio, D., Murray, K., et al. (2018). Structure-based inhibitors of tau aggregation. *Nat. Chem.* 10, 170–176. doi: 10.1038/nchem.2889
- Sengupta, U., Nilson, A. N., and Kayed, R. (2016). The role of amyloid- β oligomers in toxicity, propagation and immunotherapy. *EBioMedicine* 6, 42–49. doi: 10.1016/j.ebiom.2016.03.035
- Shafiei, S. S., Guerrero-Muñoz, M. J., and Castillo-Carranza, D. L. (2017). Tau oligomers: cytotoxicity, propagation and mitochondrial damage. *Front. Aging Neurosci.* 9:83. doi: 10.3389/fnagi.2017.00083
- Sharma, S., Sarkar, S., Paul, S. S., Roy, S., and Chattopadhyay, K. (2013). A small molecule chemical chaperone optimizes its unfolded state contraction and denaturant like properties. *Sci. Rep.* 3:3525. doi: 10.1038/srep03525
- Shiraki, K., Kudou, M., Fujiwara, S., Imanaka, T., and Takagi, M. (2002). Biophysical effect of amino acids on the prevention of protein aggregation. *J. Biochem.* 132, 591–595. doi: 10.1093/oxfordjournals.jbchem.a003261
- Shristi, A. (2014). Developing arginine as an inhibitor for α -Synuclein aggregation: an innovative therapy to combat Parkinson's disease. *Asian J. Sci. Technol.* 5, 615–619.
- Shukla, D., and Trout, B. L. (2010). Interaction of arginine with proteins and the mechanism by which it inhibits aggregation. *J. Phys. Chem. B* 114, 13426–13438. doi: 10.1021/jp108399g
- Sievers, S. A., Karanicolas, J., Chang, H. W., Zhao, A., Jiang, L., Zirafi, O., et al. (2011). Structure-based design of non-natural amino-acid inhibitors of amyloid fibril formation. *Nature* 475, 96–100. doi: 10.1038/nature10154
- Singh, V., Patel, K. A., Sharma, R. K., Patil, P. R., Joshi, A. S., Parihar, R., et al. (2019). Discovery of arginine ethyl ester as polyglutamine aggregation inhibitor: conformational transitioning of huntingtin N-terminus augments aggregation suppression. *ACS Chem. Neurosci.* 10, 3969–3985. doi: 10.1021/acscchemneuro.9b00167
- Slade, D. J., Fang, P., Dreyton, C. J., Zhang, Y., Fuhrmann, J., Rempel, D., et al. (2015). Protein arginine deiminase 2 binds calcium in an ordered fashion: implications for inhibitor design. *ACS Chem. Biol.* 10, 1043–1053. doi: 10.1021/cb500933j
- Smirnova, E., Safenkova, I., Stein-Margolina, B., Shubin, V., and Gurvits, B. (2013). L-arginine induces protein aggregation and transformation of supramolecular structures of the aggregates. *Amino Acids* 45, 845–855. doi: 10.1007/s00726-013-1528-7
- Soto, C., Sigurdsson, E. M., Morelli, L., Kumar, R. A., Castaño, E. M., and Frangione, B. (1998). Beta-sheet breaker peptides inhibit fibrillogenesis in a rat brain model of amyloidosis: implications for Alzheimer's therapy. *Nat. Med.* 4, 822–826. doi: 10.1038/nm0798-822
- Stancu, I. C., Vasconcelos, B., Terwel, D., and Dewachter, I. (2014). Models of β -amyloid induced Tau-pathology: the long and "folded" road to understand the mechanism. *Mol. Neurodegener.* 9:51. doi: 10.1186/1750-1326-9-51
- Tesei, G., Vazdar, M., Jensen, M. R., Craggell, C., Mason, P. E., Heyda, J., et al. (2017). Self-association of a highly charged arginine-rich cell-penetrating peptide. *Proc. Natl. Acad. Sci. U S A* 114, 11428–11433. doi: 10.1073/pnas.1712078114
- Thal, D. R., and Fändrich, M. (2015). Protein aggregation in Alzheimer's disease: A β and τ and their potential roles in the pathogenesis of AD. *Acta Neuropathol.* 129, 163–165. doi: 10.1007/s00401-015-1387-2
- Tsumoto, K., Umetsu, M., Kumagai, I., Ejima, D., Philo, J. S., and Arakawa, T. (2004). Role of arginine in protein refolding, solubilization and purification. *Biotechnol. Prog.* 20, 1301–1308. doi: 10.1021/bp0498793
- Twohig, D., and Nielsen, H. M. (2019). α -synuclein in the pathophysiology of Alzheimer's disease. *Mol. Neurodegener.* 14:23. doi: 10.1186/s13024-019-0320-x
- Vagenende, V., Han, A. X., Mueller, M., and Trout, B. L. (2013). Protein-associated cation clusters in aqueous arginine solutions and their effects on protein stability and size. *ACS Chem. Biol.* 8, 416–422. doi: 10.1021/cb300440x
- Valerio, M., Porcelli, F., Zbilut, J. P., Giuliani, A., Manetti, C., and Conti, F. (2008). pH effects on the conformational preferences of amyloid beta-peptide (1–40) in HFIP aqueous solution by NMR spectroscopy. *Chem. Med. Chem.* 3, 833–843. doi: 10.1002/cmdc.200700324
- van Groen, T., Wiesehan, K., Funke, S. A., Kadish, I., Nagel-Steger, L., and Willbold, D. (2008). Reduction of Alzheimer's disease amyloid plaque load in transgenic mice by D3, A D-enantiomeric peptide identified by mirror image phage display. *Chem. Med. Chem.* 3, 1848–1852. doi: 10.1002/cmdc.200800273
- Varughese, M. M., and Newman, J. (2012). Inhibitory effects of arginine on the aggregation of bovine insulin. *J. Biophys.* 2012:434289. doi: 10.1155/2012/434289
- Vazdar, M., Heyda, J., Mason, P. E., Tesei, G., Allolio, C., Lund, M., et al. (2018). Arginine "magic": guanidinium like-charge ion pairing from aqueous salts to cell penetrating peptides. *Acc. Chem. Res.* 51, 1455–1464. doi: 10.1021/acs.accounts.8b00098
- Vershinin, M., Carter, B. C., Razafsky, D. S., King, S. J., and Gross, S. P. (2007). Multiple-motor based transport and its regulation by tau. *Proc. Natl. Acad. Sci. U S A* 104, 87–92. doi: 10.1073/pnas.0607919104
- Viet, M. H., Ngo, S. T., Lam, N. S., and Li, M. S. (2011). Inhibition of aggregation of amyloid peptides by beta-sheet breaker peptides and their binding affinity. *J. Phys. Chem. B* 115, 7433–7446. doi: 10.1021/jp1116728
- von Bergen, M., Barghorn, S., Biernat, J., Mandelkow, E. M., and Mandelkow, E. (2005). Tau aggregation is driven by a transition from random coil to beta sheet structure. *Biochim. Biophys. Acta* 1739, 158–166. doi: 10.1016/j.bbdis.2004.09.010
- Wang, L. L., Song, Y. P., Mi, J. H., and Ding, M. L. (2021). Peptidyl arginine deiminase 4 and its potential role in Alzheimer's disease. *Med. Hypotheses* 146:110466. doi: 10.1016/j.mehy.2020.110466
- Wang, R., and Reddy, P. H. (2017). Role of glutamate and NMDA receptors in Alzheimer's disease. *J. Alzheimers Dis.* 57, 1041–1048. doi: 10.3233/JAD-160763
- Wang, S., and Wang, Y. (2013). Peptidylarginine deiminases in citrullination, gene regulation, health and pathogenesis. *Biochim. Biophys. Acta* 1829, 1126–1135. doi: 10.1016/j.bbarm.2013.07.003
- Wascher, T. C., Posch, K., Wallner, S., Hermetter, A., Kostner, G. M., and Graier, W. F. (1997). Vascular effects of L-arginine: anything beyond a substrate for the NO-synthase. *Biochem. Biophys. Res. Commun.* 234, 35–38. doi: 10.1006/bbrc.1997.9994
- Watanabe, K., Nakamura, K., Akikusa, S., Okada, T., Kodaka, M., Konakahara, T., et al. (2002). Inhibitors of fibril formation and cytotoxicity of beta-amyloid peptide composed of KLVFF recognition element and flexible hydrophilic disrupting element. *Biochem. Biophys. Res. Commun.* 290, 121–124. doi: 10.1006/bbrc.2001.6191
- Weingarten, M. D., Lockwood, A. H., Hwo, S. Y., and Kirschner, M. W. (1975). A protein factor essential for microtubule assembly. *Proc. Natl. Acad. Sci. U S A* 72, 1858–1862. doi: 10.1073/pnas.72.5.1858
- Welander, H., Fränberg, J., Graff, C., Sundström, E., Winblad, B., and Tjernberg, L. O. (2009). Abeta43 is more frequent than Abeta40 in amyloid plaque cores from Alzheimer disease brains. *J. Neurochem.* 110, 697–706. doi: 10.1111/j.1471-4159.2009.06170.x
- Weller, J., and Budson, A. (2018). Current understanding of Alzheimer's disease diagnosis and treatment. *F1000Res.* 7:F1000 Faculty Rev-1161. doi: 10.12688/f1000research.14506.1
- Wiesehan, K., Buder, K., Linke, R. P., Patt, S., Stoldt, M., Unger, E., et al. (2003). Selection of D-amino-acid peptides that bind to Alzheimer's disease amyloid peptide abeta1–42 by mirror image phage display. *Chembiochem* 4, 748–753. doi: 10.1002/cbic.200300631
- Williamson, R., Scales, T., Clark, B. R., Gibb, G., Reynolds, C. H., Kellie, S., et al. (2002). Rapid tyrosine phosphorylation of neuronal proteins including tau and focal adhesion kinase in response to amyloid-beta peptide exposure: involvement of Src family protein kinases. *J. Neurosci.* 22, 10–20. doi: 10.1523/JNEUROSCI.22-01-00010.2002
- Wolff, M., Zhang-Haagen, B., Decker, C., Barz, B., Schneider, M., Biehl, R., et al. (2017). A β 42 pentamers/hexamers are the smallest detectable oligomers in solution. *Sci. Rep.* 7:2493. doi: 10.1038/s41598-017-02370-3
- Xu, B., Jacobs, M. I., Kostko, O., and Ahmed, M. (2017). Guanidinium group remains protonated in a strongly basic arginine solution. *Chemphyschem* 18, 1503–1506. doi: 10.1002/cphc.201700197

- Yankner, B. A., and Lu, T. (2009). Amyloid beta-protein toxicity and the pathogenesis of Alzheimer disease. *J. Biol. Chem.* 284, 4755–4759. doi: 10.1074/jbc.R800018200
- Zhang, T., Gering, I., Kutzsche, J., Nagel-Steger, L., and Willbold, D. (2019). Toward the mode of action of the clinical stage all-d-enantiomeric peptide RD2 on A β 42 aggregation. *ACS Chem. Neurosci.* 10, 4800–4809. doi: 10.1021/acscchemneuro.9b00458
- Zhang, X., Zhang, X., Zhong, M., Zhao, P., Guo, C., Li, Y., et al. (2020). Selection of a d-enantiomeric peptide specifically binding to PHF6 for inhibiting tau aggregation in transgenic mice. *ACS Chem. Neurosci.* 11, 4240–4253. doi: 10.1021/acscchemneuro.0c00518
- Zhao, W., and Ai, H. (2018). Effect of pH on A β 42 monomer and fibril-like oligomers-decoding in silico of the roles of pK values of charged residues. *Chemphyschem* 19, 1103–1116. doi: 10.1002/cphc.201701384
- Zhao, Y., and Zhao, B. (2013). Oxidative stress and the pathogenesis of Alzheimer's disease. *Oxid. Med. Cell Longev.* 2013:316523. doi: 10.1155/2013/316523
- Zheng, H., and Koo, E. H. (2011). Biology and pathophysiology of the amyloid precursor protein. *Mol. Neurodegener.* 6:27. doi: 10.1186/1750-1326-6-27
- Zheng, J., Liu, C., Sawaya, M. R., Vadla, B., Khan, S., Woods, R. J., et al. (2011). Macrocyclic β -sheet peptides that inhibit the aggregation of a tau-protein-derived hexapeptide. *J. Am. Chem. Soc.* 133, 3144–3157. doi: 10.1021/ja110545h
- Ziehm, T., Brener, O., van Groen, T., Kadish, I., Frenzel, D., Tusche, M., et al. (2016). Increase of positive net charge and conformational rigidity enhances the efficacy of d-enantiomeric peptides designed to eliminate cytotoxic A β species. *ACS Chem. Neurosci.* 7, 1088–1096. doi: 10.1021/acscchemneuro.6b00047

Conflict of Interest: BM is a named inventor of several patent applications regarding the use of CARPs as neuroprotective agents, and a shareholder in Argenica Therapeutics, a company developing R18 as a neurotherapeutic.

The remaining author declares the absence of any commercial or financial relationships that could be construed as a potential conflict of interest.

Publisher's Note: All claims expressed in this article are solely those of the authors and do not necessarily represent those of their affiliated organizations, or those of the publisher, the editors and the reviewers. Any product that may be evaluated in this article, or claim that may be made by its manufacturer, is not guaranteed or endorsed by the publisher.

Copyright © 2021 Mamsa and Meloni. This is an open-access article distributed under the terms of the Creative Commons Attribution License (CC BY). The use, distribution or reproduction in other forums is permitted, provided the original author(s) and the copyright owner(s) are credited and that the original publication in this journal is cited, in accordance with accepted academic practice. No use, distribution or reproduction is permitted which does not comply with these terms.

Advantages of publishing in Frontiers



OPEN ACCESS

Articles are free to read
for greatest visibility
and readership



FAST PUBLICATION

Around 90 days
from submission
to decision



HIGH QUALITY PEER-REVIEW

Rigorous, collaborative,
and constructive
peer-review



TRANSPARENT PEER-REVIEW

Editors and reviewers
acknowledged by name
on published articles

Frontiers

Avenue du Tribunal-Fédéral 34
1005 Lausanne | Switzerland

Visit us: www.frontiersin.org

Contact us: frontiersin.org/about/contact



REPRODUCIBILITY OF RESEARCH

Support open data
and methods to enhance
research reproducibility



DIGITAL PUBLISHING

Articles designed
for optimal readership
across devices



FOLLOW US

@frontiersin



IMPACT METRICS

Advanced article metrics
track visibility across
digital media



EXTENSIVE PROMOTION

Marketing
and promotion
of impactful research



LOOP RESEARCH NETWORK

Our network
increases your
article's readership